Astrophysics and Space Science Library 413

Henri M.J. Boffin
Giovanni Carraro
Giacomo Beccari *Editors*

Ecology of Blue Straggler Stars

ASSL

Springer

Ecology of Blue Straggler Stars

Astrophysics and Space Science Library

More information about this series at
http://www.springer.com/series/5664

Henri M. J. Boffin • Giovanni Carraro •
Giacomo Beccari
Editors

Ecology of Blue Straggler Stars

Springer

Editors
Henri M. J. Boffin
Giovanni Carraro
ESO Vitacura
Santiago de Chile
Chile

Giacomo Beccari
ESO
Garching bei München
Germany

ISSN 0067-0057 ISSN 2214-7985 (electronic)
ISBN 978-3-662-44433-7 ISBN 978-3-662-44434-4 (eBook)
DOI 10.1007/978-3-662-44434-4
Springer Heidelberg New York Dordrecht London

Library of Congress Control Number: 2014957414

Cover illustration: The centre of the globular cluster Messier 4, as seen with the Hubble Space Telescope. Globular clusters are the first place where blue straggler stars were discovered and are still ideally suited to study them, even though we now have found these strange objects in many different places. Credit: ESA/Hubble & NASA

Printed on acid-free paper

Springer is part of Springer Science+Business Media (www.springer.com)

Ah—but I was so much older then; I'm younger than that now

Bob Dylan

Foreword

Don't be fooled: even though the idea of this book arose from the *Ecology of Blue Stragglers* workshop which took place at the ESO headquarters in Santiago, Chile, this is not the proceedings of the conference. The editors, indeed, have from the start decided to produce the first ever textbook on this important subject. This book, therefore, will provide an invaluable resource to students and researchers interested in this rich, yet far from understood, stage in stellar evolution.

The book begins with a deep review of the observational status of blue straggler stars (BSS) distributed in several chapters dealing with blue straggler stars (BSS) in clusters, nearby dwarf irregular galaxies, and the field. The picture that emerges from the observations confirms the earlier impressions that the BSS phenomenon is somehow related to binarity. Having firmly established the observational status of BSS, the book then goes on to summarise the essential aspects of the theory of BSS genesis, which seems intimately related to mass transfer between binary components, such that the evolution of both the mass-donor and mass-accreting stars is changed by the mass transfer process. Even more spectacularly, in order to reconcile the theory with the observations, it seems necessary to invoke two channels for the formation of BSS: mass transfer via the canonical Roche overflow, and a merger of the two components. This opens a completely new way of understanding stellar evolution that is not limited to low-mass stars, but seems to be ubiquitous across the entire Hertzsprung–Russell diagram. This has profound consequences in our understanding of stellar populations in galaxies, which are also described in this timely and comprehensive book.

VLT Programme Scientist Jorge Melnick

Preface

The existence of blue straggler stars (BSS), which appear younger, hotter, and more massive than their siblings, is at odds with a simple picture of stellar evolution, as such stars should have exhausted their nuclear fuel and evolved long ago to become cooling white dwarfs. As such, BSS could just be some quirks but in fact their understanding requires a deep knowledge of many different areas in astronomy, from stellar evolution through cluster dynamics, from chemical abundances to stellar populations. In November 2012, a workshop on this important topic took place at the ESO Chilean headquarters in Santiago. The many topics covered at this workshop were introduced by very comprehensive invited reviews, providing a unique and insightful view on the field. These reviews have now become chapters of the first ever book on BSS.

The book starts with an introduction about stellar evolution that should be of use to students or researchers from different fields. The following chapter, by R. Cannon, covers the history of the field. It reminds us that the first discovery of blue straggler stars was made in 1953 by Alan Sandage in the globular cluster M3. The germ of the idea that BSS are due to binaries was planted by no-one else than Fred Hoyle, 2 years only after their discoveries, as well as by John Crawford the same year, and then further by William McCrea in 1964.

The following chapters are dedicated to a review of the observational evidences, clearly demonstrating that BSS are ubiquitous: they exist in globular clusters (F. Ferraro and colleagues), open clusters (R. Mathieu and A. Geller), and nearby dwarf galaxies (Y. Momany). Field blue stragglers have also been identified from their anomalous kinematics and chemical abundances (G. Preston).

R. Mathieu and A. Geller present the incredible fine study of the BSS population in the open cluster NGC 188, allowing his colleagues and him to do, as they call it, "micro-astronomics", i.e. determining the binary frequency and orbital parameter's (period, eccentricity and secondary mass) distributions. G. Preston shows what we know of BSS in the field, and the conclusion is that BSS in the field and in open clusters present a high binary fraction, with orbital periods of 1,000 days, small orbital eccentricities and typical secondary masses of 0.5 $M_{\odot}$. Whether this is

similar to the population of BSS in globular clusters is still unknown, but such properties are most likely the result of mass transfer from an AGB star, which is also responsible for the formation of peculiar red giants. The fact that most field BSS are chemically enriched in s-process elements—the exact signature of peculiar red giants!—is thus perhaps no surprise, even though much more work is required to connect the two categories of stars.

F. Ferraro and his group present the challenges linked with observing these relatively faint stars in over-crowded stellar regions as the globular cluster cores. Blue straggler stars are a common population found in each globular cluster properly observed, with some clusters (e.g. M80) having more than 100 BSS identified! This allows for a comparative analysis of BSS in globular clusters with different physical parameters showing the deep connection that is emerging between the BSS properties and the parent cluster dynamical evolution. Y. Monamy takes us to even larger scales and presents the populations of BSS in dwarf galaxies, looking in details at their radial distribution and luminosity function. The following chapters are devoted to the theory and the interpretation of the data. Boffin reviews the mass transfer by wind scenario in binary systems, while N. Ivanova covers Roche lobe overflow. If the latter mass transfer scenario is most likely to occur in the very short period systems (with orbital period of a few days or less), the crucial question is to know in which conditions the mass transfer from an AGB star could be stable, so as to avoid the common-envelope phase, thought to cause a dramatic shrinkage of the orbit and so unable to explain the long orbital periods observed in open clusters.

Further, H. Perets and M. Davies present the possible formation channels for BSS in their various environments, S. McMillan reviews the dynamical evolution of globular clusters and how BSS fit into the picture, while C. Knigge and A. Sills make detailed confrontations between theory and observations. In some cases, data exist that are so precise as to get detailed information on the characteristics of some blue straggler systems—mass, temperature and luminosity—so as to confront them with evolutionary tracks and mass transfer modelling. The conclusion is that it is still unclear how to produce BSS with their observed luminosities, much too low for their mass, or how one can even produce BSS with such high masses. Similarly, although it is generally assumed that two mechanisms are responsible for blue straggler stars—merger and mass transfer (both of which are operating in the same cluster)—the exact preponderance of one mechanism over the other is clearly depending on the cluster's property, that is, the *blue straggler's ecology*.

The last chapter by Y. Xin and L. Deng shows the importance of BSS in stellar population synthesis, and how these can dramatically alter the observables of distant systems—their neglect could lead to large errors in the inferred properties of galaxies.

The few good reviews about BSS date back from the 1990s and are completely outdated. No book existed on this important topic. We have now remedied to this situation and we hope this will bring even more researchers to this exciting field of study.

Santiago de Chile, Chile — Henri Boffin
Santiago de Chile, Chile — Giovanni Carraro
Garching bei München, Germany — Giacomo Beccari

Contents

Chapter 1
Introduction to the Theory of Stellar Evolution

Giacomo Beccari and Giovanni Carraro

1.1 The Pre-Main Sequence Phase

Stars form from the collapse and the fragmentation of molecular clouds. This is possible under physical conditions that induce a local instability in the cloud. In term of mass, the limit of stability is called Jeans mass. This critical mass depends on the thermodynamic variables described by the equation:

$$M_{Jeans} \propto T^{3/2}\rho^{-1/2}, \tag{1.1}$$

making the cold and dense clouds of molecular hydrogen the ideal environment in which the gravitational collapse occurs.

In reality, the collapse of a cloud with a mass of few hundred solar masses is responsible of the formation of stellar associations. The following discussion focuses on the behaviour of a single star.

The outcome of the collapse of the molecular gas is a fully convective protostar in hydrostatic equilibrium. As such, it compensates the lose of energy due to radiation by contracting, following the virial theorem. The contraction causes a temperature rise in the core of the structure. As a consequence the opacity κ (the laws of Kramers describe a dependency of type $\kappa \propto T^{-3.5}$) and the module of the radiative gradient decrease. The latter is defined as:

$$\frac{dT}{dr} = -\frac{3}{4ac}\frac{\kappa\rho F}{T^3}, \tag{1.2}$$

where F is the flux emitted and ρ is the density of the structure.

G. Beccari (✉) • G. Carraro
European Southern Observatory, Alonso de Cordova 3107, Santiago de Chile, Chile
e-mail: gbeccari@eso.org; gcarraro@eso.org

H.M.J. Boffin et al. (eds.), *Ecology of Blue Straggler Stars*, Astrophysics and Space Science Library 413, DOI 10.1007/978-3-662-44434-4_1

The Schwarzschild criterion states that the convection is triggered when the radiative gradient is greater in magnitude, than the adiabatic lapse rate. Hence, the effect of the irradiation of the protostar is to gradually erase the convection inside its structure.

In the Hertzsprung–Russell (HR) diagram, i.e. the log T_{eff}—log L diagram, where T_{eff} is the surface temperature of a star and L its bolometric luminosity, this results in the protostar departure from the so-called *Hayashi track*. The latter is defined as the evolutionary path traced by a fully convective structure in hydrostatic equilibrium.

At this point, the protostar continues to contract and the temperature in the nucleus continues to increase until it becomes sufficiently high ($T \simeq 10^7$ K) to trigger the reactions of nuclear burning of hydrogen. At this stage the star reaches the Zero Age Main Sequence (ZAMS, see Fig. 1.1).

It is important to know that $M_{lim} \simeq 0.08$ M$_\odot$ represents the mass limit below which the physical conditions needed for the activation of nuclear reactions are not reached. Hence, this value represents the minimum mass for an object to become a star. Any object of mass lower than M_{lim} will be a brown dwarf or a planet.

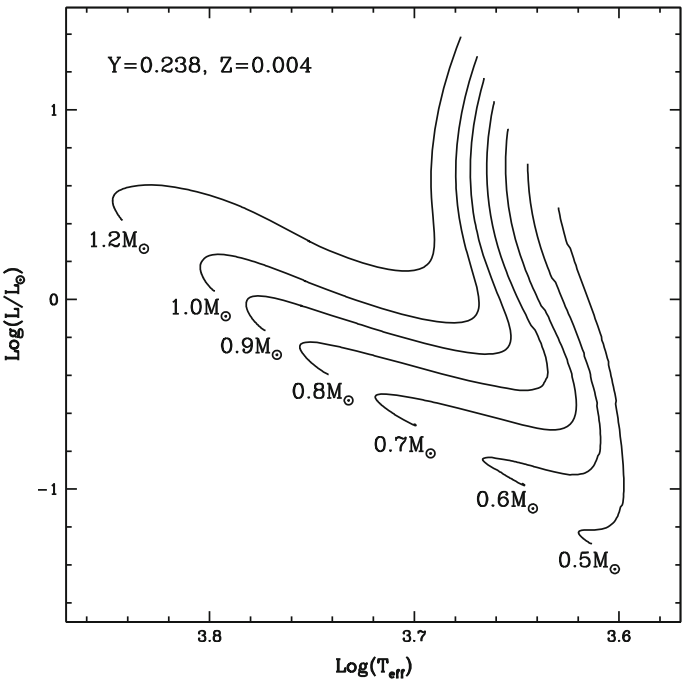

Fig. 1.1 A set of Pre-Main Sequence tracks in a HR diagram (theoretical models from Tognelli et al. 2011). The masses of the PMS objects are reported in the figure

1.2 The Main Sequence

The Main Sequence (MS) is defined as the stage during which a star burns hydrogen in its nucleus. This is the longest evolutionary phase in the life of a star. Such burning may occur through two different mechanisms: either through the proton–proton (PP) chain, or through the Carbon–Nitrogen–Oxygen (CNO) cycle. The two types of combustion have very different impacts on the stellar structure: stars that produce energy via the PP chain, in fact, are characterised by a radiative core and a convective envelope, while stars that consume hydrogen through the CNO cycle have a convective core and a radiative envelope.

Both processes consume four hydrogen nuclei to give as net product an helium nucleus. As a consequence the energetic budget involved in both processes is very similar. Nevertheless, from the equations:

$$\varepsilon_{pp} \propto \rho X^2 T_6^4 \tag{1.3}$$

$$\varepsilon_{CNO} \propto \rho X T_6^{16}, \tag{1.4}$$

where X is the mass fraction of hydrogen and T_6 is the temperature expressed in millions of Kelvin, it is clear that the reactions have very different temperature dependences. Hence, at lower temperatures the PP chain dominates, but with rising temperatures there is a sudden transition to dominance by the CNO cycle, which has an energy production rate that varies strongly with temperature. This is why the CNO cycle is more important for more massive stars: their interior temperatures are higher, thus favouring the CNO cycle.

Moreover, since:

$$\frac{dL}{dr} = 4\pi r^2 \rho(r) \varepsilon, \tag{1.5}$$

during the CNO cycle the luminosity and hence the flux emitted is very high and, as a consequence of the Schwarzschild criterion, the convention is activated in the stellar nucleus. The opposite happens in the case of a PP chain.

Typically, the value of mass that separates these two behaviours is $\sim 1.2\,\mathrm{M}_\odot$. It should however be noted that, in most cases both burning channels are active. The distinction in the two cases simply describes the predominance of one channel over the other, depending on the temperature that is reached in the core (see Fig. 1.2).

The entire evolution of a star on the MS is then characterised by the consumption of hydrogen in the core with the production of helium. As a consequence, the average molecular weight, defined as

$$\mu = \frac{1}{(2X + 0.75Y + 0.5Z)}, \tag{1.6}$$

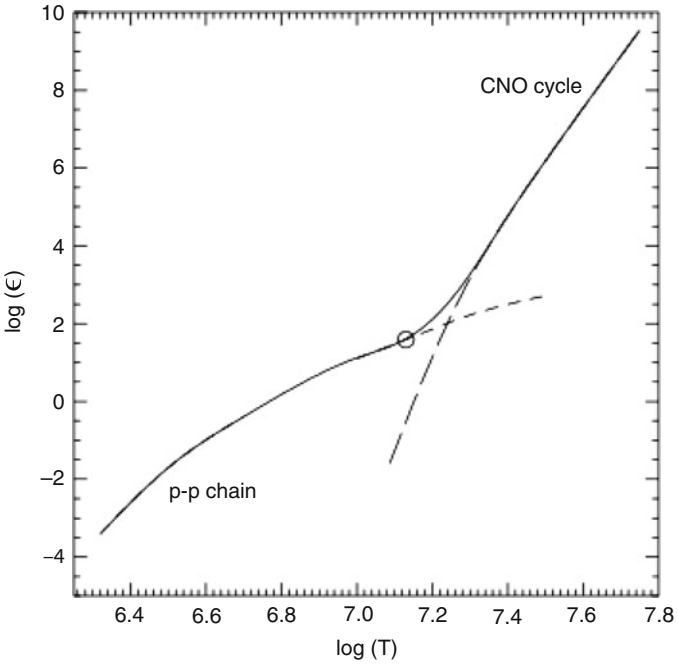

Fig. 1.2 Efficiency of the PP chain and CNO cycle as a function of the temperature. The picture is reproduced from Salaris and Cassisi (2005) with permission from the authors

where Y is the helium mass fraction and Z the mass fraction of all the other elements[1] increases. As a result, considering as valid the approximation of non-degenerate gas (necessary to build stable cycles of thermonuclear reactions), the pressure decreases and the core slowly contracts. Both the density and the temperature in the core—and thus also the efficiency of the nuclear reactions—increase as a consequence of the contraction. The effect of all this is, again, an increase of the flux emitted, with the consequent introduction of convective motions in the stellar interiors. It is in this way, then, that the star starts its ascent on the subgiant branch (SGB).

1.3 The Combustion of Hydrogen in a Shell: The Sub and Red Giant Branches

The evolutionary path of a star after the consumption of the hydrogen in the core depends of its mass.

[1] Z is called in astronomy the *metallicity*, and is given by $Z = 1 - X - Y$.

The first important distinction to be considered is that between stars of mass less than or greater than $\sim$1.2 $M_\odot$ or, as previously described, between stars with or without a convective core.

The effect of convection is to smooth any gradients of chemical abundances in the region where it is active. This means that the hydrogen in the radiative nuclei is exhausted only in the innermost region, while in the regions immediately adjacent there are already the conditions to trigger the reactions of hydrogen burning in thick shells. Convective nuclei are characterised by the presence of extensive regions, above the nucleus itself, in which the availability of fuel is low. Before it can ignite the hydrogen burning in the shell, which in this case is more distant and colder, the structure must contract and heat up to a temperature of $\sim 10^7$ K.

This translates along the evolutionary tracks on the HR diagram, in a continuous sequence in the case of low mass stars and in a broken line, characterised by a "hook", for stars in which the convection is dominant (Fig. 1.3). During this phase the gravitational energy is the only source of energy.

Once turned on, the shell becomes the main energy source of the star in terms of luminosity: a nucleus of inert helium has formed at the centre as the temperatures are not high enough to activate the helium burning (T $\sim 1.5 \cdot 10^8$ K).

However, the shell proceeds consuming hydrogen outward of the stellar structure, and as consequence, inert helium is deposited in the core. If the core is in conditions of perfect gas, it remains isothermal until its mass does not exceed the critical value of the mass of Schonberg–Chandrasekhar (M_{SC}): when this occurs, or when $M_{core} > 0.12 M_{star}$, the core shrinks until the activation of the helium-burning reaction, also called reaction 3α.

As the shell keeps on burning hydrogen along the stellar structure, it also gets progressively thinner. The structure responds by expanding and cooling at the surface. At this stage the stars move in the HR diagram to the regions dominated by convection, which is indeed penetrating the stellar volume from the outside. When the star is sufficiently close to the Hayashi track, the SGB phase ends.

The stellar structure is not able to reach and/or overcome the Hayashi track which is by definition suitable for fully convective structures. The structure responds to the solicitations from the shell by rapidly increasing its luminosity and its radius (Fig. 1.3). As a consequence the temperature at the surface decreases, and thus it begins the Red Giant Branch (RGB) phase.

It is important to notice that the time needed for a star to reach this evolutionary stage depends on the initial mass of the star itself. In particular, if a star is very massive ($M > 6\ M_\odot$), the mass of its core at the end of the MS is already greater than M_{SC}, and thus the duration of the phase of RGB is extremely short.

For intermediate massive stars ($2.2\ M_\odot < M < 6\ M_\odot$), the RGB phase is slower because it is necessary that the shell generates enough helium to exceed the value of critical mass and the core can start to contract.

The situation is different if the star has initial mass $<2.2\ M_\odot$: in this case, in fact, the structure develops a core only partially degenerate that continues to increase its mass while remaining practically isothermal (shrinks very slowly). This, of course,

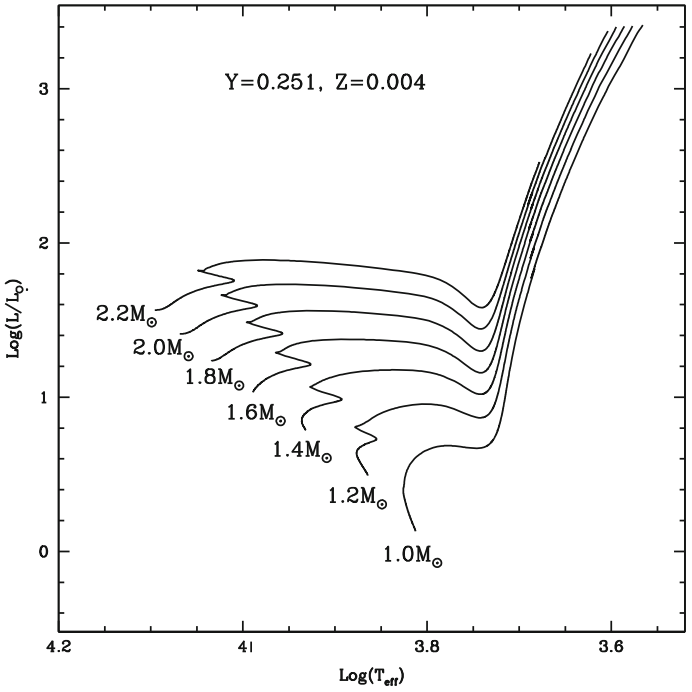

Fig. 1.3 Evolutionary tracks at a given metallicity showing the SGB and RGB phases for stars at different masses (as indicated in the figure; theoretical models from Pietrinferni et al. 2006)

slows down the nuclear heating and indeed the nucleus is able to trigger the 3α reaction only after an extremely long time.

Shortly after the beginning of the RGB, the first event of chemical mixing experienced by a star after the initiation of nuclear reactions takes place: the so called first *dredge-up*. The convection, penetrating into the areas affected by the CNO cycle, brings some of its products to the surface, causing the alterations of the chemical composition. In particular, the surface abundances of He and N increase, while those of C and O decrease proportionally to the characteristic times of nuclear reactions in the CNO cycle.

From this point onwards the shell starts to approach the limit reached by the convection which tends to recede. A discontinuity in the profile of hydrogen remains in correspondence with this limit, which results in an important characteristic along the evolutionary track: the so called *RGB bump*. When the shell, in fact, is located in proximity of the discontinuity, it encounters a region in which the average molecular weight μ is suddenly lower; since the luminosity of the shell, L_{shell} obeys the relation

$$L_{shell} \propto T \propto \mu^{7.5}, \tag{1.7}$$

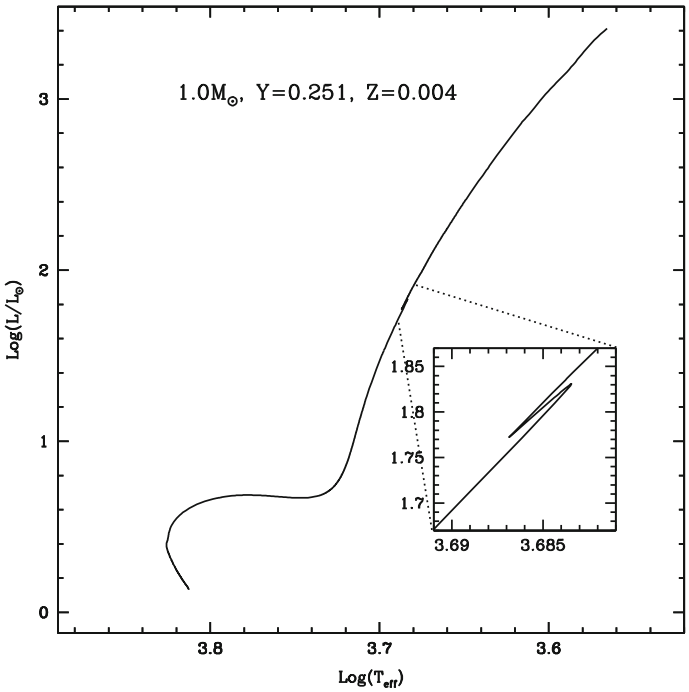

Fig. 1.4 The behaviour of an evolutionary track at the RGB bump is show in the inset box together with a 1 $M_\odot$ track (theoretical model from Pietrinferni et al. 2006)

then a reverse is visible in the evolutionary track on the HR diagram. The RGB stars then move back along the evolutionary track once the shell leaves the discontinuity behind (Fig. 1.4).

This theoretical sequence is observationally witnessed by an increase of density of stars in a small region along the RGB, created by the fact that a star spends a relatively long time in a short range of luminosity and temperature.

The luminosity of the RGB bump is therefore a critical observable allowing one to understand how deep the convection pushed into the stellar interiors.

After the bump, the stars move very rapidly along the RGB up to the last point of this evolutionary sequence: the *RGB tip*.

It is important to emphasise again the golden rule that the initial mass of the star is driving the evolution of the star itself along these firsts evolutionary stages: massive stars ($M > 15\ M_\odot$), for example, do not experience the phase of RGB, as the core is already sufficiently massive to contract and warm up to the quick triggering of the 3α reaction. The stars of intermediate mass ($2\ M_\odot < M < 15\ M_\odot$) develop a short RGB, so that it is not theoretically expected for the stars to pass to the stage of RGB bump. The core, in fact, reaches a temperature of $T \simeq 1.5 \cdot 10^8$ K, required to trigger the helium-burning before the shell reaches the discontinuity of the profile of hydrogen. For low mass stars ($M < 2.2\ M_\odot$), finally, the RGB has the greatest

importance. In fact, it is widespread in brightness and lasts longer, which results in a very populated and bright giant branch in the observed colour-magnitude diagram.

1.4 The Helium-Burning in the Core: The Horizontal Branch

Keeping in mind the distinction on the initial mass proposed in the previous section, it is clear that for massive stars the fusion of the helium core happens rapidly and in a continuous manner with respect to the previous stage of burning, without producing important features on evolutionary tracks. The situation is very different for the intermediate and low-mass stars.

As described above, because of the combustion of hydrogen in the core, stars of initial mass $<2.2M_{\odot}$ develop a semi-degenerate core, which accretes mass from the shell during the RGB phase without contracting and remaining isothermal. The partial degeneration of the environment has two important effects: the temperature of the combustion of helium is lowered and the ability of contraction of the core decreases, delaying the triggering of the 3α reaction. Moreover, the initiation of the 3α reaction in a degenerated environment causes a thermonuclear runaway. This is the consequence of the lack of the negative feedback between temperature and pressure, as (in non-relativistic degenerate environment):

$$P \propto \rho^{5/3}. \tag{1.8}$$

The ignition of the helium burning is, for these reasons, semi-explosive and is generally referred to as the *He-flash*.

This evolutionary stage is defined as a flash since the release of energy is almost instantaneous and sizable, corresponding to about 10^{11} $L_{\odot}$. Nevertheless, this energy is used for the expansion of the semi-degenerate stellar structure and for the removal of the degeneration itself.

In particular, the helium flash is nothing but a series of flash that are repeated until the degeneration of the nucleus is completely removed and the stable burning of helium is performed in conditions of perfect gas.

In detail, the flash will originate in the following way: first, the star that is evolving along the RGB is characterised by conditions of density and temperature such as to enable the interaction between the photons produced in the nucleus and the degenerate electrons, according to the relation

$$\gamma + e^{-} \longrightarrow e^{-} + \nu + \bar{\nu}. \tag{1.9}$$

The neutrinos produced, having a small cross section, tend to leave the structure subtracting energy. In particular the inner regions tend to cool more rapidly and, consequently, in the core of the star forms a reverse gradient of temperature that causes the ignition of the first flash in the outer area of the core. The sudden release of energy massively increases the flux emitted and the convective motions that are

established expand the structure by partly removing the degeneracy. What remains is a small semi-degenerate core that undergoes the same process repeatedly until the degeneracy is removed completely and creates the conditions that allow the stable process of helium burning in a perfect gas.

It is important to specify that the He-flash is still not the phase of helium burning: only 5 % of that element is consumed during the flash.

The stable helium burning in the core according to the reaction 3α

$$^4\text{He} + ^4\text{He} \longrightarrow ^8\text{Be} \tag{1.10}$$

$$^8\text{Be} + ^4\text{He} \longrightarrow ^{12}\text{C} + \gamma, \tag{1.11}$$

starts along the so called *Zero Age Horizontal Branch* (ZAHB) defined, in the HR diagram, as the locus of points in which a star is positioned, in a very short time ($\sim 10^6$ years), once the helium flash is finished. Notice that the ZAHB is located on the HR diagram at a lower luminosity with respect to the tip of the RGB, as a consequence of the expansion and relaxation of the nucleus of the stars after the He-flash.

It should be noted that for low mass stars the helium flash happens when the mass of the degenerate core is 0.5 $M_\odot$. This is a key ingredient to understand where a star positions itself on the ZAHB.

For stars of intermediate mass, however, the core is not in degenerate conditions and turns on the reactions of helium-burning once it exceeds the mass M_{SC} and when the ignition temperatures are reached. Even in this case, however, the evolutionary tracks decrease in luminosity with respect to the end point of the RGB. The shell, which keeps the dominant role in terms of emission, is pushed towards the outer and colder regions, where the efficiency ϵ decreases.

The positioning of a star on the ZAHB depends on the ratio between the mass of the nucleus and the total mass of the star. In this sense, the ZAHB (as for the ZAMS) represents a sequence in mass (see Fig. 1.5).

Since the low-mass stars reach the tip of the RGB at constant mass of the nucleus, the location of these stars on the HB depends only on the mass of the envelope. In particular, the higher this value, and therefore the greater is the total mass of the star, the redder the point of the ZAHB in which it is positioned. In fact a thicker envelope is able to "shield" better the star, which then appears cooler and redder. For these same reasons, stars of intermediate mass do not describe a real sequence on the HR diagram: they locate themselves in the reddest part of the ZAHB and constitute the so-called *He-clump*.

When the luminosity of the shell dominates with respect to the emission from the nucleus, the evolutionary track moves towards the bluest regions of the colour magnitude diagram. Conversely, if it is the core that dominates, the stellar structure tends to expand, to cool and the tracks then moves towards the convective zone of the HR diagram, i.e. towards the Hayashi's track (Fig. 1.5). At the end of the HB phase, when the helium in the core is exhausted, the star moves towards the *Asymptotic Giant Branch* (AGB).

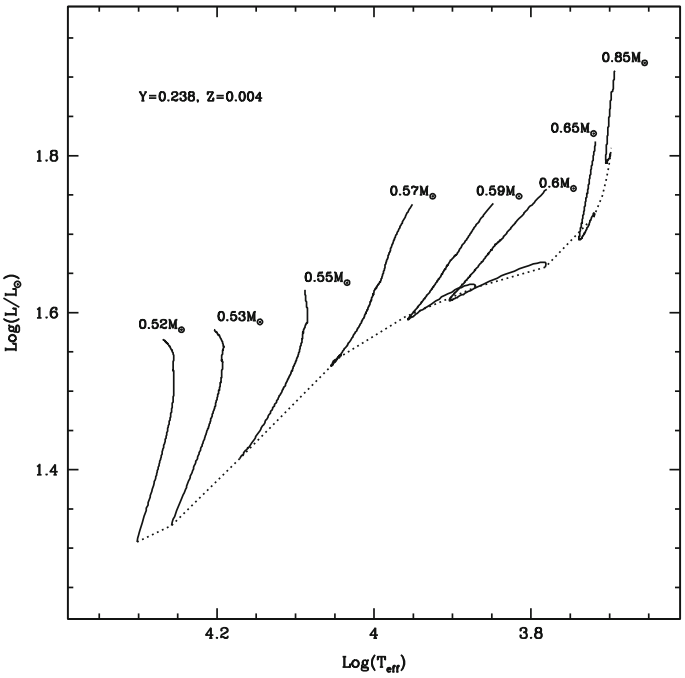

Fig. 1.5 Theoretical ZAHB (*dashed line*) with a progenitor of $M = 0.9\mathrm{M}_{\odot}$. The models are taken from Castellani et al. (2003)

1.5 Two Burning Shells: The AGB

At the end of the HB phase, the core of the stars, consisting of carbon and oxygen, becomes extremely compact being formed by a smaller number of atoms, and therefore warmer. The same properties are shared by the adjacent regions, and consequently it is possible to turn on the helium-burning reaction in a shell.

Once again the trigger occurs in a region partially degenerate and therefore leads to the release of a huge amount of energy. The first flash that is generated traces on the HR diagram the so-called stretch of Early AGB (EAGB, see Fig. 1.6).

During the EAGB the shell of hydrogen, still on, continues to deposit helium in the layer that separates it from the core of C–O, making it more and more degenerate. As already discussed, the degeneracy lowers the ignition temperature of the helium until the shell lights up in a semi-explosive way. The emission of energy, this time of approximately 10^6 $\mathrm{L}_{\odot}$, translates in the expansion of the inter-shell that removes the degeneracy and pushes the shell of hydrogen towards the outer and colder regions, reducing the luminosity. The shell of helium becomes dominant, and continues to deposit CO on the core, making it more and more degenerate. At the same time the inter-shell stops progressively to expand until the shell of hydrogen returns to dominate.

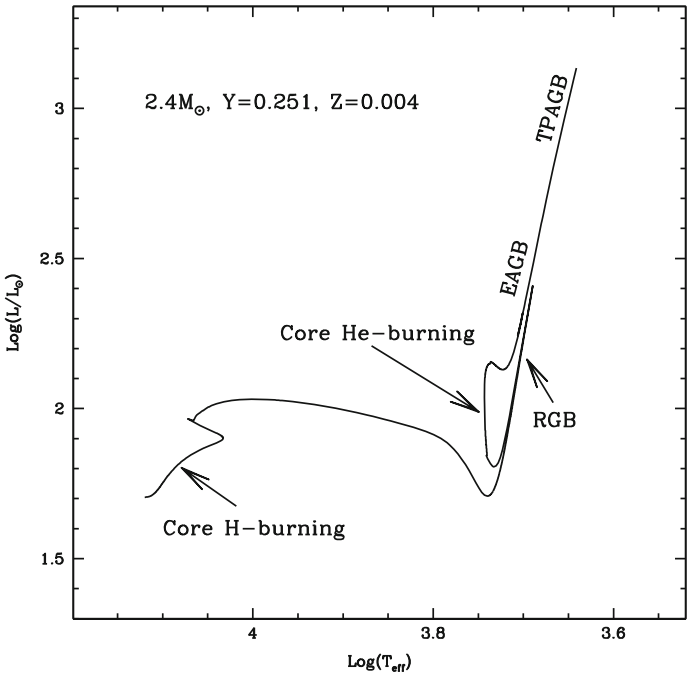

Fig. 1.6 Theoretical evolutionary track for an intermediate massive star (2.4 $M_{\odot}$; theoretical model from Pietrinferni et al. 2006)

During this phase of EAGB, the stars in the mass range $M > 4.6\ M_{\odot}$, can experience the second chemical mixing process. As already mentioned, the expansion of the structure allow the convection layers to penetrate from the outside. If this is sufficiently deep to arrive to the inter-shell, it can bring at the surface elements such as He, C, N, O, which are the products of combustion of hydrogen. In this sense, the second dredge-up is extremely similar to the first.

The next phase is called Thermally Pulsing AGB (TPAGB) and substantially is the cyclic repetition of the phenomena that have occurred during the EAGB, which can be just considered as the first of these thermal pulses. The fundamental process that occurs during TPAGB is the third dredge-up. Since the convection is penetrating from the outside (following the cooling of the envelope) and at the same time it must be expanding from the inside (thanks to the thermal pulse), it may happen that, during the inactivity of the shell of hydrogen, the two convective streams are in contact. In this case, therefore, the mixing involves extremely profound regions of the star (∼75 % of the structure) and generates chemical signatures that differ form those characterising the other two dredge-ups, such as an increase of the abundance of carbon at the surface.

During the entire duration of the AGB phase, the stars may be affected by phenomena of substantial mass loss. This is due to the fact that the envelope of these

stars is expanded and cold as ever during the other phases of evolution: therefore the formation of layers of molecules and dust becomes possible, layers which are then removed as stellar wind by the effect of radiation pressure.

These phenomena of mass loss become even more important when considered from the point of view of the chemistry of the medium in which stellar populations evolve. Besides the two dredge-ups, in fact, other peculiar chemical events take place during the AGB. One of these is the production of s-process elements by neutron capture reactions. During the thermal pulse in the intershell, convection remixes isotopes such as ^{14}N and ^{4}He that may come in contact and react, giving rise to nuclear chains such as:

$$^{14}\mathrm{N} + ^{4}\mathrm{He} \longrightarrow ^{18}\mathrm{F} + \gamma \tag{1.12}$$

$$^{18}\mathrm{F} \longrightarrow ^{18}\mathrm{O} + \mathrm{e}^{+} + \nu \tag{1.13}$$

$$^{18}\mathrm{O} + ^{4}\mathrm{He} \longrightarrow ^{22}\mathrm{Ne} + \gamma \tag{1.14}$$

$$^{22}\mathrm{Ne} + ^{4}\mathrm{He} \longrightarrow ^{25}\mathrm{Mg} + n. \tag{1.15}$$

These reactions require temperatures $T > 3.5 \cdot 10^8$ K to complete and only stars of mass $M > 3\ \mathrm{M}_\odot$ satisfy such a requirement. Free neutrons that are created are then captured and contribute to form s-elements that are quickly brought to the surface thanks to the dredge-up and are then dispersed in the interstellar medium through the above-mentioned events of mass loss. They then become the important tracers for AGB stars of this type.

In lower-mass AGB stars, the intershell region does not reach the required temperature to start the chemical reaction involved in this chain. However, in AGB stars with mass $<3\ \mathrm{M}_\odot$ another reaction that can act as an alternative source of neutrons is $^{13}\mathrm{C}(\alpha, \mathrm{n})^{16}\mathrm{O}$. This reaction requires a temperature of $\sim 9 \cdot 10^7$ K to operate.

Another mechanism that can be established during these phases is the so-called *hot bottom burning*: stars of mass $M > 5\ \mathrm{M}_\odot$ reach, at the base of the convective envelope, temperatures able to trigger the secondary cycles of the CNO cycle. These proton capture reactions, through the creation of N, O, F, Ne, Na, Mg, may proceed until the formation of aluminum, and as for the s-elements, these elements enrich the interstellar medium with proportions corresponding to the characteristic times of the reaction itself. This event might be at the origin of the peculiar anti-correlations between some chemical abundances (such as Na and O, or Mg and Al) which characterise all the galactic globular clusters observed to date.

After about a dozen thermal pulses, the latest expansion is sufficient to allow the release of the outermost layers around the nucleus of CO which is rapidly becoming fully degenerate. With this phase, known as post-AGB, the nuclear-active evolution of the stars ends leading to the final stages of a star's life (Fig. 1.7).

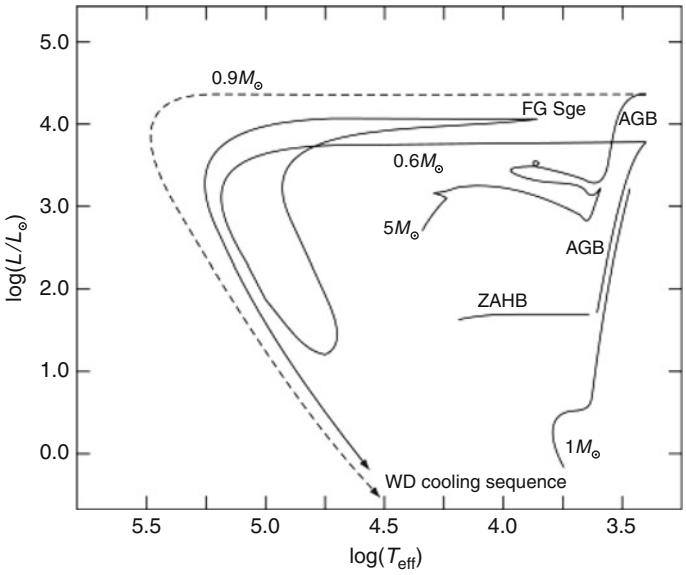

Fig. 1.7 Post ZAMS evolutionary tracks for intermediate and low mass stars. The picture is reproduced from Salaris and Cassisi (2005) with the permission of the authors

1.6 The Final Stages of the Evolution of the Stars

As for the entire evolution of the star, the latest stages depend on its initial mass. As for objects of mass less than 0.3 $M_\odot$ (but still greater than the aforementioned limit of 0.08 $M_\odot$), once the hydrogen is exhausted and its burning is finished, they fail to trigger the burning of the helium in the core. They simply cool as helium white dwarfs. It 's important to specify that objects of this type should not be currently observable, since such very low mass stars evolve off the MS after about 20 Gyr. However several have been observed and the explanation of their nature is linked to phenomena of interaction between two stars in a binary system: when one of the two companions, expanding, reaches its Roche lobe limit, it starts to transfer matter to the secondary. If the primary was evolving along the RGB and loses the entire envelope, what remains is just a helium white dwarf.

Let us now consider stars of mass M between 0.3 $M_\odot < M < 8\ M_\odot$. After the stage of planetary nebula—a brief swan song where the outer shell is ionised by the very hot core, once the outermost layers are dispersed, what remains is a completely degenerate CO. Its destiny is to follow the so-called cooling sequence of a white dwarf. The key feature of a white dwarf is to be in conditions of density and temperature that makes it a structure completely degenerate. As such, it is supported

by the pressure of degenerate electrons. In addition, the mass and radius are linked by a relationship of the type:

$$MR^{1/3} = constant, \tag{1.16}$$

meaning that the more massive a white dwarf is, the smaller it is. Finally, there is a critical value of the mass, called the *Chandrasekhar mass* ($\sim$1.44 $M_\odot$, see e.g. Shu 1982), beyond which the structure is no longer able to maintain equilibrium.

If this limit is exceeded, the structure would collapse to become a completely degenerate system supported by the pressure of degenerate neutrons, or a neutron star.

The white dwarfs have structures which are almost isothermal. The internal temperature is around 10^7 K (only the outermost layer, which constitutes 1 % of the total thickness, is located at a temperature of 10^4–10^5 K), and these objects evolve by cooling down at constant radius. To describe such cooling sequences in the HR diagram, we must firstly consider that, from the mass-radius relation and the Stefan–Boltzmann equation, we have:

$$\log \frac{L}{L_\odot} = 4 \log \frac{T}{T_\odot} - \frac{2}{3} \log \frac{M}{M_\odot} + c, \tag{1.17}$$

meaning that at a given temperature, the more massive a white dwarf is, the less luminous it is. Furthermore, from the equation of radiative transport combined with the equation of hydrostatic equilibrium, we get:

$$L \propto \frac{M_{WD}}{\mathrm{M}_\odot} \frac{\mu T^{7/2}}{Z(1+X)}, \tag{1.18}$$

where the brightness of the white dwarf is due to the residual energy of the components of ions of the structure. Finally, comparing this relation to the time derivative of the thermal energy of the ions, a time-temperature relation derives, which replaced in the previous one gives:

$$L_{WD} = L_0 \left(1 + \frac{5t}{2\tau}\right)^{-7/5}, \tag{1.19}$$

where τ is the characteristic cooling time for a structure of this type. In light of these laws and of the fact that the minimum mass of a white dwarf, according to what already described, is about 0.5 $M_\odot$, a population of white dwarfs in a observed colour-magnitude diagram describes a sequence characterised by a "turn off" that could be used as an indicator of age, but that unfortunately is also very weak and difficult to observe (Fig. 1.8).

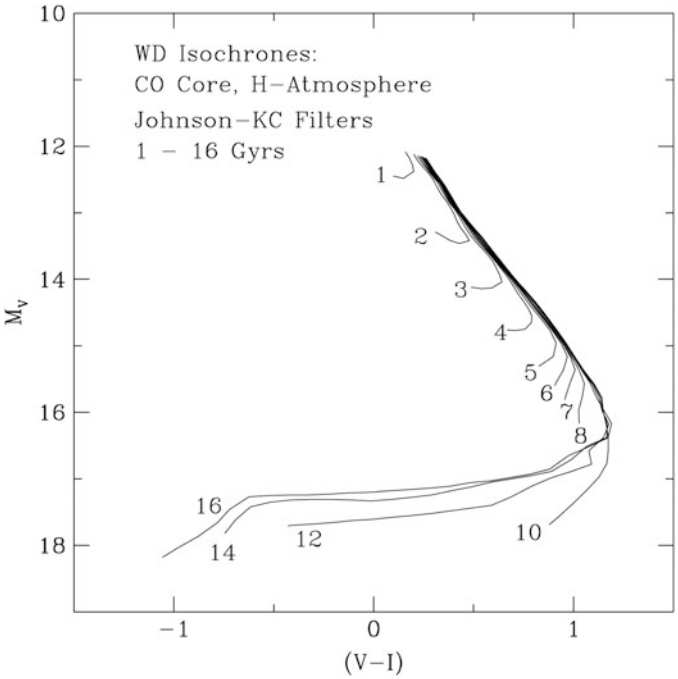

Fig. 1.8 Isochrones in Johnson–Kron/Cousins filters describing the turn off along the white dwarf's cooling sequence. Isochrone ages are indicated. The image is reproduced from Richer et al. (2000) by permission of the AAS

The final stages of the evolution of stars in the mass range $8\ M_\odot < M < 11\ M_\odot$ is quite uncertain. This uncertainty is due to the fact that in this mass range the nucleus of CO formed after the AGB is not completely degenerate. In these conditions, therefore, the trigger of the carbon burning happens in an environment partially cooled by neutrinos, just the same as during the He-flash. If this occurs, the subsequent evolution is quite similar to that of the AGB. Hence, the combustion in a shell of carbon starts, followed by several flashes until the complete removal of the degeneration. The similarity is such that we define this phase as a phase of *super-AGB*.

However, a second scenario considers the possibility that reactions of electron capture become active within the nucleus with the effect to remove the degenerate electrons supporting the stellar structure. With the mass of the core being similar to the Chandrasekhar limit, the structure will collapse to form a neutron star, in a process analogous to that of the core-collapse supernovae but with much less energy.

It remains, finally, to describe the final stages for mass stars $M > 11\ M_\odot$. In these stars, the high mass ensures the ignition of all the nuclear reactions subsequent to those of hydrogen in a non-degenerate environment, up to the reactions that produce ^{56}Fe. At this point, with the formation of a core of iron completely degenerate, the

internal temperature has reached values of about 10^{10} K, sufficient to activate the process of photo-disintegration of iron nuclei, namely:

$$^{56}Fe + \gamma \longrightarrow 13\,^{4}\mathrm{He} + 4n \tag{1.20}$$

and very quickly

$$^{4}He + \gamma \longrightarrow 2p^{+} + 2n. \tag{1.21}$$

These free protons trigger what in astroparticle physics is called the URCA process

$$p^{+} + e^{-} \longrightarrow n + \nu \tag{1.22}$$

and the support provided by the degenerate electrons is removed. The internal supply of the process leads to the collapse of the core. When the density becomes about $10^{14}\,\mathrm{g\,cm^{-3}}$, the collapse stops and a shock wave expels the remaining outer layers, causing a core-collapse supernova (SN). It is important to note that the high flow of free neutrons allows the formation, by neutron capture, of r-process elements, which become a fundamental tracer for this type of supernovae (which in the old spectral classification are defined as Type II SNe), and that about 99 % of the total energy is lost through the emission neutrino. The remnant of this explosion depends, once again, on the initial mass of the star: in general, for masses up to 25 $M_{\odot}$, a neutron star remains after the explosion of a supernova. For masses above this limit, we have the formation of a black hole.

Acknowledgements The authors have used as primary references to prepare this chapter the seminal works of Castellani (1985) and Salaris and Cassisi (2005). It is a pleasure to thank these authors for their exhaustive and illuminating works.

References

Castellani, V.: Astrofisica Stellare. Zanichelli, Bologna (1985)
Castellani, V., Degl'Innocenti, S., Marconi, M., Prada Moroni, P. G., & Sestito, P.: A&A **404**, 645 (2003)
Pietrinferni, Cassisi, Salaris & Castelli: ApJ **642**, 797 (2006)
Richer, H. B., Hansen, B., Limongi, M., et al.: ApJ **529**, 318 (2000)
Salaris, M., & Cassisi, S.: Evolution of Stars and Stellar Populations, Wiley-VCH (2005)
Shu, F. H.: Journal of the British Astronomical Association **93**, 45 (1982)
Tognelli, Prada Moroni, Degl'Innocenti: A& A **533**, A109 (2011)

Chapter 2
Blue Straggler Stars: Early Observations That Failed to Solve the Problem

Russell D. Cannon

2.1 Introduction

The editors asked me to summarise what must amount to prehistory for many of today's readers. My aim is to review the data and ideas that were circulating from Sandage's (1953) original discovery of "anomalous blue stars" in the globular cluster M3, up until about 1992, when what seems to have been the only previous meeting devoted to Blue Straggler Stars (BSSs) was held at the *Space Telescope Science Institute*. Fortunately, the participants at that somewhat informal "Journal Club" meeting persuaded the organisers that it would be worthwhile to publish the proceedings (Sarajedini 1993). I refer readers to that publication, which captures the state of BSS research 20 years ago, and in particular to the introductory paper by Livio (1993) and the concluding summary by Trimble (1993). Papers by Paresce (1963) and Guhathakurta et al. (1963) reported the discovery of new populations of BSSs in the cores of some globular clusters, using the *Hubble Space Telescope* in its original de-focused state, which marked a major new development in the field.

The subtitle of Livio's review (1993), "The Failure of Occam's Razor", essentially says it all. Several plausible and some rather implausible hypotheses had been put forward to explain BSSs, with the most popular involving binary stars transferring mass or merging. It seems that many ways of making BSSs do sometimes occur in nature, although most routes are rare. Much of the confusion probably arose because the purely descriptive but unphysical term "Blue Straggler" came to mean different things to different people.

A few quotations illustrate how perceptions of blue stragglers evolved over four decades. Sandage, who was involved in many of the key observations, changed his

R.D. Cannon (✉)
Australian Astronomical Observatory, PO Box 915, North Ryde, NSW 1670, Australia
e-mail: rdc@aao.gov.au

H.M.J. Boffin et al. (eds.), *Ecology of Blue Straggler Stars*, Astrophysics and Space Science Library 413, DOI 10.1007/978-3-662-44434-4_2

mind several times regarding their significance or even reality (Sect. 2.2). Spinrad (1966) wrote, with considerable prescience:

> The few blue stragglers in M67 are usually dismissed — M67 would then make a perfect model for Baade's Galactic Centre Population.

Precisely how to include BSSs in modelling distant galaxies remains a key issue today. In an early review of BSSs data and explanations, Wheeler (1979) wrote:

> . . . blue stragglers remain one of the unexplained oddities of astronomical lore.

Several other reviews of blue stragglers appeared in the early 1990s (e.g., Saffer 1993). Trimble (1992) concluded that:

> All in all, blue stragglers seem to be both inadequately understood and insufficiently appreciated.

Piet Hut and eight eminent co-authors (Hut et al. 1992) focused specifically on the role of binary stars, including BSSs, in globular clusters, based on a meeting of theorists and observers at Princeton in 1991. Their abstract ends with

> . . . the fascinating interplay between stellar evolution and stellar dynamics which drives globular cluster evolution.

Stryker (1993) concluded that

> Progress has certainly been made in the last 40 years, but BSSs remain an intriguing challenge,

while Bailyn (1995) concentrated on the critical importance of binary stars in the dynamical evolution of globular clusters. He too provided some pertinent quotes:

> . . . every kind of object. . . can be made in at least two different ways, all of which are likely to be significant. . .

and

> Efforts to provide simple explanations for the full range of observed phenomena appear doomed to failure.

Evidently blue stragglers had gradually risen in status, from being either an annoying or intriguing curiosity to becoming an important factor in the evolution of star clusters and galaxies that may well have cosmological significance.

By 1992 there was no longer any doubt about the existence of blue stragglers but it was far from clear how many different formation mechanisms were involved or how many different classes of BSSs existed, while their wider significance for stellar evolution and a full understanding of stellar systems was just starting to be discussed.

Given the existence of several thorough reviews published in the early 1990s, my main focus here will be on the earlier period up to about 1970. Here, I have drawn upon an unpublished chapter of my 1968 PhD thesis that dealt with the BSSs in a sample of five old open clusters. This work is described in a "summary of a summary" given at a Herstmonceux Conference and is sometimes referred to as "Cannon 1968" although it is hardly a proper publication. This is typical of the

problems faced in trying to track down even one's own publications in the pre-digital age: many papers appear in obscure journals or observatory publications that are often not accessible online. Even the origin of the name "blue straggler" is uncertain (Trimble 1993: see Sect. 2.2.2 below).

2.2 The *Classical* Blue Stragglers

2.2.1 Globular Clusters

The discovery of BSSs came with Sandage's first Colour-Magnitude Diagram (CMD) of M3 (Sandage 1953), part of his PhD work (Fig. 2.1). M3 shows all the major features that characterise the CMDs of globular clusters: it led directly to much of our understanding of stellar evolution, starting from an "Observational Approach to Stellar Evolution" by Sandage himself (Sandage 1957). M3 also contains a group of blue stars lying above the main sequence turn-off (MSTO), apparently younger than the bulk of the cluster stars. They did not look like a single second population of younger stars, nor did they appear related to the Blue Horizontal Branch (BHB). A minor worry was that the majority of the initial sample lay in one quadrant, a good example of the often misleading properties of small samples (Eggen and Sandage 1964: discussion between Schwarzschild and Sandage).

For almost 20 years M3 remained the only convincing example of a globular cluster with BSSs, until Arp and Hartwick (1971) looked at M71. Cannon (1968)

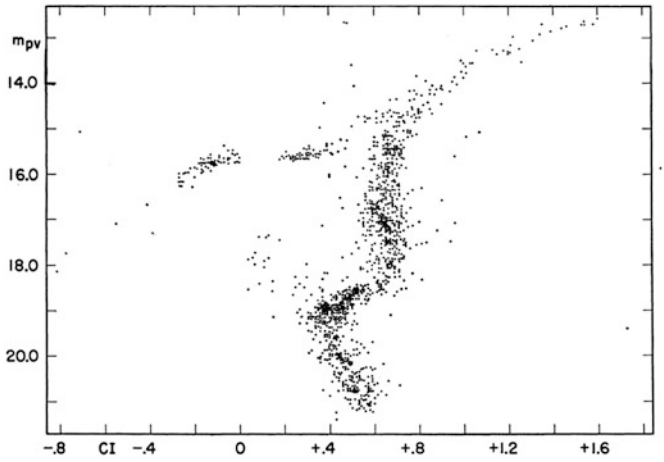

Fig. 2.1 Sandage's first CMD of the globular cluster M3 (Sandage 1953), showing blue stars lying above the main sequence turn-off near $m_{pv} \approx 18$, CI $\approx +0.2$. Reprinted with permission from the AAS

listed eight globular clusters with CMDs that might have revealed BSSs but only M92 (Arp et al. 1953) had sufficiently accurate photometry for enough stars to reveal just one potential BSS, indicating a much smaller population than in M3, relative to subgiants at the same magnitudes. By 1992, the situation was very different, with lists of over 400 BSSs in more than 20 globular clusters (Sarajedini 1993; Fusi Pecci et al. 1993).

2.2.2 The Older Open Clusters

Meanwhile, blue stars above the MSTO had been found in several intermediate-age and old open clusters, with (modern) ages in the range 0.5 to about 8 Gyrs. The earliest and still one of the best examples was NGC 7789 (Burbidge and Sandage 1958) with over 30 such stars, most of which seemed likely to be cluster members on statistical grounds (Fig. 2.2). As in M3, the large sample of BSSs in NGC 7789 do not lie on a well-defined sequence, as would be expected for a single much younger stellar population [familiar nowadays for example in the Carina Dwarf Spheroidal galaxy (Smecker-Hane et al. 1996)].

As an aside, Trimble (1993) set a challenge for someone to discover a reference to the term "blue straggler" prior to 1965. Javier Ahumada reminded us about NGC 7789 during the Ecology of Blue Straggler Stars workshop and probably deserves the glass of wine referred to by Trimble, although George Preston who was present at both meetings was not sure who should provide the prize. A search of the NASA ADS database confirms that Burbidge and Sandage (1958) were the first to use the name in print. My personal recollection is that "blue straggler" was in common use by the mid-1960s.

The much sparser cluster NGC 752 (Roman 1955) contains a single A0 star with a radial velocity and proper motion consistent with cluster membership. Arp and Cuffey (1962) compared the CMD for NGC 2158 with those of NGC 7789 and NGC 752, the first group of "intermediate-age clusters" (ages from about one to a few billion years). They all have characteristic red giant clumps and contain BSSs. Other intermediate-age clusters with BSSs that have proper motions consistent with cluster membership include NGC 2477 (Eggen and Stoy 1961) and NGC 6633 (Hiltner et al. 1958).

The oldest open clusters, such as M67, NGC 188 and NGC 6791, have ages between about five and ten billion years. They have CMDs qualitatively similar to those of globular clusters, with continuous subgiant and giant branches. M67 (Johnson and Sandage 1955) also contained blue stars, but in this case the situation was confused because the same stars could be interpreted as either anomalous main sequence stars or the analogues of globular cluster BHB stars (Fig. 2.3, left panel). Eggen and Sandage (1964) produced a more accurate CMD (Fig. 2.3, right). In addition to improved photometry, they used proper motions (Murray et al. 1965) to cull non-members from the sample. It is apparent that M67 contains a few stars that may be similar to the BSSs in M3, but it is difficult to distinguish between them

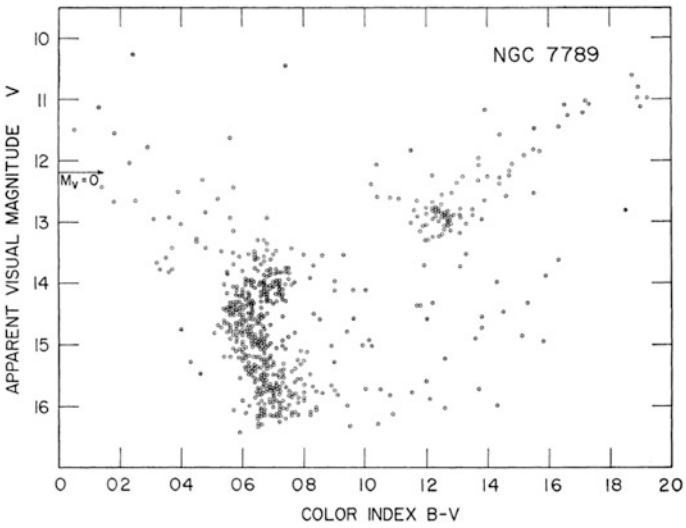

Fig. 2.2 The first CMD for a rich intermediate-age open cluster, NGC 7789 (Burbidge and Sandage 1958). This shows a substantial population of *blue stragglers* in the upper left-hand corner, well above the main sequence turn-off. Reprinted with permission from the AAS

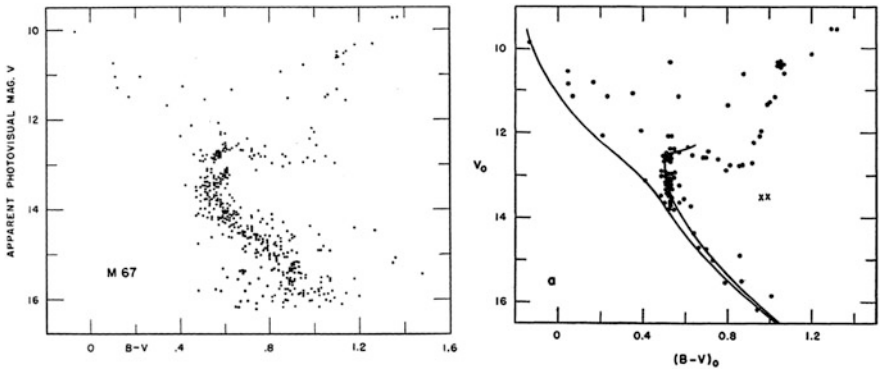

Fig. 2.3 CMDs of the old open cluster M67 by Johnson and Sandage (1955) (*left*) and later (*right*) by Eggen and Sandage (1964), with improved photometry and some non-members omitted. Reprinted with permission from the AAS

and possible analogues of globular cluster BHB stars, as noted by Pesch (1967), who checked that most of the potential BSSs had radial velocities consistent with cluster membership. Sargent (1968) also took spectra and found that the brightest BHB candidate in M67, star Fagerholm 81 in the extreme top left corner of the plots in Fig. 2.3, had the gravity and hence high mass expected for a main sequence star at its location in the CMD, while the next three hottest stars had masses similar to stars on the upper main sequence, consistent with their being BHB stars. However,

Bond and Perry (1971) obtained Strömgren photometry and disagreed with this latter conclusion, finding that all of these blue stars had relatively high masses and were genuine BSSs.

Sandage (1962) produced the first CMD of NGC 188, one of the oldest open clusters. Its CMD is similar to that of M67 but with a fainter MSTO. This too had blue stars above the MSTO, with a larger magnitude gap between most of these and an ill-defined sparse clump of red giants so that there is less confusion with possible BHB stars. Sandage initially concluded that the blue stars were probably not cluster members because they did not seem to be concentrated towards the cluster centre. In a later paper with better photometry over a wider field, Eggen and Sandage (1969) decided that at least some probably were BSS cluster members. NGC 188 is discussed in much more detail in Chap. 3.

For my PhD work I studied a sample of old open clusters (Cannon 1968), using proper motions to remove field stars from their CMDs. This involved measuring matched pairs of photographic plates taken several decades apart. As often happens in astronomy, the program was determined by the available data. I was presented with a collection of photographs of star clusters from the Mount Wilson 60-inch reflector, taken by Adriaan van Maanen circa 1920, together with modern repeats taken by Richard Woolley and Andrew Murray in 1961.

Eventually I had *clean* CMDs for six clusters, all of which contained BSSs. These were M67 (Murray et al. 1965), NGC 188 (Cannon 1968), NGC 6939 (Cannon and Lloyd 1969), NGC 2420 (Cannon 1970), NGC 752 and NGC 7789 (both unpublished). An analysis of the red giant clump stars was published (Cannon and Lloyd 1970) but the BSS analysis never was. The two main results were that virtually all of the BSSs lay within the Population I hydrogen-burning main sequence, between the zero-age main sequence (ZAMS) and the Schönberg–Chandrasekhar limit, and almost all of them lay less than two magnitudes above the MSTO in each cluster. The BSSs were spread across the main sequence band, with no evidence for a concentration at the level of the horizontal branch. Thus all the data were consistent with them having formed by binary mass exchange. Their distribution in magnitude and colour was consistent with simple models of the likely outcome of mass exchange, based on interpolation between a few published evolutionary tracks for single stars (Iben 1967) with two free parameters, the initial mass ratio of the binary and the fraction of mass retained by the system.

The cluster NGC 6791 is an interesting case, straddling the boundary between open and globular clusters. Kinman (1965) showed that it has a CMD similar to those of M67 and NGC 188 (Fig. 2.4). It is one of the oldest known open clusters (Meynet et al. 1993). However, its "blue straggler" sequence is more yellow than blue, being shifted significantly redward from the main sequence. The reality of this shift has been confirmed in a very similar CMD using modern CCD photometry (Montgomery et al. 1994) and with cluster membership confirmed by proper motions (Cudworth and Anthony-Twarog 1993).

Very recently, NGC 6791 has received a great deal of attention, because it is the oldest known metal-rich cluster, with age $\sim$8 Gyr and [Fe/H] $\sim +0.4$, and it lies in

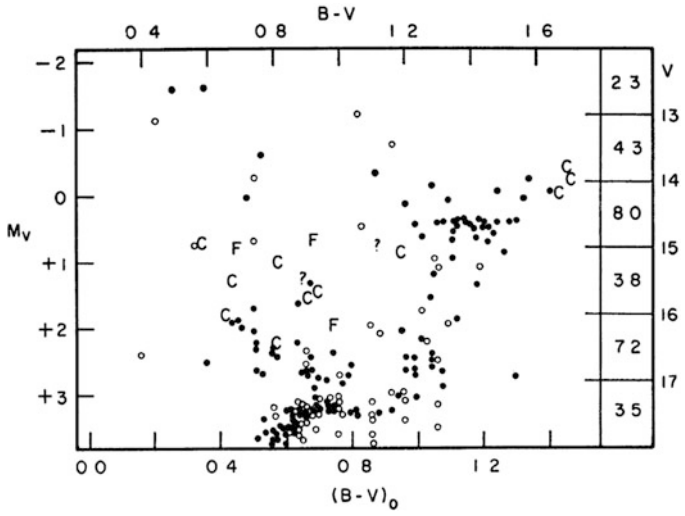

Fig. 2.4 The first CMD of the very old open cluster NGC 6791 (Kinman 1965). The letters "C" and "F" denote probable cluster members and field stars respectively, based on their radial velocities. Reprinted with permission from the AAS

the region of sky covered by the NASA's *Kepler* satellite. As such it was the subject of 25 published papers in 2011–2012. It contains BHB stars as well as BSSs, but perhaps most importantly the *Kepler* data provide information on the core masses and mass loss from asteroseismology of individual stars (Miglio et al. 2012; Cohen and Sarajedini 2012).

2.2.3 Younger Open Clusters and BSSs in the Field

It was realised early on that there were BSSs in younger clusters, but this branch has been more focused on the detailed study of individual relatively bright stars than on their CMDs. Few young clusters are populous enough to have many BSSs, and the "classical" definition based on the CMD only works when the spread in star formation times is small compared with the overall age of a cluster.

Eggen and Herbig (1964) and Eggen and Iben (1988) looked for BSSs within "moving groups" of stars. This concept fell out of favour for some time, but is rapidly reappearing in the context of galaxy formation and the accretion of companion galaxies, and within the framework of "Galactic Archaeology" (Freeman and Bland-Hawthorn 2002). A major compilation of BSSs in all open clusters has been put together by Ahumada and Lapasset (2007).

Blue stragglers must exist among the field stars in the Galaxy but finding them in the metal rich populations is difficult unless they have some characteristic other than being too young, for example as Algol-type systems (Sect. 2.3.1). However, they can

be identified as hot metal-poor stars, as demonstrated for by Bond and McConnell (1971) and by Preston (1994; see also Chap. 4).

2.3 Early Ideas on the Origin of Blue Stragglers

To summarise, the essential properties of "classical" blue stragglers were that they are members of star clusters that lie on the main sequence but above the age-dependent turn-off defined by the majority of the stars in a cluster. Hence they seemed to be either younger or rejuvenated stars, or the consequence of some unusual process.

The data described in Sect. 2.2 illustrate some fundamental problems in pinning down BSSs. Globular clusters are very populous and can give large samples of rare types of star in well-defined locations in the CMD, and cluster membership can often be inferred only statistically. However, their BSSs are relatively faint, which may no longer be such a serious problem for photometry but still puts a limit on the amount and precision of high dispersion spectroscopic data. It is also difficult to obtain comparable data for complete samples of stars in the dense central cores of globular clusters and in the sparse outer regions. By contrast, open clusters are generally closer but much less populous, which means that better data can be obtained but often for only very small samples of BSSs. Open clusters also suffer more from interstellar dust and reddening, and from contamination by field stars so that accurate proper motions and radial velocities are needed to confirm cluster membership.

2.3.1 Blue Stragglers and Algol-Type Eclipsing Binaries

Although most BSSs were almost by definition members of clusters, it was quickly realised that they might be related to the Algol-type binary stars. These are short period eclipsing binaries in which the brighter and more massive star is located near the ZAMS, while the fainter companion looks more highly evolved and hence older. However, they are too common to be the result of chance captures and must be coeval: the explanation is mass exchange.

Many astronomers of my generation were familiar with this concept thanks to a popular astronomy text by Hoyle (1955). It was presented in more detail by Crawford (1955) and by Kopal (1956), who was puzzled by the preponderance of secondaries filling their Roche lobes in Algol systems. Morton (1960) made the first modern stellar evolution calculations and demonstrated that the mass transfer process would normally be unstable and hence short-lived.

The possible link between BSSs and Algols was discussed at one of the first IAU Colloquia, on *Star Clusters and Stellar Evolution*[1] in 1962 (Eggen and Sandage 1964).

The work of McCrea (1964) is probably the most cited reference for Algol-type mass exchange as the origin of BSSs; Smak (1966) developed similar ideas. Later, Algol variables were found among cluster BSSs. For example, Niss et al. (1978) discovered the probable eclipsing variable NJL 5 in Omega Centauri and Margon and Cannon (1989) showed that it was a radial velocity member of the cluster. However, repeated attempts to determine the velocity amplitude accurately or to detect the spectrum of the secondary component were unsuccessful. It was a bit too faint for the 4-m telescopes and spectrographs available at that time.

2.3.2 Other Possible Explanations for BSSs

While binary mass exchange was the early favourite explanation for the formation of BSSs and remains one of the most popular today—now strongly supported by a lot of evidence—some stragglers do not fit that simple picture and many variants have been proposed. Fagerholm 81, the brightest BSS in M67 (Fig. 2.3), is almost three magnitudes above the MSTO and is too bright to have been formed from two main sequence stars. Presumably this required multiple mass transfers or collisions involving binary stars. Direct collisions between single stars are probably too rare to explain most BSSs, but Leonard (1989) argued that binary star collisions should be much more efficient in low-density environments. Ferraro et al. (1993) provided convincing observational evidence for two distinct populations of BSSs in M3, one centrally concentrated and the other much more extended, which may well indicate two different formation mechanisms.

By comparison, several possible mechanisms that involved single stars were either discredited or believed to be much rarer: these included delayed or late star formation, stars whose main sequence lifetime had been extended by large scale mixing (Wheeler 1979), highly evolved stars that happened to land close to the standard main sequence, tidally captured Galactic field stars, or Bondi–Hoyle gas accretion from the ISM. Most of the reviews cited in Sect. 2.1 list the various hypotheses and discuss their relative merits.

[1] A virtually verbatim transcript of the recorded proceedings of this meeting, held at the Royal Greenwich Observatory (RGO) while it was located at Herstmonceux Castle in Sussex, was published in 1964. The meeting is usually said to have been in 1963 but internal evidence points to 1962, a date recently confirmed by Bob Dickens (private communication, 2012). Although this and other Royal Observatory Bulletins are listed in the ADS, the text seems not to be available.

2.4 Expanding the Definition of BSSs, 1970–1990

While observations of the relatively bright blue stragglers in open clusters dominated the literature up to about 1970, the emphasis then shifted towards globular clusters. This was probably a consequence of the advent of a new generation of 4m-class telescopes, and then of CCDs from about 1980 onwards, which hugely increased the power of those telescopes. Coincidentally, the small area and slow readout of early CCDs made them difficult to use for accurate photometry of extended open clusters but they were well-matched to compact dense globular clusters. CCDs also opened up the field of spectroscopy of globular cluster stars, with a further large boost in telescope power when multi-fiber systems began to become available by 1990.

There were already fundamental flaws in the original definition of BSSs, since it only applied directly to stars in clusters and was not based on physically meaningful parameters. The term "red giant" works well because such stars are intrinsically redder (cooler) and bigger (larger radius) than most other stars. The "blueness" of blue stragglers is only relative to the MSTO, and many of the mechanisms devised to explain them can (and probably do) produce stars well below the turn-off that do not *straggle*.

In addition, new discoveries gradually led to a complete revision of the importance of binary stars in star clusters, particularly in the cores of globular clusters. In the mid-1970s came the discovery of low-mass X-ray binaries and cataclysmic variables in many globular clusters (Pooley et al. 2003). A decade later it was found that millisecond pulsars, also believed to originate in binary systems, were exceptionally common in some clusters, most notably 47 Tucanae (Manchester 2001). It became apparent that binary stars must be both created and destroyed in cluster cores. It also became clear that these mechanisms were of fundamental dynamical importance for understanding the evolution of clusters and the process of core collapse that had long puzzled theorists (Bailyn 1995).

Conclusions

All these different perspectives on binary stars and BSSs mean that today probably everyone has a different mental picture of what is meant by the term "blue straggler". It is to be hoped that one outcome of this book will be some guidelines on distinguishing between different types and specifying whether "blue straggler" is being used to define some particular stars or a formation process.

In parallel with the rapid evolution of ideas on BSSs, there has been a radical revision of ideas on the importance of the cluster environment for understanding the complex chemical abundance patterns seen within and between different clusters. The old paradigm that clusters were simple stellar

(continued)

systems that provided ideal tests for stellar evolution theory is no longer tenable. Although most clusters do seem to be made from material that is homogeneous in the relative abundance of iron and other heavy elements that dominate the opacity in the surface layers, there are large variations in the CNO group of elements and a few others such as Na. Moreover, very accurate faint photometry, mainly from HST, has shown that there are multiple stellar populations within some clusters. The exceptional cluster Omega Centauri (NGC 5139) is now regarded as perhaps the remnant core or bulge of a dwarf galaxy accreted by our Galaxy. It also appears that the abundances variations observed within many clusters are not representative of stars in the general field (Kraft 1994). Our standard theories of stellar evolution have been *fine tuned* to fit globular clusters and may not be the whole story.

In any event, it will be difficult to synthesise high redshift galaxies without a complete prescriptive theory of star formation and evolution: BSSs are just one problem among several (the initial mass function; mass loss and horizontal branch structure; asymptotic giant branch evolution, supernovae and the return of processed material to the interstellar medium). Xin et al. (2011) have shown that BSSs can be numerous enough to contribute $\sim$10 % to the integrated light of star clusters at short wavelengths (see also Chap. 14 in this volume).

References

Ahumada, J. A, Lapasset, E.: A&A **463**, 789 (2007)
Arp, H. C., Baum, W. A., Sandage, A. R.: AJ **58**, 4 (1953)
Arp, H. C., Cuffey, J.: ApJ **136**, 51 (1962)
Arp, H. C., Hartwick, F. D. A.: ApJ **167**, 499 (1971)
Bailyn, C. D.: ARA&A **33**, 133 (1995)
Bond, H. E., McConnell, D. J.: ApJ **165**, 51, (1971)
Bond, H. E ., Perry C.L.: PASP **83**, 6388, (1971)
Burbidge, E. M., Sandage, A. R.: ApJ **128**, 174, (1958)
Cannon, R. D.: Observatory **88**, 201, (1968)
Cannon, R. D.: MNRAS **150**, 111, (1970)
Cannon, R. D., Lloyd, C.: MNRAS **144**, 449, (1969)
Cannon, R. D., Lloyd, C.: MNRAS **150**, 279, (1970)
Cohen, R.E., Sarajedini, A.: MNRAS **419**, 342, (2012)
Crawford, J. A.: ApJ **121**, 71, (1955)
Cudworth, K. M., Anthony-Twarog B. J.: BAAS **25**, 1454, (1993)
Eggen, O. J., Herbig G. H.: Roy Obs Bull No. **82**, 89, (1964)
Eggen, O. J., Iben I.: AJ **96**, 635, (1988)
Eggen, O. J., Sandage, A. R., ApJ **140**, 130, (1964)
Eggen, O. J., Sandage, A. R., ApJ **158**, 669, (1969)
Eggen, O. J., Stoy, R. H.: Roy Obs Bull No. **24**, (1961)
Ferraro, F. R., et al.: AJ **106**, 2324, (1993)

Freeman, K. C., Bland-Hawthorn, J., ARA&A, **40**, 487, (2002)
Fusi Pecci, F., Ferraro, F., Cacciari, C.: PASP, **53**, 97, (1993)
Guhathakurta, P. et al.: PASP **53**, 60, (1963)
Hiltner, W A, Iriarte B, Johnson H. L.: ApJ **127**, 539, (1958)
Hoyle, .F.: Mercury, **1961**, 1, (1955)
Hut, P. et al.: PASP **104**, 981, (1992)
Iben, I.: ApJ **147**, 650, (1967)
Johnson, H. L., Sandage A. R.: ApJ **121**, 616, (1955)
Kinman, T. D.: ApJ **142**, 655, (1965)
Kopal, Z.: AnAp **19**, 298, (1956)
Kraft, R. P.: PASP **106**, 553, 1994)
Leonard, P. J. T.: AJ **98**, 217, (1989)
Livio, M.: PASP **53**, 3, (1993)
Manchester, R. N.: PASP **18**, 1, (2001)
Margon, B., Cannon R. D.: Observatory **109**, 82, (1989)
McCrea, W. H.: MNRAS **128** ,147, (1964)
Meynet, G., Mermilliod, J.-C . Maeder, A.: A&AS **98**, 477, (1993)
Miglio, A. et al, MNRAS **419**, 2077, (2012)
Montgomery, K. A., Janes, K. A., Phelps, R. L.: AJ **108**, 585, (1994)
Morton, D. C.: ApJ **132**, 146, (1960)
Murray, C. A., Corben, P. M., Allchorn, M. R.: Roy Obs Bull **91**, 1, (1965)
Niss, B., Jorgensen, H. E., Laustsen, A.: A&AS **32**, 387, (1978)
Paresce, F.: PASP **53**, 30, (1963)
Pesch, P.: ApJ **148**, 781, (1967)
Pooley, D. et al.: ApJ **591**, L131, (2003)
Preston, G. W., Beers, T. C., Shectman, S. A. et al.: AJ **108**, 538, (1994)
Roman, N. G.: ApJ **121**, 454,(1955)
Saffer, R.A.: Introduction to “Blue Stragglers”. ASP Conf. Ser. **53** (1993)
Sandage, A. R.: AJ **58**, 61, (1953)
Sandage, A. R.: ApJ **126**, 326, (1957)
Sandage, A. R.: ApJ **135**,333, (1962)
Sarajedini, A.: PASP **53**, 14, (1993)
Sargent, W.L. W.: ApJ **152**, 885, (1968)
Smak, J.: Acta Astron. **16**, 25, (1966)
Smecker-Hane, T. A. et al.: PASP**98**, 328, (1996)
Spinrad, H.: PASP **78**, 367, (1966)
Stryker, L. L.: PASP **105**, 1081, (1993)
Trimble, V.: PASP **104**, 1, (1992)
Trimble, V.: PASP **53**, 155, (1993)
Wheeler, J. C.: ApJ **234**, 569, (1979)
Xin, Y. et al.: MNRAS **411**, 761, (2011)

Chapter 3
The Blue Stragglers of the Old Open Cluster NGC 188

Robert D. Mathieu and Aaron M. Geller

3.1 Blue Stragglers in Open Clusters

While the photometric study of the globular cluster M3 (Sandage 1953) is often cited as the seminal photometric discovery of blue stragglers, the demonstration of blue stragglers in the open cluster M67 comes soon thereafter in the classic paper of Johnson and Sandage (1955).

Since then blue stragglers have been found in large numbers of open clusters. For example, Ahumada and Lapasset (2007) identify 1887 blue straggler candidates in 427 open clusters, and provide a catalog with a wide array of data for these blue straggler candidates. Ahumada and Lapasset (1995) did macroscopic analyses searching for trends across the open cluster blue straggler populations (using an earlier version of the catalogue), to which the reader is recommended.

As often in science, understanding is gained by combining both macroscopic and microscopic perspectives. Since the discovery paper of Johnson and Sandage (1955), M67 has been a primary laboratory for detailed and fruitful studies of a specific set of blue stragglers (e.g. Mathys 1991; Mathieu and Latham 1986; Leonard and Linnell 1992; Latham 2007).

Recently we have developed a new laboratory, the old open cluster NGC 188. The 20 blue stragglers of this cluster have proven a rich vein that we have mined deeply. Here we first present a comprehensive observational picture of these blue

R.D. Mathieu (✉)
Department of Astronomy, University of Wisconsin-Madison, Madison, WI 53726, USA
e-mail: mathieu@astro.wisc.edu

A.M. Geller
Center for Interdisciplinary Exploration and Research in Astrophysics (CIERA) and Department of Physics and Astronomy, Northwestern University, 2145 Sheridan Rd, Evanston, IL 60208, USA
e-mail: a-geller@northwestern.edu

H.M.J. Boffin et al. (eds.), *Ecology of Blue Straggler Stars*, Astrophysics and Space Science Library 413, DOI 10.1007/978-3-662-44434-4_3

stragglers, followed by comparison of the actual blue stragglers with the products of N-body simulations of NGC 188. Ultimately we suggest that most of the blue stragglers in NGC 188 are the result of mass-transfer processes, quite likely joined by contributions from both collision and merger formation channels.

3.1.1 The Open Cluster NGC 188

The open cluster NGC 188 is one of the richest old open clusters in the Galaxy. A recent proper-motion study finds that NGC 188 contains about 1,500 cluster members down to a magnitude of $V = 21$ (0.5 $M_\odot$) within a 17 pc radius (13 core radii) in projection (Platais et al. 2003). Its old age (7 Gyr), reasonable proximity to the Sun (2 kpc) and low reddening ($E(B-V) = 0.09$; distance and reddening from Sarajedini et al. 1999) have attracted observational studies for more than 50 years. Together these have yielded a wealth of astrophysical data that provides a broad foundation from which to study a dynamically evolved open cluster.

NGC 188 also includes a rich population of 20 blue stragglers,[1] as shown in Fig. 3.1. Importantly, because of the age and solar metallicity of NGC 188, these blue stragglers are in fact not blue—they are late-F and early-G stars with effective temperatures ranging from 6,000 to 6,500 K. The significance of this lies first in permitting the measurement of highly precise radial velocities for these blue stragglers, yielding all of the results to be reported here, and then more broadly in placing the interpretation of these blue stragglers in the context of our rich understanding of the astrophysics of late-type stars.

3.1.2 The WIYN Open Cluster Study and Radial Velocities

The WIYN Observatory 3.5-m telescope combines sizable aperture, wide field of view and excellent image quality. Instrumented with a multi-object spectrograph providing intermediate spectral resolution (R $\sim$ 15,000–20,000) and a large

[1] Our previous papers identified 21 blue stragglers. Recently we found an error in the photometry for WOCS ID 1947 in Platais et al. (2003). In fact star 1947 is a giant; data from the AAVSO Photometric All Sky Survey (APASS) yield $V = 12.54$ and $(B-V) = 1.29$. We have updated appropriately all of the figures and accounting here. We also note that there are two proper-motion members (WOCS IDs 4230 and 4447 from Platais et al. 2003) in the blue-straggler region of the colour-magnitude diagram for which we are unable to derive precise radial-velocity measurements due to rapid rotation. Both stars are likely members ($\geq$90 %) based on proper motions. Our mean radial velocities for both stars place them somewhat outside of the cluster velocity distribution, but we are not sufficiently confident in the radial-velocity measurement errors to report on their membership probability. WOCS ID 4230 is an X-ray source (S27, Gondoin 2005) and a radial-velocity variable. WOCS ID 4447 does not appear to be a radial-velocity variable.

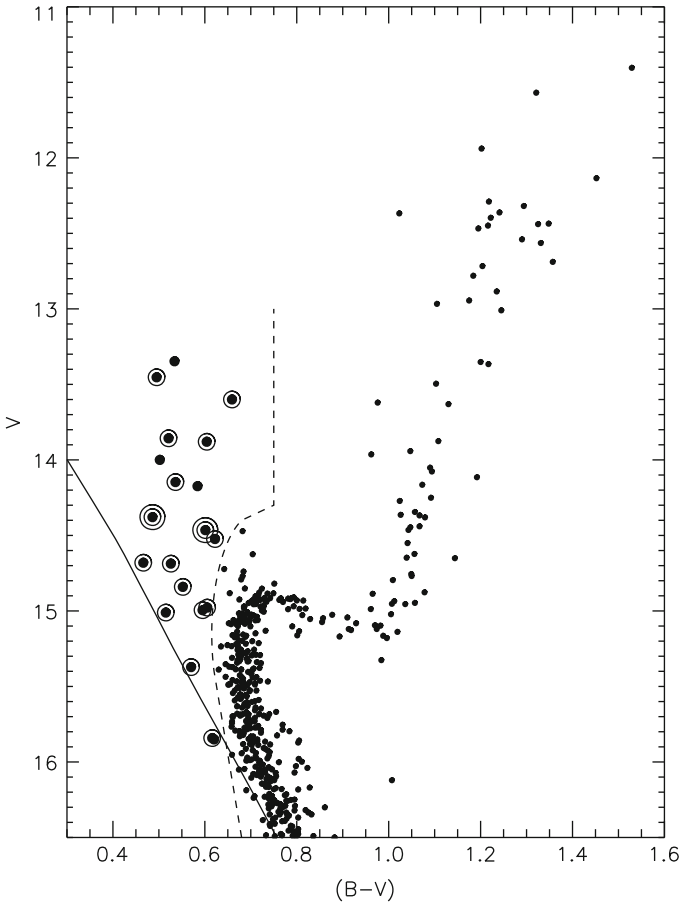

Fig. 3.1 Colour-magnitude diagram for NGC 188. The 20 blue stragglers are shown as larger black dots and are identified as being to the left of the *dashed line* at a given magnitude. The line is drawn so as to not include binaries comprising two normal stars from the cluster turn-off region. For reference, we also show the zero-age main sequence (*solid line*). Updated from Mathieu and Geller (2009)

format CCD imager, it is optimally suited for studies of open clusters. The WIYN Open Cluster Study (WOCS) is a broad collaboration of investigators within and beyond the WIYN consortium who together seek to (1) produce comprehensive photometric, astrometric and spectroscopic data for a select set of new fundamental open clusters, including NGC 188, and (2) address key astrophysical problems with these data (Mathieu 2000).

The primary role of the WOCS team at the University of Wisconsin–Madison has been to acquire time-series, precise ($\sigma = 0.4$ km s^{-1}) radial-velocity measurements for nearly complete samples of solar-type main-sequence stars, giants, and blue stragglers in each of the WOCS clusters. Specifically, radial-velocity measurements

are obtained for well-defined samples of stars having $(B-V)_o > 0.4$ and $V \leq 16.5$ within 30 arcmin of the cluster's centre.

For NGC 188 specifically, the availability of the WOCS deep wide-field proper-motion study allowed straightforward definition of a sample of 1498 stars satisfying these criteria. To date we have 10,046 radial-velocity measurements of 1,151 stars over 39 years, including at least three radial-velocity measurements[2] for essentially all of the 630 stars with non-zero proper-motion membership probabilities and $V \leq 16.5$. Most of these data can be found in Geller et al. (2008).

All 20 blue stragglers yield precise radial-velocity measurements, and each has been observed at least six times over at least 3.3 years. The discoveries from these data comprise the first half of this chapter.

3.2 Observational Findings from the Blue Stragglers in NGC 188

3.2.1 Binary Frequency

Remarkably, the binary frequency ($P < 10^4$ days)[3] among the 20 blue stragglers is 80 % ± 20 %. This binary frequency is more than three times larger than the observed NGC 188 solar-type main-sequence binary frequency of 23 % in the same period range (Mathieu and Geller 2009; Geller and Mathieu 2012).

Only four of the blue stragglers are not detected as spectroscopic binaries. Our incompleteness studies indicate a 24 % chance of having one undetected binary with a period less than 10^4 days, with the incompleteness function rising rapidly toward 10^4 days. Thus it is possible that some of these non-velocity-variable blue stragglers are long-period binaries, perhaps even in this period regime.

All of the blue-straggler spectroscopic binaries now have yielded orbital solutions.[4] Two are double-lined with very short periods, to which we will return.

3.2.2 Orbital Period and Eccentricity Distributions

The distributions of two astrophysically important orbital parameters—period and eccentricity—are often displayed in an $e - \log P$ diagram, as shown in Fig. 3.2

[2]We gratefully acknowledge the extensive radial-velocity observations of Hugh Harris and Robert McClure and their collaborators Roger Griffin and James Gunn, who from 1973 through 1996, executed a radial-velocity survey of 77 stars in NGC 188 and kindly merged their data with ours.

[3]Our Monte Carlo analysis indicates a detection limit for binaries of 10^4 days, and a completeness limit for binary orbital solutions of 3,000 days (Geller and Mathieu 2012).

[4]One of the orbital solutions has not been previously published. The orbital parameters for WOCS ID 8104 are given in Table 3.1.

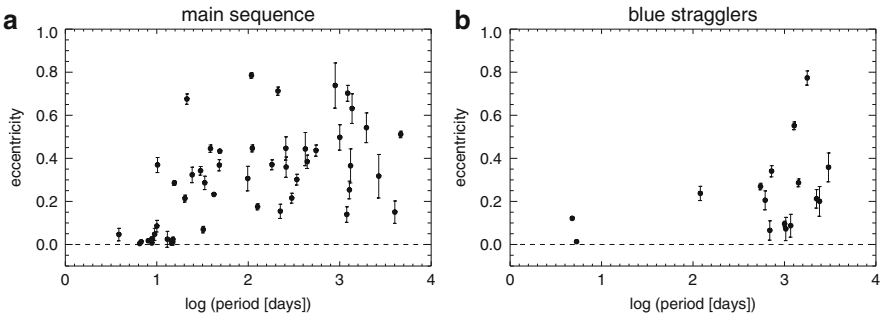

Fig. 3.2 Plots of orbital eccentricity against log period for the NGC 188 solar-type main-sequence binary stars (*left panel*) and for the blue-straggler binary stars (*right panel*). Updated from Mathieu and Geller (2009)

Table 3.1 Orbital parameters for WOCS ID 8104

Parameter	Value
P (days)	2,410 ± 110
γ (km s^{-1})	−41.2± 0.3
K (km s^{-1})	5.5 ± 0.4
e	0.20 ± 0.07
ω (deg)	267 ± 21
$T0$ (HJD—2,400,000 days)	55,390 ± 150
$a \sin i$ (10^6 km)	178 ± 12
$f(m)$ ($M_\odot$)	0.039 ± 0.008
σ (km s^{-1})	0.7
N	19

for both the solar-type main-sequence binary stars and the blue-straggler binary stars.

The period distribution of the blue-straggler binaries is notably different from that of the main-sequence binaries. Most of the blue-straggler binaries have orbital periods within a half-decade of 1,000 days, whereas the main-sequence binaries in NGC 188 (and in other open clusters and the Galactic field) populate all periods from this period domain down to only a few days.

Comparison with the longest period binaries detected among the NGC 188 solar-type stars—which certainly extend to longer periods (e.g., Raghavan et al. 2010)—confirms that the upper limit on the blue straggler orbital periods is likely an observational limit. Again, some of the four "single" blue stragglers may have companions at longer periods.

The eccentricity distribution of the long-period ($P > 100$ days) blue stragglers also differs from the solar-type binaries; the mean eccentricity for the long-period blue-straggler binaries is 0.27 ± 0.05, while the mean eccentricity for similar main-sequence binaries is higher at 0.42 ± 0.04. The formal likelihood of the

two distributions being the same is <1 % (updated from Geller and Mathieu 2012; Mathieu and Geller 2009).

Of special physical significance are the three long-period binaries with eccentricity measurements consistent with circular orbits. None of the solar-type main-sequence binaries with periods longer than the tidal circularisation period of 14.5 days (Meibom and Mathieu 2005) show such low orbital eccentricities, and they are similarly rare among solar-type binaries in other clusters and the field. Tidal circularisation at such long periods would strongly suggest the earlier presence of an evolved star—and possibly mass transfer—in each of these blue straggler binaries.

Even so, most of the long-period blue-straggler binaries do have substantial orbital eccentricities, which as we will see later pose an interesting challenge to mass-transfer scenarios for the formation of blue stragglers.

The two double-lined binaries are also notable for their uniquely short periods (4.8 days and 5.3 days) among the NGC 188 blue stragglers (Fig. 3.2), which later in the chapter we attribute to dynamical encounters for at least one if not both cases. In addition, WOCS ID 5078 has a non-zero orbital eccentricity of 0.12, despite having an orbital period of 4.8 days, well below the tidal circularisation period of 14.5 days. Interestingly, the blue-straggler binary F190 in M67 has remarkably similar orbital properties (Milone and Latham 1992).

Eccentricities of these small magnitudes could be excited by an as yet undetected tertiary companion. Non-zero orbital eccentricities are also expected for the products of stellar dynamical encounters, although higher eccentricities are favoured. Interestingly, such a dynamical origin would require the encounter to have been more recent than the short tidal circularisation timescale at these small orbital periods.

3.2.3 Secondary-Star Mass Distribution

Only two of the blue-straggler binaries are double-lined; for the other 14 our information about the secondary stars derives only from the mass functions of single-lined orbital solutions. Given the unknown inclination, and indeed the poorly known masses of the blue straggler primary stars, standard statistical techniques (Mazeh and Goldberg 1992) must be used to determine the mass distribution of the secondary stars of these blue-straggler binaries. As noted earlier, the double-lined systems are astrophysically distinct from the longer period single-lined binaries, and so we do not include them in the analysis here but discuss them separately in Sect. 3.2.6.

The secondary-star mass distribution of the long-period ($\sim$1,000 days) blue-straggler binaries is shown in Fig. 3.3. It too is noteworthy, in this case for its narrowness around a peak near 0.5 $M_{\odot}$ (Geller and Mathieu 2011). This distribution is markedly (and formally) distinct from the secondary mass distribution of the NGC 188 solar-type main-sequence binaries, which is consistent with a single-star initial mass function (Fig. 3.3; Geller and Mathieu 2012).

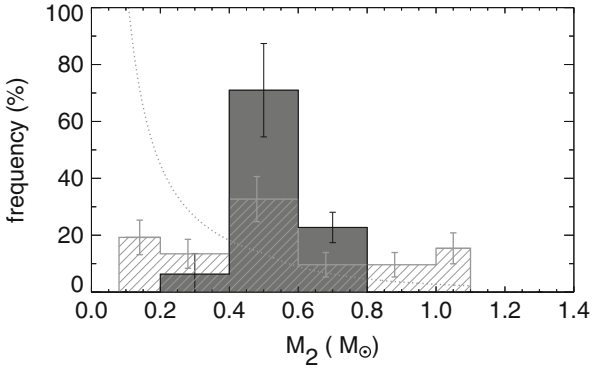

Fig. 3.3 Secondary-star mass distribution for the 13 blue straggler binaries in NGC 188 with periods of order 1,000 days. For comparison, we also plot (*dashed line*) an initial mass function for single stars with masses between 0.08 and 1.1 $M_{\odot}$ (from the hydrogen-burning limit to the current main-sequence turn-off mass in NGC 188). This distribution is similar to that of the secondary masses of the NGC 188 main-sequence binaries. The grey hatched histogram shows the field tertiary mass distribution, evolved to 7 Gyr in isolation (discussed in Sect. 3.3.5.1). Updated from Geller and Mathieu (2011)

That the distribution peaks near 0.5 $M_{\odot}$ likely has important physical significance, since this is also the expected mass of carbon–oxygen white dwarfs left behind after mass transfer from an asymptotic giant branch star.

Such asymptotic giant branch cores would not be expected to have masses lower than 0.4 $M_{\odot}$, this being the core mass that solar-type stars develop at the top of the red giant branch. While the distribution in Fig. 3.3 is statistical, the suggestion of one or two cases with lower secondary star masses might point toward occasional red-giant mass transfer.

The 120-day period of blue straggler WOCS ID 5379, not included in the analysis for Fig. 3.3, is particularly suggestive of a red-giant-branch mass-transfer origin. The mass function for this system is consistent with the theoretical prediction of a helium white dwarf companion with a mass of 0.25–0.5 $M_{\odot}$ as the remnant of red-giant-branch mass transfer. *Hubble Space Telescope* far-ultraviolet photometric observations have detected light from a white dwarf companion (next section), but as yet its mass is not determined.

3.2.4 Detection of White Dwarf Companions

The white dwarfs suggested by the secondary-mass distribution are detectable at far-ultraviolet wavelengths, if they are young enough ($t < 0.4$ Gyr) and therefore hot enough ($T > 12{,}000$ K) to be substantially bluer than the blue stragglers themselves.

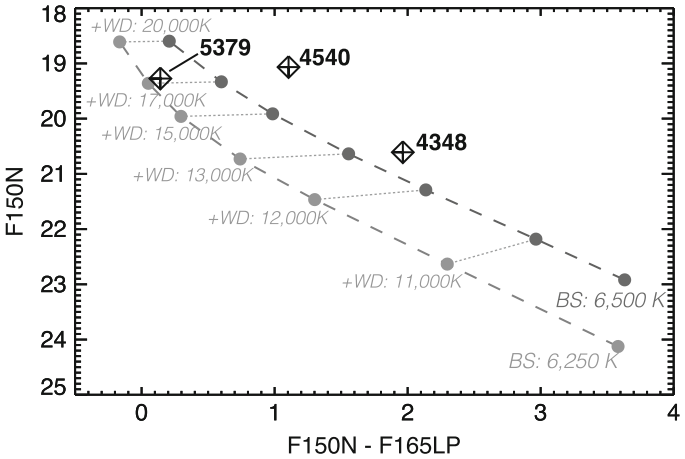

Fig. 3.4 Far-ultraviolet colour-magnitude diagram showing the positions of three detected NGC 188 blue stragglers. F150N is a derived bandpass centered on 1,554 Å with a width of 140 Å; F165LP is a bandpass peaking at 1,700 Å, extending from 1,650 Å with a long-pass extension to ∼1,850 Å. The detected blue stragglers are shown as diamonds (2σ error bars are approximately the same size as the symbols). All three blue stragglers are also detected in F140N, a derived narrow bandpass centered on 1,417 Å. Synthetic blue-straggler—white-dwarf binaries are shown as light grey (6,250 K blue straggler) and dark grey (6,500 K blue straggler) tracks with increasing temperature of white dwarf companions, as labeled (Gosnell et al. 2014)

We have observed each of the NGC 188 blue stragglers with the *Hubble Space Telescope* ACS/SBC camera. These data are currently under analysis (N. Gosnell, PhD dissertation, in progress), but already there are three unambiguous detections of white dwarfs, as shown in Fig. 3.4.

The observed far-ultraviolet fluxes imply white dwarf temperatures in excess of 12,000 K and thus white dwarf ages younger than ∼300 Myr (Bergeron et al. 2001). Such ages are negligibly small compared to the 7 Gyr age of NGC 188. Thus, in a mass-transfer formation scenario, that mass transfer has only very recently ended for these three blue stragglers.

3.2.5 Stellar Rotational Velocities

The spectra obtained for radial-velocity measurements also yield measurements of projected rotation velocities,[5] $v \sin i$. The theoretical expectations for blue-straggler rotation velocities are not well defined, but all current formation scenarios can

[5]Given our spectral resolution of 20 km s^{-1}, we only measure upper limits for stars with $v \sin i <$ 10 km s^{-1}.

plausibly spin up the blue stragglers. In Fig. 3.5 we show the colour-magnitude diagram of NGC 188 with projected rotation velocities indicated by size of symbol. None of the main-sequence stars have measurable $v \sin i$, as expected for solar-type stars at 7 Gyr. The rapidly spinning giant is a well-known FK Comae star. Such stars have been suggested to be recent merger products, perhaps from common-envelope evolution, although this scenario has challenges.

In contrast to the main-sequence stars, several of the blue stragglers show measurable rotation, in some cases higher than $v \sin i = 50$ km s^{-1}. For comparison with main-sequence stars of the same effective temperature, we also show in Fig. 3.5 a similar colour-magnitude diagram of the 2.5 Gyr cluster NGC 6819. Although at this younger age a few of the main-sequence stars show detectable rotation, they do so at a lower frequency than among the NGC 188 blue stragglers and none have $v \sin i$ as large as 50 km s^{-1}.

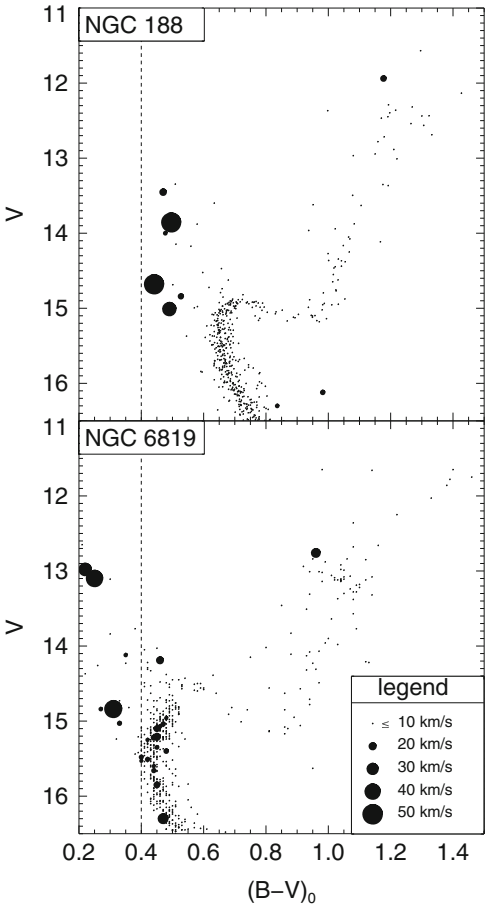

Fig. 3.5 Colour-magnitude diagrams of NGC 188 and the 2.5 Gyr cluster NGC 6819, in which the point sizes correspond to the projected rotational velocities ($v \sin i$) for each star, as indicated. We plot only cluster members, and we have removed close binaries whose periods are less than the corresponding tidal circularisation periods, so the $v \sin i$ values shown have not been affected by tidal evolution. The *dashed line* at $(B - V)_o = 0.4$ is to guide the eye in comparing the $v \sin i$ values of stars of similar colours in the two clusters. Updated from Mathieu and Geller (2009)

Thus the observations show that at least some NGC 188 blue stragglers are rotating more rapidly than normal main-sequence stars at 7 Gyr, and also are more rapidly rotating than main-sequence stars of the same effective temperature at 2.5 Gyr. From the point of view of theoretical predictions, it is not evident whether these blue stragglers are rotating fast or slow. In collision scenarios the more probable high impact parameters likely leave products with spins approaching break-up velocity (Sills et al. 2005), and so the current rotation velocities would require a substantial spin-down mechanism. Likewise, the coalescence of two main-sequence stars is thought to lead to rapid rotation (Webbink 1976). Mass transfer onto a normal main-sequence may also act to substantially spin-up the product, as predicted in certain situations (Eggleton 2011).

Interestingly, the NGC 188 blue-straggler rotation rates seem to decrease with decreasing surface temperature, as also found for normal main-sequence stars spanning the same temperature range. The spin-down of normal stars is associated with the presence of surface convective zones and magnetic fields, and the onset of stellar winds with decreasing surface temperature. The magnetised winds transport away angular momentum on timescales of several hundred million years. Whether blue stragglers of these same surface temperatures also have surface convection zones or magnetic fields is unknown. If the blue stragglers do not have effective mechanisms by which to lose angular momentum, this may place serious challenges before formation mechanisms—such as collisions and merger—that are thought to produce very rapidly rotating products from the pre-event orbital angular momentum. Alternatively, if the internal structures, magnetic fields and winds of blue stragglers mimic normal main-sequence stars, with commensurate spin-down times, then that some blue stragglers have not yet spun down will place upper limits on their ages.

3.2.6 Spatial Distribution

One of the more striking results of studies of globular cluster blue stragglers has been the discovery of bimodal spatial distributions that show maxima in blue straggler surface density, relative to normal stars, in both the cluster cores and halos, with minima in between. These have been attributed to dynamical friction causing the blue stragglers out to intermediate radii to sink to the cluster centres, while the timescales of similar processes in the halos are longer than the cluster ages (see Chap. 5).

A similar distribution of blue stragglers is found in NGC 188, as shown in Fig. 3.6. Note the break in the blue straggler distribution at about seven arcmin radius (three core radii). This distribution shows a centrally concentrated population, within about five core radii, and a halo population extending to the edge of the cluster. We discuss this distribution further in Sect. 3.3.

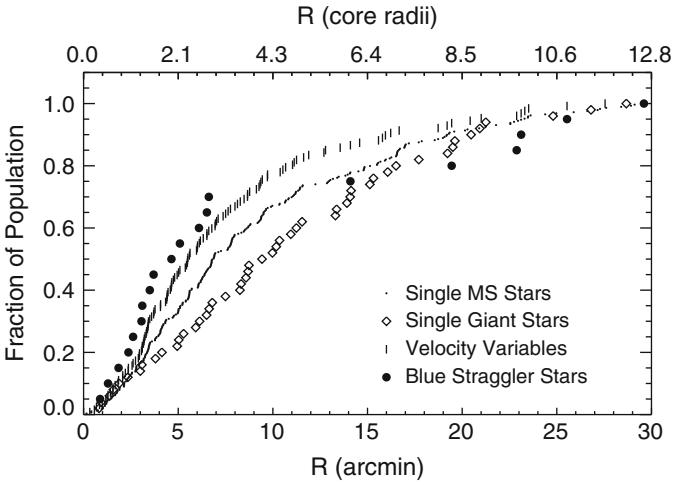

Fig. 3.6 Cumulative spatial distribution of the single main-sequence stars, single giant stars, velocity-variable (binary) stars and blue stragglers in NGC 188. Updated from Geller et al. (2008)

3.2.7 Blue-Straggler Masses

Typically, blue-straggler masses have been derived from stellar evolution tracks for normal stars. However, the distributions of the blue stragglers in colour-magnitude diagrams do not mimic normal main-sequence stars, and in fact many do not lie between the zero-age and the terminal-age main sequences. So the appropriateness of normal stellar evolution models is not clear, and more recently researchers have sought to build evolutionary tracks that begin with initial conditions appropriate to the several current blue straggler formation scenarios, as discussed elsewhere in this book (see Chaps. 12 and 14).

Of course, what is needed are dynamical mass measurements for blue stragglers. The double-lined blue straggler binary WOCS ID 5078 takes a valuable step in this direction; its analysis is shown graphically in Fig. 3.7. Spectroscopic analysis of the light from the secondary star shows it to have an effective temperature of 5,850 K $\pm$ 250 K (2σ). Presuming it to be a main-sequence star, the consequent mass of the secondary star is between 0.94 and 1.08 $M_{\odot}$. The mass ratio from the orbital solution is $q = 0.678$, and so the primary star mass is between 1.39 and 1.59 $M_{\odot}$.

Figure 3.7 shows the combined light of the system, and the deconvolved light of the blue-straggler primary star as a function of candidate main-sequence secondary stars within the permitted temperature range. Compared to a standard set of normal-star evolutionary tracks, the maximum inferred mass for the primary star is between 1.2 and 1.3 $M_{\odot}$. The indication then is that the normal stellar evolution models underestimate the mass of this blue straggler by roughly 15 %.

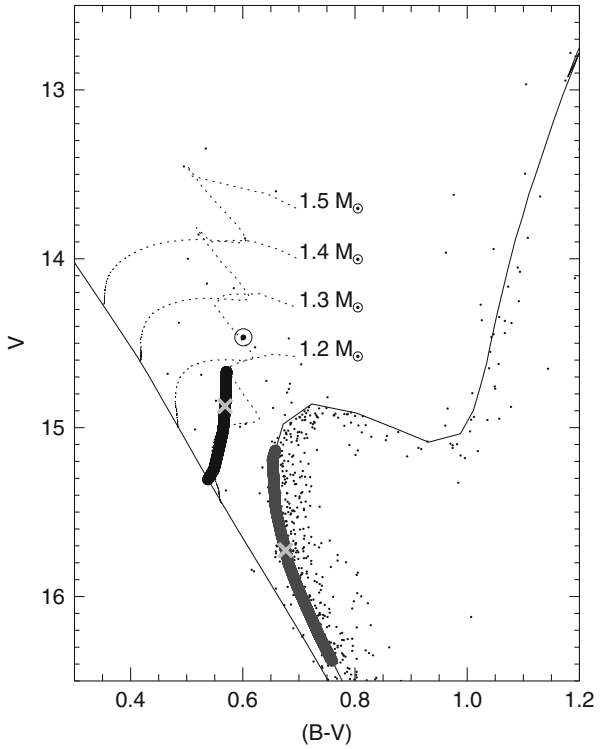

Fig. 3.7 Colour-magnitude diagram showing the loci of possible locations for the components of the blue straggler binary WOCS ID 5078. Cluster members are shown in the *small black points*, and 5078 is *circled*. We also show a zero-age main sequence and a 7 Gyr isochrone in the *thin solid lines*, and evolutionary tracks for 1.2, 1.3, 1.4, and 1.5 $M_{\odot}$ stars in the *dotted lines*, respectively (Marigo et al. 2008). The *thick gray line* shows the locus of potential secondary stars, and the *thick black line* shows the locus of potential primary stars. The derived effective temperature of 5,850 K for the secondary implies a mass of 1.02 $M_{\odot}$; we plot the location of a nominal secondary star, and the location of the associated primary, with the *light gray crosses*. Given the kinematic mass ratio of $q = 0.678 \pm 0.009$ and this secondary mass, the blue straggler mass would be 1.5 $M_{\odot}$. Yet the blue straggler is significantly less luminous than a normal 1.5 $M_{\odot}$ star at any point in its evolution. From Geller and Mathieu (2012)

We next briefly leave NGC 188 to draw attention to a particularly important double-lined eclipsing blue straggler in M67, S1082 (van den Berg et al. 2001; Sandquist et al. 2003). Goranskij et al. (1992) showed S1082 to have partial eclipses with a period of 1.07 days. Oddly for such a short-period eclipsing binary, radial-velocity studies of S1082 had found only very small velocity variability and no sign of a period consistent with the photometric period. The puzzle was resolved when it was shown that the system consists of (at least) three stars, comprising both a short-period eclipsing binary and a more luminous blue straggler in a long-period orbit (van den Berg et al. 2001; Sandquist et al. 2003).

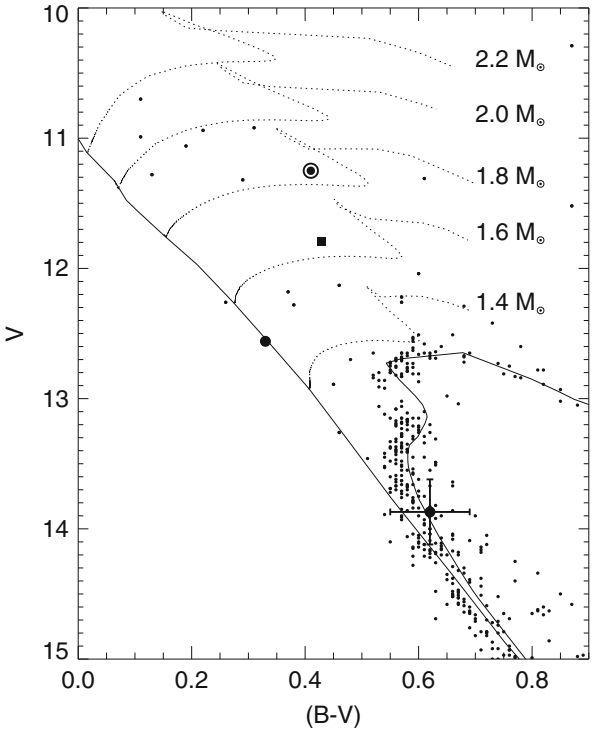

Fig. 3.8 Colour-magnitude diagram of M67 showing the locations of (i) the combined light of blue straggler system S1082 (*circled dot*), (ii) the tertiary blue straggler (*square*); and (iii) the primary and secondary of the 1.07-day eclipsing binary based on the Sandquist et al. (2003) solution (*dots*). The photometric errors on the primary and tertiary fall within the plotted symbols; error bars are shown for the secondary. Adapted from Sandquist et al. (2003)

Figure 3.8 shows the colour-magnitude location of the two components of the eclipsing binary as found[6] by Sandquist et al. (2003). Each star currently falls near the zero-age main sequence, one as a blue straggler and one seemingly as a normal main-sequence star. Both stars become remarkable when associated with their dynamical masses. For the primary star, van den Berg et al. (2001) find a mass of $2.70 \pm 0.38\ M_{\odot}$ and Sandquist et al. (2003) find a mass of $2.52 \pm 0.38\ M_{\odot}$. As shown in Fig. 3.8, both of these dynamical masses greatly exceed the photometric mass of $1.5\ M_{\odot}$ from stellar evolutionary tracks.

Even more surprising is the mass of the secondary star in the eclipsing binary, which photometrically would appear to be a normal main-sequence star below the cluster turnoff. Van den Berg et al. (2001) find a mass of $1.70 \pm 0.27\ M_{\odot}$ and Sandquist et al. (2003) find a mass of $1.58 \pm 0.27\ M_{\odot}$. However, the turnoff mass of M67 is only $1.3\ M_{\odot}$! The expected mass for the secondary star based on the zero-age main sequence is $1.1\ M_{\odot}$.

[6]The colour-magnitude locations found for the stars in the eclipsing binary are substantially different between van den Berg et al. (2001) and Sandquist et al. (2003), largely the result of Sandquist et al. (2003) including spectroscopically derived effective temperatures in their analyses. This system merits additional careful study.

Formally the high mass measurement of the secondary is less than a 2σ deviation from the zero-age-main-sequence prediction. In addition, the crucial radial-velocity measurements for this system are difficult because of both the luminous tertiary and rotational line broadening. So we must be careful that our interpretations and conclusions do not outstrip the security of the result. But the indication of very underluminous stars in this blue-straggler binary is interesting enough to merit substantially more observational work being applied to S1082, seeking especially higher-precision mass determinations.

In closing, these systems are hopefully only beginning to tell the story of blue straggler masses. Both WOCS ID 5078 and S1082 have rather short orbital periods. There is no evidence that they are not detached binaries currently, and indeed all of the stars fit within their Roche lobes. Still, the implications of these findings regarding the accuracy of stellar evolution masses for blue stragglers found in wide binaries or as single stars are not yet clear. Even so, these two blue-straggler binaries present us with three underluminous stars that would seem to suggest that the standard stellar interiors theory of our undergraduate and graduate courses may not apply.

3.2.8 Insights from Two Notable Blue Straggler Systems

The double-lined blue straggler WOCS ID 7782 may shed valuable light on the dynamical evolution of blue-straggler binaries. The key observational finding is a mass ratio of 1.005. In addition, spectroscopic analysis yields effective temperatures for the primary and secondary stars of 6,500 and 6,325 K, respectively. These effective temperatures are both hotter than the main-sequence turnoff surface temperature of 5,900 K. In short, this binary comprises two blue stragglers.

No single blue-straggler formation mechanism currently under consideration is capable of forming two blue stragglers simultaneously in a 5.3-day period binary. Thus we interpret 7782 as evidence for exchanges of stars in one or more resonant dynamical encounters. For specificity, consider a dynamical encounter between two of the current long-period blue straggler binaries. That such an encounter would yield a closer binary comprising the two most massive stars in the encounter (i.e., the two blue stragglers) is a probable outcome, although such a short period may be challenging (Sect. 3.3.3.2).

At least one of the original companion stars would need to be ejected in order to remove energy from the system. The other companion star might do the same, or still be orbiting the blue straggler binary as an as yet undetected distant tertiary.

It is also possible that only one of the initial systems contained a blue straggler, and the second one was formed by a collision during the dynamical encounter. And

perhaps most likely, this system may have formed as a consequence of multiple dynamical encounters.[7]

These dynamical scenarios are consistent with the fact that 7782 is in the cluster halo, ten core radii from the centre. Momentum conservation in high-energy dynamical encounters often leads to ejections of the products from the cluster core, if not from the cluster.

Additionally, in these dynamical exchange scenarios the two blue stragglers need not have formed at the same time, and indeed their different surface temperatures might be indicative of different evolutionary ages. For example, we were able to model the system with two 1.25 $M_\odot$ stars having an age difference of about two gigayears. Given such dynamical exchanges, the current binary system may say very little about the formation mechanism of either blue straggler. At the same time, it is worth noting that these exchange scenarios do not evidently explain the near identity of the masses of the two blue stragglers.

S1082 in M67 also leads us to consider a sequence of dynamical encounters. We introduced this multiple-star system in Sect. 3.2.7 in the context of the mass determinations of the eclipsing binary components; here we consider the formation of the entire system. First, we remind that the total mass of the 1.07-day period binary is measured to be 4.1–4.4 $M_\odot$ (with an uncertainty of 0.5 $M_\odot$). The turnoff mass of M67 is 1.3 $M_\odot$. So mass contributions from at least three and likely four cluster stars are needed to create this binary. The mass of the blue-straggler primary star alone is found to be 2.5–2.7 $M_\odot$, comparable to essentially the entire masses of two turnoff stars. The mass of the secondary star is found to be 1.6–1.7 $M_\odot$. Clearly this blue straggler binary is not the simple product of a mass transfer event.

In addition, the system includes another blue straggler, itself in a 1,200-day period orbit. As the most luminous star in the system, it possibly is also the most massive star. No companion to this blue straggler has been detected in the optical, though this blue straggler may be bound to the 1.07-day binary. Landsman et al. (1998) found S1082 to be overluminous at far-ultraviolet wavelengths and suggest the presence of a hot underluminous companion. Should this be the dynamical companion, this long-period blue straggler binary would become intriguingly similar to the long-period blue straggler binaries in NGC 188.

Neither van den Berg et al. (2001) nor Sandquist et al. (2003) found a convincing formation path for the system, and we have done no better. We agree that the measured masses, if confirmed, strongly put forward one or more of the stars in S1082 as collision products, which in itself makes the system important as a case study. Furthermore, we see no way to form the tight binary except through a progression of dynamical encounters among multiple systems within some of which these collisions happen. Dynamical encounters favour leaving the most massive stars in the binary products, which would advantage discovery of binaries like those

[7]To get a sense of the diverse dynamical stories possible for blue stragglers in clusters, the reader is recommended to the short stories told in Table 5 of Hurley et al. (2002). Case 1613 is a particular favorite of the authors.

in S1082. Furthermore, collision products tend to be underluminous (Sills et al. 2001). On the other hand, time is precious. If both stars in the close binary are highly underluminous as a result of being out of thermal equilibrium, they would remain so only for a thermal timescale. This leaves very little time, and thus likelihood, for creating the stars and the binary in more than one encounter.

If the long-period blue straggler binary in S1082 in fact is not physically associated with the close binary, then it may be a mass-transfer product much like we suggest later for the long-period binaries in NGC 188 (although it is not clear that an asymptotic giant mass transfer history could produce such a luminous blue straggler given the 2.5 $M_\odot$ mass measurement of its less luminous neighbour). If they are associated, an all the more challenging series of events is required involving at least six stars. Again, the primary challenge is time, which is constrained possibly by the thermal timescales for both components of the close binary and certainly by the lifetimes of both blue stragglers.

Of course, it is puzzles such as these that make science fun, and hopefully yield unexpected discoveries. For the moment, we draw several overarching conclusions from the blue stragglers WOCS ID 7782 and S1082. First, these systems are arguably among the best observational evidence that the stellar exchanges in dynamical encounters long predicted by theory in fact occur. Second, these systems—as do many *N*-body simulations—caution us that the properties of any given binary within which a blue straggler is found may bear little information about the formation mechanism of the blue straggler. And third, the systems—especially S1082—rather strongly suggest that stellar collisions do occur during resonant dynamical encounters of multiple systems in star clusters.

3.2.9 Summary

In the past few years the 20 blue stragglers of NGC 188 have yielded a remarkable amount of information about the nature of blue stragglers in an old open cluster. Specifically, this blue straggler population is characterised by:

- A binary frequency of 80 % for P $<10^4$ days;
- Typical orbital periods around 1,000 days;
- Typical secondary star masses of 0.5 $M_\odot$;
- At least some white dwarf companion stars;
- Modestly rapid rotation;
- A bimodal radial spatial distribution;
- Dynamical masses greater than standard stellar evolution masses (short-period binaries)
- Underluminosity for dynamical masses (short-period binaries).

While the comprehensive scope of these results is powerful in themselves, they are further strengthened by corroborating studies. Many of these properties have also been found for the blue stragglers in the 4.5 Gyr open cluster M67 (e.g., Latham

2007). They also were foreshadowed by studies of the blue stragglers in the field (e.g., Carney et al. 2001 and Chap. 4).

And so our microscopic perspective of the NGC 188 blue stragglers is rich with information. We now turn to the implications of this knowledge on the formation of blue stragglers.

3.3 Blue Straggler Formation Within an *N*-Body Model of NGC 188

Current theories argue that blue stragglers form from main-sequence stars that, through interactions with an additional star or stars, gain enough mass to exceed the cluster turnoff mass. The three currently favoured hypotheses for obtaining this extra mass are mass transfer (McCrea 1964; Chen and Han 2008b), mergers (Webbink 1976; Chen and Han 2008a) and collisions (Hills and Day 1976; Sills et al. 2005). In this section we briefly describe these formation mechanisms, and then compare with observations their predictions for the binary properties of blue stragglers based on a sophisticated *N*-body model of NGC 188 (Geller et al. 2013).

3.3.1 The NGC 188 N-Body Model

Today, *N*-body codes (e.g., `NBODY6`, Aarseth 2003; `Starlab`, Hut 2003) are capable of simulating the dynamical evolution of actual open clusters from near birth across a Hubble time, including primordial populations of tens of thousands of stars and large frequencies of binaries (and triples). Stellar evolution and detailed prescriptions for binary-star evolution are modeled self-consistently with the stellar dynamics, allowing for blue-straggler formation through all of the proposed mechanisms.

A detailed description of the NGC 188 model can be found in Geller et al. (2013); we briefly summarise the method here. We use the `NBODY6` code, which includes stellar and binary evolution (Hurley et al. 2000, 2002), to generate 20 unique realisations of NGC 188. For each realisation we randomly choose the initial stellar and binary parameters (e.g., positions, velocities, binary orbital periods, eccentricities, etc.) from empirically defined distributions, producing 20 unique initial stellar populations. Each of these primordial populations is then evolved for seven gigayears. For the analyses discussed below we combine the 20 simulations to reduce stochastic effects, especially for relatively small stellar populations like blue stragglers.

Importantly, we employ the observed solar-type main-sequence binaries of the young (150 Myr) open cluster M35 (Geller et al. 2010) to guide our choices for the initial binary frequency and distributions of orbital elements and masses, supple-

mented with observations of field solar-type binaries (Raghavan et al. 2010) where necessary. These empirical initial binary conditions replace often-used theoretical distributions, which in many aspects don't match observed binary populations in real open clusters, both young (e.g., M35 at 150 Myr; Geller et al. 2013) and old (e.g., NGC 188 at 7 Gyr; Geller and Mathieu 2012). The importance of defining an accurate initial binary population is paramount for accurate blue-straggler production (see Sect. 3.3.4.1), as all viable blue-straggler formation mechanisms in open clusters begin from binary stars.

Crucially, we find that the empirically defined initial binaries evolve within the model to reproduce well the observed NGC 188 main-sequence solar-type binary frequency and distributions of orbital parameters at seven gigayears. In addition, the NGC 188 model matches the observed cluster mass, central density and radial-density distribution. Thus, the NGC 188 model accurately reproduces the environment in which the true NGC 188 blue stragglers formed.

Blue stragglers are identified in the model as stars that are at least 2 % more massive than the turnoff mass at a given age. We use an integrated sample of blue stragglers in our analyses of the NGC 188 model. This sample contains all blue stragglers present at each ∼30 Myr snapshot interval between 6 and 7.5 Gyr within all 20 simulations. This integrated sample of blue stragglers reduces the stochastic fluctuations in blue straggler production and also weights the sample by the time that a given blue straggler spends in a specific binary, at a specific cluster radius, etc.

3.3.2 Formation Channels for Blue Stragglers in the NGC 188 Model

Here we briefly describe the mass-transfer, merger and collision blue-straggler formation mechanisms and their implementation in the NGC 188 model. We refer the reader to the Chaps. 7, 8, 9, and 11 in this volume for more extensive discussions of these formation mechanisms, and to Hurley et al. (2002) for further details on the implementation of these formation channels in `NBODY6`.

3.3.2.1 Mass Transfer

Mass transfer through Roche Lobe Overflow (RLOF) is typically divided into three regimes, known as Cases A, B and C, based on the evolutionary state of the donor star (Kippenhahn and Weigert 1967; see also Paczyński 1971). Specifically, Case A mass transfer occurs when the donor is a main-sequence star; Case B mass transfer occurs when the donor is on the red giant branch; and Case C mass transfer occurs when the donor is on the asymptotic giant branch. In `NBODY6`, a blue straggler can be formed through mass transfer when the accretor is a main-sequence star and

accepts enough material to increase its mass above that of the cluster turnoff. If both the donor and accretor are on the main sequence, Case A mass transfer is believed to result in the coalescence (i.e. merger) of the two stars (e.g., Chen and Han 2008a), and in NBODY6 binaries that come into contact are merged. Therefore, we include Case A mass transfer systems in the merger category, and from hereon we will use the term "mass transfer" to refer specifically to Cases B and C.

In NBODY6, RLOF transferring mass from a giant on a dynamical time-scale leads to a common-envelope episode. It is assumed that no mass is accreted, and therefore no blue straggler is formed. As in many binary-population synthesis models (e.g., Hurley et al. 2002; Belczynski et al. 2008), NBODY6 employs a "critical mass ratio" value, q_c, to determine whether a given binary will undergo thermal or nuclear mass transfer (i.e., stable) or dynamical mass transfer (i.e., unstable). If $q_1 = M_{\rm donor}/M_{\rm accretor} > q_c$, the binary undergoes dynamical mass transfer, and otherwise mass transfer is stable.

The key point here, which we will return to below, is that in NBODY6 Case B and Case C mass transfer can only produce a blue straggler if the mass transfer is stable. Given stable mass transfer, Case B mass transfer leaves a He white dwarf companion bound to the blue straggler, while Case C mass transfer leaves a Carbon-Oxygen white dwarf companion.

3.3.2.2 Mergers

We use the term merger to describe the coalescence of two members of a tight binary to form a single star. If the combined mass is large enough, a blue straggler can be produced by the merger of two main-sequence stars, which is often the result of Case A mass transfer. Nelson and Eggleton (2001) study in detail the large variety of Case A mass-transfer scenarios. In general, a close binary composed of two main-sequence stars can come into contact and subsequently merge through stellar evolution processes or due to the loss of orbital angular momentum (e.g. through magnetic braking).

As discussed by Perets in this volume (Chap. 11), triple systems may increase the merger rate through a process involving Kozai cycles and tidal friction, known as the KCTF mechanism (Perets and Fabrycky 2009). The KCTF mechanism is parametrised in NBODY6 based on the analytical development of Mardling and Aarseth (2001). In general, if the KCTF mechanism forms a blue straggler, it will be in a binary with the original tertiary companion.

3.3.2.3 Collisions

We use the term collision to refer to a direct physical impact of two (or more) stars that subsequently combine to become a single star. Unlike the merger and mass-transfer mechanisms, collisions require the dynamical environment of a star cluster (or a dynamically unstable multiple-star system; Perets and Kratter 2012). In open

clusters like NGC 188, essentially all collisions occur during dynamical encounters involving at least one binary (or higher-order system), as the cross section for a direct single–single collision to occur is prohibitively small.

In NBODY6, a collision (or a merger) product is assumed to be fully mixed and to achieve thermal equilibrium rapidly, becoming a new main-sequence star in equilibrium upon creation (Hurley et al. 2002). This is most likely an oversimplification, as detailed models show that collision products may not be in thermal equilibrium and furthermore may not be fully mixed (Sills et al. 2005; Glebbeek et al. 2008). These simplifications will affect the lifetimes and luminosities of blue stragglers formed by collisions (and mergers), but will likely not impact their binary properties.

3.3.3 Implications for the Origins of the NGC 188 Blue Stragglers

The remarkable combination of comprehensive observations and sophisticated N-body modeling enables us to investigate the origins of the NGC 188 blue stragglers in great detail. The binary properties of the blue stragglers, both frequency and distributions of orbital parameters and secondary masses, are keys to unlocking the mystery of blue straggler origins.

Here we divide the discussion to focus first on the 14 NGC 188 blue stragglers in long-period (>100 days) binaries, all of which are single-lined. Then we discuss the two NGC 188 blue stragglers in short-period binaries, both of which are double-lined. Finally we briefly discuss the four NGC 188 blue stragglers that do not exhibit detectable radial-velocity variations.

3.3.3.1 The NGC 188 Blue Stragglers in Long-Period Binaries

Fourteen of the 20 blue stragglers in NGC 188 are found in long-period binaries. One of these blue stragglers has an orbital period near 100 days, and the rest have orbital periods near 1,000 days. We first discuss the blue stragglers in 1,000-day binaries.

In Figs. 3.9, 3.10, and 3.11, we compare the observed binary properties of these NGC 188 blue stragglers to the predictions from the N-body model for blue stragglers in binaries formed by collisions, by mergers and by mass transfer. We did not include primordial triples in the NGC 188 model, and, although triples do form dynamically within the model, they are so few that the rate of KCTF blue-straggler formation is negligible. Therefore the predictions for merger products from the NGC 188 model reflect blue stragglers produced by mergers within binaries.

As can be seen in Fig. 3.9, the NGC 188 model predicts that mergers form essentially no blue stragglers in binaries with periods near 1,000 days. Nearly all of the merger blue stragglers in the model that are within binaries with periods

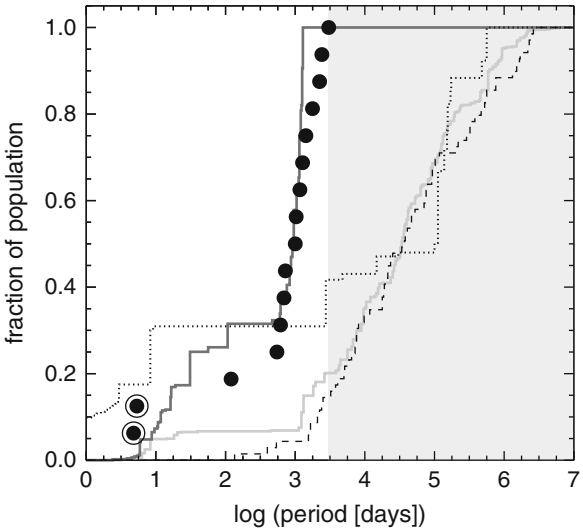

Fig. 3.9 Cumulative distributions of orbital period for observed blue-straggler binaries in NGC 188 (*black points*) as compared to blue-straggler binaries in the NGC 188 model (mass transfer origin: *solid dark gray line*; collision origin: *solid light gray line*; merger origin: *dotted line*) and tertiaries from the field triple population (*dashed line*). We include model blue-straggler binaries of any period, and the gray-filled region marks periods beyond our observational completeness limit of 3,000 days for orbital solutions. The two double-lined blue stragglers in NGC 188 are *circled*. Updated from Geller and Mathieu (2012)

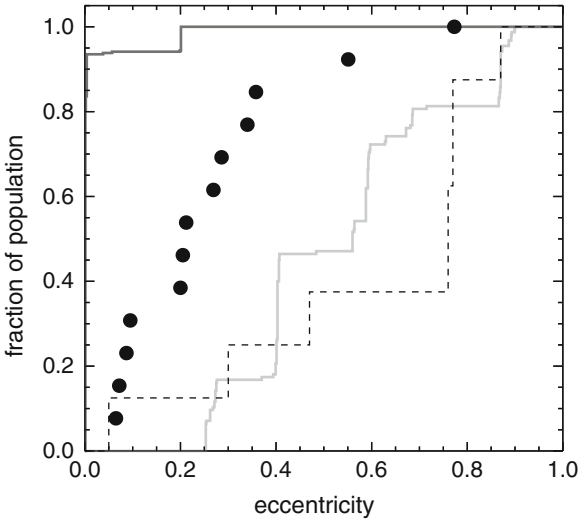

Fig. 3.10 Cumulative distributions of orbital eccentricity comparing the observed NGC 188 blue stragglers binaries with periods near 1,000 days (*black points*) with predictions from the NGC 188 model for the collision and mass-transfer hypotheses, and the field triple population. All line styles and symbols are the same as in Fig. 3.9. Updated from Geller and Mathieu (2012)

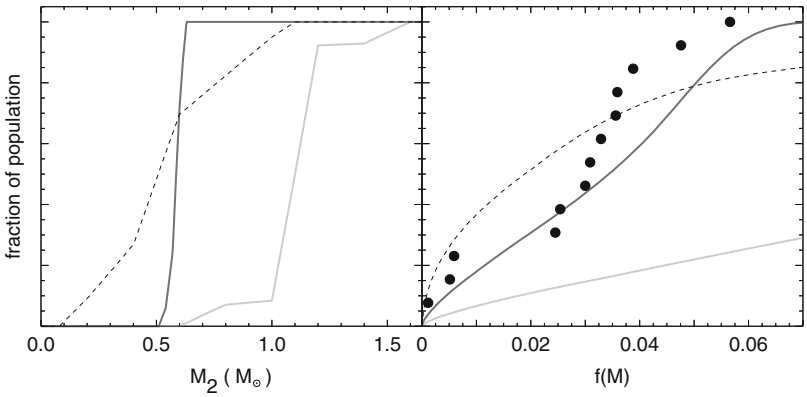

Fig. 3.11 *Left*: Cumulative companion-mass distributions drawn from the NGC 188 model blue-straggler binaries with periods between 500 days and 3,000 days sorted by mass transfer origin (*dark gray line*) and collision origin (*light gray line*), and the evolved tertiary-mass distribution for field triples (*dashed line*; (Tokovinin 1997), see Sect. 3.3.5.1 for selection criteria). *Right*: Cumulative mass-function distributions, using the same line styles for the respective samples, and also including the observed mass functions for NGC 188 blue straggler in binaries with periods near 1,000 days (*black points*). Updated from Geller and Mathieu (2012)

less than 3,000 days are short-period contact systems that will eventually merge to form single blue stragglers. The vast majority of merger blue stragglers in wider binaries (mostly beyond our detection limit) formed through subsequent exchange encounters. The two populations are also distinguishable in orbital eccentricity; the very-short-period contact systems have zero eccentricities and the long-period exchange systems have high eccentricities.

Only the collision and mass-transfer mechanisms produce blue stragglers in binaries with periods near 1,000 days. The predicted binary properties of blue stragglers formed by these two mechanisms are strikingly different.

The collision mechanism predicts that 80 % of the companions to long-period blue stragglers are main-sequence stars, with most having masses near that of the cluster turnoff (1.1 $M_{\odot}$). This outcome reflects the tendency of dynamical-encounter products to retain the most massive stars. Such companions are far more massive than observed for the NGC 188 long-period blue straggler binaries (Fig. 3.3). A Kolmogorov–Smirnov test rules out at >99 % confidence the hypothesis that the observed mass functions are drawn from a parent population of collisional origin (Fig. 3.11). Additionally, the collision mechanism predicts far too high a frequency of high-eccentricity orbits (Fig. 3.10). The eccentricity distribution for the blue stragglers formed by collisions in the N-body model is distinct from the observed distribution for the long-period NGC 188 blue stragglers with >99 % confidence (Geller and Mathieu 2011). Therefore we rule out a primarily collisional origin for the NGC 188 blue stragglers in binaries with periods near 1,000 days at very high confidence.

All of the blue stragglers in the model that formed from mass transfer are members of binaries with periods less than 3,000 days, securely detectable in our observations. Nearly all have white dwarf companions with masses between 0.5 and 0.6 $M_{\odot}$ (Fig. 3.11). These predictions agree well with our observations of the NGC 188 blue stragglers in long-period binaries. Most of the mass-transfer products in the NGC 188 model have periods near 1,000 days and derive from Case C mass transfer. A smaller subset of the mass-transfer products from the model derive from Case B mass transfer and have helium white dwarf companions with shorter orbital periods. These latter blue stragglers in the model may correspond to the one single-lined blue straggler in NGC 188 with an orbital period near 100 days and a mass function consistent with a low-mass companion.

However, nearly all of the blue stragglers that formed by mass transfer in the NGC 188 model have circular orbits, while only three of the long-period NGC 188 blue stragglers have orbits consistent with being circular (the rest having a range of non-zero eccentricities). In NBODY6 (as well as many other modeling codes), tides are assumed to rapidly circularise the binary orbit during mass transfer. The NGC 188 model shows that dynamical encounters after the formation of blue stragglers by mass transfer are not sufficient to induce the number of observed eccentric blue straggler binaries. The three circular, long-period, single-lined NGC 188 blue stragglers are very likely candidates for the mass-transfer formation mechanism. If mass transfer is also responsible for the formation of the remaining long-period blue stragglers in NGC 188, then some form of "eccentricity pumping" during the mass-transfer phase may be required. Indeed, recent theoretical work suggests that mass transfer will not always lead to circular orbits (Soker 2000; Bonačić Marinović et al. 2008; Sepinsky et al. 2009; Lajoie and Sills 2011). Further development of these eccentricity pumping theories, and the inclusion of these mechanisms in models like NBODY6, are highly desired.

Furthermore, because of their isolation the field blue stragglers discussed by Preston in this volume (Chap. 4) are thought to derive primarily from mass transfer (Carney et al. 2005, 2001). Yet they also display non-zero eccentricities. Completion of our *HST* survey for white dwarf companions to the NGC 188 blue stragglers will be very important for determining if the eccentric binaries in fact derive from mass transfer. For now, the eccentricity distribution predicted by the mass-transfer mechanism appears to be uncertain.

A second discrepancy between the model predictions for the mass-transfer hypothesis and NGC 188 observations is that less than 10 % of the blue stragglers present in the model at the age of NGC 188 formed by mass transfer, while 70 % (14/20) of the NGC 188 blue stragglers are in long-period binaries. One hypothesis is that the efficiency of mass transfer is severely underestimated in the *N*-body model, and we discuss this in detail in Sect. 3.3.5.

We conclude that of the blue-straggler formation channels that are active in the NGC 188 model, only the mass-transfer mechanism produces blue straggler binaries whose orbital properties and secondary stars are closely consistent with the observed NGC 188 blue stragglers in long-period binaries. However none of the formation channels, as implemented in NBODY6, can fully explain both the observed frequency and the binary properties of these NGC 188 blue stragglers.

3.3.3.2 The NGC 188 Blue Stragglers in Short-Period Binaries

Both of the NGC 188 blue stragglers in short-period ($P < 10$ days) binaries are double-lined systems, one with a main-sequence companion near the cluster turnoff (WOCS ID 5078) and the other comprised of two blue stragglers (WOCS ID 7782). The NGC 188 N-body model struggles to produce blue-straggler binaries with these characteristics. Between 6 and 7.5 Gyr in the model, there are no blue stragglers in detached binaries with periods less than 10 days and companion masses greater than 0.9 $M_{\odot}$. There are only two such systems present at earlier times in all 20 simulations. Furthermore there are only three blue straggler—blue straggler binaries in the NGC 188 model (out of 20 simulations) between 6 and 7.5 Gyr with short enough periods to have been detected as binaries. These all have periods much greater than 10 days, and two were only bound for <30 Myr (one snapshot interval). Another four blue straggler—blue straggler binaries are present in the model, but with periods beyond our observational detection limit. All of these blue straggler—blue straggler systems in the model were involved in exchange encounters that brought together into a binary two blue stragglers formed elsewhere. Moreover, neither 5078 nor 7782 can be explained through isolated blue straggler formation mechanisms (like mass transfer, binary mergers or the KCTF mechanism).

We conjecture that the evolutionary histories of these short-period NGC 188 blue-straggler binaries involve dynamical encounters, despite being unable to produce similar systems in our NGC 188 model. Detailed observations of the binary properties of blue stragglers in additional open clusters are needed to determine whether such blue stragglers are typical or anomalous. Of the few blue straggler populations already studied at this level of detail, there are two blue stragglers in short-period binaries in the field (Carney et al. 2001) and two blue stragglers in short-period binaries in M67 (Latham 2007). The short-period field blue stragglers are both single lined with small mass functions, and so may not have massive companions (maintaining the possibility of Case B mass transfer, for example). One of the short-period M67 blue stragglers is single-lined, and the other is S1082 (discussed in Sects. 3.2.7 and 3.2.8). We note that the Hurley et al. (2005) M67 model did not produce a system like S1082; indeed their model had no blue stragglers in higher-order systems at the age of M67 (although they only ran one simulation). Thus both NGC 188 and M67 have blue stragglers in short-period binaries with massive companions which N-body models do not readily produce.

3.3.3.3 The Non-Radial-Velocity-Variable Blue Stragglers in NGC 188

There are four blue stragglers in NGC 188 that currently do not show significant radial-velocity variability. In any given simulation within the NGC 188 model, we find on average five blue stragglers at the age of NGC 188 that do not have detectable binary companions (one of which, on average, is in a very wide binary, while the rest are single). The origins of these blue stragglers in the model are split roughly equally between mergers and collisions.

The NGC 188 model predicts that blue stragglers produced by either mergers or collisions will be primarily single blue stragglers. About 9 % of the blue stragglers formed by mergers in the model have binary companions (4 % with orbital periods below our detection threshold of 10^4 days). About 12 % of the blue stragglers formed by collisions have orbital periods below our detection threshold, and only 33 % of the blue stragglers formed by collisions in the model have binary companions at any period. Many of these single collision products formed with very wide companions that were quickly ionised by dynamical encounters.

Interestingly, nearly half of the blue stragglers that formed through collisions were members of dynamically formed hierarchical triple systems (often with a primordial binary as the inner system) during the snapshot interval prior to becoming a blue straggler. The wider orbit of the tertiary companion increases the cross section for a stellar encounter, and the blue stragglers form through collisions during the consequent dynamical interactions.

In short, the N-body model produces roughly the same number of non-radial-velocity-variable blue stragglers as is observed in the true cluster, and predicts that the majority of these are indeed single.

3.3.4 Outstanding Questions and Missing Pieces in the N-Body Model

Despite closely reproducing observations of the solar-type main-sequence stellar population of the cluster, the NGC 188 model predicts significantly fewer blue stragglers at the age of NGC 188 than are observed. There are 20 blue stragglers in NGC 188, 16 of which are in binaries with periods $<10^4$ days. In contrast, the integrated blue straggler sample of the model counts only 6 blue stragglers at the age of NGC 188, one of which is in a detectable binary. This deficit in blue straggler production rate indicates that the theory in the N-body model remains incomplete. We discuss here possible points for improvement.

The formation of blue stragglers rests on the cluster binary population. One hypothesis to explain the overall paucity of blue stragglers is that the choice of the initial binary population in the model is incorrect for NGC 188. We discuss this in Sect. 3.3.4.1.

When comparing the integrated blue-straggler population of the NGC 188 model to the observed NGC 188 blue stragglers, we find agreement in the shapes of the distributions of binary orbital periods (Fig. 3.12), eccentricities and companion masses. The agreement derives from the model distributions being dominated by blue stragglers formed by mass transfer; 60 % of the blue stragglers in binaries with periods <3,000 days in the integrated sample of the model derive from the mass-transfer mechanism. Therefore, a second hypothesis for the low number of blue stragglers is that the model underproduces blue stragglers through mass transfer specifically, which we discuss in Sect. 3.3.5.

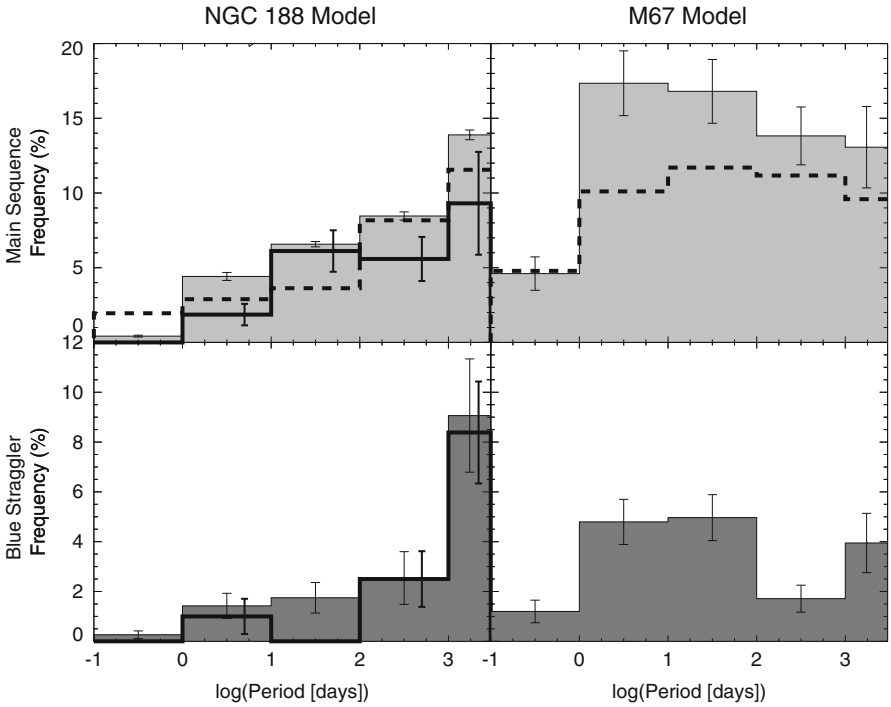

Fig. 3.12 Comparison of the solar-type main sequence (*top*) and blue straggler (*bottom*) binary orbital period distributions in the Geller et al. (2013) *N*-body model of NGC 188 at 7 Gyr (*left*) to those of the Hurley et al. (2005) *N*-body model of M67 at 4 Gyr (*right*). In the *left panels*, the *solid black histograms* show the observed NGC 188 main-sequence and blue-straggler binary orbital period distributions from Geller and Mathieu (2012); the main-sequence distribution is corrected for incompleteness. The *dashed lines* in the *top panels* show the initial distributions from the respective models. In all panels, the last bin is corrected for the smaller bin size. The Hurley et al. model begins with a significantly larger frequency of short-period binaries than are observed in NGC 188 (or included in the NGC 188 model). Adapted from Geller and Mathieu (2012) and Geller et al. (2013), and we refer the reader to these two references for similar comparisons of the observed and simulated eccentricity and companion-mass distributions

Finally, the low frequency of dynamically formed triples in the NGC 188 model as compared to the observed frequencies of triples in the Galactic field and in a few open clusters suggest that NGC 188 may have formed with a population of primordial triples. These triples, not included in the NGC 188 model, may contribute to blue straggler production, for example through the KCTF mechanism. We discuss this hypothesis in Sect. 3.3.5.1.

3.3.4.1 The Importance of an Accurate Initial Binary Population

The characteristics of the initial binary population can have a strong impact on the production rates of blue stragglers. As a case in point, we compare

the NGC 188 model to the Hurley et al. (2005) model of M67 (created using NBODY4, which is very similar to NBODY6, and has no significant differences in the treatment of blue stragglers.). The Hurley et al. model produces 20 blue stragglers at the age of M67, roughly three times the number of blue stragglers produced by the NGC 188 model at the same age (despite the NGC 188 model having a larger total mass). The difference between the blue straggler production rates in these two models is tied to their very different initial binary populations.

The Hurley et al. model began with a 50 % binary frequency (integrated over all periods) and typical theoretical distributions of key binary properties: a uniform distribution in log periods and a thermal eccentricity distribution (which were subsequently evolved through the Kroupa (1995) pre-main-sequence evolution algorithm). These initial distributions have a significantly higher frequency of short-period binaries than the NGC 188 model (Fig. 3.12).

As a consequence, the frequency of main-sequence solar-type binaries with periods $<10^4$ days at 4 Gyr in the Hurley et al. model is 64 %, as compared to 28 % at 4 Gyr in the NGC 188 model and much higher than the spectroscopic binary frequency in NGC 188 itself (or M67; Latham 2007). The overly high binary frequency in the Hurley et al. model is a direct result of its initially uniform distribution in log P. We also find significant discrepancies between the distributions of binary orbital parameters in the Hurley et al. model and our observations of the NGC 188 binaries (Geller and Mathieu 2012). The empirical initial conditions used in the NGC 188 model remedy these discrepancies.

The higher frequency of short-period binaries increases blue straggler production through all mechanisms, enabling the Hurley et al. model to match the number of blue stragglers in M67. Interestingly, the relative rates of blue-straggler formation through the different mechanisms are roughly the same as in the NGC 188 model; 10 % of the blue stragglers in the M67 model at 4 Gyr formed through mass transfer, 40 % formed through collisions and 50 % formed through mergers. As a result, the frequency of detectable blue straggler binaries in the Hurley et al. model is only 30 %. Furthermore, of these detectable binaries a large fraction are found with short periods and high eccentricities, which is not observed in either NGC 188 or M67.

Thus, although the Hurley et al. model produces roughly the correct number of blue stragglers found in NGC 188 and M67, the model fails to reproduce the blue-straggler (or main-sequence) binary properties as a result of the unrealistic initial binary population.

On the other hand, a more realistic initial binary population in the NGC 188 model, which evolves to match the observed main-sequence binaries of the true cluster, does not reproduce the observed number of blue stragglers. We have attempted adjusting the parameters of the initial binary population and cluster central density, but we cannot simultaneously reproduce the number and binary properties of the NGC 188 blue stragglers, the binary properties of the NGC 188 solar-type main-sequence stars, and the 7 Gyr cluster structure.

3.3.5 *Efficiency of Mass Transfer in the N-Body Model*

Our observations of the NGC 188 blue stragglers in long-period binaries—which represent 70 % of the entire NGC 188 blue straggler population—suggest that most, if not all, were formed by mass transfer. Yet, the mass-transfer mechanism is woefully inefficient at producing blue stragglers in the N-body model. On average, less than one blue straggler at the age of NGC 188 is produced by mass transfer in the model. Even evolving the initial binary population in isolation (disregarding stellar encounters or escape from the cluster, both of which tend to decrease the number of blue stragglers in the cluster formed by mass transfer), we cannot produce the 14 NGC 188 blue stragglers in long-period binaries through the mass-transfer mechanism. If mass transfer is indeed responsible for producing these NGC 188 blue stragglers in long-period binaries, then the physics of mass transfer in `NBODY6` (and models using similar binary evolution prescriptions) is not accurate.

As described in Sect. 3.3.2.1 (and Hurley et al. 2002), during RLOF `NBODY6` compares a critical mass ratio, q_c, to the binary mass ratio, q_1, to determine whether a given binary will go through mass transfer on a thermal or nuclear timescale (i.e., stable), or a dynamical timescale (i.e., unstable). Moreover, for a given binary undergoing RLOF, the parameter q_c determines whether a blue straggler can be created or whether the system will go through a common-envelope episode and not produce a blue straggler. Thus in terms of creating blue stragglers through mass transfer, q_c is a key parameter in the model.

However, the value of q_c for a given binary is highly uncertain and depends on how conservative is the mass transfer. For a given binary, different developments in the literature (e.g., Hjellming and Webbink 1987; Hurley et al. 2002; Chen and Han 2008a; Chen and Han 2008b; Belczynski et al. 2008) provide different q_c values (by a factor of a few). There is also growing theoretical evidence that this standard q_c parameterization may not match predictions from more detailed binary mass-transfer models (Woods and Ivanova 2011; Passy et al. 2012; see also Chap. 8).

In the NGC 188 model, we employ the Hjellming and Webbink (1987) formula and do not account for non-conservative mass transfer explicitly in the calculation of q_c. The result of this method is to send the vast majority of possible proto-blue-straggler systems undergoing RLOF through the common-envelope channel, and thereby to produce a population of main-sequence—white dwarf binaries in circular orbits with periods of a few hundreds to thousands of days (see Fig. 9 in Geller et al. 2013). Such long-period circular binaries are not observed amongst the true solar-type main-sequence binary population in NGC 188 (nor in the Galactic field or any other open cluster binary population).

We suggest that these systems may, in reality, undergo stable mass transfer to produce blue stragglers. On average, there are 9 such binaries in the model at the age of NGC 188 that perhaps should instead have undergone Case C (or B) mass transfer, and thereby become blue stragglers with white dwarf companions orbiting at long periods. If these spurious common-envelope products were converted to mass-transfer blue stragglers, the resulting frequency and binary properties of

the NGC 188 model blue stragglers would nearly reproduce the blue straggler population of the true cluster. These specific systems in the NGC 188 model are prime candidates for follow-up through detailed binary evolution models to determine whether indeed they should go through stable or unstable mass transfer.

In summary, the combination of (1) the deficit of blue stragglers formed by mass transfer, compared to the 14 NGC 188 blue stragglers with binary properties indicative of a mass transfer origin, and (2) the excess of spurious long-period circular solar-type main-sequence—white-dwarf binaries suggests that the physics of mass transfer as incorporated in the N-body model is not yet accurate. The efficiency of stable mass transfer may be significantly underestimated in `NBODY6` and in other codes that use similar binary evolution procedures.

3.3.5.1 Primordial Triples and the KCTF Formation Channel

An alternative hypothesis to explain the paucity of blue stragglers in the NGC 188 model is that the model is missing a population of primordial hierarchical triples. We did not include primordial triples in the NGC 188 model, although triples do form dynamically and their subsequent dynamical evolution is modeled in detail. However, the frequency of dynamically formed triples is never high enough to reproduce the observed frequencies of triples in the Galactic field or in the few open clusters where such data are available. Although we know very little about the triple population of NGC 188, if the cluster currently has a similar frequency of triples as observed for solar-type stars in the field, then our N-body model indicates that the cluster must have formed with these triples in its primordial population.

Because triples may be important for blue straggler production through the KCTF mechanism and through collisions resulting from dynamical encounters, we performed a few additional models of the cluster with increased numbers of primordial triples (Geller et al. 2013). We included ad hoc triple populations, associating solar-type main-sequence binaries having periods between 2 days and 50 days with solar-type tertiaries at periods of 700–3,000 days in an attempt to maximise the contribution of the KCTF mechanism in particular to blue stragglers at periods near 1,000 days at seven gigayears.

Even with this "optimised" triple population, we find that including primordial triples does not dramatically increase the number of blue stragglers at the age of NGC 188. Placing every solar-type main-sequence binary with an orbital period between 2 days and 50 days in a triple (roughly 200 systems in total) on average only results in a total of 7–8 blue stragglers at the age of NGC 188 (as compared to an average of 6 blue stragglers in the NGC 188 model without primordial triples).

However, the inclusion of primordial triples does dramatically increase the detectable blue-straggler binary frequency, up to 80 % for our model with 200 triples. The majority of these additional blue-straggler binaries formed the blue stragglers through collisions during stellar encounters involving primordial triples, after which the newly formed blue stragglers managed to retain companions from the encounter at detectable orbital periods. Thus triples may in fact play an important

role in producing blue-straggler binaries through collisions (as was suggested by Mathieu and Geller 2009 and Leigh and Sills 2011).

Only about 25 % of these detectable blue-straggler binaries formed in relative isolation through Kozai-induced processes. It is possible that the Mardling and Aarseth (2001) analytic development for modeling Kozai oscillations and tidal processes in triple stars, which is employed in NBODY6, may underestimate the efficiency of KCTF blue straggler production. Further investigation into this possibility is needed, as are additional N-body models with more varied populations of primordial triples—ideally based directly on observations of triple populations in open clusters. At least in our current NGC 188 N-body simulations with NBODY6, the KCTF mechanism is not a significant contributor to blue straggler production.

In the absence of a secure treatment in NBODY6, here we explore the KCTF theoretical prediction that blue-straggler companions should derive from the primordial tertiary population. Specifically, we compare the orbital parameters and masses for the long-period NGC 188 blue straggler binaries to those of observed triple stars. Very little is currently known about the triple populations in open clusters. As a proxy, we compare with the triples observed in the solar neighbourhood from the Multiple Star Catalogue (MSC; Tokovinin 1997). The MSC is not a complete sample, but is representative of field triples and is currently the largest sample of triples available in the literature. We select from the MSC all triples that have inner binaries with masses and orbital parameters that could conceivably merge to form blue stragglers similar to those in NGC 188. Specifically we select triples with inner binaries of total masses between 1.2 and 2.2 $M_\odot$ (i.e., from just above the turnoff mass to twice the turnoff mass of NGC 188), inner orbital periods less than 10 days, and outer orbital periods less than 3,000 days.

The outer-period distribution for this sample of triples is consistent with the periods of the long-period NGC 188 blue stragglers (although the majority of triples have much larger periods; see Fig. 3.9). A subset of eight triples from this sample also have eccentricity measurements, shown in Fig. 3.10. Their eccentricity distribution is shifted to larger eccentricities than observed for the NGC 188 blue stragglers, at the 97 % confidence level.

The distributions of companion masses for this sample of MSC triples are shown in Figs. 3.3 and 3.11, evolved to the age of NGC 188. Geller and Mathieu (2011) show that if we draw companions to the NGC 188 blue stragglers from the MSC tertiary mass distribution, there is only a 1.8 % probability that they would both reproduce the observed mass function distribution of the NGC 188 blue stragglers in long-period binaries and result in all single-lined systems. Thus both the companion masses and eccentricities of the NGC 188 blue stragglers are inconsistent with those of the tertiaries of solar-type field triple systems in the MSC.

In summary, the KCTF channel encounters difficulties in explaining the observed properties of the NGC 188 blue stragglers in long-period binaries. The KCTF mechanism does not operate efficiently in our N-body models that include large populations of primordial triples, producing far less than the 14 observed NGC 188 blue stragglers in long-period binaries. Instead triples in our models contribute to blue straggler formation primarily through collisions resulting from

stellar encounters. It is possible that this low KCTF efficiency is a failing of the implementation of KCTF in NBODY6. However, potential KCTF progenitors in the observed triple population of the solar neighborhood also predict companions that are too massive and orbits that are too eccentric to explain the binary orbital properties of the NGC 188 blue stragglers in long-period binaries.

3.3.5.2 Bimodal Blue-Straggler Spatial Distributions

As discussed in Sect. 3.2.6, NGC 188 has a bimodal blue-straggler radial distribution reminiscent of those observed in many globular clusters. The NGC 188 model does not show this same structure in the blue-straggler radial distribution. At the age of NGC 188, the blue stragglers in the model are centrally concentrated, and there is not a distinct halo population like that observed in the true cluster. Only 17 % of the simulated blue stragglers are found outside of 5 pc at the age of NGC 188, as compared to 30 % in the true cluster.

This lack of a detectable bimodal radial distribution for the blue stragglers in the NGC 188 model may correspond with the overall paucity of blue stragglers discussed above, in that the model appears to underproduce blue stragglers through non-dynamical formation channels (e.g., mass transfer or the KCTF mechanism). Blue stragglers formed through such channels may form throughout the cluster, including the halo. This result should be revisited when the model more accurately reproduces the cluster blue straggler number.

Interestingly, though, the binary frequencies and distributions of orbital parameters for the NGC 188 core and halo blue stragglers are statistically indistinguishable. This finding suggests that the bimodal blue straggler radial distribution seen in NGC 188 is not the result of distinct formation channels.

3.3.6 Summary of Findings from N-Body Modeling of NGC 188

Our NGC 188 *N*-body model provides detailed predictions for the binary properties of blue stragglers formed by different formation processes. As is often the case, when one looks in greater detail at a problem, both answers and questions arise. We will focus first on the predictions from the model that appear most secure. Specifically, the NGC 188 *N*-body model predicts that within a rich open cluster after several gigayears of dynamical evolution:

- Blue stragglers produced by mass transfer will have a very high binary frequency (100 % in the NGC 188 model, all with orbital periods $<10^4$ days and most near 1,000 days). Except for the very few mass-transfer blue stragglers that undergo exchange encounters, these blue stragglers are predicted to have white-dwarf companions (the remnant cores of the donor stars). Most of these mass-

transfer blue stragglers form by Case C mass transfer and have CO white-dwarf companions that have masses between roughly 0.5 and 0.6 $M_\odot$; a smaller subset form through Case B mass transfer and have He WD companions with masses below 0.5 $M_\odot$.

- Blue stragglers produced by collisions will have a low binary frequency (12 % with orbital periods $<10^4$ days, and 33 % over all periods), and those that are in binaries with orbital periods around 1,000 days tend to have high eccentricities and companions with masses near that of the cluster turnoff.
- Blue stragglers produced by binary mergers will also have a low binary frequency (4 % with orbital periods $<10^4$ days, and 9 % over all periods), and those that are in binaries are either in short-period contact systems on their way towards merging or in long-period eccentric binaries produced by exchange encounters. Essentially no blue stragglers produced by mergers in binaries will be found with periods near 1,000 days.

Our comparisons between these predictions and our observations of the NGC 188 blue stragglers rule out at very high confidence an origin through collisions for the NGC 188 blue stragglers in binaries with periods near 1,000 days (which comprise 70 % of the NGC 188 blue stragglers). Mergers strictly within binaries also cannot produce blue stragglers in long-period binaries. Only the mass-transfer and KCTF mechanisms naturally produce blue stragglers in binaries with periods near 1,000 days.

The mass-transfer predictions for the secondary-star masses are closely consistent with the observed companion mass distributions. The recently detected white dwarf companions for some of the NGC 188 blue stragglers also agree with model predictions for an origin through mass transfer.

However, the mass-transfer production rate in the model was too low to reproduce accurately the number of blue stragglers. We suggest this reflects on the implemented mass-transfer theory, and in particular that detailed binary models are necessary to define the boundary between stable and unstable mass transfer. The orbital eccentricity distribution predicted by the mass-transfer mechanism also remains a key open question.

The NGC 188 blue stragglers in short-period binaries were most likely involved in previous close stellar encounters. We suspect that some or all of these blue stragglers were formed prior to their current binary configurations. However, the NGC 188 model struggles to produce blue stragglers with these binary characteristics.

Finally, the model does predict the same number of single (or very-long-period binary) blue stragglers as we observe in NGC 188. Roughly half of these blue stragglers in the model came from collisions with the remainder from binary mergers.

We conclude that the binary properties of the NGC 188 blue stragglers in long-period binaries are most closely reproduced by the mass-transfer mechanism. However, a combination of formation channels (indeed, perhaps all channels) are likely required to reproduce the full blue straggler population of NGC 188.

Conclusions

From a dynamical perspective, open clusters represent valuable laboratories that are intermediate between the high-density cores of many globular clusters and the collisionless environment of the Galactic field.

The recent deep mining of the open cluster NGC 188, and before that M67, yields a rich description of blue stragglers in old clusters, as summarised in Sect. 3.2.9. The overarching conclusion from this observational work is that open cluster blue stragglers are primarily binary systems, with the strong implication that their origins are inextricably linked to the rich primordial binary populations of open clusters.

The predominance of orbital periods near 1,000 days combined with a secondary mass distribution narrowly peaked at white-dwarf-like masses, as well as recent detections of white dwarf companions among several NGC 188 blue stragglers, point to most blue stragglers in old open clusters forming through mass transfer in binaries having asymptotic branch primary stars. Several remarkable short-period double-lined binaries point to subsequent dynamical exchange encounters modifying the blue straggler population after formation, and provide at least one example of a likely collisional origin for a blue straggler.

The observations open critical questions and new opportunities. The origin of the spin angular momentum of blue stragglers is unknown; the modest rotation rates are neither near break-up velocities as some theories predict nor like those of similar effective-temperature stars at ages of several gigayears. The few dynamical mass measurements find the blue stragglers (in short-period binaries) to be underluminous compared to normal evolutionary tracks, in one instance by as much as a factor of a few. Finally, the white-dwarf detections indicate effective temperatures that correspond to ages of several hundred megayears. In contrast to the age of NGC 188, these blue stragglers were formed "yesterday". With determination of the white-dwarf masses and thus the evolutionary states of the donor stars, these blue stragglers provide opportunities for detailed modeling of their mass transfer origins.

Extensive N-body modeling of NGC 188 with empirical initial conditions is able to reproduce the properties of the cluster, including the main-sequence solar-type binary population that is so critical to blue-straggler formation rates. The current models also reproduce well the binary orbital properties of the blue stragglers. However, they fall well short of producing the observed number of blue stragglers or their very high binary frequency.

Again, this challenge is at the same time an opportunity to improve essential physics within stellar and cluster evolution. In the case of the low blue-straggler formation rate in the current models, our analyses suggest that this is the result of an inaccurate parameterization of red-giant and

(continued)

asymptotic-giant mass transfer. This feature of the model also produces an excess of main-sequence—white-dwarf long-period binaries not observed in the cluster, with numbers comparable to the deficit of blue stragglers. Demanding that the main-sequence stars in these binaries actually become blue stragglers informs the relative rates of common-envelope versus mass-transfer evolution.

The progenitors of these spurious main-sequence—white-dwarf long-period binaries from the NGC 188 model offer ideal test cases for detailed binary evolution models investigating the stability of mass transfer and blue straggler production. Furthermore, with increasing computational speeds and recent software advances (like MESA (Paxton et al. 2011) and AMUSE (McMillan et al. 2012)), future N-body star cluster simulations may include "live" binary models for systems undergoing RLOF, and perhaps "live" collision models as well, thereby avoiding many of the assumptions necessary for the parameterised models we use today.

Still, within the current N-body framework, we cannot yet simultaneously reproduce all of the observed properties of the NGC 188 blue stragglers along with the cluster mass, central density, radial structure, main-sequence binary population, etc. Thus the challenge remains: to reproduce the observed NGC 188 blue straggler population within a coherent N-body model of the cluster.

References

Ahumada, J., Lapasset, E.: A&AS **109**, 375 (1995)
Ahumada, J., Lapasset, E.: A&A **463**, 789 (2007)
Aarseth, S. J.: Gravitational N-Body Simulations, Cambridge University Press (2003)
Belczynski, K., Kalogera, V., Rasio, F., Taam, R. E., Zezas, A., Bulik, T., Maccarone, T. J., Ivanova, N.: ApJS **174**, 223 (2008)
Bergeron, P., Leggett, S. K., Ruiz, M. T.: ApJS **133**, 413 (2001)
Bonačić Marinović, A. A., Glebbeek, E., Pols, O. R.: A&A **480**, 797 (2008)
Carney, B. W., Latham, D. W., Laird, J. B.: AJ **129**, 466 (2005)
Carney, B. W., Latham, D. W., Laird, J. B., Grant, C. E., Morse, J. A.: AJ **122**, 3419 (2001)
Chen, X., Han, Z.: MNRAS **384**, 1263 (2008a)
Chen, X., Han, Z.: MNRAS **387**, 1416 (2008b)
Eggleton, P. P.: Evolutionary Processes in Binary and Multiple Stars, Cambridge University Press (2011)
Geller, A. M., Hurley, J. R., Mathieu, R. D.: AJ **145**, 8 (2013)
Geller, A. M., Mathieu, R. D.: AJ **144**, 54 (2012)
Geller, A. M., Mathieu, R. D.: Nature **478**, 356 (2011)
Geller, A. M., Mathieu, R. D., Braden, E. K., et al.: AJ **139**, 1383 (2010)
Geller, A. M., Mathieu, R. D., Harris, H. C., McClure, R. D.: AJ **135**, 2264 (2008)
Glebbeek, E., Pols, O. R., Hurley, J. R.: A&A **488**, 1007 (2008)
Gondoin, P.: A&A **438**, 291 (2005)

Goranskij, V. P., Kusakin, A. V., Mironov, A. V., Moshkaljov, V. G., Pas-tukhova, E. N.: Astr. Astroph. Trans. **2**, 201 (1992)
Gosnell, N. M., Mathieu, R. D., Geller, A. M., , et al.: ApJL **783**, 8 (2014)
Hills, J. G., Day, C. A.: ApJL **17**, 87 (1976)
Hjellming, M. S., Webbink, R. F.: ApJ **318**, 794 (1987)
Hurley, J. R., Pols, O. R., Tout, C. A.: MNRAS **315**, 543 (2000)
Hurley, J. R., Tout, C. A., Pols, O. R.: MNRAS **329**, 897 (2002)
Hurley, J. R., Pols, O. R., Aarseth, S.J., Tout, C. A.: MNRAS **363**, 293 (2005)
Hut, P.: in Astrophysical Supercomputing using Particle Simulations, IAU Symposium 208, p. 331 (2003)
Johnson, H. L., Sandage, A. R.: ApJ **121**, 616 (1955)
Kippenhahn, R., Weigert, A.: Zeit Astrophys. **65**, 251 (1967)
Kroupa, P.: MNRAS **277**, 1507 (1995)
Lajoie, C.-P., Sills, A.: ApJ **726**, 67 (2011)
Latham, D. W.: Highlights Astron. **14**, 444 (2007)
Landsman, W., Bohlin, R. C., Neff, S. G., O'Connell, R. W. , Roberts, M. S. , Smith, A. M., Stecher, T. P.: AJ **116**, 789 (1998)
Leigh, N., Sills, A.: MNRAS **410**, 2370 (2011)
Leonard, P. J. T., Linnell, A. P.: AJ **103**, 1928 (1992)
Mardling, R. A., Aarseth, S. J.: MNRAS **321**, 398 (2001)
Marigo, P., Girardi, L., Bressan, A., et al.: A&A **482**, 883 (2008)
Mathieu, R. D.: in Stellar Clusters and Associations: Convection, Rotation, and Dynamos, ASPC 198, p. 517 (2000)
Mathieu, R. D., Geller, A. M., Nature **462**, 1032 (2009)
Mathieu, R. D., Latham, D. W.: AJ **92**, 1364 (1986)
Mathys, G.: A&A **245**, 467 (1991)
Mazeh, T., Goldberg, D.: ApJ **394**, 592 (1992)
McCrea, M. W.: MNRAS **128**, 147 (1964)
McMillan, S., Portegies Zwart, S., van Elteren, A., Whitehead, A.: in Advances in Computational Astrophysics: Methods, Tools, and Outcome, ASPC 453, p. 129 (2012)
Meibom, S., Mathieu, R. D.: ApJ **620**, 970 (2005)
Milone, A. A. E., Latham, D. W.: in Evolutionary Processes in Interacting Binary Stars, IAU Symp. 151, p. 475 (1992)
Nelson, C. A., Eggleton, P. P.: ApJ **552**, 664 (2001)
Paczyński, B.: ARA&A **9**, 183 (1971)
Passy, J.-C., Herwig, F., Paxton, B.: ApJ **760**, 90 (2012)
Paxton, B., Bildsten, L., Dotter, A., Herwig, F., Lesaffre, P., Timmes, F.: ApJS **192**, 3 (2011)
Perets, H. B., Fabrycky, D. C.: ApJ **697**, 1048 (2009)
Perets, H. B., Kratter, K. M.: ApJ **760**, 99 (2012)
Platais, I., Kozhurina-Platais, V., Mathieu, R. D., Girard, T. M., van Altena, W. F.: AJ **126**, 2922 (2003)
Raghavan, D., McAlister, H. A., Henry, T. J., et al.: ApJS **190**, 1 (2010)
Sandage, A. R.: AJ **58**, 61 (1953)
Sandquist, E. L., Latham, D. W., Shetrone, M. D., Milone, A. A. E.: AJ **125**, 810 (2003)
Sarajedini, A., von Hippel, T., Kozhurina-Platais, V., Demarque, P.: AJ **188**, 2894 (1999)
Sepinsky, J.F., Willems, B., Kalogera, V., Rasio, F.A.: ApJ **702**, 1387 (2009)
Sills, A., Adams, T., Davies, M. B.: MNRAS **358**, 716 (2005)
Sills, A., Faber, J. A., Lombardi, Jr., J. C., Rasio, F. A., Warren, A. R.: ApJ **548**, 323 (2001)
Soker, N.: A&A **357**, 557 (2000)
Tokovinin, A. A.: A&AS **124**, 75 (1997)
van den Berg, M., Orosz, J. , Verbunt, F., Stassun, K.: A&A **375**, 375 (2001)
Webbink, R.F.: ApJ **209**, 829 (1976)
Woods, T. E., Ivanova, N.: ApJL **739**, 48 (2011)

Chapter 4
Field Blue Stragglers and Related Mass Transfer Issues

George W. Preston

4.1 Introduction

I view field blue stragglers (FBS) through the prism of an aging observer. This chapter contains my impressions and perspectives about the current state of knowledge about FBSSs, drawn from an extensive literature that I searched with the aid of the *NASA Astrophysics Data System*,[1] and *Google*. The search prior to 2000 is spotty and I make no claim of completeness. In documenting various topics I tried to use references that acknowledge important earlier investigations.

It is not possible to construct a sensible story about blue stragglers in the Galactic field without reference to their occurrence in globular clusters where they were first identified, or in Milky Way satellites where they are now being discovered. I have tried to minimise discussion of these topics, which are treated at length elsewhere in this book. I include discussions of theoretical work (with diffidence) only when such work has an immediate impact on the interpretation of observations.

4.1.1 Historical Developments in First Part of the Twentieth Century

My point of view in this presentation is that McCrea's (1964) mass transfer produces the bulk of metal-poor FBS in the Galactic halo, so my history is largely confined

[1] http://adsabs.harvard.edu/abstract_service.html.

G.W. Preston (✉)
Carnegie Observatories, 813 Sana Barbara Street, Pasadena, CA 91101, USA
e-mail: gwp@obs.carnegiescience.edu

H.M.J. Boffin et al. (eds.), *Ecology of Blue Straggler Stars*, Astrophysics and Space Science Library 413, DOI 10.1007/978-3-662-44434-4_4

to this process. The earliest reference to "mass transfer" generated by my search engines is that of Kuiper (1941), who introduced Roche lobe overflow (RLOF) in his analysis of β Lyrae. Kuiper (1941), with characteristic modesty, refers to his own unpublished work conducted prior to his PhD thesis (1932) thusly:

> . . . , a stream of matter from M_A to M_B is likely to set in. . .

And later,

> . . . the degree of contact increases very considerably during the process of **mass transfer**. . .

In the 1930–1940s Otto Struve assembled a stable of luminaries at Yerkes Observatory (Chandrasekhar, Greenstein, Henyey, Herzberg, Kuiper, Morgan, München, Strömgren). Though Kuiper had already established himself as an authority in binary stars, Struve (1941) directed the attack on β Lyrae by Kuiper and his colleagues at Yerkes (see Sahade and Wood 1978 for details). For Struve β Lyrae was an obsession. He once confided to me that his goal (sadly, never-to-be-realised) was to spend his retirement at a modest telescope in the backyard of his home in the Berkeley hills, observing the endless spectroscopic variations produced by the gas-stream escaping from the outer Lagrangian point L_2.

Following WWII, Kopal (1955) invented the definitive binary classification scheme that persists to this day (detached, semi-detached, common envelope—see Chap. 7), and in 1967 groups led by Kippenhahn (Göttingen), Paczynski (Warsaw), and Plavec (Ondrejov) began detailed exploration of the consequences of stellar evolution within the confines of a Roche potential. Kippenhahn and Weigert (1967) gave us cases A, B, and C, and Paczynski (1967) is generally credited with resolving the Algol paradox, for which Paczynski (1967) gave this gracious tribute:

> May I say that until today it was the theory of close binaries that lagged behind the observations. Today we have a historical moment when the problem of the existence of semi-detached systems has been essentially solved theoretically.

McCrea (1964) worked largely aloof from developments in continental Europe. His seminal paper, directed specifically to the "extended main sequence of some stellar clusters", made no reference to Sandage's paper (1953) nor to any of the research referred to in the paragraph above, and it was his only publication about binary stars. However, I know that he had an abiding interest in binary stars, because a decade earlier I, then a graduate student, attended a number of his lectures devoted to problems of interacting binaries during his tenure as a Visiting Professor at Berkeley in 1956. McCrea was invited to Berkeley by (*who else?*) my mentor Otto Struve!

Speculations about the origin of blue stragglers in the halo field are inextricably linked to ideas about the origin of the Galactic halo itself. In addition to an origin *in situ*, via ELS (Eggen et al. 1962) and its various possible aftermaths, two additional hypotheses have been advanced. I (Preston 1994a) suggested that a modest fraction of them arise from capture of Galactic satellites similar to the present-day Carina dSph, where they abound as part of an intermediate-age population (Smecker-Hane et al. 1994) or an even younger "blue-plume" (Monelli et al. 2004). Gnedin

and Ostriker (1997), on the other hand, calculated that the destruction time-scale for Galactic globular clusters (hereafter GCs) is comparable to their lifetimes, and therefore that remnants of now-largely-destroyed primordial clusters might constitute a substantial fraction of the spheroid (bulge/halo) stellar population. I shall return to these issues in Sect. 4.5 below.

4.2 Identification of BSS

4.2.1 The Metal-Poor Halo

The observational requirements for selection of (apparently young) halo FBSSs are parameters that (a) identify stars with the metallicity of the parent population and (b) sort them unambiguously by age. The first of these two parameters must cull halo stars from the much more numerous, metal-rich, and age-heterogeneous populations of the thick and thin discs. Note that there are complications here because of the overlapping abundance distributions of the three principal Galactic populations. The second parameter must separate the "young" FBSSs from the bulk of their older main sequence cousins. If we ignore well-known details about the behavior of O and Na (Carretta et al. 2009), and the poorly-constrained and indirectly inferred He content (Buzzoni et al. 1983), the gross chemical compositions of most GCs are homogeneous, and their ages can be estimated by fits of isochrones (there is a plethora of these in the literature) to the stellar distributions in colour-magnitude diagrams (CMD). The fits are characterised most sensitively by colours of the main sequence turnoffs (MSTO). Because of the great ages of GCs the variation of turnoff colour with age is small, $d(B-V)/dt \sim 0.008\,\mathrm{dex\,Gyr^{-1}}$ (Yi et al. 2001). For this reason a number of small and not-so-small effects mask the age effect: interstellar (IS) reddening, chemical composition, including [Fe/H], and [alpha/Fe], and (assumed) He, the choice of mixing-length parameter, and the effects of radiation pressure and gravitational settling on stellar models. These effects combine to produce a blurred lower bound for temperature-sensitive colour indices of halo main sequence stars.

4.2.1.1 Photometric Criteria: UBV

The *UBV* photometric system identifies FBSSs (Preston et al. 1994b) with reasonable success because $U-B$ is a sensitive metallicity indicator (Wallerstein and Carlsoln 1960; Wildey et al. 1962; Melbourne 1960), and $B-V$ is an adequate, though not ideal, temperature indicator (Buser and Kurucz 1978; Van den Bergh and Clem 2003). The manner in which the *UBV* two-colour diagram isolates FBS candidates is indicated in Fig. 4.1 taken from Preston et al. (1994b), which utilised photometry (Preston et al. 1991) of the HK search for metal-poor stars (Beers et al. 1992).

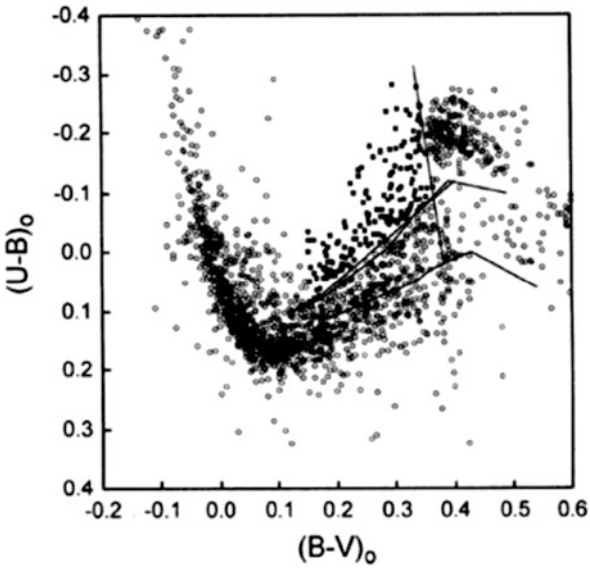

Fig. 4.1 FBSSs in the *UBV* two-colour plane lie in a triangular region blueward of a steeply-inclined blanketing vector that extends upward from the intrinsic two colour-relation for solar-type stars near $(B-V)_o = 0.38$, and above a linearised MS relation for [Fe/H] $= -1$. This figure is reproduced from Preston et al. (1994b) with permission from the Astronomical Journal

A steeply inclined blanketing vector extending upward from the intrinsic two-colour relation for solar-type stars (Wildey et al. 1962) near $(B-V)_o = 0.38$ separates FBS candidates from the dense clump of metal-poor "subwarfs" near $(B-V)_o = 0.4$, $(U-B)_o = -0.2$. The UBV system fails below $(B-V)_o = 0.15$ ($T_{eff} > 7700$ K), where line blanketing becomes too small to act as an effective abundance indicator. Temperature-dependent blanketing vectors (Wildey et al. 1962) were used to construct a linear lower bound for [Fe/H] $= -1$. The success of this lower bound can be judged by the plot of space motions versus [Fe/H] values derived from spectrum analysis by Preston and Sneden (2000, hereafter PS00) of FBSSs in Fig. 4.2, reproduced from Bragaglia et al. (2005).

Figure 4.2 exhibits at once the strength and weakness of the $U-B$ abundance discriminant. A clear majority of the stars (the red symbols and most of the green symbols) have spaces velocities and abundances ([Fe/H] < -1.2) associated with the halo. However, the lower bound failed to eliminate a significant number of stars with [Fe/H] > -1.0. This failure can be attributed in part at least to photometric errors and the vertical density gradient $dn/d(U-B)$ near the lower bound in Fig. 4.1 which combine to provide net spillover of metal-rich stars into the FBS domain. New abundances for stars in the PS00 survey derived from spectra with superior signal-to-noise ratios (S/N) and resolution (Bragaglia et al. 2005) are plotted against those of PS00 in Fig. 4.3. The solid 45-degree line indicates 1:1 correspondence.

Bragaglia et al. (2005) obtain abundances systematically lower than PS00 by $\sim$0.15 dex. Scatter in this regression contributes to blurring of the lower boundary of the FBS domain.

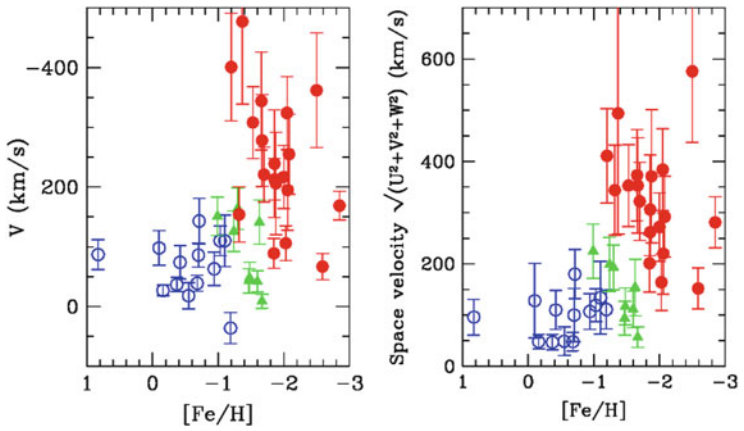

Fig. 4.2 Galactic rotation vector (*left panel*) and space velocity (*right panel*) versus [Fe/H] for the PS00 sample of FBSSs. The figure is reproduced from Bragaglia et al. (2005) with permission from the IAU

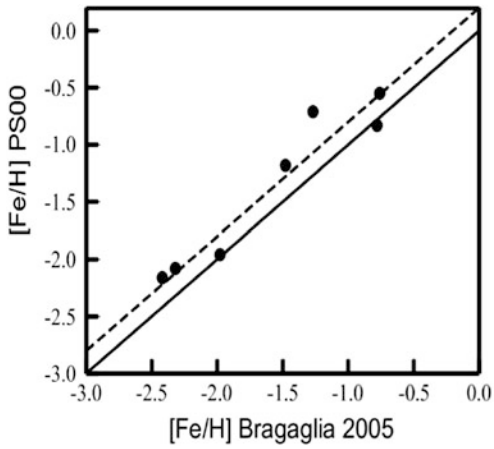

Fig. 4.3 [Fe/H] values of PS00 versus those of Bragaglia et al. (2005)

There is a bright side to this otherwise dreary discussion. The binary fraction of stars in the PS00 survey with thick disc abundances ([Fe/H] > -1) is marginally higher, 0.76, than the fraction, 0.69, for stars with [Fe/H] < -1 and markedly higher than the spectroscopic binary fractions, $\sim$0.15, of the normal stars of the halo (Latham et al. 2002) and disc near the sun (Duquennoy and Mayor 1991). Evidently, mild $(U - B)$ excesses properly select mildly metal-deficient FBSSs in the thick disc. This result suggests that the bulk of the thick disc stars have similar ages, i.e., the thick disc does not contain a significant component of normal A-type and early F-type stars. Most of the known FBSSs near the solar circle have been identified by

UBV photometry. For additions to the list of FBS candidates at distances less than about 2 kpc subsequent to Preston et al. (1994b), see the compilation by Wilhelm et al. (1999a).

4.2.1.2 Photometric Criteria: SDSS *ugr*

Numerous FBS candidates have been identified in the distant halo by use of the $(u-g, g-r)$ equivalent of the $(U-B, B-V)$ diagram shown in Fig. 4.1 (Yanny et al. 2000; Sirko et al. 2004). Noting that the conversion of $(u-g)$ to $(U-B)$ is not well-defined, Yanny et al. (2000) tentatively identify 2,715 FBSSs and 1,493 BHB stars. Sirko et al. (2004), finding that *ugr* photometry did not separate BHB and FBS satisfactorily, preferred the use of Balmer lines as described in Sect. 4.2.1.5 below.

FBSSs enter most discussions of BHB stars as a nuisance population that complicates the calculation of space densities of BHB stars. I have found little discussion of the apparent FBS population (e.g., space densities, Galactic distribution, clumping, specific frequency, abundance distribution) in the SDSS literature. More about this possibility in Sect. 4.4.1 below.

4.2.1.3 Other Photometric Criteria

Morrison et al. (2000) used the Washington photometric system to search for halo substructure produced by satellite accretion. They chose BMP stars (Preston 1994a), of which FBSSs are a subset, as one of their halo tracers. Using Washington $M-T_2$ as a temperature indicator they found 23 BMP to $V = 19$ in an area of 2.75 deg^2 in accord with expectations (see their Fig. 2). In their discussion apparent magnitude, which limits the sample to heights far above the Galactic plane, isolates stars with low [Fe/H].

FBS candidates have been identified in the Strömgren photometric surveys of Olsen (1979, 1980) who lists 84 candidates in the summary tables of his two papers. Stetson (1991) identifies 15 possible metal-poor FBSSs in his Table 9. I found it difficult to assess the reliability of these assignments mainly because of the confusing graphical displays of results. It is my impression that Strömgren filters are not ideal tools for wholesale identification of FBS. Narrow bandwidths of the filters are a major drawback.

4.2.1.4 Hybrid Spectro-Photometric Methods

Pier (1983) pioneered the identification of bona fide metal-poor blue horizontal branch stars (BHB) of the halo field and, thus indirectly, FBS stars by use of $B-V$ as a temperature coordinate, the equivalent width of the CaII K line as an abundance indicator, and the widths of Balmer lines as a gravity (luminosity)

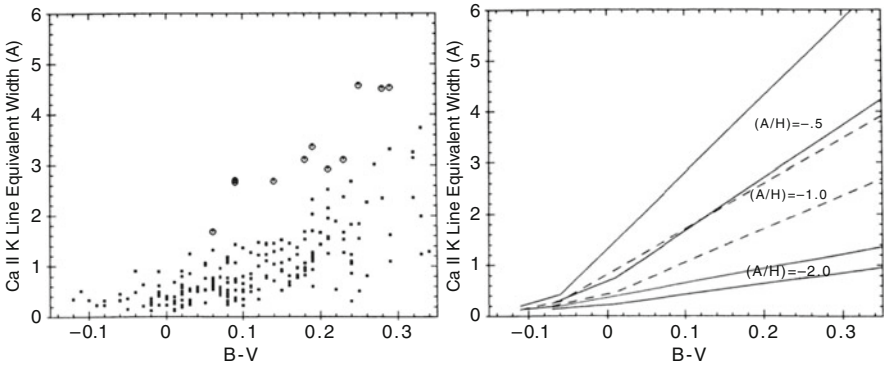

Fig. 4.4 (*Left panel*) Equivalent widths of CaII (K) for candidate BHB stars versus unreddened $B-V$ colour taken from Pier (1983); (*right panel*) abundance calibration of CaII (K) by Manduca and Bell (1978). The figures are reproduced with permission of the AAS

indicator. Following Searle and Rodgers (1966), he estimated metal abundances by calibration of the CaII K line as shown by the diagrams in Fig. 4.4, hereafter *BVK* diagrams.

The left panel contains measured equivalent widths. The right panel contains a calibration provided by Manduca and Bell (1978). Again following Searle and Rodgers (1966), Pier (1983) showed that FBSSs and BHB stars could be disentangled in a HB candidate list by use of $D_{0.2}$, the full width of a Balmer line (here Hδ) at a depth 20 % below the local continuum level. How well this works is illustrated in Fig. 4.5. Here, as in several examples to follow, the FBS are treated as a nuisance to be removed from a BHB dataset.

Wilhelm et al. (1999a; method) and Wilhelm et al. (1999b; results) compiled a list of 416 probable metal-poor FBSSs identified in the North and South hemisphere HK surveys (Beers et al. 1988, 1996). Tools of the trade include *UBV* photometry, the *BVK* diagram, and $D_{0.2}$.

Kinman et al. (1994) use another hybrid method to separate BHB stars from FBSSs among AF stars of the Case Low-Dispersion Northern Survey (Sanduleak 1988). Their classification criteria are: (1) a $(u-B)_K$ colour (Strömgren u filter and Johnson B filter) that measures the size of the Balmer jump, (2) a spectrophotometric index λ that measures steepness of the Balmer jump, and (3) the parameter $D_{0.2}$. The success with which these parameters separate BHB stars and FBSSs is shown in Figs. 4.6 and 4.7.

Concordance of classification assignments based on these three parameters is reassuring. Kinman et al. (1994) found that more than half of the A- and F-type stars fainter than $V = 13.0$ and with $(B-V)_0 < 0.23$ are not BHB stars, but have surface gravities more like those expected for main-sequence stars. They remark that the more metal-poor of these are likely to be the blue metal-poor (BMP) stars discussed by Preston (1994a).

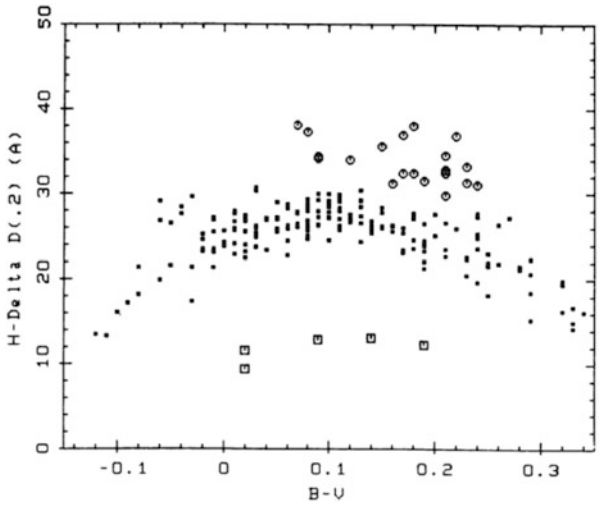

Fig. 4.5 $D_{0.2}$, width of Hδ at depth 0.2 below the local continuum, plotted versus unreddened $B-V$ for candidate BHB stars by Pier (1983). Stars with main sequence gravities (*open circles*) are clearly separated from BHB stars (*filled circles*). The figure is reproduced with permission of the AAS

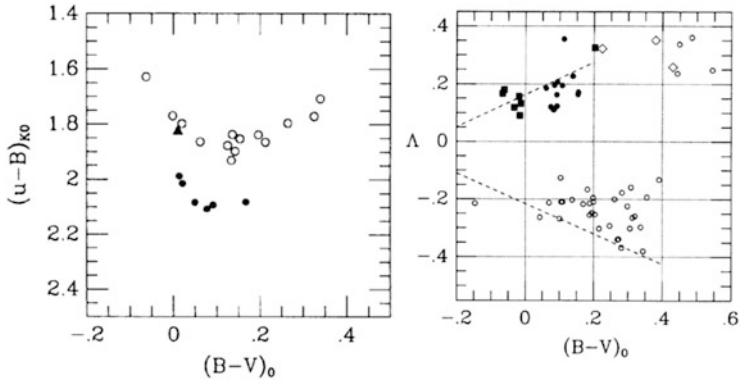

Fig. 4.6 (*Left panel*) The special 2-colour diagram of Kinman et al. (1994) uses the Strömgren u filter to effect a clean separation of HB stars (*filled circles*) from main sequence stars (*open circles*); (*right panel*) measures steepness of the Balmer jump. The figures are reproduced with permission of the AAS

Flynn et al. (1994) compared the performance of Strömgren $c1$, $(b-y)$ and $D_{0.2}$, $(B-V)$ photometry to separate BHB from FBS . They concluded that both systems work but that the $D(0.2)$, $B-V$ system made more efficient use of telescope time.

Finally, Carney et al. (1994) found a few ($n=6$) FBSSs in their radial velocity survey of high proper motion stars. $(B-V)$ is their temperature parameter. They derived abundances by matching their spectra to a grid of synthetic spectra. The low proper motion limits, $0.2''$ year^{-1}, of the Giclas and Luyten surveys from which

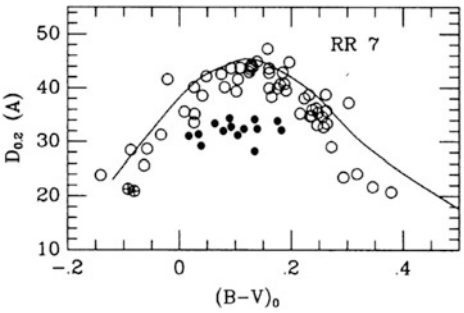

Fig. 4.7 $D_{0.2}$, defined as the mean of the widths of Hγ and Hδ at depth 0.2 below local continuum versus $(B-V)_o$. *Open and filled circles* denote MS and HB stars, respectively. This figure is reproduced with permission of the AAS

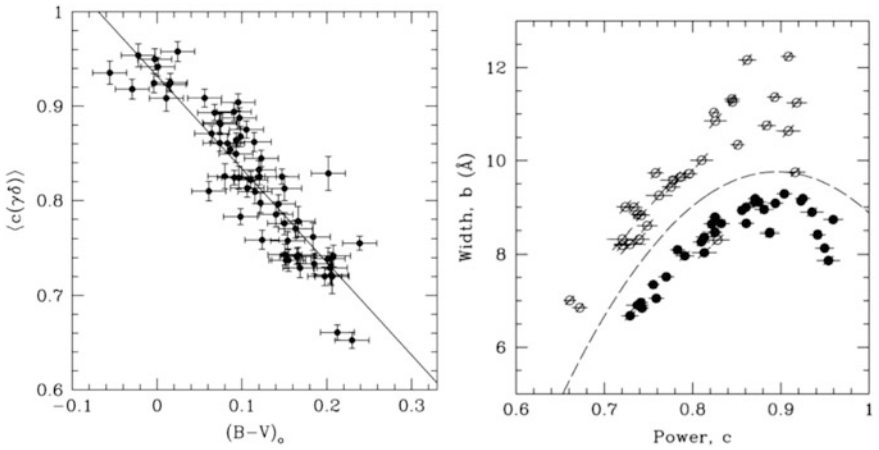

Fig. 4.8 (*Left panel*) A plot of the Sérsic exponent c versus $(B-V)_o$ taken from Clewley et al. (2002); (*right panel*) the Sérsic scaled-width parameter b, effects an excellent separation of FBSSs (*open circles*) and BHB stars (*filled circles*). The figure is reproduced with permission of Monthly Notices of the Royal Astronomical Society

their sample was drawn confines the Carney et al. (1994) survey to a small volume of space in which only a few FBSSs are expected.

4.2.1.5 Spectroscopic Criteria

In a most refreshing example of cross fertilisation in astronomy Clewley et al. (2002) borrowed the Sérsic (1968) function from extragalactic astronomy to make analytical fits of observed Balmer line profiles in A-type stars. They use the Sérsic scale-width parameter b and exponent c to derive gravities and temperatures of A-type stars. Figure 4.8 shows that the Sérsic exponent c is well-correlated with

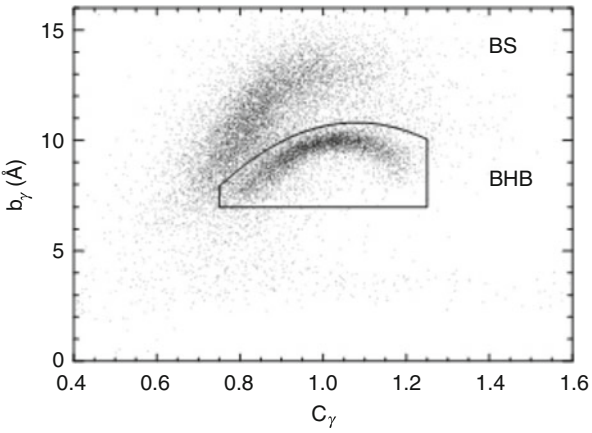

Fig. 4.9 The Sérsic parameters b and c, employed by Xue et al. (2011), effect a clear separation of FBS and BHB stars in the data of SDSS. The figure is reproduced with permission of the AAS

$(B-V)_o$, hence, temperature. The scale-width parameter b effects a clean gravity separation of metal-poor main sequence and BHB stars. The *BVK* diagram provides abundances. Brown et al. (2005) compare the various hybrid methods for isolation of BHB stars from FBSSs (see their Fig. 5) from which it is evident that the Sérsic parameters do the best job.

Xue et al. (2011) used a similar application of the Sérsic function to effect a clean separation of FBSSs from BHB stars as shown in Fig. 4.9, where the Sérsic b and c parameters were derived from measurements of Hγ. Recall that c is a temperature parameter, b is a gravity parameter (the surface gravities of FBSSs exceed those of BHB stars by approximately one order-of-magnitude). Because Xue et al. (2011) were primarily interested in kinematic substructure, they confined their analysis to the BHB stars. However, the FBS sample contains a wealth of additional untapped information about the stellar content of the halo.

Figure 4.9 contains about 5,000 BHB stars. No count of FBSSs was given. I guess conservatively by inspection that the number of FBSSs is comparable (recall Dustin Hoffman's count of toothpicks in the movie "Rainman"). An unknown fraction of the latter may be in as yet unidentified accretion streams.

This remarkable database can be used to resolve the Galactic halo BMP population into FBSSs formed in situ and FBSSs accreted from satellites. Recall that [α/Fe] is systematically low by $\sim$0.2 dex at all [Fe/H] in the red giants of dwarf spheroidal satellites of the Milky Way relative to the bulk of Galactic halo stars. This is illustrated in Fig. 4.10 taken from Venn (2004), where black boxes denote red giants in the dwarf spheroidal galaxies Carina, Draco, Fornax, Leo I, Sculptor, Sextans, and Ursa Minor (Geisler et al. 2005; Shetrone et al. 2001, 2003), and the small circles denote various species of Galactic stars.

Note further that two of the three $\alpha-$elements used to construct Fig. 4.10 possess prominent lines (Mg b, CaII K) that can be measured with modest spectral resolution, say $R = 5{,}000$. Finally, note that an early exploration (PS00) yields promising results (see Sect. 4.6 below). This is a project ready to go.

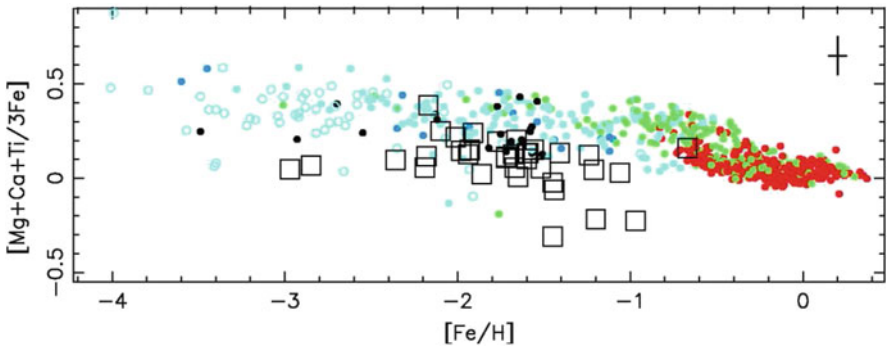

Fig. 4.10 The [α/Fe] values of red giants (*boxes*) in several dSph satellites of the Milky Way are systematically lower than the values for various species of Galactic stars (*circles*) in this compilation taken from Venn (2004). The figure is reproduced with permission of the AAS

4.2.2 FBS of the Thick/Thin Disc

If McCrea's mass transfer produces most of the FBSSs, then we must be surrounded by lots of them in the thick/thin discs. From an assemblage of star counts Sandage (1987) estimated stellar densities of the thin disc, thick disc, and halo to be in the proportions 200:22:1. Scaling the local metal-poor FBS number density, ∼350 kpc^{-3}, at the solar circle, by 100 in round numbers, we expect ∼35,000 disc FBSSs brighter than V ∼14.5, of which approximately 140 should be in the Henry Draper catalogue, and 10 in Olsen's surveys which were limited to $V < 8.3$. By this reckoning Olsen found too many disc FBSSs (see Sect. 4.2.1.3 above).

A convincing procedure for wholesale identification of disc FBSSs, simpler in its application than detailed one-by-one analysis (Fuhrmann and Bernkopf 1999; Fuhrmann et al. 2011), has yet to be devised. Perhaps, in view of the high binary fraction, 0.76, among PS00 sample stars with [Fe/H] > -1, we should revisit the *UBV* identification criteria.

4.3 Group Properties of Metal-Poor FBS

This section is devoted to a number of characteristics of metal-poor FBSSs that set them apart from other stellar groups. The first, to which all others are subsidiary, are the colour boundaries which define the group. The boundaries are defined in a number of photometric systems.

4.3.1 Colour Boundaries

In all practical cases the red (cool) boundary of the blue straggler domain is defined to be at or near the colour of the MSTO of the stellar system in which they occur,

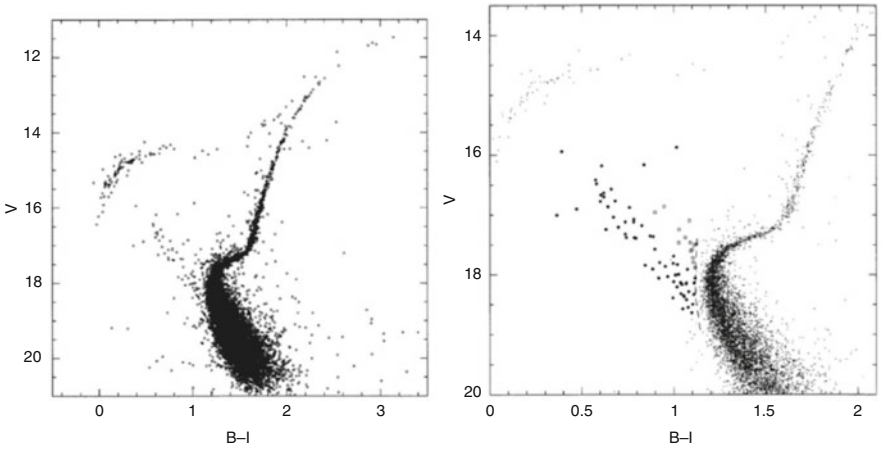

Fig. 4.11 (*Left panel*) The photometry of Mandushev et al. (1997) clearly shows that a sequence of blue stragglers merges with the main sequence below the MSTO in the GC M55; *(right panel)* the dashed line slightly blueward of the MSTO artificially truncates the sequence of mass-transfer binaries. The figure is reproduced with permission of the AAS

i.e., the boundary of the group is defined by stars which are not members of the group. Such a definition leads to the artificial edge in the beautiful photometry of NGC 6809 (Mandushev et al. 1997) indicated by the dashed curve in the right panel of Fig. 4.11.

An obvious (to me) sequence of mass transfer binaries extends continuously into the single-star main sequence in the left panel. Such a red extension was a natural ingredient of the PS00 toy model, and the more sophisticated applications of Eggleton's code (1973) by, for example, Tian et al. (2006) and Chen and Han (2009) who, however, did not make calculations for old metal-poor systems considered here. Ryan et al. (2001, 2002) reach the same conclusion, arguing that Li-deficient binaries with greater-than-average axial rotation below the MSTO should be regarded as mass-transfer binaries.

A second logical defect of this definition is dramatised by considering the MSTO $(B-V)_o$ values for two well-studied clusters each of which contains BSS. The clusters M67, and NGC 5466 have MSTO $(B-V)_o$ values of 0.50 (Van den Bergh et al. 2010) and 0.39 (Beccari et al. 2009), a large difference, comparable to the entire colour range of the FBSSs, due primarily to the $\sim$2 dex difference in metallicity. FBSSs with this range in metallicity are common in the halo/disc field, where there are no MSTOs to guide us.

What we realise from this cluster comparison is that there is no one-size-fits-all red (low temperature) boundary to the FBS domain. Furthermore, the field contains sizable numbers of FBSSs with abundances well below the low limit, [Fe/H] ~ -2.5, of the globular cluster population, and a fraction of these are CEMP-s stars, formed by mass transfer from AGB companions, that pay no heed to the MSTO; outstanding, indubitable examples are CS 22964-161 (Thompson et al.

2008) and CS 22949-008 (Masseron et al. 2012). An even larger fraction is formed by mass transfer from ordinary RGB companions. As we shall see in Sect. 4.6 below, knowledge of the amounts of mass transferred, whether by Roche lobe overflow (RLOF) or wind accretion is now or will soon become important for estimation of dilution of the accreted mass by the receiver envelope, for calculating changes in dilution modified by thermohaline mixing, for accurate calculation of the efficiency of wind accretion in the variety of scenarios posed by binaries with different orbital parameters, and for reconciliation of the relative numbers of MS and giant CEMP-s stars.

It is possible to generalise the cool boundary for metal-poor FBSSs by converting it to a parameter that can be calculated for each star, rather than a parameter defined for the whole group. Because of the large ages of metal-poor halo stars, MSTO colour varies only slowly with age, $d(B-V)/dt \sim 0.008\,\mathrm{mag\,Gyr^{-1}}$ (Yi et al. 2001). Therefore, with negligible error we may adopt a single, canonical age, say 13.5 Gyr, for the parent populations of all the individual metal-poor FBSSs. The MSTO $B-V$ values of the Y^2 isochrones (Yi et al. 2001) for age 13.5 Gyr are shown in Fig. 4.12.

[Fe/H] values and the $\Delta(B-V)$ colour displacements of each star from their respective MSTOs then yield *lower limits* to the accreted masses via $\Delta M/\Delta(B-V)$. *Lower limits* are the best that can be achieved, because the initial masses of the receivers, hence their initial $B-V$ colours, are unknown: they may lie within a considerable range of values at or below their MSTO values (PS00, Ryan et al. 2002). The [Fe/H] values of several FBSSs now under abundance scrutiny lie on $-3.5 < \mathrm{[Fe/H]} < -1.5$, which, from Fig. 4.12, corresponds to a range in MSTO $B-V$ colour of ∼0.08 mag. The individual displacements $\Delta(B-V)$ can be converted to accreted masses by values $\Delta M/\Delta(B-V)$ derived from isochrones, typically $\sim -1.5\,\mathrm{M_\odot\,mag^{-1}}$. I calculated accreted masses in this manner for several FBSSs of interest in Sect. 4.6 below.

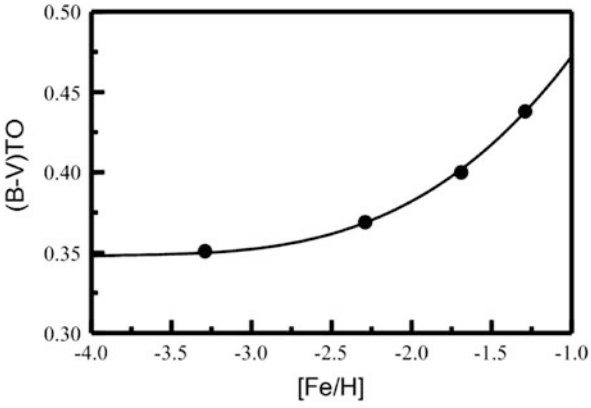

Fig. 4.12 The $B-V$ colour of the MSTO versus [Fe/H] for an age of 13.5 Gyr interpolated among the isochrones of Yi et al. (2001) by use of a 3rd order polynomial

4.3.2 *Specific Frequencies*

To estimate the incidence of FBSSs in their parent population we (Preston et al. 1994b) introduced specific frequencies, S_{BMP}, defined as the ratio of space densities of BMP and HB stars near the solar circle. HB stars are a convenient reference population because both theory and observation support the notion that HB density is closely proportional to total population density. The HB models of Lee and Demarque (1990) with typical halo abundance $Z = 0.0004$ have lifetimes that range from 0.90×10^8 years for mass $M/M_\odot = 0.52$ to 1.14×10^8 years for mass $M/M_\odot = 0.76$, and the average number ratio, 1.38, of HB stars to red giants more luminous than the horizontal branch in metal-poor globular clusters (Buzzoni et al. 1983; Zoccali et al. 2000) has a standard deviation of only 0.15. Lower RGB stars with luminosities comparable to those of BSSs (Bolte et al. 1993) or MS stars near the turnoff (Chen and Han 2009) are not options in the halo field, because such stars cannot be identified unambiguously. We (Preston et al. 1994b) used our high value $S_{BMP} = 8$ relative to the values <1 for BSSs in globular clusters to conclude that cluster-type BSSs are a minor constituent of the BMP population, and suggested an extra-Galactic origin. We were overly enthusiastic. Subsequent recognition of the high binary fraction among BMP stars (PS00) produces a lower specific frequency for FBSSs, $S_{BMP} = 4.0$, that is nevertheless an order-of-magnitude larger than those of the halo globular clusters, as shown in Fig. 4.13. Notice that S_{BMP} values are conspicuously larger in the sparse globular clusters of the outer halo, identified by name in the right panel of Fig. 4.13.

The marked decreases with increasing cluster Luminosity (mass) and the King (King 1966) concentration parameter c played key roles in formulation of the

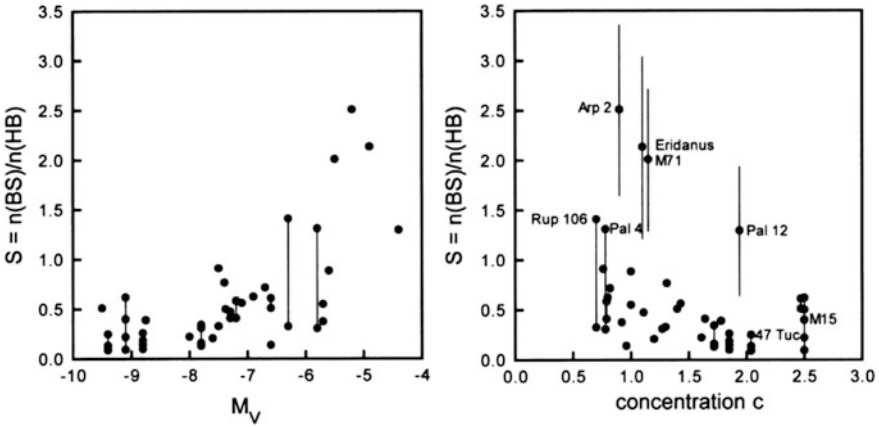

Fig. 4.13 (*Left panel*) Specific frequency of BSSs versus GC absolute visual magnitude. (*Right panel*) Specific frequency of BS stars versus King concentration parameter. The figures, taken from PS00, are reproduced with permission from the AAS

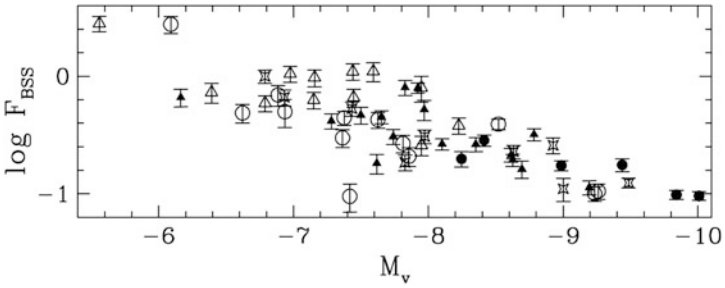

Fig. 4.14 Logarithmic specific frequency of BSSs in globular clusters based on the HST data of Piotto et al. (2004). This figure is reproduced with permission from the AAS

view that collisional disruption of long period (wide) binaries (Leonard 1989; Horton et al. 2001), by far the most numerous in the orbital period distribution of Duquennoy and Mayor (1991), accompanied by merger of the much less numerous short-period binaries (Mateo et al. 1990) are the two physical processes responsible for the low specific frequencies of BSSs in GCs relative to the field. Piotto et al. (2004) confirmed the correlation of specific frequency with absolute luminosity and the relatively low specific frequencies with their elegant HST data for 56 GCs shown in Fig. 4.14. The upper bound to specific frequency among the oldest open clusters extended the correlation essentially to the field value of PS00 (De Marchi 2006).

The disruption of wide binaries in M22 is contested by Côté et al. (1996), *in spite of the fact that their own 22 yr search led to a marked deficiency of such binaries relative to the Galactic field*. A related situation was encountered by Mayor et al. (1996) in ω Cen, who reported that only 2 of 32 CEMP stars in that cluster are spectroscopic binaries, contrary to the expectations of McClure and Woodsworth (1990). At issue is whether CEMP stars in these two clusters are produced by McCrea-type star-by-star mass transfer or by pollution of intra-cluster gas during evolution of a previous generation of stars. This topic has a fascinating history (Hesser et al. 1977; Norris and Freeman 1983; Vanture et al. 1994; Marino et al. 2009; Marino et al. 2012) beyond the purview of this chapter.

4.3.3 The Distinguishing Characteristics of FBS Binary Orbits

The orbital characteristics of FBSSs, discussed at length by PS00 and Carney et al. (2001), are these:

(a) the mass functions of FBSSs are smaller by a factor of two than those for binaries of the disc (Duquennoy and Mayor 1991) and high proper motion samples (Latham et al. 2002) as illustrated by the cumulative distributions in the left panel of Fig. 4.15. McClure and Woodsworth (1990) encountered a similar situation in their comparison of their gCH binaries with normal GK

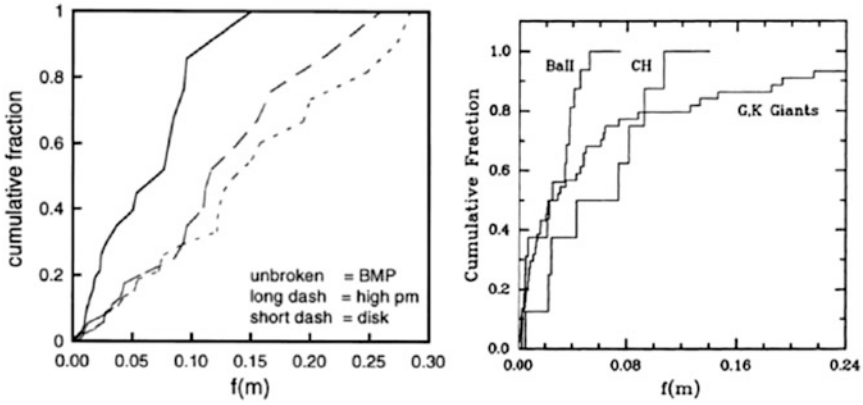

Fig. 4.15 (*Left panel*) The cumulative distribution of mass functions for FBS binaries is compared to those for ordinary binaries of the disc and halo. The figure, taken from PS00, is reproduced with permission from the AAS. (*Right panel*) The cumulative distributions of mass functions for Ba star binaries and CH-giant binaries are compared to those for ordinary G–K giant binaries. The figure, taken from McClure and Woodsworth (1990), is reproduced with permission from the AAS

giant binaries. Comparisons of the cumulative distributions for these samples are reproduced in the right panel of Fig. 4.15. Both comparisons are consistent with the idea that FBS and gCH binaries have secondaries (white dwarfs) whose masses are systematically lower than the companion masses of their normal counterparts.

(b) There is a deficit of short-period binaries and an excess of orbital eccentricities less than 0.2 among FBSSs (PS00) and CH stars (McClure and Woodsworth 1990, McClure 1997) compared to disc binaries (Duquennoy and Mayor 1991) and high proper motion binaries (Latham et al. 2002). Figure 4.16 illustrates these comparisons of FBS binaries (middle panel) to their carbon-star cousins (bottom panel) and to the parent populations from which both are drawn (top panel). Straight-line segments join alternative orbital solutions for a number of FBS binaries obtained by PS00. Such alias periods, three of them for three of the stars, were an unfortunate, inevitable consequence imposed by annual/biennial observing trips to Chile. I included these alternatives in the middle panel of Fig. 4.16 to assure the reader that the conclusions about periods and eccentricities are not sensitive to which alternatives are chosen.

It is commonly accepted that periods lengthen during conservative mass transfer after the mass of the donor falls below that of the receiver (Hilditch 2001) and that such mass transfer circularises orbits. However, Sepinsky et al. (2007, 2009, 2010) have revisited mass transfer with and without mass loss in binaries with eccentric orbits and obtain a wide variety of outcomes that depend on initial conditions. Even in the conservative case periods and eccentricities may either increase or decrease on time scales that range from a few million

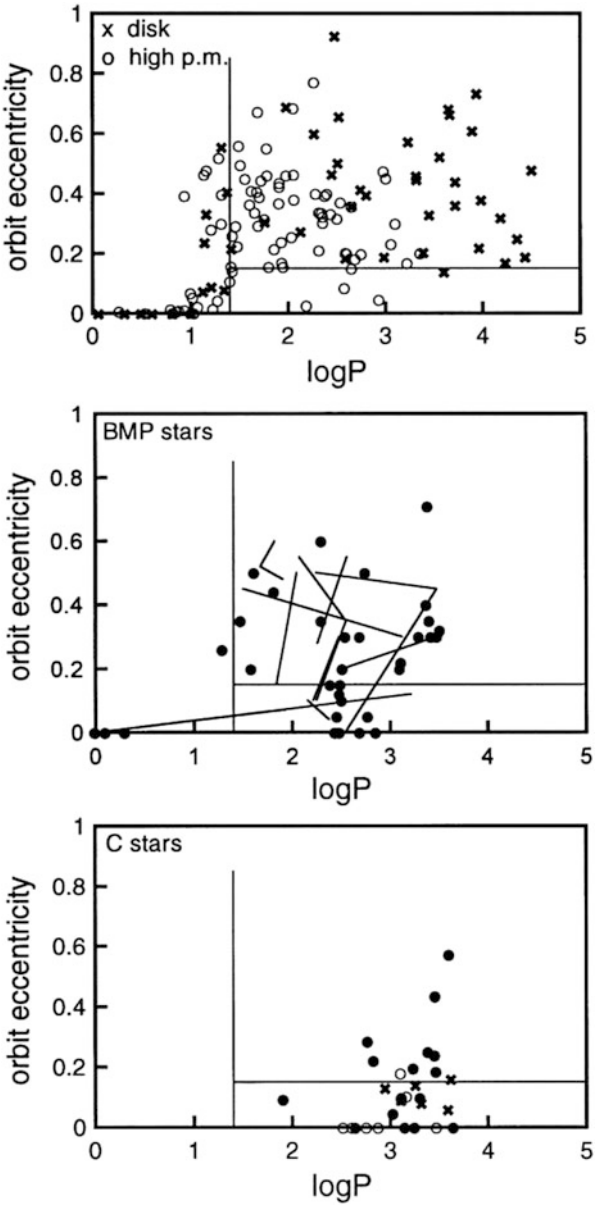

Fig. 4.16 Orbital eccentricity versus logarithm of orbital period for (*top panel*) ordinary binaries of the disc (*crosses*) and high proper motion samples (*open circles*); (*middle panel*) FBSSs of PS00; (*bottom panel*) Ba stars (*filled circles*) and CH giants (*open circles*). The figures, taken from PS00, are reproduced with permission from the AAS

years to a Hubble time. FBSSs and CEMP-s stars provide a rich database with which to test these recent theoretical developments.

(c) Finally, PS00 found no double-lined spectroscopic binaries (SB2) among their FBSSs while SB2 comprise 20 % of the binaries in the high proper motion sample of Latham et al. (2002). The absence of detectable secondaries among FBS binaries is a natural consequence of the mass transfer hypothesis. I (Preston 1994a) did discover one extremely metal-poor SB2, CS 22873-139 and deduced an age of 8 Gyr from a discussion of the observed colours, suggesting that this binary came to the Milky Way from a satellite like the Carina dSph. This result was challenged by Spite et al. (2000) who derived a lower T_{eff} from the Hα profile. Interestingly, however, they also found low [α/Fe] $\sim$0 and did not detect lithium—results expected for a BSS accreted from a dSph (see Fig. 4.10 and the discussion in Sect. 4.6.2)

To summarise: the orbital characteristics of the FBS binaries are distinctly different from the ordinary binaries of their parent populations with regard to mass functions, orbital periods, orbital eccentricities, and incidence of detectable secondaries. FBS binaries are a species *sui generis*.

4.4 Galactic Distribution

4.4.1 Smooth Halo Field

SDSS-based studies have identified thousands of FBSSs widely dispersed over the distant halo (see Figs. 4.4 and 4.10). These FBSSs have been identified primarily for the purpose of isolating pure BHB samples; they have not been used, to my knowledge, in investigations of halo structure. The compilation of BSSs in GC by Sarajedini (1993) displayed in Fig. 4.17 allows estimation of their utility for such purposes.

For simplicity of presentation I did not use the much busier update of this diagram in Cohen and Sarajedini (2012). Supposing that the ranges of age and chemical composition in the GC sample are similar to those encountered in the halo, I estimate from inspection of Fig. 4.17 that the standard deviation of M_V for FBSSs on $0.0 < (B-V)_o < 0.4$ is $\sigma < 0.5$ mag., which translates to 25 % errors in distances to individual stars. The range of galacto-centric distances over which SDSS FBS data could be used to calculate space densities is $\sim$20 kpc, so my gloss on the situation is that FBSSs may be useful for investigations of space density on such length scales. How useful they might be would require more careful error analysis. Nevertheless, FBS have not been entirely discounted for such purposes. Univane et al. (1996) used star counts blue-ward of the classical halo turnoff at $B-V \sim 0.4$ to estimate that $\sim$10 % of the halo could be attributed to accretion of intermediate-age satellites.

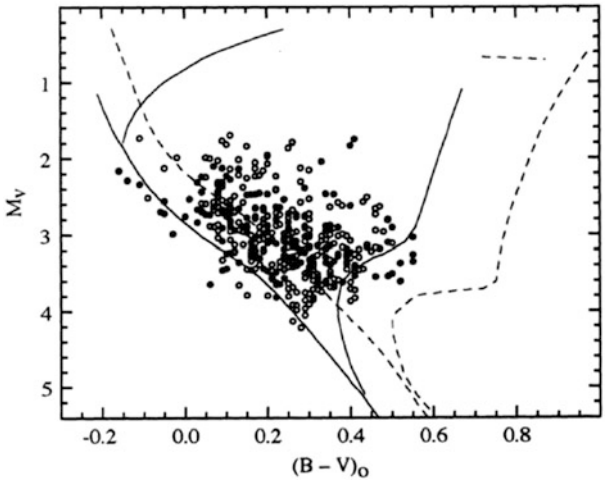

Fig. 4.17 A composite colour-magnitude diagram from GC BSSs taken from Sarajedini (1993). This figure is reproduced with permission of the Publications of the Astronomical Society of the Pacific

4.4.2 The Galactic Bulge

Recently Clarkson et al. (2011) reported the discovery of BSSs in the Galactic Bulge. They identify BSSs produced by mergers of W UMa stars that follow the path of AW UMa (Paczynski et al. 2007) to FK Com (Bopp and Stencel 1981). They use these BSSs to place a conservative upper limit on the percentage of genuinely young stars in their sample. Such young stars have interesting consequences for the history of the Bulge. The strong resemblance of the Bulge observational material to that of Mateo et al. (1990) for the GC NGC 5466, indicated by the side-by-side CMDs of NGC 5466 and the Bulge sample in Fig. 4.18, invites a common explanation for at least a portion of the bulge BSSs.

The ratios of variable to constant BSSs in the two CMDs, $5/30 = 0.167$ and $3/29 = 0.103$, are statistically indistinguishable. From admittedly shaky estimates of BS and W UMa lifetimes, Mateo et al. (1990) concluded that all of the BSSs in NGC 5466 can be understood as mergers of W UMa stars. This conclusion, coupled with the great preponderance of long-period binaries in the distribution of Duquennoy and Mayor (1991), provides a convenient rationale for the disparate specific frequencies of BSSs in GCs and the halo field.

Clarkson et al. (2011), working with a much more complicated dataset, cautiously reach a suitably more modest conclusion, namely, that the Bulge BS population with $P < 10$ days comprises at *most half* of all bulge BS binaries. This is more or less consistent with their specific frequency for Bulge BSSs, $\sim$1.23, which is markedly smaller than that of the halo field. If (almost) all the remainder are BSS

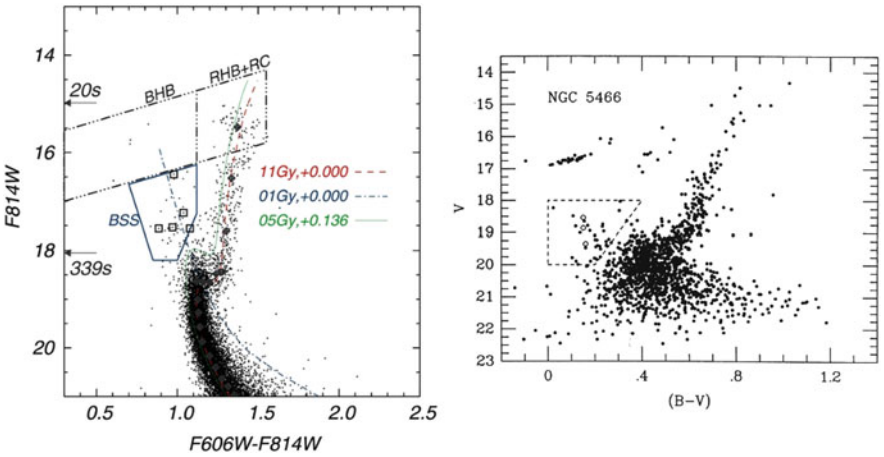

Fig. 4.18 (*Left panel*) Colour-magnitude diagram of the Galactic Bulge sample of Clarkson et al. (2011). W UMa stars in the field are denoted by *boxes*; (*right panel*) colour-magnitude diagram of the GC NGC 5466 studied by Mateo et al. (1990). W UMa stars are indicated by *open circles*. These figures are reproduced with permission from the AAS

binaries of longer period, an expectation based on halo experience, they arrive at an upper limit of $\sim$3 % for the young (<5 Gyr) population of the bulge. Bensby et al. (2012) argue for the existence of an intermediate-age population based on spectral analysis of Bulge dwarfs observed during microlensing events. The age distribution of stars in the Bulge has arisen once again, like the Phoenix, as a new direction for research.

4.4.3 Halo Streams

Morrison et al. (2000) included BMP stars in their list of tracers to investigate structure in the halo produced by satellite accretion, but I could find no subsequent results based on their use. Newberg et al. (2009) identified a new polar-orbit stream (*Cetus Polar Stream*) spatially coincident with the Sagittarius trailing tidal trail, but with systematically lower metallicity ([Fe/H] $= -2.1$), in which the specific frequency of BSSs differs from that in Sagittarius. More recently Koposov et al. (2011) claim that the BSSs belong mainly to Sagittarius and the BHB belong mainly to the Cetus stream. This conclusion requires gross, unlikely differences in specific frequencies of the two streams. Streams in the halo is a fascinating but difficult subject in its infancy, so interpretation of results best awaits further investigation

4.5 Metal-Rich A-Type Stars Above the Galactic Plane: Another Inconvenient Truth

No review of FBSSs would be complete without a digression to the metal-rich A-type stars far above the Galactic plane. The existence of such stars was first recognised by Perry (1969) who sought to determine the force law perpendicular to the Galactic plane by use of early A-type main sequence stars near the north Galactic pole, for which accurate distances could be derived from suitably calibrated Strömgren photometry. Perry (1969) constructed a density distribution perpendicular to the plane, shown in the left panel of Fig. 4.19, that produced an unbelievable force law.

He was obliged to consider that the A-type stars more than 400 pc above the plane were a mixture of two populations. This result prompted Rodgers (1971) to investigate the A-type stars at the south Galactic pole (SGP) identified by Philip and Sanduleak (1968). He identified 21 stars on $-0.04 < (B-V)_o < 0.32$ with "normal" abundances of calcium and thought of no satisfactory explanation. A decade later Rodgers et al. (1983) confirmed Rodgers (1971) first abundances, used their radial velocities and a believable force law (Oort 1960; Innanen 1966) to calculate Z_{max} values that range from 1.5 to 8 kpc. They hypothesised that these stars were formed during a recent ($<10^9$ years ago) collision with a gas-rich satellite galaxy.

Lance (1988a,b) investigated this speculation anew by compiling a catalogue of 305 early type stars brighter than $V = 15$ in 218 deg^2 at the SGP. From Strömgren photometry and the *byK* equivalent of Pier's (1983) *BVK* diagram she identified 29 Population I A-type stars which lie in $1 < z(kpc) < 11$ and $-0.6 <$ [Ca/H] < 0.2, and have radial velocity dispersion $\sigma = 62\,\mathrm{km\,s^{-1}}$. The density distribution of her stars at the SGP shown in the right panel of Fig. 4.19 bear the same two-slope signature of Perry's distribution in the left panel. The locations of these 29 stars in

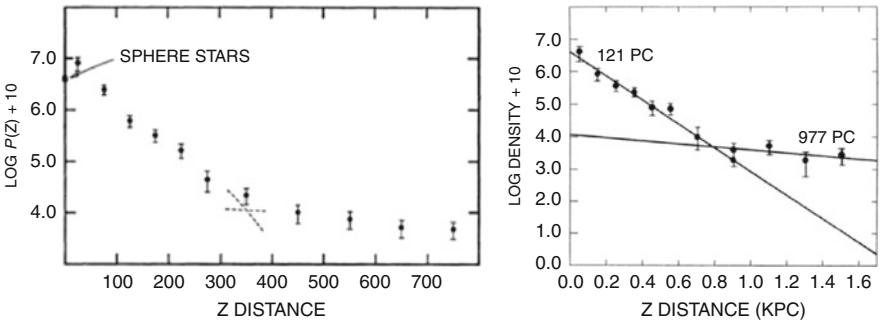

Fig. 4.19 Space densities of early A-type stars near the North and South Galactic Poles versus distance from the Galactic plane according to: *left panel*, Perry (1969); *right panel*, Lance (1988b). The figures are reproduced with permission from the AAS

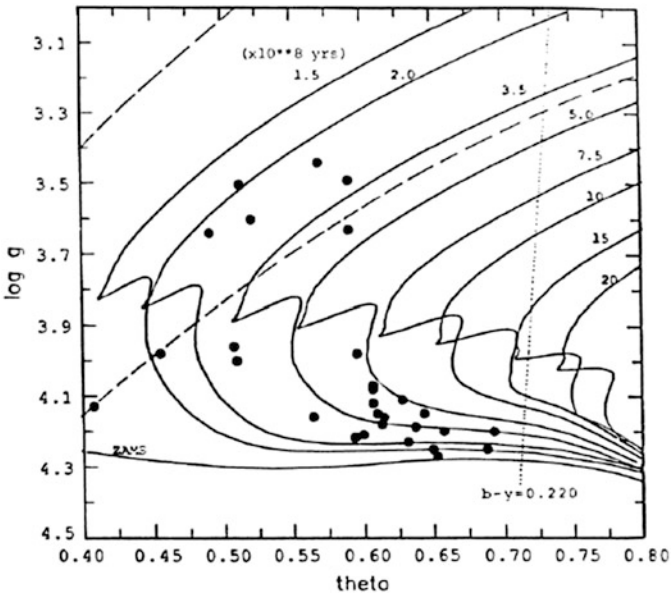

Fig. 4.20 Locations of early A-type stars among RYI isochrones, according to Lance (1988b). This figure is reproduced with permission from the AAS

the grid of revised Yale Isochrones (Green et al. 1987) translated to the (log g, Θ) plane ($\Theta = 5040/T_{eff}$) and displayed in Fig. 4.20 indicate ages less than 0.6 Gyr.

After considering various alternatives, Lance arrived at the earlier conclusion of Rodgers et al. (1983): about 0.6 Gyr ago a slightly metal-poor, but still gas-rich, satellite merged with the disc of the Galaxy. During the collision stars formed "*that do not partake of the usual age-abundance-kinematics relationships shown by other Galactic stellar groupings*" (Lance *verbatim*).

So far as I am aware, Lance's work has never been refuted. Rather, it simply has been ignored because, I suspect, her results do not conform to current dogma about Milky Way satellite encounters. According to ADS her paper (Lance 1988b) has received a total of 56 citations in 24 years, the last being 5 years ago in 2007. In contemporary vernacular, the astronomical community "*never lets facts stand in the way of a good idea*".

4.6 Abundance Issues

Three abundance topics are of particular importance for FBSSs: (a) Li (and Be) as diagnostics of deep mixing in FBSSs and in the RGB/AGB antecedents of their present white dwarf companions (b) the α-elements as possible discriminants for

satellite accretion, and (c) neutron-capture elements as constraints on AGB models, thermohaline convection, and dilution.

4.6.1 Lithium

Lithium deficiencies in blue stragglers of various ilks relative to those of the Spite plateau (Spite and Spite 1982) have been recognised for two decades (Pritchet and Glaspey 1991; Hobbs and Mathieu 1991; Glaspey et al. 1994; Carney et al. 2005). More recently Boesgaard (2007) have added Be deficiencies to the problem. Because ^{7}Li is burned to ^{4}He ash at temperatures greater than $\sim 2 \times 10^{6}$ K, Li deficits are widely believed to be consequences of mixing processes that are plausible consequences of collision, merger, or mass transfer from a cool giant. These mixers are by no means the only possibilities. Pinsonneault et al. (1999, 2002) consider rotation-driven circulation, while Ryan et al. (2002) discuss rotation produced by angular momentum transfer during binary mass transfer. They suggest that such transfer could produce the rapid axial rotations (sic!), $v \sin i$ values of 8.3, 7.6, and 5.5 km s^{-1}, of three Li-deficient stars below the MSTO. This suggestion can be reframed as an hypothesis amenable to observational test. Finally, in consideration of the "Lithium Dip" in young stellar populations (Boesgaard and Tripico 1986), it was, perhaps, inevitable that radiative levitation, gravitational settling (Michaud and Charbonneau 1991), and associated mass-loss (Dearborn and Schramm 1997) would be investigated.

The link between blue stragglers and the small fraction of Li-deficient stars below the MSTO, required by observation (Mandushev et al. 1997), is a natural consequence of power-law mass spectra adopted for the initial primaries and secondaries of primordial binaries used in the toy model of PS00. This link was also noted by Ryan et al. (2001, 2002). Worry by Ryan et al. (2001, 2002) that some Li deficient MS stars are not known binaries will only become a real problem after these stars have been subjected to the same careful long-timescale scrutiny accorded the disc (Duquennoy and Mayor 1991), halo (Latham et al. 2002), and BMP (PS00) samples. Norris et al. (1997) note that Li deficiency is not always accompanied by AGB carbon and s-process enrichments. For some unstated reason they do not consider the rational possibility that mass transfer from ordinary RGB companions will deplete Li without affecting other [X/Fe].

Most recently Masseron et al. (2012) have made an extensive investigation of Li in CEMP-s stars. Among the several important issues addressed in their paper is the unequivocal demonstration, provided by CS 22949-008, that mass transfer binaries populate the main sequence well below the MSTO. Equally interesting, they present a detailed discussion of the role of dilution, as parameterised by Gallino and his colleagues (Bisterzo et al. 2012) and modified by thermohaline mixing (Vauclair 2004), in creating the dispersion of Li abundance in the Spite plateau. Detailed discussion of their results is beyond the scope of this review; I only note that they (Masseron et al. 2012) provide yet another empirical argument for the notion that

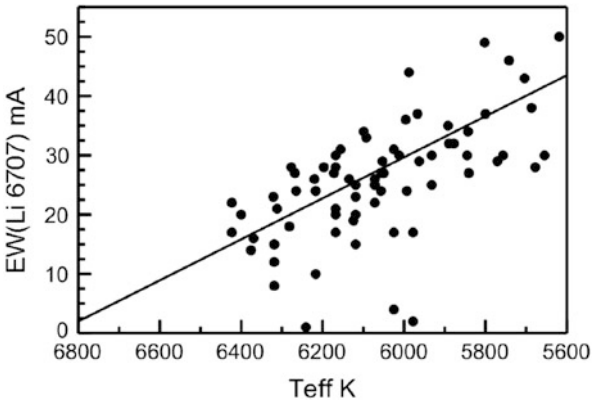

Fig. 4.21 A plot of equivalent width of Li I (6,707 Å) versus effective temperature for the main sequence stars studied by Thorburn (1994)

FBSSs represent an extension of the family of mass transfer binaries to locations above (hotter than) the MSTO. Finally, Glebbeek et al. (2010) calculated surface abundances of blue straggler models and comment that it may be possible to use Li as a tracer to distinguish between formation by mass transfer and formation by collision.

One caution about detection of Li in FBSSs should be mentioned. Due to increasing ionisation of Li I (ionisation potential= 5.4eV) the strength of Li I 6707Å decreases steadily at temperatures above MSTO values, as shown in Fig. 4.21, a plot of equivalent width of Li I 6707Å versus T_{eff} along the Spite plateau made from data in Table 2 of Thorburn (1994). Linear extrapolation into the FBS region by use of the line drawn through the data in Fig. 4.21 indicates that equivalent widths for normal Spite-plateau abundances fall below 10 mÅ at $T_{eff} > 6{,}500$ K. Considering that most of the FBSSs found in the HK and HES surveys are fainter than $V = 14$, detection of Li with the requisite resolution ($R > 25{,}000$) and signal-to-noise ratio (S/N> 50) in most FBSSs can only be accomplished with large telescopes.

4.6.2 Alpha/Fe

The relatively lower values of [α/Fe] found for red giants in Milky Way satellite galaxies (see Fig. 4.10 in Sect. 4.2 above) suggests the possibility that [α/Fe] might serve as a discriminant with which to distinguish FBSSs accreted from Milky Way satellites from FBSSs home-grown in the halo. The data for FBSSs, summarised in Table 4.1, indicate that this might be so. I sorted the data in Table 7 of PS00 first into two groups by metal abundance at [Fe/H]= -1 and then into binary and constant velocity groups within each abundance group. I calculated average values of [α/Fe] for these four groups, first treating Mg and Ca as the α-elements in column 4 of Table 4.1, and then including Ti, frequently treated as an α-element, in column 6.

Table 4.1 [α/Fe] behavior among FBSSs

			$< [MgCa/Fe] >$	$< [MgCa/Fe] >$	$< [MgCaTi/Fe] >$	$< [MgCaTi/Fe] >$	
Population	[Fe/H]	[Fe/H]	Avg.	SD (avg)	Avg.	SD (mean)	n
SB	< -1	-1.69	0.42	0.03	0.44	0.03	23
RVC	< -1	-1.94	0.27	0.03	0.30	0.03	13
Difference			0.15	0.14			
SB	> -1	-0.45	0.24	0.07	0.25	0.06	12
RVC	> -1	-0.48	0.22	0.04	0.27	0.06	4
Difference			0.02		-0.02		

The two cases are indistinguishable. The last column of Table 4.1 contains the number of stars in each group. For the FBS stars with [Fe/H] < -1 the average [α/Fe] is lower among the constant-velocity stars by 0.15 dex. The differences in columns 4 and 6 exceed the sums of the standard deviations of the means and are comparable to the amounts by which red giants of satellite galaxies lie below Galactic stars in Fig. 4.11. The differences found for the samples with disc metallicity are insignificant. The abundances were derived from spectra of low-to moderate S/N for modest numbers of stars, so these results should be regarded as tentative. They are presented here as incentive for a definitive investigation.

Finally, we only mention that Ivans (2003), on the basis of three stars, promote the existence of yet another population of metal-poor stars ([Fe/H] ~ -2) in the Galactic halo. They are characterised by unusually low abundances of the α-elements Mg, Si, and Ca and the neutron-capture elements Sr, Y, and Ba, and other peculiarities in abundances of the Fe-peak group. One of the three stars, CS 22966-043, that define this putative new population is a pulsating binary blue straggler (Preston and Landolt 1999).

4.6.3 The Neutron-Capture Elements

Bisterzo et al. (2012) have interpreted the abundances of 94 s-process enriched metal-poor C-stars, the CEMP-s stars, by comparison with appropriate AGB models. I confine my discussion below to 4 FBSSs among the 27 MS stars in their sample. To interpret the observed abundances of any CEMP-s star the following parameters must be specified: (a) chemical abundances, [X/Fe], in the envelopes, hence ejecta, of various AGB models, (b) a set of standard abundances for the companion star, (c) the mass of ejecta captured by the companion, and (d) the envelope mass of the receiving star into which AGB ejecta are mixed.

If mixing were confined to the diminutive convective envelope, 0.001 $M/M_{\odot}$, of a typical FBSS with $T_{eff} \sim 6{,}400$ K (Pinsonneault et al. 2001), the wind accretion of Boffin and Jorissen (1988) would be more than adequate. However, Stancliffe et al. (2007) complicated the discussion by noticing that the enhanced molecular weight of overlying He- and C-enriched AGB accreta will induce thermohaline mixing

Table 4.2 FBSSs for which minimum accreted masses can be estimated

				Star	TO	Star-TO	
Star	[Fe/H]	T_{eff}	log g	$(B-V)_0$	$(B-V)_0$	$d(B-V)_0$	$min\ M/M_\odot$
CS 22887-048	−1.70	6,500	3.35	0.353	0.408	−0.055	0.09
CS 29497-030	−2.57	7,000	4.10	0.296	0.364	−0.068	0.11
CS 29526-110	−2.06	6,800	4.10	0.322	0.386	−0.064	0.11
CS 29528-028	−2.86	6,800	4.00	0.322	0.355	−0.033	0.06

throughout ∼90 % of the mass of a typical MS star. In a rejoinder Thompson et al. (2008) argue that helium and the heavy elements settle in the surface layers of the receiver during the main-sequence lifetime (∼3 Gyr) of a typical (1.3 $M_\odot$) AGB star employed by Bisterzo et al. (2012), thus creating a stabilising μ-gradient that confines thermohaline mixing to a thin surface layer until the stabilising μ-gradient is flattened by sufficient accretion of high-μ matter. The various issues of mixing associated with CEMP-s stars are reviewed by Stancliffe et al. (2010).

Bisterzo et al. (2012) combine items (c) and (d) above into their dilution parameter, $dil = \log M_{CE}/M_{AGBacc}$, the $\log_{10}$ of the ratio of mass of the convective envelope of the receiver to the mass of AGB accreta. They then try various combinations of AGB compositions and dilution factors to achieve the best agreement between observed and predicted abundances for each star. Details of the AGB models and element-by-element model-fitting procedures are beyond my competence. I restrict my discussion to aspects of their work pertinent to the FBSSs.

Physical data for the four FBSSs studied by Bisterzo et al. (2012) are presented in Table 4.2. Column 6 contains $(B-V)_o$ values of the MSTO inferred from Y^2 isochrones for age = 13.5 Gyr and the individual stellar [Fe/H] values in column 2 by use of the curve in Fig. 4.13. Column 7 contains the amount by which each star lies blueward of its MSTO. Finally, column 8 contains the minimum accreted stellar mass inferred from the Y^2 isochrones.

They are minimum masses because there is no way to know the initial masses. These minimum masses can easily be provided by the wind accretion calculations of Boffin and Jorissen (1988), and they are more than sufficient to completely fill the surface convection zones of these stars, but they require dilution parameters of order unity if the AGB material has been mixed into ∼0.7 $M/M_\odot$ of receiver envelope. I include these calculations merely to indicate that the means are at hand to place additional observational constraints on the AGB models used to explain CEMP-s stars.

4.6.4 How Many Evolved Mass-Transfer Binaries Are There?

This topic was belabored by me earlier (Preston 2009). To estimate the amount of mass transferred requires a theory of accretion. Boffin and Jorissen (1988), in a limited exploration of their parameter space, concluded that accretion in an AGB wind could produce a Ba star like classic ζ Capricorni (Böhm-Vitense

1980). Subsequently, Han et al. (1995) and Theuns et al. (1996) concurred that accretion from an AGB wind might produce Ba star and CH star companions in binaries with periods up to 100,000 days or more, a range that extends beyond the frequency maximum, near P = 50,000 days, for F- and G-type dwarfs in the solar neighbourhood (Duquennoy and Mayor 1991). On the other hand, Boffin and Zaćs (1994) observed that overabundances of s-process elements decline systematically with increasing orbital period (separation), as they must, in a recognisable albeit imperfect correlation. Their results are in qualitative agreement with those of Jorissen et al. (2000) who found a steep drop in numbers of Ba star spectroscopic binaries with P > 3,000 days, the number falling to zero at 10,000 days. Failure to find such binaries is not a radial-velocity precision problem, but it may be an observer persistence problem. The K_1 value of a 0.8 $M_\odot$ star in a 10,000 days orbit with a 0.5 $M_\odot$ white dwarf companion is 4 km s^{-1}, easily detectable by all modern high-resolution spectrographs, if someone has the patience to monitor radial velocities on a 30-year timescale. My gloss on all of this is that any census of CEMP-s stars is conditioned by observer persistence and the sensitivity of survey detection criteria. Thresholds for detection skew the observed orbital period (size) distribution toward lower values and such bias acts to produce a discrepancy between the period distributions of Jorissen et al. (2000) and Duquennoy and Mayor (1991).

4.7 Pulsating Blue Stragglers

SX Phe stars are metal-poor pulsating blue stragglers found in GCs and the halo field. See Cohen and Sarajedini (2012) and references contained therein. The issues of SX Phe stars are complex and multifarious. I confine my attention here to only two of them.

4.7.1 Non-variable Stars in the SX Phe Instability Strip

PS00 found one large-amplitude SX Phe star and two probable low-amplitude versions (Preston and Landolt 1998, 1999) among 40 BMP binaries. They noted that other low-amplitude pulsators might contribute to the radial velocity residuals of some of their binary orbits, but it is clear from examination of velocity residuals in Fig. 7 of PS00 that velocity amplitudes of putative pulsators in many of these binaries would have to be near or below the 1 km s^{-1} level. *High-amplitude pulsators like SX Phe are a distinct minority among FBS spectroscopic binaries.*

Kepler data for the δ Scuti stars, Population I analogues of SX Phe stars, discussed by Balona and Dziembowski (2011), pre-empt all previous photometric inquires into this topic. In spite of exquisite photometric precision that permits detection of very low-amplitude (<100 ppm) variables, they find that the δ Scuti fraction of stars in the instability strip barely reaches *0.5 only in the narrow*

temperature interval 7,500 < T_{eff} (K)< 8,000, and falls to very low levels below 7,000 and above 8,500 K. *The great majority of FBSSs in the δ Sct instability strip are non-variable even by stringent Kepler standards*, a circumstance contrary to all previous experience with the instability strips of the RR Lyrae stars and classical Cepheids. This concentration to a narrow interval of T_{eff}, less than 300 K, is borne out approximately by the locations of high amplitude δ Scuti and SX Phe stars in the (M_V, T_{eff}) plane of McNamara (1997) reproduced here in the left panel of Fig. 4.22.

McNamara's narrow *High Amplitude Delta Scuti* (HADS) strip, identified by the letter "M" in the right panel of Fig. 4.22, cannot be predicted theoretically according to Petersen and Christensen-Dalsgaard (1999). Furthermore, stability analysis (Pamyatnikh 2000) does not explain the paucity of SX Phe stars within the much broader temperature boundaries (thick solid lines in the right panel of Fig. 4.22).

SX Phe stars identified in the Fornax dSph galaxy (Poretti et al. 2008) are not confined to the HADS strip of Fig. 4.22, but the stars are faint and photometric errors blur this conclusion. As in the *Kepler* field the SX Phe stars comprise only a small fraction of the total BS population of Fornax. Balona and Dziembowski (2011) suggest that unspecified damping mechanisms operate to suppress pulsation in many BSSs. According to them, "*Perhaps we need to wait for the development of*

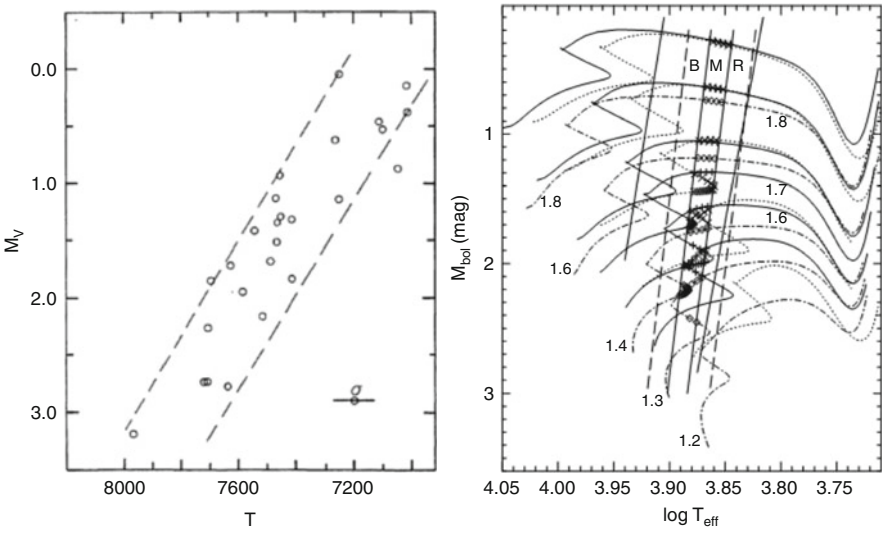

Fig. 4.22 (*Left panel*) The instability strip for δ Scuti and SX Phe stars from McNamara (1997). This figure is reproduced with permission of Publications of the Astronomical Society of the Pacific; (*right panel*) McNamara's empirical strip, indicated by "M", in the theoretical instability strip marked by *heavy solid lines*, according to Petersen and Christensen-Dalsgaard (1999). This figure is reproduced with permission of Astronomy & Astrophysics

non-linear, non-radial calculations to properly address this problem." Explanations for many SX Phe phenomena are still in disarray.

4.7.2 RRLYR-02792, Archetype of a New Kind of Mass-Transfer Pulsator

Pietrzyński et al. (2012) describe a new kind of pulsating star found in an OGLE eclipsing binary, RRLYR-02792 (Soszyński et al. 2011). Its light and radial velocity variations resemble, approximately, those of an RRb star with period $P = 0.627$ days, but its dynamical mass, 0.26 $M_\odot$, is incompatible with a location on the horizontal branch. Pietrzyński et al. (2012) believe that they have caught an Algol-type binary in a short-lived evolutionary phase following mass exchange, in which the pulsator possesses a partially degenerate helium core and a small H-shell-burning envelope. The pulsator is now shrinking as it evolves toward the hot subdwarf region at a rate compatible with the decline of its pulsation period, 8.4–2.6×10^{-6} days year^{-1}. Wonders never cease.

4.8 Odds and Ends

4.8.1 Mass Transfer in Hierarchical Triples

Approximately half of the short-period ($P < 30$ days) binaries in the solar neighbourhood reside in multiple systems (Tokovinin et al. 2006), so we expect to find them among main sequence CEMP-s stars, whether above or below the MSTO, if the statistical properties of disc and halo binary populations are similar. Apparent confirmation of such expectation is provided by CS 22964-161 (Thompson et al. 2008) and CS 22949-008 (Masseron et al. 2012), double-lined binaries in which both components are carbon and s-process enriched. Both components of CS 22964-161 have subgiant characteristics in contrast to CS 22949-008, in which both components lie well below the MSTO. In both cases the AGB donor must have been the remote third star of an hierarchical triple. This circumstance puts a lower limit on the semi-major axis of the AGB orbit, hence upper limits on the density of the AGB wind at the close binary and on the accretion of AGB gas by that binary system.

Soker (2004) initiated inquiry into the very case of interest here, wind accretion by the close binary companions of a remote AGB in an hierarchical triple system. The problem is extremely complex, requiring specification of the inclination angle of orbital planes and treatment anew of Bondi and Hoyle (1944) accretion in an AGB wind, including assumptions about cooling times and angular momentum transfer in the accretion column. With regard to the latter Davies and Pringle (1980) called attention to a conceptual problem for angular momentum transfer in an inhomogeneous medium that was not resolved in subsequent investigations by

Livio et al. (1986a,b). Accretion rates for the two binary components may differ, in which case they will possess different surface enrichments by the AGB accreta. Investigation of accretion in hierarchical triples adds a new dimension to McCrea's initial ideas.

4.8.2 Heresy

I conclude my review of issues that attend FBS and mass transfer, by brief enumeration of a few mildly disquieting observational facts.

Lithium again. After building a case for AGB enrichment of the surface layers of CS 22964-161, enrichment in gas that has endured deep mixing in cool giant atmosphere, Thompson et al. (2008) were obliged to appeal to some process by which lithium is produced in the AGB star prior to mass transfer, and by just the right amount that elevates it to the Spite plateau. Extraordinary coincidence, one may suppose. The process must be a bit less than extraordinary, because it must also account for the detection of appreciable lithium in two additional relatively bright (nearby) MS CEMP-s stars, CS 22898-027 (Thorburn and Beers 1992) and LP 706-7 (Norris et al. 1997).

The three aforementioned stars share another property illustrated in Fig. 4.23: extant observations provide no clear evidence for orbital motion. The results for

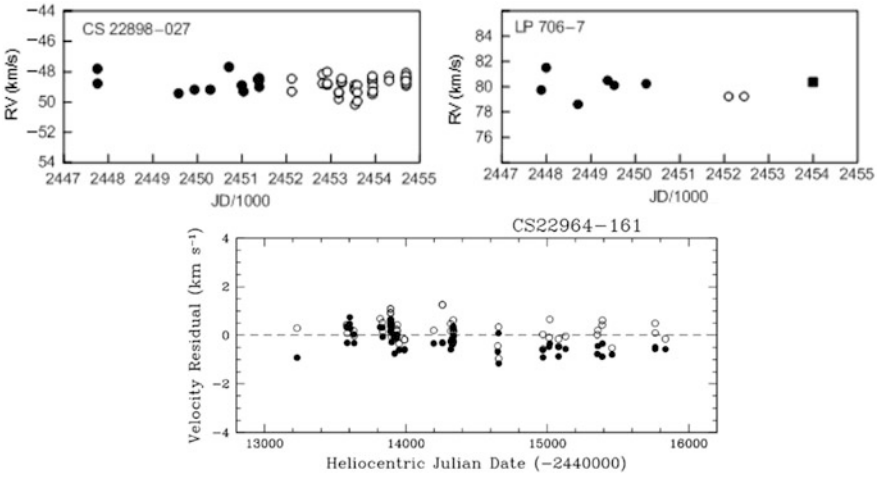

Fig. 4.23 (*Top left*) Radial velocity versus Julian Date for MS CEMP-s star CS 22898-027; (*top right*) radial; velocity versus Julian Date for the MS CEMP star LP 706-7. The figures are reproduced with permission of Publications of the Astronomical Society of Australia; (*bottom*) residuals of individual radial velocity observations of the primary (*solid circles*) and secondary (*open circles*) components of the SB2 CEMP-s system CS 22964-161 (Ian Thompson, private communication)

CS 22898-027 and LP 706-7 are taken from Preston (2009); those for CD 22964-161 are velocity residuals with respect to predictions of the binary orbit under continuing investigation by Ian Thompson (private communication). The centre of mass velocity ought to vary sooner or later, if the third AGB relic is present.

CS 22880-074 (Preston 2009) and TY Gru (Preston 2011) are additional examples of apparently misbehaving CEMP-s stars. I leave it to the reader to consider whether the radial velocity behaviours of these stars (never mind Li!) are all statistical flukes, chance consequences of small orbital inclinations, or are they warning signals about the universal AGB paradigm for production of s-process elements.

References

Balona, L. A. Dziembowski, W. A.: MNRAS **417**, 591 (2011)
Beccari, G., et al.: MmSAI, **80**, 107 (2009)
Beers, T. C., Prestoln, G. W., Shectman, S. A.: ApJS **67**, 461 (1988)
Beers, T. C., Preston, G. W., Shectman, S. A.: AJ **103**, 1987 (1992)
Beers, T. C., et. al.: ApJS **103**, 433 (1996)
Bensby, T., Feltzing, S., Gould, A., et al.: in Galactic Archaeology: Near-Field Cosmology and the Formation of the Milky Way, ASPC Vol. 458, p. 203 (2012)
Bisterzo, S., Gallino, R., Straniero, O., Cristallo, S., Käppeler, F.: MNRAS **422**, 849 (2012)
Boesgaard, A. M., Tripico, M. J.: ApJ **302**, L49 (1986)
Boesgaard, A. M.: ApJ **667**, 1196 (2007)
Boffin, H. M. J., Jorissen, A.: A&A **205**, 155 (1988)
Boffin, H. M. J., Zaćs, L.: A&A **291**, 811 (1994)
Böhm-Vitense, E.: ApJL, **239**, 79 (1980)
Bolte, M., Hesser, J. E., Stetson, P. B.: ApJL **408**, 89 (1993)
Bondi, H, Hoyle, F.: MNRAS **104**, 273 (1944)
Bopp, B. W., Stencel, R. E.: ApJL **247**, 131 (1981)
Bragaglia, A., et al.: in IAUS **228**, p. 243 (2005)
Brown, W. R. et al.: AJ **130**, 1097 (2005)
Buser, R., Kurucz, R. L.: A&A **70**, 555 (1978)
Buzzoni, A., et al.: A&A **128**, 94 (1983)
Carney et al.: AJ **107**, 2240 (1994)
Carney, B. W., et al.: AJ **122**, 3419 (2001)
Carney, B. W., Latham, D. W., Laird, J. B.: AJ **129**, 466 (2005)
Carretta, E., Bragaglia, A., Gratton, R., Lucatello, S.: A&A **505**, 139 (2009)
Chen, X., Han, Z.: in IAUS **266**, p. 333 (2009)
Clarkson, W. I., et al.: ApJ **735**, 37 (2011)
Clewley, L., et al.: MNRAS **337**, 87 (2002)
Cohen, R. E., Sarajedini, A.: MNRAS **419**, 342 (2012)
Côté, P., et al.: AJ **112**, 574 (1996)
Davies, R. E., Pringle, J. E.: MNRAS **191**, 599 (1980)
Dearborn, D. S. P., Schramm, D. N.: Proc. Nat. Acad. Sci.**94**, 4836 (1997)
De Marchi, F.: A&A **459**, 489 (2006)
Duquennoy, A., Mayor, M.: A&A **248**, 485 (1991)
Eggen, O. J., Lynden-Bell, D., Sandage, A. R.: ApJ **136**, 748 (1962)
Eggleton, P. P.: MNRAS **163**, 279 (1973)
Flynn, C., Sommer-Larsen, J., Christensen, P. R.: MNRAS **267**, 77 (1994)

Fuhrmann, K., Bernkopf: A&A **347**, 897 (1999)
Fuhrmann, K., et al.: MNRAS **416**, 391 (2011)
Geisler, D., et al.: AJ **129**, 1428 (2005)
Glaspey, J. W., Pritchet, C. J., Stetson, P. B.: AJ **108**, 271 (1994)
Glebbeek, E., et al.: in AIP Conf. Proc. 1314, p. 113 (2010)
Gnedin, O. Y., Ostriker, J. P. 1997: ApJ **474**, 223
Green, E. M., Demarque, P., King, C.: Revised Yale Isochrones and Luminosity Functions, Yale U. Press (1987)
Han, Z., et al.: MNRAS **277**, 1443 (1995)
Hesser, J. E., Hartwick, F. D. A., McClure, R. D.: ApJS **33**, 471 (1977)
Hilditch, R. W.: An Introduction to Close Binary Stars, Cambridge Univ. Press (2001)
Hobbs, L. M., Mathieu, R. D.: PASP **103**, 431 (1991)
Horton, A. J., Bate, M. R., Bonnell, I. A.: MNRAS **321**, 585 (2001)
Innanen, K.: ApJ **143**, 153 (1966)
Ivans, I. I.: ApJ 592, 906 (2003)
Jorissen, A., van Eck, S., MmSAI **71**, 645 (2000)
King, I.: AJ **71**, 64 (1966)
Kinman, T. D., Suntzeff, N. B., Kraft, R. P.: AJ **108**, 1722 (1994)
Kippenhahn, R,, Weigert, A.: Z. Astrophys. **65**, 251 (1967)
Kopal, Z.: Ann. Astrophys.**18**, 379 (1955)
Koposov, S. E., Gilmore, G., Walker, M. G., et al.: ApJ **736**, 146 (2011)
Kuiper, G. P.: ApJ **93**, 133 (1941)
Lance, C. M.: ApJS **68**, 463 (1988a)
Lance, C. M.: ApJ **334**, 927 (1988b)
Latham, D. W., et al.: AJ **124**, 1144 (2002)
Lee, Y.-W., Demarque, P.: ApJS **73**, 709 (1990)
Leonard, P. J. T.: AJ **98**, 217 (1989)
Livio, M., et al.: MNRAS **218**, 593 (1986a)
Livio, M., et al.: MNRAS **222**, 235 (1986b)
Manduca, A., Bell, R. A.: ApJ **225**, 908 (1978)
Mandushev, G. I. et al.: AJ **114**, 1060 (1997)
Marino, A. F., et al.: A&A **505**, 1099 (2009)
Marino, A. F., et al.: ApJ **746**, 14 (2012)
Masseron, T., Johnson, J. A., Lucatello, S., et al.: ApJ **751**, 14 (2012)
Mateo, M., et al.: AJ **100**, 469 (1990)
Mayor, M., Duquennoy, A., Udry, S.: in ASPC Vol. 90, p. 190 (1996)
McClure, R. D., Woodsworth, A. W.: ApJ **352**, 709 (1990)
McClure, R. D.: PASP**109**, 536 (1997)
McCrea, W. H.: MNRAS **128**, 147 (1964)
McNamara, D. H.: PASP **109**, 1221 (1997)
Melbourne, W. L.: ApJ **132**, 101 (1960)
Michaud, G, Charbonneau, P.: Sp. Sci. Rev. **57**, 1 (1991)
Monelli, M., et al.: MmSAI **75**, 114 (2004)
Morrison, H., et al.: AJ **119**, 2254 (2000)
Newberg, H. J., Yanny, B., Willet, B. A.: ApJ **700**, L61 (2009)
Norris, J., Freeman, K. C.: ApJ **266**, 130 (1983)
Norris, J. E., Ryan, S. G., Beers, T. C., Deliyannis, C. P.: ApJ **485**, 370 (1997)
Olsen, E. H.: A&AS **37**, 367 (1979)
Olsen, E. H.: A&AS **39**, 205 (1980)
Oort, J.: Bull. Astron. Inst, Neth. **15**, 45 (1960)
Paczynski, B.: in On the evolution of double stars, Obs. Royal Belgique, Communications, Serie B, No. 17, p. 122 (1967)
Paczynski, B. Sienkiewicz, Szczyiel, D. M.: MNRAS **378**, 961 (2007)
Pamyatnikh, A. A.: in ASPC Vol. 210, p. 215 (2000)

Perry, C. L.: AJ **74**, 139 (1969)
Petersen, J. O., Christensen-Dalsgaard, J.: A&A **352**, 547 (1999)
Philip, A. G. D., Sanduleak, N.: Bol. Obs. Tonanzintla y Tacubaya **4**, 253 (1968)
Pier, J. R.: ApJS **53**, 791 (1983)
Pietrzyński, G., Thompson, I. B., Gieren, W., et al.: Nature **484**, 75 (2012)
Pinsonneault, M. H., et al.: ApJ **527**, 180 (1999)
Pinsonneault, M. H., DePoy, D. L., Coffee, M.: ApJ **556**, L59 (2001)
Pinsonneault, M. H., et al.: ApJ **574**, 398 (2002)
Piotto, G., et al.: ApJ **604**, L109 (2004)
Poretti, E., et al.: ApJ **685**, 947 (2008)
Preston, G. W., Shectman, S. A., Beers, T. C.: ApJS **76**, 1001 (1991)
Preston, G. W.: AJ **108**, 2267 (1994a)
Preston, G. W., Beers, T. C., Shectman, S. A.: AJ **108**, 538 (1994b)
Preston, G. W., Landolt, A. U.: AJ **115**, 2515 (1998)
Preston, G. W., Landolt, A. U.: AJ **118**, 3006 (1999)
Preston, G. W., Sneden, C.: AJ **120**, 1014 (2000; PS00)
Preston, G. W.: PASA **26**, 372 (2009)
Preston, G. W.: AJ **141**, 6 (2011)
Pritchet, C. J., Glaspey, J. W.: ApJ **373**, 105 (1991)
Rodgers, A. W.: ApJ **165**, 581 (1971)
Rodgers, A. W, Harding, P., Sadler, E.: ApJ **244**, 912 (1983)
Ryan, S. G. et al.: ApJ **547**, 231 (2001)
Ryan, S. G. et al.: ApJ **571**, 501 (2002)
Sahade, J., Wood, F. B.: in Interacting Binary Stars, Pergamon Press, p. 1 (1978)
Sandage, A. R.: AJ **58**, 61 (1953)
Sandage, A. R.: AJ **93**, 610 (1987)
Sanduleak, N.: ApJS **66**, 309 (1988)
Sarajedini, A.: in ASPC Vol. 53, 14 (1993)
Searle, L., Rodgers, A. W.: ApJ **143**, 809 (1966)
Sepinsky, J. F., et al.: ApJ **667**, 1170 (2007)
Sepinsky, J. F., et al.: ApJ **702**, 1387 (2009)
Sepinsky, J. F., et al.: ApJ **724**, 546 (2010)
Sérsic, J. L.: Atlas de galaxias australes, Cordoba, Obs. Astronomico (1968)
Shetrone, M. D., Côté, P., Sargent, W. L. W.: ApJ **548**, 592 (2001)
Shetrone, M, et al.: AJ **125**, 684 (2003)
Sirko, E., et al.: AJ **127**, 899 (2004)
Smecker-Hane, T. A., Stetson, P. B., Hesser, J. E., Lehnert, M. D. AJ **108**, 507 (1994)
Soker, N.: MNRAS **350**, 1366 (2004)
Soszyński, I, et al.: Acta Astron. **61**, 1 (2011)
Spite, F., Spite, M.: A&A **115**, 357 (1982)
Spite, M. et al.: A&A **360**, 1077 (2000)
Stancliffe, R. J., et al.: A&A **464**, L57 (2007)
Stancliffe, R. J.: MmSAI **81**, 1064 (2010)
Stetson, P. B.: AJ **102**, 589 (1991)
Struve, O.: ApJ **93**, 104 (1941)
Theuns, T., Boffin, H. M. J., Jorissen, A.: MNRAS **280**, 1264 (1996)
Thompson, I. B., et al.: ApJ **677**, 556 (2008)
Thorburn, J. A., Beers, T. C.: BAAS **24**, 1278 (1992)
Thorburn, J. A.: ApJ **421**, 318 (1994)
Tian, B., et al.: A&A **455**, 247 (2006)
Tokovinin, A., et al.: A&A **450**, 681 (2006)
Univane, M, Wyse, R. F. G., Gilmore, G.: MNRAS **278**, 727 (1996)
VandenBergh, D. A., Clem, J. L.: AJ **126**, 778 (2003)
VandenBergh, D. A., Casagrande, L., Stetson, P. B.: AJ **140**, 1020 (2010)

Vanture, A. D., Wallerstein, G., Brown, J. A.: PASP **106**, 835 (1994)
Vauclair, S.: ApJ **605**, 874 (2004)
Venn, K. A.: AJ **128**, 1177 (2004)
Wallerstein, G. Carlsoln, M.: ApJ **132**, 276 (1960)
Wildey, et al., et al.: ApJ **135**, 94 (1962)
Wilhelm, R., et al.: AJ 117, 2308 (1999a)
Wilhelm, R., et al.: AJ 117, 2329 (1999b)
Xue, X.-X., et al.: ApJ **738**, 79 (2011)
Yanny, B., et al.: ApJ **540**, 825 (2000)
Yi, S., et al.: ApJS **136**, 417 (2001)
Zoccali, M., et al.: ApJ **538**, 239 (2000)

Chapter 5
Blue Straggler Stars in Globular Clusters: A Powerful Tool to Probe the Internal Dynamical Evolution of Stellar Systems

Francesco R. Ferraro, Barbara Lanzoni, Emanuele Dalessandro, Alessio Mucciarelli, and Loredana Lovisi

5.1 Introduction

Blue straggler stars (BSSs) in globular clusters (GCs) are commonly defined as those stars located along an extrapolation of the main sequence (MS), in a region brighter and bluer (hotter) than the turnoff (TO) point, in the optical colour-magnitude diagram (CMD; see Fig. 5.1). They were first discovered by Sandage (1953) in the external region of the Galactic GC M3. Their origin has been a mystery for many years and the puzzle of their formation is not completely solved yet.

The BSS location in the CMD suggests that they are more massive than the current cluster population (Fig. 5.1; this is also confirmed by a few mass measurements, e.g., Shara et al. 1997; Gilliland et al. 1998; Fiorentino et al. 2014). However, GCs are completely devoid of gas and any recent star formation event can be realistically ruled out. Hence the BSS origin should be searched in some mechanisms able to increase the initial mass of single stars in a sort of *rejuvenation process*. The BSS formation mechanisms are not completely understood yet, but the main leading scenarios, at present, are mass transfer (MT) processes between binary companions (McCrea 1964; Zinn and Searle 1976), possibly up to the complete coalescence of the binary system, or the merger of stars induced by collisions (COLL; Hills and Day 1976). Being more massive than the average cluster stars, BSSs suffer from the effect of dynamical friction, that makes them sink towards the cluster centre (Mapelli et al. 2004; Ferraro et al. 2012). In turn, the frequent stellar interactions occurring in the ultra-dense cores of Galactic GCs can promote both the formation and the hardening of binary systems, thus contributing to generate

F.R. Ferraro (✉) • B. Lanzoni • E. Dalessandro • A. Mucciarelli • L. Lovisi
Dipartimento di Fisica e Astronomia, Università degli Studi di Bologna, Via Ranzani 1, 40127 Bologna, Italy
e-mail: francesco.ferraro3@unibo.it

H.M.J. Boffin et al. (eds.), *Ecology of Blue Straggler Stars*, Astrophysics and Space Science Library 413, DOI 10.1007/978-3-662-44434-4_5

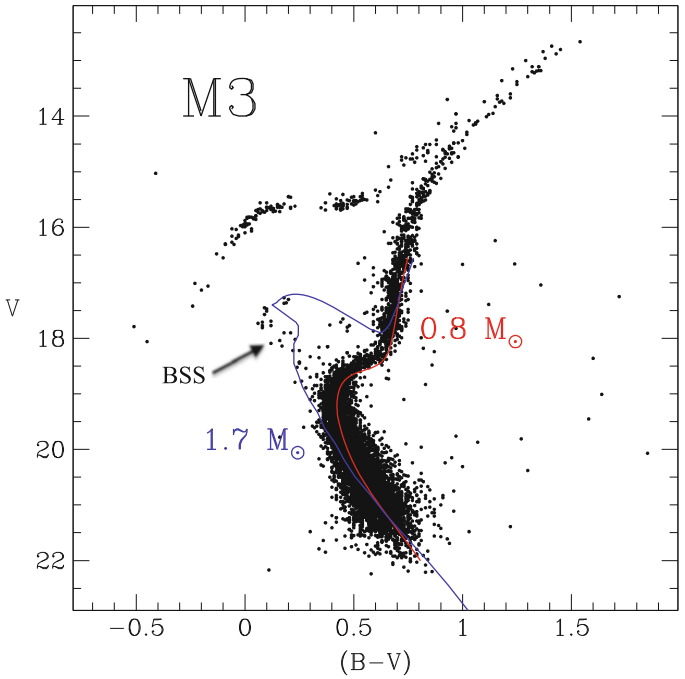

Fig. 5.1 Optical CMD of the globular cluster M3, with the location of BSSs indicated by the *arrow*. The theoretical track corresponding to 0.8 $M_{\odot}$ well reproduces the main evolutionary sequences of the cluster, while BSSs populate a region of the CMD where core hydrogen-burning stars of ∼1.7 $M_{\odot}$ are expected. From Buonanno et al. (1994)

MT-BSSs. All these considerations clearly show that BSSs represent a crucial link between standard stellar evolution and GC internal dynamics (see Bailyn 1995; Ferraro et al. 2012, and references therein).

5.2 BSS Specific Frequency and Primordial Binary Fraction

The observational and interpretative scenario of BSSs has significantly changed in the last years. In fact, for a very long time (almost 40 years) since their discovery (see Chap. 2), BSSs have been detected only in the outer regions of GCs, or in relatively loose clusters. This generated the idea that low-density environments were their *natural habitats*. However, starting from the early '90, high spatial resolution facilities allowed to properly image and discover BSSs also in the highly-crowded central regions of dense GCs (see the case of NGC 6397; Auriere et al. 1990), thus demonstrating that the previous conviction was just due to an observational bias. In particular, the advent of the *Hubble Space Telescope* (HST) represented a real turning point in BSS studies, thanks to its unprecedented spatial resolution and

imaging/spectroscopic capabilities in the ultraviolet (UV). Indeed, the pioneering observations of the central regions of 47 Tucanae (Paresce et al. 1991; Guhathakurta et al. 1994) and M15 (Ferraro and Paresce 1993), by means of the HST opened a new perspective in the study of BSSs, definitely demonstrating that they also (preferentially) populate high-density environments.

Based on these observations, the first catalogs of BSSs have been published (e.g., Fusi Pecci et al. 1992; Sarajedini 1993) and the first comparisons among different clusters have been attempted (Ferraro et al. 1995). In order to perform meaningful comparisons, various definitions of BSS specific frequencies have been proposed over time. Ferraro et al. (1993) introduced the "double normalised ratio", defined as:

$$R_{\rm BSS} = \frac{(N_{\rm BSS}/N_{\rm BSS}^{\rm tot})}{(L^{\rm sampled}/L_{tot}^{\rm sampled})}, \tag{5.1}$$

where $N_{\rm BSS}$ is the number of BSSs counted in a given cluster region, $N_{\rm BSS}^{\rm tot}$ is the total number of BSSs observed, and $L^{\rm sampled}/L_{tot}^{\rm sampled}$ is the fraction of light sampled in the same region, with respect to the total measured luminosity. The same ratio can be defined for any post-MS population. Theoretical arguments (Renzini and Fusi Pecci 1988) demonstrate that the double normalised ratio is equal to unity for any population (such as red giant branch and horizontal branch stars, RGB and HB, respectively) whose radial distribution follows that of the cluster luminosity. Other definitions of the BSS specific frequency adopted in the literature are: $S4_{\rm BSS} = N_{\rm BSS}/L_s$, where $N_{\rm BSS}$ is the number of BSSs and L_s is the sampled luminosity in units of 10^4 $L_\odot$ (Ferraro et al. 1995); $F_{\rm BSS} = N_{\rm BSS}/N_{\rm bright}$, where $N_{\rm bright}$ is the number of all the stars brighter than two magnitudes below the HB level (Bolte et al. 1993); $F_{\rm pop}^{\rm BSS} = N_{\rm BSS}/N_{\rm pop}$ (Ferraro et al. 2003), where $N_{\rm pop}$ is the number of stars belonging to a cluster "normal" population adopted as reference (generally the HB population, or a segment of the RGB or MS). Besides the different definitions, all these normalisations account for the different cluster richness (i.e., total luminosity or mass). However, as discussed in Ferraro et al. (1995), particular caution is needed when looking for correlations among BSS specific frequencies and cluster structural parameters, since the concentration parameter and central density are intrinsically related to the cluster luminosity (see, e.g., Djorgovski and Meylan 1993); hence spurious correlations can emerge simply because of the BSS "normalisation".

The largest compilations of BSSs to date have been collected for nearly 60 Galactic GCs surveyed with the HST/WFPC2 (Piotto et al. 2004; Leigh et al. 2007; Moretti et al. 2008), and for 35 clusters (Leigh et al. 2011) observed within the HST/ACS *Survey of Galactic Globular Clusters* (Sarajedini et al. 2007). These compilations, together with deep investigations in open clusters, dwarf spheroidals, and the Galactic field (see Chap. 3, 4, and 6 in this book), have significantly contributed to form the nowadays largely accepted idea that BSSs are a stellar population common to any stellar system.

With the aim of understanding how BSSs form and if their formation mechanisms depend on some cluster physical properties, the most recent catalogs have been used to search for correlations between the BSS specific frequency (or number), and

several parameters tracing the cluster structure (as luminosity, mass, central density, etc.), as well as for correlations with the collision rate and binary fraction (for recent results, see Chap. 9). Though not conclusive, this approach has provided a number of interesting results. For instance, no correlation has been found with the collisional parameter (Piotto et al. 2004; Davies et al. 2004; Leigh et al. 2007), while a strong correlation has been revealed between the number of BSSs in cluster cores and the core mass (Knigge et al. 2009; Leigh et al. 2013). These facts have been interpreted as the evidence of a binary (instead of a collisional) origin of BSSs, even in the densest environments, like the centre of post-core collapsed (PCC) clusters (Knigge et al. 2009). However, the fraction of binary systems in a sample of 59 GCs has been recently estimated from the distribution of stars along the "secondary" MS (Milone et al. 2012), thus allowing to explore directly any possible correlation between the fraction/number of BSSs and that of binaries. By using a sub-sample of 24 GCs, Milone et al. (2012) found a nice correlation between the BSS specific frequency and the binary fraction in cluster cores. This has been confirmed also by Leigh et al. (2013), who, however, obtain a much stronger correlation between the number of core BSSs and the cluster core mass. Interestingly, in Milone et al. (2012) plot, PCC clusters lie well outside the relation. This likely reflects the role that internal dynamics plays on the binary and BSS content of GCs. In fact, binary systems are subject to frequent dynamical interactions with other binaries, single stars and even multiple systems. These interactions can either bring to stellar collisions, or significantly alter the physical properties of binaries, even promoting mass transfer activity. Hence, binaries and interactions play a crucial role in both the MT and the COLL scenarios and it is probably impossible to separate the two effects just on the basis of the observed binary fraction. An exception could be represented by low density environments, where the efficiency of dynamical interactions is expected to be negligible. Very interestingly, indeed, a clear correlation between the binary and the BSS frequency has been found in a sample of 13 low density GCs ($\log \nu_0 < 3$ in units of $L_\odot/pc^3$; see Fig. 5.2 and Sollima et al. 2008). This is the cleanest evidence

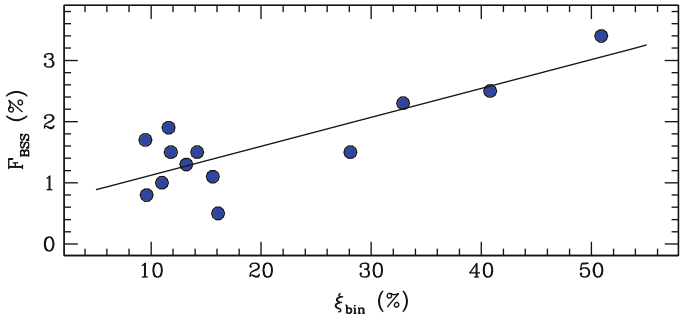

Fig. 5.2 BSS specific frequency as a function of the core binary fraction measured in a sample of low-density GCs. The best-fit linear correlation is also plotted (*solid line*). From Sollima et al. (2008)

that the unperturbed evolution of primordial binaries is the dominant BSS formation process in low-density environments (also consistently with the results obtained in open clusters; e.g., Mathieu et al. 2009).

5.3 The Ultraviolet Route to Study BSS

The systematic study of BSSs in the visible-light bands, especially in the central regions of high density clusters, is intrinsically difficult and remains problematic even when using HST. This is because the optical emission of old stellar populations is dominated by cool, bright giants. Hence, the observation of complete samples of (faint) hot stars (as BSSs, other by-products of binary system evolution, extreme blue horizontal branch stars, etc.) is quite problematic in this plane. *It is like trying to make a complete census of fire-flies, while having a clump of large light-bulbs just in front of us. In order to secure a proper counting of fire-flies one needs to switch off the lights, first!*. Moreover, in the visible-light plane, BSSs can be easily mimicked by photometric blends of subgiant branch (SGB) and RGB stars. Instead, at ultraviolet (UV) wavelengths RGB stars are very faint, while BSSs are among the brightest objects. In particular, in the UV plane BSSs are much more easily recognisable, since they define a narrow, nearly vertical sequence spanning a ∼3 mag interval (see Fig. 5.3). In the mean time, BSS-like blends are much less severe

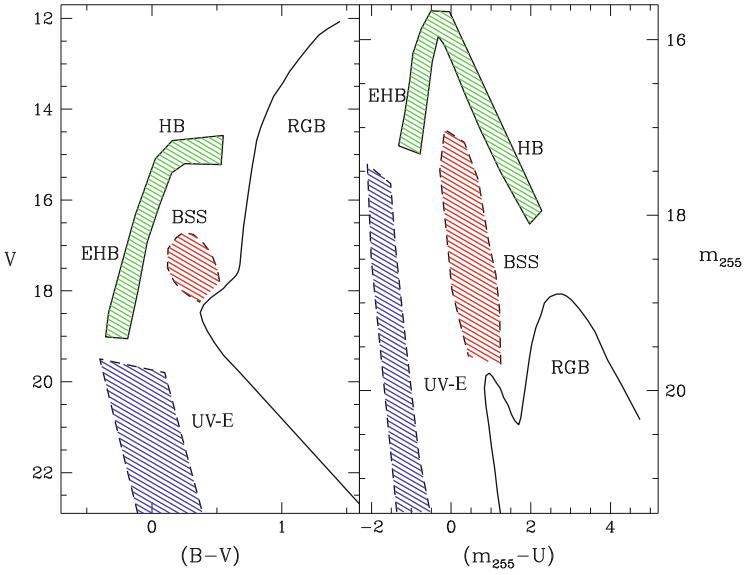

Fig. 5.3 Sketch of the stellar evolutionary sequences in the optical (*left panel*) and in the UV (*right panel*) CMDs. The loci of RGB, BSS, HB, extreme-HB stars (EHB) and stars with UV excess are marked

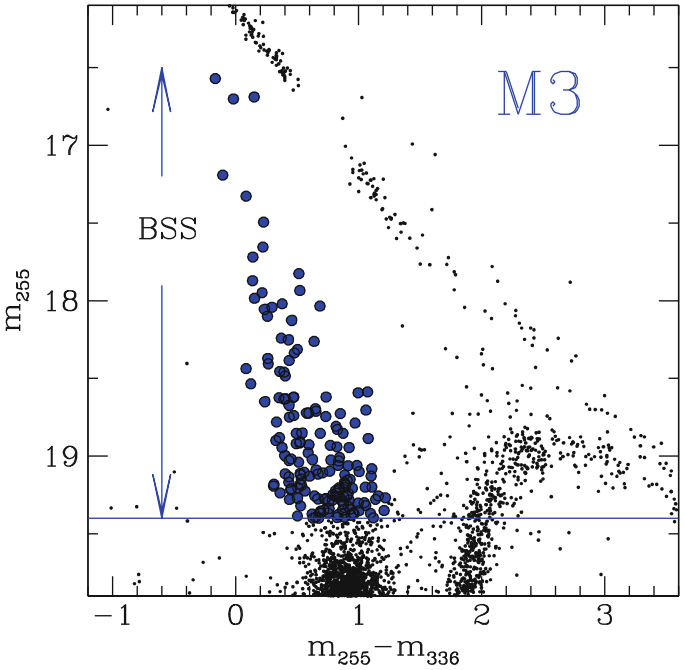

Fig. 5.4 BSS in the UV: the case of M3. The *horizontal line* at $m_{255} = 19.4$ is the assumed BSS limiting magnitude, corresponding to $\sim 5\sigma$ above the turnoff level. From Ferraro et al. (1997)

at these wavelengths because of the relative faintness of SGB and RGB stars. Indeed, the $(m_{255}, m_{255}–m_{336})$ plane has been found to be ideal for selecting BSSs even in the cores of the densest GCs.

The UV exploration of the very central region of M3 (see Ferraro et al. 1997, hereafter F97; see also Fig. 5.4) brought to the discovery of a substantial population of BSSs, at odds with the depletion claimed by Bolte et al. (1993). Since then, the central regions of a number of GCs have been explored in the UV to search for BSSs: this systematic approach allowed to put the BSS study into a more quantitative basis than ever before. Indeed a number of interesting results have been obtained from cluster-to-cluster comparisons (see Fig. 5.5). Of course the UV approach strongly favours the observation of hot objects, like HB stars (see Fig. 5.3). Hence the HB becomes the ideal reference population for the definition of the BSS specific frequency ($F_{\rm HB}^{\rm BSS}$) at these wavelengths.

By using appropriate observations in the UV (Fig. 5.5), Ferraro et al. (2003) presented a comparison of the BSS populations in the central regions of six clusters (namely NGC 288, M92, M3, M13, M80, and M10) characterised by different structural parameters. The BSS specific frequency ($N_{\rm BSS}/N_{\rm HB}$) has been found to largely vary from cluster to cluster, from 0.07 to 0.92, and it does not seem to be correlated with central density, total mass, velocity dispersion, or any other obvious cluster property (see also Piotto et al. 2004). On the other hand, this study pointed

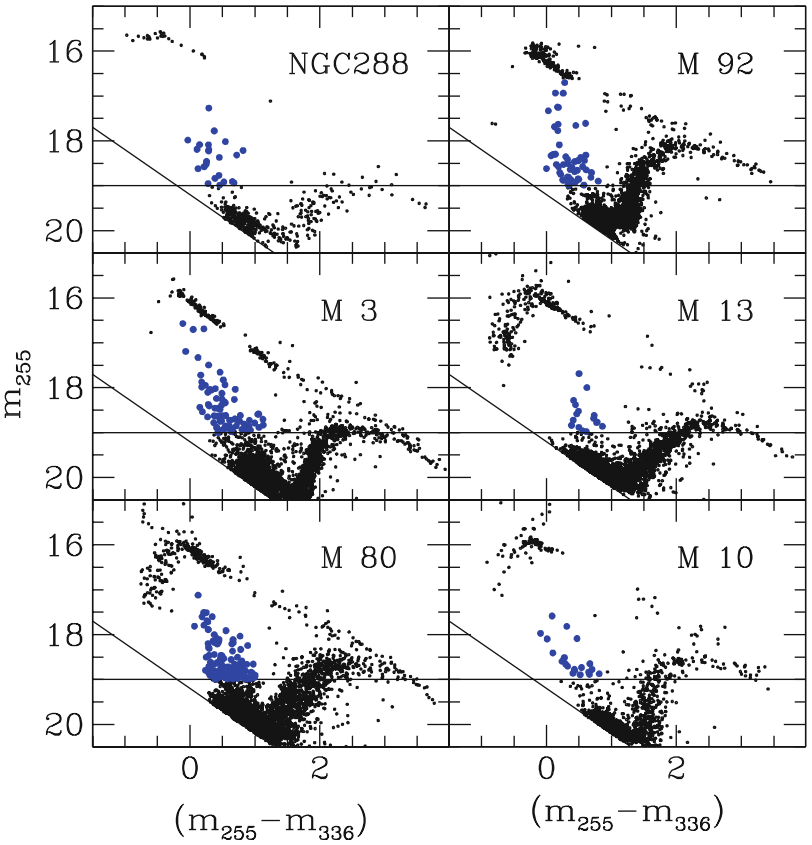

Fig. 5.5 UV CMDs of six different globular clusters (see labels), with the BSS populations highlighted as *blue circles*. The *horizontal line marks* the magnitude limit adopted for the BSS selection. From Ferraro et al. (2003)

out peculiar cases that statistical approaches (as those presented, e.g., by Piotto et al. 2004) did not bring into evidence. "Twin" clusters like M3 and M13 have been found to harbour quite different BSS populations: the specific frequency in M13 is the lowest ever measured in a GC (0.07), and it turns out to be four times lower than that measured in M3 (0.28). *What is the origin of this difference?* We (Ferraro et al. 2003) suggested that it could be related to their binary content; in particular the paucity of BSSs in M13 could be due either to a quite poor population of primordial binaries, or to the fact that most of them were destroyed during the cluster evolution. Indeed the fraction of binaries recently measured in the central regions of these two clusters (Milone et al. 2012) confirms a significant difference ($f_{\rm bin} = 0.027$ for M3, and $f_{\rm bin} = 0.005$ for M13), thus supporting the hypothesis that this is the origin of the different BSS content. One of the most interesting result is that the largest BSS specific frequency has been found in two GCs which are at the extremes

of the central density values in the analysed sample: NGC 288 and M80, with the lowest and the highest central density, respectively ($\log \rho_0 = 2.1$ and 5.8, in units of $M_\odot/pc^3$). This suggests that the two formation channels can have comparable efficiency in producing BSSs in the respective most favourable environment.

5.4 The Discovery of the Double BSS Sequence

While the proposed BSS formation mechanisms could be separately at work in clusters with different densities (Ferraro et al. 1995, 1999a), a few pieces of evidence are now emerging suggesting that they could also act simultaneously within the same cluster. Indeed the discovery of a double BSS sequence in M30 (Ferraro et al. 2009, hereafter F09) indicates that this can be the case.

By using an exceptional set of 44 high-resolution images obtained with the HST-WFPC2, F09 obtained a very high-precision CMD of the central region of the Galactic GC M30. The CMD revealed the existence of two well-separated and almost parallel sequences of BSSs (Fig. 5.6). The two sequences are similarly

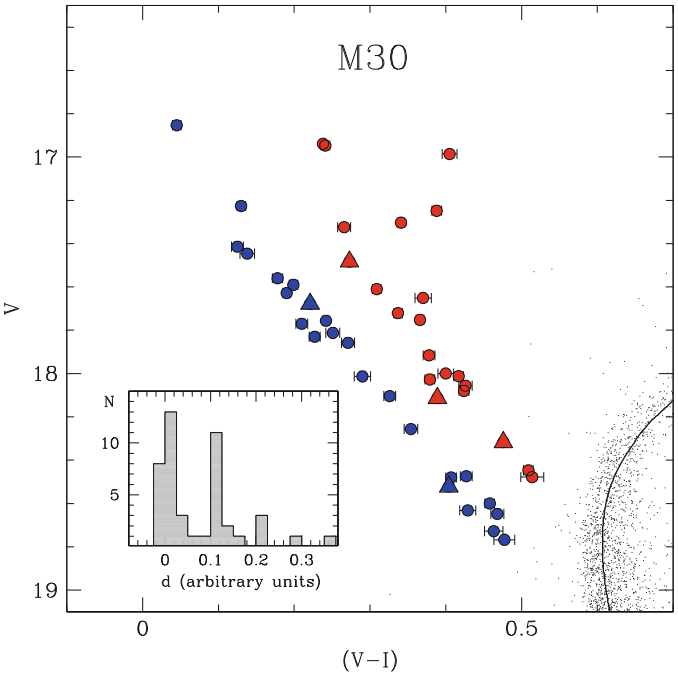

Fig. 5.6 Optical CMD of M30 zoomed in the BSS region. The two distinct sequences of BSSs are highlighted as *blue* and *red symbols*. The *inset* shows the distribution of the geometrical distances of BSSs from the straight line that best fits the blue BSS sequence. Two well-defined peaks are clearly visible, confirming that the two sequences are nearly parallel to each other. From Ferraro et al. (2009)

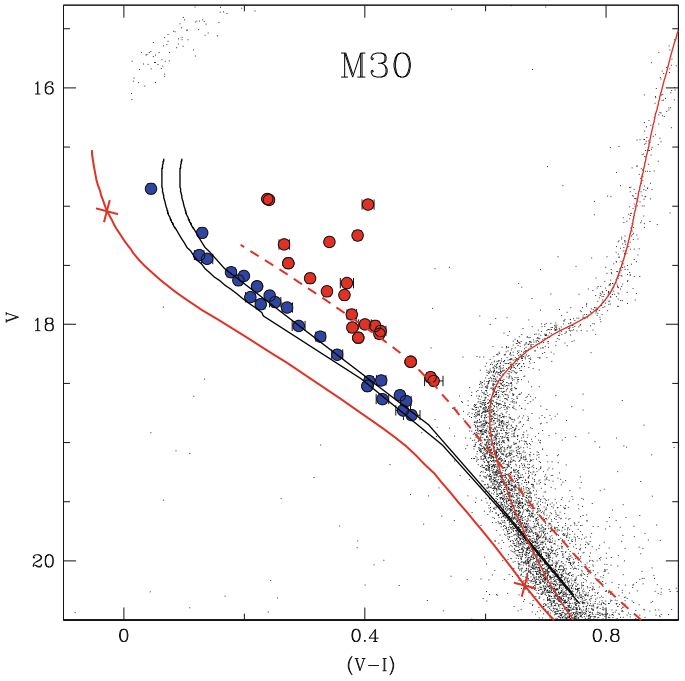

Fig. 5.7 Magnified portion of the CMD of M30. The *solid black lines* correspond to the collisional isochrones of 1 and 2 Gyr, respectively, which accurately reproduce the blue BSS sequence. The *solid red lines* correspond to the single-star isochrones of 13 Gyr (well fitting the main cluster evolutionary sequences) and 0.5 Gyr (representing the reference cluster zero-age main sequence, ZAMS). The *two crosses mark* the respective positions of a 0.8 $M_{\odot}$ star and a 1.6 $M_{\odot}$ star along the ZAMS. The *dashed red line* corresponds to the ZAMS shifted by 0.75 mag, marking the lower boundary of the locus occupied by mass-transfer binary systems. This line well reproduces the red BSS sequence. From Ferraro et al. (2009)

populated, consisting of 21 and 24 stars, respectively. *This is the very first time that such a feature has been detected in any stellar system, and it could be the signature of the cluster core collapse imprinted onto the BSS population.*

The comparison with evolutionary models of BSS formed by direct collisions of two MS stars (Sills et al. 2009) shows that the blue-BSS sequence is well fit by collisional isochrones with ages of 1–2 Gyr (black solid lines in Fig. 5.7). Instead, the red-BSS population is far too red to be properly reproduced by collisional isochrones of any age, and its origin should therefore be different. Binary evolution models (Tian et al. 2006) have shown that during the mass-transfer phase (which can last several Gyr, i.e., a significant fraction of the binary evolution time-scale), the binary population defines a sort of "low-luminosity boundary" located ∼0.75 mag above the zero-age MS in the BSS region. This is just where the red-BSS sequence is observed (red dashed line in Fig. 5.7). Hence, the BSS along the red-sequence could be binary systems still experiencing an active phase of mass-exchange.

Due to the normal stellar evolution, all BSSs will evolve toward the RGB phase. In particular, the evolved blue-BSSs will populate the region between the two observed sequences and fill the gap. Hence, the fact that two well-separated chains of stars are observed supports the hypothesis that both the blue- and the red-BSS populations have been *generated by a recent and short-lived event, instead of a continuous formation process*. Quite interestingly, M30 is classified as a PCC cluster in the original compilation of Djorgovski and King (1986), and F09 confirmed this finding by carefully re-determining the cluster density profile from deep HST images and detecting a steep power-law cusp in the innermost 5–6″ (∼0.2 pc). During the core collapse phase the central stellar density rapidly increases, bringing to a concomitant enhancement of gravitational interactions (in fact, the collisional parameter scales as $\Gamma \propto \rho_0^{1.5} r_c^2$, where r_c is the core radius). In turn, these can trigger the formation of new BSSs, both via direct stellar collisions and via mass transfer activity in dynamically shrunk binary systems. All together these considerations support a scenario where the two observed BSS populations are generated by the same dynamical event (the core collapse): the blue-BSSs arose from the enhanced stellar collision activity, while the red-BSSs are the result of the evolution of binary systems which first sank into the cluster center because of the dynamical friction (or they were already present into the cluster core), and then have been driven into the mass-transfer regime by hardening processes induced by gravitational interactions during the core collapse phase. According to this scenario, *the double BSS sequence detected in M30 dates the occurrence of the core collapse event back to 1–2 Gyr ago. If the proposed scenario is correct, this discovery opens the possibility of defining a powerful "clock" to date the occurrence of this dramatic event in a star cluster history* (see also Sect. 5.6).

Additional clues in favour of a different formation history for the BSSs belonging to the two sequences are suggested by their central concentration and specific frequency. The red-BSSs are more centrally segregated than the blue ones (Fig. 5.8), with no red-BSSs observed at $r > 30''$ (∼1.3 pc) from the cluster center. Moreover, the value of the BSS specific frequency with respect to HB stars varies significantly over the cluster extension, reaching the surprising value of ∼1.55 when only the central cusp of the star density profile ($r < 5$–$6''$) is considered. This is the highest BSS specific frequency measured in any GC (Ferraro et al. 2003), and it further supports the possibility that in M30 we are observing the effect of an enhanced gravitational interaction activity on single and binary stars.

The proposed picture leads to a testable observational prediction: the red-BSS sequence should be populated by binaries with short orbital periods. A recent paper (Knigge et al. 2009) suggested that the dominant BSS formation channel is the evolution of binary systems, independently of the dynamical state of the parent cluster. The double BSS sequence in M30 possibly shows that binary evolution alone does not paint a complete picture: dynamical processes can indeed play a major role in the formation of BSSs. Interestingly, preliminary indications of double BSS sequences have been collected for two additional clusters: M15 (Beccari et al. 2014 in preparation) and NGC 362 (Dalessandro et al. 2013). Moreover, detailed

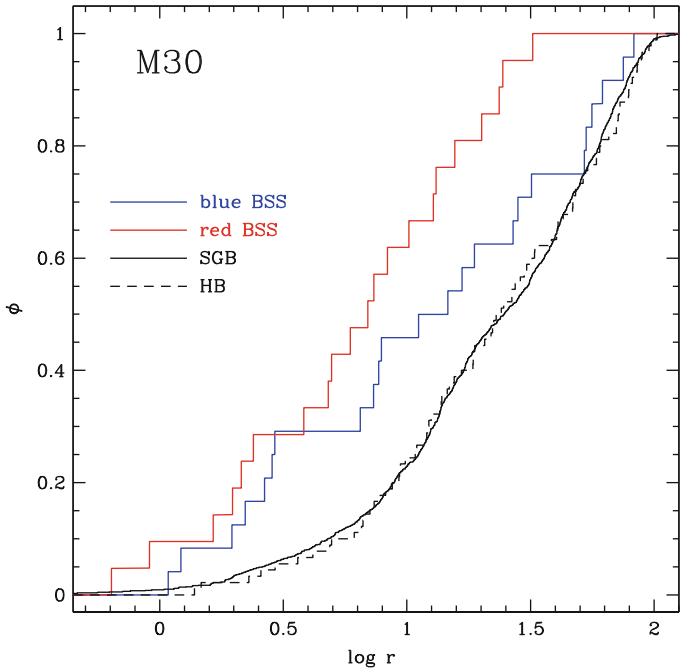

Fig. 5.8 Cumulative radial distributions of red BSSs (*red line*) and blue BSSs (*blue line*), as function of the distance from the cluster centre. The distributions of subgiant branch stars (*solid black line*) and horizontal-branch stars (*dashed black line*) are also plotted, for comparison. From Ferraro et al. (2009)

spectroscopic investigations are certainly worth performing to obtain a complete characterisation of the BSS properties (orbital periods, rotation velocities, etc.). In this respect particularly promising is the search for the chemical signature of the MT process (see Sect. 5.8) for the BSSs along the red sequence.

5.5 The BSS Radial Distribution

M3 has played a fundamental role in the BSS history: not only it is the system where BSSs have been first identified (Sandage 1953), but also where their radial distribution has been studied over the entire cluster extension for the first time (F97). In fact by combining UV HST observations of the cluster central region (F97) and wide field ground-based observations in the visible-light bands (Ferraro et al. 1993; Buonanno et al. 1994), F97 presented the BSS radial distribution of M3 out to $r \sim 6'$. The result was completely unexpected: BSSs appeared to be more centrally

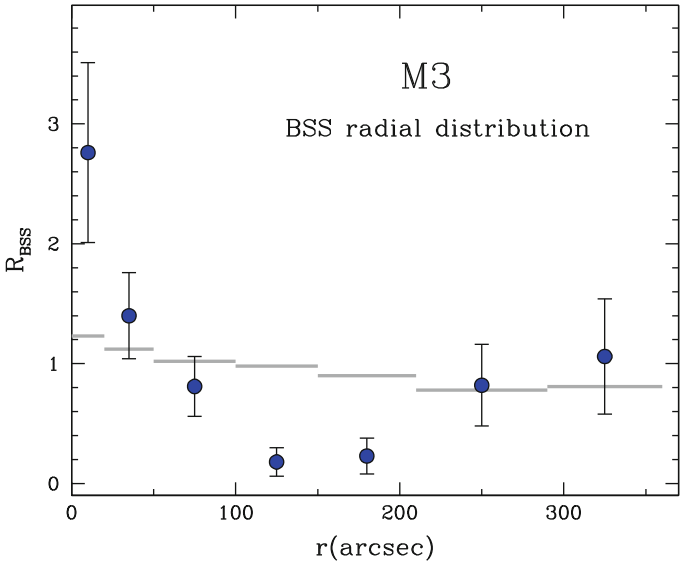

Fig. 5.9 Bimodal radial distribution of BSSs in M3. *Blue dots mark* the value of the BSS double normalised ratio as defined in Eq. (5.1), computed at various distances from the cluster centre, the *gray segments mark* the double normalised ratio of HB stars. From Ferraro et al. (1997)

concentrated than RGB stars in the cluster central regions, and less concentrated in the outskirts. The result is shown in Fig. 5.9 and it clearly shows that the radial distribution of BSSs in M3 is bimodal: it reaches a maximum in the centre of the cluster, shows a clear-cut dip in the intermediate region (at $100'' < r < 200''$), and rises again in the outer region.

Sigurdsson et al. (1994) suggested that the bimodal BSS distribution observed in M3 could be explained by assuming that all BSSs formed in the core by direct collisions (thus creating the central peak of the distribution) and some of them were kicked out from the centre by the recoil of the interactions. Those BSSs ejected to a few core radii rapidly drifted back to the centre of the cluster due to mass segregation (thus contributing to the central BSS concentration and generating the paucity of BSSs at intermediate distances of a few core radii). BSSs affected by more energetic recoils would have been kicked out to larger distances and, since they require much more time to drift back toward the core, they may account for the overabundance of BSSs observed in the cluster outskirts. However, Monte-Carlo dynamical simulations ((Mapelli et al. 2004, 2006) demonstrated that BSSs kicked out from the core either are lost from the cluster, or sink back to the centre in 1–2 Gyr only. Hence, the observed BSS bimodal distributions cannot be explained with a purely collisional population, and to accurately reproduce the external upturn of the distribution it is necessary to assume a sizable fraction ($\sim 20 - 40\,\%$) of MT-BSSs, generated in the peripheral regions where primordial binaries can evolve in isolation

and experience mass transfer processes without suffering significant interactions with other cluster stars.

While the bimodality detected in M3 was considered for years to be *peculiar*, more recent results demonstrated that this is not the case. In fact, the same observational strategy adopted by F97 in M3 has been applied to a number of other clusters, and bimodal distributions have been detected in the majority of cases ($\sim$15) studied so far. Examples can be found in: 47 Tuc (Ferraro et al. 2004) , NGC 6752 (Sabbi et al. 2004), M55 (Zaggia et al. 1997; Lanzoni et al. 2007c), M5 (Warren et al. 2006; Lanzoni et al. 2007a), NGC 6388 (Dalessandro et al. 2008a), M53 (Beccari et al. 2007). Only a few exceptions are known: M79 and M75, which do not present any external upturn (Lanzoni et al. 2007b; Contreras Ramos et al. 2012), and three clusters (ω Centauri, NGC 2419 and Palomar 14) showing a completely flat BSS radial distribution, totally consistent with that of the reference population (Ferraro et al. 2006a; Dalessandro et al. 2008b; Beccari et al. 2011, respectively). The last three cases deserve a specific comment. The flat behaviour discovered in these clusters suggests that the BSS radial distribution is not yet significantly altered by stellar interactions and by the dynamical evolution of the cluster. *Indeed, this is the cleanest evidence of the fact that these systems are not fully relaxed yet, even in the central regions*. We emphasise that this result is much more solid than any other estimate of mass segregation in these stellar systems. In fact, the degree of mass segregation is usually evaluated from star number counts along the MS, down to quite faint magnitudes where incompleteness biases can be severe (see, e.g., Anderson 2002; Jordi et al. 2009). Instead the computation of the BSS specific frequency refers to much brighter objects, as BSS and TO/RGB/HB stars.

5.6 Setting the Dynamical Clock for Stellar Systems

The entire database of available BSS radial distributions has been analysed by us (Ferraro et al. 2012, hereafter F12). Such a dataset contains 21 GCs with very different structural properties (hence possibly at different stages of their dynamical evolution), but with nearly the same chronological age (12–13 Gyr; Marín-Franch et al. 2009), with the only exception of Palomar 14 which formed $\sim$10.5 Gyr ago (Dotter et al. 2008). While significant cluster-to-cluster variations were already known, F12 discovered that once the radial distance from the centre is expressed in units of the core radius (thus to allow a meaningful comparison among the clusters), GCs can be efficiently grouped on the basis of the shape of their BSS radial distribution, and at least three families can be defined:

- *Family I*—the radial distribution of the BSS double normalised ratio ($R_{\rm BSS}$) is fully consistent with that of the reference population ($R_{\rm pop}$) over the entire cluster extension (see Fig. 5.10);
- *Family II*—the distribution of $R_{\rm BSS}$ is incompatible with that of $R_{\rm pop}$, showing a significant bimodality, with a central peak and an external upturn. At intermediate

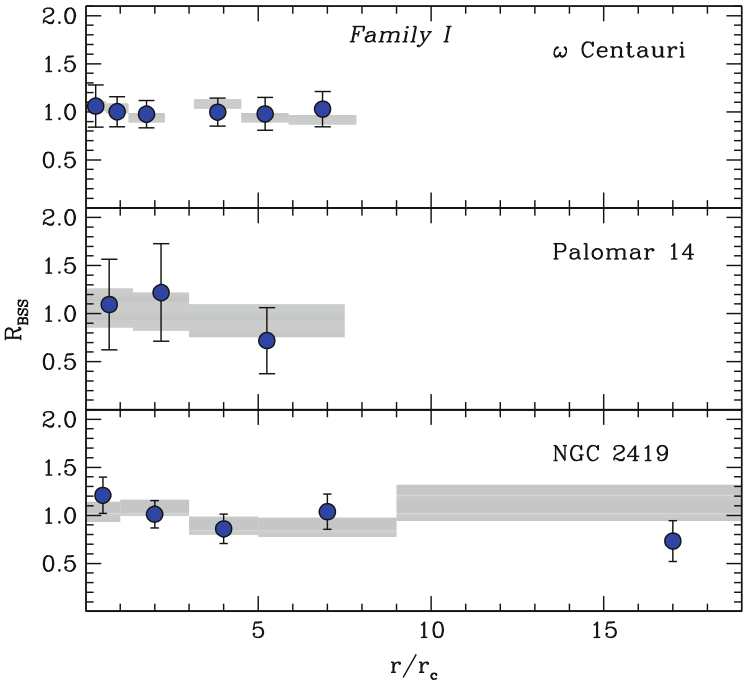

Fig. 5.10 BSS radial distribution observed in ω Centauri, Palomar 14 and NGC 2419, with the *blue circles* marking the values of $R_{\rm BSS}$, defined in Eq. (5.1). The distribution of the double normalised ratio measured for RGB or HB stars is also shown for comparison (*grey strips*). The BSS radial distribution is flat and totally consistent with that of the reference population, thus indicating a low degree of dynamical evolution for these three GCs (*Family I*). From Ferraro et al. (2012)

radii a minimum is evident and its position ($r_{\rm min}$) can be clearly defined for each sub-group (see Fig. 5.11);

- *Family III*—the radial distribution of $R_{\rm BSS}$ is still incompatible with that of the reference population, showing a well defined central peak with no external upturn (see Fig. 5.12).

Which is the physical origin of these distributions? Previous preliminary analysis (Mapelli et al. 2004, 2006; Lanzoni et al. 2007a,b) of a few clusters indicated that BSSs generated by stellar collisions mainly/only contribute to the central peak of the distribution, while the portion beyond the observed minimum is populated by MT-BSSs which are evolving in isolation in the cluster outskirt and have not yet suffered the effects of dynamical friction (see Sect. 5.5). Overall, the BSS radial distribution is primarily modelled by the long-term effect of dynamical friction acting on the cluster binary population (and its progeny) since the early stages of cluster evolution. In fact, what we call MT-BSS today is the by-product of the evolution of a $\sim$1.2 $M_\odot$ binary that has been orbiting the cluster and suffering

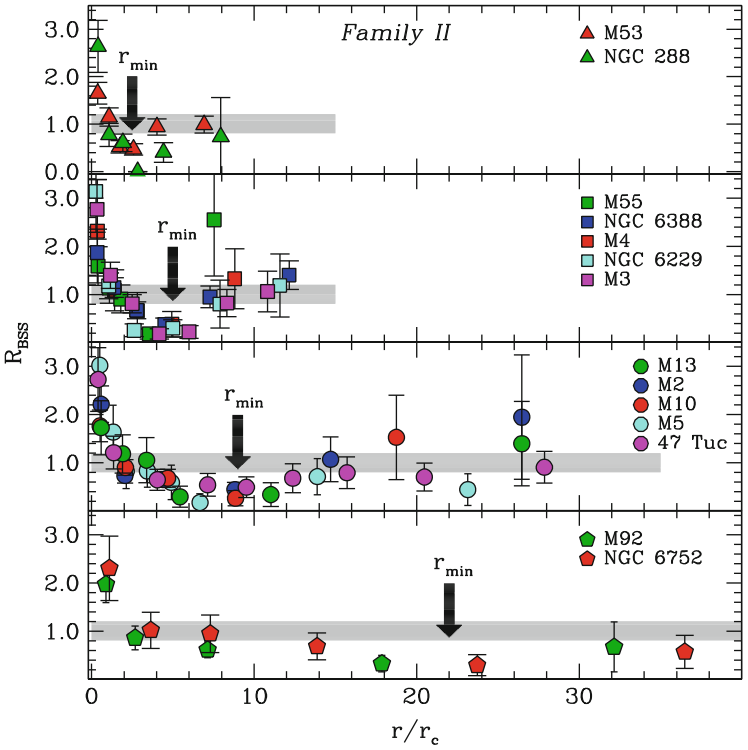

Fig. 5.11 BSS radial distribution observed in clusters of intermediate dynamical age (*Family II*). The distribution is clearly bimodal and the radial position of the minimum (marked with the *arrow* and labelled as r_{min}) clearly moves outward from *top* to *bottom*, suggesting that the bottom clusters are more dynamically evolved than the upper ones. For the sake of clarity, the grey bands schematically mark the distribution of the reference populations. From Ferraro et al. (2012)

the effects of dynamical friction for a significant fraction of the cluster lifetime. The efficiency of dynamical friction decreases for increasing radial distance from the centre, as a function of the local velocity dispersion and mass density. Hence, dynamical friction first segregates (heavy) objects orbiting close to the centre and produces a central peak in their radial distribution. As the time goes on, the effect extends to larger and larger distances, thus yielding to a region devoid of these stars (i.e., a dip in their radial distribution) that progressively propagates outward. Simple analytical estimate of the radial position of this dip turned out to be in excellent agreement with the position of the minimum in the *observed* BSS radial distributions (r_{min}), despite a number of crude approximation (see, e.g., Mapelli et al. 2006). Moreover, a progressive outward drift of r_{min} as a function of time is confirmed by the results of direct N-body simulations that follow the evolution of $\sim$1.2 $M_\odot$ objects within a reference cluster over a significant fraction of its lifetime.

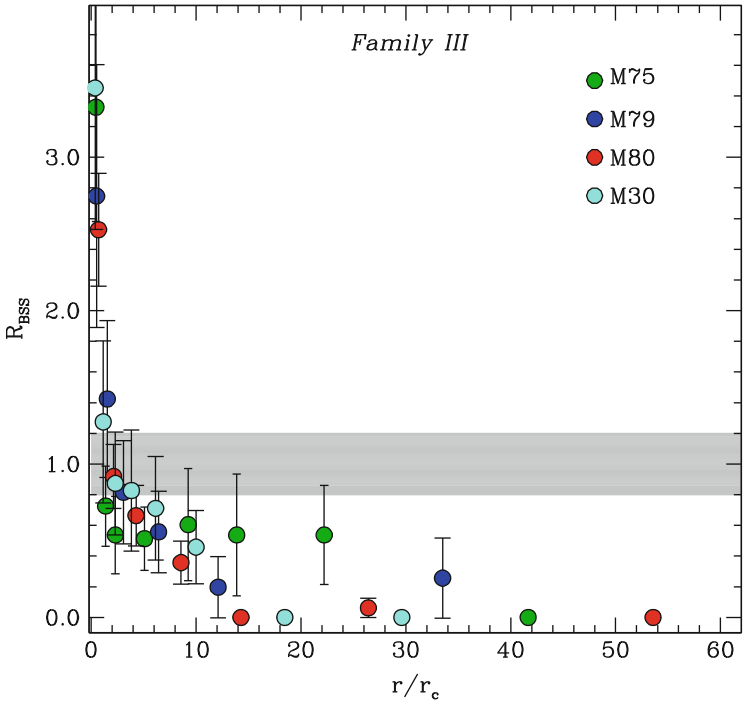

Fig. 5.12 BSS radial distribution for dynamically old clusters (*Family III*): only a central peak is visible, while the external upturn is no more present because, within the proposed scenario, the dynamical friction has been efficient out to the cluster outskirts. From Ferraro et al. (2012)

In light of these considerations, the three families defined in Figs. 5.10, 5.11, and 5.12 correspond to GCs of increasing dynamical ages. Hence, the shape of the BSS radial distribution turns out to be a powerful dynamical-age indicator. A flat BSS radial distribution (consistent with that of the reference population; see *Family I* in Fig. 5.10) indicates that dynamical friction has not played a major role yet even in the innermost regions, and the cluster is still dynamically young. This interpretation is confirmed by the absence of statistically significant dips in the BSS distributions observed in dwarf spheroidal galaxies (Mapelli et al. 2009; Monelli et al. 2012; see also Chap. 6): these are, in fact, collisionless systems where dynamical friction is expected to be highly inefficient. In more evolved clusters (*Family II*), dynamical friction starts to be effective and to segregate BSSs that are orbiting at distances still relatively close to the centre: as a consequence, a peak in the centre and a minimum at small radii appear in the distribution, while the most remote BSSs are not yet affected by the action of dynamical friction (this generates the rising branch of the observed bimodal BSS distributions; see upper panel in Fig. 5.11). Since the action of dynamical friction progressively extends to larger and larger distances

from the centre, the dip of the distribution progressively moves outward (as seen in the different groups of *Family II* clusters; Fig. 5.11, panels from top to bottom). In highly evolved systems dynamical friction already affected even the most remote BSSs, which started to gradually drift toward the centre: as a consequence, the external rising branch of the radial distribution disappears (as observed for *Family III* clusters in Fig. 5.12). All GCs with a single-peak BSS distribution can therefore be classified as "dynamically old".

Interestingly, this latter class includes M30 (see Sect. 5.4), a system that already suffered core collapse which is considered as a typical symptom of extreme dynamical evolution (Meylan and Heggie 1997). The proposed classification is also able to shed light on a number of controversial cases debated into the literature. In fact, M4 turns out to have an intermediate dynamical age, at odds with previous studies suggesting that it might be in a PCC state (Heggie and Giersz 2008). On the other hand, NGC 6752 turns out to be in a quite advanced state of dynamical evolution, in agreement with its observed double King profile indicating that the cluster core is detaching from the rest of the cluster structure (Ferraro et al. 2003). Finally this approach might provide the key to discriminate between a central density cusp due to core collapse (as for M30) and that due to the presence of an exceptional concentration of dark massive objects (neutron stars and/or the still elusive intermediate-mass black holes; see the case of NGC 6388 in Lanzoni et al. 2007, 2013, and references therein).

The quantization into distinct age-families is of course an over-simplification, while the position of $r_{\rm min}$ is found to vary with continuity as a sort of clock time-hand. This allowed F12 to define the first empirical clock able to measure the dynamical age of a stellar system from pure observational quantities (the *dynamical clock*): as the engine of a chronometer advances the clock hand to measure the time flow, in a similar way the progressive sedimentation of BSSs towards the cluster centre moves $r_{\rm min}$ outward, thus marking its dynamical age. This is indeed confirmed by the tight correlations found between the clock-hand ($r_{\rm min}$) and the central and half-mass relaxation times ($t_{\rm rc}$ and $t_{\rm rh}$, respectively), which are commonly used to measure the cluster dynamical evolution time-scales. The trend with $t_{\rm rc}$ found by F12 is shown in Fig. 5.13 and the best-fit relations is:

$$\log(t_{\rm rc}/t_{\rm H}) = -1.11 \times \log(r_{\rm min}) - 0.78 \tag{5.2}$$

where $t_{\rm H}$ is the Hubble time. Note that, while $t_{\rm rc}$ and $t_{\rm rh}$ provide an indication of the relaxation timescales at specific radial distances from the cluster centre ($r_{\rm c}$ and $r_{\rm h}$, respectively), the dynamical clock here defined provides a measure of the global dynamical evolution of the systems, because the BSS radial distribution simultaneously probes all distances from the cluster centre.

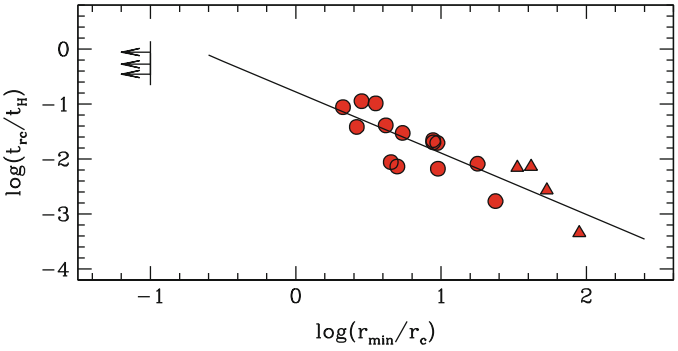

Fig. 5.13 Core relaxation time (normalised to the Hubble time t_H) as a function of the clock hand of the proposed *dynamical clock* ($r_{\rm min}$, in units of the core radius). Dynamically young systems (*Family I*) show no minimum and are plotted as lower-limit arrows at $r_{\rm min}/r_c = 0.1$. For dynamically old clusters (*Family III*, *triangles*), the distance of the farthest radial bin where no BSSs are observed has been adopted as $r_{\rm min}$. As expected for a meaningful clock, a tight anticorrelation is found: clusters with relaxation times of the order of the age of the Universe show no signs of BSS segregation (hence their BSS radial distribution is flat and $r_{\rm min}$ is not definable; see Fig. 5.10), whereas for decreasing relaxation times the radial position of the minimum increases progressively. The *solid line* corresponds to the best-fit relations, given in (5.2). From Ferraro et al. (2012)

5.7 Searching for the BSS Progeny: Evolved BSSs

Although BSSs have been routinely observed for 60 years now, no firm identification of even a single evolved BSS (E-BSS) has been obtained to date. Indirect evidence of the possible existence of E-BSSs has been derived from photometric criteria. Renzini and Fusi Pecci (1988) suggested to search for E-BSSs during their core helium burning phase, when they should appear redder and brighter than *normal* HB stars, i.e. they should be located in a region of the CMD between the HB level and the Asymptotic Giant Branch (AGB). Following this prescription Fusi Pecci and collaborators (Fusi Pecci et al. 1992) identified a few E-BSS candidates in several clusters with predominantly blue HBs, where the likelihood of confusing E-BSSs with true HB or evolved HB stars was minimised. Following the same prescription, F97 identified a sample of E-BSS candidates in M3 (see upper panel in Fig. 5.14), demonstrating that their radial distribution is similar to that observed for BSSs (see lower panel in Figs. 5.14 and Fig. 5.9). Similar results have been obtained by us (Ferraro et al. 1999a) in the case of M80 (Fig. 5.15). The cumulative distribution of E-BSSs is consistent with that of BSSs and significantly different from that of genuine HB + RGB stars. Indeed, the Kolmogorov-Smirnov probability that E-BSSs and BSSs are extracted from the same parent population is ∼67 %, while the same probability between E-BSSs and RGB stars decreases to only ∼1.6 %. This result confirms the expectation that E-BSSs share the same radial distribution of BSSs, both being more massive than the bulk of the cluster stars. It is interesting to note that

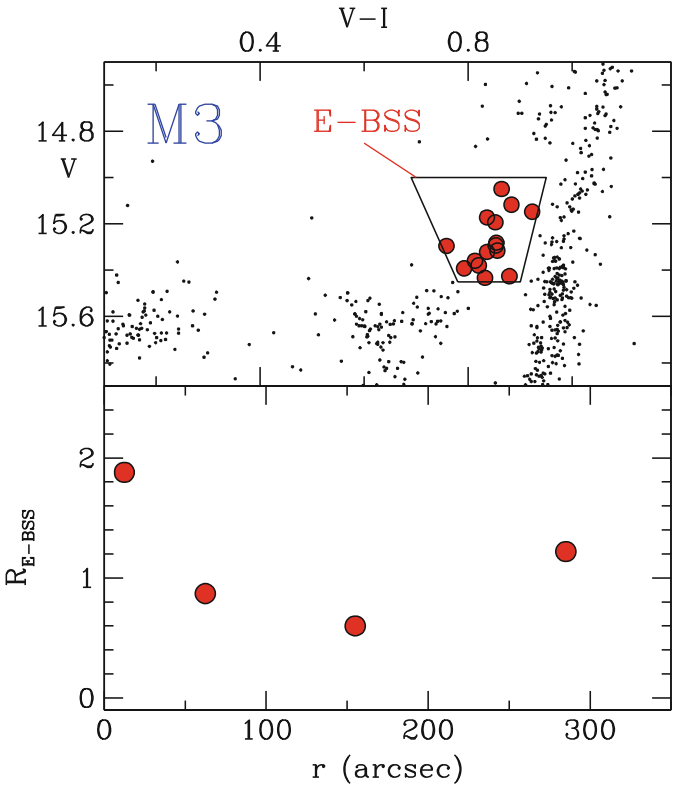

Fig. 5.14 *Upper panel*: CMD of M3 zoomed in the HB/AGB region. *Red circles* and the *box* mark the sample of candidate evolved BSSs. *Lower panel*: Double normalised ratio computed for the sample of candidate E-BSSs. A bimodality similar to that found for BSSs (see Fig. 5.9) is clearly visible. From Ferraro et al. (1997)

the ratio between the number of bright BSSs and that of E-BSSs is $N_{\rm bBSS}/N_{\rm EBSS} \approx 6.5$ in both GCs (Ferraro et al. 1997, 1999a). An approximate estimate of the lifetime ratio between BSSs (i.e., BSSs in the MS evolutionary stage) and their progeny can be obtained from the ratio between the total number of BSSs and that of E-BSSs. This turns out to range between 11 and 16, thus suggesting that we should expect 1 E-BSS ever 13 genuine BSSs. Indeed this is in very good agreement with the predictions of recent theoretical models of E-BSSs (Sills et al. 2009).

More recently, we (Beccari et al. 2006) discovered a very promising signature of the existence of BSS descendants along the AGB of 47 Tuc: a *significant excess* of stars which are *more centrally segregated* than the RGB and HB populations has been found in the AGB region of the CMD (Fig. 5.16). Within $1'$ from the cluster centre $\sim$53 "AGB stars" are counted, while only $\sim$38 such objects are predicted on the basis of the HB star number counts and the post-MS evolutionary timescales (Renzini and Fusi Pecci 1988): this makes an excess of $\sim$40 %! Because of the

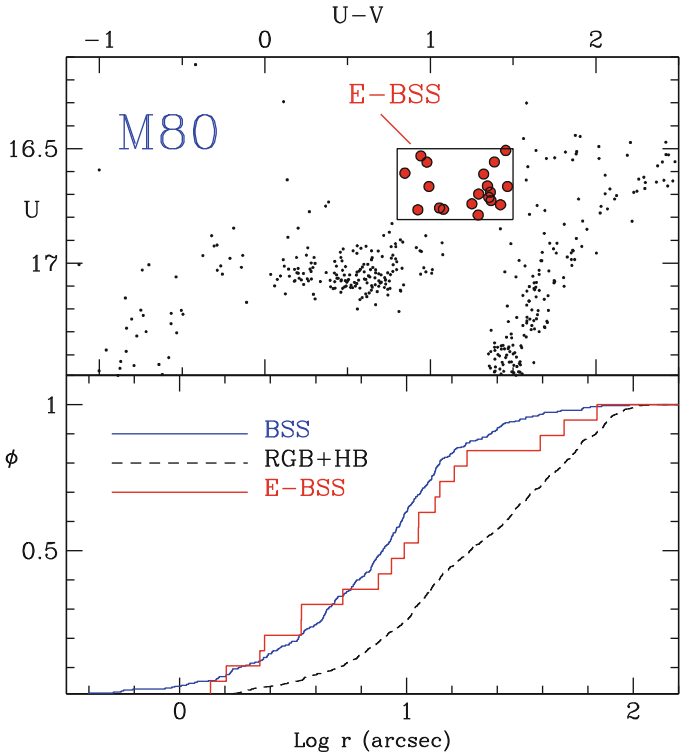

Fig. 5.15 *Upper panel*: CMD of M80 zoomed in the HB/AGB region. *Red circles* and the *box* mark the sample of candidate evolved BSSs. *Lower panel*: Cumulative radial distribution of BSSs (*blue line*), RGB + HB stars (*black dashed line*) and candidate evolved BSSs (*red line*). Clearly, E-BSSs share the same radial distribution of BSSs and are significantly more segregated than normal cluster stars (RGB and HB stars). From Ferraro et al. (1999a)

typical low stellar mass along the AGB ($M \sim 0.6\ M_{\odot}$), this feature is hardly understandable in terms of a mass segregation effect on these stars. Instead it is very likely due to a sample of more massive objects, that, given the large population of BSSs in 47 Tuc, most probably are the BSS descendants. Indeed, the comparison with theoretical tracks (Pietrinferni et al. 2006) and collisional models (Sills et al. 2009) shows that the AGB population of 47 Tuc can be significantly contaminated by stars with masses typical of BSSs (between $\sim$1.1 and $\sim$1.6 $M_{\odot}$), which are currently experiencing the first ascending RGB (Fig. 5.16).

These photometric indications are very promising. Ongoing spectroscopic follow-ups of E-BSS candidates selected in these three clusters will allow the first clear cut detection of the BSS progeny. Indeed due to their higher mass, E-BSSs are expected to be distinguishable from genuine AGB stars on the basis of their higher values of the surface gravity. Also their rotational and chemical composition will be measured, thus providing the first ever collected information about the physical

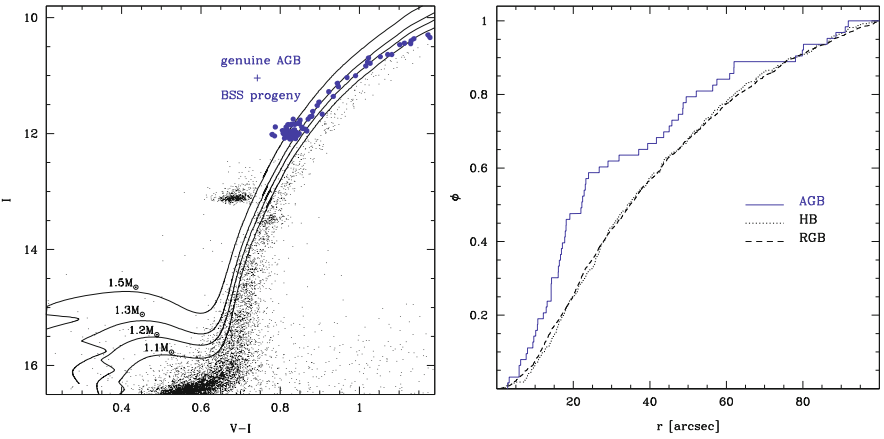

Fig. 5.16 *Left panel*: Portion of the CMD of 47 Tucanae above the MS-TO. *Blue circles* highlight the AGB population, which is suspected to be severely contaminated by a sample of E-BSSs. *Solid lines* are theoretical tracks from Pietrinferni et al. (2006) for stars with masses ranging between 1.1 $M_{\odot}$ and 1.5 $M_{\odot}$ (see labels), showing that the RGB phase of these massive objects is well superposed to the AGB sequence of the cluster. *Right panel*: Cumulative radial distribution of the AGB population, likely contaminated by E-BSSs (*blue solid line*), compared to that of HB stars (*black dotted line*) and RGB stars (*black dashed line*). Clearly, the "AGB" population is significantly more segregated than normal cluster stars, as expected if it is contaminated by more massive objects, as E-BSSs. From Beccari et al. (2006)

properties of these peculiar stars during evolutionary paths subsequent to the core hydrogen burning phase. In turn, these are new, precious ingredients for the current and future theoretical modeling of these exotica.

5.8 Chemical and Kinematical Properties of BSSs

Theoretical models still predict conflicting results on the expected properties of BSSs generated by different production channels. In fact, high rotational velocities are expected for both MT-BSSs (Sarna and de Greve 1996) and COL-BSSs (Benz and Hills 1987), but braking mechanisms like magnetic braking or disk locking have been suggested to subsequently slow down the stars, with timescales and efficiencies which are still unknown (Leonard and Livio 1995; Sills et al. 2005). Concerning the chemical surface abundances, hydrodynamic simulations (Lombardi et al. 1995) have shown that very little mixing is expected to occur between the inner cores and the outer envelopes of the colliding stars. On the other hand, signatures of mixing with incomplete CN-burning products are expected at the surface of BSSs formed via the MT channel, since the gas at the BSS surface is expected to come from deep regions of the donor star, where the CNO burning occurred (Sarna and de Greve 1996).

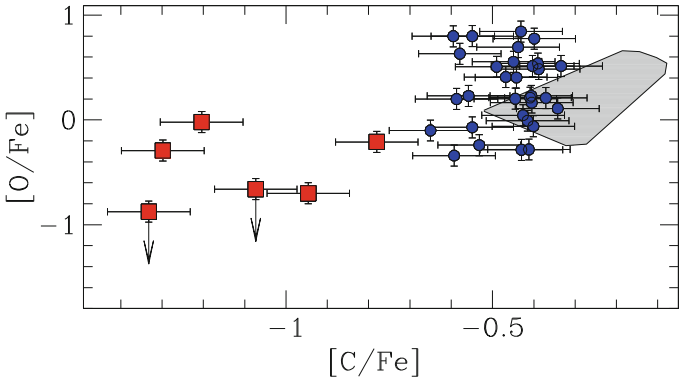

Fig. 5.17 [O/Fe] ratio as a function of [C/Fe] for the sample of 43 BSSs observed in 47 Tuc. Normal BSSs are marked with *blue circles*, while CO-depleted BSSs are marked with *filled red squares*. The *gray region* corresponds to the location of the 12 TO stars analyzed by Carretta et al. (2005). From Ferraro et al. (2006b)

Sparse spectroscopic observations provided the first set of physical properties of BSSs (effective temperature, mass, rotation velocity, etc.; see De Marco et al. 2005), but a systematic survey of basic parameters and surface abundance patterns was lacking, particularly in GCs. Recently, extensive campaigns with multiplexing spectrographs mounted at 8-m class telescopes (as *FLAMES* at the *ESO-VLT*) allowed to measure the chemical and kinematic properties for representative numbers of BSSs in a sample of Galactic GCs. The selected clusters differ in dynamical state, metallicity and density, thus providing an ideal sample for testing any possible link between the properties of BSSs and those of the host cluster. Indeed these observations represent a gold mine of information, providing the first characterisation of the structural properties of BSSs in GCs.

The first results of this search have led to an exciting discovery: by measuring the surface abundance patterns of 43 BSSs in 47 Tuc, we (Ferraro et al. 2006b) discovered a sub-population of BSSs with a significant depletion of carbon and oxygen, with respect to the dominant population (see Fig. 5.17). This evidence is interpreted as the presence of CNO burning products on the BSS surface, coming from the core of a deeply peeled parent star, as expected in the case of the MT formation channel. Thus, such a discovery in 47 Tuc could be the first detection of a chemical signature clearly pointing to the MT formation process for BSSs in a GC. Moreover, these observations have shown that (1) most of the BSSs are slow rotators; (2) the CO-depleted BSSs and the few BSSs with $v \sin i > 10$ km/s appear to be "less evolved" than the others: they all lie within a narrow strip at the faint-end of the BSS luminosity distribution in the CMD (see Fig. 5.18); (3) some of them are W UMa binaries, further suggesting that the evolution of these systems could be a viable channel for the formation of BSSs in GCs.

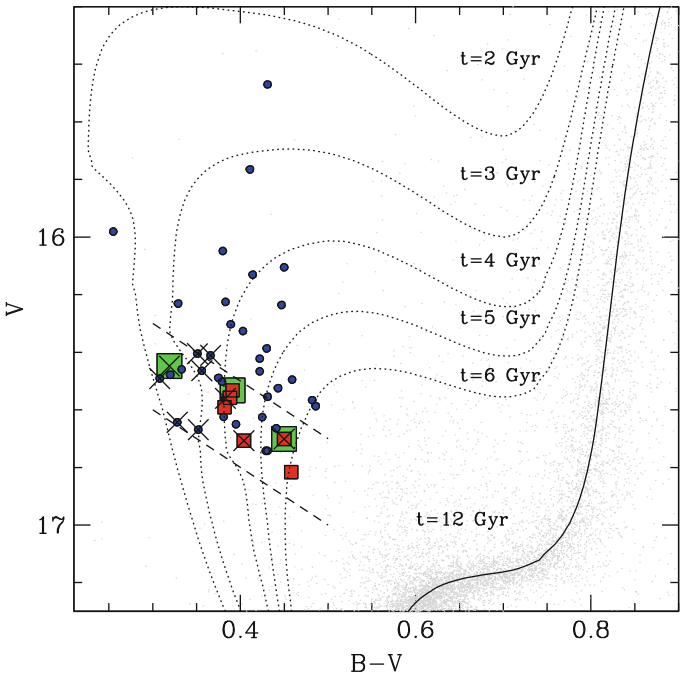

Fig. 5.18 CMD of 47 Tuc zoomed in the BSS region. BSSs showing no chemical anomalies are marked with *blue circles*, while CO-depleted BSSs are shown as *red squares*. Isochrones of different ages (from 2 to 12 Gyr) from Cariulo et al. (2003) are overplotted for comparison. The three W UMa systems and the 10 BSSs rotating with $v \sin i > 10$ km/s are highlighted with *large green squares* and *large crosses*, respectively

Which is the scenario emerging from these observations? In the early stage of mass transfer in W UMa systems (*Stage-1*), unprocessed material could be transferred and the resulting star would have normal C–O abundances (see Fig. 5.19). As the transfer continues, the accreted material could come from regions processed by the CNO cycle. Hence, first C and then both C and O would appear depleted (*Stage-2*). Thus it is possible to find depleted C, normal O BSSs/W UMa stars. After the merger, the star would appear as a CO-depleted non-variable BSS (*Stage-3*). In the sample studied in 47 Tuc, two or three BSSs are found in *Stage-2*, and 4 in *Stage-3*. The number of BSSs with CO depletion and the presence of W UMa systems show that the MT channel is active even in a high-density cluster like 47 Tuc: at least 15 % of the BSSs are being produced by MT.

The distribution of rotational velocities provide additional clues to this scenario. In fact, most BSSs in the 47 Tuc sample are slow rotators (Ferraro et al. 2006b), with velocities compatible with those measured in unperturbed TO stars (Lucatello and Gratton 2003). In particular, among the three BSSs identified as W UMa systems, one is found to be a rapid rotator and two are intermediate-slow rotators. This seems

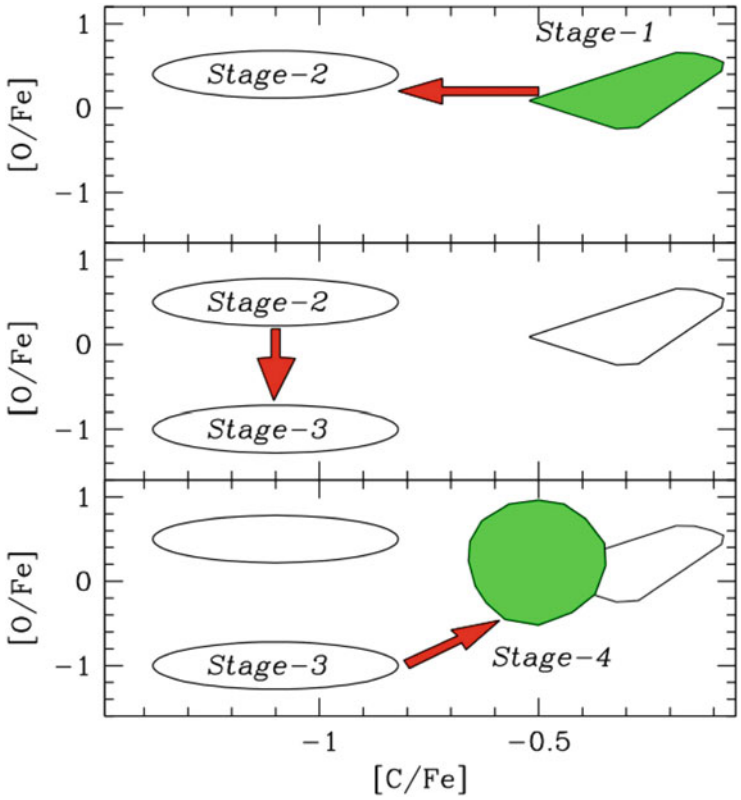

Fig. 5.19 Suggested evolution of BSSs in the [O/Fe]–[C/Fe] diagram. The four different stages discussed in the text are shown

at odds with what is expected, especially for W UMa systems which are predicted to be rapid rotators, but, of course, different inclination angles may play a role. In any case, from their location in the CMD, all the fastest BSSs are presumably the most recently born (see Fig. 5.18). This is also the region of C–O depletion and the W UMa behavior. The cooler, older BSSs rotate more slowly and have "normal" C–O abundances. Hence, this might suggest that during the evolution some mixing occurred and the rotation slows down. While rotational mixing ordinarily increases CNO anomalies, in MT-BSSs the C–O depleted material overlies the material with normal abundances and chemical anomalies are therefore reduced. C and possibly O would still below, but less so than a MT-BSS at birth (Stage-4 in Fig. 5.19). Indeed, the bulk of the 47 Tuc sample has C roughly one half of that of the TO stars (however, this could be due to systematics, since C in TO stars has been measured from different lines with respect to BSSs). Future observations will hopefully clarify this issue.

A similar study has now been extended to other clusters and up to now more than 180 BSS in 6 GCs (namely 47 Tuc, M4, NGC 6397, M30, NGC6752 and ωCen) have been observed (Ferraro et al. 2006b; Lovisi et al. 2010, 2012, 2013a; Mucciarelli et al. 2014, ApJ, submitted). Unfortunately, however, these observations provided the first observational evidence that radiative levitation affects not only HB stars hotter than 11,000 K (Quievy et al. 2009), but also BSSs hotter than $T > 8{,}000$ K (Lovisi et al. 2012). The effect is clearly traced by the value of the metallicity measured on the surface of the hottest BSSs, which is systematically and significantly larger than that of the parent cluster (Lovisi et al. 2012). Of course, in presence of radiative levitation the measured chemical abundances cannot be interpreted in the context of the BSS formation channels and the occurrence of this process in the hottest (and brightest) BSSs has *de facto* hampered the possibility of putting the result found in 47 Tuc onto a more solid statistical base. In fact the observable pool of "safe BSSs" (i.e. those cooler than 8,000 K) is quite limited in number, or too faint for the capabilities of the current generation of high-resolution spectrographs ($V \lesssim 18$–18.5). The results obtained from the few BSSs not affected by radiative levitation are the following: no chemical anomalies have been found in the sample of 11 BSSs measured in M4 (Lovisi et al. 2010), only one depleted BSS has been found in M30 (Lovisi et al. 2013b), and possibly one or two have been observed in ω Centauri (Mucciarelli et al. 2014, ApJ, submitted). Within the limitations of small number statistics, the collected data confirm that the percentage of CO-depleted BSSs is small (of the order of 10 %), thus indicating either that CO-depletion is only temporarily visible on the BSS surface (and then it is cleaned up by the subsequent evolution), or that the specific formation channel generating this feature has a limited efficiency in GCs.

A quite intriguing result seems instead to emerge from the measurement of the BSS rotational velocities: in M4, we (Lovisi et al. 2010) found that $\sim$40 % of the measured BSSs are fast rotators, with rotational velocities $v \sin i > 50$ km/s (see Fig. 5.20). *This is the largest frequency of rapidly rotating BSSs ever detected in a GC.* Interesting enough, while a similar fraction has been found in ω Cen (Mucciarelli et al. 2014, ApJ, submitted), significantly different results have been found in 47 Tuc, NGC 6397 and M30, where almost all (92–94 %) BSSs rotate slowly ($v \sin i < 20$ km/s; Ferraro et al. 2006b; Lovisi et al. 2012). These results suggest a possible correlation between the total fraction of rapidly spinning BSSs and the density of the host cluster: in fact, GCs with the largest fraction of fast rotators are also the loosest in our sample ($\log \rho_0 = 3.91$ and 3.43 in units of $M_\odot/pc^3$ for M4 and ω Cen, compared to $\log \rho_0 = 5.20$ for 47 Tuc and the very high central densities of the PCC clusters NGC 6397 and M30; McLaughlin and van der Marel 2005). The total fraction of fast rotating BSSs in the M4 + ω Cen sample is $\sim$33 %, whereas it is only $\sim$4 % in the higher-density sample of 47 Tuc+NGC 6397+M30 (see Fig. 5.21). If confirmed, this would be the first evidence of a direct link between the BSS physical properties and the characteristics of the host cluster, and it could lead to interesting scenarios never explored before. These results indicate that

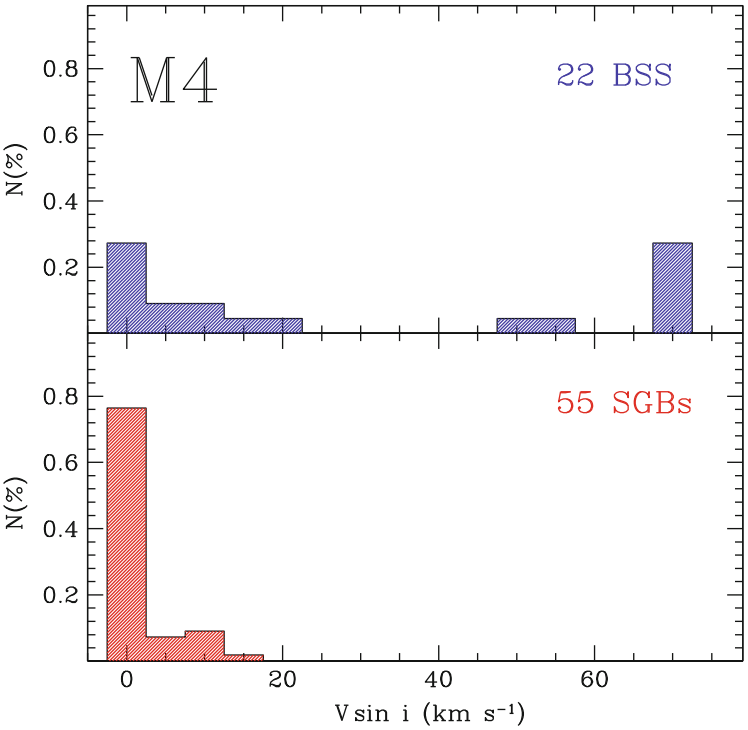

Fig. 5.20 Distribution of rotational velocities measured for 22 BSSs (*upper panel*) and 55 SGB stars (*lower panel*) in the GC M4. Six BSSs have $v \sin i \geq 70$ km/s and are all plotted in a single bin. Eight BSSs have been classified as fast rotators (i.e., with $v \sin i > 50$ km/s) and represent the largest sample (40 % of the total) of rapidly rotating BSSs ever measured in a GC. From Lovisi et al. (2010)

some braking mechanism (either magnetic braking or disk locking, as proposed by Leonard and Livio (1995) and Sills et al. (2005), or something different/additional) could somehow depend on the parent cluster environment. For instance, recurrent stellar interactions might be efficient in decreasing the BSS rotational velocities, while in loose GCs, where stellar interactions are less frequent, the initial rotational velocities of BSSs might be preserved and a larger fraction of fast rotators should be observable.

While the mystery of BSS formation is not completely solved yet, detailed photometric and spectroscopic observations of these puzzling stars are providing crucial information about their physical properties, also shedding new light on the global dynamical evolution of stellar systems.

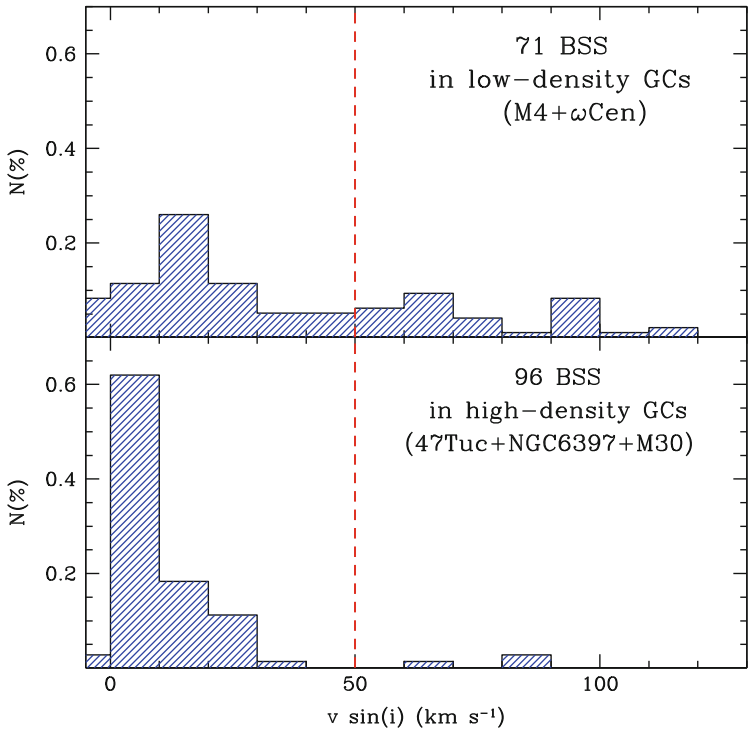

Fig. 5.21 Distribution of rotational velocities of 71 BSSs observed in low-density GCs (*upper panel*) and 96 BSSs in high-density GCs (*lower panel*). A systematic difference is apparent, possibly suggesting that some braking mechanism is active in high-density environments, while rapid rotation can last longer in low-density clusters. Adapted from Lovisi et al. (2010, 2012)

Acknowledgements Most of the results discussed in this chapter have been obtained within the project *Cosmic-Lab* (PI: Ferraro, see http://www.cosmic-lab.eu), a 5-year project funded by the European European Research Council under the 2010 *Advanced Grant* call (contract ERC-2010-AdG-267675). We warmly thank the other team members involved in this research: Giacomo Beccari, Paolo Miocchi, Mario Pasquato, Nicoletta Sanna and Rodrigo Contreras Ramos. The authors dedicate this chapter to the memory of Bob Rood, a pioneer in the theory of the evolution of low mass stars and a dear friend who shared our enthusiasm for the BSS topic and who unexpectedly passed away on 2 November 2011.

References

Anderson, J.: Omega Centauri, A Unique Window into Astrophysics, ASP 265, 87 (2002)
Auriere, M., Lauzeral, C., Ortolani, S.: Nature **344**, 638 (1990)
Bailyn, C. D.: A&ARA **33**, 133 (1995)
Beccari, G., Ferraro, F. R., Lanzoni, B., Bellazzini, M.: ApJL **652**, L121 (2006)
Beccari. G., et al.: ApJ **679**, 712 (2007)

Beccari, G., Sollima, A., Ferraro, F. R., et al.: ApJL **737**, L3 (2011)
Beccari, G., Ferraro F. R., et al.: in preparation (2014)
Benz, W., Hills, J. G.: ApJ **323**, 614 (1987)
Bolte, M., Hesser, J. E., Stetson, P. B.: ApJL **408**, L89 (1993)
Buonanno, R., Corsi, C.E., Buzzoni, A., Cacciari, C., Ferraro, F.R., Fusi Pecci, F.: A&A **290**, 69 (1994)
Cariulo, P., Degl'Innocenti, S. Castellani, V.: A&A **412**, 1121 (2003)
Carretta, E., Gratton, R. G., Lucatello, S., Bragaglia, A., Bonifacio, P.: A&A **433**, 597 (2005)
Contreras Ramos, R., Ferraro, F. R., Dalessandro, E., Lanzoni, B., Rood, R. T.: ApJ **748**, 91 (2012)
Dalessandro, E., et al.: ApJ **677**, 1069 (2008a)
Dalessandro, E., et al.: ApJ **681**, 311 (2008b)
Dalessandro, E., Ferraro, F. R., Massari, D., et al.: ApJ **778**, 135 (2013)
Davies, M. B., Piotto, G., de Angeli, F.: MNRAS **349**, 129 (2004)
De Marco, O., et al.: ApJ **632**, 894 (2005)
Djorgovski, S., Meylan, G.: Structure and Dynamics of Globular Clusters, ASP 50, 325 (1993)
Djorgovski, S., King, I. R.: ApJL **305**, L61 (1986)
Dotter, A., Sarajedini, A., Yang, S.-C.: AJ **136**, 1407 (2008)
Ferraro, F. R., Paresce, F.: AJ **106**,154 (1993)
Ferraro F. R., Pecci F. F., Cacciari C., Corsi C., Buonanno R., Fahlman G. G., Richer H. B.: AJ **106**, 2324 (1993)
Ferraro, F. R., Fusi Pecci, F., Bellazzini, M.: A&A **294**, 80 (1995)
Ferraro, F. R., et al.: Paltrinieri, B., Fusi Pecci, F., Cacciari, C., Dorman, B., Rood, R. T., Buonanno, R., Corsi, C. E., Burgarella, D., Laget, M.: A&A **324**, 915 (1997; F97)
Ferraro, F. R., Paltrinieri, B., Rood, R. T., Dorman, B.: ApJ **522**, 983 (1999a)
Ferraro, F. R., Sills, A., Rood, R. T., Paltrinieri, B., Buonanno, R. : ApJ **588**, 464 (2003)
Ferraro, F. R., Possenti, A., Sabbi, E., et al.: ApJ **595**, 179 (2003)
Ferraro, F. R., Beccari, G., Rood, R. T., Bellazzini, M., Sills, A., Sabbi, E.: ApJ **603**, 127 (2004)
Ferraro, F. R., Sollima, A., Rood, R. T., Origlia, L., Pancino, E., Bellazzini, M.: ApJ **638**, 433 (2006a)
Ferraro, F. R., et al.: ApJ **647**, L53 (2006b)
Ferraro, F. R., Beccari, G., Dalessandro, E., et al.: Nature **462**, 1028 (2009; F09)
Ferraro, F. R., Lanzoni, B., Dalessandro, E., et al.: Nature **492**, 393 (2012; F12)
Fiorentino, G., Lanzoni, B., Dalessandro, E., Ferraro, F. R., Bono, G., Marconi, M.: ApJ **783**, 34 (2014)
Fusi Pecci, F., Ferraro, F. R., Corsi, C. E., Cacciari, C., Buonanno, R.: ApJ **104**, 1831 (1992)
Guhathakurta, P., Yanny, B., Bahcall, J. N., Schneider, D. P.: ApJ **108**, 1786 (1994)
Gilliland, R. L., Bono, G., Edmonds, P. D., et al.: ApJ **507**, 818 (1998)
Heggie, D. C., Giersz, M.: MNRAS **389**, 1858 (2008)
Hills, J. G., Day, C. A.: ApJL **17**, 87 (1976)
Jordi, K., Grebel, E. K., Hilker, M., et al.: AJ **137**, 4586 (2009)
Knigge, C., Leigh, N., Sills, A.: Nature **457**, 288 (2009)
Lanzoni, B., Dalessandro, E., Ferraro, F. R., Mancini, C., Beccari, G., Rood, R. T., Mapelli, M., Sigurdsson, S.: ApJ **663**, 267 (2007a)
Lanzoni, B., et al.: ApJ **663**, 1040 (2007b)
Lanzoni, B., et al.: ApJ **670**, 1065 (2007c)
Lanzoni, B., Dalessandro, E., Ferraro, F. R., et al.: ApJL **668**, L139 (2007)
Lanzoni, B., Mucciarelli, A., Origlia, L., et al.: ApJ **769**, 107 (2013)
Leigh, N., Sills, A., Knigge, C.: ApJ **661**, 210 (2007)
Leigh, N., Sills, A., Knigge, C.: MNRAS **415**, 3771 (2011)
Leigh, N., Knigge, C., Sills, A., et al.: MNRAS **428**, 897 (2013)
Leonard, P. J. T., Livio, M.: ApJL **447**, 121 (1995)
Lombardi, J. C. Jr., Rasio, F. A., Shapiro, S. L.: ApJL **445**, 117 (1995)
Lovisi, L., Mucciarelli, A., Ferraro, F. R., et al.: ApJL **719**, 121 (2010)
Lovisi, L., Mucciarelli, A., Lanzoni, B., et al.: ApJ **754**, 91 (2012)

Lovisi, L., Mucciarelli, A., Dalessandro, E., Ferraro, F. R., Lanzoni, B.: ApJ **778**, 64 (2013a)
Lovisi, L., Mucciarelli, A., Lanzoni, B., Ferraro, F. R., Dalessandro, E., Monaco, L.: ApJ **722**, 148 (2013b)
Lucatello, S., Gratton, R.G.: A&A **406**, L691 (2003)
Mapelli, M., Sigurdsson, S., Colpi, M., Ferraro, F. R., Possenti, A., Rood, R. T., Sills, A., Beccari, G.: ApJL **605**, 29 (2004)
Mapelli, M., Sigurdsson, S., Ferraro, F. R., Colpi, M., Possenti, A., Lanzoni, B.: MNRAS **373**, 361 (2006)
Mapelli, M., Ripamonti, E., Battaglia, G., et al.: MNRAS **396**, 1771 (2009)
Marín-Franch, A., Aparicio, A., Piotto, G., et al.: ApJ **694**, 1498 (2009)
Mathieu, R. D., Geller, A. M.: Nature **462**, 1032 (2009)
McCrea, W. H.: MNRAS **128**, 147 (1964)
McLaughlin, D. E., van der Marel, R. P.: A&A **161**, 304 (2005)
Meylan, G., Heggie, D. C.: A&A Rev. **8**, 1 (1997)
Milone, A. P., Piotto, G., Bedin, L. R., et al.: A&A **540**, A16 (2012)
Monelli, M., Cassisi, S., Mapelli, M., et al.: ApJ **744**, 157 (2012)
Moretti, A., de Angeli, F., Piotto, G.: A&A **483**, 183 (2008)
Mucciarelli A., Lovisi L., Ferraro F. R., Dalessandro E., Lanzoni B., Monaco L.: ApJ submitted (2014)
Paresce, F., Meylan, G., Shara, M., et al.: Nature **352**, 297 (1991)
Pietrinferni, A., Cassisi, S., Salaris, M., Castelli, F.: ApJ **642**, 797 (2006)
Piotto, G., et al.: ApJ **604**, L109 (2004)
Quievy, D., Charbonneau, P., Michaud, G., Richer, J.: A&A **500**, 1163 (2009)
Renzini, A., Fusi Pecci, F.: A&ARA **26**, 199 (1988)
Sabbi, E., Ferraro, F. R., Sills, A., Rood, R. T.: ApJ **617**, 1296 (2004)
Sandage A. R.: AJ **58**, 61 (1953)
Sarajedini, A.: Blue Stragglers, ASP **53**, 14 (1993)
Sarajedini, A., Bedin, L. R., Chaboyer, B., et al.: AJ **133**, 1658 (2007)
Sarna, M. J., de Greve, J. P.: QJRAS **37**, 11 (1996)
Shara, M. M., Saffer, R. A., Livio, M.: ApJ **489**, L59 (1997)
Sigurdsson, S., Davies, M.B., Bolte, M.: ApJL **431**, 115 (1994)
Sills, A., Adams, T., Davies, M. B.: MNRAS **358**, 716 (2005)
Sills, A., Karakas, A., Lattanzio, J.: ApJ **692**, 1411 (2009)
Sollima, A. et al.: A&A **481**, 701 (2008)
Tian, B., Deng, L., Han, Z., Zhang, X. B.: A&A **455**, 247 (2006)
Warren, S. R., Sandquist, E. L., Bolte, M.: ApJ **648**, 1026 (2006)
Zaggia, S. R., Piotto, G. Capaccioli M.: A&A **327**, 1004 (1997)
Zinn, R., Searle, L.: ApJ **209**, 734 (1976)

Chapter 6
The Blue Straggler Population in Dwarf Galaxies

Yazan Momany

6.1 Introduction

6.1.1 Blue Stragglers in Globular Clusters

Ever since their first identification in M3 by Sandage (1953), the term *Blue Stragglers* (BSS) refers to the population of stars that are relatively brighter and bluer than the cluster's main sequence (MS) turn-off point. Several decades after, globular clusters remain the ideal environment where BSS can be identified with certain *ease*. Indeed, the family of Galactic globular clusters typically shows a turn-off mass of $\sim$0.8 $M_{\odot}$, being mostly coeval and $\gtrsim$ 10 Gyr old (Marín-Franch et al. 2009). Thus, the identification of a $\sim$1.2–1.5 $M_{\odot}$ hot stellar population, *nowadays*, is unexpected since such high mass stars would have evolved already in a $\gtrsim$10 Gyr system; thereafter the *"straggler"* term.

In the context of globular clusters studies the last decade has brought a new wave of interest in these presumably *dead systems* (see Chap. 5). In particular, thanks to the accumulating evidence of: (a) systematic chemical abundance anomalies (Carretta et al. 2009); coupled with (b) detection of multiple and discrete red giant branches and/or main sequences (Milone et al. 2013), the idea that multiple stellar populations coexist within *a* single cluster is taking the upper hand (Renzini 2013). This clearly defies the old text-book definition of globular clusters (i.e. *ancient, coeval and chemically homogeneous systems*).

For what concerns the BSS identification in globular clusters one may wonder if admitting the multiple populations scenario would leave some space for the presence

Y. Momany (✉)
European Southern Observatory, Alonso de Cordova 3107, Santiago, Chile

INAF, Oss. Astronomico di Padova, Vicolo dell'Osservatorio 5, 35122 Padova, Italy
e-mail: ymomany@eso.org

H.M.J. Boffin et al. (eds.), *Ecology of Blue Straggler Stars*, Astrophysics and Space Science Library 413, DOI 10.1007/978-3-662-44434-4_6

of a "young" population (BSS), the answer is *no*. Indeed, and based on our current understanding, the complexity of multiple epochs of star formation within globular clusters is always limited to the first $\lesssim$1 Gyr since the formation epoch of the cluster (some $\sim$13 Gyr time ago). Thus, and despite these chemical anomalies and multiple generations of stars, there is still no room to accommodate for the presence of a 1.2–1.5 $M_{\odot}$ hot/blue stellar population (i.e. BSS) within the *standard single-star* evolution in globular clusters.

The origin of the BSS is usually sought as either the products of (a) dynamical interactions; or (b) binary evolution (see Chap. 5). The dynamical origin for BSS foresees a *continuous* production of collisional binaries (Hills and Day 1976) between single and/or binary MS stars throughout the life of the stellar system. On the other hand, the most likely BSS formation scenario is that involving binary evolution. In this case the origin of the fresh hydrogen that "rejuvenates" the BSS is mass transfer (McCrea 1964). In particular, mass transfer occurs when the evolved primary (now invisible) fills its Roche lobe and processed material overflows to the secondary MS (which *now* constitutes the BSS visible component). Within the binary evolution scenario, BSS can also be formed via the coalescence of a binary system made by two "normal" MS stars at the TO level.

6.1.2 The Importance of Dwarf Galaxies

Dwarf galaxies represent the dominant population, by number, of the present-day universe and galaxy clusters. These low-mass galaxies are *not* simply scaled-down versions of giant systems. Indeed, they hold the keys for a deeper understanding of galaxy formation, chemical evolution, star formation processes and dark matter content. In the framework of hierarchical clustering scenarios such as in cold dark matter models (Blumenthal et al. 1984) dwarf galaxies would have been the first objects to be formed, that would later contribute to the assembling of larger systems (White and Rees 1978). The resultant picture is one in which the dwarfs observed nowadays are those which survived merging events. There are a number of factors that contribute to making the Local Group ($d \lesssim 1.1$ Mpc) a unique laboratory for astronomers; first its dwarf members are close enough to enable determining age, metallicity and their star formation histories from their *resolved stellar populations*. Second, the Local Group comprises dwarf galaxies of such variety of morphological types, masses, ages, spatial distributions and metallicities that they are statistically representative of other dwarf populations present in other environments, nearby groups or clusters. The two aforementioned properties qualify dwarf galaxies as optimal cases for "*near-field cosmology*".

When studying the Blue Stragglers properties in the resolved stellar populations of nearby dwarf galaxies one soon realises a basic limitation: a meaningful analysis is possible only for those galaxies whose imaging surveys reach at least $\sim$1 magnitude below the old main-sequence turnoff level. Consequently, the current sample of "*useful*" Local Group dwarf galaxies is limited to systems within $D_{\odot} \approx 900$ kpc,

where the upper limit is set by the Tucana *dwarf spheroidal* galaxy survey by the *Hubble Space Telescope*. Nevertheless, one should appreciate that addressing the BSS population in such a distant system implies availing a photometric catalogue with a reasonable photometric completeness level at $I \approx 29.0$, which is a major challenge already.

6.1.3 Dwarf Galaxies vs Globular Clusters

It is important to recall that the *fuzzy*, almost featureless dwarf galaxies still represent a different class of objects on their own, which is fundamentally different from that of globular clusters. Misgeld and Hilker (2011) searched for *Fundamental Plane* relations for systems ranging from faint galaxies and star clusters of only a few hundred solar masses up to giant ellipticals 10^{12} $M_\odot$. Their analysis (see Fig. 6.1) shows a clear dichotomy between the *galaxy* and *star cluster* family. It is straightforward to qualify globular clusters as members of the *star cluster* family,

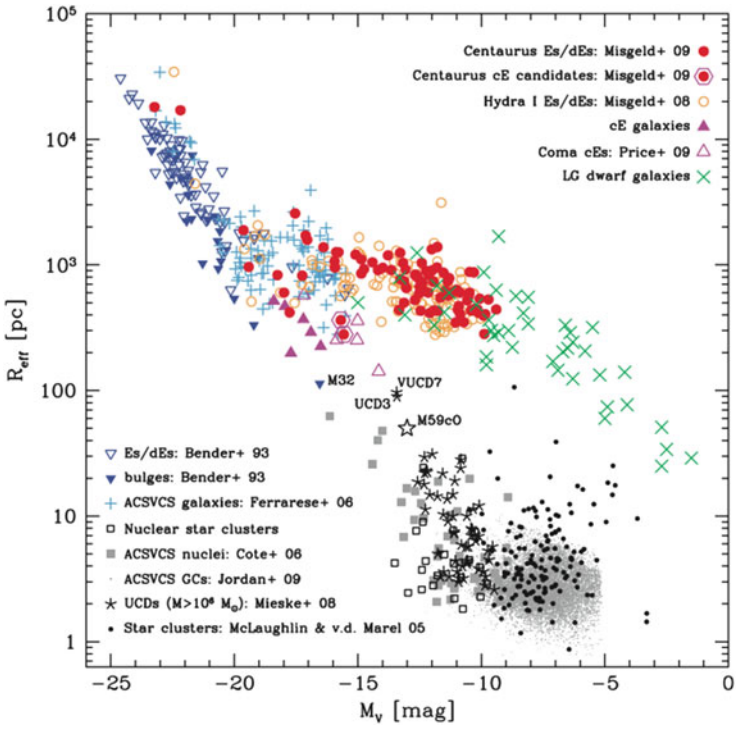

Fig. 6.1 The effective radius (R_{eff}[pc]) *vs* absolute V-band magnitude (M_V) for the family of stellar systems covering a range of ten magnitudes in mass. This figure is reproduced from Misgeld and Hilker (2011) with permission by the RAS

and that dwarf galaxies occupy the faint tail of the galaxy group. In particular, and over several orders of magnitudes ($-10 \lesssim M_V \lesssim -5$), the typical effective radius of globular clusters (∼3–10 pc) and dwarf galaxies (few hundreds to ∼1,000 pc) does not vary significantly with mass.

One may argue that the faintest dwarf galaxies reach low effective radii that are *too close* to typical values of the clusters group, thereby defying the *galaxy* definition. Clearly, these are not *ordinary* dwarf galaxies (e.g. Segue I has $M_V \sim -1.5$ and a $M/L \sim 3{,}000$) rather they probably represent a class of objects losing dynamical equilibrium and close to disruption (Gilmore et al. 2007; Niederste-Ostholt et al. 2009). Nevertheless, these ultra-faint dwarfs (whose total luminosities can be less than that of individual red giants) show kinematic and metallicity evidence that unambiguously support the dwarf galaxy classification (Willman and Strader 2012) and as such their BSS population (when present) should be included in any review. This is particularly, important because the sample of ultra-faint dwarfs is expected to rise thanks to forthcoming Southern hemisphere surveys (e.g. *Skymapper*[1]; Keller et al. 2012).

6.2 BSS Identification in Dwarf Galaxies

Colour-magnitude diagrams of typically old dwarf spheroidal galaxies show the presence of a well-separated blue plume of stars that very much resembles an old BSS population, as that observed in globular and open clusters (see the early studies of Mateo et al. 1991, 1995). However, in the context of dwarf galaxies one cannot exclude that blue plume stars may include genuinely young main sequence (MS) stars, i.e. a residual star forming activity. The BSS–young MS ambiguity is simply a hard quest (see discussions in Hurley-Keller et al. 1998; Aparicio et al. 2001; Carrera et al. 2002).

Photometric techniques like the $(U - B)$, $(B - V)$ colour–colour diagram are widely used for Galactic Halo BSS and horizontal branch (HB) studies. Respectively, the two colours are proxies for metallicity and temperature and are useful in separating Halo BSS from blue horizontal branch stars. This technique, however, is not necessary for dwarf galaxies studies, because the dwarf galaxies stellar populations are basically projected at the same distance from us. Thus the disentangling of the BSS population in dwarf galaxies relies entirely on the colour-magnitude diagram (as is the case for Galactic globular and open clusters), and consists of a selection region within certain luminosity and colour boundaries.

The luminosity function of BSS in globular clusters has been found to increase from a luminosity cutoff at $M_V \sim 1.9$ down to $M_V \sim 4.0$, at the ancient MS turn-off level (Fusi Pecci et al. 1992) while the temperature of BSS are between ∼6,000–7,500 K. An examination of Fig. 6.2 shows that the colour and luminosity

[1] http://rsaa.anu.edu.au/observatories/siding-spring-observatory/telescopes/skymapper.

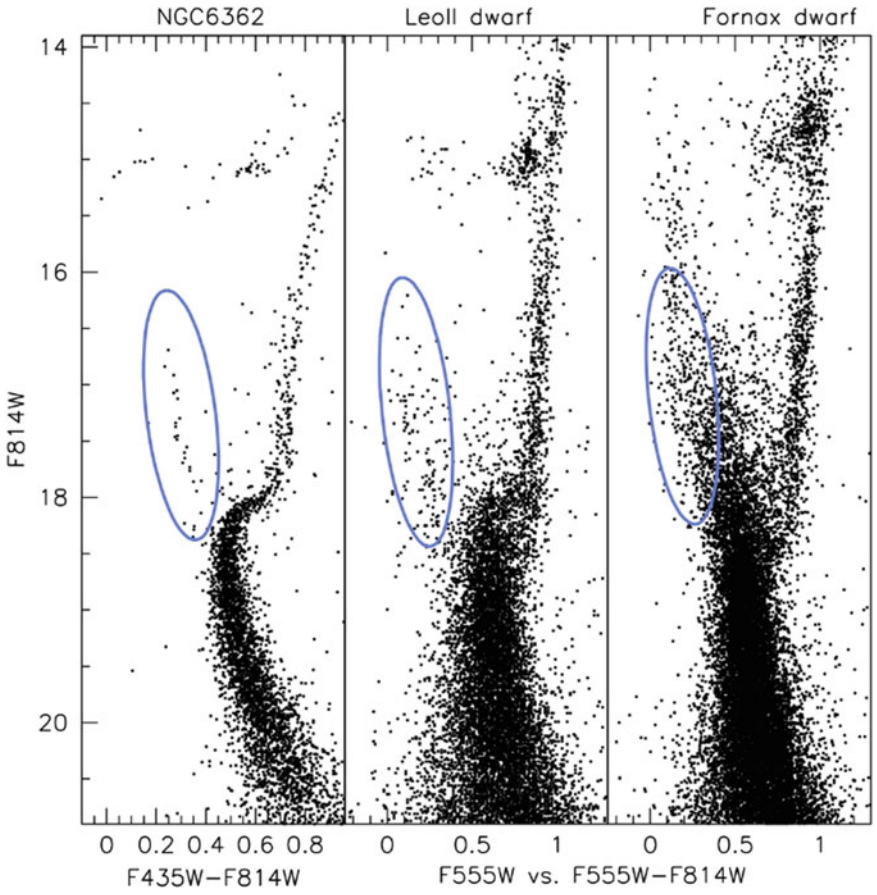

Fig. 6.2 From *left* to *right the panels* show the colour-magnitude diagram of NGC 6362 (Piotto et al. 2002), Leo II dwarf galaxy (Held 2005), and Fornax dwarf galaxy (Holtzman et al. 2006). The ellipse approximately traces the BSS region in NGC 6362 and Leo II, whereas for the Fornax dwarf contamination by the young stars forbids reliable BSS estimates

extensions of the Leo II blue plume population falls within the BSS limits in globular clusters. On the other hand, the right panel of Fig. 6.2 summarises the *BSS–young stars* ambiguity in dwarf galaxies. The Fornax dwarf galaxy is known to host a recent star formation episode, that occurred some 200 Myr ago (Saviane et al. 2000), and the diagram from the *HST* survey (Holtzman et al. 2006) shows that in such cases one *cannot* properly reach the ancient MS turn-off level without the inclusion of contaminant young stars. Thus, the selection of a dwarf galaxies sample for BSS studies must filter out all those galaxies that *do not* allow a clear detection of the ancient MS turn-off level.

In this regards, one should bear in mind that the fainter end of the BSS sequence extends to $\sim$0.6 magnitude *below* the ancient MS turn-off level (e.g. the case of

M55 by Mandushev et al. 1997). Given the small number statistics of the BSS stars in dwarf galaxies, we caution that a conservative BSS selection region (i.e. a bright $M_V \sim 3.0$ cutoff that does not reach the ancient main sequence turn-off level) would heavily under-estimate the BSS frequency in dwarf galaxies. For example, Mapelli et al. (2007) (using a conservative BSS selection regions) derive a fraction of HB stars over BSS of $F_{HB}^{BSS} = log(N_{BSS}/N_{HB}) \approx -0.65$ for the Draco and Ursa Minor dwarf galaxies. This is well below the value derived in Momany et al. (2007) of $F_{HB}^{BSS} \approx +0.1$, based, however, on deeper and more complete photometric catalogues that allowed reaching the oldest turn-off level. We note that our BSS frequencies (Momany et al. 2007) for the two galaxies were recently confirmed by Zhao et al. (2012) (see also the discussion in Clarkson et al. 2011). Admittedly however, there exists no standardised selection process ultimately defining the BSS selection region for dwarf galaxies, and much is left to the discretion of the investigators.

6.2.1 The BSS Identification in the Galactic Halo

The low-density environment of dwarf galaxies is very similar to that of the Galactic Halo, hence it is no surprise that a comparison between their BSS populations is made. In the absence of kinematic and chemical studies of BSS in dwarf galaxies, the comparison to the Galactic Halo BSS properties is limited only to the BSS specific frequency. In this regards, it is worth to spend a few words on the identification of the Galactic Halo BSS. The chapter by Preston (Chap. 4) reports a detailed presentation of the (a) photometric; (b) spectro-photometric; and (c) spectroscopic criteria used to extract and *disentangle* the BSS from the horizontal branch population. The spectroscopic survey by Preston and Sneden (2000) remains a reference point for Milky Way field *blue metal-poor* (BSS) studies, and they conclude that over 60 % of their sample is made up by binaries, and that at least 50 % of their blue metal-poor sample are BSS. We all refer to their results for the BSS frequency in the Galactic Halo: $N_{BSS}/N_{BHB} = 4$.

The Halo BSS frequency however has been derived relying on a composite sample of only 62 blue metal-poor stars that are: (a) distributed at different line of sights; (b) at different distances; and most importantly, (c) for which no observational BSS-HB star-by-star correspondence can be established (see also Ferraro et al. 2006). Most importantly, one has to bear in mind that the normalised horizontal branch population is limited to the blue HB *only*, as these are the only HB component that can be disentangled from the Thin/Thick Disc population. On the other hand, the majority of BSS frequency studies for globular clusters and dwarf galaxies refer to the *entire* HB population, i.e. including the blue, the variable and the red components of the HB. Consequently, one has to bear in mind that the adopted $log(N_{BSS}/N_{BHB}) \approx 0.6$ value for the Galactic Halo is actually a *high* upper limit, as indeed the inclusion of red horizontal branch stars would lower this value. Indeed, a simple check of the M31 Halo stellar populations, as recently

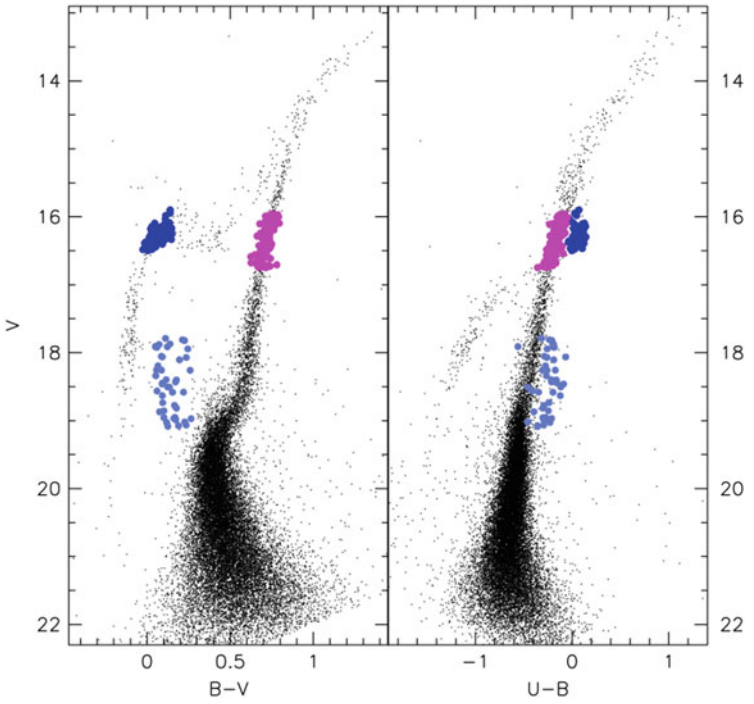

Fig. 6.3 *HST* colour-magnitude diagrams of NGC 7078 in the F336W, F439W and F555W filters, showing a selection of BSS, horizontal and red giant branch populations. The *right panel* shows the same selection in the $(U - B)$ plane, highlighting how the BSS and horizontal branch stars (sharing almost the same temperature) display the so-called *red-incursion* (Momany et al. 2003), which is an instrumental effect

surveyed by the Hubble space telescope, shows a conspicuous red horizontal branch population (see Fig. 2 in Brown et al. 2008). Clearly, one has to account for differences in the star formation and chemical enrichment histories of the two spiral galaxies, nevertheless the Halo stellar populations of the two galaxies cannot be very dissimilar.

Lastly, we point to an often neglected effect when surveying the Galactic Halo for BSS populations. Figure 6.3 displays the HST colour-magnitude diagram of NGC 7078. The left panel shows a typical selection of BSS, HB, and RGB populations and these are later searched in the V, $(U - B)$ plane (right panel). The later diagrams shows the un-expected and un-physical feature (the so-called *red-incursion,* see Momany et al. 2003) where blue HB stars *can* appear redder than their red giant equivalents. This feature has been explained as due to a particular dependence of the adopted U filter (in any given photometric system) and whether it encompasses the Balmer jump. Figure 6.3 shows that the *red-incursion* affects also the BSS population, which ends up at redder colours with respect to red giants at the same luminosity level. The occurrence and extent of the *red-incursion* shows a

dependence of the employed U and B filters on the star's effective temperature, gravity, and metallicity. In particular, the *red-incursion* is stronger (i.e. shows *redder* extent) for lower metallicities stars (see Fig. 5 of Momany et al. 2003). Thus, photometric techniques employing U, B filters for BSS and HB surveys in the Galactic Halo should take this into account.

6.3 BSS Specific Frequency in Dwarf Galaxies

6.3.1 The Dwarf Galaxies Sample

The large on-sky projection of the closest dwarf galaxies and the faintness of the BSS in the distant ones preclude the availability of *a single homogeneous and large-area* photometric data-set addressing the BSS population. Although a significant effort has been devoted to such purpose (e.g. the HST/WFPC2 archival survey by Holtzman et al. 2006) the small field of view of the HST may veil some important spatial distribution gradients of specific stellar populations. For example the Leo I *HST* study of Gallart et al. (1999) did not show the presence of the blue horizontal (HB) branch population, and this led to the conclusion that LeoI might have delayed its first epoch of star formation. However, a *wide-area* coverage by Held et al. (2000) *did* reveal a conspicuous, ancient, HB population. Thus, in the context of BSS studies, spatial distribution gradients are important and should be to accounted for by wide-area surveys.

For example, the largest available catalogue for the Sagittarius dwarf galaxy is that of Monaco et al. (2003), covering $\sim 1^\circ$ square degree. However, the Sagittarius dwarf has a core radius of $\sim 3.7^\circ$, thus the above-mentioned catalogue (Monaco et al. 2003) covers only $\sim 3.5\,\%$ of the galaxy, or $\sim 6\,\%$ of its stellar populations. Hence, any estimate of its BSS frequency is to be taken with caution, especially that the inner $\sim 14' \times 14'$ region has to be excluded to account for the coincidence of the galaxy's centre with the position of its globular cluster M54. Moreover, a delicate aspect of estimating the BSS frequency involves estimating the Galactic foreground/background contribution in the covered area. This is particularly important for galaxies in certain line of sights (e.g. the Sagittarius dwarf suffering severe Galactic Bulge contamination). To estimate the Galactic contribution in a homogeneous way the *TRILEGAL* code (Girardi et al. 2005) was used. This online tool provides synthetic stellar photometry of the Milky Way components (Disc, Halo, and Bulge), and star counts were performed on the simulated diagrams (using the same selection boxes) and these subtracted from the observed HB and BSS star counts for the dwarf galaxies.

There are 12 dwarf galaxies for which a reliable BSS frequency could be determined. The basic properties of the selected galaxies (taken from Mateo 1998; McConnachie 2012) are summarised in Table 6.1, and respectively report the absolute visual magnitude, the absolute distance modulus, the reddening, the central

Table 6.1 Basic properties of dwarf galaxies for which the BSS frequency could be reliably derived

Name	M_V	$Log(F_{HB}^{BSS})$	$\sigma_{Log(F_{HB}^{BSS})}$	$(m-M)_\circ$	$E_{(B-V)}$	μ_V(mag/□″)	$r_h(')$	$M_\star(10^6 M_\odot)$
Bootes	−5.8	0.26	0.15	18.9	0.000	28.05	12.6	0.029
Ursa Major	−6.8	0.20	0.18	17.1	0.150	27.80	11.3	0.014
Draco	−8.6	0.09	0.15	19.5	0.030	25.30	10.0	0.290
Ursa Minor	−8.9	0.13	0.13	19.0	0.030	25.50	8.2	0.290
Sextans	−9.5	0.05	0.12	19.7	0.040	26.20	27.8	0.440
Sculptor	−9.8	0.01	0.13	19.7	0.000	23.70	11.3	0.230
LeoII	−10.1	−0.01	0.09	21.6	0.030	24.00	2.6	0.740
Sagittarius	−13.5	−0.26	0.26	17.1	0.150	25.40	342.0	21.00
Cetus	−10.1	0.05	0.05	24.5	0.030	25.00	3.2	2.600
Tucana	−9.5	0.02	0.04	24.7	0.030	25.00	1.1	0.560
Leo IV	−5.0	0.49	0.16	20.9	0.026	27.50	4.6	0.019
Hercules	−6.4	0.21	0.17	20.6	0.063	27.20	8.6	0.037

V surface brightness, the core and half-light radius and the stellar mass of the galaxy. The BSS specific frequency—calculated as $F_{HB}^{BSS} = \log(N_{Bss}/N_{HB})$—is reported in column 3. We emphasise that: (a) photometric incompleteness corrections; (b) foreground/background subtraction; (c) possible overlap between old and intermediate age stellar population around the HB level; and (d) confusion between BSS and normal MS stars, are *unavoidable* sources of error that affect any analysis addressing the BSS frequency in dwarf galaxies. The reported error bars (reported in column 4) account for the propagation of the Poisson errors on the star counts, but mostly reflect the dependence on the uncertainty in properly defining the HB and BSS selection boxes. In particular, the reported BSS specific frequency have been either taken directly from the literature (as is the case for the Cetus and Tucana dwarf galaxies, Monelli et al. 2012) or from estimates based on photometric catalogues made available for the following objects: (a) Sextans (Lee et al. 2003); (b) Ursa Minor (Carrera et al. 2002); (c) Sculptor (Rizzi et al. 2003b); (d) Ursa Major by Willman et al. (2005); (e) Bootes (Belokurov et al. 2006); (f) Sagittarius by Monaco et al. (2003); (g) Leo II (Held 2005); (h) Draco (Aparicio et al. 2001); and (i) Leo IV and Hercules by Milone (*priv. comm.*, based on *HST* diagrams).

6.3.2 The F_{HB}^{BSS}–M_V Anti-correlation

For a wider perspective on the BSS specific frequency in dwarf galaxies, a comparison is made with that derived for Galactic globular and open clusters. Of the original compilation of BSS in Galactic open cluster by de Marchi et al. (2006) we filter out clusters for which less than two BSS stars were found. On the other hand, the original compilation of ∼3,000 BSS in 56 Galactic globular clusters by Piotto et al. (2004) was complemented by BSS frequencies for three interesting

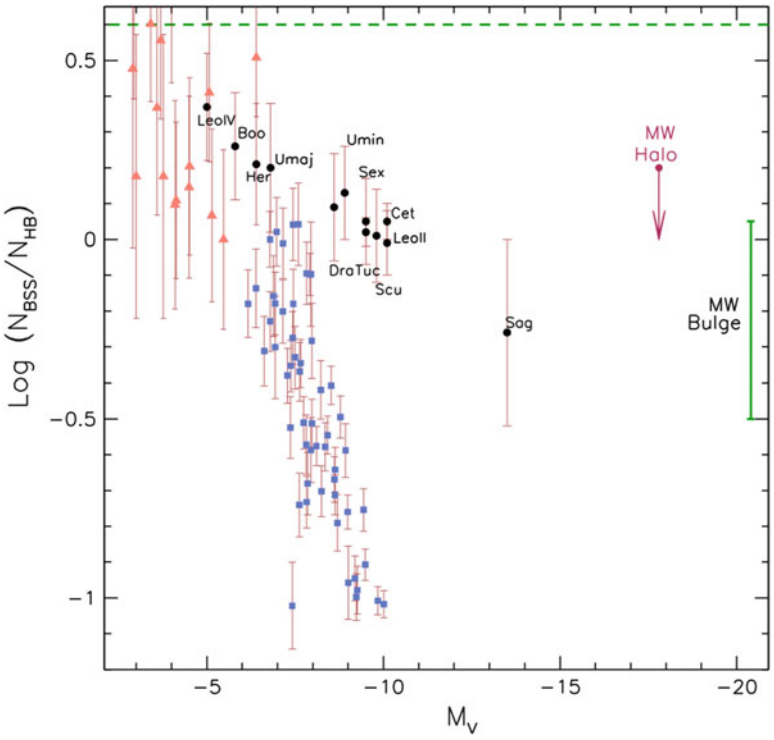

Fig. 6.4 The BSS frequency (F_{HB}^{BSS}) *vs* M_V diagram for globular clusters (Piotto et al. 2004), open clusters (de Marchi et al. 2006), and dwarf galaxies (Momany et al. 2007). The *horizontal line* shows the mean BSS frequency as derived for the Milky Way field stars by Preston and Sneden (2000). The range of the BSS frequency for the Milky Way Bulge (Clarkson et al. 2011) is shown as a bar at $M_V = -20.4$. A preliminary *upper limit* for the Milky Way Halo BSS frequency (as normalised to *only* the blue horizontal branch stars) is shown at $M_V = -17.8$

additional clusters, namely: (a) NGC 1841 (Saviane et al. 2003), which is the Large Magellanic Cloud (LMC) most metal-poor and most distant (10 kpc from the LMC bar) cluster; (b) NGC 2419, which is a massive Milky Way cluster at 90 kpc from the Galactic centre, suspected to be a dwarf galaxy; and (c) ω Cen, which is the most enigmatic Milky Way cluster, also suspected to be an extra-Galactic dwarf galaxy. The three data-points are based on deep *HST*/ACS, WFPC2 and ACS archival data, respectively. Focusing our attention only on the BSS frequency of Galactic globular cluster, in particular for the three additional clusters, Fig. 6.4 shows that the so-called F_{HB}^{BSS}–M_V anti-correlation (Piotto et al. 2004; Davies et al. 2004) is basically *universal* for all globular clusters, regardless of their specific complexity and origin. The observed anti-correlation implies that more massive globular clusters are surprisingly BSS-deficient, as if their high collision rate had no correlation with the production of collisional binaries. In particular, the F_{HB}^{BSS}–M_V anti-correlation was explained by Davies et al. (2004) (see also Mapelli et al. 2004,

2006) in the following manner: the number of BSS produced via collisions tends to increase with cluster mass, becoming the dominant formation channel for clusters with $M_V \leq -8.8$. On the other hand, the BSS number originating from primordial binaries should decrease with increasing cluster mass. Accounting for these two opposite trends and binary evolution, the models by Davies et al. (2004) reproduce the observed BSS population, whose total number seems independent of the cluster mass.

When plotting the BSS frequency in dwarf galaxies, Fig. 6.4 shows the following general trends: (a) dwarf galaxies with $M_V \leq -8.0$ possess a relatively higher BSS frequency with respect to globular clusters with similar luminosities; and (b) the lowest luminosity dwarf galaxies with $-8.0 \leq M_V \leq -5.0$ show BSS frequencies that are fully compatible with that observed in open clusters. This compatibility between dwarf galaxies and open clusters may suggest that there exists a "saturation" in the BSS frequency (at $F_{HB}^{BSS} \approx 0.3 - 0.4$) for the lowest luminosity systems (both for open clusters and dwarf galaxies). In this regards, we note that the globular clusters distribution shows an abrupt cut at $M_V \sim -6.0$. This is only a selection effect, and we remind the reader that there are a dozen of clusters with $M_V \gtrsim -6.0$ that were not included in the Piotto et al. (2004) survey. It is of great importance to fill this gap and test the hypothesis that all stellar systems show a saturation of the BSS frequency at $F_{HB}^{BSS} \approx 0.3 - 0.4$.

There is a hint of such *universal upper limit* in the study by Sollima et al. (2008) who derive high BSS frequencies for three clusters with $M_V \approx -5.0$. Similarly, Santana et al. (2012) derive high BSS frequencies for the faintest tail of the globular clusters at $M_V \approx -5.0$. Unfortunately, these clusters could not be added to Fig. 6.4 because Sollima et al. (2008) normalised their BSS star counts with respect to the main sequence stars, while the study of Santana et al. (2012) used the red giant branch stars.

Overall, the dwarf galaxies sample shows a hint of a proper F_{HB}^{BSS}–M_V anti-correlation. In (Momany et al. 2007), and relying on a smaller sample of 8 galaxies, the statistical significance of a F_{HB}^{BSS}–M_V anti-correlation was explored, and the probability that a random sample of uncorrelated experimental data points would have yielded a linear-correlation coefficient of 0.984 was found to be extremely low ($\leq 10^{-6}$). With respect to the above (Momany et al. 2007) study, the present dwarf galaxy sample has four new solid entries, that populate the extreme ends of the dwarf galaxies luminosity distribution. The BSS frequency for the Tucana and Cetus dwarfs at around $M_V \approx -10.0$ are taken directly from Monelli et al. (2012), whereas for the Leo IV and Hercules at around $M_V = -5.0$, the frequencies were derived. Repeating the same exercise, the statistical significance of the hinted F_{HB}^{BSS}–M_V anti-correlation still holds. Nevertheless, it is populating the dwarf galaxy sample with the ultra-faint dwarfs with $M_V \approx -4.0$ that the anti-correlation can be firmly established. In this regards, we note the extreme difficulty in the process of identification of BSS samples in such galaxies, as this heavily relies on the quality of photometric catalogues. For example, the BSS frequency for the Leo IV and Hercules dwarf galaxies was derived only thanks to yet unpublished *Hubble Space Telescope* deep diagrams that reveal with confidence the presence of

BSS in these systems. On the other hand, ground-based observations of the same two galaxies did not allow a reliable estimate of the BSS frequency.

Lastly, one should also keep in mind that for the ultra-faint dwarf galaxies even the absolute luminosity of the system is subject to significant variations, i.e. the inclusion or not of few red giant stars (whose census become very sensitive to foreground contamination) has reflected on changes of the order of $\sim$0.6 magnitude for some galaxies.

The Specific Case of the Carina Dwarf Galaxy Previously we emphasised the obvious need to exclude the group of gas-rich, star forming dwarf galaxies from our sample. To this constraint, one can also add the group of dwarf galaxies with known, dominant, intermediate-age population. Indeed, the presence of intermediate age population of around $\sim$5 Gyr would inevitably interfere with the BSS selection process and impose the shifting of the BSS box to brighter magnitudes. A perfect example of such a case is the Carina dwarf galaxy. The colour-magnitude diagrams of Hurley-Keller et al. (1998) and Bono et al. (2010) show clearly the presence of multiple subgiant branches separated by $\sim 0.5 - 0.8$ magnitude. The Carina star formation history reconstructed by Rizzi et al. (2003a) shows that the bulk of the star formation has taken place in an episode at around $\sim$6 Gyr. Deriving a BSS frequency for Carina (as done for the other galaxies but with the limitation of not reaching the faintest turn-off level) results in a *lower* limit of $F_{HB}^{BSS} = 0.4$, which at $M_V = -9.1$ would *still* reflect a high BSS frequency with respect to other dwarf galaxies of similar luminosity (e.g. the Tucana dwarf at $M_V = -9.5$ has $F_{HB}^{BSS} = 0.0$). This has triggered the use of the F_{HB}^{BSS}–M_V anti-correlation as a diagnostic for the presence of young stellar populations in other galaxies. For example, examining the diagrams of the Canes Venatici I dwarf ($M_V = -8.6$), Martin et al. (2008) estimate the BSS/blue plume frequency to be $F_{HB}^{BSS} = 0.5$, and along with arguments concerning the spatial distribution of this population they conclude that it is best understood as a young stellar population.

The Specific Case of the Milky Way Bulge Thanks to recent and multi-epoch *Hubble Space Telescope* observations of the Galactic Bulge, Clarkson et al. (2011) beautifully managed to proper-motion decontaminate the Bulge stellar populations from the foreground disc contribution. Their goal was to investigate the presence (or not) of a genuine young stellar population in the Galactic Bulge. The cleaned colour-magnitude diagram however resembles that of a typical old stellar population with a scarce population of seemingly BSS. They (Clarkson et al. 2011) estimate the BSS specific frequency and (as done in this and many studies) use the convention of normalising the BSS numbers as a function of the entire horizontal branch population. Assuming a $M_V = -20.4$ for the Bulge they conclude that the limits of their BSS frequency is consistent (see Fig. 6.4) with the general trend displayed by the F_{HB}^{BSS}–M_V anti-correlation, suggested in our earlier work (Momany et al. 2007). The addition of the Bulge extends the F_{HB}^{BSS}–M_V anti-correlation by over 7 magnitudes to the extreme massive systems. As emphasised by Clarkson et al. (2011), the interpretation of this agreement remains unclear and awaits further confirmation of the anti-correlation itself.

Lastly, availing recent *SEGUE* survey results for BSS and blue-HB candidates (Santucci R., priv. comm.), a rough and preliminary BSS frequency for the Galactic Halo of $F_{BHB}^{BSS} \sim 0.2$ was derived involving 9,000 and 5,600 stars. To assign an absolute luminosity of the Galactic Halo, we roughly assume that the family of Galactic globular clusters contribute by 1 % of the total luminosity, and derive $M_V \sim -17.8$. As argued in Sect. 6.2.1, normalising the BSS star counts to only blue-HB stars would provide a strong upper limit. Nonetheless, we add this point to Fig. 6.4 for comparison purposes and speculate that the Galactic Halo BSS frequency might approach values of $F_{HB}^{BSS} \sim 0.0$ and lower. All together, the addition of four new dwarf galaxies, along with that of the Galactic Bulge and evidence from the Anomalous Cepheid frequency (see Sec. 6.6) seem to confirm the F_{HB}^{BSS}–M_V anti-correlation.

6.3.3 The Significance of the Anti-correlation

The blue plume of dwarf galaxies (currently not experimenting star formation episodes) does not allow clear cut indications on whether it represents: (a) a genuine BSS population (as that observed in globular clusters); (b) a young population of recently ($\leq$2 Gyr) formed stars; or (c) a combination of both. To tackle this ambiguous problem, and given the faintness of the blue plume stars, one could only address the number frequency of this population and search for general trends as a function of the parent galaxy parameters. To attempt such analysis, one *must* tacitly assume that the blue plume is made of a genuine BSS population (perform the BSS star counts and normalisation) and then search for a correlation, say, with the parent galaxy luminosity (a proxy of mass). Should the assumption be incorrect—and the blue plume population is instead made of (or contaminated by) young MS stars—then one would expect to find a *correlation* between the BSS frequency and the galaxy luminosity (i.e. more massive galaxies tend to preserve a low level of residual star formation rate and hence possess a larger fraction of young stars). On the other hand, a flat BSS frequency distribution would need an ad hoc scenario where more massive galaxies *conspire* and coordinate their star formation rate in a way to mimic a rather flat "BSS" frequency. Instead, and with all necessary caution, we find hints of an *anti-correlation*. This is unexpected and points to a genuine BSS origin of the blue plume in the studied galaxies. The fact that globular clusters do show a similar anti-correlation makes it easier to suggest that whatever mechanism is at work in globular clusters *might* be responsible for the milder anti-correlation seen in the dwarf galaxies. Granted the above, does the scenario envisaged by Davies et al. (2004) apply also for dwarf galaxies?

The above question implies answering "*do dwarf galaxies harbour a significant population of collisional binaries at all*?" The answer is *no*. This lies in the intrinsic properties of dwarf galaxies and their differences from globular clusters. Indeed, it is enough to recall that the central luminosity density of a dwarf galaxy (e.g. Ursa Minor: 0.006 $L_\odot$ pc^{-3} at $M_V = -8.9$) is several orders of magnitudes lower

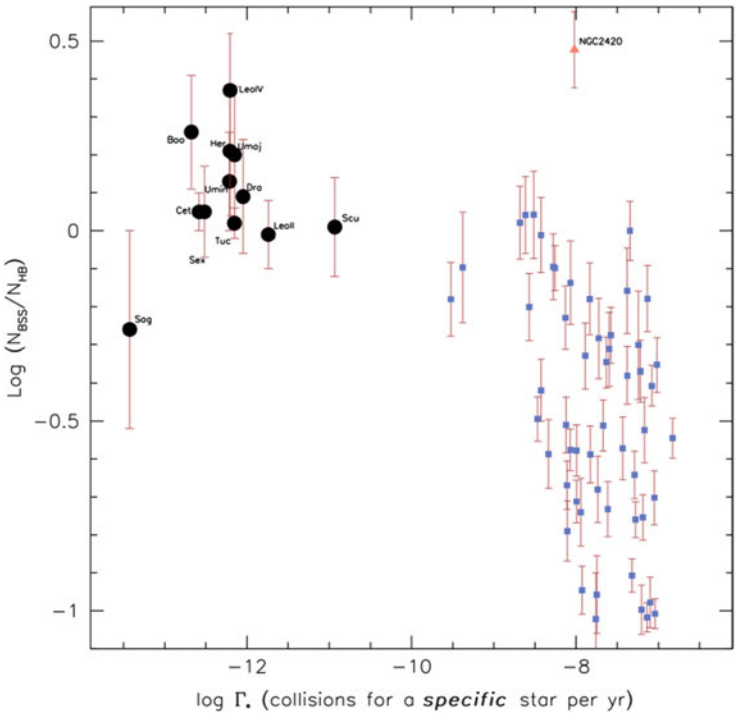

Fig. 6.5 The BSS frequency as a function of the stellar collision factor for a specific star per year. Globular clusters are plotted as *filled squares*, while dwarf galaxies are plotted as *filled circles*. The *filled triangle* is that of an open cluster

than that found in a typical globular cluster (e.g. NGC 7089: $\sim$8,000 $L_{\odot}$ pc^{-3} at $M_V = -9.0$). This implies that the collisional parameter of dwarf galaxies is very low, and unambiguously point to the much slower dynamical evolution of dwarf galaxies. To further emphasise this last point, in Fig. 6.5 we show F_{HB}^{BSS} as a function of a *calculated* quantity: the stellar specific collision parameter ($log\Gamma_{\star}$: the number of collisions per specific star per year). More specifically, following Piotto et al. (2004), we estimate $log\Gamma_{\star}$ from the systems's central surface density and core size. To these, we could add the $log\Gamma_{\star}$ corresponding value of an open cluster, thanks to parameters provided by Giovanni Carraro (priv. comm.).

The mean collisional parameter of the 12 studied galaxies is -11.5. The lowest value is that for the Sagittarius dwarf, and this is probably due to its very extended galaxy core. Compared with the mean value of $\log \Gamma_{\star} = -7.5$ for the globular clusters sample, the estimated number of collisions per specific star per year in a dwarf galaxy is 10^{-5} times lower. This almost *precludes* the occurrence of collisional binaries in dwarf galaxies, and one may conclude that genuine BSS sequences in dwarf galaxies are mainly made of primordial binaries. Moreover, the overall $\log \Gamma_{\star}$ distribution of the dwarf galaxies shows no obvious correlation with

the BSS frequency. This is in good agreement with the observational fact (see Piotto et al. 2004) that the collisional parameter of globular clusters also do not show any correlation with the BSS frequency.

The flatter slope of the potential anti-correlation in dwarf galaxies may be understood in terms of the almost lack of collisional—BSS: i.e. neither created nor destroyed. Moreover, not all primordial binaries, now present in a dwarf galaxy, turn into or are already in the form of BSS. In particular, it is the low exchange encounter probabilities in environments like the Galactic Halo or dwarf galaxies that guarantees a friendly environment and a slower consumption/evolution of primordial binary systems. The BSS production (via evolution off the MS of the primary and the consequent mass transfer to the secondary that may become a BSS) is still taking place in the present epoch and this can explain the high frequency of primordial BSS in dwarf galaxies as well as the Galactic Halo.

6.4 The BSS Radial Distribution and Luminosity Function in Dwarf Galaxies

As argued in the previous section, the collisional rate of dwarf galaxies is 10^{-5} times lower than in globular clusters. This practically precludes the BSS *collisional* formation channel in dwarf galaxies, thereby supporting solely the *mass-transfer* binaries channel. This conclusion can be confirmed or refuted by examining the radial distribution and luminosity functions of the BSS population in dwarf galaxies. Indeed, models of the globular clusters BSS that are *thought* to originate via the *collisional* channel foresee specific radial distribution and luminosity functions signature, and such signatures can be verified in dwarf galaxies.

6.4.1 Radial Distribution

Thanks to their high density cores, globular clusters are the ideal environment where collisional BSS can, and *must*, form. Interestingly, the BSS radial distribution of the majority of globular clusters is bimodal (Fusi Pecci et al. 1992; Ferraro et al. 1997; Zaggia et al. 1997; Lanzoni et al. 2007a; Beccari et al. 2008): showing a central peak, followed by a gradual decrease until reaching a minimum at intermediate radii, and then showing a rise at the clusters periphery. This bimodality was explained (Mapelli et al. 2004, 2006) by the joint contribution of: (a) *collisional* binaries, naturally produced in the highest density regions of the parent cluster, thereby responsible for the central peak; and (b) *mass-transfer* binaries which, left peacefully to evolve in the cluster outskirts, avoid sinking towards the cluster centre, and produce the outer peak. A minority of globular clusters (Lanzoni et al. 2007b; Beccari et al. 2011) do not show the external rise and are expected to be poor in

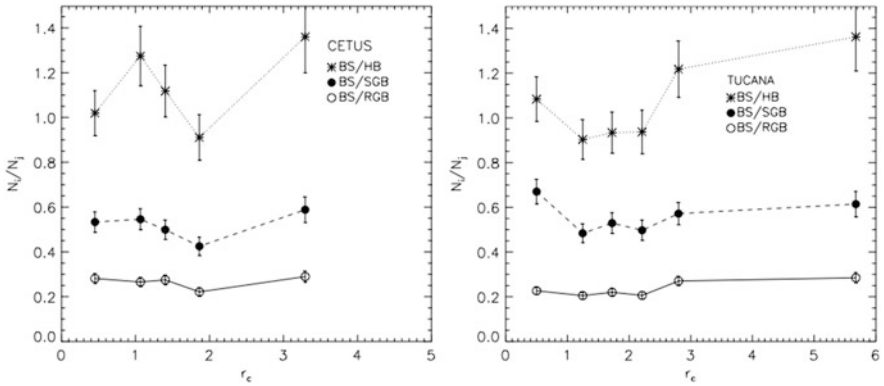

Fig. 6.6 The BSS radial distribution as a function of the core galacto-centric radius for the Cetus (*left*) and Tucana (*right*) dwarf galaxies. The absence of a central peak points to the lack of collisional BSS in dwarf galaxies. This figure is reproduced from Monelli et al. (2012) with permission by the AAS

mass-transfer BSS. Overall, *all* globular clusters show a central peak in their BSS radial distribution and this is attributed to the production of *collisional* BSS.

The wide-field imaging study of the Draco and Ursa Minor dwarf galaxies by Mapelli et al. (2007) shows clearly that the radial distribution of the BSS population is *flat* (see also Carrera et al. 2002), and hardly consistent with a central peak like that observed in globular clusters. If ever, the BSS populations in this study (Mapelli et al. 2007) show a hint of a decrease in the central regions. Mapelli et al. (2007) conclude that the BSS in the Draco and Ursa Minor dwarf galaxies have radial distributions that are consistent with the expectations of their models of *mass-transfer* BSS (Mapelli et al. 2004, 2006) . Similar results were obtained for the case of the Sculptor dwarf by Mapelli et al. (2009), and Cetus and Tucana by Monelli et al. (2012). Figure 6.6 shows an excellent example of flat BSS distributions in the Cetus and Tucana dwarf galaxies (from Monelli et al. 2012).

6.4.2 *Luminosity Function*

Monkman et al. (2006) find that *bright* BSS stars in 47 Tuc tend to be more centrally concentrated. The central distribution of these bright BSS stars strengthen the idea of a collisional origin. Indeed, the collisional formation channel should allow the final product (the BSS star) to retain a large fraction of the original masses involved in the collisions, hence the brighter luminosities. In terms of the luminosity function, this translates into a correlation between the BSS luminosities and their radial distribution. Should the dwarf galaxy lack the presence of collisional binaries (as we have argued) one expects no correlation between an inner and outer BSS luminosity functions.

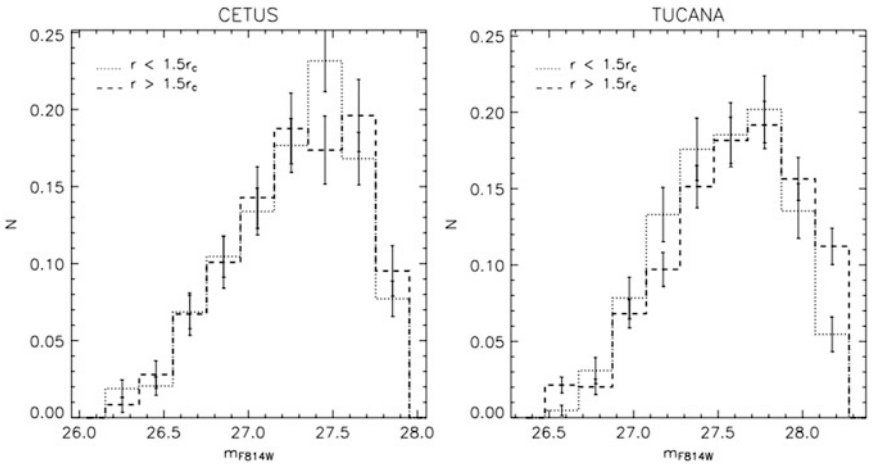

Fig. 6.7 The BSS normalised luminosity functions in the Cetus and Tucana dwarf galaxies. The *different lines* refer to the BSS stars within (*dotted*) and outside (*dashed*) $1.5 \times r_c$ from the galaxies centres. The agreement between the two luminosity functions (for both galaxies) hints to the absence of collisional—BSS in dwarf galaxies. This figure is reproduced from Monelli et al. (2012) with permission by the AAS

This hypothesis was tested by Mapelli et al. for the Draco, Ursa Minor dwarf galaxies and for Sculptor (Mapelli et al. 2009, 2007), and by Monelli et al. (2012) for the Cetus and Tucana dwarfs. With the only exception of Sextans (Lee et al. 2003), all these studies proved the absence of a correlation between the BSS luminosity function and the radial distribution. This is best illustrated in Fig. 6.7 taken from Monelli et al. (2012). For each galaxy, two BSS luminosity functions were derived and compared. The excellent agreement between the inner and outer $1.5 \times r_c$ selections points to the absence of collisional binaries products, thereby confirming the mass-transfer binaries as the sole origin of BSS in dwarf galaxies.

6.5 Variable BSS in Dwarf Galaxies

SX Phoenicis (SX Phe) are a class of Population II pulsating variables that exhibit short period ($P < 0.1$ days) variations, having spectral types between A2 and F5. SX Phe variables are particularly interesting because the region in the colour-magnitude diagram where they cross the instability strip coincides with the BSS location for globular clusters. Indeed, all SX Phe variables in globular clusters are BSS stars. SX Phe are, however, ∼1–2.5 magnitudes fainter than RR Lyrae and therefore, in the context of distant dwarf galaxies studies, are harder to detect. Mateo et al. (1998) and Poretti (1999) were the first to report on SX Phe in the Carina dwarf galaxy.

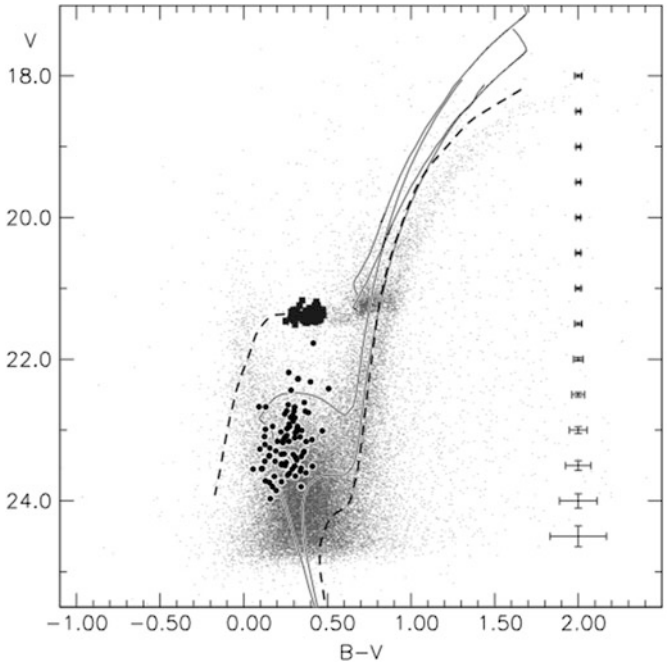

Fig. 6.8 The colour-magnitude diagram of the Fornax dwarf galaxy. *Highlighted with heavy squares* are the RR Lyrae, while the sample of 85 SX Phe variables are *highlighted with heavy filled circles*. This figure is reproduced from Poretti et al. (2008) with permission by the AAS

Poretti et al. (2008) presented an intensive survey of the Fornax dwarf (a galaxy known to harbour recent star formation activity and a predominately intermediate age population). Figure 6.8 shows how the group of 85 SX Phe variables is coincident with the expected BSS location and, at the same time, immersed within the blue plume of young stars. Examining the period–luminosity relation for the SX Phe sample, Poretti et al. (2008) conclude that the observed scatter exceeds their observational errors and propose a physical rather than an instrumental origin for this scatter. Using the period-luminosity plane, they reported the first identification of a peculiar group of *sub-luminous* extra-Galactic SX Phe variables. The presence of the sub-luminous SX Phe was confirmed by Cohen and Sarajedini (2012) in the Carina dwarf, NGC 2419 and ω Cen. Poretti et al. (2008) cautiously speculate that the *sub-luminous* variables could be the results of merging of a close binary system, and present arguments in favour for this scenario. Clearly, more observations are needed to confirm this scenario. However, this may open a new field where BSS can be disentangled (via their variability signature) in star forming dwarf galaxies.

6.6 The Progeny of BSS

During their core-helium burning phase, the progeny of the BSS population (i.e. evolved-BSS, hereafter E-BSS) are expected to pile up in a particular location in the colour-magnitude diagram: bluer than the red giant branch and brighter than normal horizontal branch stars. Renzini and Fusi Pecci (1988) were the first to suggest the presence of E-BSS. Interestingly, the occurrence of E-BSS is independent of the formation channel of the BSS (Sills et al. 2009). Ferraro et al. (1999) performed a systematic search for E-BSS, and Fig. 6.9 shows their ultraviolet diagram of M80 where the E-BSS population is clearly present and highlighted by the open box. They derive $N_{BSS}/N_{E-BSS} = 16$.

The right panel of Fig. 6.9 shows the detection of a vertical extension in correspondence of the red HB region in the Cetus and Tucana dwarf galaxies. In the context of dwarf galaxies, this sequence is usually referred to as *vertical-clump* (Gallart et al. 1999): helium-burning stars of few hundred Myr to 1–2 Gyr old population. Monelli et al. (2010) use their best reconstruction of the Cetus star formation history, and derive a $N_{BSS}/N_{E-BSS} = 12$ and 10 upon simulated and observed diagrams, respectively. The agreement between the empirical and synthetic values for the Cetus dwarf, and the value derived by Ferraro et al. (1999) all point to a correct identification of the *same* evolved BSS population in the two different systems. We repeated the exercise for the LeoII dwarf galaxy and derive

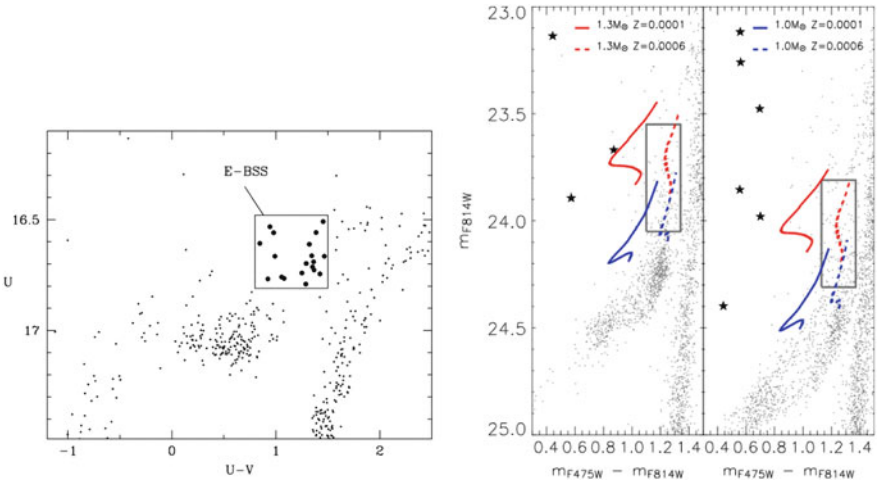

Fig. 6.9 The *left panel* displays the *HST* ultraviolet U, $(U-V)$ diagram of M80 where the progeny of BSS are identified within the *open box*. The *right panel* displays the optical diagram of the Cetus and Tucana dwarf galaxies, where the boxes also highlight the E-BSS population. The *filled stars* are the identified Anomalous Cepheid variables, detected by Bernard et al. (2009). The left and right figures are reproduced from Monelli et al. (2012), and Ferraro et al. (1999), respectively, with permission by the AAS

$N_{BSS}/N_{E-BSS} = 9$, again indicating a correct identification of E-BSS in dwarf galaxies.

The Case of Anomalous Cepheids Dwarf galaxies (whether *purely ancient* systems like Ursa Minor or intermediate-age ones like LeoI) are known to host a peculiar class of Cepheid variables known as Anomalous Cepheids (ACs). RR Lyrae and ACs are core helium-burning pulsational variables passing through the instability strip and co-exist in low-metallicity systems. However, ACs are two to three times more massive than RR Lyrae (Renzini et al. 1977; Fiorentino et al. 2006). The origin of ACs is sought as either due to: (a) relatively young (∼1–6 Gyr) single stars; or (b) the progeny of BSS, formed through mass transfer in primordial (10 Gyr) binary systems. The early study of Renzini et al. (1977) shows how the chances of survival of such primordial binaries are strictly correlated with the stellar density of the parent system: ACs are easily destroyed via dynamical encounters in high density environments like globular clusters. On the other hand, the low stellar densities of dwarf galaxies offer a peaceful environment and allow the system to evolve. This 1977 prediction is proven correct by the continuous and successful surveys of ACs in dwarf galaxies—e.g. Bernard et al. (2009) for the detection of 8 and 6 ACs in Cetus and Tucana, and Fiorentino et al. (2012) for the detection of 51 ACs in Leo I. Most interestingly, the prediction of the almost *lack* of ACs in globular clusters still holds as well. The exception being the detection of a *single* AC detected in NGC 5466 (Zinn and Dahn 1976), which *is* a low-density cluster.

Fiorentino and Monelli (2012) complemented the earlier studies by Mateo et al. (1995) and Pritzl et al. (2002) and reinvestigated the correlation between the ACs frequency and the absolute visual luminosity of the parent galaxy. Figure 6.10

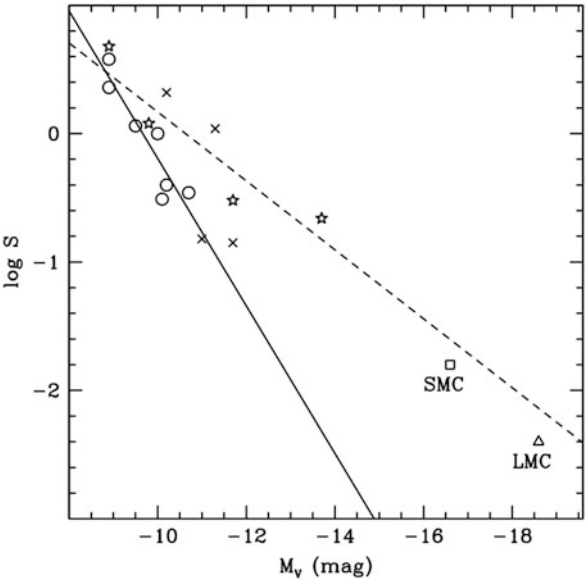

Fig. 6.10 The Anomalous Cepheid frequency (*log S*, per $10^5 L_{\odot}$) as a function of the M_V of the parent dwarf galaxy (i.e. the *ACs frequency—M_V anti-correlation*). *Open circles* highlight purely ancient galaxies while starred symbols indicate galaxies with large intermediate-age populations. The *solid line* shows an excellent fit to only the ancient systems (included in this review). This figure is reproduced from Fiorentino and Monelli (2012) with permission by Astronomy & Astrophysics, © ESO

displays the Anomalous Cepheid frequency (log S, per $10^5 L_\odot$) as a function of the M_V of the parent dwarf galaxy. Open circles show purely ancient galaxies while starred symbols indicate galaxies with large intermediate-age populations. The sample of Fiorentino et al. (2012) of ancient galaxies includes: Ursa Minor, Draco, Sculptor, Leo II, Sextans, Tucana and Cetus (all of which are included in the present BSS study) confirm that these possess a genuine BSS population. Figure 6.10 shows that for these galaxies there exists a clear anti-correlation between the ACs frequency and the luminosity of the parent galaxy. The solid line shows the fit to *only* the ancient systems while the dashed line is the fit for the intermediate-age galaxies. The interpretation of the apparent ACs frequency–M_V anti-correlations for the two groups is not straightforward. However, intermediate-age galaxies systematically show higher ACs frequencies, and this goes along with the fact that these systems can host ACs originating from two different channels (i.e. recently formed young stars as well as evolving primordial binaries). Fiorentino and Monelli (2012) note, however, that for their sample of ancient systems one expects to find ACs originating *only* through the binary channel, and therefore imply that binary systems have a higher chance of survival in low-mass galaxies.

Conclusions

During the workshop, George Preston proposed us a nice definition of blue straggler stars:

> BSS are a subset of the interacting-binary field stars whose end products are hotter than the main sequence turn-off of the parent stellar population.

In his 1993 review Stryker (1993) concludes

> This makes forming conclusion about the origin of BS in dwarf galaxies difficult, if not impossible, at the present time.

Twenty years after, I believe that the recent imaging surveys of these distant systems have allowed us to get a deeper insight on the general properties and origin of their BSS population. Indeed, and thanks to the new generations of ground and space-based telescopes, the star formation and chemical enrichment history for the majority of Local Group galaxies have been derived. This has allowed us to scrutinise and filter-out those galaxies with hints of recent star formation activity. Consequently, clean samples of "ancient" galaxies are available to address the *BSS-young stars* ambiguity in a reasonable manner.

Our current understanding of the possible BSS formation channels are mass-transfer binaries, collisions and mergers, and all three channels must manifest themselves in globular clusters. The central peak of the BSS radial distribution is *still* best explained as a signature of collisional BSS. Similarly, the segregation of the brighter BSS in the cluster centres is also attributed

(continued)

to collisional BSS. Assuming that the previous two interpretations are true, one can confidently affirm that both these collisional BSS *"signatures"* are lacking in dwarf galaxies. This proves the long-suspected prediction that BSS in dwarf galaxies form preferentially through mass-transfer binaries, as is the case for the Galactic Halo.

Figure 6.4 shows that the lowest luminosity dwarf galaxies with $-8.0 \leq M_V \leq -5.0$ have BSS frequencies that are in perfect agreement with that observed in Galactic open clusters. Evidence that the lowest-luminosity globular clusters share the same BSS frequency as in open clusters *and* dwarf galaxies allow us to suggest that there exists an *empirical upper limit* to the BSS frequency in *any* given stellar system. Figure 6.4 also shows that the BSS frequency in dwarf galaxies with $M_V \approx -9.0$ is *higher* than that of globular clusters at the same luminosity. This is in perfect agreement with the notion that higher density environments, with their higher collisional rates, perturb the evolution of mass transfer in primordial binaries and end up being BSS deficient. Dwarf galaxies on the other hand offer a more friendly environment for mass-transfer binaries and tend to preserve their initial binary population. The recent derivation of the BSS frequency in the Galactic Bulge, and arguments presented for the BSS frequency in the Galactic Halo, seem to provide more evidence for the dwarf galaxies *BSS frequency–M_V anti-correlation*. The mechanism responsible for the decreasing BSS frequency with increasing mass remains unclear, and awaits further confirmation of the *anti-correlation.* Interestingly, a *tight* and *strong* anti-correlation (Fig. 6.10) has been observed between the frequency of Anomalous Cepheids (a progeny of BSS) and M_V for ancient dwarf galaxies with $-11.0 \leq M_V \leq -9.0$.

All together, I believe that the past few years have been very fruitful for the study of BSS in dwarf galaxies, and the best (deeper imaging and kinematic and chemical surveys) are yet to come.

Acknowledgements I would like to thank S. Zaggia for valuable comments. H. Boffin and G. Carraro are warmly thanked for organising a wonderful workshop.

References

Aparicio, A., Carrera, R., Martínez-Delgado, D.: AJ **122**, 2524 (2001)
Beccari, G., Pulone, L., Ferraro, F. R., et al.: MemSAI **79**, 360 (2008)
Beccari, G., Sollima, A., Ferraro, F. R., et al.: ApJL **737**, 3 (2011)
Belokurov, V., Zucker, D. B., Evans, N. W., et al.: ApJL **647**, 111 (2006)
Bernard, E. J., Monelli, M., Gallart, C., et al.: ApJ **699**, 1742 (2009)
Blumenthal, G. R., Faber, S. M., Primack, J. R., Rees, M. J.: Nature **311**, 517 (1984)
Bono, G., Stetson, P. B., Walker, A. R., et al.: PASP **122**, 651 (2010)
Brown, T. M., Beaton, R., Chiba, M., et al.: ApJL **685**, 121 (2008)

Carrera, R., Aparicio, A., Martínez-Delgado, D., & Alonso-García, J.: AJ **123**, 3199 (2002)
Carretta, E., Bragaglia, A., Gratton, R. G., et al.: A&A **505**, 117 (2009)
Clarkson, W. I., Sahu, K. C., Anderson, J., et al.: ApJ **735**, 37 (2011)
Cohen, R. E. Sarajedini, A.: **419**, 342 (2012)
Davies, M. B., Piotto, G., de Angeli, F.: **349**, 129 (2004)
de Marchi, F., de Angeli, F., Piotto, G., Carraro, G., Davies, M. B.: A&A **459**, 489 (2006)
Ferraro, F. R., Paltrinieri, B., Fusi Pecci, F., et al.: A&A **324**, 915 (1997)
Ferraro, F. R., Paltrinieri, B., Rood, R. T., Dorman, B.: ApJ **522**, 983 (1999)
Ferraro, F. R., Sollima, A., Rood, R. T., et al.: ApJ **638**, 433 (2006)
Fiorentino, G., Limongi, M., Caputo, F., Marconi, M.: A&A **460**, 155 (2006)
Fiorentino, G. Monelli, M.: A&A **540**, A102 (2012)
Fiorentino, G., Stetson, P. B., Monelli, M., et al.: ApJL **759**, 12 (2012)
Fusi Pecci, F., Ferraro, F. R., Corsi, C. E., Cacciari, C., & Buonanno, R.: AJ **104**, 1831 (1992)
Gallart, C., Freedman, W. L., Mateo, M., et al.: ApJ **514**, 665 (1999)
Gilmore, G., Wilkinson, M. I., Wyse, R. F. G., et al.: ApJ **663**, 948 (2007)
Girardi, L., Groenewegen, M. A. T., Hatziminaoglou, E., da Costa, L.: A&A **436**, 895 (2005)
Held, E. V.: , in IAU Colloq. 198: Near-fields cosmology with dwarf elliptical galaxies, p. 11 (2005)
Held, E. V., Saviane, I., Momany, Y., Carraro, G.: ApJL **530**, 85 (2000)
Hills, J. G. Day, C. A.: ApJL **17**, 87 (1976)
Holtzman, J. A., Afonso, C., Dolphin, A.: ApJS **166**, 534 (2006)
Hurley-Keller, D., Mateo, M., Nemec, J.: AJ **115**, 1840 (1998)
Keller, S. C., Skymapper Team, Aegis Team: in Galactic Archaeology: Near-Field Cosmology and the Formation of the Milky Way, ASPC 458, p. 409 (2012)
Lanzoni, B., Dalessandro, E., Ferraro, F. R., et al.: ApJ **663**, 267 (2007a)
Lanzoni, B., Sanna, N., Ferraro, F. R., et al.: ApJ **663**, 1040 (2007b)
Lee, M. G., Park, H. S., Park, J.-H., et al.: AJ **126**, 2840 (2003)
Mandushev, G. I., Fahlman, G. G., Richer, H. B., Thompson, I. B.: AJ **114**, 1060 (1997)
Mapelli, M., Ripamonti, E., Battaglia, G., et al.: MNRAS **396**, 1771 (2009)
Mapelli, M., Ripamonti, E., Tolstoy, E., et al.: MNRAS **380**, 1127 (2007)
Mapelli, M., Sigurdsson, S., Colpi, M., et al.: ApJL **605**, 29 (2004)
Mapelli, M., Sigurdsson, S., Ferraro, F. R., et al.: MNRAS **373**, 361 (2006)
Marín-Franch, A., Aparicio, A., Piotto, G., et al.: ApJ **694**, 1498 (2009)
Martin, N. F., Coleman, M. G., De Jong, J. T. A., et al.: ApJL **672**, 13 (2008)
Mateo, M., Fischer, P., Krzeminski, W.: AJ **110**, 2166 (1995)
Mateo, M., Hurley-Keller, D., Nemec, J.: AJ **115**, 1856 (1998)
Mateo, M., Nemec, J., Irwin, M., McMahon, R.: AJ **101**, 892 (1991)
Mateo, M. L.: ARA&A **36**, 435 (1998)
McConnachie, A. W.: AJ **144**, 4 (2012)
McCrea, W. H.: MNRAS **128**, 147 (1964)
Milone, A. P., Marino, A. F., Piotto, G., et al.: ApJ **767**, 120 (2013)
Misgeld, I. Hilker, M.: MNRAS **414**, 3699 (2011)
Momany, Y., Cassisi, S., Piotto, G., et al.: A&A **407**, 303 (2003)
Momany, Y., Held, E. V., Saviane, I., et al.: A&A **468**, 973 (2007)
Monaco, L., Bellazzini, M., Ferraro, F. R., Pancino, E.: ApJL **597**, 25 (2003)
Monelli, M., Cassisi, S., Mapelli, M., et al.: ApJ **744**, 157 (2012)
Monelli, M., Hidalgo, S. L., Stetson, P. B., et al.: ApJ **720**, 1225 (2010)
Monkman, E., Sills, A., Howell, J., et al.: ApJ **650**, 195 (2006)
Niederste-Ostholt, M., Belokurov, V., Evans, N. W., et al.: MNRAS **398**, 1771 (2009)
Piotto, G., De Angeli, F., King, I. R., et al.: ApJL **604**, 109 (2004)
Piotto, G., de Angeli, F., Recio Blanco, A., et al.: in Observed HR Diagrams and Stellar Evolution, ASPC 274, p. 282 (2002)
Poretti, E.: A&A **343**, 385 (1999)
Poretti, E., Clementini, G., Held, E. V., et al.: ApJ **685**, 947 (2008)
Preston, G. W. Sneden, C.: AJ **120**, 1014 (2000)

Pritzl, B. J., Armandroff, T. E., Jacoby, G. H., Da Costa, G. S.: AJ **124**, 1464 (2002)
Renzini, A.: MmSAI **84**, 162 (2013)
Renzini, A. Fusi Pecci, F.: ARA&A **26**, 199 (1988)
Renzini, A., Mengel, J. G., Sweigart, A. V.: A&A **56**, 369 (1977)
Rizzi, L., Held, E. V., Bertelli, G., Saviane, I.: ApJL **589**, 85 (2003a)
Rizzi, L., Held, E. V., Momany, Y., et al.: MmSAI **74**, 510 (2003b)
Sandage, A. R.: AJ **58**, 61 (1953)
Santana, F. A., Muñoz, R. R., Geha, M., et al.: in Galactic Archaeology: Near-Field Cosmology and the Formation of the Milky Way, ASPC 458, p. 339 (2012)
Saviane, I., Held, E. V., Bertelli, G.: A&A **355**, 56 (2000)
Saviane, I., Rosenberg, A., Aparicio, A., Piotto, G.: in New Horizons in Globular Cluster, ASPC 296, p. 402 (2003)
Sills, A., Karakas, A., Lattanzio, J.: ApJ **692**, 1411 (2009)
Sollima, A., Lanzoni, B., Beccari, G., Ferraro, F. R., Fusi Pecci, F.: A&A **481**, 701 (2008)
Stryker, L. L.: PASP **105**, 1081 (1993)
White, S. D. M. Rees, M. J.: MNRAS **183**, 341 (1978)
Willman, B., Dalcanton, J. J., Martinez-Delgado, D., et al.: ApJL **626**, 85 (2005)
Willman, B. Strader, J.: AJ **144**, 76 (2012)
Zaggia, S. R., Piotto, G., Capaccioli, M.: A&A **327**, 1004 (1997)
Zhao, Z., Okamoto, S., Arimoto, N., Aoki, W., Kodama, T.: in Galactic Archaeology: Near-Field Cosmology and the Formation of the Milky Way, ASPC 458, p. 349 (2012)
Zinn, R. Dahn, C. C.: AJ **81**, 527 (1976)

Chapter 7
Mass Transfer by Stellar Wind

Henri M.J. Boffin

7.1 Stars in Couple

A large fraction of stars are found in binary or multiple systems. This fraction is dependent on the mass of the primary (i.e., the more luminous of the two stars), and is about 40–50 % for solar-like stars (Raghavan et al. 2010) and 70 % for A stars (De Rosa et al. 2014), while it is even higher for more massive stars (which are not considered in this chapter). When close enough, the stars in a binary system may interact through tidal forces, mass and angular momentum transfer. What is "close enough"? To answer this requires to introduce the concept of Roche lobe.

To do this, we consider the simplified case of a system containing two stars, of mass M_1 and M_2, *in a circular orbit* and with a separation a. Kepler's third law tells us that the orbital period P is then given by

$$P = \frac{2\pi}{\omega} = 2\pi \sqrt{\frac{a^3}{G(M_1 + M_2)}}, \tag{7.1}$$

where ω is the orbital angular velocity and G is the gravitational constant. If we assume that the two stars are points and that *their rotation is synchronised with the orbital motion*, the potential Φ in the rotating system with the centre of mass at the origin is given by

$$\Phi = -\frac{q}{1+q}\frac{1}{r_1} - \frac{1}{1+q}\frac{1}{r_2} - \frac{1}{2}(x^2 + y^2). \tag{7.2}$$

H.M.J. Boffin (✉)
ESO, Alonso de Cordóba 3107, Vitacura, Santiago 190001, Chile
e-mail: hboffin@eso.org

H.M.J. Boffin et al. (eds.), *Ecology of Blue Straggler Stars*, Astrophysics and Space Science Library 413, DOI 10.1007/978-3-662-44434-4_7

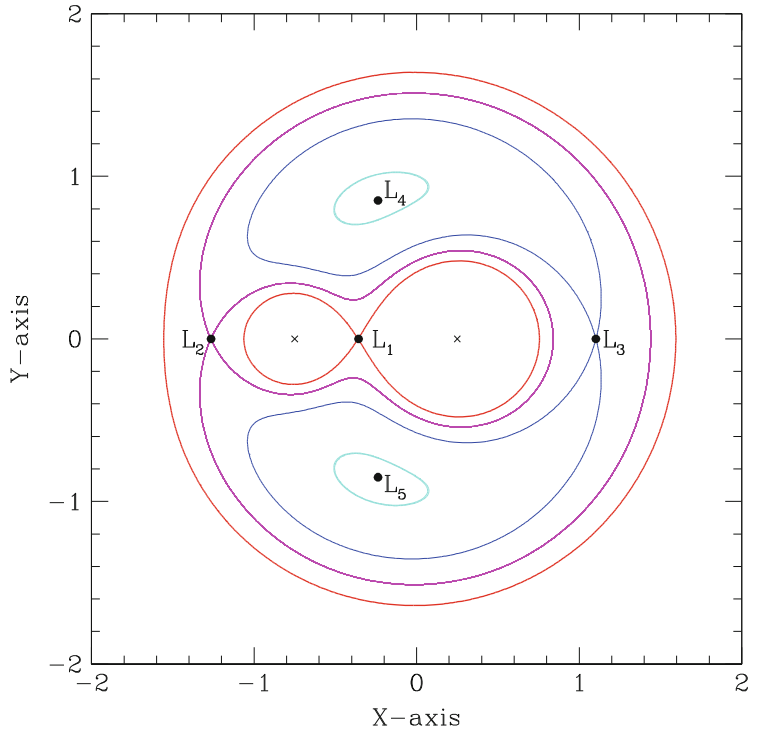

Fig. 7.1 Equipotentials in the orbital plane of a binary system with $q = 3$. The rotating reference's origin is the centre of mass of the system, and the positions of the two stars are indicated by *crosses*. The Lagrangian equilibrium points, L_1 to L_5, are also indicated

Here, x is along the line joining the two stars, while y is perpendicular to x in the orbital plane and z is perpendicular to the orbital plane, q is the mass ratio, $q = M_1/M_2$, and r_i is the distance to star i, given by

$$r_i = \sqrt{(x - x_i)^2 + y^2 + z^2}, \tag{7.3}$$

and $x_1 = 1/(1 + q)$ while $x_2 = -q/(1 + q)$. In the above, we have assumed the usual normalisation, $a = G = M_1 + M_2 = 1$.

Equipotentials as represented by Eq. (7.2) correspond to loci of constant pressure, which means that a star in a binary system will take their shape. An example of the resulting equipotentials in the orbital plane ($z = 0$) for a binary with a mass ratio of three is shown in Fig. 7.1. There are five equilibrium points where the gradient of the potential is zero, and those points are called the Lagrangian points (L_1, L_2 and L_3 are aligned on the x-axis and are unstable). The equipotential passing through the inner Lagrangian point L_1 is essential in the study of binary stars. It is called the Roche equipotential and it defines, around each of the two stars, a pear-shaped region, called *Roche lobe*. This region represents the maximum radius

a star can reach before there will be mass transfer. If both stars are well within their Roche lobe, the system is called *detached*. In this case, both stars will mostly keep a spherical shape and there is a limited interaction between them. If either the separation between the two stars decreases (and thus the Roche lobes as well) or if the radius of the stars increases (due to stellar evolution), one of the star—generally the most massive as this is the one that will evolve faster—will fill its Roche lobe, taking a pear shape. The system is then *semi-detached*, and mass transfer takes place: material will flow from the Roche lobe filling star to its companion via the inner Lagrangian point L_1. Such mass transfer is called *Roche lobe overflow* (RLOF). In some particular cases, e.g. in W UMa, the mass transfer results in both stars filling their Roche lobes and the system is then called *in contact*, both stars being surrounded by a *common envelope* (Kopal 1955). Note that when the star fills a large fraction of its Roche lobe, tidal effects become very strong, and the star's rotation become synchronised with the orbital motion on a short timescale, while the orbit will quickly circularise as well. This justifies the assumptions made in the definition of the Roche lobe, although it is important to realise that they may not be always fulfilled.

The position of the L_1 point is given by (Plavec and Kratochvil 1964):

$$x_{L_1} = \frac{1}{1+q} - (0.5 + 0.227\ \log q). \tag{7.4}$$

One also usually defines the Roche lobe radius, R_L as the radius of a sphere whose volume equals the volume of the Roche lobe itself. Some useful approximations for the Roche lobe radius around star 1 were derived by Paczyński (1971) from the values tabulated by (Kopal 1959)

$$R_L = \quad 0.462\, a \left(\frac{q}{1+q}\right)^{\frac{1}{3}} \qquad q < 0.523 \tag{7.5}$$

$$R_L = a\ (0.38 + 0.2 \log q) \qquad 0.523 < q < 20, \tag{7.6}$$

and, later, by (Eggleton 1983)

$$R_L = \frac{0.49\, q^{\frac{2}{3}}}{0.6\, q^{\frac{2}{3}} + \ln(1 + q^{\frac{1}{3}})}\, a. \tag{7.7}$$

The Roche lobe radius around star 2 is obtained by replacing q by $1/q$.

Here, we will only deal with systems containing low- and intermediate-mass stars, i.e., stars in the range $0.8 < M < 8\ \mathrm{M}_\odot$, as these are the only one relevant to blue straggler stars. The typical maximum radius such a star will reach on the first giant branch (RGB) is about 200 $\mathrm{R}_\odot$ for stars below about 1.3–1.5 $\mathrm{M}_\odot$, but only 30 $\mathrm{R}_\odot$ to ∼100 $\mathrm{R}_\odot$ for stars between 2 and 3 $\mathrm{M}_\odot$. On the other hand, the radius such stars can reach on the asymptotic giant branch (AGB) is of several hundreds of solar radii, especially during the last phases, when the AGB undergoes thermal

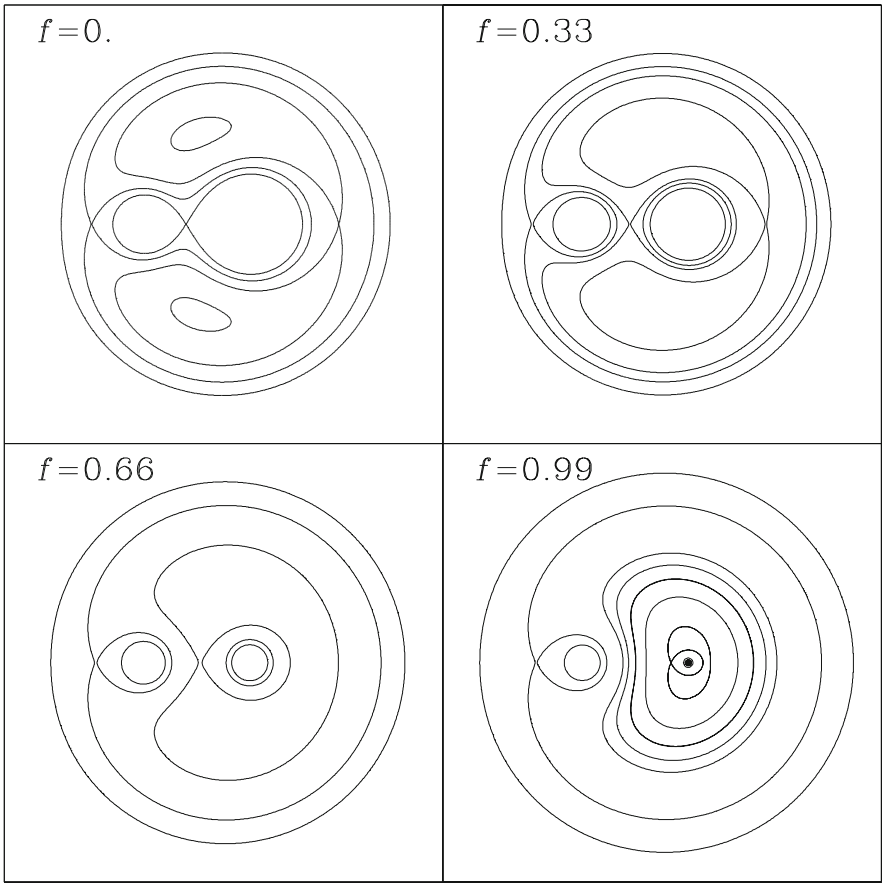

Fig. 7.2 Same as Fig. 7.1 for the case of a reduced effective gravity due to the mass loss by stellar wind. The gravity of the primary is multiplied by a factor $1. - f$, where f takes the values 0, 0.33, 0.66, and 0.99. As can be seen, for large values of f, the shapes of the Roche lobes change dramatically, and one can no more define the usual Lagrangian points. This will affect the way matter is transferred from one star to the other

pulses. In these cases, the maximum radius can reach up to 800 $R_\odot$ for stars above 3 $M_\odot$. Thus, except for the less massive stars, a star can avoid to fill its Roche lobe if the initial orbital period is above, say, 50–200 days. For the less massive stars, Roche lobe overflow could in principle happen for periods up to 1,000 days! And in all cases, RLOF could happen on the AGB—at least in the very last phases of this evolution—for orbital periods up to 10–20 years! We will see later, however, that even in this case, it is most likely that prior to the RLOF, there will be an extensive phase of wind mass transfer.

The description above may need some modification when dealing with red giants. Such stars will indeed lose mass (see below) through stellar wind. The exact way

this happens in AGB stars is still far from understood, although it generally assumes that pulsation is pushing material far enough away from the star for dust to condense and radiation pressure onto these dust grains will lead to the mass loss. This implies that the effective gravity of the star has been reduced—multiplied by $(1-f)$, where f is an unknown factor between 0 and 1. This reduced gravity will change the shape of Roche lobes as already shown by Schuerman (1972) and more recently by Dermine et al. (2009). Figure 7.2 shows the effect this has on the equipotentials and thus on the way mass will be transferred. Whether this is actually taking place in binary systems is still open to debate.

7.2 Wind Mass Transfer

In this chapter, we are concerned with the case of detached binaries, that is, both stars are well within their Roche lobe. The case of Roche lobe overflow is covered in Chap. 8.

Being detached does not imply that there is no mass transfer. Indeed, stars undergo regular mass loss, via a stellar wind, and in such case, a fraction of the mass lost may also be captured by the companion, which will thereby gain mass and angular momentum. The Sun is losing mass at a rate of 10^{-14} $M_\odot$ year^{-1}—a value too small to be of any interest in the evolution of binary stars. At such a rate, over 10 billion years only 10^{-4} $M_\odot$ would have been lost and if the Sun had a binary companion, only a fraction of it would have been accreted, hardly worth mentioning. But there are phases in the lives of solar-like stars where the mass loss by wind could be much stronger. Similarly, high mass, i.e. O and B, stars, experience much higher mass loss rates by wind.

Red giants with luminosity of 50–200 $L_\odot$ have mass loss rates of a few 10^{-10} to 10^{-8} $M_\odot$ year^{-1}, while AGB stars will lose more, and in their final stages, as carbon stars, they may lose between 10^{-7} and 10^{-4} $M_\odot$ year^{-1}. Such massive mass loss will have quite an impact on the evolution of the binary system.

7.2.1 The Bondi–Hoyle–Lyttleton Model

The simplest problem to consider in the framework of wind accretion is that of a star of mass M moving with velocity v_∞ in a homogeneous, uniform and inviscid cloud of density ρ_∞. Far away from the object, the pressure forces will be small and the matter will follow a free Keplerian orbit. Approaching the gravitational mass, the particle trajectories are deflected and, behind the object, a region forms where particles collide and increase the density. In this region, pressure effects become important. This problem was first considered by Hoyle and Lyttleton (1939) who studied the effect of interstellar matter accretion by the Sun on the Earth climate! They assumed a cold gas, and therefore neglected any pressure effect. In this model,

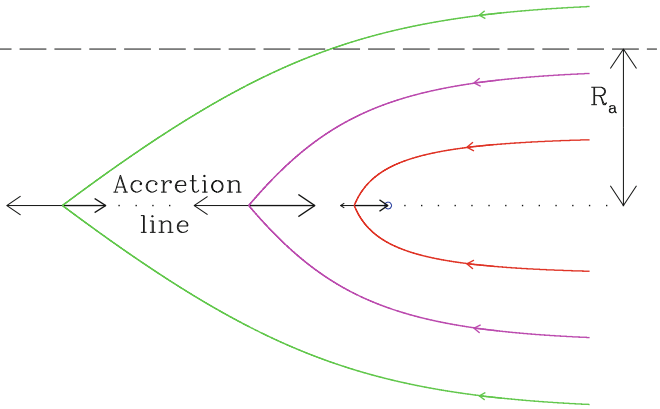

Fig. 7.3 Hoyle–Lyttleton representation of the wind accretion process: a star (indicated by the *blue circle*) moves inside a cloud of cold gas. The accretion radius is defined as the largest distance from the star, where the x-velocity behind the star (and the sole velocity after collision; indicated by the *arrows*) is equal to the escape velocity (represented by the *bold arrows*). All material within the accretion radius is supposed to be accreted by the star

gravitationally deflected material passing on one side of the star collides with material passing on the opposite side, thereby cancelling its transverse velocity and forming an "accretion line" behind the star. The material from this accretion line that has a velocity below the local escape velocity from the star will be accreted (Fig. 7.3), leading to a mass accretion rate $\dot{M}_{HL}$:

$$\dot{M}_{HL} = \pi R_A^2 \rho_\infty v_\infty, \tag{7.8}$$

where the accretion radius R_A is given by

$$R_A = 2\,\frac{GM}{v_\infty^2}. \tag{7.9}$$

This result is only valid for hypersonic flows, i.e., $v_\infty \gg c_\infty$, the sound velocity at infinity. Later, Bondi and Hoyle (1944) included some limited pressure effects (making the accretion line, an "accretion column"), and showed that Eq. (7.9) is an upper limit, and that the actual accretion rate is given by

$$\dot{M} = \alpha \dot{M}_{HL},$$

where α is an efficiency parameter of the order of unity. Physically, α represents the location of the stagnation point in units of the accretion radius. In the Bondi and Hoyle formalism, this position cannot be determined exactly.

Bondi (1952) studied the complementary case of a pressure dominated flow, namely a stationary, spherically symmetric accretion with $v_\infty = 0$. The accretion

rate in a steady state is not uniquely determined but the model does provide a maximum accretion rate $\dot{M}_B$:

$$\dot{M}_B = \lambda \pi R_B^2 \rho_\infty c_\infty, \tag{7.10}$$

where the Bondi radius is given by Eq. (7.9) but with the sound speed at infinity c_∞ replacing v_∞. Here λ ranges between 0.25 and 1.12, with the exact value depending on the polytropic index of the gas. Bondi then proposed an interpolation formula for the intermediate cases, which is the most widely used Bondi–Hoyle accretion rate:

$$\dot{M}_{BH} = \alpha \pi R_A^2 \rho_\infty v_\infty \left(\frac{\mathscr{M}_\infty^2}{1 + \mathscr{M}_\infty^2} \right)^{3/2}, \tag{7.11}$$

where $\mathscr{M}_\infty = v_\infty / c_\infty$ is the Mach number.

The theoretically predicted accretion rate $\dot{M}_{BH}$ in the Bondi–Hoyle model has been extensively tested against numerical simulations by, e.g., Hunt (1971), Matsuda et al. (1987, 1992), Boffin and Anzer (1994), Ruffert (1994), Shima et al. (1998) and Isaka et al. (2006). These show that the accretion line is only present transiently as, soon, pressure effects will create a shock upstream of the star (Fig. 7.4). Still, the theoretical and numerical rates agree to within 10–20 %.

When dealing with binary systems, Boffin and Jorissen (1998) replaced v_∞ by $\sqrt{v_w^2 + v_{\rm orb}^2}$, where v_w is the wind speed and $v_{\rm orb}$ is the orbital velocity. The density ρ_∞ is computed from assuming a spherical mass loss from the primary and averaging over one orbit, $\dot{M}_w = 4\pi \rho_\infty a^2 \sqrt{1 - e^2} v_w$. This then leads to a mass transfer rate, β:

$$\beta = -\frac{\dot{M}_{\rm acc}}{\dot{M}_w} = \alpha \frac{1}{\sqrt{1 - e^2}} \left(\frac{q}{1 + q} \right)^2 \frac{v_{\rm orb}^4}{v_w \left(v_w^2 + v_{\rm orb}^2 + c^2 \right)^{3/2}}. \tag{7.12}$$

One can see that in the case of a fast wind (the only case when this equation is formally valid), $v_w^2 \gg v_{\rm orb}^2 + c^2$, we have

$$\beta \propto \left(\frac{v_{\rm orb}}{v_w} \right)^4, \tag{7.13}$$

while in the case $v_{\rm orb} \;\; v_w, \; c$,

$$\beta \propto \frac{v_{\rm orb}}{v_w}, \tag{7.14}$$

which could lead to the unphysical case $\beta > 1$.

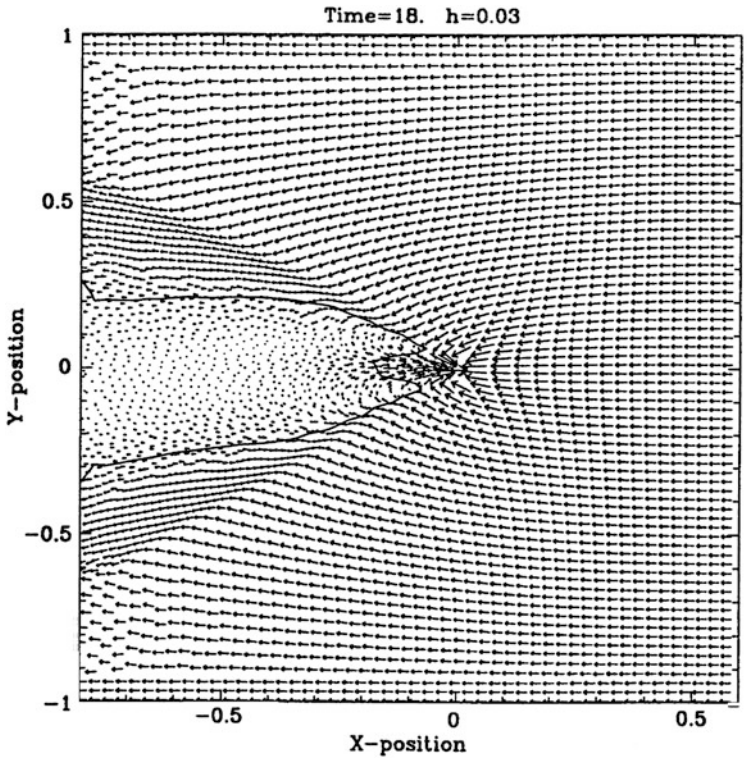

Fig. 7.4 Two-dimensional numerical simulation of a Bondi–Hoyle accretion at Mach 3. The *arrows* illustrate the velocity field, while the *thick line* represents the contour of Mach $= 1$. A shock has been formed but there is still a stagnation point clearly visible, defining the accretion radius. Reproduced with permission from Fig. 1 of Boffin and Anzer (1994)

7.3 Wind Accretion in Binary Systems

The Bondi–Hoyle formulation [Eq. (7.12)] is very widely used—in particular in population synthesis calculations, despite the fact that, while it may be valid when the orbital velocity is much smaller than the wind velocity, i.e. in ζ Aurigae and O-type binaries, it has been shown since two decades that it does not apply to binary systems containing a red giant. In such systems indeed, and unless the system is very wide, the wind velocity (5–30 km/s, depending on the evolutionary stage) of a red giant is smaller than or of the order of magnitude of the orbital velocity, and the binary motion becomes important in determining the flow structure. This, has in turn, also a big impact on the mass accretion rate.

This was first shown by Theuns and Jorissen (1993), Boffin et al. (1994) and Theuns et al. (1996) who clearly demonstrated that the flow structure of a mass-losing AGB star in a 3 AU system was very different from what one expects for a Bondi–Hoyle accretion flow (Fig. 7.5), with the presence of a large spiral. Such

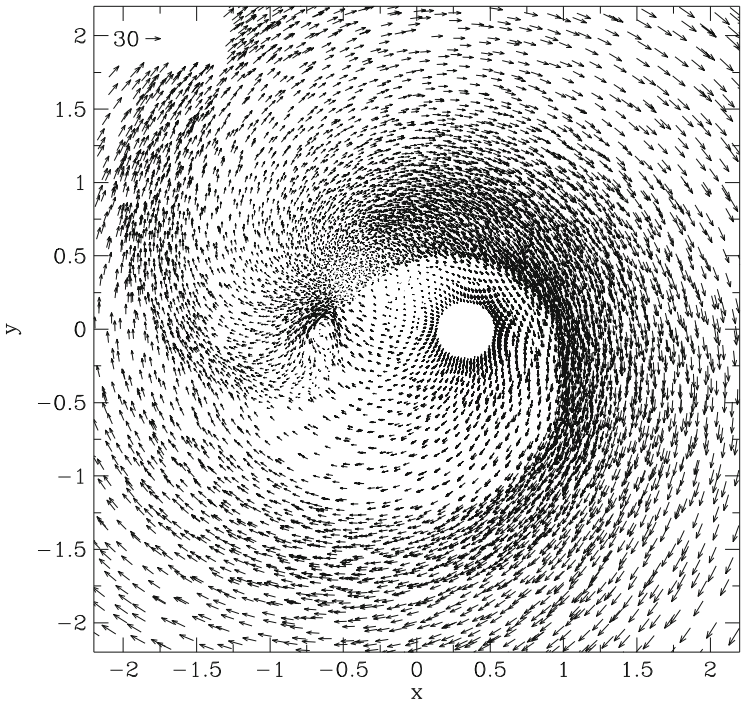

Fig. 7.5 Numerical simulations of mass transfer in a 3 AU binary system, where the primary looses mass through a slow wind. A clear spiral structure is seen in the orbital plane, and the flow is therefore much different from what one expects for a normal Bondi–Hoyle flow, due to the effect of the centrifugal force. Reproduced from Theuns et al. (1996)

spirals have since then been detected observationally by HST in the carbon star AFL3068 (Morris et al. 2006) and with ALMA in R Scl (Maercker et al. 2012). Such a different flow structure also impact the mass accretion rate and Theuns et al. (1996) found a mass accretion rate β of the order 1 % in the adiabatic case, and 8 % for the isothermal case. In the adiabatic case, *this is about ten to twenty times smaller than the theoretical estimates* based on the Bondi–Hoyle prescription, i.e. $\alpha \sim 0.05$–0.1.

A more extensive study was done by Nagae et al. (2004) who explored the full parameter space, varying the wind velocity with respect to the orbital speed, in the case of $q = 1$ (Fig. 7.6). They characterised the flow by the mean normal velocity of the wind on the critical Roche surface of the mass-losing star, v_R. When $v_R < 0.4 v_{\rm orb}$, they obtained Roche-lobe over-flow (RLOF), while for $v_R > 0.7 v_{\rm orb}$ they observed wind accretion. Very complex flow patterns in between these two extreme cases were found. They also found that the mass accreted by the accreting star is roughly *a factor 5 smaller than what would be naively deduced from the Bondi–Hoyle–Lyttleton formalism* (Fig. 7.7).

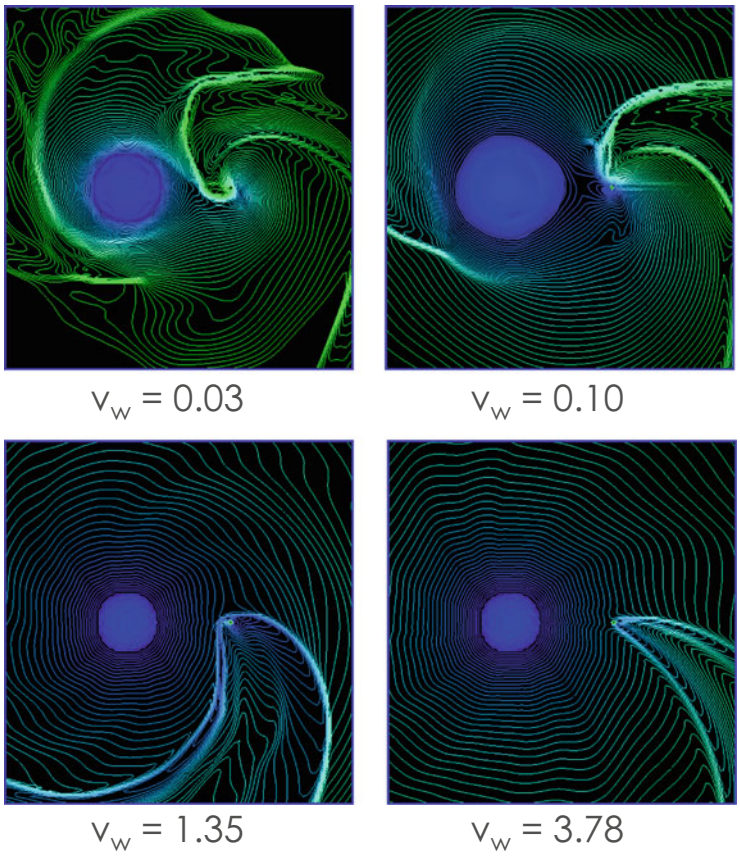

Fig. 7.6 Numerical simulations of mass transfer in a binary system, for various wind speed, v_w, in units of the orbital velocity. The low velocity case shows resemblance to a Roche lobe overflow, although mass also escape through the outer Lagrangian point, while the higher velocity case are reminiscent of ζ Aurigae systems. Adapted from Nagae et al. (2004)

For low v_R, they constructed an empirical formula for the mass accretion ratio given by

$$\beta = 0.18 \times 10^{-0.75 v_R / v_{\rm orb}}. \tag{7.15}$$

For larger v_R they obtain another empirical formula for the mass accretion ratio

$$\beta = 0.05 \left(\frac{v_{\rm orb}}{v_R} \right)^4, \tag{7.16}$$

indicating that in the case $q = 1$ they studied, $\alpha = 0.2$ in Eq. (7.12).

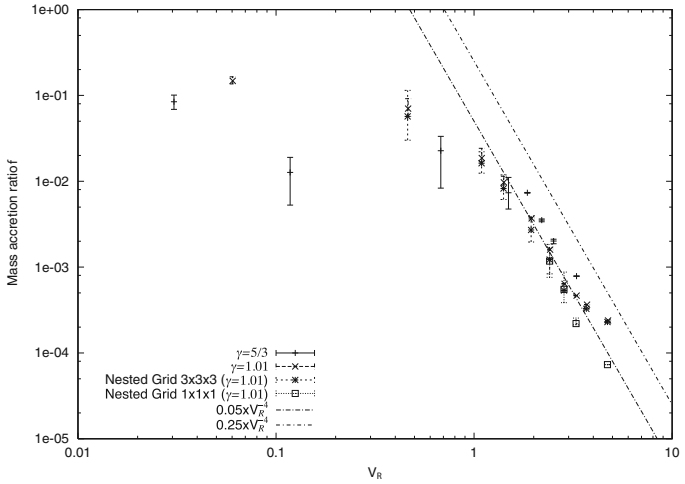

Fig. 7.7 Log–log plot of the mass accretion ratio as a function of the wind velocity at the position of the Roche lobe. The *upper line* shows a simple Bondi–Hoyle–Lyttleton formula with $\alpha = 1$. The *lower dashed line* shows another empirical formula $f = 0.05 v_R^{-4}$, i.e. 20 % the Bondi–Hoyle value. Reproduced with permission from Nagae et al. (2004)

7.3.1 Chemical Pollution

The accretion of material from an evolved star, whose surface composition has been modified from its initial composition (which we can safely assume is also the one of its companion), will lead to chemical pollution. This is for example the case if mass is transferred from an AGB star which already went through thermal pulses and is enriched in carbon and s-process elements. As shown by Boffin and Jorissen (1988) and Theuns et al. (1996), the pollution of the envelope of the accreting star depends on

- the amount of mass ΔM_2 accreted from the wind,
- the dilution factor, $\mathscr{F}$, of the accreted matter in the envelope of mass $M_{2,env}$, i.e., $\mathscr{F} = \Delta M_2/(M_{2,env} + \Delta M_2)$, and
- the difference in chemical composition between the accreted matter and that of the envelope.

Note that one can generally safely assume that the accreted matter has been fully mixed in the envelope. The overabundance f_i of element i in the envelope of the accreting star (i.e., the ratio between the abundance after completion of the accretion and mixing processes, and the abundance in the primordial envelope) is related to its overabundance g_i in the wind (i.e., in the AGB atmosphere) through the relation

$$f_i = \frac{g_i \Delta M_2 + M_{2,env}}{\Delta M_2 + M_{2,env}} \equiv g_i \mathscr{F} + (1 - \mathscr{F}). \tag{7.17}$$

7.3.2 Orbital Parameters Evolution

The mass lost from the system, carrying with it angular momentum, and the mass transferred from one star to the other, will lead to a change in the orbital parameters. Boffin and Jorissen (1988) presented a first analysis of this changes, based on the formalism of Huang (1956). This was revisited by Theuns et al. (1996) who derived:

$$\frac{\dot{a}}{a} = -\frac{\dot{M}_1 + \dot{M}_2}{M_1 + M_2} - 2\frac{F_y}{M_2 v_{\rm orb}}, \tag{7.18}$$

$$\frac{\dot{P}}{P} = -2\frac{\dot{M}_1 + \dot{M}_2}{M_1 + M_2} - 3\frac{F_y}{M_2 v_{\rm orb}}, \tag{7.19}$$

$$\frac{\dot{e}}{e} = -\frac{1}{2}\frac{\dot{M}_2}{M_2} + \frac{3}{2}\frac{F_y}{M_2 v_{\rm orb}}, \tag{7.20}$$

where F_y is the tangential component of the total force, including gravity and accretion of linear momentum.

Karakas et al. (2000) propose a different set of equations

$$\frac{\dot{a}}{a} = -\frac{\dot{M}_1}{M_1 + M_2} - \left(\frac{1 + e^2}{M_1 + M_2} + \frac{2 - e^2}{M_2}\right)\frac{\dot{M}_2}{1 - e^2}, \tag{7.21}$$

$$\frac{\dot{e}}{e} = -\dot{M}_2\left(\frac{1}{M_1 + M_2} + \frac{1}{2M_2}\right). \tag{7.22}$$

In the approximation that little mass is gained, i.e. $\dot{M}_2 \approx 0$, the above equations lead to a widening of the orbit and no change in eccentricity. This is what lead Boffin et al. (1993) to propose that barium stars have evolved from normal red giants at constant eccentricity, and only their orbital period increased. The resulting change in orbital period according to Eq. (7.21) for no mass accretion is thus

$$\frac{P}{P_0} = \left(\frac{M_{1,0} + M_2}{M_1 + M_2}\right)^2, \tag{7.23}$$

where it is assumed that $M_{2,0} = M_2$. Thus, assuming an initial binary system containing a 3 $M_\odot$ AGB star and a 1.5 $M_\odot$ companion with an initial period of 3 years (to avoid Roche lobe overflow by the AGB), leads to a final orbital period of 13.77 years when the AGB became a 0.6 $M_\odot$ white dwarf. It is therefore difficult to explain the orbital periods below 10 years by such mechanisms. To explain shorter systems, one would thus need either to have consequent mass accretion or to have extra angular momentum loss (see Sect. 7.3.4). If there is mass accretion, then the variation of the period is given by (assuming $e = 0$)

$$\frac{P}{P_0} = \left(\frac{M_{1,0} + M_{2,0}}{M_1 + M_2}\right)^2 \left(\frac{M_{2,0}}{M_2}\right)^2, \tag{7.24}$$

so that starting from an initial period of 3 years, we have a final period of 5.2, 3.5, 2.4 and 1.7 years, when accreting 20, 30, 40 or 50 %, respectively. This may be particularly relevant for blue straggler stars that have most likely accreted a large fraction of their mass (see Chap. 3). Those seen in the open cluster NGC 188 have current orbital period around 1,000 days. They could have thus been the result of wind mass transfer coming from wider systems, if they accreted enough mass.

7.3.3 Spin-Up of Accretor

The companion star may accrete spin angular momentum from the wind, which may alter its rotational velocity. Packett (1981) showed that a star needs to accrete only a few percent of its own mass from a Keplerian accretion disc to be spun up to the equatorial centrifugal limit, essentially because stellar moments of inertia are generally much smaller than MR^2. Theuns et al. (1996) found that in their simulations of wind accretion in a binary system there is a net accretion of spin momentum, in such a way that the accreting star tends to be spun up if it is in synchronous rotation to begin with (see also Jeffries and Stevens 1996). This could explain the rapid rotation of some barium stars, such as HD 165141 (Jorissen et al. 1995), as well as the barium-enriched central stars of planetary nebulae (see Sect. 7.4.3).

7.3.4 Angular Momentum Loss

As shown above, an isotropic mass loss from the mass-losing star without any accretion will lead to an increase in the semi-major axis. When the angular momentum loss is large enough, however, Hachisu et al. (1999) showed that the system can shrink. They use this property to provide a wider channel for symbiotic systems to become Type Ia supernovae. The symbiotic binary system they consider consists of a white dwarf and a mass-losing red giant. If the white dwarf accretes enough of the wind from the giant, it could reach the Chandrasekhar limit and explode as a Type Ia supernova. An essential part of the validity of this single-degenerate channel resides in the fact that the required close white dwarf—red giant binary can form from a very wide binary. They reach their conclusion after noticing that a system, where one of the components has a wind whose velocity is smaller or on the order of the orbital velocity, takes away the orbital angular momentum effectively, hence shrinking the orbit. Jahanara et al. (2005) made detailed three-dimensional hydrodynamic calculations of mass transfer in an interacting binary

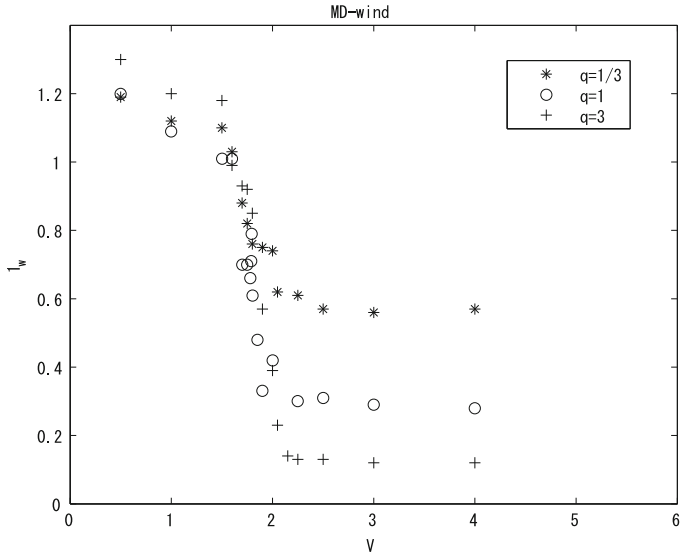

Fig. 7.8 The specific angular momentum loss l_w is shown as a function of the outflowing velocity on the surface of the mass-losing star, V. Three mass ratios, $q = 1/3$, 1, and 3, are examined. The specific angular momentum loss decreases from about 1–1.2 at low V (RLOF) to 0.1–0.5 at high V (wind type flow). For very fast wind, i.e., when $V > 2$, all the cases approach an asymptotic value. Reproduced with permission from Jahanara et al. (2005)

system in which one component undergoes mass loss through a wind, for various values of the mass ratio. They were particularly interested in looking at the amount of specific angular momentum of gas escaping the system (l_w) in order to see if the scenario of Hachisu et al. (1999) was valid.

The isotropic mass loss assumes that $l_w \equiv l_{w,s} = 1/(1+q)^2$, easily derivable from assuming that all the mass lost carries the angular momentum of the mass-losing star. Jahanara et al. (2005) found (Fig. 7.8) that for high wind velocities one reaches such limiting value for mass ratios smaller than one, but for higher q they obtain larger values than predicted—by a factor two for $q = 3$ and a factor of five for $q = 7$. For low wind velocities, moreover, the specific angular momentum does not vary greatly as a function of the mass ratio and is much higher than the value predicted by this simple formula. They obtain the following fit for the specific angular momentum loss:

$$l = 0.25 + \frac{0.12}{v_R + 0.02} \qquad q = 1 \tag{7.25}$$

$$l = 0.12 + \frac{0.12}{v_R + 0.02} \qquad q = 3, \tag{7.26}$$

where v_R is the velocity of the gas at the Roche radius.

The possibility that the specific angular momentum loss can be much larger than the canonical value has important consequences on the variations of the orbital parameters. We can write the variation of the semi-major axis $\dot{a}$ as a function of the angular momentum loss $\dot{J}$ (for $e = 0$):

$$\frac{\dot{a}}{a} = 2\frac{\dot{J}}{J} + \frac{\dot{M}_1 + \dot{M}_2}{M_1 + M_2} - 2\frac{\dot{M}_1}{M_1} - 2\frac{\dot{M}_2}{M_2}. \tag{7.27}$$

Writing the angular momentum loss, $\dot{J}$, in function of the dimensionless specific angular momentum loss, l_w, i.e. $\dot{J} = l_w a^2 \Omega(\dot{M}_1 + \dot{M}_2)$, we have:

$$\frac{\dot{a}}{a} = \frac{\dot{M}_1 + \dot{M}_2}{M_1 + M_2} + 2\frac{\dot{M}_1}{M_1}\left(l_w - 1 + l_w\frac{M_1}{M_2}\right) + 2\frac{\dot{M}_2}{M_2}\left(l_w - 1 + l_w\frac{M_2}{M_1}\right). \tag{7.28}$$

Neglecting the mass accreted, we have

$$\frac{\dot{a}}{a} = \left(\frac{M_1}{M_1 + M_2} + 2\frac{M_1 + M_2}{M_2}l_w - 2\right)\frac{\dot{M}_1}{M_1} \equiv L(q)\frac{\dot{M}_1}{M_1}. \tag{7.29}$$

With a value of $l_w \sim 1$, the function in front of $\dot{M}_1/M_1$ would be positive, hence the orbit would shrink, because $\dot{M}_1 < 0$. As seen above, $l_w \approx 1$ is a plausible value for low wind speed flows. From Eq. (7.29),

$$L(q) = \frac{q}{1+q} + 2l_w(1+q) - 2, \tag{7.30}$$

so that for the system to shrink we need to have $L(q) > 0$ and, hence,

$$l_w > \frac{1}{2}\frac{2+q}{(1+q)^2}.$$

From the results of the numerical simulations of Jahanara et al. (2005), as shown by Eq. (7.26), it appears that the system would shrink—when assuming no mass accretion—when the wind speed at the Roche lobe is smaller than about one ($q = 1$) and three ($q = 3$) times the orbital velocity. One can also show that the conclusion still holds, when the mass ratio is larger or equal to one, when mass accretion is taken into account. This makes the symbiotic channel for Type Ia supernovae a plausible one and could also dramatically help explain the existence of Barium stars and other Peculiar Red Giants with orbital periods below, say, 1,000 days (see, e.g., Abate et al. 2013).

It still remains to be seen what would be the evolution of the eccentricity caused by this specific angular momentum loss, but in any case, it seems clear that binary population synthesis codes should take these corrected values for mass accretion and angular momentum loss into account when trying to explain post-AGB systems.

7.4 The Zoo of Peculiar Stars

7.4.1 Barium and Related Stars

Barium stars constitute about 1 % of G–K giants that show in their spectra a very strong BaII 4554 line. The group was defined by Bidelman and Keenan (1951) from inspection of low resolution spectrograms. These authors also called attention to some other prominent features in the spectra of those stars, namely the enhancement of all BaII lines, of the 5165 C_2 band, as well as of the G-band due to CH. In addition, some bands of CN are also enhanced. An index of the strength of the BaII 4554 line has been introduced by Warner (1974): the line strength is estimated visually on a scale from 1 (weak) to 5 (strong). Abundance analyses of the atmosphere of barium stars have shown that elements with $Z \leq 38$ behave as in normal giants, except carbon which is enhanced. Heavier elements up to Ba ($Z = 56$) are enhanced, and still heavier elements are generally not enhanced. This is the typical behaviour expected from the s-process, one of the two processes of neutron captures on iron-peak elements. The s- (or slow-) process takes in particular place during the thermal pulses on the upper-Asymptotic Giant Branch (AGB).

CH stars present also strong bands of CH, the enhancement being larger than in barium stars. Most of the metallic lines are weakened, but heavy elements are enhanced. Other carbonated molecules, like C_2 and CN are also strengthened.

In S stars, the BaII lines are enhanced, as are the SrII lines. However, S stars are of later type than the barium stars (around M0) and, therefore, exhibit ZrO bands.

F str4077 stars were discovered by Bidelman (1981) on the basis of objective-prism spectra. Those F-type main sequence stars have normal or deficient abundance of the iron-peak elements, but overabundance of the s-process elements. They are now commonly included, together with CH subgiants, in the class of dwarf barium stars (Lü 1991). Other carbon-rich dwarfs are also known (see, e.g., Lambert 1985; Jaschek and Jaschek 1987; Gray et al. 2011). In barium stars, the overabundance of s-process elements over the solar value, ranges from a factor 2 (mild barium stars) to a factor 30 (strong barium stars). In CH stars, this enhancement is still larger, up to 100 sometimes.

Thus barium and related stars present carbon and s-process element enhancements, which are typical of evolved AGB stars, but they are in an evolutionary stage prior to the AGB. This apparent paradox can be solved only by assuming that these peculiar stars are all binaries. And indeed, in the early 1980s, McClure et al. (1983) found that barium stars seemed to belong to binary systems, a conclusion further confirmed by McClure and Woodsworth (1990), Jorissen and Boffin (1992), Jorissen and Mayor (1992) and Jorissen et al. (1998). These systems have orbital periods in the range 80 days to several years. Jorissen and Mayor (1992) also found that non-Mira S stars are predominantly binary systems with similar periods. The companion in these systems are all thought to be white dwarf, i.e., the remnant of a former AGB (Böhm-Vitense et al. 1984; Webbink 1988). As clearly emphasised by Eggleton (1992),

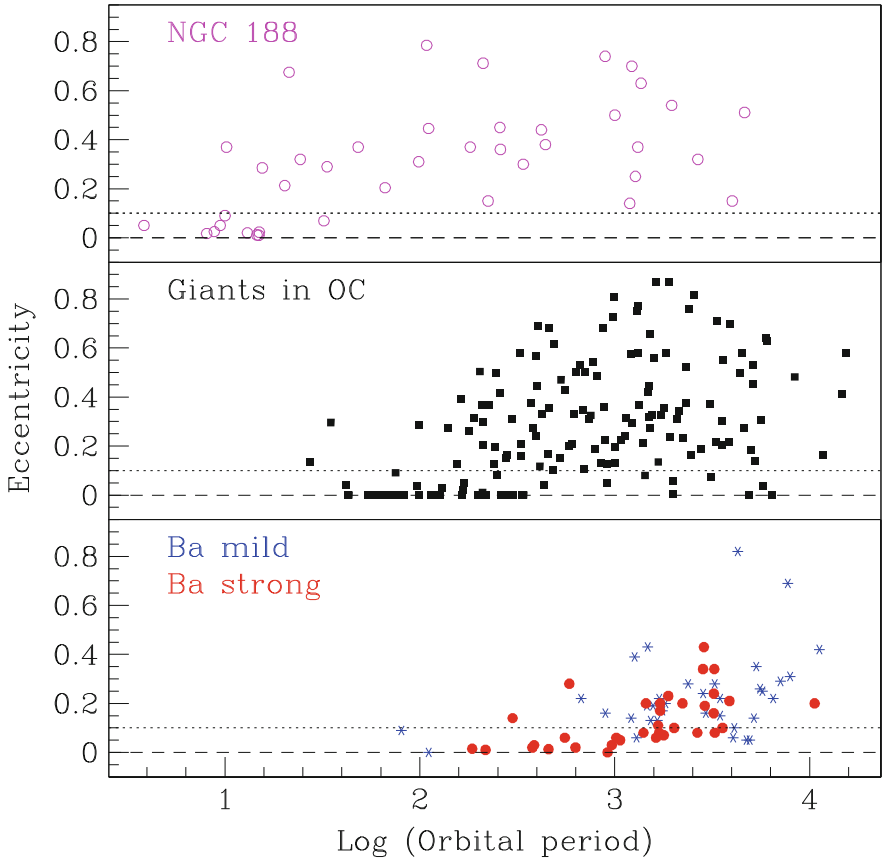

Fig. 7.9 Eccentricity-period (in days) diagrams for various samples. The *upper panel* shows the main-sequence stars in the open cluster NGC 188 (from Geller et al. 2009; see also Chap. 3); the *middle panel* shows red giant spectroscopic binaries in open clusters (from Mermilliod et al. 2007); while the *lower panel* shows a compilation of orbital elements for mild and strong barium stars. The *dotted line* shows the limit $e = 0.1$

Barium stars have a claim to be considered the most important class of binaries to have emerged in the last few decades. This is partly because their putative progenitors are intrinsically common, and partly because they themselves are quite common, i.e. they appear to have to be the fairly normal outcome of evolution in a binary with period in the range 1–10 yrs.

A striking property of barium stars is that they have non-circular orbits, even though they have eccentricities smaller than normal systems (Boffin et al. 1992, 1993). Figure 7.9 shows the eccentricity-orbital period diagrams for several samples of stars. The upper panel shows the main sequence stars in the old open cluster NGC 188 (Chap. 3) and is typical of main sequence spectroscopic binaries. It shows that such systems have almost any eccentricity at a given period with two exceptions: the

closest of all systems have been circularised by tidal forces, while for periods above ∼50 days, there are no binary systems with eccentricity below 0.1 (dotted line). When looking at the sample of red giants in open clusters (Mermilliod et al. 2007), we can see that all the shortest period systems have disappeared due to RLOF—they will have undergone mass transfer and most likely a common envelope phase (see Chap. 8), and the red giant is now stripped of its mass and appears as a (He) white dwarf. The circularisation period has increased given the larger radii of red giants and, although there is a general trend for longer systems to be more eccentric, the eccentricity is quite large on average. A few systems occupy the large P—small e region in the plane, and this is most likely because these are post-mass transfer systems, containing a red giant and a white dwarf. The third panel shows the diagram for barium stars and it is clear that although *most systems are not circularised*, the average eccentricity is much smaller than for normal giants. Several systems also occupy the large P—small e region. The fact that the orbits of barium stars are generally not circularised may indicate that these systems avoided a phase of RLOF, or that some eccentricity-pumping mechanism was excited after the RLOF. It is very interesting to compare the $e - \log P$ diagram of barium stars with that of blue straggler stars in NGC 188, as shown in Fig. 3.2 in Chap. 3. The striking resemblance may point to a common origin for these blue straggler stars and barium stars. In this respect, it would be useful to know if *any of the blue straggler stars in NGC 188 are s-process and/or carbon enriched*.

Boffin and Jorissen (1988) devised a model of wind accretion from an AGB star to explain barium and related stars. They assumed a binary system with a wide enough orbit in which the AGB star is transferring mass via a stellar wind to a main sequence companion which becomes polluted in carbon and s-process elements. The AGB then evolves into a white dwarf while the companion will appear as a carbon or barium dwarf and, when on the giant branch, as a peculiar red giant. This model seems to reproduce the bulk properties of bariums stars (Jorissen and Boffin 1992; Boffin and Začs 1994), although there is still a debate in the literature as to how these systems avoided RLOF and have their current non-zero eccentricity. The discussion above as shown, however, that it is possible to end up with the current orbital periods, even if the progenitors systems were much wider, and several studies have also shown that it is possible to reproduce the eccentricity distribution of barium stars (Karakas et al. 2000; Bonačić Marinović et al. 2008).

The important features of the Boffin and Jorissen wind accretion model is that it is able to explain:

- the existence of barium stars with very long orbital periods;
- the existence of a weak correlation between s-process enhancement and orbital period;
- the non-circular orbits of long period systems; and
- the existence of dwarf barium stars.

Boffin and Jorissen assumed the Bondi–Hoyle mass accretion rate, Eq. (7.12) (in fact, they implemented the idea!). Boffin and Začs (1994) showed, however, that even if the mass accretion rate was lower than that derived by this approximate

formula, i.e., of a few percents only as shown above, it was still enough to explain the pollution of most barium stars. The initial model of Boffin and Jorissen (1988) fails, however, to explain most small period barium star systems with orbital period below, say, 1,000 days. The existence of such systems was always a problem since if one takes the value of the specific angular momentum given by the spherically symmetric wind, one finds that the system will widen. Things changes when one takes into account the specific angular momentum loss as computed by Jahanara et al. (2005). If the present system has a period below 1,000 days, say, then for typical masses in a barium system, its present separation is roughly 2.5 AU, implying with the canonical value of $l_{w,s}$ an initial semi-major axis of less than 1 AU. This is too small to hope to fit an asymptotic giant branch star without having Roche-lobe overflow. With the value of the specific angular momentum loss found by Jahanara et al. (2005), the system did not expand, but instead shrank by a factor 3 to 10, depending on the ratio of the wind speed to the orbital velocity. Interestingly, Brookshaw and Tavani (1993) also emphasise the importance of angular momentum loss in the evolution of binary systems and the fact that the often used approximation $l_w = l_{w,s}$ can lead to wrong conclusions, in particular in X-ray binaries.

7.4.2 Symbiotic Stars and the Case of SS Lep

Symbiotic stars are a class of bright, variable red giant stars, whose composite spectrum present typical absorption features of a cool star on top of strong hydrogen and helium emission lines, linked to the presence of a hot star and a nebula. It is now well established that such a "symbiosis" is linked to the fact that these stars are active binary systems, with orbital periods between a hundred days and several years. Symbiotic stars are de facto the low- and intermediate-mass interacting binaries with the longest orbital periods and the largest component separations. They are thus excellent laboratories to study a large range of very poorly understood physical processes (Mikolajewska 2007).

One of the main questions related to symbiotic stars is how the mass transfer takes place: by stellar wind, through Roche-lobe overflow or through some intermediate process? Answering this question indeed requires being able to compare the radius of the stars to the Roche lobe radius. Optical interferometry can achieve this and in particular Blind et al. (2011) used this unique ability to study in unprecedented detail the interacting binary system SS Leporis.

SS Leporis is composed of an evolved M giant and an A star in a 260-day orbit, and presents the most striking effect of mass transfer, the "Algol" paradox; that is, the M giant is less massive than the A star. The latter is unusually luminous and surrounded by an expanding shell, certainly as the result of accretion. The observation of regular outbursts and of ultraviolet activity from the A star shell are further hints that mass transfer is currently ongoing.

SS Lep was observed during the commissioning of the PIONIER visitor instrument at the Very Large Telescope Interferometer. Blind et al. (2011) were able

to detect the two components of SS Lep as they moved across their orbit and to measure the diameter of the red giant in the system (∼2.2 milli-arcseconds). By reconstructing the visual orbit and combining it with the previous spectroscopic one, they could further constrain the parameters of the two stars.

The M giant is found to have a mass of 1.3 $M_\odot$, while the less evolved A star has a mass twice as large: thus a clear mass reversal must have taken place, with more than 0.7 $M_\odot$ having been transferred from one star to the other. The results also indicate that the M giant only fills around 85 ± 3 % of its Roche lobe, which means that the mass transfer in this system is most likely by a wind and not by RLOF. It is useful to note that given the rather low mass loss from the giant in SS Lep, the Roche lobe will not be much affected, as the f parameter (cf. Sect. 7.1) is most likely only of order 0.01–0.1, leading to a decrease of the Roche lobe by 1–4 % only.

Podsiadlowski and Mohamed (2007) suggest the possibility of a new mode of mass transfer—the wind Roche lobe overflow—where a slow wind fills the Roche lobe. This is in effect the low wind velocity case of Nagae et al. (2004); see Fig. 7.6. Because the wind speed in M giants is rather small (around 10–15 km/s) and lower than the orbital one for SS Lep ($v_{\rm orb} = 48$ km/s), we expect it to be in the particular case of a wind Roche lobe overflow, where a substantial part of the stellar wind can be accreted. The simulations of Nagae et al. (2004) show that at least 10 % of the M giant wind could be accreted in SS Lep. Abate et al. (2013) find much larger mass transfer, up to 50 %. The mass transfer cannot be fully conservative though, as matter will generally also escape through the outer Lagrangian point.

However, it is still difficult to explain the current system state with normal stellar-wind rates, which are too low. Indeed, before the AGB phase, the typical mass-loss rates are around ~ 1–2×10^{-8} $M_\odot$ year^{-1} at the normal (e.g., Reimers) rate. The M giant (with an expected initial mass > 2.2 $M_\odot$) should have lost only a few hundredths of a solar mass before reaching the AGB, whereas we expect it to have lost at least 0.9 $M_\odot$. As the M star is on the AGB since only a few million years—and will stay there for a few million years more at most—it cannot have lost much mass since then. There is, however, some evidence of enhanced wind mass loss of giants in binaries compared to single giants of the same spectral type (Jorissen 2003; Mikolajewska 2007). From a theoretical point of view, the presence of a companion reduces the effective gravity of the mass-losing star, thus enhancing the mass loss. In the case of SS Lep, the superbly called companion-reinforced attrition process ("CRAP") of tidally enhanced stellar wind (Tout and Eggleton 1988) allows a mass loss rate 150 times higher[1] than the Reimers rate, i.e. $\sim 2.4 \times 10^{-6}$ $M_\odot$ year^{-1}.

[1]The CRAP supposes that the typical mass loss, $\dot{M}_R$, is tidally enhanced by the companion and Tout and Eggleton (1988) propose the following *ad hoc* formula:

$$\dot{M} = \dot{M}_R \left\{ 1 + B \times min \left[\left(\frac{R}{R_L} \right)^6 , \frac{1}{2^6} \right] \right\} , \tag{7.31}$$

with $B \approx 10^4$. It is important to note that the existence of many different kinds of binary systems seem to require the CRAP to work, with different values of B, however.

Quite noteworthy, Bonačić Marinović et al. (2008) and Karakas et al. (2000) also had to invoke some tidally-enhanced mass loss from the AGB star to provide an explanation for the eccentricities of most barium star systems. And so did Abate et al. (2013) to explain carbon-enhanced metal-poor stars.

Blind et al. (2011) were able to reproduce the current state of SS Lep, when including wind RLOF and the CRAP. They started with a system having an initial period of 160 days and initial masses $M_{M,0} = 2.28$ M$_\odot$, $M_{A,0} = 1.85$ M$_\odot$. For about 1 Gyr, the system evolves without much change, and the primary star starts its ascent of the AGB. After 2.8 Myr, the masses and period have reached the currently observed values, with about 0.1 M$_\odot$ having been lost by the system, and forming some circumbinary disc. The mass loss and transfer occurred mostly during the last 500,000 years, with a mass loss $\sim 10^{-6}$ M$_\odot$ year^{-1}. During the whole process, the Roche lobe radius around the M star remained similar, the lowest value being 74 R$_\odot$. No RLOF should thus have happened, unless the initial eccentricity was very high. More detailed simulations (L. Siess, priv. comm.) seem to question the exact details of this scenario, but it should be working in a broad sense.

Boffin et al. (2014a) conducted a mini-survey of symbiotic stars with PIONIER and found that for the three stars with the shortest orbital periods (i.e., HD 352, FG Ser and HD 190658), the giants are filling (or are close to filling) their Roche lobes, while the other three studied stars (V1261 Ori, ER Del, and AG Peg) have filling factors in the range 0.2–0.55, i.e., the star is well within its Roche lobe. They also tentatively propose (Boffin et al. 2014b) that the systems which apparently fill their Roche lobes are those that contain a main-sequence companion or a helium white dwarf (WD), and not a carbon/oxygen (CO) WD.

7.4.3 The Fellowship of the Ring

A small group of planetary nebulae (PNe) are known to harbour binary central stars where a subgiant or giant companion is enriched in carbon and s-process elements (see Boffin and Miszalski 2011; Miszalski et al. 2012 and ref. therein). These are the progenitors of the barium stars, caught during the short-lived phase ($\sim 10^4$ years) when the PN ejected by the white dwarf is still visible. These cool central stars are those of the (unfortunately) denominated A 35-type (Bond et al. 1993). The initial list included A 35, LoTr 1 and LoTr 5 which have rapidly rotating subgiants or giants accompanied by very hot white dwarfs peaking at UV wavelengths ($T_{\rm eff} \geq 100$ kK). Since these initial discoveries, Bond et al. (2003) added WeBo 1 to the list while Frew (2008) raised suspicions that the nebula of A 35 may not be anymore a bona-fide PN, even if it is likely to have passed through a PN phase at some stage to create the stellar abundances currently observed (hence, the group should be named differently!). Further additions of HD 330036 and AS 201 may be drawn from barium enhanced yellow or D'-type symbiotic stars which show extended nebulae, but the classification of such objects as PNe is controversial (Corradi 2003; Jorissen et al. 2005). On the other hand, Tyndall et al. (2013) showed

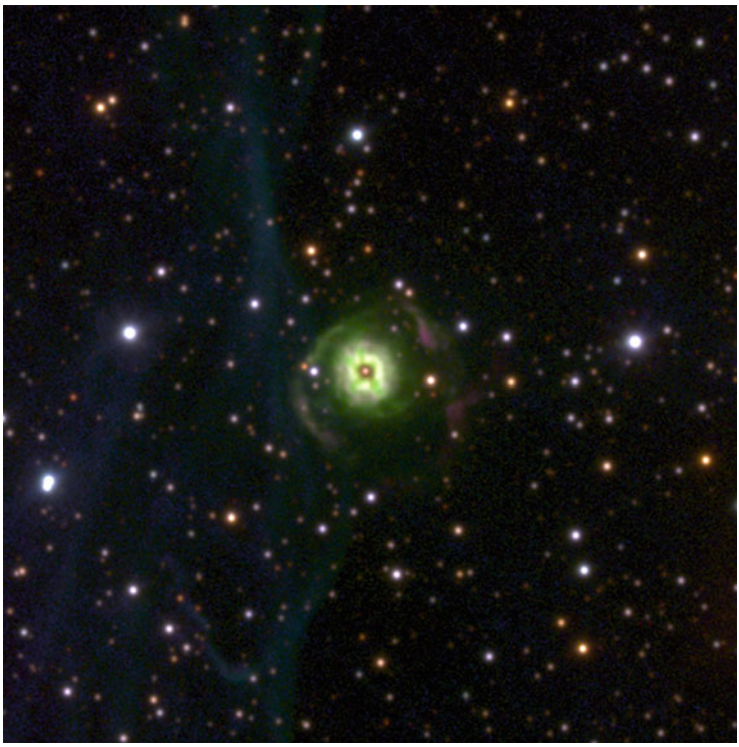

Fig. 7.10 VLT FORS2 colour-composite image of Hen 2-39 made from Hα+[N II] (*red*), [O III] (*green*) and [O II] (*blue*). Reproduced with permission from Miszalski et al. (2013a)

that the cool central star of LoTr 1 is not enhanced in barium and is therefore not a real member of the group. It is also interesting to note that van Winckel et al. (2014) reported the first detection of orbital motion in LoTr5. Despite a 1807-day coverage, a full period was not yet covered, indicating that the orbital period may be as much as 10 years. This makes for a direct link with barium stars.

Miszalski et al. (2012) present UV and optical observations of the *diamond ring* PN A 70 (PN G038.1−25.4) that prove the existence of a barium star binary CSPN. The apparent morphology of A 70 is that of a ring nebula, although on closer inspection the [O III] image shows a ridged appearance similar to Sp 1 which is a bipolar torus viewed close to pole-on.

More recently, Miszalski et al. (2013a) also showed that the cool central star of the planetary nebula Hen 2-39 (Fig. 7.10) is carbon and s-process enriched. Weak Ca II K emission is detected, indicating some chromospheric activity may be present. Time-resolved photometry revealed a short-term periodicity, indicating that the nucleus of Hen 2-39 is a fast rotating giant (with a period of a few days), consistent with the periods found for similar stars. These include 5.9 days for LoTr 5 and 4.7 days for WeBo 1. A rotation period of 6.4 days was also determined for LoTr

1 (Tyndall et al. 2013). Given our discussion in Sect. 7.3.3, one could conjecture that these stars were spun-up during a wind accretion phase.

A significant carbon enhancement of [C/H] $= 0.42 \pm 0.02$ dex is required to fit the observed spectrum of Hen 2-39. The iron abundance was found to be close to solar while barium is clearly overabundant, [Ba/Fe] $= 1.50 \pm 0.25$ dex. Miszalski et al. (2013a) found that it was possible to reproduce such pollution, using 1.8 $M_\odot$ as the initial mass for the AGB star and assuming that the polluted star accreted about 0.5 $M_\odot$ from it during the last thermal pulses. This implies quasi-conservative mass transfer at this stage.

The nebula shows an apparent ring-like morphology as also seen in the other PNe with barium CSPNe, WeBo 1 and A 70. It seems therefore clear that the morphology must be the outcome of the mass transfer episode—most likely by wind—that led to the pollution of the cool central star in carbon and s-process elements. As such, LoTr 5, WeBo 1, A 70, and Hen 2-39 belong to a *Fellowship of the Ring*, all progenitors of barium stars. Their further study should bring detailed knowledge on the wind mass transfer. Moreover, the short time spent during the PN phase makes barium CSPNe a potentially very powerful platform for studying AGB nucleosynthesis in that we simultaneously see both the polluted s-process-rich cool star and the nebula ejected by the polluting star.

7.4.4 *Evidence for Wind Accretion Before Common-Envelope Evolution*

The existence of barium central stars to planetary nebulae constitutes the only firm evidence for mass transfer and accretion onto non-WD companions in PNe. Observations of close binary central stars, i.e. those that have passed through a common-envelope (CE) phase and have orbital periods less than ∼1–2 days (e.g., De Marco 2009; Miszalski et al. 2009), show no evidence for rapid variability (flickering) or spectroscopic features that could be attributed to accretion.

The presence of collimated outflows or jets surrounding several systems (e.g., Boffin et al. 2012) possibly launched from an accretion disc that is no longer present may be indirect evidence for accretion, either prior to the common envelope phase via wind accretion from the AGB primary, during the start of the CE infall phase or perhaps even after the CE phase. Long-slit observations of some jets around post-CE nebulae indicate the jets were probably ejected before their main nebulae (Boffin et al. 2012; Corradi et al. 2011; Mitchell et al. 2007; Miszalski et al. 2011). Another fundamental clue comes from point-symmetric outflows of PNe. Simulations can recreate these complex outflows with a precessing accretion disc around the secondary launching jets (e.g., Cliffe et al. 1995; Raga et al. 2009). While there are multiple examples of such PNe, none were known to have a binary nucleus until the landmark discovery of a post-CE binary nucleus in the archetype of this class Fleming 1 (Boffin et al. 2012). The characteristics of Fleming 1 indicate

that wind accretion (with the formation of a disc) must have happened *before* a CE episode.

However, the clearest proof for accretion would be a polluted main-sequence companion with an atmosphere strongly enriched by accreted material. Miszalski et al. (2013b) report the detection of a carbon dwarf secondary in the post-CE central star binary in the Necklace planetary nebula (PN G054.2−03.4) as the first firm proof for a previous accretion phase. These authors found that to reproduce the observed carbon enhancement, they need to accrete between 0.03 and 0.35 $M_\odot$, depending on the mass of the star, in a binary system with initial orbital period between 500 and 2,000 days. The current period of the system, 1.16 day, clearly proves that the system underwent a common-envelope phase. The most advanced simulations of the spiral-in part of the CE phase by Ricker and Taam (2012) and Passy et al. (2012) predict a negligible amount of mass accretion (10^{-3} $M_\odot$). The accretion is therefore most likely to have occurred before the CE phase via wind accretion, a process that simulations predict to form an accretion disc around the companion (e.g., Theuns et al. 1996). Since the jets of the Necklace are also observed to be older than the main PN (Corradi et al. 2011), they were probably launched from such a disc.

The initial period estimated for the system is typical of symbiotic stars, where substantial wind accretion on to companions is known to occur. A small CE efficiency would then produce a dramatic decrease in the orbital period to the current value. The Necklace nebula is therefore a real **Rosetta Stone** for the study of mass transfer.

Acknowledgements It is a pleasure to thank my many collaborators over the years for exciting work on this topic: A. Acker, U. Anzer, N. Blind, J.-P. Berger, N. Cerf, R. L. M. Corradi, H. Fujiwara, I. Hachisu, H. Isaka, B. Jahanara, D. Jones, A. Jorissen, J.-B. Le Bouquin, T. Matsuda, B. Miszalski, M. Mitsumoto, T. Nagae, K. Oka, G. Paulus, E. Shima, T. Theuns, A. A. Tyndall, and L. Začs

References

Abate, C., Pols, O. R., Izzard, R. G., Mohamed, S. S., de Mink, S. E.: A&A **552**, A26 (2013)
Bidelman, W. P.: AJ **86**, 553 (1981)
Bidelman, W. P., Keenan, P. C.: ApJ **114**, 473 (1951)
Blind, N., Boffin, H. M. J., Berger, J.-P., Le Bouquin, J.-B., Mérand, A., Lazareff, B., Zins, G.: A&A **536**, A55 (2011)
Boffin, H. M. J., Anzer, U.: A&A **284**, 1026 (1994)
Boffin, H. M. J., Cerf, N., Paulus, G.: A&A **271**, 125 (1993)
Boffin, H. M. J., Hillen, M., Berger, J. P., et al.: A&A **564**, A1 (2014a)
Boffin, H. M. J., Blind, N., Hillen, M., et al.: Messenger **156** (2014b)
Boffin, H. M. J., Jorissen, A.: A&A **205**, 155 (1988)
Boffin, H. M. J., Miszalski, B.: in Evolution of Compact Binaries, ASPC **447**, p. 159 (2011)
Boffin, H. M. J., Miszalski, B., Rauch, T., et al.: Science **338**, 773 (2012)
Boffin, H. M. J., Paulus, G., Cerf, N.: in Binaries as Tracers of Star Formation, Cambridge Univ. Press, p. 26 (1992)

Boffin, H. M. J., Theuns, T., Jorissen, A.: MmSAI **65**, 1199 (1994)
Boffin, H. M. J., Začs, L.: A&A **291**, 811 (1994)
Böhm-Vitense, E., Nemec, J., Proffitt, C.: ApJ **278**, 726 (1984)
Bonačić Marinović, A. A., Glebbeek, E., Pols, O. R.: A&A **480**, 797 (2008)
Bond, H. E., Ciardullo, R., Meakes, M. G.: in Planetary Nebulae, ASPC **155**, 397 (1993)
Bond, H. E., Pollacco, D. L., Webbink, R. F.: AJ **125**, 260 (2003)
Bondi, H.: MNRAS **114**, 195 (1952)
Bondi, H., Hoyle, F.: MNRAS **104**, 273 (1944)
Brookshaw, L., Tavani, M.: ApJ **410**, 719 (1993)
Cliffe, J. A., Frank, A., Livio, M., Jones, T. W.: ApJL **447**, 49 (1995)
Corradi, R. L. M.: in Symbiotic Stars Probing Stellar Evolution, ASPC **303**, 393 (2003)
Corradi, R. L. M., Sabin, L., Miszalski, B., et al.: MNRAS **410**, 1349 (2011)
De Marco, O.: PASP **121**, 316 (2009)
Dermine, T., Jorissen, A., Siess, L., Frankowski, A: A& A **507**, 891 (2009)
De Rosa, R. J., Patience, J., Wilson, P. A., et al.: MNRAS **437**, 1216 (2014)
Eggleton, P. P.: ApJ **268**, 368 (1983)
Eggleton, P. P.: in Evolutionary Processes in Interacting Binary Stars, IAU Symp. 151, Kluwer Academic Publishers, p. 167 (1992)
Frew, D. J.: Ph.D. Thesis, Macquarie University (2008)
Geller, A. M., Mathieu, R. D., Harris, H. C., McClure, R. D.: AJ **137**, 3743 (2009)
Gray, R. O., McGahee, C. E., Griffin, R. E. M., & Corbally, C. J.: AJ **141**, 160 (2011)
Hachisu, I., Kato, M., Nomoto, K.: ApJ **522**, 487 (1999)
Hoyle, F., Lyttleton, R.A.: Proc. Cam. Phil. Soc. **35**, 405 (1939)
Huang, S.S.: AJ **61**, 49 (1956)
Hunt, R.: MNRAS **154**, 141 (1971)
Isaka, H., Matsuda, T., Boffin, H. M. J.: PThPh **116**, 1069 (2006)
Jaschek, C., Jaschek, M.: The classification of stars, Cambridge University Press (1987)
Jahanara, B., Mitsumoto, M., Oka, K., Matsuda, T., Hachisu, I., Boffin, H. M. J.: A&A **441**, 589 (2005)
Jeffries, R. D., Stevens, I. R.: MNRAS **279**, 180 (1996)
Jorissen, A.: in Symbiotic Stars Probing Stellar Evolution, ASPC **303**, 25 (2003)
Jorissen, A., Boffin, H. M. J.: in Binaries as tracers of stellar formation, Cambridge Univ. Press, p. 110 (1992)
Jorissen, A., Mayor, M.: A&A **260**, 115 (1992)
Jorissen, A., Hennen, O., Mayor, M., Bruch, A., Sterken, C.: A&A **301**, 707 (1995)
Jorissen, A., Van Eck, S., Mayor, M., Udry, S.: A&A **332**, 877 (1998)
Jorissen, A., Začs, L., Udry, S., Lindgren, H., Musaev, F. A.: A&A **441**, 1135 (2005)
Karakas, A. I., Tout, C. A., & Lattanzio, J. C.: MNRAS **316**, 689 (2000)
Kopal, Z.: Ann. Astrophys.**18**, 379 (1955)
Kopal, Z.: Close binary systems, The International Astrophysics Series, Chapman & Hall (1959)
Lambert, D. L.: in Cool Stars with Excesses of Heavy-elements, p. 191 (1985)
Lü, P. K.: AJ **101**, 2229 (1991)
Matsuda, T., Inoue, M., Sawada, K.: MNRAS **226**, 785 (1987)
Matsuda, T., Ishii, T., Sekino, N., Sawada, K., Shima, E., Livio, M., Anzer, U.: MNRAS **255**, 183 (1992)
Maercker, M., Mohamed, S., Vlemmings, W. H. T., et al.: Nature **490**, 232 (2012)
McClure, R. D., Fletcher, J. M., Nemec, J. M.: ApJL **238**, 35 (1983)
McClure, R. D., Woodsworth, A. W.: ApJ **352**, 709 (1990)
Mermilliod, J.-C., Andersen, J., Latham, D. W., Mayor, M.: A&A **473**, 829 (2007)
Mikolajewska, J.: Baltic Astronomy **16**, 1 (2007)
Mitchell, D. L., Pollacco, D., O'Brien, T. J., et al.: MNRAS **374**, 1404 (2007)
Miszalski, B., Acker, A., Moffat, A. F. J., Parker, Q. A., & Udalski, A.: A&A **496**, 813 (2009)
Miszalski, B., Jones, D., Rodríguez-Gil, P., et al.: A&A **531**, A158 (2011)

Miszalski, B., Boffin, H. M. J., Frew, D. J., Acker, A., Köppen, J., Moffat, A. F. J., Parker, Q. A.: MNRAS **419**, 39 (2012)
Miszalski, B., Boffin, H. M. J., Jones, D., et al.: MNRAS **436**, 3068 (2013)
Miszalski, B., Boffin, H. M. J., Corradi, R. L. M.: MNRAS **428**, L39 (2013)
Morris, M., Sahai, R., Matthews, K., et al.: in Planetary Nebulae in our Galaxy and Beyond, ASPC **234**, p. 469 (2006)
Nagae, T., Oka, K., Matsuda, T., Fujiwara, H., Hachisu, I., Boffin, H. M. J.: A&A **419**, 335 (2004)
Packett, W.: A&A **102**, 17 (1981)
Paczyński, B.: ARA&A **9**, 183 (1971)
Passy, J.-C., De Marco, O., Fryer, C. L., et al.: ApJ **744**, 52 (2012)
Plavec, M., Kratochvil, P.: Bulletin of the Astronomical Institutes of Czechoslovakia **15,** 165 (1964)
Podsiadlowski, P., Mohamed, S. 2007, Baltic Astronomy **16**, 26 (2007)
Raga, A. C., Esquivel, A., Velázquez, P. F., et al.: ApJL **707**, L6 (2009)
Raghavan, D., McAlister, H. A., Henry, T. J., et al.: ApJS **190**, 1 (2010)
Ricker, P. M., Taam, R. E.: ApJ **746**, 74 (2012)
Ruffert, M.: ApJ **427**, 342 (1994)
Schuerman, D. W.: Ap&SS **19**, 351 (1972)
Shima, E., Matsuda, T., Anzer, U., Boerner, G., Boffin, H. M. J.: A&A **337**, 311 (1998)
Theuns, T., Boffin, H. M. J., Jorissen, A.: MNRAS **280**, 1264 (1996)
Theuns, T. & Jorissen, A.: MNRAS **265**, 946 (1993)
Tout, C. A. & Eggleton, P. P.: MNRAS **231**, 823 (1988)
Tyndall, A. A., Jones, D., Boffin, H. M. J., et al.: MNRAS **436**, 2082 (2013)
Van Winckel, H., Jorissen, A., Exter, K., et al.: A&A **563**, L10 (2014)
Warner, B.: MNRAS **129**, 263 (1974)
Webbink, R. F.: in Critical Observations vs. Physical Models for Close Binary Systems, Gordon and Breach Science Publishers, p. 403 (1988)

Chapter 8
Binary Evolution: Roche Lobe Overflow and Blue Stragglers

Natalia Ivanova

8.1 Introduction

As we have seen in Chap. 7, when a star (the donor) in a binary system has a radius larger than some critical value, called the Roche lobe, it will transfer mass to its companion (the accretor), through Roche lobe overflow (RLOF). Both the beginning of the RLOF and its outcome depend strongly on what *kind* of a donor had started the mass transfer. Several characteristics are commonly considered to be most important for predicting the outcome:

1. the evolutionary status of the donor—this implies its complete internal structure;
2. the structure of the donor's envelope;
3. the mass ratio of the binary;
4. the type of the accretor

All these properties are intrinsically responsible for the stability of the mass transfer and for its final product.

As opposed to those governing features, the mass transfer can also be discussed in terms of its case. The **case** of the mass transfer is simply a *classification* of the mass transfer by the evolutionary status of the donor as the following:

- **Case A**—during hydrogen (H) burning in the core of the donor.
- **Case B**—after exhaustion of hydrogen in the center of the donor.
- **Case C**—after exhaustion of central helium (He) burning.

The case A and the case B were first introduced by Kippenhahn and Weigert (1967), and the case C was later introduced by Lauterborn (1970) (he cited Kippenhahn and

N. Ivanova (✉)
University of Alberta, Edmonton, AB, Canada T6G 2G7
e-mail: nata.ivanova@ualberta.ca

H.M.J. Boffin et al. (eds.), *Ecology of Blue Straggler Stars*, Astrophysics and Space Science Library 413, DOI 10.1007/978-3-662-44434-4_8

Weigert 1967 for the compete A–B–C classification, however no traces of the case C discussion there could be found). Interesting, that when the case C was introduced, the specific clarification for the case B was made that the central He burning has not yet started. This left the central He core burning in limbo for the purpose of this simple classification, and in literature it has been filed variably as cases B or C.

Nonetheless, it is important to realise that the specific case of the mass transfer by itself does not imply whether the mass transfer would be stable or not, as it was based on the current nuclear energy source. The evolutionary stage and internal structure of the donor are more important in determining what object could be left at the end of the mass transfer *if* the initial stability and the timescale of the initiated mass transfer are known by other means. The structure of the inner layers may affect the stability of the mass transfer later on, for example, when the initial core becomes exposed (for further details see Sect. 8.4.2.4). It is the structure of the donor's envelope that affects the initial stability.

Any of the cases of the mass transfer could start with any type of donor's envelope—either radiative or convective envelope (see Fig. 8.1 for a typical radius evolution), especially considering that case C *might* include the He core burning stage. On the other hand, RLOF might not start at some of evolutionary stages. For instance, unless the binary has been perturbed so as to shrink, a donor usually cannot have RLOF if its radius at this moment is smaller than at any moment of the donor's life before (otherwise it would have undergone the RLOF earlier). To alter that, an angular momentum loss from the binary needs to occur. While the donor evolves, its timescales for the next evolutionary stages speed up compared to main sequence lifetime. Coupled with the donor's wind mass loss, this usually prevents the start of

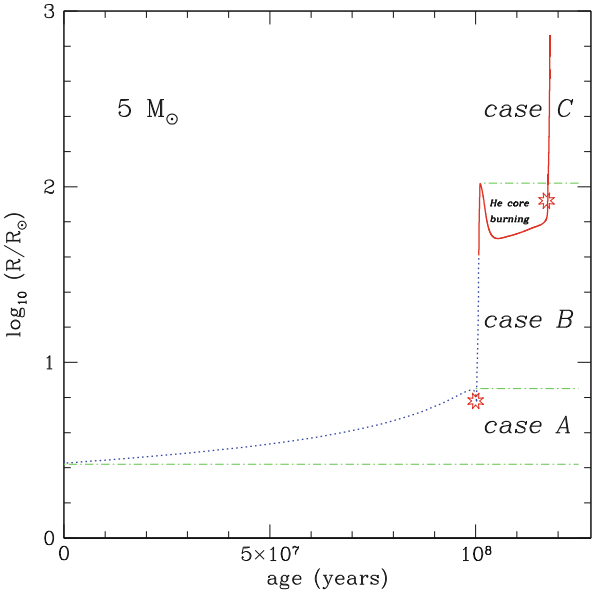

Fig. 8.1 Evolution of the radius of a single star of 5 $M_\odot$ (metallicity $Z = 0.02$). The *dotted* (*blue*) *line* indicates that the star has radiative envelope and *solid* (*red*) *line* indicates that the star has a convective envelope. Two "star" symbols indicate when hydrogen is exhausted in the core and when helium is exhausted in the core. *Green dash-dotted lines* separate the cases of the mass transfer in an assumption that a binary does not shrink

the mass transfer if a potential donor has contracted during, e.g., its He core burning (see Fig. 8.1).

8.2 Stability of the Mass Transfer: The Global Condition

When a donor starts it mass transfer, two things happen at the same time. First, a mass-loosing star changes its radius. The response of the donor radius $R_{\rm d}$ to the mass-loss can be written as $R_{\rm d} \propto M^{\zeta_*}$. During the mass transfer, bits of the donor's material either move from one star to another, or they are lost from the system. Angular momentum then could be transferred to a companion, or to a circumbinary disc, or again it could be lost from the binary system via magnetic braking, or gravitational wave radiation, or simply with the lost material. The Roche lobe's response to the mass loss can be written as $R_{\rm L} \propto M^{\zeta_{\rm L}}$. These two responses are known as mass-radius exponents and were first introduced in Webbink (1985) (see also Hjellming and Webbink 1987 for more details).

$$\zeta_{\rm L} \equiv \frac{d \log R_{\rm L}}{d \log M} \,. \tag{8.1}$$

$$\zeta_* \equiv \left(\frac{\partial \log R_{\rm d}}{\partial \log M} \right) \,. \tag{8.2}$$

In the last exponent, the changes of the donor radius are only due to its evolution and the mass loss.

In order to continue the mass transfer *stably*, the donor must remain within its Roche lobe. Hence, the stability of the mass transfer depends on the donor's response to the mass loss (this is implicit in ζ_*) and on how conservative the process is and what are angular momentum loss processes in this binary (this is implicit in $\zeta_{\rm L}$). Then

$$\begin{aligned} &\zeta_* \geq \zeta_{\rm L} \iff \text{stability of the mass transfer ;} \\ &\zeta_* < \zeta_{\rm L} \iff \text{instability of the mass transfer.} \end{aligned} \tag{8.3}$$

The larger ζ_*, the more stable the mass transfer is.

This condition—due to the donor response—represents only one of the possible situations leading to the unstable mass transfer. Unstable mass transfer can also be a result of the *accretor's* response on a too fast mass transfer. For example, too fast accretion rate can reincarnate a white dwarf into a red giant (Nomoto et al. 1979), or build up of a "trapped" envelope around a neutron star during a super-Eddington mass-transfer (Begelman 1979). More discussion on these cases can be found in Ivanova et al. (2013). Here we will only provide an example that is more applicable

for blue straggler formation: an accretor can overfill its own Roche lobe, due to its evolution, while mass transfer from the primary is still continuing. When the spin angular momentum of the system is more than a third of its orbital angular momentum, the system is secularly unstable with respect to mass transfer. This is known as the Darwin instability (Darwin 1879; Hut 1980).

8.3 Roche Lobe Response

As mentioned in Chap. 7, the Roche lobe radius is given by (Eggleton 1983):

$$\frac{R_{\rm L}}{a} = \frac{0.49q^{2/3}}{0.6q^{2/3} + \ln(1+q^{1/3})} \,. \tag{8.4}$$

Here q is the mass ratio ($q = M_{\rm d}/M_{\rm a}$, where $M_{\rm a}$ is the accretor mass) and a is the binary's orbital separation. For the useful range of mass ratios $0.1 < q < 10$, this Roche lobe radius also can be further approximated as (Eggleton 2006):

$$\frac{R_{\rm L}}{a} \approx 0.44\frac{q^{0.33}}{(1+q)^{0.2}} \,. \tag{8.5}$$

The response of the Roche lobe in the case when the mass transfer is fully conservative—neither mass nor angular momentum is lost from the binary—is then (Tout et al. 1997)

$$\zeta_{\rm L} = 2.13q - 1.67 \,. \tag{8.6}$$

The mass transfer will become unstable if the mass ratio is higher than the critical value:

$$q > q_{\rm crit} = \frac{\zeta_*}{2.13} + 0.788 \,. \tag{8.7}$$

$q_{\rm crit}$ provides a useful way to estimate roughly whether the mass transfer would be stable or unstable. We emphasise, however, that the intrinsic condition of dynamically unstable mass transfer is given by the donor response, ζ_*, and is only expressed via $q_{\rm crit}$. This is frequently forgotten and $q_{\rm crit}$ is used at face value only, despite the fact that the donor's response, even for the same class of donors, varies.

As opposed to *conservative* mass transfer, a mass transfer evolution where mass or angular momentum is taken away from the system and, hence, is not conserved has been named *liberal* (Eggleton 2000). A great amount of details on how $\zeta_{\rm L}$ changes in cases of various modes of mass and angular momentum loss can be found in Soberman et al. (1997). We only consider here the next most important case,

when only a fraction of the transferred material, β, is accreted onto $M_{\rm a}$ (with $\beta = 1$ implying that the mass transfer is fully conservative). Equation (8.1) expands as

$$\zeta_L = \frac{\partial \ln a}{\partial \ln m_{\rm d}} + \frac{\partial \ln(R_L/a)}{\partial \ln q}\frac{\partial \ln q}{\partial \ln m_{\rm d}} \,. \tag{8.8}$$

Here $\partial \ln a / \partial \ln m$ is solely due to the mass loss or transfer:

$$\frac{\partial \ln a}{\partial \ln m_{\rm d}} = \frac{m_{\rm a}}{\dot{m}_{\rm d}}\frac{\dot{a}}{a} = \frac{2q^2 - 2 - q(1-\beta)}{q+1} \,. \tag{8.9}$$

The second term consists of the mass ratio response to the change in donor mass,

$$\frac{\partial \ln q}{\partial \ln m_{\rm d}} = 1 + \beta q, \tag{8.10}$$

and the Roche lobe response to the change in mass ratio, which can be found using Eggleton's approximation (Eggleton 1983):

$$\frac{\partial \ln(R_L/a)}{\partial \ln q} = \frac{2}{3} - \frac{q^{1/3}}{3}\frac{1.2q^{1/3} + 1/(1+q^{1/3})}{0.6q^{2/3} + \ln(1+q^{1/3})} \,. \tag{8.11}$$

The derivations above are important to show that if the mass transfer is becoming non-conservative ($\beta < 1$), the value of $\zeta_{\rm L}$ is decreasing. This implies that non-conservative mass transfer is stable over a larger range of mass ratios than conservative mass transfer.

8.4 Donor's Response

8.4.1 Timescales

If a star suddenly loses mass, then both hydrostatic and thermal equilibria are disturbed, and a star starts to readjust its structure in order to recover both equilibria. The readjustment of the internal structure results in the star's radius evolution and, hence, can be described using ζ_*.

Hydrostatic Readjustment The donor's dynamical timescale is usually much smaller than its thermal timescale, $\tau_{\rm dyn} \ll \tau_{\rm KH}$. Therefore, the initial donor's response to mass loss can be expected to be almost adiabatic. Here we clarify that the term "adiabatic" in this context means that the entropy of each mass shell of the donor remains the same as at the start of the mass loss, as they are considered to have no time to exchange energy with their neighbour layers—in other words, the entropy profile of the donor is frozen (note the difference with the usual use of the term adiabatic, where it implies that the entropy of the whole systems is conserved).

This response for the immediate stability on a dynamical timescale is known as the adiabatic mass-radius exponent (Webbink 1985):

$$\zeta_{\rm ad} \equiv \left(\frac{\partial \log R_{\rm d}}{\partial \log M}\right)_{\rm ad} \quad \Rightarrow \quad \text{if } \zeta_{\rm L} \leq \zeta_{\rm ad}, \text{ the mass transfer is dynamically stable.} \tag{8.12}$$

The mass transfer is dynamically stable if the donor shrinks within its Roche lobe on $\tau_{\rm dyn}$.

Thermal Readjustment At the same time, the donor will attempt to recover its thermal equilibrium, readjusting its internal structure to obtain a radius that is appropriate for its new decreased mass. This response is known as thermal-equilibrium mass-radius exponent (Webbink 1985):

$$\zeta_{\rm eq} \equiv \left(\frac{\partial \log R_{\rm d}}{\partial \log M}\right)_{\rm eq} \Rightarrow \begin{cases} \text{if } \zeta_{\rm eq} < \zeta_{\rm L} \leq \zeta_{\rm ad}, & \text{thermal timescale mass transfer.} \\ \text{if } \zeta_{\rm L} \leq \min(\zeta_{\rm eq}, \zeta_{\rm ad}), & \text{secularly stable mass transfer.} \end{cases} \tag{8.13}$$

If the new equilibrium radius after the mass loss is smaller than the new Roche lobe radius, $\zeta_{\rm L} \leq \min(\zeta_{\rm eq}, \zeta_{\rm ad})$, the donor remains in both thermal and hydrostatic equilibrium all the time. The mass transfer is then secularly stable and proceeds on a timescale that is independent of the donor envelope's thermal and dynamical responses, but is dictated by other processes (e.g., orbital angular momentum evolution, or nuclear evolution of the donor).

If new equilibrium radius is larger than the Roche lobe radius, but $\zeta_{\rm L} \leq \zeta_{\rm ad}$, the mass transfer will be driven by continuous thermal readjustment that would keep pushing the star's radius so as to overfill its Roche lobe. It is a *stable* mass transfer although it proceeds from a donor that is out of thermal equilibrium. Indeed, suppose that the mass transfer is unstable, and has started to increase exponentially. Then the reaction of the donor will be determined by $\zeta_{\rm ad}$, and since the mass transfer is dynamically stable, the donor will shrink inside its Roche lobe, decreasing the mass transfer rate.

Superadiabatic Readjustment Although it has become a norm to analyse the donor's response on two widely separated timescales, in *real* stars the thermal readjustment of the outer layers of a donor could occur on a very short timescale. If $\tau_{\rm KH,surf} < \tau_{\rm ML} = M_{\rm d}/\dot{M}_{\rm d}$, the surface layers are capable to keep rebuilding their thermal structure during the mass transfer (Woods and Ivanova 2011). While hydrodynamic readjustment still takes place, this readjustment cannot be treated as adiabatic. The donor's response in this case, $\zeta_{\rm sad}$, is defined by the entropy profile that the donor is constantly restoring at its surface during the mass loss, and is function of the mass loss rate. At very high mass rates, $\zeta_{\rm sad} \rightarrow \zeta_{\rm ad}$. At the mass loss rates closer to thermal, $\dot{M}_{\rm KH} = M_{\rm don}/\tau_{\rm KH}$, the response $\zeta_{\rm sad} \rightarrow \zeta_{\rm eq}$. Since donor's response is not anymore adiabatic, the mass transfer then could be stable

even if $\zeta_{\rm L} > \zeta_{\rm ad}$. $\zeta_{\rm sad}$ is function of the mass loss rate and can only be obtained by performing stellar calculations.

$$\zeta_{\rm sad}(\dot{M}) \equiv \left(\frac{\partial \log R_{\rm d}}{\partial \log M}\right)_{\dot{\rm M}} \Rightarrow \text{if } \zeta_{\rm L} \leq \zeta_{\rm sad}, \text{the mass transfer is dynamically stable.} \tag{8.14}$$

8.4.2 Envelope's Structure

8.4.2.1 Adiabatic Response

Convective Envelope For a non-degenerate and fully ionised ideal gas, during an *adiabatic* motion of a convective eddy, pressure and density are related as $P\rho^{-\Gamma_1} =$ constant, with the adiabatic exponent $\Gamma_1 = 5/3$. Since this condition is satisfied everywhere inside a convective zone, a fully convective star can be considered as an isentropic polytrope of index $n = 1.5$. Giant stars, which possess large outer convective envelopes, are also often described as polytropes. Since giants are not fully convective and contain a radiative core, additional considerations could include composite polytropes, where the inner part was treated as a polytrope of $n = 3$, and condensed polytropes, while the core is a point mass.

The property of the polytrope of index $n = 1.5$ is that its radius increases when its masses decreases, $\zeta_{\rm n=1.5} = -1/3$. This response is the adiabatic response of a fully-convective low-mass main sequence star, or a limiting case of the adiabatic response of a giant star. With hydrodynamics simulations, it was also found that the presence of the core, as in the case of either composite or condensed polytropes, increases the value of $\zeta_{\rm ad}$ (Hjellming and Webbink 1987; Soberman et al. 1997), implying that, in accordance to the criterion (8.12), the stability of the mass transfer *increases* as the star evolves on the red giant branch. If $M_{\rm c}$ is the core mass of the donor and $m = M_{\rm c}/M_{\rm d}$, then (see Soberman et al. 1997):

$$\zeta_{\rm ad} = \frac{2}{3}\left(\frac{m}{1-m}\right) - \frac{1}{3}\left(\frac{1-m}{1+2m}\right) - 0.03m + 0.2\left[\frac{m}{1+(1-m)^{-6}}\right]. \tag{8.15}$$

The effect of the core is non-negligible: $\zeta_{\rm ad}$ is positive when $m \gtrsim 0.2$ (see Fig. 8.2).

Radiative Envelope By definition, radiative layers are stable against convection, and, hence, the temperature gradient is $\nabla \left(\equiv \frac{\partial \ln T}{\partial \ln P}\right) < \nabla_{\rm ad} = 0.4$. For an ideal gas, it can be shown that

$$s(m) \propto \rho^{(\frac{5}{3}\nabla - \frac{2}{3})/(1-\nabla)}. \tag{8.16}$$

If the temperature gradient $\nabla < 0.4$, the entropy is growing towards the surface. If some mass is removed, then a layer with a lower entropy is exposed. In an adiabatic case, this implies that if a star attains hydrostatic equilibrium and regains

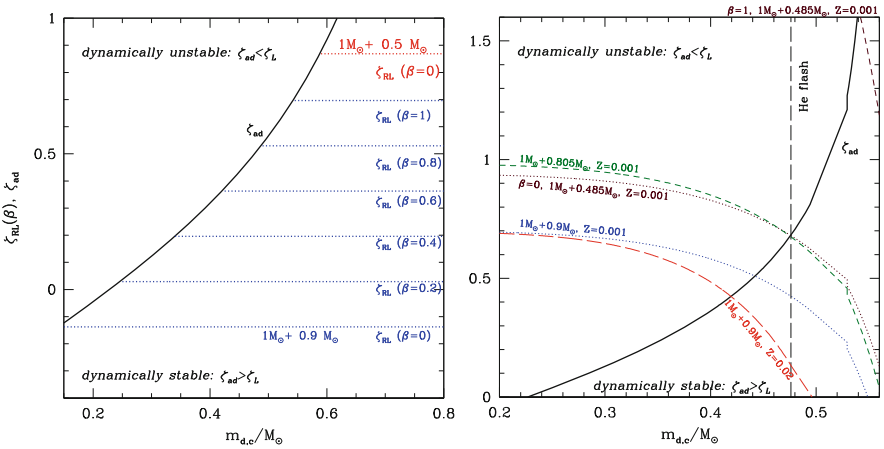

Fig. 8.2 Comparison of adiabatic and Roche-lobe mass-radius exponents. *Left panel*: a red giant of 1 $M_\odot$ of solar metallicity $Z = 0.02$ evolved without any mass loss, with companions of $0.9 M_\odot$ and 0.5 $M_\odot$, as a function of the red-giant core mass and for different cases of mass conservation β. *Right panel*: red giants of 1 $M_\odot$ with $Z = 0.02, 0.001$, evolved with wind-mass loss. *Dashed line* indicates where giants evolve through the He flash. $\zeta_{\rm ad}$ is calculated using (8.15)

the same surface pressure as before, the density of the outer layers will be larger than previously, and the donor shrinks. Hence for radiative donors, $\zeta_{\rm ad} \gg 0$.

8.4.2.2 Equilibrium Response

The equilibrium response depends on the evolutionary state of the donor. For low-mass giants, the thermal structure is almost independent from the envelope mass and is a function of the core mass, so $\zeta_{\rm eq} = 0$. For main sequence stars, the response is dictated by the mass-radius relation and is usually positive for all donor types. For example, for zero-age main sequence stars $\zeta_{\rm eq}$ is at least 0.57 (Demircan and Kahraman 1991), and it grows as the donor approaches the terminal main sequence. Note, that these values are applicable only for the start of the mass transfer.

8.4.2.3 Superadiabatic Response

This is the response of the donor on the mass loss that proceeds on a timescale longer than $\tau_{\rm dyn}$ but shorter than $\tau_{\rm KH}$. Arguably, this is the most important response for determining the mass transfer stability. In fact, in stellar codes, the decision on whether a star is experiencing dynamically unstable mass loss is often done when the mass loss is still $\lesssim 10^{-3}$ $M_\odot$ per year, but only because stellar codes often cannot converge on a star that looses mass at a faster rate. Note that this mass transfer rate is still several orders of magnitude slower than if it would

be on a real dynamical timescale, which is presumed for an ideal adiabatic response.

The understanding of superadiabatic response is most important for the cases of the mass transfer which are deemed to be unstable if adiabatic response is considered. Radiative donors have $\zeta_{\rm ad} \gg 0$ and are widely accepted to be more stable than convective donors, so we will consider here the superadiabatic response for convective donors only.

Why it is called "superadiabatic response"? The entropy profile in convective stars is not as simplistic as was discussed above in Sect. 8.4.2.1. Closer to the surface, the energy transport by convection is becoming not efficient enough to transport all the luminosity, and the transfer of energy by radiation starts to play a role (the region is still convectively unstable). The temperature gradient is now determined by both energy transport mechanisms, and its value is now somewhere between the adiabatic temperature gradient and the radiative temperature gradient $\nabla_{\rm ad} < \nabla < \nabla_{\rm rad}$, hence, it is called *superadiabatic*. In this region, the entropy of the material is becoming *smaller* than in the adiabatic convective envelope beneath it—see also (8.16). The convective envelope appears to be covered by a thin superadiabatic blanket.

If mass is removed from this entropy profile in an adiabatic regime, the envelope is momentarily expanding by a large fraction of its radius. For example, a 1 $M_\odot$ giant would expand by as much as ∼25 % (see Fig. 8.3). This dramatic expansion after removing a tiny mass from the surface ($<10^{-4}$ $M_\odot$) demonstrates that a simplified star with a constant entropy profile in the envelope, up to the surface, as

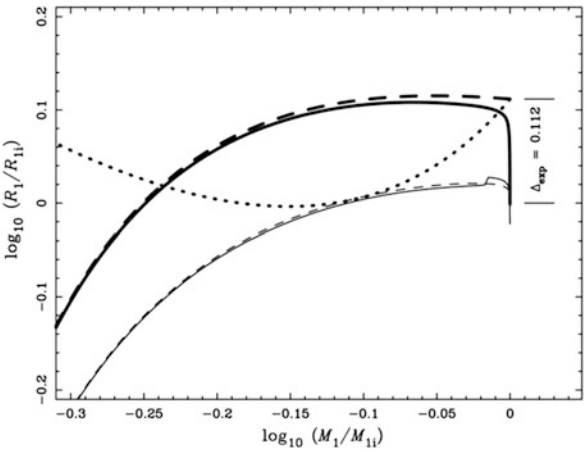

Fig. 8.3 Adiabatic mass-loss sequences for *true* (*thick solid lines*) stellar models and *pseudo-models* (i.e. adiabatic models; *thick dashed lines*) of a 1 $M_\odot$ star near the tip of the giant branch. $\nabla_{\rm exp}$ is the prompt initial expansion resulting from the removal of superadiabatic surface layers. Also shown are the Roche lobe radii within true and pseudo-models (*thin solid* and *dashed lines*, respectively) at which the mass-loss rate would reach $\dot{M}_{\rm KH}$. Critical initial mass ratio at which mass transfer rate reaches $\dot{M}_{\rm KH}$ for the pseudo-model is shown by the heavy dotted curve (reproduced from Ge et al. 2010 by permission of the AAS)

was considered in Sect. 8.4.2.1, finds a very different hydrostatic equilibrium than a normal giant of almost the same mass, and the role of the superadiabatic layer in finding that new equilibrium, and hence $\zeta_{\rm ad}$, could be enormous. The applicability of the adiabatic approach is therefore quite questionable.

Woods and Ivanova (2011) investigated how giant envelopes are responding in realistic stellar models when fast mass loss proceeds. They found that if the superadiabatic layer is resolved, the mass transfer could be stable in systems with larger mass ratio than would be predicted by the polytropic approach (in the considered systems, $q_{\rm crit} \sim 1.5$ instead of $\sim$0.8 as derived when using the adiabatic approximation). They also found that real giants will often contract while the adiabatic response, given by (8.15), predicts an expansion. A giant would start to expand only at the very high mass loss rate, $\gtrsim 0.1\,{\rm M}_\odot\,{\rm year}^{-1}$, and this expansion is much smaller than predicted by the adiabtic approach—less than 1 % of its radius.

These effects were observed in two fairly different stellar codes. One code is Lagrangian, a standard *Henyey-type* code developed by Podsiadlowski et al. (2002) from what was originally described in Kippenhahn et al. (1967); the current state of the code and input physics can be found in Ivanova (2003) and Ivanova and Taam (2004).

The second code is a non-Lagrangian code *STARS/ev*, originally developed by Eggleton (Eggleton 1971, 1972, 1973; Eggleton et al. 1973, and with updates as described in Pols et al. 1995; Glebbeek et al. 2008; Eggleton et al. 2011 and references therein). The contraction of the giants upon the mass loss was also confirmed by Passy et al. (2012) using yet another stellar code, *MESA* (Paxton et al. 2011, 2013).

Nonetheless, even though three different stellar codes reproduced qualitatively the same result—the giant's contraction upon rapid mass loss—it is not clear if *any* of the existing stellar codes is capable of producing a valid result in this regime. The caveat is that the continuous re-establishment of the surface superadiabatic layer proceeds on a timescale shorter than a convective eddy turnover time. In this case the commonly accepted convection treatment (the mixing length theory) may not be further applicable (Pavlovskii and Ivanova 2013).

8.4.2.4 Sudden Change of the Donor's Response: Delayed Dynamical Instability

This is the case of a dynamical instability that follows a period of a stable mass transfer. It occurs if the donor's response ζ_* *suddenly* drops during the mass transfer and become smaller than $\zeta_{\rm L}$. It usually takes place in initially radiative donors, when the mass loss ripped enough of the donor's material to reach layers where the convective core was and where the entropy is still nearly constant (for a more extended discussion, see e.g. Ge et al. 2010).

Since the first phase of the mass transfer proceeds roughly on a thermal timescale and its rate is a function of the mass ratio, the entropy of the inner layers might change compared to the initial profile. Hence the response ζ_*, as a function of the

current donor mass, will depend on the history of the mass transfer. The prediction of when exactly the delayed dynamical instability (DDI) could start is impossible by considering the initial donor only, but requires detailed stellar modeling.

Some rough values of $q_{\rm crit}$ separating the binaries that will experience a DDI and those proceeding with a stable mass transfer are known from previously performed calculations (for example, see Ivanova and Taam 2004; Ge et al. 2010) but vary from code to code; $q_{\rm crit} \gtrsim 3$.

8.4.2.5 Donor's Pulsations

Red giants are known to have intrinsic pulsations (for a review, see Christensen-Dalsgaard 2012, and the references therein). When hydrostatic equilibrium is perturbed due to mass loss, and a giant attempts to restore it, these intrinsic pulsations might be amplified. Indeed, it was shown (Pavlovskii and Ivanova 2013) that the initiation of the mass loss causes mass-loss induced pulsations, where the radius amplitude could be about 1 % of the star's radius, $\delta R \sim 0.01 R$. While this radius increase may seem small, the mass loss rate during RLOF is a strong function of the fractional radius excess of the donor, $\dot{M} \propto (\delta R/R)^3$. Hence, mass-loss induced pulsations could affect the rate of mass transfer during RLOF as well as the initial stability of the mass transfer.

8.5 The Donor's Response and the Consequences for the Mass Transfer Stability

8.5.1 Initial Stability

8.5.1.1 Fully Conservative Mass Transfer

In a binary star, the initial mass ratio $q > 1$, implying that the initial $\zeta_{\rm L} > 0.46$ in the case of a fully conservative mass transfer (see (8.6) above). A comparison with values of $\zeta_{\rm ad}$ shows that donors with convective envelopes are expected to start the mass transfer in a dynamically unstable way. The dynamical instability could be avoided in a second episode of the mass transfer, if $q < 0.8$ at the second RLOF.

Donors with radiative envelopes have $\zeta_{\rm ad} \gg 0$ and they can avoid dynamical instability at the start of mass transfer for a large range of mass ratios. Mass transfer will unavoidably be dynamically unstable from the very beginning for systems with radiative donors and $q_{\rm crit} \gtrsim 10$ due to the Darwin instability.

8.5.1.2 Non-conservative Mass Transfer

As follows from (8.9) and (8.10), if mass is lost from the system, the stability of the mass transfer is increasing. This can be demonstrated using a simple "toy" model,

where $\zeta_{\rm ad}$ (obtained using 8.15) is compared to $\zeta_{\rm L}$, for a 1 $M_\odot$ giant with two different companions, 0.9 $M_\odot$ and 0.5 $M_\odot$, and assuming that different fractions of transferred mass can be accreted (see Fig. 8.2, left panel). It can be seen that a low-mass giant in a binary with a 0.9 $M_\odot$ companion cannot have both stable and fully conservative mass transfer while it is a red giant (core mass $M_{\rm c} \lesssim 0.47\ M_\odot$). The stability of the mass transfer can only be achieved if $\beta \lesssim 0.6$. A fully non-conservative mass transfer ($\beta = 0$) will be stable in a binary consisting of a 1 $M_\odot + 0.9\ M_\odot$ starts, whatever the red-giant core mass. The critical mass ratio for $\beta = 0$ is larger by $\sim$40 % than for a fully conservative case for the same donor.

8.5.1.3 Mass Loss Prior to RLOF

The "toy" model used a star evolved without wind mass loss. Loosing mass through winds prior to RLOF reduces the relative envelope mass, increases the donor's $\zeta_{\rm ad}$ and makes the mass transfer stable for a larger range of donor's radii (or core masses, which are tightly related to the radii for low-mass giants). For example, a red giant of initial 1 $M_\odot$ could have a stable and fully conservative mass transfer onto a donor of 0.9 $M_\odot$ once it developed a core $M_{\rm c} \geq 0.42\ M_\odot$ (see Fig. 8.2, right panel). Low-mass giants of lower metallicity, as in metal-poor globular clusters, would lose less mass through wind. Hence, the stability of the mass transfer in metal-poor globular clusters can only be achieved for a smaller range of initial binary parameters.

8.5.2 Stability of the Ensuing Mass Transfer

In order to have a dynamically stable mass transfer, the condition for stability must be satisfied not only at the start of the mass transfer, but during the whole duration of the mass transfer. In population synthesis studies, especially where a parameterisation is used for stellar codes to speed up calculations, the instability is evaluated only at the start of the mass transfer (e.g. Hurley et al. 2002; Belczynski et al. 2008). It is partially justified, as in simple cases $\zeta_{\rm L}$ is decreasing as the mass transfer proceeds (e.g., if the mass transfer is fully conservative), hence the stability of the mass transfer is expected to only increase after it started.

The noticeable exception that is usually taken into account is the DDI. For DDI, population studies accept some value for $q_{\rm crit}$, and for all systems with $q > q_{\rm crit}$ the mass transfer is considered to be unstable (e.g., Belczynski et al. 2008) (note, however, that the mass transfer in reality would become unstable only after a significant fraction of the donor is transferred on its thermal time scale). While population synthesis codes accept some strict value, the exact value of the critical mass ratio varies between the code and depends on considered systems. For example, Ivanova and Taam (2004) found $q_{\rm crit} \approx 2.9-3.1$ on one sample of donors, while Ge et al. (2010) found this value to be higher, $q_{\rm crit} > 3.5$, on another sample

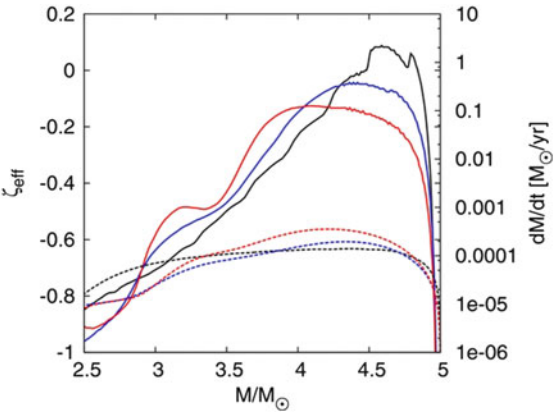

Fig. 8.4 Evolution of the effective radial response of the donor (*solid lines*) and mass loss $\dot{M}$ (*dashed lines*) during the mass transfer, for a 5 $M_\odot$ + 5 $M_\odot$ binary with a donor radius of 50 $R_\odot$ (*black*, highest peak), 68 $R_\odot$ (*blue*, middle), and 85 $R_\odot$ (*red*, lower) with a point mass companion (reproduced from Woods and Ivanova 2011 by permission from the AAS)

of donors.[1] This classic DDI scenario is assumed to happen to donors with radiative envelopes and convective cores.

The change of the donor's response, however, could occur in other cases, not only in the classic DDI case. In convective giants, ζ_* is not constant during the mass transfer (see Fig. 8.4), and its value can go down after an insignificant fraction of the envelope has been already transferred. The particular example shown in Fig. 8.4 adopted fully conservative mass transfer but was nonetheless stable, despite the fact that the polytropic argument would predict all of them being unstable—and any non-conservation would improve stability even further. However, the important point here is that even in giants with convective envelope the response of their envelope is changing with time. Subsequently, it is possible that for any convective donor there is a $q_{\rm crit,DDI}$ such that for mass ratios $q > q_{\rm crit,DDI}$ but $q < q_{\rm crit}$, the DDI arises. In these systems, a period of initial stable mass transfer will increase the survivability of the binary once dynamical instability (common envelope) occurs, since a fraction of the envelope was removed at the expense of "nuclear" energy during the donor's evolution.

8.5.3 Stable or Not Stable?

The determination of whether dynamical instability takes place at the start of the mass transfer or a DDI takes place during the mass transfer, hits the same problem: even detailed binary stellar codes are numerically limited by their abilities to converge a donor that experiences fast mass loss. The mass transfer is usually declared to be dynamically unstable if its value exceeds some adopted critical value for the mass transfer rate, different for various codes, and depends on what a code is

[1] We note also that in their approach DDI was based on a frozen entropy profile.

capable of handling. Taking a too low value may lead to wrong conclusions—e.g., 10^{-3} $M_\odot$ year^{-1}. Note that this is a mass transfer rate that is by several orders of magnitude larger than in the dynamical regime. This inability of a stellar code to converge does not imply that dynamical mass transfer—in other words, that a star is not capable anymore to remain in hydrostatic equilibrium—has indeed occurred. There are mass transfer sequences where thermal time scale mass transfer rate from a giant donor approaches 10^{-2} $M_\odot$ year^{-1} (still 100 times slower than dynamical timescale), and then the donor recovers and continues the mass transfer on a nuclear time scale.

In addition to problem with the convergence of the donor, the converged solution might be intrinsically incorrect, depending on what physics was taken into account. While many stellar codes now include a component that takes into account structural changes on a dynamical timescale, convection is for instance considered in the approximation known as mixing length theory, which can break down when significant changes happen on a timescale comparable to a convective eddy turnover time (Pavlovskii and Ivanova 2013).

8.5.4 Three-Dimensional Problem

The RLOF process in a binary system is intrinsically a three-dimensional (3D) problem, while all the possible criteria of mass transfer instability described above are valid only for one-dimensional, spherically symmetric stars. While there are simulations of three-dimensional behaviour of the stream after it had already left L_1 (e.g. Yukawa et al. 1997), there is no fully self-consistent simulations yet of the start of the RLOF in 3D, where the RLOF is truly driven by binary evolution.

Most 3D studies of RLOF binaries are rather devoted to the understanding of the common envelope evolution. Hence, the topic under investigation is not the stability, but instability and its consequences. Since evolution-driven RLOF takes place on a timescale much longer than the dynamical timescale (hydrodynamical codes are not capable of treating events on timescale much longer than a dynamical timescale unless proper stellar physics, especially for energy transfer, is added), the start of the common envelope is usually artificially enforced. Example of enforcement include starting with initial Roche lobe overflow, or starting with initially asynchronised companions and allowing tidal forces to drive the coalescence (Passy et al. 2012; Ricker and Taam 2012).

Recently, one of the Smoothed Particle Hydrodynamics (SPH) codes was specifically modified to study stability of the mass transfer, by introducing a proper treatment of synchronised binaries, including cases where a companion could be just reaching its RLOF (Lombardi et al. 2011). In recent calculations using that code Avendano Nandez et al. (in preparation) considered a binary system that consisted of a 8 $M_\odot$ giant and 5 $M_\odot$ black hole. The expectation for such a system (the mass ratio $q = 1.6$ is almost twice the critical mass ratio for a donor with convective

envelope) from 1D stability analysis is very firm—this system is destined to start the common envelope phase, i.e. a dynamical unstable RLOF. However, in the 3D simulations, this binary failed to start the dynamically unstable mass transfer. In 6 years (physical time) of RLOF, the average mass transfer rate in the simulation was $\sim 0.02\ M_\odot\ \text{year}^{-1}$; most of the transferred mass did not stay within the black hole's Roche lobe: $0.084\ M_\odot$ was ejected from the binary to infinity and $0.025\ M_\odot$ went into a circumbinary disc. This example clearly suggests that criteria based on 1D stellar calculations cannot be final, and mass transfer in real 3D stars could be stable for a much larger range of mass ratios, whether this is due to strong liberal evolution, or different from spherically symmetric case donor's response.

8.6 The Accretor's Response and Consequences for Mass Transfer Stability

During RLOF, the donor's material, once leaving the nozzle at the L_1, proceeds towards the accretor in the form of a stream. The stream's trajectory is more-or-less ballistic (for vertical structure and trajectory of an isothermal stream see Lubow and Shu 1976 and for an adiabatic stream see Ivanova et al. 2002). The material in the stream:

1. has the chemical composition of the donor;
2. carries angular momentum from L_1;
3. *may* have the entropy of the donor's material.

The transfer of a donor's composition may create a specific signature that could help to identify a star formed through mass transfer, but it does not affect the stability of the ongoing mass transfer. The stream's angular momentum and entropy may, however, affect it.

8.6.1 The Stream's Angular Momentum

After leaving L_1, the stream conserves its angular momentum J_s for as long as its trajectory is unperturbed from interacting with some other material. Depending on the sizes of the accretor and of its Roche lobe, the stream could either collide with itself, forming an accretion disc around the accretor at the circularisation radius $R_\text{circ} = J_\text{s}^2/GM_\text{a}$, or, if the accretor's radius $R_\text{a} > R_\text{circ}$, the stream can hit the accretor directly, transferring to the accretor its angular momentum.

If an accretion disc is formed, as can be expected in relatively wide binary systems that proceed with a case B or a case C mass transfer or if the accretor is a white dwarf, a neutron star, or a black hole, the accretor is not necessarily gaining

angular momentum. But in case of a direct impact, the accretor can be quickly spun up. It can be estimated that the accretor can reach *critical rotation*—defined when the centrifugal force equals the gravitational force and the star is no more bound—after accreting just a few per cent of its mass (Packet 1981). This raises for blue stragglers formed via case A or early case B mass transfer the same problem as in the case of blue stragglers formed via collisions: how to get rid of the angular momentum? (not to mention that the physics of stars that are close to critical rotation is poorly understood, see, e.g., for a review Langer et al. 2008).

A possible solution is that the stream is not able to transfer all its angular momentum to the accretor. Indirect evidence, for instance, suggests that it is hard to recreate the distribution of observed Algol systems with mass ratios in the range 0.4–0.6 with fully conservative mass transfer (van Rensbergen et al. 2008). Also, magneto-hydrodynamic simulations presented in Raymer (2012) showed that the stream that would be normally expected to have a direct impact, is deflected, where the deflected formation is taking away most of the stream angular momentum. In addition to resolving the problem with the excess of the angular momentum in the accretor, stream's deflection also stabilizes the mass transfer.

8.6.2 The Accretor's Response

Let us consider the case of stable mass transfer, operating on a thermal timescale. For as long as the mass of the donor remains larger than the mass of the accretor, the accretor's thermal timescale is longer than that of the donor (this is valid at the start of both cases A and B mass transfers, or for as long as both companions remain main sequence stars). The accretor, just like the donor, has to readjust to its new mass, but the timescale at which it has to readjust is shorter than its thermal timescale. The accretor, hence, will be brought out of its thermal equilibrium.

This accretor's response on a timescale shorter than its thermal timescale can be considered as the reverse of a rapid mass loss from the donor (adiabatic response, though in reality this response will be closer to superadiabatic response): if the accretor has a radiative envelope, it can be expected to expand upon the mass accretion, while if the accretor has a convective envelope, it can be expected to contract upon the mass accretion. For example, an initially radiative donor is expected to be both more luminous and more expanded than a star of the same mass in thermal equilibrium. For sufficiently high accretion rates, an accretor then might even overfill its Roche lobe, forming a contact binary.

A contact binary could also be formed during nuclear timescale mass transfer, when then accretor's expansion takes place due to its evolution off the main sequence. Other possibilities, as was mentioned before, include a white dwarf's reincarnation into a red giant and the formation of a "trapping" envelope around a neutron star. However, none of these situations leads to formation of a blue straggler.

8.6.3 *Donor's Entropy and the Accretor's Response*

The accretor's response onto mass accretion, as described above, has been confirmed by binary calculations (e.g., Nelson and Eggleton 2001). These calculations, however, made two simplifications: the accreting material had the surface composition and entropy (as well as temperature) of the surface material of the accretor, not of the donor. More recent evolutionary codes include *thermohaline mixing* (e.g. Stancliffe and Glebbeek 2008), and are capable to add material of different chemical composition in a proper way. Adding material with different entropy remains a problem. It is also unclear what exactly should be the entropy of the accreting material: (a) the stream does not necessarily keep the same entropy as the donor while it is in the ballistic phase; (b) the stream could be shock-heated during its impact with the accretor.

So why is the entropy of the material during the accretion (and hence the entropy profile of the accretor) a problem? It must be clarified that, especially in the case of blue straggler formation, this is an entirely different issue from the entropy profile of a collision product. In the latter case, the entropy profile of the collision product is created by *simplified entropy sorting* (Lombardi et al. 2002), with mandatory positive entropy gradient. This profile then defines an initial, out-of-thermal equilibrium, stellar model of a blue straggler, which is then further evolved with a stellar code.

On the other hand, accretion of material with different entropy creates an entropy discontinuity in the accretor's envelope. The physics of this discontinuity is closely related to the problem of a transitional layer in contact binaries and is not yet fully understood (see, e.g., discussion in Shu et al. 1980).

8.7 How Well Do We Understand Stable Mass Transfer?

We can express the change of the donor's radius as due to the evolutionary change and to the thermal equilibrium's response on the mass loss:

$$\frac{\dot{R}_\mathrm{d}}{R_\mathrm{d}} = \left(\frac{\dot{R}_\mathrm{d}}{R_\mathrm{d}}\right)_\mathrm{ev} + \zeta_\mathrm{eq}\frac{\dot{M}_\mathrm{d}}{M_\mathrm{d}} \,. \tag{8.17}$$

The change of the Roche lobe radius can be expressed as due to the response on the mass transfer, and to the losses of the orbital angular momentum without the mass transfer:

$$\frac{\dot{R}_\mathrm{L}}{R_\mathrm{L}} = \left(\frac{\dot{R}_\mathrm{d}}{R_\mathrm{d}}\right)_\mathrm{aml} + \zeta_\mathrm{L}\frac{\dot{M}_\mathrm{d}}{M_\mathrm{d}} \,. \tag{8.18}$$

In the absence of mass transfer, at constant q, $R_{\rm L}$ is simply proportional to a, and the change of the orbital angular momentum J is $2\dot{J}/J = \dot{a}/a$. Then the mass transfer rate can be found from

$$-\frac{\dot{M}_{\rm d}}{M_{\rm d}} = \frac{1}{\zeta_{\rm eq} - \zeta_{\rm L}} \left[\left(\frac{\dot{R}_{\rm d}}{R_{\rm d}} \right)_{\rm ev} - 2\frac{\dot{J}}{J} \right] . \tag{8.19}$$

The best systems to test our understanding of stable mass transfer are low-mass X-ray binaries with neutron star accretors, where we can obtain the mass transfer rates from the observed X-ray luminosities with uncertainties to only within a factor of 3 (in't Zand et al. 2007). Nonetheless, for low-mass X-ray binaries with non-degenerate donors, the observed mass transfer rates do disagree with theoretically obtained "most likely" mass transfer rates by more than an order of magnitude (Podsiadlowski et al. 2002), with observed systems having usually much higher mass transfer rate (see Fig. 8.5).

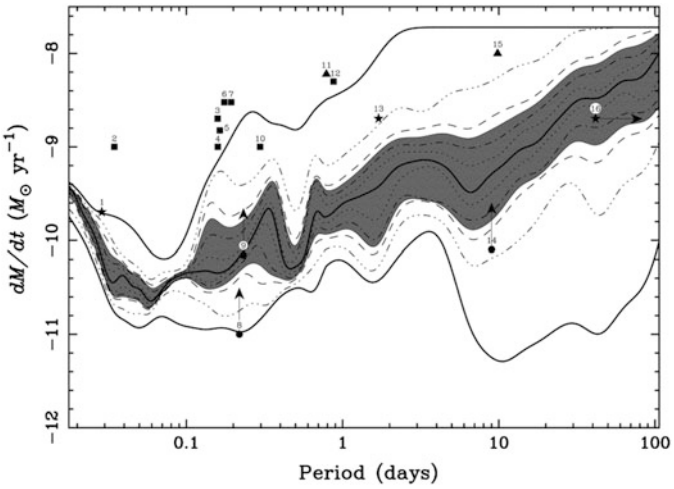

Fig. 8.5 Cumulative (smoothed) probability distribution for the mass accretion rate onto a neutron star primary as a function of orbital period for 100 binary calculations (with equal weighting for all sequences). The *thick*, solid central curve gives the median mass accretion rate; the pairs of curves moving progressively outward from the median curve include 20, 40, 60, 80, and 98 % of the distribution, respectively. The *shaded region* contains 50 % of all systems around the median. The *symbols* indicate the mass transfer rates of selected observed X-ray binaries (*triangles*: Z sources; *squares*: atoll sources; *stars*: X-ray pulsars; *circles*: systems with accretion disc coronae [lower limits]). The individual systems are (in ascending order of orbital period, as given in *parentheses*) (*1*) 1626-67 (0.69 h), (*2*) 1916-053 (0.83 h), (*3*) 1636-536 (3.8 h), (*4*) 0748-676 (3.82 h), (*5*) 1254-690 (3.93 h), (*6*) GX 9+9 (4.2 h), (*7*) 1735-555 (4.65 h), (*8*) 2129+470 (5.24 h), (*9*) 1822-37 (5.57 h), (*10*) 1658-29 (7.11 h), (*11*) Sco X-1 (18.9 h), (*12*), 1624-590 (21 h), (*13*) Her X-1 (40.8 h), (*14*) 0921-630 (216 h), (*15*) Cyg X-2 (236 h), and (*16*) GX 1+4 (greater than 1,000 h) (reproduced from Podsiadlowski et al. 2002 by permission from the AAS)

The situation is relatively better in the case of ultra-compact X-ray binaries—low-mass X-ray binaries with white-dwarf donors. There, the orbital angular momentum loss is via gravitational wave radiation and is understood much better than angular momentum loss with non-degenerate donors in wide systems. The adiabatic response is simply $\zeta_{\rm ad} = -1/3$. A further improvement was obtained by considering the effect of the final entropy on $\zeta_{\rm ad}$ in white dwarf remnants (Deloye and Bildsten 2003). While most of the ultra-compact X-ray binaries do match very well the theoretically obtained mass transfer rates, there are three systems that have mass transfer rate almost two orders of magnitude higher than theoretically predicted, and one system where the mass transfer is much lower than theoretically predicted (Heinke et al. 2013).

Discrepancies between theory and too high mass transfer rates for some ultra-compact X-ray binaries may indicate that the donors are not remnants of white dwarfs (Pavlovskii and Ivanova 2013; Heinke et al. 2013). Otherwise, it can be stated that the theory of the stable mass transfer in systems with a well known mechanism of angular momentum loss (for instance, via gravitational wave radiation) and a well understood simple donor's response (as with degenerate donors where $\zeta_{\rm ad} = -1/3$) agrees with observations very well. However, for the cases applicable to blue straggler formation, where the mass transfer proceeds from a non-degenerate donor, especially from main sequence and early giant donors, the theory of the stable mass transfer is yet far from matching the observations well.

8.8 RLOF and Blue Stragglers Formation

In this section we discuss *how* blue stragglers can be formed as a result of RLOF, while the overview of population studies and rates can be found in Chap. 12.

8.8.1 Case A and Early Case B

Here we consider the cases when the mass transfer resulting in a blue straggler formation occurred before the donor developed a deep convective envelope. From the analysis above, binary systems with low-mass primaries are expected to either have thermal timescale mass transfer, or experience DDI. A more precise mapping of the actual mass transfer with the initial binary parameters (primary mass, mass ratio and orbital period) can be done only using binary stellar codes.

Nelson and Eggleton (2001) performed an extensive study of the Case A and early case B mass transfers for a wide variety of initial binary systems, with primary masses from 0.9 to 50 $M_\odot$, initial mass ratios up to $\log_{10} q = 0.5 (q \sim 3.16)$, and with periods ranging from the contact period at the zero-age main sequence, $P_{\rm zams}$ up to $\log_{10} P/P_{\rm zams} = 0.75 (P \sim 5.6\ P_{\rm zams})$. This extensive library of models was created to explain Algol systems. However, the first episode of mass transfer, whether it was found to be stable or unstable, creates a blue straggler. This study

therefore provides good insight on when the formed blue stragglers remain in a binary, and when they are formed as single blue stragglers.

Analysing this study, it can be accessed that single blue stragglers that can be present in globular clusters (with relatively low masses of initial primaries, $<2\,M_\odot$), could be formed both via case A and case B mass transfers. The first condition that determines whether a binary would merge and produce a single blue straggler is the initial period $P \gtrsim 2-3\ P_{\rm zams}$, where the larger period is for the more massive primaries. Most of those binaries were found to have rapidly rising above thermal timescale case B mass transfer. The second condition is the initial mass ratio. First of all, this study adopted the fact that any initial mass ratio that is larger than $\sim$3.16 would likely lead to DDI and the merging of the system; these binaries were not calculated. In the binary calculations done, binaries with primaries $\sim 1\ M_\odot$ and with as small mass ratio as two were found to start dynamic timescale case A mass transfer and quickly enter into contact, before the secondary could accrete enough to appear as a blue struggler. At the contact, the calculations were stopped and further fate of the systems (merger or long-term contact) was not determined.

It must be noted that even though the AD and BD cases described above were declared to be dynamical, there are not really such. The adopted criterion for defining whether the mass transfer is dynamical was very soft, with the mass transfer rate being just 10 times more than that of a thermal timescale mass transfer, which for main sequence donors implies many orders of magnitude less than realistic dynamical timescale mass transfer. All the mentioned studies on DDI adopted fully conservative mass transfer, and as discussed previously, any non-conservation could change the boundary between the formation of a blue straggler in a binary and a single blue straggler to a lower value of q.

Blue stragglers that are typical for globular cluster conditions and that remain in their original binaries could be formed via AS ("slow" evolution to contact), AG (first contact is on the giant branch), AR (rapid contact), AL and BL (two cases of "late overtaking" scenario, where the secondary also overfills its Roche lobe) types of the evolution. AR evolution towards blue straggler formation is rare though as it can occur only with primaries close to $2\ M_\odot$ and for most initial mass ratios, the companion does not gain enough mass to appear as a blue straggler. A couple of typical examples of binary mass transfer sequences, cases AS and AL, are shown in Fig. 8.6 (note that the stars that are shown are more massive than stars present in *now* globular clusters, but less massive stars would evolve via scenarios qualitatively similar to the ones shown). AS, AL and BL cases usually took place in binaries that had initial mass ratios smaller than 2 (at $q > 2$, AD takes place), AR takes place in binaries with primaries having a mass close to $2\ M_\odot$ and $q > 2$. Most of the binaries that have case A or case B mass transfer towards a blue straggler formation have first thermal time-scale mass transfer, producing both components being strongly out of their thermal equilibrium. The primary after the mass transfer, if it remains a main-sequence star, would be out of thermal equilibrium for a long time—a blue straggler in this case could be in a binary where the lower-mass companion is out of thermal equilibrium.

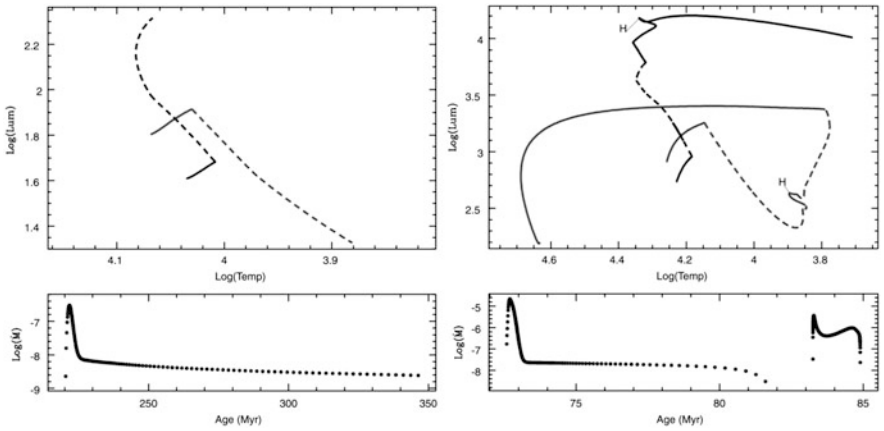

Fig. 8.6 Examples of Case A evolution that result in the formation of a contact binary containing a blue straggler. *Left panel:* Case AS—slow evolution to contact. This particular system consisted initially of 2.8 $M_\odot$ + 2.5 $M_\odot$ stars with initial period ∼1.6 P_{zams}. *Right panel:* Case AL—late overtaking. This particular system consisted initially of 5.6 $M_\odot$ + 5 $M_\odot$ stars with initial period ∼4 P_{zams}. "H" denotes the end of the main sequence for each star (reproduced from Nelson and Eggleton 2001 with permission by the AAS)

While we have an overall understanding of how blue stragglers could be formed via case A and case B mass transfers, theory is still far from predicting exact numbers and binary configurations. To test the theory with observations, we need to compare predicted with observed blue straggler populations. Blue stragglers in globular clusters are contaminated by those formed via collisions, and blue stragglers in a field are not easy to distinguish. However, many of the blue stragglers formed via case A and case B mass transfers are precursors of Algol systems, which are much easier to be observationally detected, and, hence, we can test out the theory on Algol systems. It was shown that theoretically obtained distributions and numbers of Algols still do not match well with observations (e.g., van Rensbergen et al. 2011). The important outcome of Algol's studies is that the observed distributions cannot be matched by conservative evolution, though liberal evolution does not reproduce Algols fairly well neither (also note that less conservative mass transfer is less effective in the production of blue stragglers—by definition, a blue straggler is a star more massive than its parent population, i.e. it should have gained enough mass in a binary system).

8.8.2 Late Case B/Case C

Here we consider the cases when mass transfer that resulted in the formation of a blue straggler has started from a donor with a well developed convective envelope. From the analysis above, binary systems with low-mass giant primaries,

in conservative evolution, are expected to start dynamically unstable mass transfer for most case B mass transfers. In many cases, a binary would survive common envelope evolution, but a main sequence companion is not capable of accreting during a common envelope phase enough material to appear as a blue straggler (Hjellming and Taam 1991).

As discussed above, due to wind mass loss, metal-rich globular clusters are more likely to form blue stragglers via conservative case B mass transfer than metal-poor globular clusters—in this case, the stripped red giant core would be close to $0.47\,M_{\odot}$.

Case C mass transfer is expected to be stable in globular clusters of all metallicities and will lead to the formation of long-orbital-period blue stragglers (case C also can be unstable, however, this occur for such mass ratios that a companion is unlikely to appear as a blue straggler).

The stated above expectations were based on an adiabatic response of giant donors. With superadiabatic response taken into account, blue stragglers can be formed via stable case B mass transfers from giant donors with smaller core masses. Similar effect is achieved by non-conservation (though again note the caveat: with non-conservative mass transfer it is easier to have stable mass transfer, but harder to accrete enough to become a blue straggler).

Liberal mass transfer from red giant donors to non-degenerate companions has been discussed in Woods et al. (2012), especially its implications and importance for the avoidance of the dynamically unstable mass transfer from a primary (this is the first of the two episodes of the mass transfer that eventually forms a double white dwarf system). The same channel that produces double white dwarfs also produces long-orbital-period blue stragglers at its first leg.

Forming a blue straggler could also be a precursor for hot sub-dwarf formation (for a recent review, see Geier 2013). Case B channel can produce wide systems with massive white dwarfs, but only if the case B mass transfer is liberal and/or the giant's response is superadiabatic would we be able to find at least some blue stragglers in a relatively "narrow"-wide system ($P \lesssim 100$ days) with a low-mass white dwarf ($\lesssim 0.25\,M_{\odot}$). In this respect, it is interesting to note the recent discovery of a stripped red giant with a mass of $0.23 \pm 0.03\,M_{\odot}$, in an eclipsing binary system and with an A-type companion (Maxted et al. 2011), though the period of this binary is very short to be a characteristic late case B. Finally, as was mentioned in Sect. 8.7, the mass transfer rates in binaries with early giant donors are among the least well understood.

8.8.3 Role of Globular Cluster Dynamics on the RLOF

In globular clusters, dynamical encounters could replace an original binary companion by a more massive one and/or increase the binary's eccentricity. Those perturbation, however, do not affect the previously described stability and rate of the mass transfer once it has started. A more interesting deviation from most field

binaries is that a binary that contains a potential blue straggler is much more likely to be a member of a dynamically formed hierarchical triple.

A fraction of dynamically formed hierarchically stable triples, those that have inclinations of the orbit $\gtrsim 39°$, could be affected by the Kozai mechanism (Kozai 1962; Innanen et al. 1997). Such Kozai mechanism causes large variations in the eccentricity and inclination of the binary orbits and, especially if coupled with tidal friction, could drive the inner binary of the triple system to RLOF and/or merger (Eggleton and Kisseleva-Eggleton 2006; Fabrycky and Tremaine 2007). If triple induced RLOF leads to a merger, it can form about 10 % of blue stragglers in a globular cluster (Ivanova 2008), but whether it will be a merger or a mass transfer requires further understanding of the evolution of contact binaries (Eggleton 2012).

Acknowledgements N. Ivanova acknowledges support from NSERC Discovery and Canada Research Chairs programs.

References

Begelman, M. C.: MNRAS **187**, 237 (1979)
Belczynski, K., Kalogera, V., Rasio, F. A. et al.: ApJS **174**, 223 (2008)
Christensen-Dalsgaard, J.: in Progress in Solar/Stellar Physics with Helio- and Asteroseismology, ASP Conf. **462**, 503 (2012)
Darwin, G. H.: Proc. Roy. Soc. London **29**, 168 (1879)
Deloye, C. J., Bildsten, L.: ApJ **598**, 1217 (2003)
Demircan, O., Kahraman, G.: Ap&SS **181**, 313 (1991)
Eggleton, P. P.: MNRAS **151**, 351 (1971)
Eggleton, P. P.: MNRAS **156**, 361 (1972)
Eggleton, P. P.: MNRAS **163**, 279 (1973)
Eggleton, P. P.: ApJ **268**, 368 (1983)
Eggleton, P. P.: New Astronomy Reviews **44**, 111 (2000)
Eggleton, P. P.: Evolutionary Processes in Binary and Multiple Stars, Cambridge University Press (2006)
Eggleton, P. P.: Journal of Astronomy and Space Sciences **29**, 145 (2012)
Eggleton, P. P., Faulkner, J., Flannery, B. P.: A&A **23**, 325 (1973)
Eggleton, P. P., Kisseleva-Eggleton, L.: Ap&SS **304**, 75 (2006)
Eggleton, P. P., Tout, C., Pols, O. R., et al.: STARS: A Stellar Evolution Code, Astrophysics Source Code Library (2011)
Fabrycky, D., Tremaine, S.: ApJ **669**, 1298 (2007)
H. Ge, M. S. Hjellming, R. F. Webbink, X. Chen, Z. Han: ApJ **717**, 724 (2010)
Geier, S.: European Physical Journal Web of Conferences **43**, 4001 (2013)
Glebbeek, E., Pols, O. R., Hurley, J. R.: A&A **488**, 1007 (2008)
Heinke, C. O., Ivanova, N., Engel, M. C., et al.: ApJ **768**, 184 (2013)
Hjellming, M. S., Webbink, R. F.: ApJ **318**, 794 (1987)
Hjellming, M. S., Taam, R. E.: ApJ **370**, 709 (1991)
Hurley, J. R., Tout, C. A., Pols, O. R.: MNRAS **329**, 897 (2002)
Hut, P.: A&A **92**, 167 (1980)
in't Zand, J. J. M., Jonker, P. G. , Markwardt, C.B.: A&A **465**, 953 (2007)
Innanen, K. A., Zheng, J. Q., Mikkola, S., Valtonen, M. J.: AJ **113**, 1915 (1997)
Ivanova, N.: DPhil Thesis (2003)

Ivanova, N.: in Multiple Stars Across the H-R Diagram, ESO Symp., Springer-Verlag, p. 101 (2008)
Ivanova, N., Podsiadlowski, P., Spruit, H.: MNRAS **334**, 819 (2002)
Ivanova, N., Taam, R.E.: ApJ **601**, 1058 (2004)
Ivanova, N., Justham, S., Chen, X., et al.: A&A Rev. **21**, 59 (2013)
Kippenhahn, R., Weigert, A.: ZAp **65**, 251 (1967)
Kippenhahn, R., Weigert, A., Hofmeister, E.: Mth. Comp. Phys. **7**, 129 (1967)
Kozai, Y.: AJ **67**, 591 (1962)
Langer, N., Cantiello, M., Yoon, S.-C., et al.: in IAU Symposium 250, pp-167 (2008)
Lauterborn, D.: A&A **7**, 150 (1970)
Lombardi, Jr., J. C., Warren, J.S., Rasio, F. A. , Sills, A., Warren, A. R.: ApJ **568**, 939 (2002)
Lombardi, Jr., J. C. , Holtzman, W., Dooley, K. L. , Gearity, K., Kalogera, V., Rasio, F. A.: ApJ **737**, 49 (2011)
Lubow, S. H., Shu, F. H.: ApJL **207**, L53 (1976)
Maxted, P. F. L., Anderson, D. ., Burleigh, M. R., et al.: MNRAS **418**, 1156 (2011)
Nelson, C. A., Eggleton, P. P.: ApJ **552**, 664 (2001)
Nomoto, K., Nariai, K., Sugimoto, D.: PASJ **31**, 287 (1979)
Packet, W.: A&A **102**, 17 (1981)
Passy, J. C., Herwig, F., Paxton, B.: ApJ **760**, 90 (2012)
Passy, J.C., De Marco, O., Fryer, C.L., et al.: ApJ **744**, 52 (2012)
Pavlovskii, K., Ivanova, N.: CASCA meeting (2013)
Pavlovskii, K., Ivanova, N.: in IAU Symposium 291, 468 (2013)
Pavlovskii, K., Ivanova, N.: in IAU Symposium, 290, 293 (2013)
Paxton, B., Bildsten, L., Dotter, A., et al.: ApJS **192**, 3 (2011)
Paxton, B., Cantiello, M., Arras, P., et al.: ApJS **208**, 4 (2013)
Podsiadlowski, P., Rappaport, S., Pfahl, E. D.: ApJ **565**, 1107 (2002)
Pols, O. R., Tout, C. A. , Eggleton, P. P., Han, Z.: MNRAS **274**, 964 (1995)
Raymer, E.: MNRAS **427**, 1702 (2012)
Ricker, P. M., Taam, R. E.: ApJ **746**, 74 (2012)
Shu, F. H., Lubow, S. H., Anderson, L.: ApJ , **239**, 937 (1980)
Soberman, G. E., Phinney, , E. S., van den Heuvel, E. P. J.: A&A **327**, 620 (1997)
Stancliffe, R. J., Glebbeek, E.: MNRAS **389**, 1828 (2008)
Tout, C. A., Aarseth, S. J., Pols, O. R., Eggleton, P. P.: MNRAS **291**, 732 (1997)
van Rensbergen, W., De Greve, J.P., De Loore, C., Mennekens, N.: A&A **487**, 1129 (2008)
van Rensbergen, W., De Greve,J.P., Mennekens, N., Jansen, K. , de Loore, C.: A&A,**528**, A16 (2011)
Webbink, R.F.: in Stellar evolution and binaries, Cambridge University Press, p. 39 (1985)
Woods, T.E., Ivanova, N.: ApJL **739**, L48 (2011)
Woods, T.E., Ivanova, N. , van der Sluys, M.V. , Chaichenets, S. : ApJ **744**, 12 (2012)
Yukawa, H., Boffin, H. M. J., Matsuda, T. : MNRAS **292**, 321 (1997)

Chapter 9
Formation Channels for Blue Straggler Stars

Melvyn B. Davies

9.1 Introduction

As has been discussed earlier in this book, blue stragglers sit on the main sequence but above the current turn-off mass. Their existence is at first surprising: one would have expected these stars to have evolved off the main sequence and become white dwarfs some time ago. How could a subset of stars somehow forget to evolve off the main sequence? In this chapter, we will focus on two, distinct, alternatives for blue straggler production: direct collisions between two stars (leading to their merger), and mass transfer (or merger) between two stars as part of natural evolution within a binary system. We will see that both formation mechanisms probably occur, at least in some clusters. One should also note that stellar mergers can occur also in triples as the inner binary is driven into contact by the action of the third star via the Kozai effect (Perets and Fabrycky 2009). This pathway is discussed in detail in Chap. 11.

We begin by outlining some of the key concepts and ideas which will be discussed in more detail in later sections of this chapter:

(a) Stellar collisions occur often in the cores of dense stellar clusters
Physical collisions between stars occur interestingly-often in the cores of the densest star clusters. Most of the collisions occur whilst the stars are on the main sequence. Because the relative speed of the stars within stellar clusters is much smaller than their surface escape speeds, collisions between two main-sequence stars will lead to their merger with only a very small amount of mass loss.

(b) The post-collision evolution of merger products is complex
The post-collision evolution of merger products is complex, with many uncertainties. Merger products typically contain a relatively large amount of angular

M.B. Davies (✉)
Department of Astronomy and Theoretical Physics, Lund University, Lund, Sweden
e-mail: mbd@astro.lu.se

H.M.J. Boffin et al. (eds.), *Ecology of Blue Straggler Stars*, Astrophysics and Space Science Library 413, DOI 10.1007/978-3-662-44434-4_9

momentum. In other words, the stars will be rotating sufficiently rapidly that they may be significantly non-spherical. Mixing within the merger product is critical when one considers the refueling of the core with unburned hydrogen and thus calculations of the lifetime of the merger product.

(c) Encounters involving binary stars can be as frequent as those involving only single stars

A binary poses a much larger target for encounters than single stars. Thus even if only a small fraction of stars are contained in binaries, the event rate for strong encounters between binaries and single stars can be comparable to (or possibly even in some cases exceed) the event rate for encounters between two single stars. Stellar collisions will occur in a subset of encounters involving binaries thus potentially producing blue stragglers. Stellar collisions occurring during encounters between two binaries will be important in less-dense clusters.

(d) Blue stragglers may also be produced through the natural evolution of isolated binaries

In the case of very tight binaries, angular momentum loss via winds may drive the two stars together forming a merger product not very different from that formed via collisional mergers. Alternatively when the primary star evolves, it may fill its Roche lobe and transfer mass on to the secondary star. If the mass transfer is stable, this may add sufficient mass to the secondary to convert it into a blue straggler.

(e) The observed blue straggler population is probably a combination of those formed via mergers and those formed from the evolution of binaries

Blue stragglers can be formed either via mergers (as the outcome of collisions) or via mass transfer (or merger) as an outcome of isolated-binary evolution. We will see that a combination of both formation channels probably occurs in most globular clusters, whilst binary evolution is most likely to be more important in less-dense clusters such as open clusters, and in the halo.

This chapter is arranged as follows. In Sect. 9.2, we review stellar collisions considering the collision rate within clusters, which types of stars are likely to be involved in collisions, and their immediate outcome. We review the post-collision evolution of merger products in Sect. 9.3. In Sect. 9.4, we describe encounters between binary star systems and single stars or other binaries. The evolution of isolated binaries is dealt with in Sect. 9.5, where we consider the effect of mass transfer on enhancing the mass of the secondary star, potentially converting it into a blue straggler. In Sect. 9.6 we consider the blue straggler population which may be produced as a combination of those formed via collisions and those formed via mass transfer as part of the evolution of binaries.

9.2 Stellar Collisions

In order for collisions to contribute significantly to the observed blue straggler population, we need a number of conditions to be satisfied: (1) collisions must occur at interesting rates within stellar clusters; (2) collisions must lead to the

merger of stars; (3) the merger product must look like a moderately-massive main sequence star (i.e. consistent with observations); and (4) the merger products must have a sufficiently long lifetime to produce a sufficiently large population of blue stragglers. We consider points (1) and (2) in this section, and points (3) and (4) in Sect. 9.3.

We begin by calculating the stellar encounter rate within clusters. The cross section for two stars, having a relative velocity at infinity of V_∞, to pass within a distance $R_{\rm min}$ is given by

$$\sigma = \pi R_{\rm min}^2 \left(1 + \frac{V^2}{V_\infty^2}\right) , \tag{9.1}$$

where V is the relative velocity of the two stars at closest approach in a parabolic encounter (i.e. $V^2 = 2G(M_1 + M_2)/R_{\rm min}$, where M_1 and M_2 are the masses of the two stars). The second term is due to the attractive gravitational force, and is referred to as gravitational focussing. In the regime where $V \ll V_\infty$ (as might be the case in galactic nuclei with extremely high velocity dispersions), we recover the result, $\sigma \propto R_{\rm min}^2$. However, if $V \gg V_\infty$ as will be the case in systems with low velocity dispersions, such as globular and open clusters, $\sigma \propto R_{\rm min}$. This will have consequences for the relative frequency of collisions at various stages of stellar evolution as we will see below.

One may estimate the timescale for a given star to undergo an encounter with another star, $\tau_{\rm coll} = 1/n\sigma v$. For clusters with low velocity dispersions, we thus obtain

$$\tau_{\rm coll} \simeq 10^{11}{\rm year} \left(\frac{10^5 {\rm pc}^{-3}}{n}\right) \left(\frac{V_\infty}{10{\rm km/s}}\right) \left(\frac{R_\odot}{R_{\rm min}}\right) \left(\frac{M_\odot}{M}\right) , \tag{9.2}$$

where n is the number density of single stars of mass M. For an encounter between two single stars to be hydrodynamically interesting, we typically require $R_{\rm min} \sim 3R_\star$ for $V_\infty = 10$ km/s (see for example, Davies et al. 1991). We thus see that for typical globular clusters, where $n \sim 10^5$ stars/pc^3, up to 10 % of the stars in the cluster cores will have undergone a collision at some point during the lifetime of the cluster.

Stars spend a large fraction of their life on the main sequence, where helium is produced through fusion of hydrogen within their cores. Once the hydrogen fuel is exhausted, stars then evolve off the main sequence and move towards the red giant branch where hydrogen fusion reactions occur in a shell above a contracting helium core, as the surrounding envelope expands to about 100 $R_\odot$. For low-mass stars, once helium ignition occurs within the core, the star shrinks to about 10 $R_\odot$ as it stays on the horizontal branch, fusing helium into carbon in its core. Post-horizontal branch, the star evolves up the asymptotic giant branch, expanding to length scales of around 300 $R_\odot$. Low-mass stars then eject their envelopes

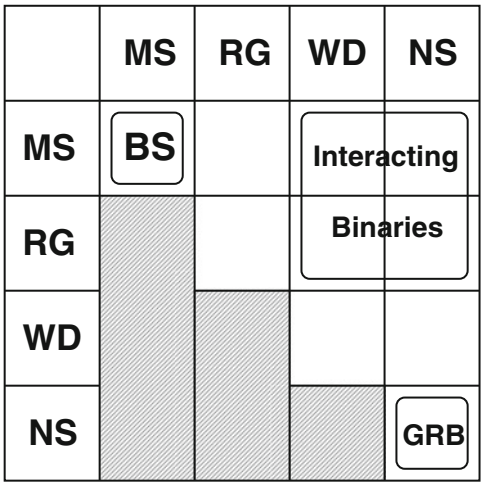

Fig. 9.1 Plot showing the grid of possible collisions between various stellar species: main sequence stars (MS), red giants (RG), white dwarfs (WD) and neutron stars (NS). Collisions between two main sequence stars may produce at least some of the observed blue stragglers (BS). Collisions between either main sequence stars or red giants and white dwarfs or neutron stars may produce interacting binaries (cataclysmic variables and low-mass X-ray binaries). Encounters involving two neutron stars could potentially produce gamma-ray bursts (GRB)

producing a white dwarf, whilst stars more massive than 8 $M_\odot$ will explode as a core-collapse supernova, leaving either a neutron star or (for the most massive stars) a stellar mass black hole (see Chap. 1 for a more detailed discussion).

It is possible for stars to be involved in collisions during all of the phases of stellar evolution described above, as shown in Fig. 9.1. Of interest to us here are the collisions involving two main sequence stars which may produce at least some of the observed blue stragglers.

We consider now when stars are most likely to be involved in collisions. One may integrate the collision rate equation over the entire lifetime of a cluster to calculate the expected number of collisions $n_{\rm coll}$ for a particular star:

$$n_{\rm coll}(t) = \int_0^t \Gamma_{\rm coll} dt = n \int_0^t \sigma(R_\star) V_\infty dt \,, \tag{9.3}$$

where $\Gamma_{\rm coll}$ is the collision rate for the star and $\sigma(R_\star)$ is the collision cross section [as given in Eq. (9.1) with the minimum distance $R_{\rm min}$ set to the stellar radius $R_\star$] which will change as a function of time as the star evolves (and its radius changes).

The number density of stars in a cluster n is assumed to be constant throughout the evolution of the star. The result of such a calculation is show in Fig. 9.2, where we plot the normalised expected number of collisions as a function of stellar radius for 0.4 $M_\odot$ stars in a globular cluster (stellar radius is used here as it easily shows the various phases of stellar evolution). The frequency of collisions when the star

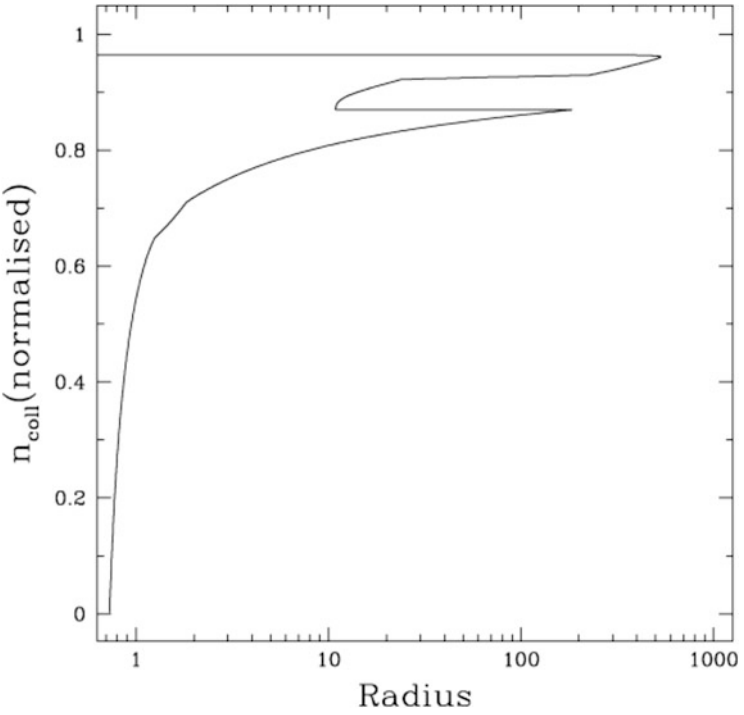

Fig. 9.2 The cumulative number of collisions as a function of stellar radius (in solar units) for 0.4 $M_\odot$ mass stars in a globular cluster. The expected number of collisions has been normalised so that the total number of collisions over the entire cluster lifetime is one. The various phases of stellar evolution are clear from this plot: the main sequence phase ending when the stellar radius is few solar radii, the red giant phase extending up to a radius ∼200 $R_\odot$, the star has a radius ∼10–20 $R_\odot$ on the horizontal branch, then expands again to over 300 $R_\odot$ on the asymptotic giant branch. The results obtained for 0.6 and 0.8 $M_\odot$ models are very similar (Figure 1 from Sills et al. 2005, reproduced with permission)

is large are somewhat reduced because of the effects of gravitational focussing as the cross section $\sigma(R_\star) \propto R_\star$ rather than $R_\star^2$. From Fig. 9.2, we can see that some 60–70 % of collisions will occur whilst the star is on the main sequence, a further 20 % or so occur whilst the star is ascending the giant branch, 10 % whilst the star is on the horizontal branch and a little less than 10 % on the asymptotic giant branch. We thus conclude that the majority of collisions will occur whilst the star is on the main sequence.

We consider now the immediate outcomes of collisions between two main sequence stars. Such collisions are complex events. Understanding them well requires fully 3D computational hydrodynamic simulations. Much work has been done modelling such collisions, particularly involving low-mass main-sequence stars with relatively-low velocities, which are relevant for the encounters of interest

to us in globular clusters (including Benz and Hills 1987; Lombardi et al. 1995, 1996, 2002; Sills et al. 2002).

There are two speeds to consider in a stellar collision: the relative speed of the two stars at infinity V_∞ and the surface escape speeds of the stars ($V_{\rm esc} = \sqrt{2GM_\star/R_\star}$). For globular clusters, $V_\infty \simeq 10$ km/s. In comparison, for low-mass main-sequence stars, $V_{\rm esc} \simeq 600$ km/s. We should not be surprised therefore to find that collisions in globular clusters lead to mergers having little mass loss (typically 1–10 % of mass is lost; e.g., Benz and Hills 1987, 1992) as the ejection of a small fraction of the total mass can carry off the (small) positive energy contained in the collision. Snapshots of a typical collision between two low-mass main-sequence stars is shown in Fig. 9.3. The stars quickly merge, with little mass loss, although the merged object does contain (unsurprisingly) considerable angular momentum. The post-collision evolution of such a merged object is complex, and will be discussed in the next section. The energy lost in a head-on impact is equivalent

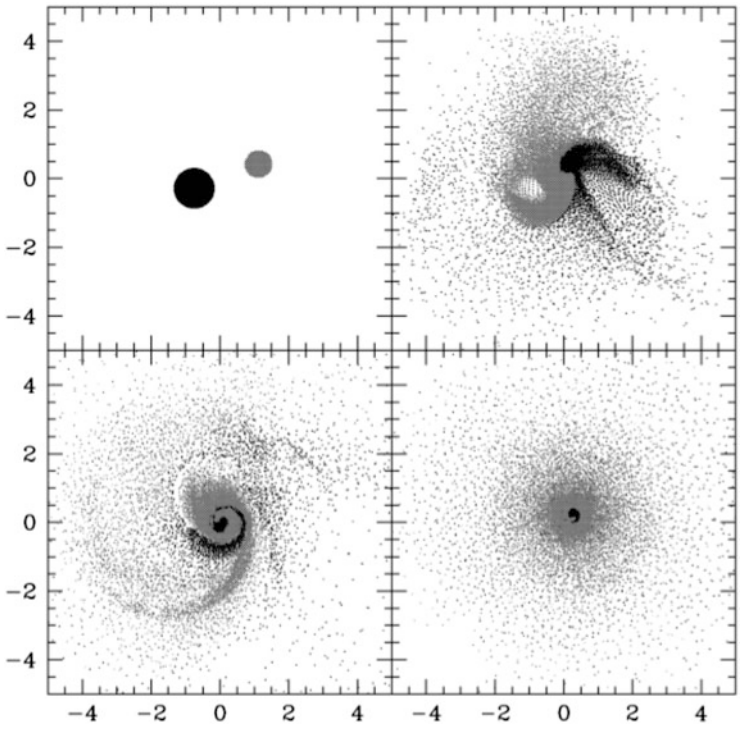

Fig. 9.3 Snapshots of a collision between a 0.6 $M_\odot$ main sequence star (*black dots*) and a 0.4 $M_\odot$ main sequence star (*grey dots*). The minimum distance between the stars in the initial collision was 0.255 $R_\odot$, equal to $0.25(R_1 + R_2)$ and the stars had a relative speed at infinity $V_\infty = 10$ km/s. The colours represent the density of the gas in the plane of the encounter (Figure 2 from Sills et al. 2005, reproduced with permission)

to $\delta V_\infty \sim 100\,\mathrm{km/s}$. Stars will become bound even for close encounters which do not (initially) lead to physical collisions, with the minimum distance to capture $R_{\mathrm{capt}} \sim 3R_\star$. Indeed, such a capture mechanism has been invoked as a way to produce the population of low-mass X-ray binaries in globular clusters, where in this case a passing neutron star captures a main sequence star via tidal interactions (Fabian et al. 1975).

9.3 Post-Collision Evolution

The subsequent evolution of the merger product is complicated, though much modelling work has been done—see, for example, Glebbeek and Pols (2008), Glebbeek et al. (2008), Sandquist et al. (1997) and Sills et al. (1997, 2001, 2005, 2009). Even though most of the material is bound in a single merged object, it will not immediately appear as a main-sequence star. The incoming kinetic energy of the impact has been converted into thermal energy, the merger product is out of virial equilibrium and will expand. One is interested to learn about the extent of the expansion and the timescales involved for it to return to the main sequence, if indeed it does so. The object typically contains significant angular momentum as most collisions are relatively grazing so the merger product contains the angular momentum from the trajectories of the two stars. Indeed many merger products initially contain too much angular momentum to contract down to the main sequence. By considering angular momentum loss through either disc- or wind-locking, it was shown that both methods allow the merger product to shed sufficient angular momentum to contract down to the main sequence (Sills et al. 2005).

In modelling the evolution, one is also concerned about how much mixing takes place within the star. Will the core be refueled with a fresh supply of hydrogen to thus extend the life of the blue straggler? The distribution of matter in low-mass main sequence stars in illustrated in Fig. 9.4 where we show the redistribution of material within the stars as an outcome of both head-on and off-axis collisions (Sills et al. 2005). If collisions were to lead to the complete mixing of material, then we would see that the four columns of the initial structure would be completely mixed in the collision products. In other words, the inner mass quartile of the collision product would contain equal amounts of material from each of the four mass quartiles from the initial structure. This is not seen. Indeed, only a very small amount of material in the central mass quartile of the collision products is drawn from outer regions of the pre-collision stars (very little mixing is seen also in the work of Sandquist et al. 1997; Sills et al. 1997). Slightly more mixing is seen in off-axis collisions than in head-on collisions (see also Sills et al. 2001). Mixing is important when one considers the lifetime of the collision product: collisions involving main sequence stars close to the turn-off mass, will contain relatively small amounts of unburned hydrogen in their cores. The lifetime of the collision products will be short unless fresh hydrogen can be brought in to the core of the

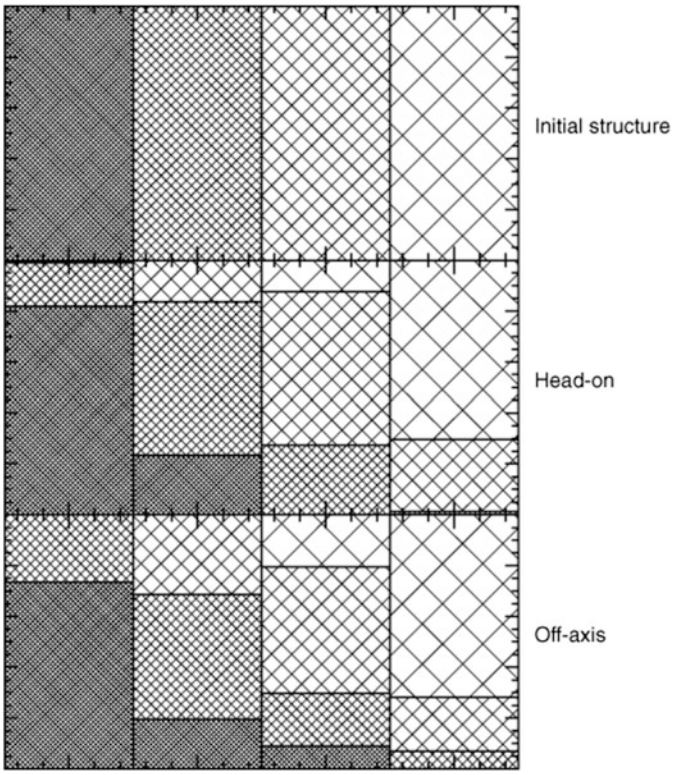

Fig. 9.4 A plot showing the mixing of material which occurs in head-on and off-axis collisions between two low-mass main sequence stars. The four columns in each plot represent four equally-spaced mass bins (Figure 3 from Sills et al. 2005, reproduced with permission)

merger product. Indeed, recent work suggests that blue stragglers have somewhat shorter lifetimes than regular main-sequence stars of similar masses (Sills et al. 2013).

9.4 Encounters Involving Binary Stars

In this section we consider the role played by encounters involving binary stars in producing blue stragglers. Binaries are larger targets than single stars within stellar clusters. Interesting encounters occur when a star passes within a distance roughly equal to the size of the binary. Hence, the time scale for encounters is given by

$$\tau_{2+1} \simeq 10^{11}\text{year}\left(\frac{10^5 pc^{-3}}{n}\right)\left(\frac{V_\infty}{10km/s}\right)\left(\frac{R_\odot}{a_{\rm bin}}\right)\left(\frac{M_\odot}{M}\right) . \quad (9.4)$$

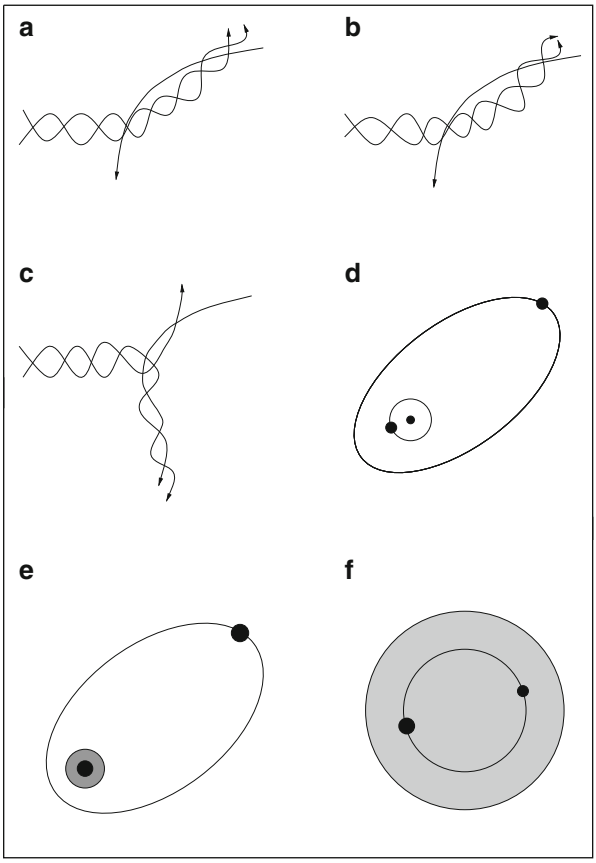

Fig. 9.5 Possible outcomes of encounters between a binary and a single star: (**a**) a fly-by occurs where the binary's orbit is changed, (**b**) the fly-by leads to the merger of the two stars in the binary, (**c**) the intruding star exchanges into the binary, (**d**) the system forms a (transient) triple system, (**e**) two of the stars merge and remain bound to the third star, and (**f**) a common envelope system is formed where two of the stars orbit inside a gaseous envelope made from the third star

One can see how encounters between binaries and single stars can be as frequent as encounters between two single stars. For example, if a cluster possesses a binary fraction of around 0.05, then the encounter rates will be similar for binaries of separation $a_{\rm bin} \sim 60$ R$_\odot$. There are many outcomes possible for encounters involving binaries as illustrated in Fig. 9.5: fly-bys occur where the binary retains its stellar components although the binding energy and eccentricity of the binary orbit may change; fly-bys may lead to the merger of the two stars within the binary; an intruder star may exchange into the binary with typically the least massive of the three stars being ejected; the system may form a (transient) triple system; two of the stars may merge but remain bound to the third star; or a common envelope system may form where two of the stars orbit inside a gaseous envelope made from the third star.

For us here, considering blue straggler production in stellar clusters, we are particularly interested in the fifth possible outcome, where two stars merge. The outcomes for such mergers are likely to be similar to those seen for collisions between two single stars as described earlier.

We will now consider some general concepts concerning binary–single encounters. If binaries are sufficiently wide, encounters with single stars will tend to break them up as the kinetic energy contained in the incoming star exceeds the binding energy of the binary. Such binaries are referred to in the literature as *soft*. Whereas binaries which are more tightly bound and are thus resilient to break-up are known as *hard*. The separation of the stars in a binary sitting on the hard-soft boundary depends on the masses of the stars in the binary, and the mass of the incoming star. Assuming that all stars are of one solar mass, the binary separation for a system on the hard-soft boundary is given approximately by $a_{\rm hs} \simeq 6{\rm AU}(V_\infty/10\,{\rm km\,s^{-1}})^{-2}$. Encounters tend to break up soft binaries, whereas hard binaries get harder (i.e. more bound). They are also left with a thermal distribution of eccentricities, where the distribution follows $dn/de = 2e$. As stated earlier, in exchange encounters it is most often the least massive of the three stars which is ejected.

Thus, encounters involving binaries will tend to increase the mass of the stellar components within binaries; a fact which will become important later in this chapter when we compare the blue straggler formation rates in clusters produced from the evolution of primordial binaries to the rate due to collisions and mergers.

The fraction of binary–single encounters which lead to collisions between stars is a function of the binary separation. For binaries having separations around 1 AU, the fraction of strong binary–single encounters where two stars pass within some distance $r_{\rm min}$ is found, through numerical experimentation, to be $f \propto (r_{\rm min}/a_{\rm bin})^\gamma$ where $\gamma \simeq 1/2$ (Davies et al. 1993, 1994). So, for example, collisions and mergers occur in 10–20 % of encounters involving solar-like stars and a binary of separation 1 AU. Thus stellar mergers occurring during a binary–single encounter may make a significant contribution to the total merger rate within a stellar cluster providing the binary fraction is large. In typical globular clusters, where the binary fraction is perhaps around 10 % or smaller (e.g., Milone et al. 2012), the collision rate derived from single–single collisions is likely to exceed that derived from encounters involving binaries.

We now consider encounters involving *two* binaries. The cross section for some kind of strong interaction for binary–binary encounters is in fact roughly the same as for binary–single encounters: we require that the binaries pass within a distance roughly comparable to the size of the binaries. However the fraction of strong encounters leading to physical collisions is larger. This can be seen simply by reflecting that when we have four bodies (i.e. two binaries) involved in a complex encounter the number of distinct pairs $n_4 = 4(4-1)/2 = 6$ whereas for three bodies (i.e. a binary and a single star), the number of pairs is $n_3 = 3(3-1)/2 = 3$. Thus, we have a much greater chance that at least one pair will suffer a close passage during the whole encounter. Typically a binary–binary encounter quickly resolves itself into a (transient or stable) triple and a single star. Such an encounter is shown in Fig. 9.6.

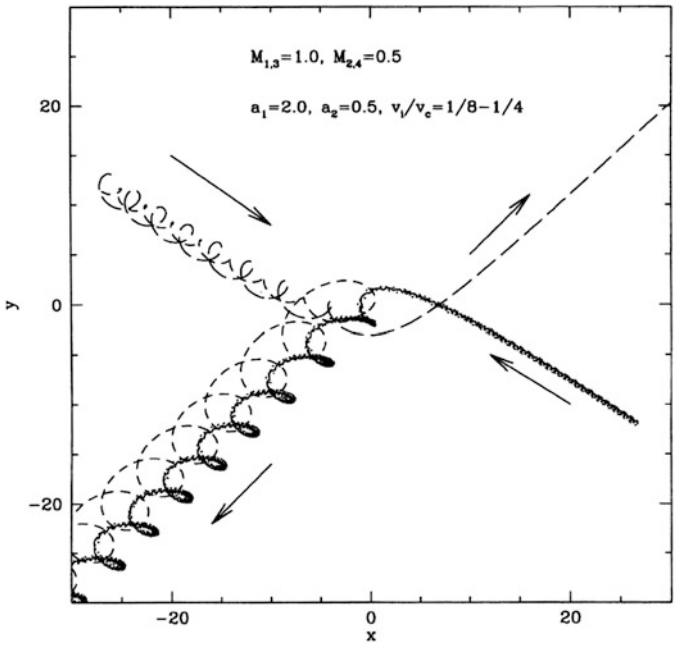

Fig. 9.6 An example of a binary–binary encounter, in this case producing a hierarchical triple and a single star (Figure 3 from Bacon et al. 1996, reproduced with permission)

In sparse clusters, with lower number densities of stars, collisions between two single stars may be rare. In such cases, collisions occurring during the interaction between two binaries may dominate. There are several papers which contain calculations of cross sections for various outcomes (binary break-ups, exchange encounters, and stellar collisions): including Bacon et al. (1996), Davies et al. (1993), Davies et al. (1994), Heggie (1975), Hut et al. (1992), Hut and Verbunt (1983), Leonard (1989) and Sigurdsson and Phinney (1993).

Binaries are, in many ways, a fossil fuel of globular clusters. Through close encounters with single stars or other binaries, they are broken up or ground down, processed, and sometimes ejected from clusters. Those not formed in clusters' cores will sink into the core (as they are heavier than the average star) and there undergo close encounters. The fate of binaries within a cluster is shown in Fig. 9.7, taken from Hut et al. (1992), who used a simple model to follow a population of primordial binaries within a cluster, allowing them to sink into the cluster core, suffer encounters, be ejected from the core, or the entire cluster. They found that about half of the binaries will be broken up (often termed "ionisation")—in fact often by encounters with other binaries. Others will be involved in collisions or would be hardened to the point where the two stars in the binary would merge. A very small fraction will escape from the cluster.

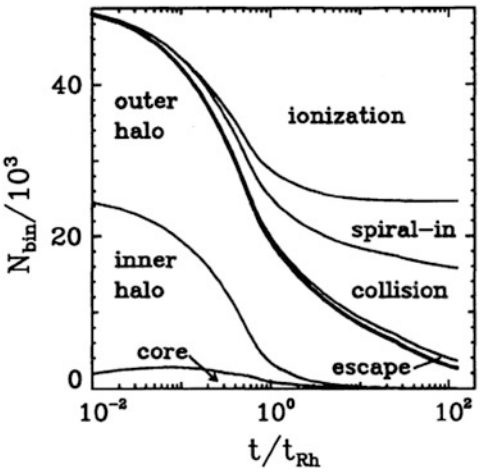

Fig. 9.7 The location and fate of binaries within a stellar cluster, containing initially 50,000 binaries. The *left-hand side of the figure* shows the location of any surviving binaries as a function of time (in units of the half-mass relaxation time). The *right-hand side of the figure* shows the fate of those binaries which have not survived: break-up (ionisation), stars merging (spiral-in and collision), and those (few) escaping from the cluster (Figure 3 from Hut et al. 1992, reproduced with permission)

9.5 Making Blue Stragglers via Binary Evolution

In this section we consider the formation of blue stragglers through the evolution of stellar binaries, where either the two stars spiral together and merge as angular momentum is lost via stellar winds, or where mass transfer occurs from one (evolved) star to the other. Both processes may produce stars more massive than the current turn-off, providing in the first case the total mass of the two stars exceeds the current turn-off, and in the second case providing the mass transferred from the primary to the secondary increases the mass of the secondary above that of the turn-off mass of the cluster.

Tight binaries, where the separation is only a few times larger than main sequence stars, may merge as angular momentum is lost via stellar winds (Vilhu 1982). The subsequent evolution of the merger product is likely to be rather similar to that described earlier for objects produced via stellar collisions. Here, as before, the object is likely to be spinning rapidly, perhaps leading to global circulation within the merged object which may help refuel the core with unburnt hydrogen. Clearly the merger product will be a single star, unless the tight binary is itself a component of a wider binary (see Perets and Fabrycky 2009 and Chap. 11).

We consider now the evolution of binaries which are too wide to merge via angular momentum loss from stellar winds. In such systems, mass may flow from

the primary to the secondary star when the former evolves off the main sequence, expanding up the giant branch and filling its so-called Roche lobe where material at the primary's surface flows toward the secondary star (McCrea 1964). This mass transfer may be stable, in the sense that the mass transfer rate does not grow rapidly, and the system evolves steadily as the primary evolves up the giant branch (as illustrated schematically in Fig. 9.8). In such a case, the secondary will gain mass from the primary.

Alternatively, the mass transfer can be unstable: the rate increases to the point where a very rapid mass transfer occurs with a large fraction of the primary's

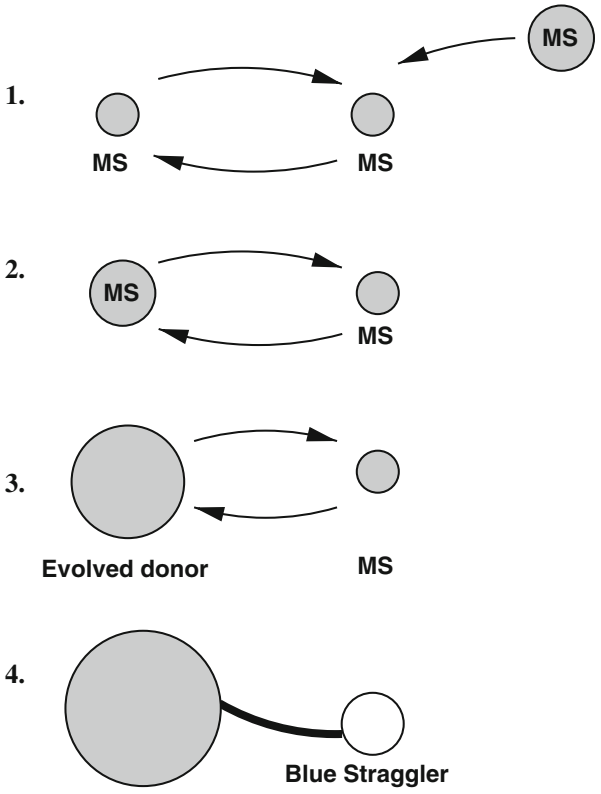

Fig. 9.8 The evolutionary pathway to produce blue straggler stars (BSSs) through mass transfer in wide binaries in globular clusters. A more massive main sequence star exchanges into a binary containing two main sequence stars (phase 1). The typical primary mass after encounters in a sufficiently crowded cluster is $M_1 \simeq 1.5$–$3M_\odot$ (Davies and Hansen 1998). This primary evolves off the main sequence and fills its Roche lobe (phase 3). The secondary gains mass from the primary becoming a BSS (phase 4) at a time roughly equal to the main sequence lifetime of the donor star. Hence BSSs have formed earlier in binaries containing more-massive primaries (i.e. in high collision rate clusters). Given the finite lifetime of BSSs, the BSS population in the most crowded clusters today could be lower than in very sparse clusters (Figure 4 from Davies et al. 2004, reproduced with permission)

envelope engulfing the secondary forming what is know as a common envelope system where the core of the primary and the secondary star orbit inside this envelope of gas. In this case, the core of the primary and the secondary star will spiral together, dumping energy and angular momentum into the surrounding envelope which will be ejected.

In order to compute whether mass transfer is unstable, one has to consider the response of the donor star to its mass loss and compare this to how the size of the Roche lobe changes as mass is transferred (see Chap. 8 for a more detailed discussion). Mass transfer will be unstable when the ratio of the donor radius to the Roche lobe radius increases, in other words, when the star overfills its Roche lobe by increasing amounts.

If the mass transfer is *conservative*, meaning that mass transfers from one star to the other without any loss of material (or angular momentum) via stellar winds, then the separation of a binary will increase if the donor is less-massive than the receiving star, and decrease if the donor is more-massive than the receiving star. One can see that systems containing more massive donors will often be unstable, as once filling their Roche lobes, the donors will overflow their Roche lobes more and more, leading to extremely high rates of mass transfer.

By definition, in the case considered here, the donor is the primary in the binary and will thus be more massive than the secondary (mass-receiving) star. However, for systems with an initial mass ratio close to unity, it could be that in some systems an initial phase of mass transfer could change the mass ratio such that the donor is now the less massive star in the binary. What follows is then a phase of stable mass transfer where the envelope of the primary is slowly transferred to the secondary star (on stellar evolutionary timescales) whilst the separation of the binary increases.

Providing mass transfer occurs on the giant branch, one would expect to see at the end of this mass transfer a rejuvenated secondary star (now the more massive star in the system) orbiting around some form of white dwarf (the former core of the primary). The binary separation being a few times larger than red giant radii.

In Fig. 9.9[1] we plot the binary properties of both solar-type main-sequence stars and blue stragglers observed in the open cluster NGC 188 (Mathieu and Geller 2009; see also Chap. 3). Interestingly, the vast majority of the blue stragglers are in relatively *wide* binaries. This strongly suggests that these systems have passed through a period of stable mass transfer from a star evolving up the red-giant branch as described above. This is also consistent with the observations in the field that blue stragglers are in wide binaries (Carney et al. 2001; Preston and Sneden 2000; Sneden et al. 2003).

[1]This is a repetition of Fig. 3.2, reproduced here for the convenience of the reader.

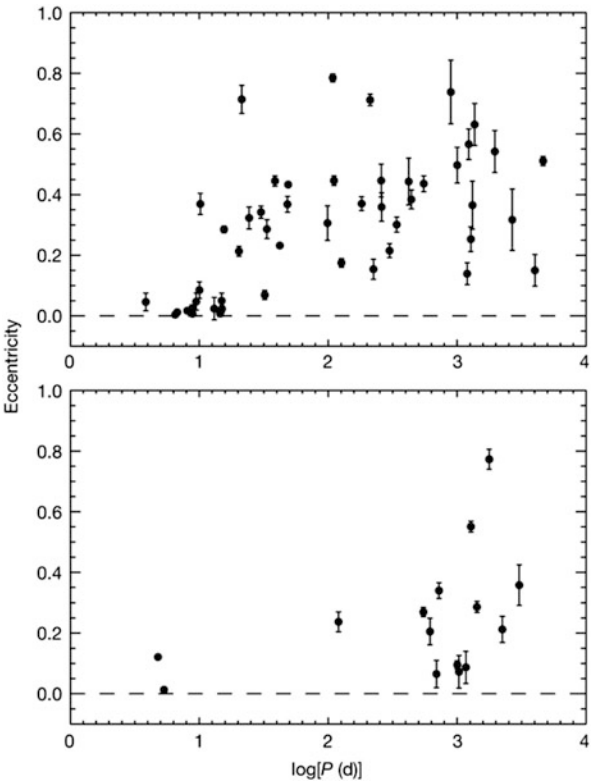

Fig. 9.9 Distribution of solar-type main sequence binaries seen in the open cluster NGC 188 (*upper figure*), and the binary population for blue stragglers in NGC 188 (*lower figure*) (Figure 2 from MG09, reproduced with permission)

9.6 Comparing Primordial and Collisional Formation Rates in Clusters

We may compute how the blue straggler production rate scales with cluster mass, assuming all blue stragglers are made via the two-body collisions described above, and that these collisions occur exclusively within the dense core.

The stellar collision rate within the cluster core is given by $\Gamma_{\rm coll} \propto \rho^2 r_{\rm c}^3/\sigma$, where ρ is the mass density of stars within the cluster core, $r_{\rm c}$ is the core radius, and σ is the velocity dispersion of the stars which is $\propto \sqrt{M_{\rm tot}/r_{\rm h}}$, where $M_{\rm tot}$ is the cluster total mass and $r_{\rm h}$ is the radius containing half of the cluster's total mass. Also the cluster's core mass $M_{\rm c} \propto \rho r_{\rm c}^3$. Hence we have

$$\Gamma_{\rm coll} \propto \frac{\rho^2 r_{\rm c}^3}{\sigma} \propto \frac{\rho^2 r_{\rm c}^3}{\sqrt{M_{\rm tot}/r_{\rm h}}} \propto \frac{M_{\rm c}^2 r_{\rm c}^{-3}}{\sqrt{M_{\rm tot}/r_{\rm h}}} \propto \frac{f_{\rm c}^2 r_{\rm h}^{1/2}}{r_{\rm c}^3} M_{\rm tot}^{3/2}\,, \tag{9.5}$$

where $f_c = M_c/M_{tot}$. Assuming for simplicity f_c, r_c, and r_h are the same for all clusters, we see that $\Gamma_{coll} \propto M_{tot}^{1.5}$. Clearly f_c, r_c, and r_h all vary between clusters, though this simply produces a spread around the relationship. In other words, if all the blue stragglers in globular clusters really were produced via two-body collisions, then we would expect to see that the number of blue stragglers increases with cluster mass as

$$N_{bs,coll} \propto M_{tot}^{1.5}\,, \tag{9.6}$$

This is not seen in the observed systems as illustrated in Fig. 9.10 where we see that the number of blue stragglers is relatively independent of cluster mass (see also Piotto et al. 2004).

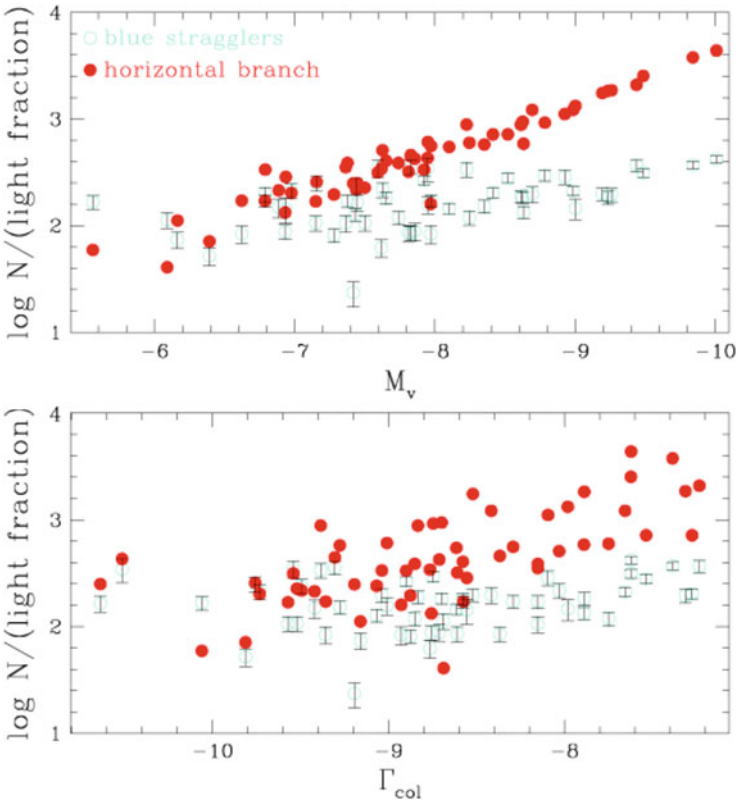

Fig. 9.10 The estimated total number of blue stragglers and horizontal branch stars in the sample of 56 globular clusters as a function of cluster total magnitude M_V (*top panel*) and stellar collision rate (*bottom panel*). See Piotto et al. (2004) for more details (Figure 1 from Davies et al. 2004, reproduced with permission)

We consider now the production of blue stragglers via binary evolution, either through the merger of the two components of a binary, or via mass transfer from the primary to the secondary as the primary evolves off the main sequence. In order for such a process to produce the blue stragglers we see today, the mass of the merger product, or mass transfer enhanced secondary, must exceed the current turn-off mass. The merger or mass transfer event must also have occurred relatively recently, i.e. less than the blue straggler lifetime ago. If we assume here that the merger or mass transfer is driven by the evolution of the primary off the main sequence, then this is equivalent to requiring that the primary mass subtracted by the current cluster turn-off mass is less than some amount. For example, if we take a blue straggler lifetime of one gigayear, and a turn-off mass today of 0.8 $M_\odot$, then we require that the primary mass is in the range 0.8 $M_\odot \leq M_1 \leq 0.816\ M_\odot$. We note that this is a rather narrow range of masses (due to the very strong mass dependence of main-sequence lifetimes). Typically, only a small fraction of binaries will satisfy this condition. If we consider a binary population where stars are drawn from a reasonable Initial Mass Function (IMF; in our case, from Eggleton et al. 1989), then we find that the fraction of binaries making a blue straggler seen today would be $f_{\rm bs} \simeq 0.006$. If the binaries which produce blue stragglers are allowed to evolve in globular clusters without any interactions with other stars, then we would simply expect that the number of blue stragglers derived from these primordial binaries would be proportional to the cluster mass:

$$N_{\rm bs,bin} \propto f_{\rm bs,bin} M_{\rm tot} \tag{9.7}$$

where $f_{\rm bs,bin}$ is the fraction of the original binary population contributing to the blue straggler population today, i.e. those with primaries in the mass range 0.8 $M_\odot \leq M_1 \leq 0.816\ M_\odot$.

Let us assume that the two mechanisms described above are the only two contributing to the observed blue straggler population seen in globular clusters. How could their combination produce a population which is relatively independent of cluster mass, given the mass dependencies described in Eqs. (9.6) and (9.7)?

The key point here is that dynamical interactions occur within the stellar cluster which will alter the binary population: (1) exchange encounters with single stars occur where less-massive stars in binaries are replaced by more-massive single stars; (2) stellar collisions may occur during binary–single encounters (see Fig. 9.5) which lead to mergers and may remove the binary from the population; (3) some binaries may be destroyed by binary–binary encounters.

Thus in more massive clusters, the binaries will on average have experienced more close encounters with single stars and binaries. Binary–single encounters scale with cluster mass in the same way as two-body collisions seen in equation (9.6). From exchange encounters, the binaries will tend to contain more massive stars today. This will *reduce* the fraction of binaries contributing to the blue straggler population today, as more of the primaries in the binaries will have evolved off

the main sequence too long ago in the past: the blue stragglers they produced have been and gone by today (Davies et al. 2004). However, as pointed out by Knigge (private communication; see also Chap. 13), stellar evolution may reduce this effect as stars will have evolved, becoming (less-massive) compact remnants before they encounter binaries. If the binaries are in mass-segregated stellar cluster cores, more of the stars they encounter will be massive and thus more massive stars will exchange into binaries before they evolve. Even if this effect is limited, binary destruction via stellar collisions and binary–binary encounters may be equally effective in reducing the blue-straggler population derived from binaries. The destruction of binaries via these two mechanisms is shown in Fig. 9.7 (see also Hut et al. 1992). Observational evidence for lower binary fractions in more massive clusters (and thus, on average those having more dynamical interactions) has been reported by Milone et al. (2012).

Combining the contribution from stellar collisions and that from binaries, we have

$$N_{\rm bs} = k_{\rm bs,coll} M_{\rm tot}^{3/2} + k_{\rm bs,bin} f_{\rm bs,bin}(M_{\rm tot}) M_{\rm tot} \ , \tag{9.8}$$

where $k_{\rm bs,coll}$ and $k_{\rm bs,bin}$ are suitably chosen constants. $f_{\rm bs,bin}(M_{\rm tot})$ has been determined through Monte Carlo calculations of binary–single encounters including only the effects of exchange encounters, not including the effects of stellar evolution (Davies et al. 2004).

The number of blue stragglers expected as a function of absolute cluster magnitude is shown in Fig. 9.11. Here we have assumed a mass-to-light ratio $M/L_V = 3$, and have taken reasonable values for the two constants (see Davies et al. 2004). Including the effects of stellar evolution could reduce the effect due to exchanges, but the binary population will also be reduced via stellar collisions during binary–single encounters and by binary destruction during binary–binary encounters. The net effect is likely to be the same: in environments where interactions with other stars and binaries are sufficiently frequent, the contribution to the blue straggler population made by binaries is reduced. We see that the blue straggler population derived from binaries dominates for most clusters and that direct collisions only become important for clusters brighter than $M_{\rm v} = -9$ (or equivalently a mass, $M_{\rm tot} = 10^6$ M$_\odot$). Indeed, by considering the number of blue stragglers found in cluster cores and comparing this to the total stellar mass contained in cluster cores, Knigge et al. (2009) concluded that most blue stragglers come from binary systems—but see also Leigh et al. (2013).

It is important to recall that the trend shown in Fig. 9.11 has been derived assuming average cluster properties (the dependence on cluster mass given in Eq. (9.6) assumed for example that all clusters have the same core and half-mass radii). There will be outliers to the distribution shown here. Nonetheless, the turnover in the blue straggler population derived from primordial binaries seen here due to encounters with single stars (and perhaps also binary destruction through stellar collisions and binary–binary encounters) does explain the observed,

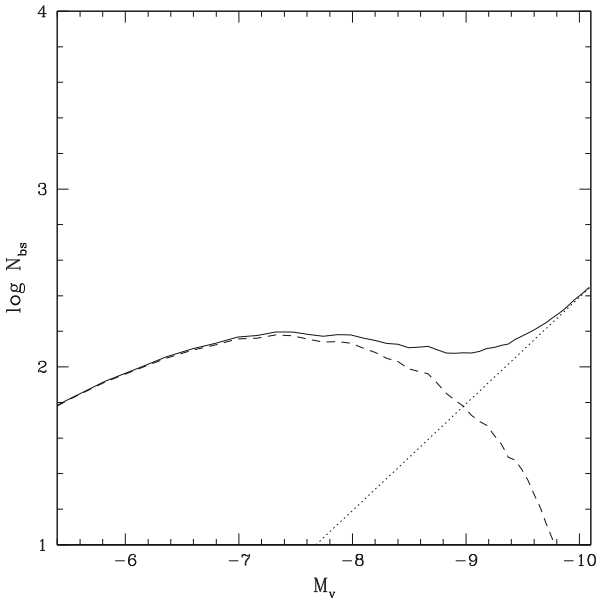

Fig. 9.11 The number of BSSs produced over the last Gyr as a function of absolute cluster luminosity, M_V , assuming $M/L_V = 3$ for all clusters. The contribution from primordial systems is shown with a *dashed line*, whilst those produced via collisions (involving either two single stars or binaries) is shown as a *dotted line*. The total is given as a *solid line* (Figure 6 from Davies et al. 2004, reproduced with permission)

relatively flat, blue straggler population. There is observational evidence that two formation channels for blue stragglers occur in at least one globular cluster—M30—as two distinct blue-straggler sequences have been observed (Ferraro et al. 2009).

It should also be noted that the *specific* frequency of blue stragglers seen in clusters (i.e. the number per unit mass) is in fact *less* than one would obtain for binaries in the field. This is because binary–single encounters (and binary–binary encounters) act to reduce the fraction of binaries contributing to the blue straggler population today. Thus the largest specific frequency of blue stragglers derived from binaries will occur in low-density environments where no such encounters are expected: in the low-density haloes of clusters and in field of the Galaxy. Indeed, this is consistent with observations of blue stragglers seen in the Galactic halo (Carney et al. 2001; Preston and Sneden 2000; Sneden et al. 2003) and also in open clusters, where the observed population follows that expected if it is derived from primordial binaries which have undergone mass transfer, as shown in Fig. 9.12 (de Marchi et al. 2006).

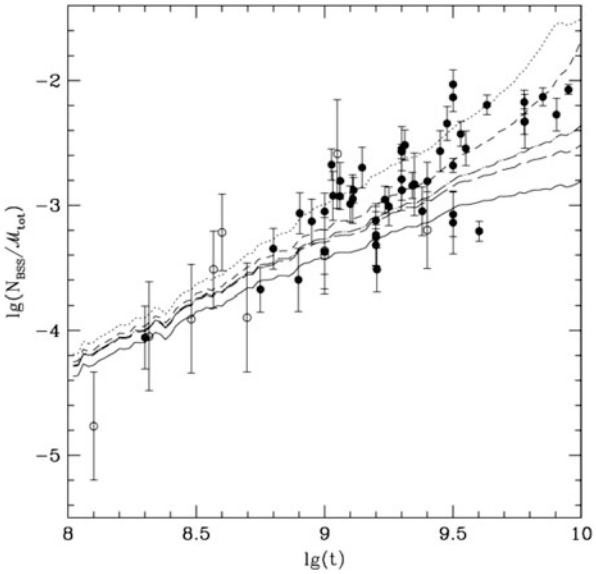

Fig. 9.12 Comparison between the expected number of blue stragglers and the number observed in open clusters. The *solid line* represents the model given in de Marchi et al. (2006) where it is assumed that the observed blue stragglers are derived from primordial binaries which have undergone mass-transfer. *Dotted*, *dashed*, *dot-dashed* and *long-dashed curves* reproduce respectively the expected values obtained taking into account the evaporation of stars from clusters following the models of Tanikawa and Fukushige (2005) with 2k, 8k, 32k, and 131k N-body models (Figure 8 from de Marchi et al. 2006, reproduced with permission)

Acknowledgements This book is the result of a meeting held at ESO, Chile. I thank the local organisers for their hospitality. I thank Christian Knigge for pointing out the importance of stellar evolution when considering the evolution of a population of binaries within a stellar cluster.

References

Bacon, D., Sigurdsson, S., Davies, M. B.: MNRAS **281**, 830 (1996)
Benz, W. , Hills, J. G.: ApJ **323**, 614 (1987)
Benz, W. , Hills, J. G.: ApJ **389**, 546 (1992)
Carney, B. W., Latham, D. W., Laird, J. B., Grant, C. E., Morse, J. A.: AJ **122**, 3419 (2001)
Davies, M. B., Benz, W., Hills, J. G.: ApJ **381**, 449 (1991)
Davies, M. B., Benz, W., Hills, J. G.: ApJ **411**, 285 (1993)
Davies, M. B., Benz, W., Hills, J. G.: ApJ **424**, 870 (1994)
Davies, M. B. , Hansen, B. M. S.: MNRAS **301**, 15 (1998)
Davies, M. B., Piotto, G., de Angeli, F.: MNRAS **349**, 129 (2004)
de Marchi, F., de Angeli, F., Piotto, G., Carraro, G., Davies, M. B.: A&A **459**, 489 (2006)
Eggleton, P. P., Fitchett, M. J., Tout, C. A.: ApJ **347**, 998 (1989)
Fabian, A. C., Pringle, J. E., Rees, M. J.: MNRAS **172**, 15P (1975)
Ferraro, F. R., Beccari, G., Dalessandro, E., et al.: Nature **462**, 1028 (2009)

Glebbeek, E. , Pols, O. R.: A&A **488**, 1017 (2008)
Glebbeek, E., Pols, O. R., Hurley, J. R.: A&A **488**, 1007 (2008)
Heggie, D. C.: MNRAS **173**, 729 (1975)
Hut, P., McMillan, S., Goodman, J., et al.: PASP **104**, 981 (1992)
Hut, P., McMillan, S., Romani, R. W.: ApJ **389**, 527 (1992)
Hut, P. , Verbunt, F.: Nature **301**, 587 (1983)
Knigge, C., Leigh, N., Sills, A.: Nature **457**, 288 (2009)
Leigh, N., Knigge, C., Sills, A., et al.: MNRAS **428**, 897 (2013)
Leonard, P. J. T.: AJ **98**, 217 (1989)
Lombardi, Jr., J. C., Rasio, F. A., Shapiro, S. L.: ApJ **445**, L117 (1995)
Lombardi, Jr., J. C., Rasio, F. A., Shapiro, S. L.: ApJ **468**, 797(1996)
Lombardi, Jr., J. C., Warren, J. S., Rasio, F. A., Sills, A., Warren, A. R.: ApJ **568**, 939 (2002)
Mathieu, R. D. , Geller, A. M.: Nature **462**, 1032 (2009)
McCrea, W. H.: MNRAS **128**, 147 (1964)
Milone, A. P., Piotto, G., Bedin, L. R., et al.: A&A **540**, A16 (2012)
Perets, H. B. , Fabrycky, D. C.: ApJ **697**, 1048 (2009)
Piotto, G., De Angeli, F., King, I. R., et al.: ApJ **604**, L109 (2004)
Preston, G. W. , Sneden, C.: AJ **120**, 1014 (2000)
Sandquist, E. L., Bolte, M., Hernquist, L.: ApJ **477**, 335 (1997)
Sigurdsson, S. , Phinney, E. S.: ApJ **415**, 631(1993)
Sills, A., Adams, T., Davies, M. B.: MNRAS **358**, 716 (2005)
Sills, A., Adams, T., Davies, M. B., Bate, M. R.: MNRAS **332**, 49 (2002)
Sills, A., Faber, J. A., Lombardi, Jr., J. C., Rasio, F. A., Warren, A. R.: ApJ **548**, 323 (2001)
Sills, A., Glebbeek, E., Chatterjee, S., Rasio, F. A.: ApJ **777**, 105 (2013)
Sills, A., Karakas, A., Lattanzio, J.: ApJ **692**, 1411 (2009)
Sills, A., Lombardi, Jr., J. C., Bailyn, C. D., et al.: ApJ **487**, 290 (1997)
Sneden, C., Preston, G. W., Cowan, J. J.: ApJ **592**, 504 (2003)
Tanikawa, A. , Fukushige, T.: PASJ **57**, 155 (2005)
Vilhu, O.: A&A **109**, 17 (1982)

Chapter 10
Dynamical Processes in Globular Clusters

Stephen L.W. McMillan

10.1 Introduction

Globular clusters have long been regarded as near-perfect laboratories for studies of stellar physics and stellar dynamics. Some reasons (and complications) are:

- they are isolated in space (but not all clusters are found in galactic halos—many disk and bulge clusters are known, and dynamical friction has probably transported many clusters into the Galactic Centre)
- they contain coeval stars (but many clusters are now known to contain multiple stellar populations indicating several distinct phases of star formation)
- they contain virtually no gas or dust (today, that is—at early times, gas dynamical processes dominated their evolution)
- they are nearly spherical (although several are measurably flattened by rotation and/or tidal effects)

These systems thus represent a relatively—although not perfectly—"clean" realisation of the classical N-body problem

$$\mathbf{a}_i \equiv \ddot{\mathbf{x}}_i = \sum_{j \neq i}^{N} G m_j \frac{\mathbf{x}_j - \mathbf{x}_i}{\left|\mathbf{x}_j - \mathbf{x}_i\right|^3}, \quad i = 1, \ldots, N. \tag{10.1}$$

We begin our study of cluster dynamics by ignoring complicating factors such as gas dynamics, stellar evolution, mass loss, etc., and focus on the pure N-body problem, much as it might have been described by Newton. We define timescales and other

S.L.W. McMillan (✉)
Department of Physics, Drexel University, Philadelphia, PA 19104, USA
e-mail: steve@physics.drexel.edu

H.M.J. Boffin et al. (eds.), *Ecology of Blue Straggler Stars*, Astrophysics and Space Science Library 413, DOI 10.1007/978-3-662-44434-4_10

units, discuss the fundamental dynamical processes driving cluster evolution, and present some basic terminology relevant to cluster dynamics.

10.2 Virial Equilibrium

Star clusters have no static equilibrium configuration similar to that found in a fluid system such as a star. Stars are in constant motion. However, in dynamical equilibrium, at any given location in the cluster there are as many stars moving inward as moving outward—that is, there is no net radial stellar flux.

10.2.1 The Virial Theorem

A convenient global restatement of dynamical equilibrium involves the "radial moment of inertia" of the system

$$I = \sum_{i=1}^{N} m_i \, r_i^2, \tag{10.2}$$

where $r_i = |\mathbf{x}_i|$. Differentiating, we find

$$\ddot{I} = 2 \sum_{i=1}^{N} m_i \left(v_i^2 + \mathbf{x}_i \cdot \mathbf{a}_i \right). \tag{10.3}$$

Setting $\ddot{I} = 0$ as our definition of dynamical equilibrium, we have

$$\sum_{i=1}^{N} m_i \, v_i^2 + \sum_{i=1}^{N} m_i \, \mathbf{x}_i \cdot \mathbf{a}_i \; = \; 0. \tag{10.4}$$

The first term is simply twice the total kinetic energy of the system, $2K$. The second is easily shown to be

$$U = -\sum_{i=1}^{N} \sum_{j>i}^{N} \frac{G m_i m_j}{\left| \mathbf{x}_j - \mathbf{x}_i \right|}, \tag{10.5}$$

the total potential energy of the system. Thus we obtain the (scalar) Virial Theorem

$$2K + U = 0. \tag{10.6}$$

If this relation holds the cluster is said to be in virial equilibrium. Since the total energy is $E = K + U$ (< 0), in virial equilibrium we have

$$K = -E, \quad U = 2E. \tag{10.7}$$

10.2.2 Length and Time Scales

We can define some characteristic physical scales for a system in virial equilibrium [Eq. (10.6)]. For a cluster of total mass M, the virial radius, R_{vir}, is defined as

$$R_{vir} \equiv -\frac{GM^2}{2U} = -\frac{GM^2}{4E}. \tag{10.8}$$

It defines a characteristic length scale for the cluster. It is typically comparable to the cluster half-mass radius, R_h, the radius of the sphere centred on the cluster enclosing half of the cluster's total mass. The two radii are often used interchangeably, although they are distinct physical quantities. Spitzer (1987) notes that $R_{vir} \approx 0.8 R_h$ for a broad range of common cluster models.

The cluster dynamical time (or "crossing time"), t_{dyn}, is

$$\begin{aligned} t_{dyn} &\equiv \left(\frac{GM}{{R_{vir}}^3}\right)^{-1/2} = \frac{GM^{5/2}}{(-4E)^{3/2}} \\ &= 0.47\ \mathrm{Myr} \left(\frac{M}{10^6\ \mathrm{M}_\odot}\right)^{-1/2} \left(\frac{R_{vir}}{10\ \mathrm{pc}}\right)^{3/2}. \end{aligned} \tag{10.9}$$

The second forms of this and the previous expression conveniently define R_{vir} and t_{dyn} in terms of conserved quantities. The dynamical time is the characteristic orbital or free-fall time of a cluster. It is also the timescale on which an initially non-equilibrium cluster will establish virial equilibrium. Since t_{dyn} is generally short compared to all other dynamical timescales of interest, we assume virial equilibrium in all that follows.

Finally, the cluster-wide velocity dispersion $\langle v^2 \rangle$ is

$$\begin{aligned} \langle v^2 \rangle &= \frac{2K}{M} = \frac{GM}{2R_{vir}} \\ &= (14.7\ \mathrm{km/s})^2 \left(\frac{M}{10^6\ \mathrm{M}_\odot}\right) \left(\frac{R_{vir}}{10\ \mathrm{pc}}\right)^{-1}. \end{aligned} \tag{10.10}$$

Dynamicists commonly write the total kinetic energy K in terms of the "thermodynamic" quantity kT, defined by

$$K = \tfrac{3}{2}NkT \tag{10.11}$$

so

$$kT = \tfrac{1}{3}\langle m\rangle\langle v^2\rangle = -\frac{2E}{3N} \quad \text{in virial equilibrium,} \tag{10.12}$$

where $\langle m\rangle = M/N$ is the mean stellar mass.

Since gravity has no preferred scale, it is convenient to work in a system of dimensionless units such that all bulk cluster properties are of order unity. A system in widespread use, described in Heggie and Mathieu (1986), has $G = 1, M = 1$, and $E = -\frac{1}{4}$, so $R_{vir} = 1, t_{dyn} = 1$, and $\langle v^2\rangle = \frac{1}{2}$.

10.3 Relaxation

The long-term evolution of a star in hydrostatic equilibrium is driven by thermal and nuclear processes that transfer energy throughout the star and generate energy in the core. In a star cluster, thermal evolution is driven by two-body relaxation, while energy may be generated by a number of mechanisms, as discussed below.

To a first approximation (Fig. 10.1a), stars orbiting in a cluster move on relatively smooth orbits determined by the bulk mean-field gravitational potential of the system as a whole. However, stars occasionally experience close encounters with one another, changing their orbital parameters and transferring energy from one to the other (see Fig. 10.1b). This thermalising process allows energy to flow around the stellar system.

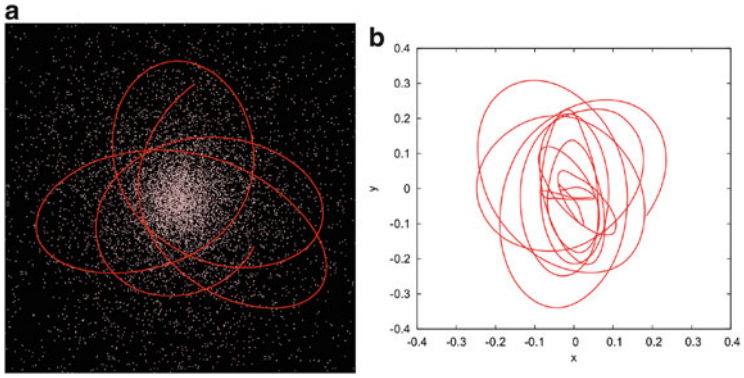

Fig. 10.1 (**a**) A typical smooth orbit in a 10,000-body system. The scale of this figure is ± 1 N-body units. (**b**) An orbit closer to the centre shows generally smooth behaviour, but also has a few sharp "kinks" associated with close encounters in the dense core

10.3.1 Two-Body Scattering

Our basic approximation here is the assumption that encounters between stars can be treated as isolated two-body scattering events. This is permissible because the scale of two-body encounters is generally much less than the scale of the system, so we can talk sensibly about stellar velocities at "infinity" in a scattering calculation without having to worry about the large-scale motion of stars around the cluster.

Imagine two stars of masses M_1 and M_2 approaching one another on unbound trajectories with relative velocity at infinity v_∞ and impact parameter b (Fig. 10.2). The solution for the relative orbit $\mathbf{r} = \mathbf{x}_1 - \mathbf{x}_2$ is

$$r(1 + e\cos\theta) = a(e^2 - 1),$$

where (with $m = M_1 + M_2$), $a = Gm/{v_\infty}^2$ is the semi-major axis, and $e = \sqrt{1 + (bv_\infty/Gm)^2}$ is the eccentricity. The deflection angle is $\psi = \pi - 2\theta_1$, where

$$\tan\theta_1 = \frac{b{v_\infty}^2}{Gm}. \tag{10.13}$$

Thus the impact parameter corresponding to a 90° scattering, $\psi = \pi/2$ or $\theta_1 = \pi/4$, is

$$b_{90} = \frac{Gm}{{v_\infty}^2}. \tag{10.14}$$

More generally, for encounters in a cluster, we have $m \sim 2\langle m\rangle$ and $\langle {v_\infty}^2\rangle \sim 2\langle v^2\rangle$, and we may write

$$b_{90} \sim \frac{G\langle m\rangle}{\langle v^2\rangle}. \tag{10.15}$$

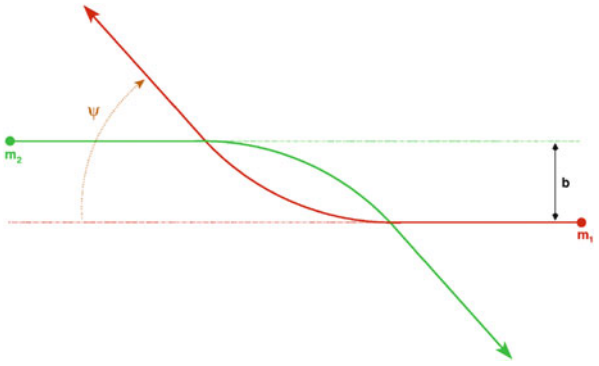

Fig. 10.2 Two stars, of masses M_1 and M_2, approach one another with impact parameter b (and relative velocity at infinity v_∞), and are deflected by an angle ψ

For $\langle m \rangle \sim 1 M_\odot$ and $\langle v^2 \rangle^{1/2} \sim 10$ km/s, Eq. (10.15) gives $b_{90} \sim 9$ AU. Combining Eqs. (10.10) and (10.15), we find $b_{90} \sim 2R_{vir}/N$.

10.3.2 Strong Encounters

The strong encounter timescale, t_s, is the time needed for a typical star to experience a 90° scattering. For a star of mass m_* moving with velocity v through a uniform field of identical stars with number density n, the cross section for a strong encounter is

$$\sigma = \pi b_{90}^2 = \frac{\pi G^2 m_*^2}{v^2}. \tag{10.16}$$

The timescale for a strong encounter is

$$t_s = (n\sigma v)^{-1} = \frac{v^3}{\pi G^2 m_*^2 n}. \tag{10.17}$$

Replacing m_* by the mean stellar mass $\langle m \rangle$, v^2 by the stellar velocity dispersion $\langle v^2 \rangle$, and writing $\langle m \rangle n = \rho$, we obtain

$$t_s = \frac{\langle v^2 \rangle^{3/2}}{\pi G^2 \langle m \rangle \rho}. \tag{10.18}$$

This is the relevant timescale for discussions of interactions involving close binaries (see Sect. 10.3.6.1 below).

10.3.3 Distant Encounters

The cross section for wide encounters, with smaller deflections $\psi \ll 1$, is much larger than that for a 90° scattering, but to estimate the cumulative effect of many small-angle deflections we must adopt a different approach. Consider again our star moving through a field of similar stars. For a single encounter with impact parameter b, the resulting velocity change transverse to the incoming velocity v may be shown to be (see, e.g., Binney and Tremaine 2008)

$$\delta v_\perp = 2v \left(\frac{b}{b_{90}} \right) \left(1 + \frac{b^2}{b_{90}^2} \right)^{-1}. \tag{10.19}$$

Integrating over repeated random encounters, we expect the mean velocity change in any direction transverse to the incoming velocity to be zero, by symmetry. However, the transverse velocity undergoes a symmetric, two-dimensional random walk, and we expect transverse velocity changes to add in quadrature, leading to a non-zero value for the mean square transverse velocity $\Delta v_\perp^2$. During a time interval δt, the number of encounters with impact parameters in the range $[b, b+db)$ is $2\pi b\, db\, n v \delta t$, so integrating over all encounters, we find

$$\begin{aligned}\Delta v_\perp^2 &= 2\pi n v \delta t \int_0^{b_{max}} b\, db\, (\delta v_\perp)^2 \\ &\approx 8\pi \delta t\, \frac{G^2 m_*^2 n}{v} \ln\left(\frac{b_{max}}{b_{90}}\right), \end{aligned} \tag{10.20}$$

where we have assumed $b_{max} \sim R_{vir} \gg b_{90}$.

We can define a two-body relaxation timescale, δt_r, as the time interval in the above expression corresponding to $\Delta v_\perp^2 = v^2$. Rearranging the equation and replacing all quantities by mean values, as above, we find

$$\delta t_r = \frac{\langle v^2 \rangle^{3/2}}{8\pi G^2 \langle m \rangle \rho \ln \Lambda}, \tag{10.21}$$

where the "Coulomb logarithm" term (the term stemming from the almost identical development found in plasma physics) has $\Lambda = R_{vir}/b_{90} = \frac{1}{2}N$, from Eqs. (10.10) and (10.15).

There is considerable ambiguity in the above definition. For example, we could equally well have used $\Delta v_\parallel^2$ as our measure of relaxation, and our procedure neglects the distribution of relative velocities of stars in a real system. In fact, all approaches and refinements yield the same functional dependence on physical parameters as Eq. (10.21), but they differ in the numerical coefficient. The expression presented in Spitzer (1987), now widely adopted as a standard definition of the term, defines the relaxation time in terms of $\Delta v_\parallel^2$, and averages over a thermal velocity distribution—the theoretical end point (not always realised in practice) of the relaxation process. The result is

$$\begin{aligned} t_r &= \frac{0.065\, \langle v^2 \rangle^{3/2}}{G^2 \langle m \rangle \rho \ln \Lambda} \\ &= 3.4\ \mathrm{Gyr} \left(\frac{\langle v^2 \rangle^{1/2}}{10\ \mathrm{km/s}}\right)^3 \left(\frac{\langle m \rangle}{\mathrm{M}_\odot}\right)^{-1} \left(\frac{\rho}{100\ \mathrm{M}_\odot \mathrm{pc}^{-3}}\right)^{-1} \left(\frac{\ln \Lambda}{10}\right)^{-1}. \end{aligned} \tag{10.22}$$

The precise definition of Λ is also the subject of a minor debate. Spitzer (1987) chooses $b_{max} = R_h$ and hence writes $\Lambda = 0.4N$. Giersz and Heggie (1994) calibrate the relaxation process using N-body simulations (see Sect. 10.5.3) and

find $\Lambda \sim 0.1N$. For systems with a significant range of stellar masses, the effective value of Λ may be considerably smaller even than this value.

Although the analysis leading to Eq. (10.22) is global in nature, it is common to find this expression used as a *local* measure of the relaxation timescale in a system.

10.3.4 Comparison of Timescales

Comparing Eqs. (10.22) and (10.18), we see that

$$\frac{t_s}{t_r} \sim 5 \ln \Lambda \sim 60 \text{ for } N \sim 10^6,$$

so distant encounters dominate over close encounters in determining the flow of energy around the system.

Spitzer (1987) defines a global relaxation timescale, often referred to as the *half-mass relaxation time*, t_{rh}, by replacing all quantities in Eq. (10.22) with their system-wide averages,

$$\begin{aligned} \langle v^2 \rangle &\rightarrow \frac{GM}{2R_{vir}} \\ \rho &\rightarrow \frac{3M}{8\pi {R_h}^3} \\ \langle m \rangle &\rightarrow \frac{M}{N}, \end{aligned}$$

obtaining

$$\begin{aligned} t_{rh} &= \frac{0.138\, N {R_h}^{3/2}}{G^{1/2} M^{1/2} \ln \Lambda} \\ &= 6.5 \text{ Gyr} \left(\frac{N}{10^6}\right) \left(\frac{M}{10^6 \mathrm{M}_\odot}\right)^{-1/2} \left(\frac{R_h}{10 \text{ pc}}\right)^{3/2} \left(\frac{\ln \Lambda}{10}\right)^{-1}. \end{aligned} \tag{10.23}$$

Hence, from Eqs. (10.9) and (10.23), we have

$$\frac{t_{rh}}{t_{dyn}} \sim \frac{N}{5 \ln \Lambda}, \tag{10.24}$$

and we see that relaxation is a slow process relative to the dynamical time for all but the smallest systems.

We note in passing that the relaxation time [Eq. (10.22)] evaluated at the half-mass radius R_h can differ significantly from the half-mass relaxation time [Eq. (10.23)]—for example, for a $W_0 = 7$ King model, the former exceeds the latter

by a factor of almost five—representing a potentially significant source of confusion in this terminology.

10.3.5 Cluster Dynamical Evolution

We can understand most aspects of the dynamical evolution of globular clusters in terms of the fundamental physics of self-gravitating systems just described.

10.3.5.1 Evaporation and Cluster Lifetimes

The relaxation time [Eq. (10.22)] is the timescale on which stars tend to establish a Maxwellian velocity distribution. A fraction ξ_e of the stars in the tail of that distribution have velocities larger than v_{esc} and therefore escape. If this high-velocity tail is refilled every t_{rh}, then the dissolution time scale is $t_{dis} \sim t_{rh}/\xi_e$. For isolated clusters, $v_{esc} = 2\langle v^2\rangle^{1/2}$ and $\xi_e = 0.0074$, implying $t_{dis} = 137\, t_{rh}$. For tidally limited clusters, ξ_e is higher since v_{esc} is lower. For a "typical" cluster density profile (with $R_h/RJ = 0.145$), Spitzer (1987) finds $\xi_e \approx 0.045$, so $t_{dis} \approx 20\, t_{rh}$.

In fact, t_{dyn} also enters into the escape rate.

Baumgardt (2001) found, for equal-mass stars, $t_{dis} \propto {t_{rh}}^{3/4} {t_{dyn}}^{1/4}$. This non-intuitive scaling of the dissolution time results from the fact that a star with sufficient energy to escape may orbit the system many times before finding one of the Lagrangian points, through which it eventually escapes (Fukushige and Heggie 2000).

Baumgardt and Makino (2003) found that this non-linear scaling of the dissolution time with the relaxation time also holds for model clusters with a stellar mass spectrum, stellar evolution, and for different types of orbits in a logarithmic potential. Their result for t_{dis} may be summarised as

$$t_{dis} \approx 2\,\mathrm{Myr} \left(\frac{N}{\ln \Lambda}\right)^{3/4} \left(\frac{R_G}{\mathrm{kpc}}\right) \left(\frac{V_G}{220\,\mathrm{km/s}}\right)^{-1} (1-\varepsilon), \tag{10.25}$$

where ε is the ellipticity of the orbit. For non-circular orbits ($\varepsilon > 0$), the galactocentric distance R_G is taken as apogalacticon, while V_G is the circular velocity, which is constant in a logarithmic potential. Lamers et al. (2005) found that, when the Coulomb logarithm is taken into account, the scaling is approximately $t_{dis} \propto N^{0.65}$ for $M \sim 10^3$–$10^6\,\mathrm{M}_\odot$.

The combined effects of mass loss by stellar evolution and dynamical evolution in the tidal field of the host galaxy have been extensively studied by a number of authors, including Chernoff and Weinberg (1990), Fukushige and Heggie (1995), Takahashi and Portegies Zwart (2000), Baumgardt and Makino (2003) and Whitehead et al. (2013). Mass loss due to stellar evolution, particularly during a cluster's early evolution (the first few hundred million years), can significantly reduce the

cluster lifetime. Cluster expansion due to this mass loss can be substantial, and may even result in complete disruption if the cluster is mass segregated before the bulk of the stellar evolution takes place (Vesperini et al. 2009).

The expansion of a mass-segregated cluster will not be homologous, as the massive (segregated) core stellar population tends to lose relatively more mass than the lower-mass halo stars. The result is a more dramatic expansion of the cluster core, with less severe effects farther out. These above studies show that when clusters expand to a half-mass radius of $\sim 0.5\, R_J$ they lose equilibrium and most of their stars overflow R_J in a few crossing times.

10.3.5.2 Core Collapse

The evaporation of high-velocity stars and the internal effects of two-body relaxation transfer energy from the inner to the outer regions of the cluster, resulting in the phenomenon of core collapse Antonov (1962), Lynden-Bell and Wood (1968), Cohn (1980), Lynden-Bell and Eggleton (1980) and Makino (1996). During this phase, the central portions of the cluster accelerate toward infinite density while the outer regions expand. The process is most easily understood by recognising that, according to the virial theorem [Eq. (10.7)], a self-gravitating system has negative specific heat—reducing its energy causes it to heat up. Hence, as relaxation transports energy from the (dynamically) warmer central core to the cooler outer regions, the core contracts and heats up as it loses energy. The time scale for the process to go to completion (i.e. a core of zero size and formally infinite density) is $t_{cc} \sim 15 t_{rh}$ for an initial Plummer sphere of identical masses. Starting with a more concentrated King (1966) distribution shortens the time of core collapse considerably (Quinlan 1996), as does a broad spectrum of masses (Inagaki and Saslaw 1985).

In systems with a mass spectrum, the dynamical evolution is accelerated by the tendency of the system to evolve toward energy equipartition, in which the velocity dispersions of stars of different masses would have $\langle m v^2 \rangle \sim$ constant. The result is mass segregation, where more massive stars slow down and sink toward the centre of the cluster on a timescale (Spitzer 1989)

$$t_{seg} \sim \frac{\langle m \rangle}{m}\, t_{rh}\,. \tag{10.26}$$

Portegies Zwart and McMillan (2002) and Gürkan et al. (2004) find that, for a typical Kroupa (2001) initial mass function, the timescale for the most massive stars to reach the centre and form a well defined high-density core is $\sim 0.2 t_{rl}$, where t_{rl} is the relaxation time [Eq. (10.22)] of the region containing a significant number of massive stars—the core of a massive cluster, or the half-mass radius of a smaller one [in which case $t_{rl} = t_{rh}$, see Eq. (10.23)].

The post-collapse phase may involve a series of large-amplitude core oscillations, driven by the same basic instability as gravothermal collapse and involving the

innermost few percent of the mass. First discovered in gas-sphere (Bettwieser and Sugimoto 1984; Goodman 1987) and later in Fokker–Planck (Cohn et al. 1989) simulations (see Sect. 10.5), their existence in simple N-body systems was subsequently confirmed by Makino (1996). Like core collapse, these gravothermal oscillations appear to be a ubiquitous phenomenon. However, they are known to be suppressed by the presence of mass spectrum, as well as by primordial binaries and other heating mechanisms, and their reality in actual globular clusters remains unclear. However, significant core oscillations have been observed in realistic simulations of globular-cluster sized systems (Heggie 2012, private communication), and the effect of these substantial variations in central density may be important for the formation and subsequent evolution of exotica such as neutron star binaries and blue stragglers (Grindlay et al. 2006).

10.3.6 Internal Heating

On longer timescales, cluster evolution is driven by the competition between relaxation and a variety of internal heating mechanisms. High core densities lead to interactions among stars and binaries. Many of these interactions can act as energy sources to the cluster on larger scales, satisfying the relaxation-driven demands of the halo and temporarily stabilising the core against collapse (Goodman and Hut 1989; Gao et al. 1991; McMillan et al. 1990; McMillan et al. 1991; Heggie and Aarseth 1992; Fregeau et al. 2003). On long time scales, these processes lead to a relatively slow (relaxation time scale) overall expansion of the cluster, with $R_{vir} \propto t^{2/3}$, a result that follows from simple considerations of the energy flux through the half-mass radius (Hénon 1965).

10.3.6.1 Binary Interactions

Binaries in star clusters may be primordial (i.e. they were present when the cluster formed, or are descended from such systems), or they can form in a variety of ways, including dissipationless stellar-dynamical processes (Spitzer 1987; Tanikawa et al. 2012) and dissipative processes such as tidal capture (Fabian et al. 1975). Regardless of how they formed, binaries are described by dynamicists as either "hard" or "soft," depending on their binding energies. A hard binary has binding energy greater than the mean stellar kinetic energy in the cluster (Heggie 1975): $|E_b| > \frac{1}{2}\langle mv^2\rangle \approx \frac{1}{2}\langle m\rangle\langle v^2\rangle$, where $\langle m\rangle$ and $\langle v^2\rangle$ are the local mean stellar mass and velocity dispersion. A binary with mass $m_b = M_1 + M_2$ and semi-major axis a_b has energy $E_b = -GM_1M_2/2a_b$, so hard binaries have $a_b < a_{\rm hard}$, where

$$a_{\rm hard} = \frac{Gm_b^2}{4\langle m\rangle\langle v^2\rangle} \approx 9.5\times10^4\, R_\odot \left(\frac{m_b}{\mathrm{M}_\odot}\right)^2 \left(\frac{\langle v^2\rangle^{1/2}}{\mathrm{km/s}}\right)^{-2}. \tag{10.27}$$

Here we have assumed that $M_1 = M_2 = \langle m \rangle$ in deriving the right-hand expression. The hard–soft distinction is often helpful when discussing dynamical interactions between binaries and other cluster members. However, since this definition of hardness depends on local cluster properties, the nomenclature changes with environment—a binary that is hard in the halo could be soft in the core.

The dynamical significance of hard binaries [see Eq. (10.27)] has been understood since the 1970s (Heggie 1975; Hills 1975; Hut and Bahcall 1983). When a hard binary interacts with another cluster star, the resultant binary (which may or may not have the same components as the original binary) tends, on average, to be harder than the original binary, making binary interactions a net heat source to the cluster. Soft binaries tend to be destroyed by encounters. For equal-mass systems, the mean energy liberated in a hard-binary encounter is proportional to E_b: $\langle \Delta E_b \rangle = \gamma E_b$, where $\gamma = 0.4$ for "resonant" interactions (Heggie 1975), and $\gamma \sim 0.2$ when wider "flybys" are taken into account (Spitzer 1987).

The liberated energy goes into the recoil of the binary and single star after the interaction. Writing the binary energy as $E_b = -hkT$ (see Sect. 10.2.2), where $h \gg 1$, the total recoil energy, in the centre of mass frame of the interaction, is γhkT. A fraction $\frac{m_b}{m_b+m}$ of this energy goes to the single star (of mass m) and $\frac{m}{m_b+m}$ to the binary. For equal-mass stars, these fractions reduce to $\frac{2}{3}$ for the single star and $\frac{1}{3}$ for the binary. Neglecting the thermal motion of the centre of mass frame, we can identify three regimes:

1. If $\frac{2}{3}\gamma hkT < \frac{1}{2}m{v_{esc}}^2 = 2m\langle v^2 \rangle = 6kT$, i.e. $h < 45$, neither the binary nor the single star acquires enough energy to escape the cluster. Binaries in this stage are kicked out of the core, then sink back by dynamical friction.
2. If $\frac{2}{3}\gamma hkT > 6kT$ but $\frac{1}{3}\gamma hkT < 4m\langle v^2 \rangle = 12kT$, i.e. $45 < h < 180$, the single star escapes, but the binary is retained.
3. If $h > 36/\gamma = 180$, both the binary and the single star are ejected.

These numbers are valid only for equal-mass stars, and are intended for illustration only. For a binary with components more massive than average, as is often the case, the threshold for single star ejection drops, while that for self-ejection increases.

The binary encounter timescale is $t_{enc} = (n\sigma\langle v^2 \rangle^{1/2})^{-1}$, where n is the local stellar density and σ is the encounter cross section [see Eq. (10.30)]. If we arbitrarily compute the binary interaction cross section as that for a flyby within 3 binary semi-major axes, consistent with the encounters contributing to the Spitzer (Spitzer 1987) value $\gamma = 0.2$, and again assume equal masses ($m_b = 2m$), we find

$$t_{enc} \sim 8ht_r, \tag{10.28}$$

where we have used Eq. (10.22) and taken $\ln \Lambda = 10$. Thus the net local heating rate per binary during the 100 % efficient phase (#1 above), when the recoil energy remains in the cluster, is

$$\gamma hkT\, {t_{enc}}^{-1} \sim 0.1kT/t_r, \tag{10.29}$$

that is, on average, each binary heats the cluster at a roughly constant rate. During phase 2, the heating rate drops to just over one-third of this value. The limiting value of one-third is not reached since the ejected single stars still heat the cluster indirectly by reducing its binding energy by a few kT. For "self-ejecting" binaries, the heating rate drops almost to zero, with only indirect heating contributing.

Binary–binary interactions also heat the cluster, although the extra degrees of freedom complicate somewhat the above discussion. If the binaries differ widely in semi-major axes, the interaction can be handled in the three-body approximation, with the harder binary considered a point mass. If the semi-major axes are more comparable, as a rule of thumb the harder binary tends to disrupt the wider one (Bacon et al. 1996).

Numerical experiments over the past three decades have unambiguously shown how initial binaries segregate to the cluster core, interact, and support the core against further collapse (McMillan et al. 1990; Heggie and Aarseth 1992). The respite is only temporary, however. Sufficiently hard binaries are ejected from the cluster by the recoil from their last interaction, and binaries may be destroyed by interactions with harder binaries, or by collisions during the interaction. For large initial binary fractions, this binary-supported phase may exceed the age of the universe or the lifetime of the cluster against tidal dissolution. However, for low initial binary fractions, as appears to have been the case for the globular clusters observed today (Milone et al. 2008), the binaries can be depleted before the cluster dissolves, and core collapse resumes (Fregeau et al. 2003).

10.3.6.2 Stellar Collisions

In systems without significant binary fractions—either initially or following the depletion of core binaries—core collapse may continue to densities at which actual stellar collisions occur. In young clusters, the density increase may be enhanced by rapid segregation of the most massive stars in the system to the cluster core. Since the escape velocity from the stellar surface greatly exceeds the *rms* speed of cluster stars, collisions are expected to lead to mergers of the stars involved, with only small fractional mass loss (Benz and Hills 1987; Freitag and Benz 2001). If the merger products did not evolve, the effect of collisions would be to dissipate kinetic energy, and hence cool the system, accelerating core collapse (Portegies Zwart et al. 1999). However, when accelerated stellar evolution is taken into account, the (time averaged) enhanced mass loss can result in a net heating effect (Chatterjee et al. 2008).

The cross section for an encounter between two objects of masses M_1 and M_2 and radii r_1 and r_2, respectively, is (Hills and Day 1976)

$$\sigma = \pi r^2 \left[1 + \frac{2Gm}{rv^2} \right], \tag{10.30}$$

where v is the relative velocity at infinity, $m = M_1 + M_2$, and $r = r_1 + r_2$. For $r \ll Gm/v^2$, as is usually the case for the objects of interest here, the encounter is dominated by the second term (gravitational focusing), and Eq. (10.30) reduces to

$$\sigma \approx 2\pi r \frac{Gm}{v^2}. \tag{10.31}$$

Collisions between unbound single stars are unlikely unless one or both of the stars is very large and/or very massive, or the local density is very high. However, the presence of a substantial binary population can significantly increase the chance of a stellar collision. The closest approach between particles in a resonant interaction may be as little as a few percent of the binary semi-major axis (Hut and Inagaki 1985), so the hardest binaries may well experience physical stellar collisions rather than hardening to the point of ejection. It is quite likely that the third star will also be engulfed in the collision product (Fregeau et al. 2004). Alternatively, before its next interaction, the binary may enter the regime in which internal processes, such as tidal circularisation and/or Roche lobe overflow, become important. The future of such a binary may be determined by the internal evolution of its component stars, rather than by further encounters.

Since binaries generally have semi-major axes much greater than the radii of the component stars, these binary-mediated collisions play important roles in determining the stellar collision rate in most clusters (Portegies Zwart and McMillan 2002), leading to significant numbers of mergers in lower-density, binary rich environments. Massive binaries in dense clusters tend to be collision targets rather than heat sources (Gürkan et al. 2004).

10.4 Multiple Stellar Populations

The discovery of multiple populations of main-sequence stars and giants in an increasing number of globular clusters (Piotto et al. 2005; Piotto 2008) has led to the realisation that these clusters are not idealised entities with single well defined stellar populations. In many systems the observed stellar populations appear to be separated by less than $\sim 10^8$ years. The existence of multiple populations suggests that a second epoch of star formation must have taken place early in the cluster's lifetime. The differences in light-element abundances suggest that the second-generation (SG) stars formed out of gas containing matter processed through high-temperature CNO cycle reactions in first-generation (FG) stars (Carretta et al. 2009a,b).

The origin of the gas from which SG stars form is still an open question. Current leading models involve AGB stars (Cottrell and Da Costa 1981; Karakas and Lattanzio 2007), rapidly rotating massive stars (Prantzos and Charbonnel 2006; Decressin et al. 2007), and massive binaries (de Mink et al. 2009, see also Renzini 2008 for a review). In order to explain the observed abundance patterns, all current

models require that "pristine" (i.e. unprocessed) gas must be included in the SG mix (see D'Ercole et al. 2010 and references therein). In addition, in order to form the numbers of SG stars observed today, the FG cluster must have been considerably more massive than it is now, and the majority of stars in the cluster initially belonged to the FG population.

Many fundamental questions concerning globular cluster star formation and cluster chemical and dynamical history are raised by the discovery of multiple populations, and they have been targets of numerous theoretical investigations (D'Ercole et al. 2008, 2010; Bekki 2011; Vesperini et al. 2011). Recently, Bastian et al. (2013) have described a scenario that avoids both the mass problem and the need for multiple star-formation episodes by considering the accretion of CNO enriched material onto still-forming protostellar discs.

In many cases, the models suggest that the SG ("enriched") population should initially be significantly more centrally concentrated than the FG stars. Decressin et al. (2008) and Vesperini et al. (2013) have studied the subsequent evolution and mixing of the two-component cluster in the first scenario. Vesperini et al. (2013) find that the timescale for complete mixing depends on the SG initial concentration, but in all cases complete mixing is expected only for clusters in advanced evolutionary phases, having lost at least 60–70 % of their mass due to two-body relaxation. These scenarios may be relevant to the properties of blue stragglers because they suggest that the FG and SG binary populations should have significantly different dynamical histories, with the SG binaries having spent much of their lives in much denser environments. One might naively expect these differences to manifest themselves in the properties of FG and SG blue stragglers, although the limited data currently available give little hint of any such effect (see Chap. 5).

10.5 Modeling Star Clusters

Although the fundamental physics is not hard to understand, simulating star clusters can be a complex numerical undertaking. Significant complications arise due to the long-range nature of the gravitational force, which means that every star in the cluster is effectively in constant communication with every other, leading to high computational cost. Further complications arise from the enormous range in spatial and temporal scales inherent in a star cluster. Computers, by the way they are constructed, have difficulty in resolving such wide ranges, and many of the software problems in simulations of self-gravitating systems arise from this basic limitation. The combination of many physical processes occurring on many scales, with high raw processing requirements, makes numerical gravitational dynamics among the most demanding and challenging areas of computational science. Here we discuss some issues involved in the numerical modeling of massive star clusters.

A broad spectrum of numerical methodologies is available for simulating the dynamical evolution of globular clusters. In approximate order of increasing

algorithmic and physical complexity, but not necessarily in increasing numerical complexity, the various methods may be summarised as follows.

- *Static Models* are self-consistent potential–density pairs for specific choices of phase-space distribution functions (Plummer 1911; King 1966; Binney and Tremaine 2008). They have been instrumental in furthering our understanding of cluster structure, and provide a framework for semi-analytical treatments of cluster dynamics. However, they do not lend themselves to detailed study of star cluster evolution, and we will not discuss them further here.
- *"Continuum" Models* treat the cluster as a quasi-static continuous fluid whose phase-space distribution function evolves under the influence of two-body relaxation and other energy sources (such as binary heating) that operate on relaxation timescales [Eq. (10.23)].
- *Monte Carlo Models* treat some or all components of the cluster as pseudo-particles whose statistical properties represent the continuum properties of the system, and whose randomly chosen interactions model relaxation and other processes driving the long-term evolution.
- *Direct N-body Models* follow the individual orbits of all stars in the system, automatically including dynamical and relaxation processes, and modeling other physical processes on a star-by-star basis.

Much of our current understanding of the evolution of star clusters comes from detailed numerical simulations, and the above techniques are used for the vast majority of simulations. Here we present a few details of these simulation techniques. We end with brief discussions of new computer hardware and the state of the art in modern simulation codes.

10.5.1 Continuum Methods

The two leading classes of continuum models are gas-sphere (Lynden-Bell and Eggleton 1980; Bettwieser and Sugimoto 1984; Deiters and Spurzem 2001) and Fokker–Planck (Cohn 1979; Shapiro 1985; Chernoff and Weinberg 1990; Drukier et al. 1992; Takahashi 1996, 1997; Takahashi and Portegies Zwart 1998) methods. They have mainly been applied to spherically symmetric systems, although axisymmetric extensions to rotating systems have also been implemented (Einsel and Spurzem 1999; Kim et al. 2002, 2004), and a few limited experiments with simplified binary treatments have also been carried out (Gao et al. 1991).

Both approaches start from the collisional Boltzmann equation as the basic description for a stellar system, then simplify it by averaging the distribution function $f(\mathbf{x}, \mathbf{v})$ in different ways. Gas-sphere methods proceed in a manner analogous to the derivation of the equations of fluid motion, taking velocity averages to construct the moments of the distribution: $\rho = \int d^3v\, f(\mathbf{x}, \mathbf{v})$, $\mathbf{u} = \int d^3v\, \mathbf{v} f(\mathbf{x}, \mathbf{v})$, $\sigma^2 = \frac{1}{3} \int d^3v\, v^2 f(\mathbf{x}, \mathbf{v})$, etc. Application of an appropriate closure condition leads to a set of equations identical to those of a classical conducting fluid, in which the

conductivity depends inversely on the local relaxation time. Fokker–Planck methods transform the Boltzmann equation by orbit-averaging all quantities and recasting the equation as a diffusion equation in $E - J$ space, where E is stellar energy and J is angular momentum. Since both E and J are conserved orbital quantities in a static, spherically symmetric system, two-body relaxation enters into the problem via the diffusion coefficients.

These methods have been of enormous value in developing and refining theoretical insights into the fundamental physical processes driving the dynamical evolution of stellar systems (Bettwieser and Sugimoto 1984). However, as the degree of realism demanded of the simulation increases—adding a mass spectrum, stellar evolution, binaries, etc.—the algorithms rapidly become cumbersome, inefficient, and of questionable validity (Portegies Zwart and Takahashi 1999).

10.5.2 Monte Carlo Methods

Depending on one's point of view, Monte Carlo methods can be regarded as particle algorithms for solving the partial differential equations arising from the continuum models, or approximate schemes for determining the long-term average gravitational interactions of a large collection of particles. The early techniques developed in the 1970s and 1980s (Spitzer and Hart 1971; Hénon 1973; Spitzer 1975; Stodolkiewicz 1982; Stodolkiewicz 1986) fall into the former category, but more recent studies (Giersz 1998, 2001, 2006; Joshi et al. 2000; Freitag and Benz 2001; Fregeau et al. 2003; Fregeau and Rasio 2007; Heggie and Giersz 2008; Giersz and Heggie 2009, 2011; Giersz et al. 2013), tend to adopt the latter view. The hybrid Monte Carlo scheme of Giersz (1998, 2001) and Giersz and Spurzem (2003) combines a gas-sphere treatment of the "background" stellar population with a Monte Carlo realisation of the orbits and interactions of binaries and other objects of interest. These approaches allowed the first simulations of an entire globular cluster, from a very early (although gas depleted) phase to complete dissolution.

Monte Carlo methods are designed for efficient computation of relaxation effects in collisional stellar systems, a task which they accomplish by reducing stellar orbits to their orbital elements—energy and angular momentum—effectively orbit averaging the motion of each star. Relaxation is modeled by randomly selecting pairs of stars and applying interactions between them in such a way that, on average, the correct rate is obtained. This may be implemented in a number of ways, but interactions are generally realised on timescales comparable to the orbit-averaged relaxation time. As a result, Monte Carlo schemes can be orders of magnitude faster than direct N-body codes. To achieve these speeds, however, the geometry of the system must be simple enough that the orbital integrals can be computed from a star's instantaneous energy and angular momentum. In practice, this limits the approach to spherically symmetric systems in virial equilibrium, and global dynamical processes occurring on relaxation (or longer) timescales.

10.5.3 N-Body Methods

N-body codes incorporate detailed descriptions of stellar dynamics at all levels, using direct integration of the individual (Newtonian) stellar equations of motion for all stars (Aarseth 2003; Heggie and Hut 2003). Their major attraction is that they are assumption-free, in the sense that all stellar interactions are automatically included to all orders, without the need for any simplifying approximations or the inclusion of additional reaction rates to model particular physical processes of interest. Thus, problems inherent to Fokker–Planck and Monte Carlo methods related to departures from virial equilibrium, spherical symmetry, statistical fluctuations, the form of (and indeed the existence of) phase space distribution functions, and the possibility of interactions not explicitly coded in advance, simply do not arise, and therefore do not require fine-tuning as in the Monte Carlo models.

The price of these advantages is computational expense. Each of the N particles must interact with every other particle a few hundred times over the course of every orbit, each interaction requires $O(N)$ force calculations, and a typical (relaxation time) run spans $O(N)$ orbits [see Eq. (10.24)]. The resulting $O(N^3)$ scaling of the total CPU time means that, even with the best time-step algorithms, integrating even a fairly small system of a few hundred thousand stars requires sustained teraflops speeds for several months (Hut et al. 1988). Radically improved performance can be achieved by writing better software, or by building faster computers (or both). However, the remarkable speed-up of N-body codes over the last four decades has been due mainly to advances in hardware.

Substantial performance improvements were realised by adopting better (individual) time stepping schemes (as opposed to earlier shared time step schemes), in which particles advance using steps appropriate to their individual orbits, rather than a single step for all. Block time step schemes (McMillan 1986; Makino et al. 2006) offer still better performance. Further gains were made by utilising neighbour schemes (Ahmad and Cohen 1973), which divide the force on every particle into irregular (rapidly varying) and regular (slowly varying) parts, due (loosely speaking) to nearby and more distant bodies. By recomputing the regular force at every particle step, but extrapolating the more expensive $O(N)$ regular force for most time steps, and recomputing it only on longer timescales, significant improvements in efficiency are realised. These schemes form the algorithmic basis for Aarseth's `NBODY6` (Aarseth 2003) and its parallel counterpart `NBODY6++` (Spurzem 1999).

The 1980s saw a major algorithmic improvement with the development of tree codes (Barnes and Hut 1986), which reduce the force calculation complexity from $O(N)$ to $O(\log N)$. However, despite their algorithmic efficiency, tree codes have not been widely used in modeling collisional systems (but see McMillan and Aarseth 1993). This may be due to lingering technical concerns about their long-term accuracy in systems dominated by relaxation processes and their performance in clusters with large dynamic ranges in densities and timescales, even though these objections may not be well founded (Moore et al. 1999; Dehnen 2000).

In recent years, meta-algorithms have been developed that enable straightforward combination of previously distinct dynamical algorithms to address new, more complex simulations. The first application of this approach permitted detailed study of the interaction between a star cluster (modeled by a direct N-body) and the surrounding galactic stellar population (modeled by a tree code) (Fujii et al. 2007; Portegies Zwart et al. 2009). This "bridge" scheme has subsequently been generalised (Pelupessy and Portegies Zwart 2012; Pelupessy et al. 2013) to couple arbitrary dynamical integration schemes, and now allows stellar- and gas-dynamical codes to be combined in ways that were previously impossible to realise.

10.5.4 Hardware Acceleration

The "GRAPE" (short for "GRAvity PipE") series of machines developed by Sugimoto and co-workers at Tokyo University (Ebisuzaki et al. 1993). represented a quantum leap in gravitational N-body simulation speed. Abandoning algorithmic sophistication in favour of simplicity and raw computing power, GRAPE systems achieved high performance by mating a fourth-order Hermite integration scheme (Makino and Aarseth 1992) with special-purpose hardware in the form of highly parallel, pipelined accelerators implementing the computation of all inter-particle forces entirely in hardware. Operationally, the GRAPE hardware was simple to program, as it merely replaced the function that computes the force on a particle by a call to hardware interface libraries, leaving the remainder of the user's N-body code unchanged.

In recent years, as in many specialty fields, the market appears to have overtaken niche hardware solutions, and *Graphics Processing Units* (GPUs) have largely replaced GRAPEs in most N-body codes. GPU accelerated codes now surpass the older GRAPE benchmarks for raw performance and price/performance by a substantial margin. Fortunately, the GRAPE-accelerated code has not been discarded, as GPUs can serve as very efficient GRAPE emulators (see Portegies Zwart et al. 2007; Hamada and Iitaka 2007; Belleman et al. 2008; Gaburov et al. 2009) for various GPU implementations of the GRAPE interface). Besides GRAPE emulation, however, the much more flexible programming model for GPUs [as well as the GRAPE-DR (Makino 2005)], means that many other kinds of algorithms can (in principle) be accelerated, although, in practice, it currently seems that CPU-intensive operations such as direct N-body force summation show substantially better acceleration than, say, tree codes running on the same hardware.

Today, GPU-enabled code lies at the heart of almost all detailed N-body simulations of star clusters and dense stellar systems. The GPU accelerated `NBODY6-GPU` (Nitadori and Aarseth 2012) represents the current state of the art in raw N-body speed on workstations, and numerous parallel, GPU-accelerated N-body codes now exist or are under development, including `HiGPUs` (Capuzzo-Dolcetta et al. 2013), `phiGPU` (Berczik et al. 2011), `ph4` (McMillan et al. 2012), and `NBODY6++` (Spurzem 1999; Spurzem et al. 2008; Wang et al. 2014) GPU

accelerated versions of sixth and eighth order extensions of the standard fourth-order Hermite scheme (Nitadori and Makino 2008), with and without neighbour schemes, are also becoming widespread.

10.5.5 The Kitchen Sink

The leading simulation programs in this field are "kitchen sink" packages that combine treatments of dynamics, stellar and binary evolution, and stellar hydrodynamics within a single simulation. Of these, the most widely used are the N-body codes NBODY (Hurley et al. 2001; Aarseth 2003; Hurley et al. 2001; Aarseth 2003), KIRA which is part of the STARLAB package (e.g. Portegies Zwart et al. 2001), the MOCCA Monte Carlo code developed by Giersz and collaborators (Giersz 1998; Heggie and Giersz 2008; Giersz and Heggie 2009; Giersz et al. 2013), and the Northwestern MC Monte Carlo code (Fregeau et al. 2003; Freitag et al. 2006; Fregeau and Rasio 2007).

Despite the differences in their handling of the large-scale dynamics, these codes all employ similar approaches to stellar and binary evolution and collisions. All use approximate descriptions of stellar evolution, generally derived from look-up tables based on the detailed evolutionary models of Eggleton et al. (1989) and (Hurley et al. 2000). They also rely on semi-analytic or heuristic rule-based treatments of binary evolution (Portegies Zwart and Verbunt 1996; Hurley et al. 2002), conceptually similar from code to code, although significantly different in detail and implementation.

In most cases, stellar collisions are implemented in the "sticky-sphere" approximation, where stars are taken to collide (and merge) if they approach within the sum of their effective radii. The radii are calibrated using hydrodynamical simulations, and in some cases mass loss is included in an approximate way. Freitag's Monte Carlo code, geared mainly to studies of galactic nuclei, interpolates encounter outcomes from a pre-computed grid of smoothed Particle Hydrodynamics (SPH) simulations (Freitag and Benz 2005). Interesting alternatives, currently only operational in AMUSE (see below), are the "Make Me A Star" package (MMAS; Lombardi et al. 2003) and its extension "Make Me a Massive Star" (MMAMS; Gaburov et al. 2008). They construct a merged stellar model by sorting the fluid elements of the original stars by entropy or density, then recomputing their equilibrium configuration, using mass loss and shock heating data derived from SPH calculations.

Small-scale dynamics of multiple stellar encounters, such as binary and higher-order encounters, are often handled by look-up from pre-computed cross sections or—more commonly—by direct integration, either in isolation or as part of a larger N-body calculation. Codes employing direct integration may also include post-Newtonian terms in the interactions between compact objects (Kupi et al. 2006).

10.5.6 The AMUSE Software Framework

The comprehensiveness of kitchen-sink codes gives them the great advantage of applicability to complex stellar systems, but also the significant disadvantage of inflexibility. By selecting such a code, one chooses a particular hard-coded combination of dynamical integrator, stellar and binary evolution schemes, collision prescription, and treatment of multiple dynamics. The structure of these codes is such that implementing a different algorithm within the larger framework is difficult at best for an expert, and impossible in practice for others.

AMUSE (the *Astrophysical Multipurpose Software Environment*) is a collaborative effort begun in 2008 designed to address this class of problem, providing a modular and extensible means of combining individual "monophysics" solvers into a unified astrophysical multiphysics simulation. The overarching goal of the project is to disentangle these components by providing a framework in which individual modules can interoperate, to facilitate experimentation and direct comparison of competing or alternative implementations of specific physical processes.

The global structure of AMUSE is illustrated in Fig. 10.3. In the AMUSE programming model, each piece of physics (advance the stellar or gas dynamics to a specified time, manage a close encounter, evolve a star, collide two stars, etc.) is implemented as a module with a standard interface onto the rest of the system, but the model details are private to each module. For example, all stellar modules include accessor functions that provide information on the mass and radius of a specified star, but the details of what a "star" actually is (an analytic formula, an entry in a look-up table, or a set of 1- or 2-D arrays describing the run of density, temperature, composition, etc.) remain internal to the module and are normally invisible to the outside.

The high-level "glue" language for AMUSE is python, chosen for its rich feature set, ease of programming and rapid prototyping, object-oriented capabilities, large

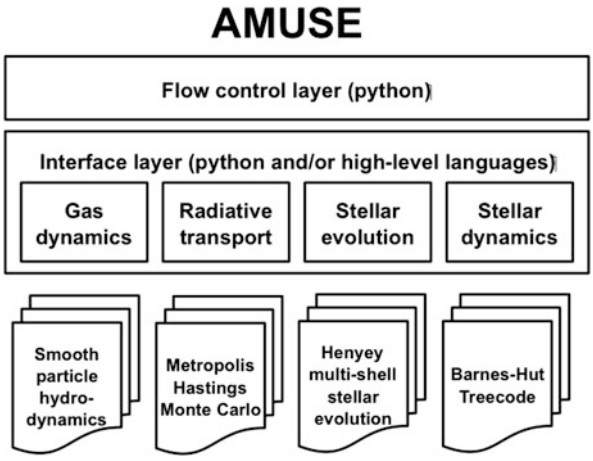

Fig. 10.3 The AMUSE environment. The top-level flow control layer is typically a custom GUI or user-written Python script that specifies the structure of the program, effectively replacing the top-level loop of a traditional program. Each of the four physics areas shown in the interface layer may be instantiated by one of several modules, allowing arbitrary combinations to be explored

user base in the astronomical community, and extensive user-written software. The design of AMUSE places no restrictions on the choice of language for any given module.

In a typical application, the top-level loop (the flow control layer in Fig. 10.3) of a simulation is written entirely in python, allowing monitoring, analysis, graphics, grid management, and other tools to be employed. The relatively low speed of the language does not significantly impact performance, because in practice virtually all of the computational load is carried by the (high-performance) physics modules.

Currently, AMUSE contains at least two (and typically more) independent modules for each physical process supported, allowing "plug and play" interchangeability between implementations. This modular approach enables, for the first time in this area of computational astrophysics, direct comparison and calibration of different implementations of the same physical processes, and facilitates experimentation in constructing new models. The integration of the parallel Message Passing Interface[1] (MPI) into AMUSE enables parallelism in all modules, allowing a serial user script to manage and transparently control modules that may themselves be parallel and/or GPU accelerated, possibly running on remote high-performance clusters.

Details on the structure and applications of AMUSE may be found on the project web site[2] and in Portegies Zwart et al. (2013) and Pelupessy et al. (2013).

References

Aarseth, S. J.: Gravitational N-Body Simulations, Cambridge University Press (2003)
Ahmad, A., Cohen, L.: J. Comp. Phys. **12**, 289 (1973)
Antonov, V. A.: Vestn. Leningr. Gros. Univ. **7**, 135 (1962)
Bacon, D., Sigurdsson, S., Davies, M. B.: MNRAS **281**, 830 (1996)
Barnes, J., Hut, P.: Nature **324**, 446 (1986)
Bastian, N., Lamers, J. G. L. M, Longmore, S. N., Goodwin, S. P., de Mink, S., Gieles, M.: MNRAS **436**, 2398 (2013)
Baumgardt, H.: MNRAS **325**, 1323 (2001)
Baumgardt, H., Makino, J.: MNRAS **340**, 227 (2003)
Bekki, K.: MNRAS **412**, 2241 (2011)
Belleman, R. G., Bédorf, J., Portegies Zwart, S. F.: New Astronomy **13**, 103 (2008)
Benz, W., Hills, J. G.: ApJ **323**, 614 (1987)
Berczik, P., Nitadori, K., Zhong, S., et al.: in Proc. 1st International Conference on High-Performance Computing, HPC-UA, p.8 (2011)
Bettwieser, E., Sugimoto, D.: MNRAS **208**, 493 (1984)
Binney, J., Tremaine, S.: Galactic Dynamics (2nd Edition), Princeton University Press (2008)
Capuzzo-Dolcetta, R., Spera, M., Punzo, D.: Journal of Computational Physics **236**, 580 (2013)
Carretta, E., Bragaglia, A., Gratton, et al.: A&A **505**, 117 (2009a)
Carretta, E., Bragaglia, A., Gratton, R., Lucatello, S.: A&A **505**, 139 (2009b)

[1] http://www.mcs.anl.gov/mpi.

[2] http://amusecode.org.

Chatterjee, S., Fregeau, J. M., Rasio, F. A.: in Dynamical Evolution of Dense Stellar Systems, IAU Symp. 246, 151 (2008)
Chernoff, D. F., Weinberg, M. D.: ApJ **351**, 121 (1990)
Cohn, H.: ApJ **234**, 1036 (1979)
Cohn, H.: ApJ **242**, 765 (1980)
Cohn, H., Hut, P., Wise, M.: ApJ **342**, 814 (1989)
Cottrell, P. L., Da Costa, G. S.: ApJ **245**, L79 (1981)
D'Ercole, A., Vesperini, E., D'Antona, F., McMillan, S. L. W., Recchi, S.: MNRAS **391**, 825 (2008)
D'Ercole, A., D'Antona, F., Ventura, P., Vesperini, E., McMillan, S. L. W.: MNRAS **407**, 854 (2010)
de Mink, S. E., Pols, O. R., Langer, N., Izzard, R. G.: A&A **507**, L1 (2009)
Decressin, T., Meynet, G., Charbonnel, C., Prantzos, N., Ekström, S.: A&A **464**, 1029 (2007)
Decressin, T., Baumgardt, H., Kroupa, P.: A&A **492**, 101 (2008)
Dehnen, W.: ApJL **536**, L39 (2000)
Deiters, S., Spurzem, R.: Astronomical and Astrophysical Transactions **20**, 47 (2001)
Drukier, G. A., Fahlman, G. G., Richer, H. B.: ApJ **386**, 106 (1992)
Ebisuzaki, T., Makino, J., Fukushige, T., Taiji, M., Sugimoto D.: PASJ **45**, 269 (1993)
Eggleton, P. P., Fitchett, M. J., Tout, C. A.: ApJ **347**, 998 (1989)
Einsel, C., Spurzem, R.: MNRAS **302**, 81 (1999)
Fabian, A. C., Pringle, J. E., Rees, M. J.: MNRAS **172**, 15P (1975)
Fregeau, J. M., Rasio, F. A.: ApJ **658**, 1047 (2007)
Fregeau, J. M., Gürkan, M. A., Joshi, K.J., Rasio, F. A.: ApJ **593**, 772 (2003)
Fregeau, J. M., Cheung, P., Portegies Zwart, S. F., Rasio, F. A.: MNRAS **352**, 1 (2004)
Freitag, M., Benz, W.: A&A **375**, 711 (2001)
Freitag, M., Benz, W.: MNRAS **358**, 1133 (2005)
Freitag, M., Rasio, F. A., Baumgardt, H.: MNRAS **368**, 121 (2006)
Fujii, M., Iwasawa, M., Funato, Y., Makino, J.: PASJ **59**, 1095 (2007)
Fukushige, T., Heggie, D. C.: MNRAS **276**, 206 (1995)
Fukushige, T., Heggie, D. C.: MNRAS **318**, 753 (2000)
Gaburov, E., Harfst, S., Portegies Zwart, S. F.: New Astronomy **14**, 630 (2009)
Gaburov, E., Lombardi, J. C., Portegies Zwart S.: MNRAS **383**, L5 (2008)
Gao, B., Goodman, J., Cohn, H., Murphy, B.: ApJ **370**, 567 (1991)
Giersz, M.: MNRAS **298**, 1239 (1998)
Giersz, M.: MNRAS **324**, 218 (2001)
Giersz, M.: MNRAS **371**, 484 (2006)
Giersz, M., Heggie, D. C.: MNRAS **268**, 257 (1994)
Giersz, M., Heggie, D. C.: MNRAS **395**, 1173 (2009)
Giersz, M., Heggie D. C.: MNRAS **410**, 2698 (2011)
Giersz, M., Heggie, D.C., Hurley, J. R., Hypki, A.: MNRAS **431**, 2184 (2013)
Giersz, M., Spurzem, R.: MNRAS **343**, 781 (2003)
Goodman, J.: ApJ **313**, 576 (1987)
Goodman, J., Hut, P.: Nature **339**, 40 (1989)
Grindlay, J. E., Portegies Zwart, S. F. McMillan, S. L. W.: Nature Physics **2**, 116 (2006)
Gürkan, M. A., Freitag, M., Rasio, F. A.: ApJ **604**, 632 (2004)
Hamada, T., Iitaka, T.: astro-ph/0703100 (2007)
Heggie, D. C.: MNRAS **173**, 729 (1975)
Heggie, D. C., Aarseth, S. J.: MNRAS **257**, 513 (1992)
Heggie, D. C., Giersz, M.: MNRAS **389**, 1858 (2008)
Heggie, D. C., Hut, P.: The Gravitational Million-Body Problem: A Multidisciplinary Approach to Star Cluster Dynamics, Cambridge University Press (2003)
Heggie, D. C., Mathieu R. D.: in The Use of Supercomputers in Stellar Dynamics, LNP Vol. 267, Springer-Verlag, p. 13 (1986)
Hénon, M.: Annales d'Astrophysique **28**, 62 (1965)

Hénon, M.: in Saas-Fee Advanced Course 3: Dynamical Structure and Evolution of Stellar Systems, Observatoire de Genéve, p. 183 (1973)
Hills, J. G.: AJ **80**, 809 (1975)
Hills, J. G, Day, C. A.: ApJL **17**, 87 (1976)
Hurley, J. R., Pols, O. R., Tout, C. A.: MNRAS **315**, 543 (2000)
Hurley, J. R., Tout, C. A., Aarseth, S. J., Pols, O. R.: MNRAS **323**, 630 (2001)
Hurley, J. R., Tout, C. A., Pols, O. R.: MNRAS **329**, 897 (2002)
Hut, P., Bahcall, J. N.: ApJ **268**, 319 (1983)
Hut, P., Inagaki, S.: ApJ **298**, 502 (1985)
Hut, P., Makino, J., McMillan, S. L. W.: Nature **336**, 31 (1988)
Inagaki, S., Saslaw, W. C.: ApJ **292**, 339 (1985)
Joshi, K. J., Rasio, F. A., Portegies Zwart, S.: ApJ **540**, 969 (2000)
Karakas, A., Lattanzio, J. C.: PASA **24**,103 (2007)
Kim. E., Einsel, C., Lee, H-M., Spurzem, R., Lee, M. G.: MNRAS **334**, 310 (2002)
Kim. E., Lee, H-M., Spurzem, R.: MNRAS **351**, 220 (2004)
King, I. R.: AJ **71**, 64 (1966)
Kroupa, P.: MNRAS **322**, 231 (2001)
Kupi, G., Amaro-Seoane, P., Spurzem, R.: MNRAS **371**, L45 (2006)
Lamers, H. J. G. L. M., Gieles, M., Portegies Zwart, S. F.: A&A **429**, 173 (2005)
Lombardi, J. C., Thrall, A. P., Deneva, J. S., Fleming, S. W., Grabowski PE.: MNRAS **345**, 762 (2003)
Lynden-Bell, D., Eggleton, P. P.: MNRAS **191**, 483 (1980)
Lynden-Bell, D., Wood, R.: MNRAS **138**, 495 (1968)
Makino, J.: ApJ **471**, 796 (1996)
Makino, J.: astro-ph/0509278 (2005)
Makino, J., Aarseth, S. J.: PASJ **44**, 141 (1992)
Makino, J., Hut, P., Kaplan, M., Saygın, H.: New Astronomy **12**, 124 (2006)
McMillan, S. L. W.: in The Use of Supercomputers in Stellar Dynamics, LNP Vol. 267, Springer-Verlag, p. 156 (1986)
McMillan, S. L. W., Aarseth, S. J.: ApJ **414**, 200 (1993)
McMillan, S. L. W., Hut, P., Makino, J.: ApJ **362**, 522 (1990)
McMillan, S. L. W., Hut, P., Makino, J.: ApJ **372**, 111 (1991)
McMillan, S., Portegies Zwart, S., van Elteren, A., Whitehead, A.: in Advances in Computational Astrophysics: methods, tools and outcomes, ASPC 435, p.129 (2012)
Milone, A. P., Piotto, G., Bedin, L. R., Sarajedini, A.: MmSAI **79**, 623 (2008)
Moore, B., Quinn, T., Governato, F., Stadel, J., Lake, G.: MNRAS **310**, 1147 (1999)
Nitadori, K., Makino, J.: New Astronomy **13**, 498 (2008)
Nitadori, K., Aarseth, S. J.: MNRAS **424**, 545 (2012)
Pelupessy, F. I., Portegies Zwart, S.: MNRAS **420**, 1503 (2012)
Pelupessy, F. I., van Elteren, A., de Vries, N., McMillan, S.L.W., Drost, N., Portegies Zwart, S.F.: A&A **557**, A84 (2013)
Piotto, G., Villanova, S., Bedin, L. R., Gratton, R., Cassisi, S., et al.: ApJ **621**, 777 (2005)
Piotto, G.: MmSAI **79**, 334 (2008)
Plummer, H. C.: MNRAS **71**, 460 (1911)
Portegies Zwart, S. F., McMillan, S. L. W.: ApJ **576**, 899 (2002)
Portegies Zwart, S. F., Takahashi, K.: Celestial Mechanics and Dynamical Astronomy **73**, 179 (1999)
Portegies Zwart, S. F., Verbunt, F.: A&A **309**, 179 (1996)
Portegies Zwart, S. F., Makino, J., McMillan, S. L. W., Hut, P.: A&A **348**, 117 (1999)
Portegies Zwart, S. F., McMillan, S. L. W., Hut, P., Makino, J.: MNRAS **321**, 199 (2001)
Portegies Zwart, S. F., McMillan, S. L. W., Harfst, S., Groen, D., Fujii, M., et al.: New Astronomy **14**, 369 (2009)
Portegies Zwart, S. F., Belleman, R. G., Geldof, P. M.: New Astronomy **12**, 641 (2007)

Portegies Zwart, S., McMillan, S. L. W., van Elteren, E., Pelupessy, I., de Vries, N.: Computer Physics Communications **184**, 456 (2013)
Prantzos, N., Charbonnel, C.: A&A **458**, 135 (2006)
Quinlan, G. D.: New Astronomy **1**, 255 (1996)
Renzini, A.: MNRAS **391**, 354 (2008)
Shapiro, S. L.: in Dynamics of Star Clusters, IAU Symp. 113, p. 373 (1985)
Spitzer, L.: in Dynamics of the Solar Systems, IAU Symp. 69, p. 3 (1975)
Spitzer, L.: Dynamical evolution of globular clusters, Princeton University Press (1987)
Spitzer, L. J.: ApJL **158**, 139 (1989)
Spitzer, L. J Hart, M. H.: ApJ **164**, 399 (1971)
Spurzem, R.: Journal of Computational and Applied Mathematics **109**, 407 (1999)
Spurzem, R., Berentzen, I., Berczik, P., Merritt, D., Amaro-Seoane, P., Harfst, S., Gualandris, A.: in The Cambridge N-Body Lectures, LNP Vol. 760, Springer-Verlag, p. 377 (2008)
Stodolkiewicz, J. S.: Acta Astron. **32**, 63 (1982)
Stodolkiewicz, J. S.: Acta Astron. **36**, 19 (1986)
Takahashi, K.: PASJ **48**, 691 (1996)
Takahashi, K.: PASJ **49**, 547 (1997)
Takahashi, K., Portegies Zwart, S. F.: ApJL **503**, 49 (1998)
Takahashi, K., Portegies Zwart, S. F.: ApJ **535**, 759 (2000)
Tanikawa, A., Hut, P., Makino, J.: New Astronomy **17**, 272 (2012)
Vesperini, E., McMillan, S. L. W., D'Antona, F., D'Ercole, A.: MNRAS **416**, 355 (2011)
Vesperini, E., McMillan, S. L. W., D'Antona, F., D'Ercole, A.: MNRAS **429**, 1913 (2013)
Vesperini, E., McMillan, S. L. W., Portegies Zwart, S.: ApJ **698**, 615 (2009)
Wang, L., Nitadori, K., Spurzem, R., Berczik, P., Aarseth S.J.: in prep. (2014)
Whitehead, A., McMillan, S. L. W., Vesperini, E., Portegies Zwart, S.: ApJ **778**, 118 (2013)

Chapter 11
The Multiple Origin of Blue Straggler Stars: Theory vs. Observations

Hagai B. Perets

11.1 Introduction

Blue straggler stars (BSSs) are stars that appear to be anomalously young compared to other stars of their population. In particular, BSSs lie along an extension of the main sequence (MS) in the colour-magnitude diagram, a region from which most of the stars of equal mass and age have already evolved. Such stars appear to be brighter and bluer than the turn-off point of the stellar population in which they were observed. Their location in the colour-magnitude diagram suggests that BSSs in old open clusters (OCs) and globular clusters (GCs) have typical masses of 1.2–1.5 $M_{\odot}$, that are significantly larger than those of normal stars in such systems. Thus, they are thought to have increased their mass during their evolution. Several mechanisms have been proposed for their formation: (a) stellar collisions due to dynamical interactions in dense stellar systems (Hills and Day 1976), (b) coalescence or mass transfer between two companions due to binary stellar evolution (McCrea 1964a), (c) induced mergers/collisions through coupled dynamical/stellar evolution in triple systems (Perets and Fabrycky 2009). The roles of each of these mechanisms in producing the observed BSS populations and their properties are still debated, as each of these scenarios were found to be successful in explaining some of the BSS observations, but fail in others.

In this review, we first discuss the observed properties of BSSs in the different environments (Sect. 11.2); we then describe the various models suggested for their formation (Sect. 11.3) and the long term evolution of BSSs in cluster environments (Sect. 11.4). Finally we compare the expectations from the different models with the known observable constraints and point out future theoretical and observational

H.B. Perets (✉)
Physics Department, Technion - Israel Institute of Technology, Haifa 32000, Israel
e-mail: hperets@physics.technion.ac.il

H.M.J. Boffin et al. (eds.), *Ecology of Blue Straggler Stars*, Astrophysics and Space Science Library 413, DOI 10.1007/978-3-662-44434-4_11

directions to advance the field (Sect. 11.5) and summarise (Sect. 11.6). Some of the subjects discussed in this review are explored in more details in other chapters of this book; and we refer the reader to these chapters when relevant. Though we discuss a wide variety of BSSs in different environments, our main discussion will focus on BSSs in old OCs and GCs which are best characterised; BSSs in other environments are discussed more briefly.

11.2 The Observed Properties of BSSs

Like any other stellar populations, BSSs are characterised through a wide variety of properties. These could be divided between intrinsic physical properties of the BSSs (mass, radii, composition, rotation, variability, temperature, luminosity); physical and orbital characteristics of multiple BSSs systems (binaries, triples); and the overall properties of the BSSs population (frequency, multiplicity, radial distribution). Another important division is between the directly observed BSS properties—e.g. colour-magnitude diagram (CMD) location—vs. inferred properties which require assumption dependent modeling (e.g. BSS mass). All of these properties may differ in different environments where BSSs are observed, and should therefore be discussed in the context of the relevant environment.

In the following we briefly discuss the observed properties of BSSs. Cases where the relevant properties are not yet well characterised/understood are specifically indicated in the table and text. An extended discussion about the observed properties of BSSs can be found in Chaps. 3 and 5.

11.2.1 Physical Properties

11.2.1.1 Masses

The masses of single BSSs are not known, and can only be inferred through interpretation of their location in colour-magnitude diagrams as well as spectroscopic data, in the context of stellar evolution models. Detailed atmospheric models could potentially provide good constraints on the mass, and such models provide mass estimates of up to twice or more the turn-off mass for the brightest BSSs (Shara et al. 1997). Stellar variability in SX Phe stars (all are BSSs in GCs) can also give various clues on the matter, and provide mass estimates up to twice and even three times the turn-off mass (Nemec et al. 1995).

However, given the complex origin and stellar evolution of BSSs, and the inherent theoretical uncertainties in these modeling such interpretation might not be very reliable. In principle, the location of BSSs in the CMD shows them to be hotter and more luminous than stars on the main sequence, leading to the current interpretation of BSSs as stars more massive than the turn-off mass of

their environment. More reliable methods make use of the dynamics of BSSs in multiple systems, where radial velocity measurements and/or eclipses can provide additional information. Even those methods can typically provide only partial data and/or constraints on the physical properties of a specific BSS. In cases where a BSS mass was determined dynamically (in double-lined spectroscopic binaries), it was found that it was underestimated by 15 % compared with the mass inferred from stellar evolution modeling of the CMD location (Geller and Mathieu 2012 and Chap. 3).

It is therefore premature to discuss a detailed mass function of BSSs. In the following we therefore refer only to the range of BSS mass inferred from the CMD, keeping in mind the potential large systematic deviations of these masses from the real BSS masses.

The CMD inferred mass function of BSSs in the OC NGC 188 (Geller and Mathieu 2012) lies in the range of 1.15–1.55 $M_\odot$ (see Chap. 3), i.e. $\Delta m = 0.15 - 0.55\ M_\odot$ more massive than the cluster turn-off mass ($\sim$1 $M_\odot$); a statistical estimate of the BSS masses based on orbital solution of binary BSSs in the cluster suggest a comparable but slightly lower mass range of 1.1–1.45 $M_\odot$ (Geller and Mathieu 2012). Among field BSSs, Carney et al. (2005) find BSSs masses in the range 0.83–1.28 $M_\odot$, i.e. $\Delta m = 0.03$–$0.48\ M_\odot$more than the turn-off mass (0.8 $M_\odot$). In other words BSSs can be significantly more massive than the turn-off mass, possibly requiring a large amount of mass accumulated onto them from an external source.

11.2.1.2 Rotation

The rotation velocities measured for BSSs extend over a wide range, showing both population of slow rotating and fast rotating stars (compared with the background population; see Lovisi et al. 2010, 2013 and Chaps. 5 and 3), with varying distributions in different clusters. Systematic study of BSS rotational velocities in different environments is still in its infancy, and more data are needed before a clear interpretation of the data can be done (e.g., rotational velocity dependence on cluster properties). Relating these data to theoretical predictions is also premature, given the contradicting theoretical results regarding BSS rotational velocities (e.g., Benz and Hills 1987; Leonard and Livio 1995; see also Chap. 12) . More theoretical as well as observational exploration is needed.

11.2.1.3 Composition

Though BSS composition could provide important constraints on their origin, e.g., showing pollution by accreted material from evolved stars, the available data is currently limited. We refer the reader to Chap. 5 as well as an overview by Lovisi et al. (2013). We will not discuss composition issues in this chapter.

11.2.2 Population Characteristics

11.2.2.1 Frequency

The overall frequency of BSSs in clusters is very small, but had typically been measured in detail only in GC cores and in open clusters. Typically, globular clusters contain a few, up to hundreds of BSSs, compared to the large numbers of stars in these clusters (few 10^5–10^6 stars), providing BSS fractions of the order of a few 10^{-5}–10^{-4}.

Simulations of BSS formation in clusters (e.g., Hypki and Giersz 2013) suggest that these fraction never become higher than these numbers even in the early evolution of a GC. A few tens of BSSs have been found in old open clusters such as M67 and NGC 188, providing a BSS fraction of a few 10^{-3}, i.e. much larger than that observed in GCs. Overall, it appears that BSS frequency is inversely proportional to the stellar density of the environment (for a more detailed discussion of these issues, see Chap. 9).

11.2.2.2 Multiplicity, Companion Type and Orbital Properties

Given the important role of binary or even triple companions in the suggested models for BSS formation, BSS multiplicity is one of their most important properties. Unfortunately, it is difficult to characterise. BSS multiplicity was studied in low mass field BSSs and in several open clusters, most notably M67 and NGC 188 (Latham 2007; Geller et al. 2008); much less is known about the multiplicity of BSSs in GCs.

Field BSSs Carney et al. (2005) used radial velocity measurements to study BSSs in the field and find their binary fraction to be high—consistent with all of the observed BSSs having companions. Their analysis shows BSSs binaries to typically have periods of 200–800 days, with low eccentricities compared with field binaries at the same period range, but distinctively not circular (see Fig. 11.1). Statistical analysis of the BSS companion masses show their mass to peak at $\sim$0.6 $M_\odot$, with none of the BSS binary companions directly observed (all binaries were single-lined spectroscopic binaries). This was interpreted as pointing to white dwarf (WD) companions and therefore to a case C mass transfer scenario for the BSS formation.

OC BSSs The on-going effort to characterise the properties of BSS populations in OCs, have provided us with very detailed knowledge[1] about their multiplicity and the orbital properties of BSS multiples (see Chap. 3 for a detailed discussion). The BSS populations in M67 and NGC 188 show many similarities. In both clusters radial-velocity studies show the BSS binary fraction is much higher than

[1] Currently, only for two OCs but ongoing study will provide similar data for additional OCs in the coming few years.

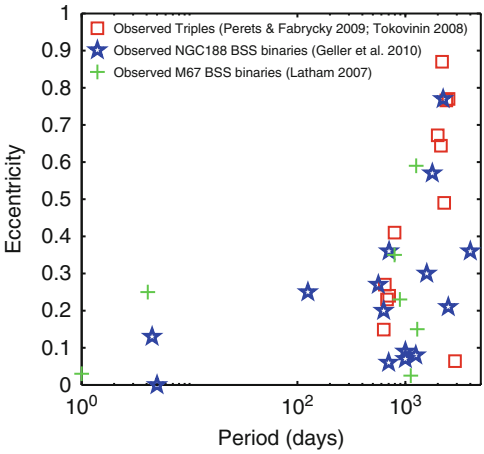

Fig. 11.1 The period-eccentricity distribution of BSS binaries in open clusters M67 and NGC 188, compared with the outer orbits or field triples with short period inner binaries

the background stellar population (60±24 and 76±22 % for M67 and NGC 188, respectively), with the locus of the period distribution extending between 700 days and 3,000 days. Though the upper limit is the observational limit, mostly due to the long time baseline required, the high binary fraction of BSSs even in this limited regime is much higher than that of field binaries (Raghavan et al. 2010), and points out to the important role of binaries. Few binary BSSs are found at shorter periods, with both cluster showing examples of peculiar double BSS binaries, and BSSs with more than twice the turn-off mass of the OC, indicating the need for many body (>3) interaction origin. The eccentricity distribution is distinctively not circular and extending higher than that observed for field BSSs, but lower than the background binary population in the clusters (Geller and Mathieu 2012; see Fig. 11.1). Statistical analysis of the companion mass shows it to peak at 0.55 $M_{\odot}$ somewhat similar to the case of field BSSs.

No systematic study of BSS binarity in GC have ever been done. However, variability surveys of several GCs suggest that the frequency of eclipsing binaries among BSSs is much higher than that of field binaries (Mateo et al. 1990; Rucinski 2000).

11.2.2.3 Radial Distribution

Some of the early studies of BSS radial distributions in clusters have already shown them to be centrally concentrated (in OCs, see Mathieu and Latham 1986; in GCs, see Auriere et al. 1990). Later studies have revealed the existence of a bi-modal radial distribution in some GCs and OCs (for the OC NGC 188, see Geller et al. 2008; in GCs, see Ferraro et al. 1997 and Chap. 5), with an inner centrally concentrated region followed by a dip in the distribution and a rise in the outer parts. The existence of a bi-modal distribution appears to depend on the cluster properties, and in particular the relaxation time, suggesting a major role of

mass segregation in determining the BSS radial distribution. It is not clear whether other stellar populations show bi-modal radial distribution, though observations of eclipsing binaries suggest that short period binaries in the GCs ω Cen and 47 Tuc may give rise to such bi-modal distributions (Weldrake et al. 2004; Weldrake et al. 2007; Perets and Fabrycky 2009).

11.2.2.4 Multiple Populations in GCs

Recently, it was shown that some GCs appear to host two distinct populations of BSSs as observed in the CMD. The origin of such multiple populations is yet to be studied in detail. We refer the reader to Chap. 5 for further discussion of this issue.

11.3 Models for Blue Straggler Star Formation

All current models for BSS formation are based on the assumption that these stars are rejuvenated through mass transfer. The difference between the models are the type of processes leading to such additional mass accumulation. All models require an external source of material and can be generally divided into three classes of mass transfer: merger, collision or accretion. Mergers occur when two MS stars, typically in a short period binary, come into contact and eventually merge together to form a more massive star containing most or all of the the mass of the mergers binary. Collisions of two MS stars are a more violent scheme where two MS stars form a merged star through a fast dynamical encounter; these could occur through the collision of two unrelated stars in a dense cluster, or possibly in unstable triple stars where two stellar companions collide. The more violent nature of these events could produce different outcomes than the more gentle merger processes, and can potentially produce BSS with different physical properties. Finally, stellar companions could shed mass through winds or Roche lobe overflow and the ensuing accretion can then rejuvenate the stars to become BSSs.

There is a wide variety of stellar systems and different types of evolutionary processes that could lead to these mass exchange scenarios; in the following we discuss these models in more detail.

11.3.1 Collisions in Dense Clusters

Early on, stellar collisions in dense clusters have been suggested as a channel for BSSs formation. This channel could play a major role in BSS formation in GCs (e.g. Chatterjee et al. 2013; Hypki and Giersz 2013, and references therein) and may contribute to the BSS population in the cores of OCs (Hurley et al. 2005); although it is not likely to serve as the dominant formation channel in OCs (Leonard 1996;

Hurley et al. 2005; Perets and Fabrycky 2009; Geller et al. 2013). Obviously, this channel is irrelevant for field BSSs, where physical collisions are extremely rare. This formation channel is discussed in more details in Chap. 9; here we provide a brief discussion and focus on the issue of binary BSSs in this context.

Collisional merger of stars is very efficient and conserves most of the mass of both merged stars for low velocity encounters as expected in OCs and GCs (Benz and Hills 1987; large mass loss could occur at impact velocities at infinity comparable to the escape velocity from the stars), allowing them to form BSSs of up to twice the turn-off mass of the cluster (or even more, if more than two stars collide).

The rate of stellar collisions is strongly dependent on the number density of stars in the cluster. Collisions can occur through the direct physical collisions between single stars in the cluster, but encounters between higher multiplicity systems are more likely to mediate most physical collisions in dense environments (Leonard 1989; Fregeau et al. 2004; Perets 2011; Leigh and Sills 2011; Chatterjee et al. 2013).

It was therefore expected that a strong correlation between the collisional parameter in GCs (see Chap. 9) and the specific frequency of BSSs should exist. A correlation with the binary fraction, given their role as collision mediators should also be apparent. However, though observations do show a correlation with the GC binary fraction, the strongest correlation is found to be with the GC mass, while no correlation is found with the calculated collisional parameter (see Leigh et al. 2013 and references therein). Most interestingly, Chatterjee et al. (2013) have recently made detailed simulations of the evolution of GCs in their BSSs populations, and found that binary mediated stellar collisions are the dominant channel for BSSs formation in dense clusters. Moreover, they find a clear, though weak correlation with the cluster collisional parameter. They suggest that the calculated collisional parameter based on observational analysis of GC properties is inaccurate, due to accumulated errors in the various observational parameters; in fact, they find no correlation between the intrinsic accurate collisional parameter calculated for their simulated GCs and an "observed" collisional parameter obtained by making use of a an observational-like analysis of the cluster properties. These results may explain the conundrum in correlation between the "observed" GC collisional properties and the BSS population which was debated over the last few years and can provide for various important pointers for new observations.

Binary–single and binary–binary encounters are very likely to leave behind a binary BSS; Chatterjee et al. (2013) find that $\sim$60 % of the BSSs in their simulations are in binaries. Studies of binary–binary and binary–single encounters (Leonard and Fahlman 1991; Leonard and Linnell 1992; Davies 1995; Fregeau et al. 2004) show that binary–binary encounters leave behind BSS with long period binary companions (most typical are at periods of 10^3–10^4 days) with an almost thermal eccentricity distribution (average eccentricity of $2/3$ and somewhat lower for the shorter period binaries). Detailed hybrid Monte-Carlo models coupled with few-body simulations of GCs also account for the later evolution of the binaries, and show the binary distribution peak at a few tenth to a few astronomical units;

only a small fraction (<10 %) have small semi-major axis comparable with typical eclipsing binaries found in GCs.

Finally, we note that none of the studies of GC evolution have accounted for primordial triples and their evolution. In addition, though dynamically formed triples have been shown to form quite frequently in GCs, and potentially play a non-negligible role in BSS formation (Ivanova 2008), their long term evolution in GCs have not been studied. Given the potentially important role of triples in mediating BSS formation (Ivanova 2008; Perets and Fabrycky 2009; Leigh and Sills 2011), this is an important direction for future theoretical studies of BSSs and other exotica in GCs.

11.3.2 Binary Evolution

Binary stellar evolution (BSSE) was one of the first models suggested for the origin of BSSs (McCrea 1964b). This general term refers to several possible scenarios and outcomes. In the BSSE model, the evolution of a stellar binary leads to mass transfer from a star to its binary companion, thereby increasing its mass, potentially a long time after its formation. A stellar binary could merge in which case the final product will include most of or all the mass of both companions; alternatively the companion might shed mass through Roche-lobe overflow (RLOF; see Chap. 8), winds or wind-RLOF (see Chap. 7) thereby transferring part, or most of its envelope to the now rejuvenated primary, leaving behind a white dwarf. Various aspects/sub-channels for the BSSE model for the formation for BSSs are discussed in various other chapters in this volume (Chaps. 7, 8, 9, and 12); here we provide a general overview for these the various sub-channels, their differences and their implications in a more general context. When applicable we will refer the reader to the relevant detailed discussions in other chapters.

Mass transfer during BSSE is traditionally divided into three categories; depending on the state of evolution of the mass donor interior (Kippenhahn and Weigert 1994): MT during the MS (case A), beyond the MS but before helium ignition (case B), or beyond helium ignition (case C). Eggleton (2006) refines case A MT into many more sub-categories (not detailed here; we refer the reader to Eggleton 2006), and redefines case B and C MT: Case B is the situation where the mass donor is in the Hertzsprung gap, with a mainly radiative atmosphere, and case C is the situation where the mass donor is on the giant branch, and therefore have a mainly convective envelope. We will not discuss these scenarios in depth, but rather remark on their main implications for BSS and its companion, and focus only on BSS formation during MT.

MT scenario are generally thought to lead to orbital circularisation. However, binary systems thought to be produced through MT many time show distinctively larger eccentricities (see Fig. 11.2), suggesting that our understanding of this process is incomplete. Some studies suggests scenarios where higher eccentricities are kept (see Dermine et al. 2013 and references therein).

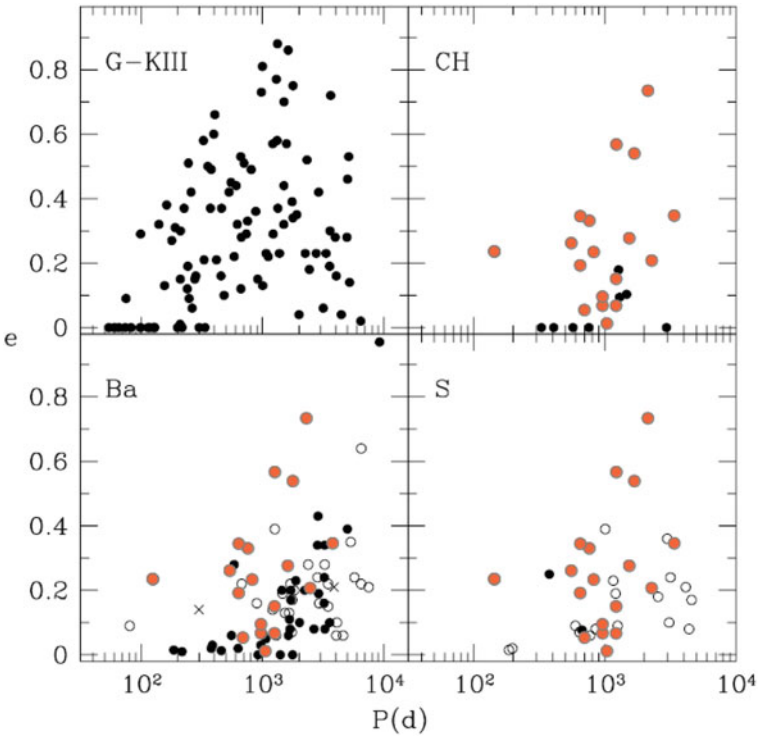

Fig. 11.2 The period-eccentricity distribution of several populations of evolved binaries, compared with the BSS binaries in M67 and NGC 188 (adapted from Jorissen et al. 1998). *Upper left panel*: Binaries involving G and K giants in open clusters (Mermilliod and Mayor 1996); *upper right panel*: CH stars (McClure and Woodsworth 1990); *lower right panel*: S stars (Jorissen et al. 1998). BSS binaries in the open clusters M67 and NGC 188 are shown as *large* (*orange*) *filled circles*. Note that although BSSs were likely to accrete more mass that the various type of polluted stars, their eccentricities are much higher than those of the polluted star binaries, even at short period of a few hundred days (the most comparable are the Ba stars); however, these are stars far more massive than the BSS binaries, whereas the CH stars with more comparable masses show significantly lower eccentricities. In other words, it appears than mass transfer does induce circularisation of binaries (though less efficiently that the typical theories suggest), as evident from the lower eccentricities observed for the polluted stars. The origin of the higher eccentricities at low periods for the BSS binaries (which accrete more mass than polluted stars) is therefore inconsistent with the overall period-eccentricity distribution of OC BSSs, suggesting that at most only small fraction of them can be explained by case C mass transfer. Mass transfer may still explain the origin of the lowest eccentricity BSS binaries observed; whereas the rest of the BSS binaries might be explained by the triple origin; see Fig. 11.1 for comparison of period-eccentricity distribution in triples

Case A MT In order for a MT to occur during the MS, the initial binary separation must be small enough for the RLOF to ensue (at most a few solar radii), given the compact radius of the companion MS star. Various processes could lead to such a close configuration, involving magnetic braking, tidal evolution or possibly also

affected by perturbations from a third companion in a triple (see Sec. 11.3.3 for the latter). In dense stellar clusters, interactions with other stars in the cluster may also results in shortening the binary period, exciting the binary eccentricity (thereby leading to a smaller peri-centre approach where effects from the first processes can become significant), or even exchange of companions to produce a new shorter period binary.

RLOF on the MS will increase the gainer mass, making it a BSS. Such evolution could lead to evolution into contact configuration (during the evolution they system could get in and out of contact, depending on the specific case), and possibly merge. A merged system will form a massive BSS, an unmerged system would form a BSS with a short period companion, which could be long lived (1–2 Gyr); contact configuration might be observed as W UMa type eclipsing binaries. Case A MT therefore lead to either single massive (on average, given the complete MT) BSS, or to a less massive (on average, given the only partial MT) BSS with a short period hydrogen burning companion (note however that the companion could be affected by the interaction, its appearance not necessarily resembling a MS star).

Case B MT In this case the evolution into RLOF occurs only following the companion evolution to Hertzsprung gap, in longer period binaries (few to tens solar radii). For significant accretion to occur leading to BSS formation, the system should not go through a common envelope stage which will eject the envelope rather than lead to mass growth. Therefore, scenarios leading to a BSS formation will leave behind a BSS with an intermediate period (few $\times$ 1–10 days) and a helium WD companion, following the mass donor stripping; see (Landsman et al. 1997) for a detailed example of such a scenario used to explain the origin of the 1040S system in the OC M67. In principle the BSS binary could also be observed during the accretion phase, but only for a relatively short time of a few hundred Myr. The BSS could be quite massive, though 0.1–0.4 $M_\odot$ of the final system mass will reside in the helium WD. Such BSSs are not likely to be observed as eclipsing binaries (due to the small radius of the WD companion, as well as the expected wide separation), unless observed during the accretion phase.

Case C MT In this case the donor star is already quite evolved, with a large radius. The initial binary period is therefore expected to be in the range of tens to a few hundreds or even 1–2 thousand days. In systems with up to a few hundred days period, a BSS could be formed through accretion, with up to $\Delta M \sim 0.2\,M_\odot$ above the turn-off mass. Stellar evolution calculations (e.g. Chen and Han 2008) suggest that binaries with larger periods can only produce BSSs very close to the turn-off mass, which are not considered as BSSs in current observational criteria. After its evolution the donor star will become a CO WD, with typical mass of 0.6 $M_\odot$.

Case D MT (Wind RLOF) Binaries with wide separations (typically >4 AU) will not evolve through RLOF, as the primary star do not fill its Roche-lobe. MT could still occur through the accretion of slow wind material ejected from an asymptotic giant branch (AGB) star. Simple calculations using Bondi-Hoyle accretion model suggest such accretion is inefficient at large separations (<15 %). However, recent

hydrodynamical simulations showed that at binary periods of ∼2,000–10,000 days, the wind can be focused by the accreting star and the accretion efficiency can be as high as 45 % (Abate et al. 2013). It is therefore potentially possible to form even massive BSS ($\Delta M > 0.4$) through this process. The leftover companions should be CO WDs, following the regular evolution of the donor star after the AGB.

11.3.3 Triple Evolution

Binary stellar evolution has been suggested early on as a channel for BSS formation through MT and mergers. In recent years, however, it was realised that triple stars can have an important, and sometime major role in affecting binary evolution. Interestingly, the evolution of triple system could mediate the production of BSSs through various different channels thereby allowing for the formation of BSSs through mergers, MT and even collisions. In the following we discuss these various channels, focusing mostly on secular evolution through Kozai–Lidov cycles, coupled with tidal friction (KCTF).

11.3.3.1 Secular Evolution Coupled with Tidal Friction

As discussed above, one of the channels for BSS formation is case A MT, through which stars in short period binary systems can transfer mass or even merge on the MS, thereby leading to the formation of massive BSSs. Such short period binaries cannot easily form following the evolution of pre-MS binary, since the pre-MS radius of stars can sometime be larger than the short period binary separation. It was therefore suggested that the formation of short period binaries is mediated by triple dynamical evolution (Kiseleva et al. 1998; Eggleton and Kiseleva-Eggleton 2001, Eggleton and Kisseleva-Eggleton 2006; Fabrycky and Tremaine 2007) coupled with tidal friction processes, as we shall discuss in the following. Following this, Perets and Fabrycky (2009) suggested that triple stars could serve as natural progenitors for BSSs, and in particular could explain the existence of eccentric and wide orbit BSS binaries observed in OCs, as triples in which the inner binary have merged, leave behind a BSS with a long period companion.

Stable triple systems require a hierarchical configuration in which two stars orbit each other in a tight "inner binary", and the third star and the inner binary orbit their common centre of mass as a wider "outer binary". Such triples are long lived, but secular evolution can sage their orbital inclination and eccentricity. A particularly important change was discovered by (Kozai 1962) and (Lidov 1962) in the context of solar system triples (Sun–asteroid–Jupiter or Sun–Earth–satellite). They found that if the inner binary initial inclination relative to the outer binary orbit is high enough, secular torques will cause its eccentricity and inclination to fluctuate out of phase with one another, leading to periodic high amplitude oscillations in the inclination and eccentricities of the triple inner binary; these are typically termed "Kozai oscillations". Lidov (1962) noted that the large oscillations in the amplitude

of the inner binary eccentricity might even lead to collision between the inner binary members. Collisions were prominent also in the first application of these dynamical concepts to triple stars. Harrington (Harrington 1968) noted that large initial inclination ($i_c \lesssim i \lesssim 180^\circ - i_c$, for a "Kozai critical angle" of $i_c \approx 40^\circ$), leads to large eccentricities, which could cause a tidal interaction, mass loss, or even collision of the members of the inner binary. Thus, Harrington (1968) reasoned that a triple star system with an inner binary mutually perpendicular to the outer binary should not exist for many secular timescales. However, as noted by Mazeh and Shaham (1979), the inner binary stars, while coming close to one another, will not merge immediately; instead, the tidal dissipation between them shortens the semi-major axis of the inner binary during these eccentricity cycles. They suggested that such inner binaries could therefore attain a very close configuration, in which mass transfer and accretion could occur, possibly forming cataclysmic variables or binary X-ray sources. Kiseleva et al. (1998) were the first to show that coupling of tidal friction to the high amplitude Kozai–Lidov secular evolution could be a highly efficient mechanism for the formation of short period binaries, as was later studied by Eggleton and Kisseleva-Eggleton (2006) and Fabrycky and Tremaine (2007); we refer to this mechanism as Kozai cycles and tidal friction (KCTF; note that the last stages of the merger are likely to be induced by magnetic braking).

Observations of short period binaries showed that more than 90 % of short period F/G/K binaries with periods of $P < 3$ days—consistent with 100 %, when considering completeness—have a third companion. The fraction gradually decreases to ∼30 % at $6 \leq P \leq 30$ days, consistent with the overall background level (∼30 % of all F/G/K binaries are triples (Raghavan et al. 2010)). These observations suggest that all short period binaries ($P < 3 - 6$ days) form in triple systems, giving credence to the KCTF formation scenario.

Perets and Fabrycky (2009) have taken the next logical step; if short period binaries are formed through KCTF evolution in triples, and short period binaries are typical progenitors of BSSs, then triples could be the natural progenitors of BSSs. In Fig. 11.3 we show an example for the KCTF scenario and the formation of short period binaries that wild later merge.

Most interesting, this basic scenario provides a wealth of unique observable predictions. These could be summarised by the following:

1. Merged short period binaries in triples will leave behind a BSS and a binary (originally the third) companion. Therefore the binary frequency of BSSs should be high, with typically wide periods, otherwise the original triple would not have been stable.
2. BSSs in short period binaries should still have a third companion on a wider orbit.
3. The BSS mass (and luminosity) can be high, and as much as twice the turn-off mass in the case a full merger of the inner binary; this is to be compared with BSSs in wide orbit binaries from case B/C MT, where a significant mass is left in the WD companion, and the MT efficiency is not expected to be high (typically at most 0.2 $M_\odot$ can be transferred to the mass accretor).

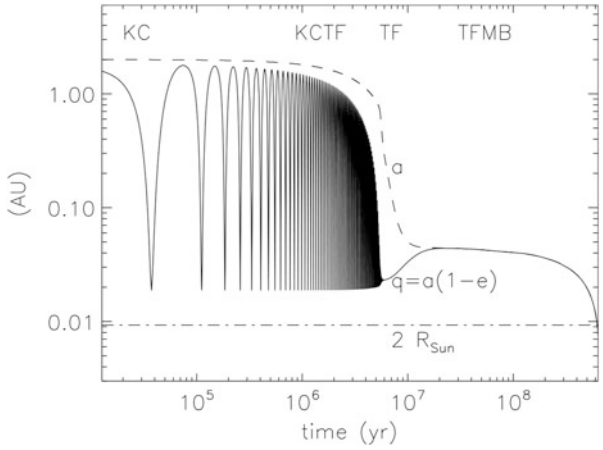

Fig. 11.3 Merger of the two stars of an inner binary, accomplished by a combination of Kozai cycles, tidal friction, and magnetic braking (reproduced from Perets and Fabrycky 2009 by permission of the AAS)

4. The period-eccentricity diagram of BSS binaries should show strong similarities to the period-eccentricity diagram of the **outer** binaries of triples with inner short period binaries. Such a comparison is shown in Fig. 11.1; it appears that such binaries should have long periods ($\gtrsim$500 days) and eccentricity distribution comparable to that of field binaries with similar periods.
5. The wide orbit companion of BSSs could be a MS star in contrast with case C or case B MT which might produce a wide orbit BSS binary, but the companion in that case must be a CO (typical mass of 0.5–0.6 $M_{\odot}$; case C) or a helium white dwarf (of 015–0.45 $M_{\odot}$; case B).

Recent studies have shown that inclined triple systems with smaller hierarchies (i.e. the outer to inner period ratio is small, of the order of a few times the critical ratio for the system stability), show quasi-periodic oscillations, similar to Kozai cycles, but more chaotic, and which can lead to large eccentricity change on dynamical timescales, and to higher eccentricities (Antonini and Perets 2012; Katz and Dong 2012, see also Hamers et al. 2013 for a related study). Such behaviour extends the Kozai-induced mergers to the small hierarchy regime, and could lead to direct collisions even without significant tidal evolution, i.e. triple dynamical evolution could lead to physical collisions and not only mergers/case A MT.

11.3.3.2 Collisions in Destabilised Triples

Recently, Perets and Kratter (2012) have suggested that stellar evolution and mass loss from the inner binaries of triples can lead to the triple destabilisation and the occurrence of collisions and close tidal encounters between the triple components.

Such triple evolution could therefore lead to the formation of BSS when two MS stars collide. However, it is not clear that such evolution could produce a significant population of BSSs, and more detailed triple stellar evolution studies are needed (see also Hamers et al. 2013 for a population synthesis calculations, but limited to wide binaries of $a > 12$ AU; much beyond observed binary BSS separations in OCs).

11.3.3.3 Accretion onto a Binary from a Third Companion

Another interesting evolutionary scenario is the case where a third companion in a triple evolves and sheds its mass on the inner binary. Such a scenario have not yet been studied in details. In principle, the transferred mass might form a common envelope around the inner binary, leading to its in-spiral and the formation of a short period binary that could later evolve to form a BSS through a case A MT. In addition, or alternatively, the mass can accrete onto the inner binary components potentially rejuvenating both of them and forming a double BSS binary with a WD third companion on a wide orbit. Whether these scenarios are physically plausible is yet to be confirmed in detailed studies (see also Chap. 4).

11.4 Long Term Dynamical Evolution of BSSs in Clusters

11.4.1 Mass Segregation in Clusters

BSSs are more luminous and bluer than the background population in which they are detected, suggesting their mass to be higher than the turn-off mass. In particular, this would make BSSs the most massive stars in stellar clusters, beside neutron stars and black holes. Dynamical friction (see Chaps. 10 and 9) leads to the segregation of the more massive stars into more centrally concentrated distribution compared with the background population of lower mass stars. Currently observed evolved stars (red giants and horizontal branch (HB) stars) have evolved off the MS only relatively recently, i.e. their mass during most of their evolution was close to the currently observed turn-off mass of the cluster, and they were among the long lived most massive stars in the cluster. Since these stars are also more massive than the typical stars in the cluster they should also be mass segregated, though slightly less than BSSs.

BSS radial distribution in clusters is typically compared with that of HB or red giant stars. However, given the relatively small difference in mass between this background population and the BSSs, it might be surprising that BSSs appear to be more segregated than these populations. In particular, Mapelli et al. (2004) and, more recently, Ferraro et al. (2012) have suggested that the bimodal radial distribution in clusters is due to the segregation of the BSSs compared with the

HB stellar population. They provided a simplified formula for the position in the cluster at which the timescale for BSS mass segregation is comparable to the cluster lifetime, and showed that it appears to be consistent with trough in the bimodal distribution of BSSs, showing this as evidence for this process. However, if one were to use the same approach on red giant stars, taking their mass to be slightly smaller than the turn-off mass of the cluster (as expected for most of their evolution), one finds that they should similarly show a trough not far from the location of the expected BSS trough. In other words a relative comparison of the two populations should not have shown a significant trough in the relative populations just due to mass segregation. The simple theoretical interpretation therefore appears to be discrepant with the observations. This might arise from the various assumptions made. For example, the assumed mass of the BSSs was taken to be 1.2 $M_{\odot}$, however, BSSs might have a much higher binary fraction than that of of the background population, consistent with several of the BSS formation channels. BSSs are therefore likely to have a binary companion, and the mass of the BSS system should therefore typically be the mass of a binary rather than the assumed mass of a single BSS. This might remedy the discrepancy described above, and not less important point out that the observed GC BSSs are likely to be binaries; an important clue about their origin. Other problem may arise from not accounting for the different lifetimes of the BSS population and that of the compared population (M. Giersz, priv. comm., 2012).

11.4.2 Dynamical Evolution of BSSs Binaries

BSSs can form through one of the evolutionary channels discussed above, leaving them either as single stars or in a multiple system, which could later change. In clusters their initial configuration could dynamically evolve through encounters with other stars in the clusters. Hurley et al. (2005) provide a detailed analysis of such later dynamical evolution observed in simulations of an open cluster, and present the diverse possibilities and outcomes of such evolution. The complicated dynamical evolution of binaries in cluster is beyond the scope of this review, but we will briefly discuss some of the main results relating to BSSs. Encounter between multiple systems typically lead to the more massive stars residing in the binary and the least massive stars being ejected. BSSs are the most massive stars in their host cluster and therefore have a higher probability to be exchanged into binaries, even if they originally formed as single BSSs. Detailed analysis of the evolution of open and globular clusters showed that the BSS binary fraction in these simulations were high, mostly due to their formation channels, but their later dynamical evolution kept them in binaries, and the majority of BSSs are found in binaries at the end of the simulations (Hurley et al. 2005; Chatterjee et al. 2013; Hypki and Giersz 2013).

Dynamical encounters between binary and single stars typically leave behind relatively eccentric binaries. Hurley et al. (2005) find the period-eccentricity diagram of BSS binaries in their simulation to be inconsistent with observations. In

particular, most of the wide binaries of 200–700 day period were typically formed though dynamical encounters, leaving behind highly eccentric binaries, whereas most observed BSS binaries reside in larger periods (>500 days) and much less eccentric orbits (see Perets and Fabrycky 2009; Geller and Mathieu 2012).

11.5 Blue Straggler Stars: Observations vs. Theory

The various theoretical expectations and observational results discussed above are summarised in Tables 11.1 and 11.2. In Table 11.1 we show a summary of the observed properties of BSSs in different environments, to be compared with the summarised theoretical predictions shown in Table 11.2. The latter include single processes, as well as results of large simulations of GCs (Chatterjee et al. 2013; Hypki and Giersz 2013) and OCs (Hurley et al. 2005; Geller et al. 2013) which include both dynamics and stellar evolution, but do not include triple stars.

In the following we briefly discuss the theoretical expectations vis-á-vis observations in the different environments.

11.5.1 Globular Clusters

Recently extensive Monte-Carlo simulations of GC evolution (Chatterjee et al. 2013; Hypki and Giersz 2013) provided for the first time detailed predictions regarding the population of BSSs in these environments. These simulations include simplified stellar evolution prescriptions and detailed account of binary dynamics and interactions. These simulations do not account for primordial or dynamically formed triples. The detailed simulations provide the overall evolution of the BSS population in GCs, but here we will focus on the final outcome at the typical age of observed GCs (∼12 Gyr). The simulations suggest that most of the currently observed BSSs today result from direct physical collisions during binary–single and binary–binary encounters. The total number of BSSs in the simulations is consistent with the observed numbers of BSSs in GCs. The BSSs are centrally concentrated, but can show a bi-modal radial distribution. The majority (∼60 %) are in binaries with a wide orbital distribution between a few days and a few thousand days, but mostly distributed at ∼100–1,000 days, with a small fraction (∼10 %) at short periods. We conclude that these results are generally consistent with the observed known properties of GC BSSs, and can explain the correlation between the binary fraction and the BSS fraction (mostly due to the dominance of collisions in binary encounters). Unfortunately, detailed knowledge of the BSS properties such as exist for a few open clusters precludes more detailed comparison (e.g., with BSS binary frequency and binary orbital properties). It is also not yet clear whether these models can explain the observed correlation of the normalised BSS fraction with the mass of the GCs (Leigh et al. 2013). In addition, the existence of a significant fraction of

Table 11.1 Summary of BSSs properties in different environments

Environment property	GC	OC	Halo	Bulge
Inferred ΔM ($M_\odot$)	0.2–0.8	0.2–0.8	0.03–0.48	
Frequency	10^{-5} to 10^{-4}	$\sim few \times 10^{-2}$	1/2,000	
Spatial distribution	Centrally concentrated and sometimes bi-model	Centrally concentrated and sometimes bi-model	–	–
Binarity	Unknown; large fraction in eclipsing binaries	High; 76 % in NGC 188 Consistent with 100 %	High; consistent with 100 %	At least 25 % are w UMa short period binaries
Companion mass	Unknown	Peaks at 0.55 $M_\odot$	$0.18 \leq M_{min} \leq 0.55$ $M_\odot$	Unknown
Period	Unknown	$P > 500$ days 10 % $P < 10$ days	167–1,576 days Typical 200–800 days	>25 % $P < 10$ days
Eccentricity	Unknown	High; $<e> \sim 0.34$	Low; $<e> \sim 0.17$	Unknown
Environmental correlates	$f_{BSS} \propto M_{cluster}$ $f_{BSS} \propto f_{bin}$	Too low statistics	–	–

Table 11.2 Summary of BSSs models and their predictions

Theoretical model Property	MT A/Merger	MT B	MT C	MT D	Collisions	Secular triples	GC models w/o triples	OC models w/o triples
ΔM_{max} ($M_\odot$)	Turn-off mass	Up to a few $M_\odot$ Below turn-off mass	<0.25 Typical < 0.15	0.5 Turn-off mass	Turn-off mass and even higher	Turn-off mass	Turn-off mass	Turn-off mass
Composition	Regular MS	Regular MS	Enriched AGB processed elements	Enriched AGB processed elements	Regular (?)	Regular MS	Combination of collision/merger and MT products	Mostly MT/merger products
Spatial distribution	–	–	–	–	Centrally concentrated	–	Centrally concentrated; can be bimodal	
Binarity	0 % (merger) High 100 % (MT)	High 100 %	High 100 %	High 100 %	High (collisions in binaries)	High 100 %	∼ 60 %	Intermediate
Companion	None (merger); MS (MT), likely w UMa type binary	Helium WD $0.1 \leq M \leq 0.45$	CO WD $0.55 \leq M \leq 0.65$	CO WD $0.55 \leq M \leq 0.65$	Any type	Any type	Any type	Mostly CO WDs

Period	$P < 3-4$ days	Typical $10 < P < 1{,}000$	Typical $300 < P < 2{,}000$	Typical $2{,}000 < P < 10^4$	Typical $10 < P < 1{,}000$	> 500 days; inferred from field triples	Typical $10 < P < 1{,}000$	Mostly large separations > 500 days
Eccentricity	Likely circular	Very low circularised	Low circularised	Somewhat low	High	typical outer binaries of triples $\langle e \rangle \sim 0.3-0.4$	High	Mostly circular (due to BSSE prescriptions?)

observed eclipsing BSSs, as discussed above, suggest a large fraction of the BSSs are in short period binaries with MS companions, inconsistent with the theoretical models. Such short period BSS binaries may arise in the triple evolution scenario where the induced formation of a short period inner binary leads to case A MT, and the BSSs to be observed as eclipsing binaries. However, at this point the data of eclipsing binaries is very sparse and detailed dedicated observational study of GC eclipsing binaries as well as theoretical study on the role of triples in GCs is required in order to resolve this issue.

11.5.2 Open Clusters

Detailed hybrid N-body/stellar evolution simulations by Hurley et al. (2005) and Geller and Mathieu (2012) were done for old OCs similar to M67 and NGC 188 for which detailed data observations exist. A detailed overview of the observations and simulation results can be found in Chap. 3. Overall they find that the number of BSSs in the simulation is less than a third of that observed and they cannot reproduce the bimodal radial distribution of BSSs observed in NGC 188; moreover the BSSs in the simulations are much more centrally concentrated than the observed ones. The BSS binary fraction in the simulations is only $\sim$15 %, but a fifth of the observed value. To quote these authors

> the deficiency in number of BSSs, the low frequency of detectable binaries among those that are formed, and the lack of a bimodal BSS radial distribution are striking failures of the model compared with the observations.

Nevertheless, Mathieu and Geller suggest that at least the orbital properties of the BSS binaries in the simulations are consistent with the observed BSS binary properties, reproducing the long periods of the BSSs, non-circular orbits and companion mass distribution. Since most of these binaries arise from case C MT scenario, they conclude that this is the likely main mechanism for the BSS production in OCs, irrespective of the other failures that might be remedied with better stellar evolution models. However, case C MT that lead to the long orbital periods with high eccentricity is highly inefficient in transferring mass, producing BSSs with typical $\Delta \mathrm{M} =\sim 0.1\ \mathrm{M}_{\odot}$, smaller than typically inferred from the CMD location of the BSSs. We therefore conclude that case C MT may explain a fraction of the observed BSSs, but it is difficult to see how it can explain the majority of the OC BSSs. That being said, our current understanding of MT in binaries is very limited, and future studies may show that more efficient MT can occur (e.g., some form of case D MT). Evolution of primordial triples may help produce the observed binary BSSs, not only naturally explaining the long orbital periods and high eccentricities (see Fig. 11.1), but also explaining the very high binary fraction, and the high mass of the BSS inferred from the CMD. Detailed cluster simulations which include significant fraction of triples and detailed accounting for KCTF are

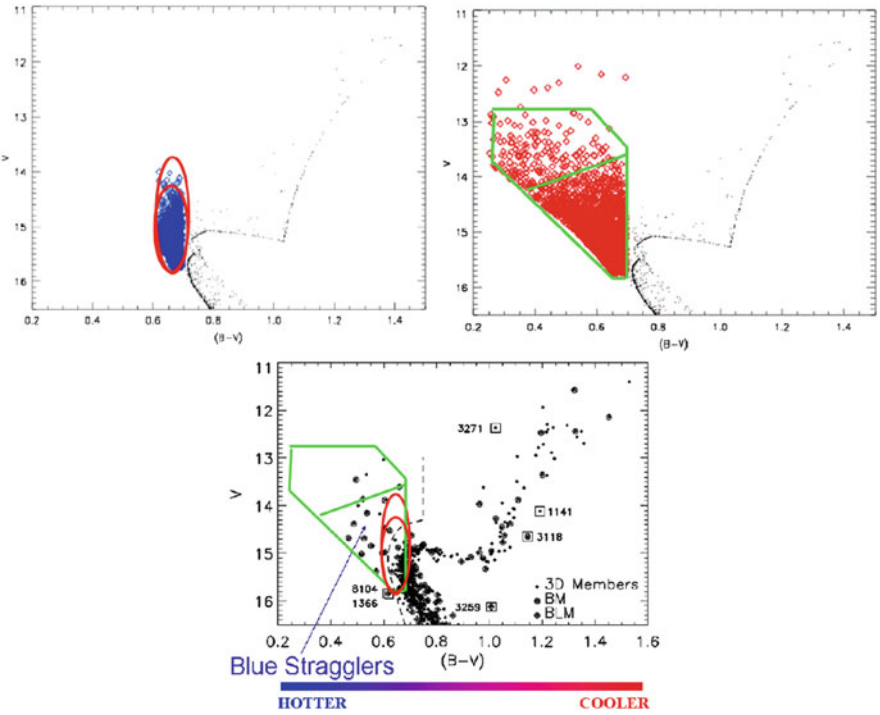

Fig. 11.4 Position of NGC 188 BSSs on the CMD. *Top left*: Population synthesis results of BSSs formed through case C mass transfer. *Top right*: Population synthesis results of BSSs formed through mergers. *Bottom*: The location of observed BSSs in the open cluster NGC 188 (Geller et al. 2008), compared with the expected location of case C mass transfer from population synthesis models (*red elipses*) and merger products from population synthesis models (*green polygons*). As can be seen, the observed BSSs are consistent with being merger products (and since most of them are in binaries, their progenitors must be triples in this case), but, for the most, are inconsistent with being case C mass transfer products. Population synthesis models were made using the BSSE code (taken from the senior thesis of M. Bailey—adviser: R. Mathieu)

needed in order to check whether a significant number of BSSs can indeed form in this way.

Figure 11.4 shows the outcome of population synthesis of evolving binaries resulting in mergers in case A MT, compared with case C MT. Case C MT can explain the wide orbits of the BSS binaries in NGC 188, but the resulting BSSs are too faint and cannot explain the observed BSS population. The CMD location of full mergers is consistent with the observed BSS population, but then a third companion must be invoked to explain the binarity of the observed BSS populations.

BSS formed through the case D MT could easily have wide orbit companions, and even their eccentricity needs not affected much. However, the expected periods for this scenario are higher than the typical periods observed for BSS binaries in OCs.

11.5.3 Field BSSs

11.5.3.1 Low Luminosity Halo BSSs

Comparing the various expectations and constraints from the currently suggested models for BSS formation, it appears that low luminosity field BSSs such as studied by Carney et al. (2005) could be fully explained by case B and C MT. Most of these BSSs are found in binary systems with periods in the range 167–1,576 day period, a typical ΔM in the range 0.03–0.48 $M_{\odot}$, with non-circular, but low eccentricity orbits. The binary companions are not seen, and are likely WDs; their minimal masses range between 0.18 and 0.55 $M_{\odot}$. Most of these properties are consistent with the predictions of the case C MT, beside the BSSs with the largest ΔM which appear to be too high compared with theoretical predictions. These, however, might serve as evidence for additional formation route, either a case B MT or triple evolution scenario. In the case B MT, larger ΔM are possible. In this case we expect BSSs with the largest ΔM to have the lowest mass companions, corresponding to helium WDs expected in the case B MT. We might also expect to generally find them at shorter periods. One peculiarity is the relatively high eccentricities of these most massive BSS binaries, which is less clear in the context of MT. This might be explained by the triple secular evolution model, in which the BSS binary eccentricities are not expected to be low, the formed BSS are massive merger products, and the most typical companions are low mass MS companions. The observed periods, however, are shorter than seen for the relevant triples in the field (see Fig. 11.1). Unfortunately, the statistics are currently too few to confirm/refute the eccentricity-mass trend.

It therefore appears that at least in the case of low luminosity field BSSs our theoretical understanding of their origin from case C MT with a contribution from case B and/or triple evolution case is fully consistent with observations. Taking this path, we can now try and learn about case B/C MT from these observations. Though the observed orbital eccentricities are not zero, they are much lower than the typical eccentricities of binaries with similar periods in the field (with the mentioned caveat for the massive BSSs), showing that binaries are circularised, though at lower rates than expected from current theories. We will discuss this issue in the context of OC BSSs.

11.5.3.2 Other Field BSSs

Other populations of BSSs exist outside stellar clusters. Their characterisation, however, is still in an early stage, and will only be briefly mentioned here.

Luminous Halo BSSs Current studies of halo BSSs focused on low luminosity BSSs, while luminous, likely more massive BSSs have hardly been studied. Massive main sequence stars do exist in the halo, as shown, for example, by the discoveries of hyper-velocity main sequence B-stars. Most of these stars are thought to be

regular main sequence stars ejected at high velocities from the Galactic Centre, while a small fraction might have been ejected from dense young clusters. Some, however, appear too young to have had the time to propagate from such locations in the Galactic Centre, or from young stellar clusters in the Galactic disc, and might have been rejuvenated through mass transfer, making them BSSs (Perets 2009). Additional observations of halo BSSs are needed in order to characterise their overall population.

Bulge BSSs Recently, the first bulge BSSs have been detected: about a quarter of them appears to be in short period W UMa type binaries (Clarkson et al. 2011). Their overall fraction compared to background HB population is consistent with that found for halo BSSs by Carney et al. (2001). The low densities in the bulge require the BSS formation to go through a binary/triple evolution interaction and not through collisions. From the large number of short period binaries, it appear that case A MT and mergers are likely the dominant channel. Given the likely origin of short period binaries in triples (Eggleton and Kisseleva-Eggleton 2006; Tokovinin et al. 2006; Fabrycky and Tremaine 2007), it is suggestive that the dominant route for BSS formation in the bulge is through triple evolution leading to mergers and case A MT (Perets and Fabrycky 2009).

11.6 Summary

Blue stragglers exist in a wide variety of environments, ranging from low density environments such as the Galactic halo and bulge through open clusters to dense globular clusters. The amount of observational data, varies widely from one environment to the other. The largest sets of data are available for GCs, however the most detailed data including specific properties of binary BSSs are of open clusters such as NGC 188 and M67, but the latter include only a small number of BSSs. The study of blue stragglers and their origin touches upon a wide range of fields, ranging from stellar evolution, stellar collisions, dynamics of few-body systems and the overall evolution of stellar clusters. Though the BSS phenomena exist in many environments, it is not yet clear whether the same processes play similar roles in their production. Current theories for the origin of BSSs include various type of mass transfer or merger products in binaries; possible direct collision origin; or induced merger/collision in secularly evolving triple systems.

The advance in complex simulation of clusters which include both dynamics and stellar evolution provide a wealth of theoretical predictions which could be compared for the first time with observations. Comparisons between the simulations and the observations suggest that the data on BSSs in GCc are consistent with the BSSs having a collisional origin mostly from binary–single and binary–binary encounters. However, given the major role of binary/triple systems in the theory of BSS formation but the lack of information on the binarity of BSSs, it is still premature to conclude that the BSS formation in GCs is well understood. Much

more detailed data are available for OCs, but current simulations show striking failure in reproducing the observed populations. The currently most likely origin of BSSs in OCs is likely a combinations of induced mergers and case A mass transfer in triples as well as case C/D mass transfer in evolved binaries. It does appear clear that collisions play at most a minor role in producing OC BSSs and binary BSSs in these environments.

Field BSSs cannot form through collisions due to the low stellar density environments. It appears that the current data on galactic halo BSSs are consistent with case B/C mass transfer, though triple secular evolution may also contribute. Less data is available for bulge BSSs, but the large fraction of eclipsing binaries among them suggest that secular triples play an important role (producing the short period binaries, that then produce BSSs through case A mass transfer and mergers). Case B/C mass transfer are also likely to play a role in those cases.

We conclude that BSSs are likely to have multiple origins both different origins in different environments, as well as combinations of various evolutionary/dynamical channels in the any given environments.

References

Abate, C., Pols, O. R., Izzard, R. G., Mohamed, S. S., de Mink S. E.: A&A **552**, A26 (2013)
Antonini, F., Perets, H. B.: ApJ **757**, 27 (2012)
Auriere, M., Lauzeral, C., Ortolani, S.: Nature **344**, 638 (1990)
Benz, W., Hills, J. G.: ApJ **323**, 614 (1987)
Carney, B. W., Latham, D. W., Laird, J. B.: AJ **129**, 466 (2005)
Carney, B. W., Latham, D. W., Laird, J. B., Grant, C. E., Morse, J. A.: AJ **122**, 3419 (2001)
Chatterjee, S., Rasio, F. A., Sills, A., Glebbeek, E.: ApJ **777**, 106 (2013)
Chen, X., Han, Z.: MNRAS **387**, 1416 (2008)
Clarkson, W. I., Sahu, K. C., Anderson, J., Rich, R. M., Smith, T. E., Brown, T. M., Bond, H. E., Livio, M., Minniti, D., Renzini, A., Zoccali, M.: ApJ **735**, 37 (2011)
Davies, M. B.: MNRAS **276**, 887 (1995)
Dermine, T., Izzard, R. G., Jorissen, A., Van Winckel, H.: A&A **551**, A50 (2013)
Eggleton, P.: Evolutionary Processes in Binary and Multiple Stars, Cambridge University Press (2006)
Eggleton, P. P., Kiseleva-Eggleton, L.: ApJ **562**, 1012 (2001)
Eggleton, P. P., Kisseleva-Eggleton, L.: Ap&SS **304**, 75 (2006)
Fabrycky, D., Tremaine, S.: ApJ **669**, 1298 (2007)
Ferraro, F. R., Lanzoni, B., Dalessandro, E., Beccari, G., Pasquato M., Miocchi, P., Rood, R. T., Sigurdsson, S., Sills, A., Vesperini E., Mapelli, M., Contreras, R., Sanna, N., Mucciarelli, A.: Nature **492**, 393 (2012)
Ferraro, F. R., Paltrinieri, B., Fusi Pecci, F., Cacciari, C., Dorman B., Rood, R. T., Buonanno, R., Corsi, C. E., Burgarella, D., Laget, M.: A&A **324**, 915 (1997)
Fregeau, J. M., Cheung, P., Portegies Zwart, S. F., Rasio, F. A.: MNRAS **352**, 1 (2004)
Geller, A. M., Hurley, J. R., Mathieu, R. D.: AJ **145**, 8 (2013)
Geller, A. M., Mathieu, R. D.: AJ **144**, 54 (2012)
Geller, A. M., Mathieu, R. D., Harris, H. C., McClure, R. D.: AJ **135**, 2264 (2008)
Hamers, A. S., Pols, O. R., Claeys, J. S. W., Nelemans, G.: MNRAS **430**, 2262 (2013)
Harrington, R. S.: AJ **73**, 190 (1968)
Hills, J. G., Day, C. A.: ApJL **17**, 87 (1976)

Hurley, J. R., Pols, O. R., Aarseth, S. J., Tout, C. A.: MNRAS **363**, 293 (2005)
Hypki, A., Giersz, M.: MNRAS **429**, 1221 (2013)
Ivanova, N.: in Multiple Stars Across the H-R Diagram Population of Dynamically Formed Triples in Dense Stellar Systems, Springer-Verlag, p. 101 (2008)
Jorissen, A., Van Eck, S., Mayor, M., Udry, S.: A&A **332**, 877 (1998)
Katz, B., Dong, S.: arXiv:1211.4584 (2012)
Kippenhahn, R., Weigert, A.: Stellar Structure and Evolution, Springer-Verlag (1994)
Kiseleva, L. G., Eggleton, P. P., Mikkola, S.: MNRAS **300**, 292 (1998)
Kozai, Y.: AJ **67**, 591 (1962)
Landsman, W., Aparicio, J., Bergeron, P., Di Stefano, R., Stecher T. P.: ApJL **481**, 93 (1997)
Latham, D. W.: Highlights of Astronomy **14**, 444 (2007)
Leigh, N., Knigge, C., Sills, A., Perets, H. B., Sarajedini, A., Glebbeek, E.: MNRAS **428**, 897 (2013)
Leigh, N., Sills, A.: MNRAS **410**, 2370 (2011)
Leonard, P. J. T.: AJ **98**, 217 (1989)
Leonard, P. J. T.: ApJ **470**, 521 (1996)
Leonard, P. J. T., Fahlman, G. G.: AJ **102**, 994 (1991)
Leonard, P. J. T., Linnell, A. P.: AJ **103**, 1928 (1992)
Leonard, P. J. T., Livio, M.: ApJL **447**, 121 (1995)
Lidov, M. L.: Planetary & Sp. Sci. **9**, 719 (1962)
Lovisi, L., Mucciarelli, A., Ferraro, F. R., Lucatello, S., Lanzoni B., Dalessandro, E., Beccari, G., Rood, R. T., Sills, A., Fusi Pecci, F., Gratton, R., Piotto, G.: ApJL **719**, 121 (2010)
Lovisi, L., Mucciarelli, A., Lanzoni, B., Ferraro, F. R., Dalessandro, E.: MmSAI **84**, 232 (2013)
Mapelli, M., Sigurdsson, S., Colpi, M., Ferraro, F. R., Possenti, A., Rood, R. T., Sills, A., Beccari, G.: ApJL **605**, 29 (2004)
Mateo, M., Harris, H. C., Nemec, J., Olszewski, E. W.: AJ **100**, 469 (1990)
Mathieu, R. D., Latham, D. W.: AJ **92**, 1364 (1986)
Mazeh, T., Shaham, J.: A&A **77**, 145 (1979)
McClure, R. D., Woodsworth, A. W.: ApJ **352**, 709 (1990)
McCrea, W. H.: MNRAS **128**, 147 (1964a)
McCrea, W. H.: MNRAS **128**, 335 (1964b)
Mermilliod, J.-C., Mayor, M.: in Cool Stars, Stellar Systems, and the Sun, ASPC 109, p. 373 (1996)
Nemec, J. M., Mateo, M., Burke, M., Olszewski, E. W.: AJ **110**, 1186 (1995)
Perets, H. B.: ApJ **698**, 1330 (2009)
Perets, H. B.: ApJL **727**, 3 (2011)
Perets, H. B., Fabrycky, D. C.: ApJ **697**, 1048 (2009)
Perets, H. B., Kratter, K. M.: ApJ **760**, 99 (2012)
Raghavan, D., McAlister, H. A., Henry, T. J., Latham, D. W., Marcy G. W., Mason, B. D., Gies, D. R., White, R. J., ten Brummelaar T. A.: ApJS **190**, 1 (2010)
Rucinski, S. M.: AJ **120**, 319 (2000)
Shara, M. M., Saffer, R. A., Livio, M.: ApJL **489**, 59 (1997)
Tokovinin, A., Thomas, S., Sterzik, M., Udry, S.: A&A **450**, 681 (2006)
Weldrake, D. T. F., Sackett, P. D., Bridges, T. J.: AJ **133**, 1447 (2007)
Weldrake, D. T. F., Sackett, P. D., Bridges, T. J., Freeman, K. C.: AJ **128**, 736 (2004)

Chapter 12
Models of Individual Blue Stragglers

Alison Sills

12.1 Introduction

As we have seen in previous chapters, blue stragglers are thought to form in both of two broad classes of formation mechanisms: through collisions or through binary mass transfer. Both processes transform two stars into a blue straggler on reasonably short timescales compared to the main sequence lifetimes of low mass stars: a head-on collision can take a few days, while stable mass transfer from main sequence stars can take much longer, up to the nuclear timescale of the stars. However, it is not enough to follow the hydrodynamic phases of either process. We must determine the structure of the proto-blue straggler at the moment when the remnant is in hydrostatic equilibrium, and then follow its evolution using a stellar evolution code for the next few billion years in order to make direct comparisons to the observed properties of blue stragglers. Those stellar evolution models are the subject of this chapter.

In the context of stellar models, it makes sense to try to define these two formation mechanisms a little more clearly. For our purposes, a collision is a short-lived and strong interaction between two stars. The situation where two previously unrelated stars move through a cluster and find themselves close enough that their radii overlap is obviously a collision, and those could be either head-on or off-axis. A similar situation during a resonant encounter involving binaries or triples can also be modelled using the same techniques as a collision. In this case the two stars might have originally been a binary, but the event that made the blue straggler was not a slow spiral-in of the two stars, but a more dramatic event caused by the

A. Sills (✉)
Department of Physics and Astronomy, McMaster University, 1280 Main Street West, Hamilton, ON, Canada L8S 4M1
e-mail: asills@mcmaster.ca

H.M.J. Boffin et al. (eds.), *Ecology of Blue Straggler Stars*, Astrophysics and Space Science Library 413, DOI 10.1007/978-3-662-44434-4_12

overall interaction of the systems. In the literature, these kinds of collisions are often called "binary-mediated". The key distinction that I would like to make is that the event which triggered the hydrodynamic phase of a collision is very short-lived, and determined by the environment in which the star finds itself. A binary mass transfer blue straggler, on the other hand, has typically gained its mass due to the orbital and nuclear evolution of the stars in a binary (or triple) system. The orbit of the system may have been modified by interactions in a cluster earlier in the binary's life, but the event which caused the system to begin transferring mass is intrinsic to the binary.

These distinctions between the two formation mechanisms drive the ways in which the blue stragglers can be modelled. A collision is a short, single event which takes two (or three) stars and transforms them into something else—but when that event is over, the star(s) return to thermal equilibrium and can be modelled using a normal stellar evolution code. The initial configuration of the gas may not be the same as a standard single star, but there will not be any more externally-imposed changes to the system. In binary mass transfer, however, the changes to the structure of the star could be happening at the same time as more mass is being added to the blue straggler. Mass transfer can happen on dynamic timescales, during which a large amount of mass is dumped onto the accretor. If the outcome of this dynamical mass transfer event is a fully detached and non-interacting binary, or the complete destruction of the donor, then the subsequent evolution of the blue straggler can be treated in a similar way that we treat the evolution of collision products. These outcomes of mass transfer are extremely unlikely, however. Typically, either a dynamical mass transfer event results in a common envelope or contact binary situation; or the mass transfer is stable and takes place on timescales that are comparable to the nuclear or thermal timescale of the star. In these cases, a standard single-star stellar evolution code is not sufficient to follow the evolution of the blue straggler and other methods are required.

In the following sections I will introduce the various methods that have been used to model both collision and binary mass transfer blue stragglers. I will outline the successes of each approach in describing particular observations, and will also discuss areas where the models are inconclusive or incomplete. In the final sections, I will describe observations of blue stragglers which could be compared to detailed stellar models, but for which the models are just starting to be available.

12.2 Collisional Models

The first hydrodynamical simulations of collisions between main sequence stars were done in the late 1980s (Benz and Hills 1987). These low resolution simulations (1,024 particles) were interpreted by the authors to show that the collision products were fully mixed. Based on these results, the first stellar evolution calculations of stellar collisions were done by Bailyn and Pinsonneault (1995). They took normal stars with masses appropriate for blue stragglers in globular clusters (0.8–1.8 $M_{\odot}$)

and evolved them with helium abundances up to $Y = 0.315$. In the same paper, the authors also approximated binary mass transfer blue stragglers as chemically inhomogeneous stars, as if they were starting their lives part-way along the normal main sequence track. Their conclusion that the outer blue stragglers in the cluster M3 are inconsistent with the collisional hypothesis, and are well-fit by the binary merger tracks needs to be re-evaluated in the light of a subsequent change in our understanding of the evolution of stellar collision products.

A decade after the Benz and Hills (1987) results, higher resolution Smoothed Particle Hydrodynamics (SPH) simulations of main sequence stellar collisions were performed (Lombardi et al. 1995, 1996) which showed that the earlier interpretation of full mixing was incorrect and that those authors had been misled by their low resolution. In fact, collision products retain a strong memory of their parent stars, with the cores of the more evolved stars ending up in the core of the collision product, and the less evolved star ends up on the outside of the collision product. Based on these simulations, Procter Sills et al. (1995) reworked the simulations of Bailyn and Pinsonneault (1995) by mapping a composition profile of an evolved low-mass star onto a higher mass star, and concluded that unmixed blue stragglers would have lifetimes that are very short, too short to explain the brightest and bluest blue stragglers in some globular clusters, particularly NGC 6397.

Sills and Lombardi (1997) realised that the structure of the collision product could be simply approximated by sorting the fluid of the two parent stars by their entropy. A stable star has entropy increasing outwards, and so we can simply compare the entropy of each shell in the two stars and place them in order from lowest to highest. Since material that has a higher mean molecular weight has a lower entropy, any material that is helium-rich will fall to the centre of the collision product. This "sort by entropy" prescription is the basis for the codes `Make Me A Star` (`MMAS`) (Lombardi et al. 2002) and `Make Me A Massive Star` (`MMAMS`) (Gaburov et al. 2008), which provide detailed stellar structure profiles of collision products for collisions between low mass and high mass stars respectively.

At the end of the hydrodynamic simulations, we are left with a ball of gas that is in hydrostatic equilibrium but not necessarily in thermal equilibrium. This configuration can be modelled by most stellar evolution codes, as long as the object is not too far out of thermal equilibrium. While "too far" is not easily quantified, the endpoints of stellar collision calculations can be used as the starting models for stellar evolution codes, with only slight modifications to treat the outer boundary conditions. Most SPH simulations (and also `MMAS`/`MMAMS`) do not have the resolution to accurately treat the very tenuous atmosphere of a star, so some extrapolation needs to be done to make a complete stellar model. However, the internal pressure, temperature, density, rotation rate, and composition of the collision product can be imported directly. This is an improvement over the early, more ad hoc models, and provides us with more certainty that we are following the evolution of a real collision product for many gigayears after the collision.

After the high resolution SPH simulations were published, a number of groups combined hydrodynamics with stellar evolution to model blue stragglers (Sandquist et al. 1997; Sills et al. 1997; Ouellette and Pritchet 1998). All groups were interested

in the properties of the collision product during the thermal-timescale contraction back to the main sequence. This phase is somewhat analogous to the pre-main sequence phase, except that the blue straggler is not chemically homogeneous and therefore does not follow the Hayashi track. The other major difference, found by all three groups, is that the collision product is stable against convection throughout this contraction phase. Therefore, there is no mixing of material into the core of the star even after the collision. As a result, collisions that involved a star at or near the turnoff in a cluster has a core which is depleted in hydrogen and therefore has a short main sequence lifetime. Collisions between stars further down the main sequence have less helium in their cores and therefore have longer lifetimes. In general, however, the evolutionary track of a blue straggler is very close to that of a normal star of the same mass. If the collision product has a helium-enriched core, it acts as if it is starting its life somewhere between the zero-age and the terminal-age main sequence. Evolutionary tracks of head-on collision products are shown in Fig. 12.1, with a comparison of tracks for normal stars of the same mass as well. These techniques were extended to stars of solar metallicity (Glebbeek et al. 2008; Glebbeek and Pols 2008), and those studies also investigated the effects of modifying the ages of the parent stars. The globular cluster studies assumed that the stars that collided were the same age as the cluster, but there is nothing special about the current time in any given cluster and collision products can have reasonably long lifetimes. Therefore, it is important to look at the difference between collision products that happened at various times in the past. Based on these detailed evolution calculations, Glebbeek and Pols (2008) presented simple formulae for the lifetimes, luminosities, temperatures, and radii of collision products compared to normal stars of the same mass.

Most of the models discussed above assumed that the collisions between stars were exactly head-on. This is extremely unlikely to actually occur, so models of off-axis collisions were also calculated by Lombardi et al. (1996) and evolved by Sills et al. (2001), and also investigated by Ouellette and Pritchet (1998). In general, the density, pressure, temperature and chemical composition profiles of a collision product do not depend much on the impact parameter of the collision (where an impact parameter of 0 is a head-on collision, and a grazing collision would have an impact parameter of 1.0 in units of the sum of the initial stellar radii $R_1 + R_2$). These quantities are dictated more by the structure of the parent stars. However, the angular momentum of the collision product increases significantly as the impact parameter increases. In all SPH simulations, the parent stars are initially not rotating. However, there is orbital angular momentum in any collision that is not directly head-on. Since the two stars become one object, the bulk of this angular momentum must end up in the collision product. Typically 1–6 % of the total mass of the system is unbound during the collision, so some angular momentum can be lost this way. However, the specific angular momentum at the surface of the parent stars is very low, and off-axis collisions lose less mass than the head-on collisions. Therefore, the collision products are rotating quite rapidly immediately after the collision. The total angular momentum of the collision products can be as much as ten times higher than normal pre-main sequence stars of comparable mass.

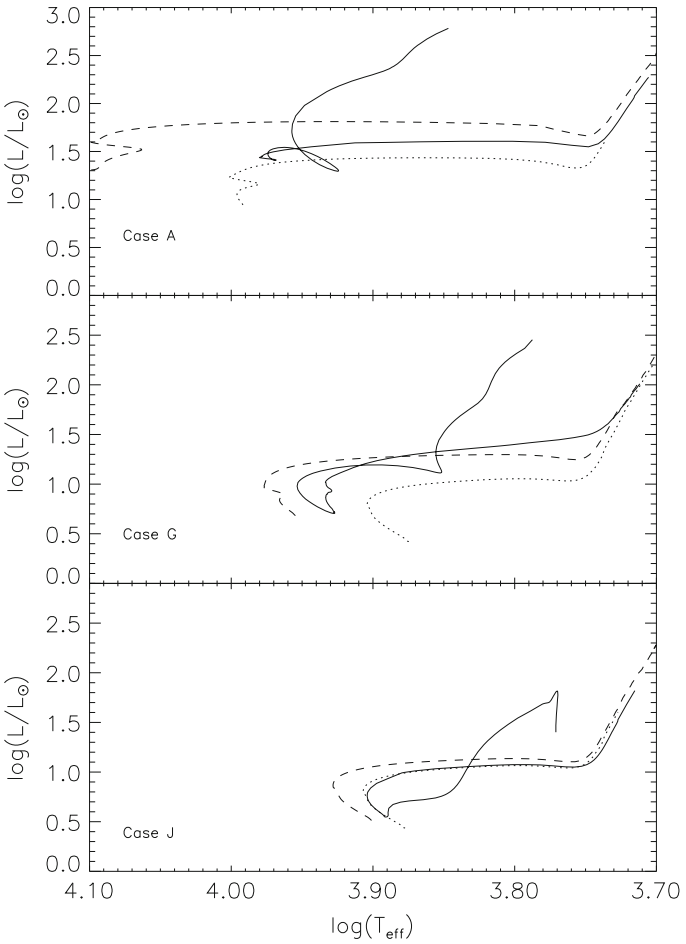

Fig. 12.1 Evolutionary tracks for a collision product (*solid line*), a star with the same mass and the composition of a normal globular cluster star (*dotted line*), and a version of the collision product which was fully mixed before evolution was started (*dashed line*). The normal and fully mixed evolutionary tracks are shown only from the zero age main sequence onwards. Case A is a collision between two turnoff-mass (0.8 $M_{\odot}$) stars; case G is a collision between a 0.8 $M_{\odot}$ star and a 0.4 $M_{\odot}$ star, and case J is a collision between two 0.6 $M_{\odot}$ stars (Figure 6 from Sills et al. 1997, reproduced by permission of the AAS)

Rapidly rotating stars are subject to a number of instabilities which can mix the stars on reasonably short timescales (Maeder et al. 2013). These instabilities also modify their angular velocity profiles, often moving the star toward solid body rotation. At the same time, the collision products are contracting towards the main sequence. If they do not have a way of losing their angular momentum, they must spin up, increasing the effectiveness of the mixing processes. Because of the large initial angular momentum, and because the stars do not have any obvious way of

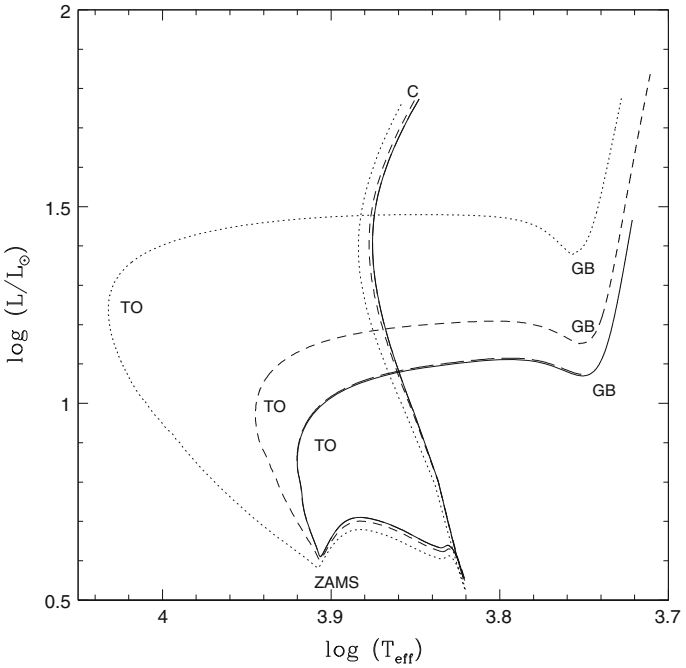

Fig. 12.2 Evolutionary tracks of the product of a collision between two 0.6 $M_{\odot}$ stars, after the angular velocity has been divided by a factor of 5 (*dotted line*), 10 (*dashed line*), 100 (*long-dashed line*), or 1,000 (*solid line*). The end of collision phase is marked with 'C', and the zero-age main sequence (ZAMS), the turnoff (TO), and the base of the giant branch (GB) are also marked (Figure 5 of Sills et al. 2001, reproduced by permission of the AAS)

losing their angular momentum (no discs, magnetic fields, or surface convective zones), the surface layers of the collision products are soon rotating more rapidly than the "break-up" velocity at that radius, where the centrifugal force is larger than the local gravity. These layers become unbound and probably fly away from the star. However, they still carry very little of the total angular momentum. The star continues to contract and spin up, and loses more and more of its mass. Under these conditions, collision products could have a final mass much less than the turnoff mass in a cluster and therefore would not be identified as blue stragglers. However, during that short life, the rotational instabilities mixed the stars so efficiently that they could become very blue, as shown in Fig. 12.2. Here, the initial angular velocity of the same collision product has been arbitrarily divided by a factor of 5, 10, 100, or 1,000, so that the collision products do not reach break-up velocities as they evolve to the main sequence and to show the effect of rotational mixing on the subsequent evolution.

The evolution of rotating collision products, under assumptions of reasonable angular momentum loss prescriptions, was suggested by Leonard and Livio (1995) and followed in detail by Sills et al. (2005). They assumed either a magnetic wind

removed angular momentum, following the formalism applied to low mass main sequence stars (e.g. Kawaler 1988), or that the star was locked magnetically to a disc for a period of time, as assumed for pre-main sequence stars (Matt and Pudritz 2005). Under either scenario, the collision products can lose an appropriate amount of angular momentum and therefore can live in the blue straggler region of the colour-magnitude diagram long enough to be observed there. However, they are still rotating fairly rapidly in this phase. Unfortunately, it is still too early to make a direct comparison between these rotation rates and the early observations of rotation rates of blue stragglers. Both the angular momentum loss prescriptions used by Sills et al. (2005) assume that the collision product has a magnetic field similar to that of the Sun and other normal, low mass (less than $\sim 1.2\,M_{\odot}$) main sequence stars. We do not know anything about the magnetic properties of blue stragglers, and it is not clear that blue stragglers (with masses between 1 and $\sim 1.8\,M_{\odot}$ in globular clusters) should be modelled in the same way as lower-mass objects.

The models of collisions between main sequence stars are concerned only with blue stragglers, and therefore the evolutionary calculations are usually ended when the star leaves the main sequence. However, we might expect to see evolved blue stragglers in globular clusters, since the main sequence lifetime of a normal star with masses like blue stragglers ($\sim 1.2 M_{\odot}$) is only a few gigayears. The best place to look for these so-called E-BSS is on the horizontal branch, since massive stars should be brighter than the standard horizontal branch and quite red. The red giant branch, on the other hand, is quite insensitive to the total mass of the star, and it is difficult to pick out unusual stars in this stage on the basis of photometry alone. Possible E-BSS have been identified in a few globular clusters. Sills et al. (2009) took collisional models and continued their evolution from the main sequence onto the asymptotic giant branch. They found that the collision products are in the same place in the colour-magnitude diagram as the E-BSS during their horizontal branch phase, as shown in Fig. 12.3. Their horizontal branch lifetimes are consistent with the observed number of E-BSS, and almost independent of mass or initial composition profile. The ratio of evolved to main sequence blue stragglers in globular clusters also points to an average blue straggler main sequence lifetime of a few gigayears.

All the collisional models discussed above have assumed that the composition of the parent stars is the same, since the stars are expected to live in the same cluster. However, our recent understanding of globular clusters has changed. Increasingly, both photometric and spectroscopic evidence is pointing to at least two populations of stars in these clusters, one with a higher helium content than the other. Many stars have the helium content expected for a normal Population II composition ($Y \sim 0.23$), but a significant fraction of the stars could have helium as high as $Y = 0.4$ or so (D'Antona et al. 2005). These two populations are expected to both be formed early in the clusters' evolution. One implication of these two populations is that collisions could happen between high helium stars, or between one high and one low helium star. If a star has a higher than normal helium content, it will be bluer and brighter than a normal star of the same mass, both of which are interesting properties for blue stragglers. Glebbeek et al. (2010) began the investigation of

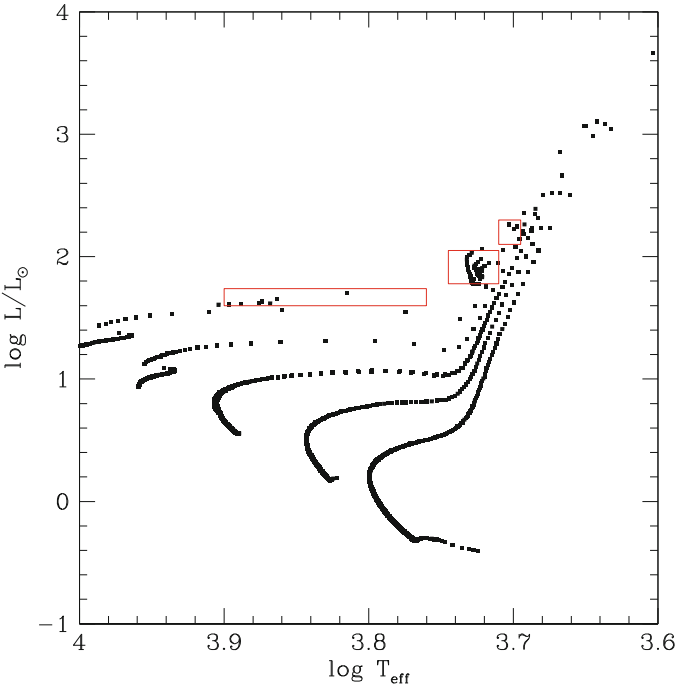

Fig. 12.3 Evolutionary tracks for all collision products for collisions which occurred 10 Gyr after the cluster was formed. The points are equally spaced at 10^7 year intervals. The boxes outline the horizontal branch, E-BSS and asymptotic giant branch regions of the CMD (Figure 11 from Sills et al. 2009, reproduced by permission of the AAS)

how a parent population of varying helium content could affect the distribution of blue stragglers in the colour-magnitude diagram. They calculated evolutionary tracks for collision products between stars drawn from two populations (normal helium and helium-rich). A sample is shown in Fig. 12.4. They found that for most clusters, the blue stragglers did not contain a large fraction of very high helium stars. However, NGC 2808's blue stragglers were better fit by a model which included both populations. These findings are consistent with the expected amount of helium enhancement in the clusters studied, suggesting that a full understanding of blue straggler populations may also require us to pay close attention to the early evolution of globular clusters.

An additional property of blue stragglers that can be determined from stellar evolutionary models is the abundances of various elements at their surfaces. The predictions of collision models is that these stars should have surface compositions which are very similar to that of normal stars, since there is little to no mixing during the collision process (Lombardi et al. 1996; Sills et al. 2001). Lithium should be depleted, because the very thin outer layers of low mass stars that are too cool for lithium burning will be ejected from the system during the collision. There may be

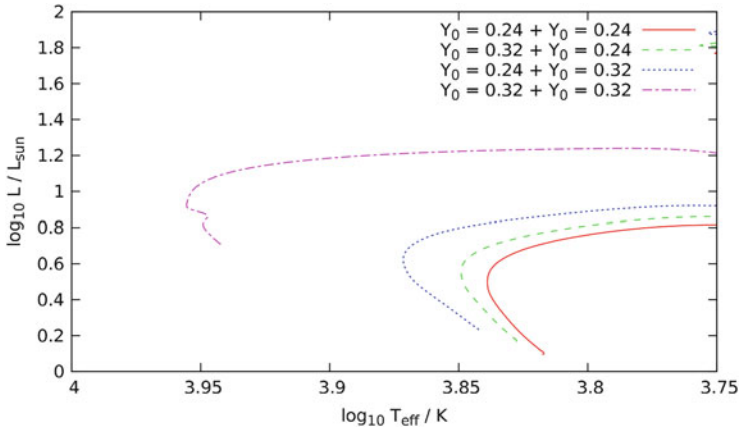

Fig. 12.4 Four evolutionary tracks of stellar collision products between a 0.6 $M_\odot$ star and a 0.4 $M_\odot$ star, with the two stars having helium abundances of either $Y = 0.24$ or 0.32. The increased helium content modifies the position of the star in the HR diagram, and also reduces the main sequence lifetime for higher helium contents (Figure 3 from Glebbeek et al. 2010, reproduced by permission of Oxford University Press on behalf of the RAS)

some slight modification of carbon and nitrogen abundances of collision products on the red giant branch (Glebbeek et al. 2008) if the collision product contained some helium-rich material below the base of the convection zone, but blue stragglers still on the main sequence will not show this signature.

When thinking about surface abundances, two effects need to be considered: first, what is the "original" surface abundance (i.e. immediately after the collision); and second, what happens to the abundances as the star evolves. There are a number of stellar processes which modify surface abundances, all of which are expected to occur in hot stars like blue stragglers under the right circumstances. Convection is a fast process which can fully mix the star to a particular depth, so if the chemical composition of the star at the depth is different than the surface, the observed abundances will change. In rapidly rotating stars, as discussed above, various instabilities can mix quickly and to greater depths than convection. Thermohaline mixing occurs when material with a high mean molecular weight lies on top of a layer of smaller mean molecular weight. This process also mixes the two layers, but on a timescale which is longer than the convective timescale. If the stellar atmosphere is radiatively stable, then gravitational settling can cause the heavier atoms to sink relative to the lighter ones, resulting in a lower observed abundance of elements relative to hydrogen. Radiative levitation works in the opposite way, to push (typically) heavier elements up due to a tighter coupling between radiation and those elements. Both gravitational settling and radiative levitation are effective on similar timescales for interesting elements like carbon, so any calculation which makes predictions of surface abundances must include both processes simultaneously.

12.3 Binary Mass Transfer Models

The other likely mechanism for creating blue stragglers is through mass transfer in a binary system. This mechanism is distinct from stellar collisions in that the two stars are in a stable orbit, and the mass transfer occurs because of some internal evolution of the stars or the system. Normally, one star's radius increases due to normal stellar evolution and the star fills its Roche lobe, or the binary orbit shrinks (e.g., due to angular momentum loss via gravitational radiation or a magnetized wind) so that mass transfer will occur. In a cluster, the binary orbit could also be modified by interactions. However, the models of the mass transfer event and the subsequent evolution of the blue straggler are always done in isolation without considering the environment surrounding the binary.

Unlike collisions, mass transfer can be a very slow process. Under some circumstances, mass can be transferred from one star to another on timescales that are comparable to the nuclear timescale of the individual stars. To model such systems, stellar evolution codes which can simultaneously evolve both stars are used. The main code used in the literature for this type of work is a modified version of Eggleton's stellar evolution code, described in detail in Nelson and Eggleton (2001). Rather than assuming that the mass of each star is fixed in time, an additional outer boundary condition is introduced so that mass can be lost if the star overfills its Roche lobe. An equivalent boundary condition is used when a star loses mass through a stellar wind, and in some instances, both a wind and Roche lobe overflow are modelled (Chen and Han 2008a). A fraction β of the material lost by the primary is accreted onto the secondary, where $\beta = 1.0$ for fully conservative mass transfer. The orbit of the binary is recalculated using the new masses and the assumption that the material carries the specific angular momentum of mass-losing star.

These codes are very robust when the mass transfer rate is reasonably low, but if the donor star is unstable to dynamical mass transfer, they can break down. For a full discussion of the conditions for stable and unstable mass transfer, see Chap. 8 in this volume. The binary evolution codes typically treat dynamical mass transfer by setting a maximum upper limit on the total amount of mass that can be transferred in any given timestep (or a maximum mass loss rate). If the parameters of the star and binary system are such that the mass transfer rates reach this maximum, one of two things are done. Either the mass loss rate is arbitrarily set to a high, but still stable, mass transfer rate (e.g. Chen and Han 2008b), or the two stars are assumed to merge and a structure for the merger product is assumed (e.g. Chen and Han 2008a). Unfortunately, various groups do not agree on the assumed structure of a dynamical merger product. Chen and Han (2008a) argue that a dynamical merger product will have the same structure as a stellar collision product, while Lu et al. (2010) assume that mergers are fully mixed.

As described in Chap. 8, Roche lobe overflow mass transfer is usually divided into three cases, following Kippenhahn and Weigert (1967) and Lauterborn (1970). Case A mass transfer occurs when the donor is on the main sequence and is typically stable on nuclear timescales. Case B mass transfer occurs a little later, after the main

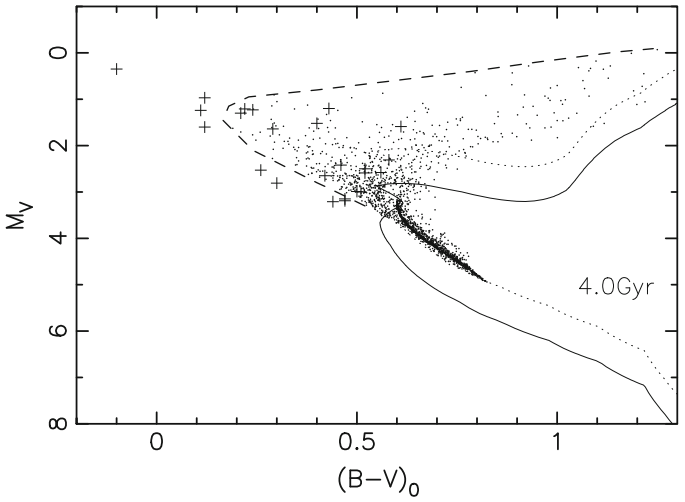

Fig. 12.5 A colour-magnitude diagram for a 4 Gyr old system showing the locations of binaries which are currently undergoing mass transfer as small dots. The *solid line* is a 4 Gyr isochrone, and the *dotted line* is that isochrone moved brighter by 0.75 magnitudes, to show where equal-mass binaries would lie. The *dashed line* gives the upper edge of the binary population. The *crosses* are the observed positions of the blue stragglers in M67 (Figure 5 from Tian et al. 2006, reproduced with permission © ESO)

sequence but before core helium ignition, and Case C is mostly when the donor is on the asymptotic giant branch. Case B and Case C mass transfer can be unstable on either dynamical or thermal timescales, depending on the structure of the envelope of the star, primarily the depth of the convective zone. All three cases are expected to contribute to the formation of blue stragglers, although the relative importance of each channel is not yet well understood.

Models of binary mass transfer products are done self-consistently if the stars do not fully merge. For example, Tian et al. (2006) follows the evolution of a 1.4 + 0.9 $M_\odot$ binary which transfers mass while the 1.4 $M_\odot$ star is on the main sequence, continues as that star becomes a giant, but ends when the mass ratio reverses, leaving a blue straggler and a helium white dwarf binary system. They also calculate a full grid of such case A mass transfer systems, with various initial masses and orbital separations. At an age of 4 Gyr (to compare to the open cluster M67), they find that many blue stragglers are still undergoing mass transfer. Both the primary and the secondary can still contribute significantly to the total luminosity of the system, and so these objects cover a very large area in the colour-magnitude diagram (Fig. 12.5). They are all above a line which is 0.75 magnitudes brighter than the Zero Age Main Sequence, and populate the area between this line and the giant branch due to blends with the second star in the system.

To study mergers, Chen and Han (2008a) looked at case A mass transfer in systems that result in a merger (based on the initial periods and masses of

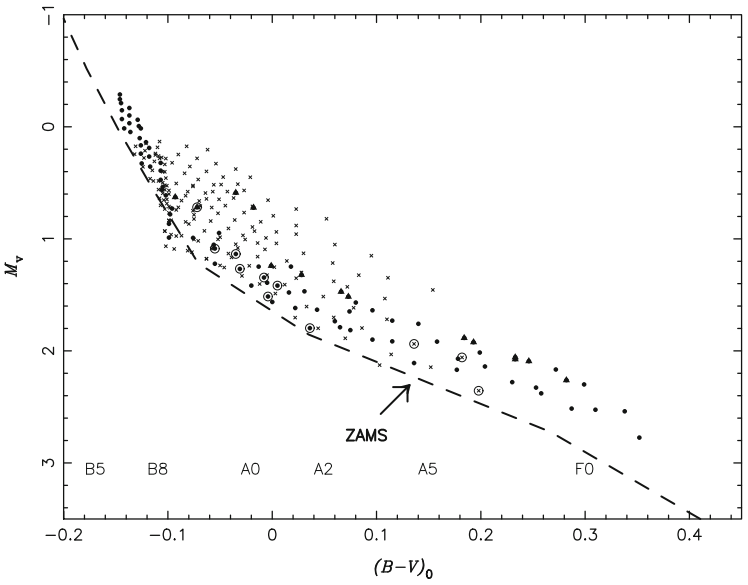

Fig. 12.6 Location of case A binary mergers in the colour-magnitude diagram. *Dots* and *crosses* represent systems which evolved quickly and slowly to contact, respectively. The *triangles* are models with very low hydrogen content. The *open symbols* are observed blue stragglers from a number of open clusters (Figure 1 from Chen and Han 2008a, reproduced by permission of Oxford University Press on behalf of the RAS)

the binary system) after a rapid (thermal timescale) or slow (nuclear timescale) evolution to contact. The evolution of these binary systems before contact was followed using the Eggleton code, under the assumption that the material from the primary is distributed homogeneously over the surface of the secondary. The evolution was stopped when contact was reached, and they assumed that the merger product has the core of the primary at the centre, and then a fully-mixed envelope which consists of the material from the secondary mixed with the envelope of the primary. These objects are then evolved using a single-star evolution model. Because the merger products can have a wide range of surface abundances but are still single stars in various stages of main sequence evolution, they all lie within about one magnitude of the Zero Age Main Sequence (Fig. 12.6). However, the hydrodynamic process of merging is not followed in detail, and these calculations assume that the merger product is in thermal equilibrium before the evolution begins. If the thermal contraction phase of a merger product is long, or if the object is like a collision product and does not fully mix the secondary into the envelope, then these evolutionary tracks need to be modified. Currently, there are not many hydrodynamic simulations of the merger of contact binaries, so we cannot definitively predict the appropriate structure of a post-mass-transfer merger.

Models of stable case B mass transfer can only be calculated when mass transfer begins when the primary is in the Hertzsprung gap (e.g., Lu et al. 2010). As the

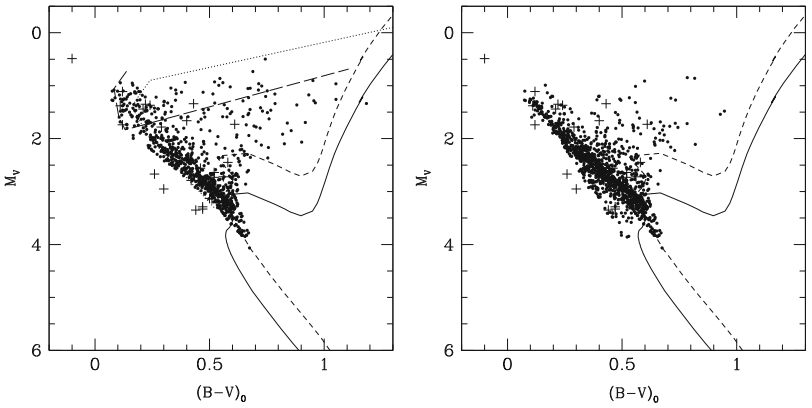

Fig. 12.7 A colour-magnitude diagram of a population of 4 Gyr old binaries undergoing case B mass transfer (*solid dots*) and blue stragglers observed in M67 (*crosses*). The conservative mass transfer parameter β is set to 1.0 in the *left panel* and 0.5 in the *right*. The *solid line* is a 4 Gyr isochrone, and the *small dashed line* is the same isochrone shifted by 0.75 magnitudes, representing the locus of equal-mass binaries. The *dotted line* gives the upper edge of the case A binary population, taken from Tian et al. (2006) (Fig. 12.5). The *long-dashed line* gives the lower bound of case B binaries with primary masses between 1.4 and 1.5 $M_\odot$ (Figure 6 from Lu et al. 2010, reproduced by permission of Oxford University Press on behalf of the RAS)

primary moves up the giant branch, it develops a larger convective envelope and quickly becomes unstable to mass transfer on a dynamical timescale. These systems will result in a merger or a common envelope system, whose evolution is not well understood (Ivanova et al. 2013). The stable case B mass transfer systems tend to be slightly bluer and brighter than the case A systems (compare Fig. 12.7 with Fig. 12.5) but still cover much of the area between the line 0.75 magnitudes above the ZAMS, and the giant branch. Few systems can lie below that line, unless the conservative mass transfer parameter β is less than one.

There are very few models of case C mass transfer applied specifically to blue stragglers. Chen and Han (2007) looked at the critical mass ratio for stable mass transfer in binaries appropriate for M67, and conclude that case C could provide a viable formation mechanism for the long-period blue stragglers in that cluster. Since the surface chemistry of AGB stars is significantly different than that of their less-evolved red giant cousins, we might expect that blue stragglers formed through case C mass transfer would show evidence of anomalous chemistry (s-process elements, for example). AGB stars also have less mass to donate to their companion to form a blue straggler, since their core is more massive than that of a red giant. And case C mass transfer must occur in wide binaries, because the system did not undergo mass transfer on the red giant branch. Other than that, the expectation is that the overall evolution will be similar to objects which are undergoing case B mass transfer.

Very little is known about the rotational properties of the products of mass transfer. The models discussed above do not include stellar rotation. It is reasonable to assume that merger products will be rotating rapidly immediately after the merger,

since the angular momentum of the orbit will have to be absorbed by the star. The subsequent evolution will depend on the structure of the object immediately after the merger, and any star which remains rapidly rotating for a substantial period of time will become more and more mixed. Since we do not see blue stragglers that have anomalously high rotation rates or extremely blue locations in the CMD, we can assume that there is some efficient angular momentum loss process for binary mergers, analogous to what must occur in stellar collision products.

Surface abundances, particularly of CNO elements, are thought to be a tracer of a binary mass transfer formation mechanism (Chen and Han 2004). If the mass transfer process exposes material which has been processed through CNO burning (from the core or a hydrogen-burning shell of a red giant), then we should see evidence for mass transfer on the surface of the blue straggler. Just like in stellar collisions, however, it is important to also consider the subsequent evolution of the surface abundances due to internal mixing. Chen and Han (2004) looked at thermohaline mixing in merger products, and concluded that the CNO signature of mass transfer would remain but that the position of the star in the colour-magnitude diagram would be affected slightly. Glebbeek et al. (2010) compare a particular collision and a binary merger from the same two parent stars, and conclude that the CNO abundances of the two stars will be similar, but that lithium may provide a better discriminant. A larger investigation of parameter space is required before we can feel confident that abundances alone can pinpoint a formation mechanism for a blue straggler.

12.4 Parametrised Models

In the context of stellar dynamics, it is very time-consuming to calculate detailed stellar evolutionary models for all stars in a system (a cluster or a galaxy). In the case of galaxies, the system is non-collisional and so stars can be treated as point masses without compromising the scientific questions that are being asked. For collisional systems such as dense star clusters, however, the physical radii of the stars as a function of time becomes important in determining the dynamical state of the system at later times. In other words, collisions can happen, and if we are to model the system correctly, direct physical collisions must be included. In addition, it can be important to track the mass of each star over time, since mass loss from stars can significantly modify the cluster potential (Hills 1980). We also want to know the luminosity and temperature of each star to create synthetic colour-magnitude diagrams. In order to capture all the stellar quantities that a stellar evolution code would give, but without doing the detailed evolution calculations, a number of codes have been developed which provide parametrised stellar evolution. In other words, the radius, temperature, luminosity, and mass of a star of a given initial mass can be determined at any time t by making use of functional fits to evolutionary tracks. The next obvious step for such codes was to combine these stellar evolution recipes with the binary evolution recipes that have

been developed for binary population synthesis codes. Processes such as Roche Lobe overflow mass transfer, common envelope evolution, wind mass transfer, and orbital energy loss by gravitational wave radiation are all parametrised. Criteria for each process to occur, and importantly the outcome of each process (in terms of the new masses, evolutionary status, and orbital elements of the binary) are given as simple formulae. These codes can also include a prescription for the outcome of direct stellar collisions.

The three main parameterized binary and stellar evolution codes used in the recent literature are `SeBa` (Portegies Zwart and Verbunt 1996), `BSE` (Hurley et al. 2002), and `StarTrack` (Belczynski et al. 2008). `BSE` is the most commonly used code, and it has been implemented into a number of stellar dynamics codes such as `NBODY4/NBODY6/NBODY7` (Aarseth 2012), `Cluster Monte Carlo` (Chatterjee et al. 2010) and `MOCCA` (Hypki and Giersz 2013) and is also available as a module in `AMUSE` (Portegies Zwart et al. 2013). `SeBa` is an integral component of the `STARLAB` code, and `StarTrack` is primarily a binary population synthesis code but has been combined with simple dynamic simulations of clusters to model the dynamical modification of binary populations in clusters (Ivanova et al. 2005).

The parametrised approach is very good for determining the overall properties of a stellar system. It does a better job than any dynamical simulation which does not include binary or collisional processes, and allows for direct comparison to observations. However, because the prescriptions for many of the binary evolutionary processes and collisions are simplified, we cannot use these parameterized codes to compare directly to individual blue stragglers. Even the details of the blue straggler populations are not treated correctly. For example, observations of blue straggler stars in NGC 188 (see Chap. 3) shows that `BSE` over-predicts the number of common envelope systems. Comparison of `BSE` results with detailed stellar evolution models of stellar collisions (Glebbeek et al. 2008) and with the observed positions of blue stragglers in the colour-magnitude diagrams of globular clusters (Sills et al. 2013) show that the `BSE` treatment of collisions overestimates their lifetime. `BSE`, which was originally formulated in the early 1990s, still assumes that collision products are fully mixed, despite the numerous papers showing that mixing is not expected either during or after the collision. Therefore, we caution against using only parametrised codes when trying to predict the properties of individual blue stragglers or blue straggler populations in clusters.

12.5 Future Directions

Models of individual blue stragglers have become more sophisticated over the past two decades. Both colliding stars and binary mass transfer have been modelled in detail using hydrodynamical techniques. Binary mergers, also known as coalescence, are usually assigned an assumed post-merger structure. All these objects are then evolved using a stellar evolution code, which, in the case of the mass transfer models, consistently treats the material which is leaving one star and accreting on

the other. The resulting evolutionary tracks are compared to the observed positions of blue stragglers in colour-magnitude diagrams to try to constrain their formation mechanism(s).

There are still a number of unanswered questions and additional observations that are yet to be investigated in the context of detailed evolutionary models. The modelling of collision products is the more mature field of the two main formation mechanisms. Even though binary mass transfer is probably a more common process, and is relevant for many objects beyond blue stragglers, there is more work to be done here. The parameter space of possible binaries is much larger and has not been fully explored. We probably understand fairly well how a mass-gaining star evolves, but the evolution of stars which fully merge after an episode of mass transfer is less clear. Are they indeed fully mixed, or does the core of the primary retain its integrity? More detailed models, although difficult, are necessary to fully understand this important contribution to blue stragglers.

One place where collisional models could be improved is through a more careful treatment of appropriate parent stars. While the idea of multiple populations with multiple helium contents may be specific to globular clusters, it may be important to include different chemical compositions in those situations. It is also important to remember that blue stragglers can have a fairly long lifetime, so they can have formed long ago when the parent stars were less evolved, and potentially more massive. The same can be said for mass transfer products, since stable mass transfer can proceed for many gigayears in some cases and so the amount of mass and its composition may not be what one would expect if we only consider stars near the current turnoff mass.

Many blue stragglers are known pulsators. They are known as SX Phoenicis stars, and are the low metallicity, low mass counterparts of δ Scuti stars. They are radial pulsators, and lie in the same instability strip as RR Lyrae stars and Cepheids. They are found in globular clusters and dwarf galaxies, and most lie on the expected period-luminosity relation (Cohen and Sarajedini 2012). There is a population of sub-luminous SX Phe stars in globular clusters which may have higher helium abundances. Whether these abundances are related to the internal structure of individual blue stragglers, or to the possibility of multiple populations in globular clusters, remains to be seen. Only a few groups have invested in detailed models of SX Phe stars (Santolamazza et al. 2001; Templeton et al. 2002), and both were more concerned with determining the location of the instability strip. We know from studies of the more common radial pulsators (RR Lyraes and Cepheids) that pulsation modes can be a powerful tool for determining fundamental stellar parameters such as their mass and chemical composition. A detailed comparison between observed pulsation modes and models may provide a way of distinguishing between various formation mechanisms, as long as those mechanisms produce stars which are substantially different in some fundamental property.

There are two pieces of physics that stellar modellers typically try to avoid: rotation and magnetic fields. Unfortunately, it seems that both effects are going to be important for both stellar collisions and binary mergers. Angular momentum loss, probably mediated by a magnetic wind or magnetic locking to a disc is needed. In

particular, magnetohydynamic simulations of collisions and of binary mergers may be needed to determine what happens to any primordial magnetic field of the parent stars. Rotational mixing is also likely to be important to the subsequent evolution of blue stragglers if they rotate even slightly faster than normal for most of their main sequence lifetime. The current rotation rates of blue stragglers are still puzzles that have not been addressed in much detail. Modellers will have to bite the bullet and include at least one of these difficult physical effects, and probably both.

References

Aarseth, S. J.: MNRAS **422**, 841 (2012)
Bailyn, C. D., Pinsonneault, M. H.: ApJ **439**, 705 (1995)
Belczynski, K., Kalogera, V., Rasio, F. A., et al.: ApJS **174**, 223 (2008)
Benz, W., Hills, J. G.: ApJ **323**, 614 (1987)
Chatterjee, S., Fregeau, J. M., Umbreit, S., Rasio, F. A.: ApJ **719**, 915 (2010)
Chen, X., Han, Z.: MNRAS **355**, 1182 (2004)
Chen, X., Han, Z.: in Unsolved Problems in Stellar Physics, AIPC Vol. 948, p. 431 (2007)
Chen, X., Han, Z.: MNRAS **384**, 1263 (2008a)
Chen, X., Han, Z.: MNRAS **387**, 1416 (2008b)
Cohen, R. E., Sarajedini, A.: MNRAS **419**, 342 (2012)
D'Antona, F., Bellazzini, M., Caloi, V., Pecci, F. F., Galleti, S., Rood, R. T.: ApJ **631**, 868 (2005)
Gaburov, E., Lombardi, J. C., Portegies Zwart, S.: MNRAS **383**, L5 (2008)
Glebbeek, E., Pols, O. R., Hurley, J. R.: A&A **488**, 1007 (2008)
Glebbeek, E., Pols, O. R.: A&A **488**, 1017 (2008)
Glebbeek, E., Sills, A., Leigh, N.: MNRAS **408**, 1267 (2010)
Glebbeek, E., Sills, A., Hu, H., Stancliffe, R. J.: in AIPC Vol. 1314, p. 113 (2010)
Hills, J. G.: ApJ **235**, 986 (1980)
Hurley, J. R., Tout, C. A., Pols, O. R.: MNRAS **329**, 897 (2002)
Hypki, A., Giersz, M.: MNRAS **429**, 1221 (2013)
Ivanova, N., Belczynski, K., Fregeau, J. M., Rasio, F. A.: MNRAS **358**, 572 (2005)
Ivanova, N., et al.: A&ARv, 21, 59 (2013)
Kawaler, S. D.: ApJ **333**, 236 (1988)
Kippenhahn, R., Weigert, A.: Zeitschrift Astron. **65**, 251 (1967)
Lauterborn, D.: A&A **7**, 150 (1970)
Leonard, P. J. T., Livio, M.: ApJL **447**, 121 (1995)
Lombardi, J. C., Jr., Rasio, F. A., Shapiro, S. L. : ApJL **445**, 117 (1995)
Lombardi, J. C., Jr., Rasio, F. A., Shapiro, S. L.: ApJ **468**, 797 (1996)
Lombardi, J. C., Jr., Warren, J. S., Rasio, F. A., Sills, A., Warren, A. R.: ApJ **568**, 939 (2002)
Lu, P., Deng, L. C., Zhang, X. B.: MNRAS **409**, 1013 (2010)
Maeder, A., Meynet, G., Lagarde, N., Charbonnel, C.: A&A **553**, A1 (2013)
Matt, S., Pudritz, R. E.: ApJ **632**, L135 (2005)
Nelson, C. A., Eggleton, P. P.: ApJ **552**, 664 (2001)
Ouellette, J. A., Pritchet, C. J.: AJ **115**, 2539 (1998)
Portegies Zwart, S. F., Verbunt, F.: A&A **309**, 179 (1996)
Portegies Zwart, S., McMillan, S. L. W., van Elteren, E., Pelupessy, I., de Vries, N.: CoPhC **183**, 456 (2013)
Procter Sills, A., Bailyn, C. D., Demarque, P.: ApJ **455**, L163 (1995)
Sandquist, E. L., Bolte, M., Hernquist, L.: ApJ **477**, 335 (1997)

Santolamazza, P., Marconi, M., Bono, G., Caputo, F., Cassisi, S., Gilliland, R. L.: ApJ **554**, 1124 (2001)
Sills, A., Lombardi, J. C., Jr.: ApJ **484**, L51 (1997)
Sills, A., Lombardi, J. C., Jr., Bailyn, C. D., Demarque, P., Rasio F. A., Shapiro S. L.: ApJ **487**, 290 (1997)
Sills, A., Faber, J. A., Lombardi, J. C., Jr., Rasio, F. A., Warren, A. R.: ApJ **548**, 323 (2001)
Sills, A., Adams, T., Davies, M. B.: MNRAS **358**, 716 (2005)
Sills, A., Karakas, A., Lattanzio, J.: ApJ **692**, 1411 (2009)
Sills A., Glebbeek, E., Chatterjee, S., Rasio, F. A.: ApJ **777**, 105 (2013)
Templeton, M., Basu, S., Demarque, P.: ApJ **576**, 963 (2002)
Tian, B., Deng, L., Han, Z., Zhang, X. B.: A&A **455**, 247 (2006)

Chapter 13
Blue Stragglers in Globular Clusters: Observations, Statistics and Physics

Christian Knigge

13.1 Straw-Man Models for Blue Straggler Formation

In order to gain some intuition, let us start by considering the two simplest distinct formation channels for blue stragglers in globular clusters. First, blue stragglers may form in the same way in clusters as they do in the Galactic field, i.e. via mass transfer or coalescence in binary systems. In this case, we may expect the number of blue stragglers in any given cluster (N_{BSS}) to scale with the number of binary stars in the cluster (N_{bin}),

$$N_{BSS} \propto N_{bin} \propto f_{bin} M_{tot}, \tag{13.1}$$

where f_{bin} is the fraction of binaries among the cluster members, and M_{tot} is the total mass of the cluster. In reality, f_{bin} should really be the fraction of *close* binaries (since only these can be the progenitors of blue stragglers), but let us assume for the moment that these two quantities track each other, so that we can ignore this subtlety.

The second possibility is that blue stragglers in globular clusters form primarily via dynamical encounters. Here, the simplest possibility is that the most important encounters are direct collisions between two single stars. In this case, the number of blue stragglers should scale with the $1 + 1$ *collision rate* ($\Gamma_{coll,1+1}$), which is determined by the conditions in the dense cluster core via

$$N_{BSS} \propto \Gamma_{coll,1+1} \propto R_c^3 n_c^2 \sigma_c^{-1}. \tag{13.2}$$

C. Knigge (✉)
Department of Physics & Astronomy, University of Southampton, Southampton SO17 1BJ, UK
e-mail: C.Knigge@soton.ac.uk

H.M.J. Boffin et al. (eds.), *Ecology of Blue Straggler Stars*, Astrophysics and Space Science Library 413, DOI 10.1007/978-3-662-44434-4_13

Here, R_c is the core radius of the cluster, n_c is the stellar density in the core, and σ_c is the core velocity dispersion (which is a measure of the characteristic speed at which stars move in the core).

These scaling relations are clearly vast oversimplifications. Perhaps most obviously, *both* channels may produce significant number of blue stragglers in globular clusters. However, more importantly, even the very distinction between binary and dynamical formation channels is something of a false dichotomy. After all, the close binaries that are the progenitors of blue stragglers in the binary evolution channel may themselves have been formed or hardened by previous dynamical encounters (e.g. Hut et al. 1992). Similarly, it is not at all obvious that the total rate of stellar collisions should be dominated by encounters between single stars. In fact, Leigh and Sills (2011) show that the rate of dynamical *encounters* is dominated by binaries (or even triples) even in environments with only modest binary (or triple) fractions (Fig. 13.1). The probability of an actual stellar *collision* occurring in such encounters

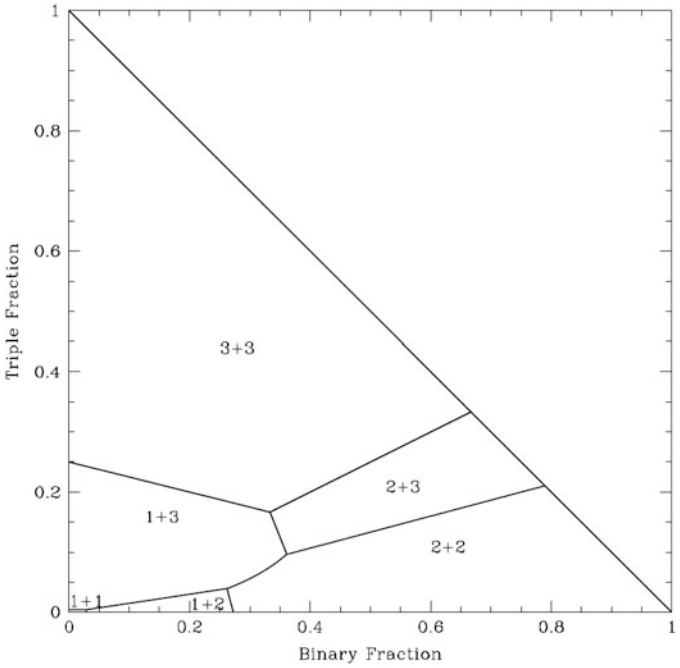

Fig. 13.1 The "phase diagram" of dynamical encounters. For any stellar population described by a particular combination of binary fraction and triple fraction, it is possible to determine which type of dynamical encounter will dominate. The plot above shows the regions of parameter space dominated by the various different encounters, assuming a particular set of characteristic binary and triple parameters. Reproduced from Figure 1 of Leigh and Sills (2011), *An analytic technique for constraining the dynamical origins of multiple star systems containing merger products*, MNRAS, 410, 2370

is discussed by Leigh and Geller (2012). Thus, in reality, the binary channel may involve dynamical encounters, and the dynamical channel may involve binaries.

Does this mean that our simple straw-man models are useless? Not at all. First, the most extreme cases one can envision within the two channels *are* basically distinct. If blue straggler formation is dominated by mass transfer in or coalescence of *primordial* binaries that have not been affected (much) by dynamical encounters, N_{BSS} will scale with N_{bin} and *not* with $\Gamma_{coll,1+1}$. Conversely, if the dominant channel is really single–single encounters, then N_{BSS} will scale with $\Gamma_{coll,1+1}$ and *not* with N_{bin}. Second, and perhaps more importantly, we might expect the basic scaling relations to be valuable even if binaries are affected by encounters and collisions involve binaries. This is particularly easy to see for the binary channel. Here, the relationship $N_{BSS} \propto N_{bin}$ should presumably hold regardless of how the relevant binaries were formed (so long as our definition of N_{bin} does, in fact, refer to the "relevant" binary population, which may be a significant challenge in practice). For example, suppose that most of the close binaries that evolve into blue stragglers have been previously hardened in three-body encounters. In this case, we would expect $N_{BSS} \propto N_{bin} \propto \Gamma_{1+2}$, where Γ_{1+2} is the $1 + 2$ *encounter* rate. Similarly, if blue stragglers are predominantly formed by direct collisions occurring during $1 + 2$ encounters, we would expect $N_{BSS} \propto P_{coll,1+2} \propto P_{coll,1+2}\Gamma_{1+2} \propto f_{bin}(a_{bin}/R_*)P_{coll,1+2}\Gamma_{coll,1+1}$, where $P_{coll,1+2}$ is the probability of a physical collision occurring during a $1 + 2$ encounter, a_{bin} is the characteristic binary separation and R_* is the characteristic stellar radius; see Leigh et al. (2013) for expressions linking the various encounter rates.

These specific examples show that, at the most basic level, the straw-man relations should remain roughly valid, even if reality is more complex than the limiting cases they formally represent. If blue straggler formation mostly involves binaries, we expect a scaling with N_{bin}; if it mostly involves encounters, we expect a scaling with $\Gamma_{coll,1+1}$. If binaries and dynamics work in tandem, N_{bin} and $\Gamma_{coll,1+1}$ will simply be less distinct quantities.

Two final, technical points are worth noting here. First, N_{bin} and $\Gamma_{coll,1+1}$ will *always* be statistically correlated, even if binaries are primordial and encounters dominated by single stars. After all, there are both more encounters and more binaries in an environment containing more stars. Davies et al. (2004) show that this effect induces a scaling of $\Gamma_{coll,1+1} \propto M_{tot}^{3/2}$, and $N_{bin} \propto f_{bin}M_{tot}$. This needs to be kept in mind when comparing N_{BSS} to either of these quantities.

Second, two different conventions are sometimes used in statistical studies of blue stragglers. The first and simplest is to use raw *numbers*, N_{BSS}, corrected (if necessary) for partial coverage of the relevant cluster. The second is to use blue straggler *frequencies*, N_{BSS}/N_{ref}, where N_{ref} refers to the number of some reference population (e.g. horizontal branch stars) in the same field of view. It is important to understand that this difference matters. In particular, the straw-man scalings we have derived above hold only for blue straggler numbers. In the collision scenario, blue straggler frequencies should scale with the *specific* encounter rate, Γ_{1+1}/M_{tot}. In

the binary scenario, blue straggler frequencies should scale simply with the binary fraction, f_{bin}.

13.2 All Theory Is Grey: Binary Coalescence and Dynamical Encounters in Practice

It is interesting to ask at this point whether there is any *empirical* evidence that the physical mechanisms we are invoking in our two basic blue straggler formation channels actually occur in nature. Let us first consider the binary channel. *Mass transfer* is, of course, a well-established process in many close binary systems, including X-ray binaries (in which the accretor is a neutron star or black hole), cataclysmic variables (in which the accretor is a white dwarf) and Algols (in which the accretor is a main sequence star). But is there also evidence that full coalescence can occur?

As it turns out, there is. It has been known for quite a long time that some binary system, and in particular the eclipsing W UMa stars, are *contact binaries*, in which *both* binary components overfill their respective Roche lobes. In many such systems, the predicted time scale for full coalescence is much shorter than a Hubble time. W UMa binaries are therefore obvious progenitor candidates for apparently single blue stragglers in the Galactic field. In fact, quite a few blue stragglers in globular clusters are known to be (in) W UMa binaries.

However, we can actually do even better. In 2008, astronomers in Japan and China discovered an apparent nova in the constellation Scorpius (Nakano et al. 2008). Follow-up observations (Mason et al. 2010) quickly revealed that Nova Sco 2008 (aka V1309 Sco) was quite an unusual transient and probably related to the rare class of "red novae" (like V838 Mon). By a huge stroke of luck, the nova happened to lie in the footprint of the OGLE microlensing survey (Udalski 2003). The pre-(and post-)eruption OGLE data of V1309 Sco is astonishing (Tylenda et al. 2011). Not only does it provide an exquisite light curve of what turns out to be a $\simeq$6 mag eruption, but it also reveals that *the system was a* $P_{orb} \simeq 1.4$ *day W UMa contact binary prior to the outburst* (Fig. 13.2)! In fact, the OGLE data is good enough to provide several accurate measurements of the orbital period in the lead-up to the eruption (Fig. 13.3). These measurements show that P_{orb} decreased significantly in just the $\simeq$6 years leading up to the outburst. The implication is that *Nova Sco 2008 represents a binary coalescence event caught in real time!*

What about dynamical encounters or direct stellar collisions in globular clusters? No such event has been unambiguously observed in real time to date. This is not surprising given the low frequency and short duration of such events. There is nevertheless very strong empirical evidence that some exotic stellar populations in globular clusters are preferentially formed in dynamical encounters.

It has been known since the 1970s that bright low-mass X-ray binaries are overabundant by a factor of $\simeq$100 in globular clusters, relative to the Galactic

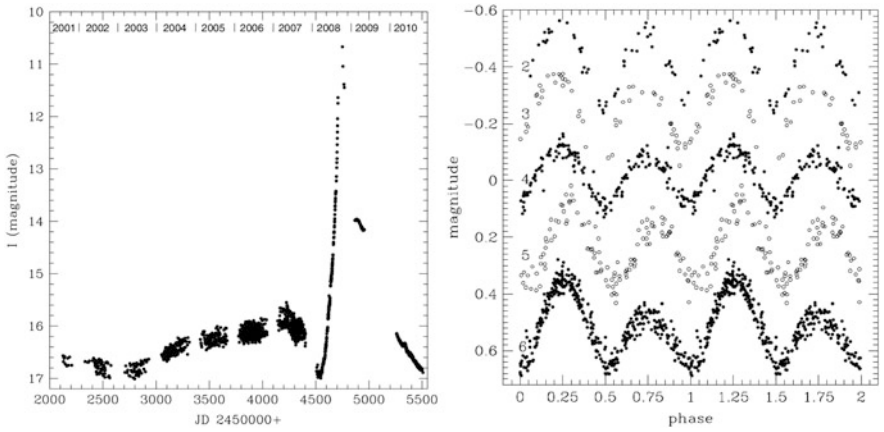

Fig. 13.2 *Left*: The long-term OGLE light curve of "Nova" Sco 2008 = V1309 Sco. *Right*: The phase-folded pre-eruption light curves of V1309 Sco for the 2002–2006 OGLE observing seasons. Reproduced from Figures 1 and 3 of Tylenda et al. (2011), *V1309 Scorpii: Merger of a Contact Binary*, A&A, 528, A114

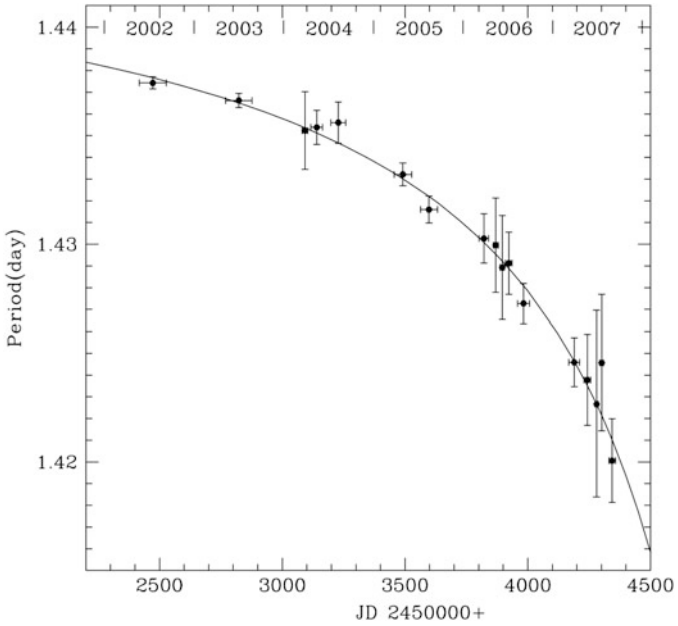

Fig. 13.3 The change in the orbital period of V1309 Sco in the years leading up to the 2008 eruption. Reproduced from Figure 2 of Tylenda et al. (2011), *V1309 Scorpii: Merger of a Contact Binary*, A&A, 528, A114

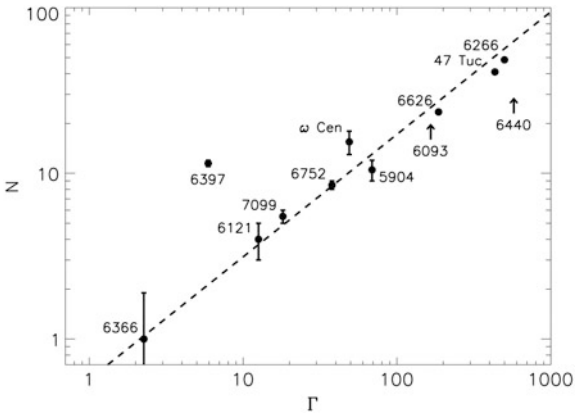

Fig. 13.4 The number of X-ray sources detected in globular cluster above $L_x \simeq 4 \times 10^{30}$ erg s^{-1} versus the normalised collision rate of the cluster. Reproduced by permission of the AAS from Fig. 2 of Pooley et al. (2003), *Dynamical Formation of Close Binaries in Globular Clusters*, ApJL, 591, L141

field. This was quickly ascribed to the availability of unique *dynamical* formation channels in globular clusters, such as 1 + 1 tidal captures (Katz 1975; Clark 1975; Fabian et al. 1975). However, observational confirmation of this idea required much more powerful X-ray telescopes and took nearly another three decades. The first convincing empirical case was made by Pooley et al. (2003), who showed that the number of moderately bright X-ray sources in a given cluster (which are dominated by a variety of accreting compact binaries) exhibits a clear scaling with the predicted dynamical collision rate in the cluster (Fig. 13.4).

Pooley and Hut (2006) later showed that, in high-collision-rate clusters, this scaling holds independently for both low-mass X-ray binaries and cataclysmic variables. However, there is also tentative evidence that, in low-collision-rate clusters, the number of these sources may instead scale with cluster mass. This suggests that the evolution of (primordial?) binaries may be sufficient to produce the few X-ray sources observed in such clusters. Our simple straw-man models thus do a rather good job in accounting for the observed number of X-ray binaries across the full range of Galactic globular clusters.

13.3 The Search for the Smoking Gun Correlation I: The Near Constancy of Blue Straggler Numbers

Let us return to blue stragglers. The first reasonably complete catalogue of blue stragglers in Galactic globular clusters was constructed and analysed by Piotto et al. (2004). This catalogue was based on an HST/WFPC2 survey that provided V and I colour-magnitude diagrams for 74 clusters (Piotto et al. 2002). Blue stragglers could be reliably selected in 56 of these clusters, yielding a total sample of nearly 3,000 stars.

The results obtained by Piotto et al. (2004) were surprising. Most importantly, they found *no* correlation between the frequency of blue stragglers and the cluster

collision rate. Moreover, they found a weak *anti-correlation* between blue straggler frequency and cluster luminosity (i.e. total mass). One potentially confounding issue in their analysis is that it is somewhat unnatural to correlate blue straggler frequencies against collision rate and total mass. As emphasised in Sect. 13.1, it is the *number* of blue stragglers that should scale linearly with these quantities in our straw-man models, not their frequency.

As it turns out, however, this issue is not the main cause of the unexpected results. Indeed, the same data base was re-analysed and interpreted by Davies et al. (2004), who showed that blue straggler *numbers* also do not correlate significantly with collision rate (Fig. 13.5; top panel). They also argued that blue straggler numbers are largely independent of total cluster mass/luminosity, although an inspection of their figure suggests that there may be a mild, positive, but sub-linear correlation between these quantities (Fig. 13.5; bottom panel).

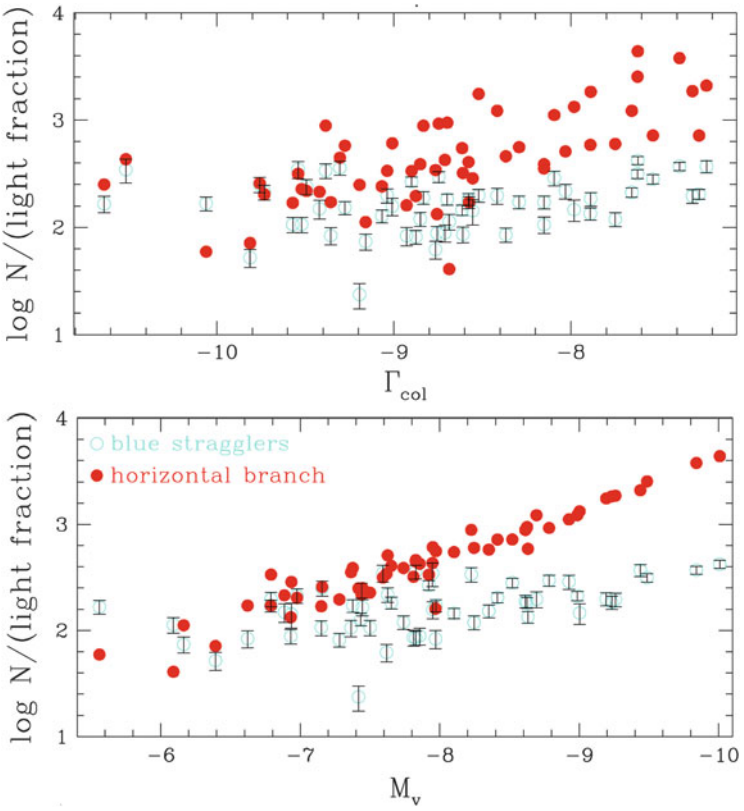

Fig. 13.5 *Top panel*: The observed number of blue stragglers and horizontal branch stars as a function of stellar collision rate. *Bottom panel*: The estimated number of blue stragglers and horizontal branch stars as a function of the absolute magnitude of the cluster. Reproduced from Fig. 1 of Davies et al. (2004), *Blue Straggler Production in Globular Clusters*, MNRAS, 348, 129

The number of horizontal branch stars does scale linearly with cluster mass or luminosity, as one would expect for a "normal" stellar population (Fig. 13.5; bottom panel). More interestingly, the number of horizontal branch stars actually also correlates with the collision rate (Fig. 13.5; top panel). This correlation is no doubt induced by the intrinsic correlation between cluster mass and collision rate (Sect. 13.1). Indeed, the scaling between horizontal branch numbers and collision rate is broadly in line with the relation we would expect in this case, i.e. $N_{HB} \propto \Gamma_{coll,1+1}^{2/3}$. But this only highlights the central mystery: apparently blue stragglers exhibit a weaker correlation with collision rate than horizontal branch stars, a population that is certainly not produced in dynamical encounters.

13.4 Do Clusters Deplete Their Reservoir of Binary Blue Straggler Progenitors?

Davies et al. (2004) suggested an interesting interpretation for the near constancy of blue straggler numbers (Fig. 13.5). Their idea invokes a combination of binaries and dynamical encounters. Specifically, they consider a binary mass transfer scenario in which blue stragglers are formed when the primary star leaves the main sequence, expands and fills its Roche lobe. This initiates mass transfer onto the secondary, which can then be converted into a blue straggler. Davies et al. note that, in dense globular clusters, each binary is likely to undergo many encounters with single stars. In each such encounter, the most likely outcome is the ejection of the least massive star, so these encounters strongly affect the mass distribution of the binary population. This, in turn, affects the ability of this population to form blue stragglers, since only systems with primaries close to the turn-off mass are viable progenitors.

The central argument put forward by Davies et al. (2004) is that, high-collision-rate clusters,[1] relatively massive stars near the cluster turn-off mass are likely to have exchanged into binaries well before the present day. Such clusters may therefore have used up their blue straggler binaries by the present day and may thus now be deficient in blue stragglers derived from the binary channel. On the other hand, blue stragglers formed via direct stellar collisions should be more numerous in these clusters. Davies et al. therefore suggest that these two effects broadly cancel. This would imply that binary-derived blue stragglers dominate in low-collision-rate clusters, while collisional blue stragglers dominate in high-collision-rate clusters, even though the absolute numbers in both types of clusters are more or less the same.

In support of this argument, Davies et al. carried out a simple simulation. In this, a set of initial ("primordial") binaries was created, in which the mass of each binary component is drawn independently from a simple initial mass function

[1] Strictly speaking, we are talking here about clusters with high *specific* collision rates, i.e. clusters in which *each binary* undergoes many encounters.

(Eggleton et al. 1989, 1990). Each binary was then subjected to a series of exchange encounters with single stars whose masses are also drawn from the same IMF. In each encounter, the least massive of the three stars involved was ejected, and the remaining two assumed to remain as a binary system. After each encounter, a system was labelled as a blue straggler if the mass of its primary satisfied $0.8\ M_\odot < M_1 < 0.816\ M_\odot$. This corresponds to the range of turn-off masses over the last 1 Gyr—a typical blue straggler life time—for a typical Galactic globular cluster.

In order to gain some insight, we have repeated their simulation. The black histogram in Fig. 13.6 shows how the fraction of blue stragglers among the simulated binaries, f_{pbs}, depends on the number of encounters a binary has undergone, N_{enc}. In agreement with their results, we see that f_{pbs} initially increases as the number of encounters goes up, but then peaks at $N_{enc} = 6$ and declines monotonically towards larger N_{enc}. The expected number of encounters in the highest collision rate clusters is larger than six over the cluster lifetime, so these results appear to suggest that binary-derived blue stragglers will indeed be rare in such clusters today.

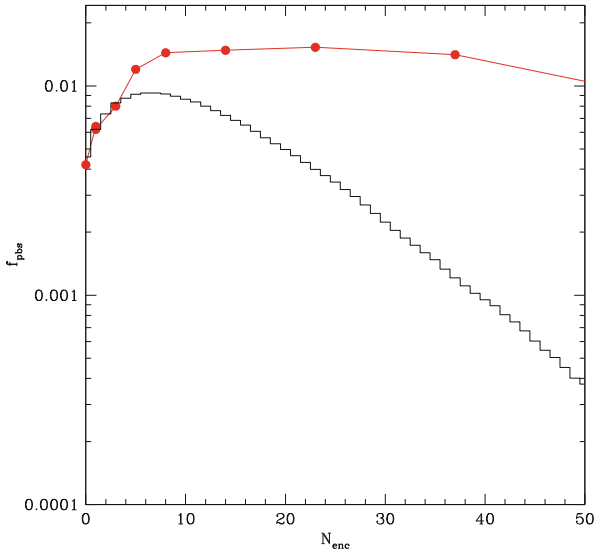

Fig. 13.6 The fraction of "blue stragglers" among a simulated binary population versus the number of encounters with single stars the binary has undergone. Blue stragglers are defined as binaries with primaries near the present-day turn-off mass. The *black line* corresponds to the case where the masses of the initial binary components, as well as the masses of the single stars the binary encounters, are drawn from an unrestricted initial mass function. This is the case considered by Davies et al. (2004). The *red line* corresponds to the case where, at each encounter, all stellar masses are replaced with a suitable compact object mass if they exceed the appropriate turn-off mass at the time of the encounter (see text for details). Note that while the black line declines fairly quickly towards large N_{enc}, the red line does not

There are, however, problems with this scenario. For example, one would still expect a scaling of blue straggler numbers with $\Gamma_{coll,1+1}$ at least for high-collision-rate clusters (which is not really observed). Moreover, since exchange encounters are required to produce even binary-derived blue stragglers in this model, we might actually still expect a scaling with $\Gamma_{coll,1+1}$ for these objects (via an intrinsic scaling with Γ_{1+2}; see Sect. 13.1).

However, the most fundamental problem with the simulation is that it assumes that all stellar masses are available for all encounters. In reality, each successive encounter represents a later time in the evolution of the cluster, so stars above the main sequence turn-off corresponding to this time will already have evolved off the main sequence. In order to test if this effect matters, we have repeated the simulation once more, but this time with a rough model for stellar evolution.

In this new calculation, we first estimate the typical time interval between encounters for a given set of representative binary and cluster parameters. This provides the time step for the simulation. We then evolve the binary population forward by allowing each binary to encounter a single star at each time step. At this point, we first check if the primary has turned off the main sequence since the last time step. If so, we assume that mass transfer has already started and that no further exchange encounters will take place. If not, we once again ask if an exchange encounter will happen. However, we now also first check if the single star the binary has encountered has turned off the main sequence. If so, we replace its mass with that of the relevant compact object.[2] Once the present day is reached, we calculate the fraction of blue stragglers in the same way as before (but excluding systems with white dwarf secondaries). We then carry out the same calculation for a wide range of assumed cluster densities (and hence collision rates), with each density corresponding to a different number of encounters between the birth of the cluster and the present day.

The results of this modified simulation are shown by the red line in Fig. 13.6. With our simplistic treatment of stellar evolution included, f_{pbs} now rises fairly quickly up to $N_{enc} \simeq 10$ and then stays nearly constant out to at least $N_{enc} \simeq 60$. The absence of a sharp decline towards high N_{enc} is actually easy to understand. In the original simulation, where all stellar masses are available in all encounters, the overall binary population quickly becomes dominated by systems with main sequence primaries more massive than 0.816 $M_\odot$. It is the increasing dominance of these systems that fundamentally causes the decline in f_{pbs} towards larger N_{enc}. But this is of course unphysical, since such systems should not exist at the present day. In the revised simulation, f_{pbs} stays high because the most massive stars in the

[2]If $M_i > 18\ M_\odot$, we assume the star has turned into a black hole, so that $M_f = 10\ M_\odot$; if $7\ M_\odot < M_i < 18\ M_\odot$, we assume the star has turned in a neutron star, so that $M_f = 1.4\ M_\odot$; finally, if $M_{to}(t) < M_i < 7\ M_\odot$, we assume the star has become a white dwarf, so that $M_f = 0.5\ M_\odot$. These mass ranges, as well as the main sequence lifetimes, are estimated using SSE (Hurley et al. 2000).

cluster (ignoring the extremely rare neutron stars and black holes) are now always stars with masses near the turn-off mass.

Davies et al. (2004) emphasised that their simulation ignored several important physical effects, and this is still true of our revised simulation as well. Some of these effects are discussed in more detail in Chap. 9. Nevertheless, the results in Fig. 13.6 suggest that the depletion of blue straggler binaries in high collision rate clusters may not offer as natural an explanation for the observed blue straggler numbers as previously envisaged.

13.5 The Search for the Smoking Gun Correlation II: The Core Mass Correlation

One obvious explanation for the lack of convincing correlations between global blue straggler numbers and cluster parameters is that both the binary and the collisional channels contribute. In particular, it seems plausible that each channel may dominate in different regions within a cluster, with collisions perhaps dominating in the dense core, and binary evolution dominating in the periphery. More generally, it seems safe to assume that if collisions/dynamics dominates blue straggler production anywhere, it will be in cluster cores. So is it possible that a cleaner picture may emerge if we focus specifically on blue stragglers found in the cores of their parent clusters?

We investigated this idea in Knigge et al. (2009), building on a new blue straggler catalogue constructed by Leigh et al. (2007, 2008). This catalogue was still based on the WFPC2 data set of Piotto et al. (2002), but included only systems found in the cluster core by a consistent photometric selection algorithm. Our hope and expectation was that the number of *core* blue stragglers *would* show a strong correlation with cluster collision rate. However, Fig. 13.7 shows that we were wrong. More in desperation than expectation we decided to also have a look at the binary hypothesis. Since no comprehensive set of empirically derived core binary fractions, $f_{bin,core}$, were available in 2009, our only option was to use the total core mass, M_{core}, as a proxy for the number of binaries in the core. This is reasonable so long as core binary fractions do not vary dramatically between clusters.

Much to our surprise, plotting $N_{BSS,core}$ vs M_{core} immediately revealed a clear correlation (Fig. 13.8). This would seem to suggest that blue stragglers are preferentially formed via the binary channel, even in dense cluster cores. However, the observed scaling is clearly sub-linear, and a fit to the data suggests $N_{BSS,core} \propto M_{core}^{0.4}$. Can this be accommodated within a simple binary scenario?

The simplest way to accomplish this is to remember that the intrinsic scaling should be with the number of binaries in the core, not just the core mass, i.e. $N_{BSS,core} \propto N_{bin,core} \propto f_{bin,core} M_{core}$ in the binary picture. Thus the observed scaling could be trivially understood if the core binary fractions themselves scale with core mass as $f_{bin,core} \propto M_{core}^{-0.6}$.

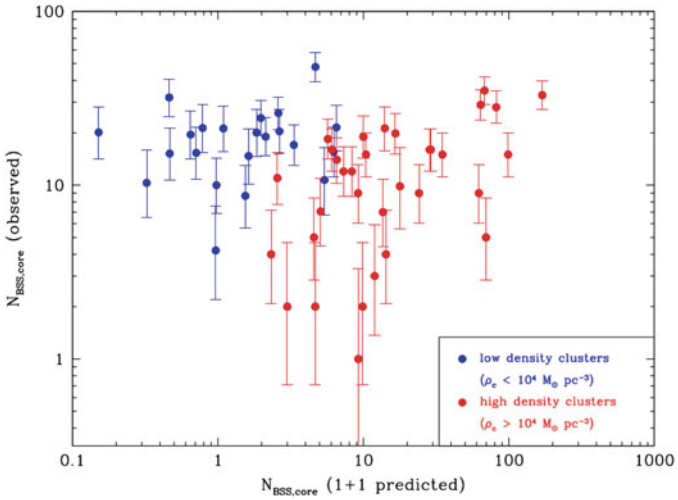

Fig. 13.7 The number of blue stragglers found in a globular cluster core versus the number expected from $1 + 1$ collisions. The latter is simply the product of the $\Gamma_{coll,1+1}$ and an assumed blue straggler lifetime (1 Gyr). *Blue points* correspond to low-density clusters, *red points* to high-density clusters (see legend). Figure reproduced from Figure 1 of Knigge et al. (2009), *A Binary Origin for Blue Stragglers in Globular Clusters*, Nature, 457, 288

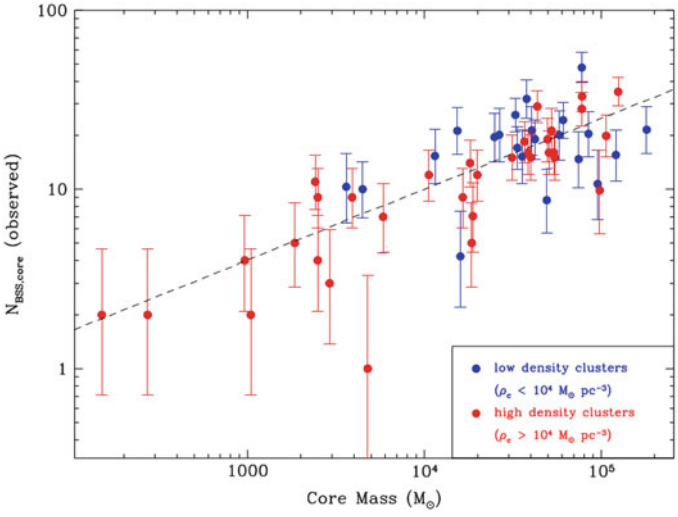

Fig. 13.8 The number of blue stragglers found in a globular cluster core versus the total mass of the core. *Blue points* correspond to low-density clusters, red points to high-density clusters (see legend). Figure reproduced from Figure 2 of Knigge et al. (2009), *A Binary Origin for Blue Stragglers in Globular Clusters*, Nature, 457, 288

As already noted above, there was no definitive set of core binary fractions available to test this prediction in 2009. However, Sollima et al. (2007, 2008) had derived empirical binary fraction for a small sample of low-density clusters and had already shown that these correlated positively with the blue straggler frequencies in these clusters. Also, Milone et al. (2008) had just obtained preliminary estimates of the core binary fractions in a larger sample of clusters, based on the HST/ACS survey of Galactic globular clusters (Sarajedini et al. 2007) and found a clear anti-correlation between core binary fractions and total cluster mass. Even though neither set of core binary fractions were suitable for combining directly with the blue straggler data base used in Knigge et al. (2009), they permitted preliminary tests for a correlation with core mass. These tests suggested that $f_{bin,core} \propto M_{core}^{-0.35}$, not too far from the expected relation, albeit with considerable scatter.

In Sect. 13.7, we will consider whether more recent, higher quality observations confirm, refute or modify these results. However, in 2009, our conclusion was that blue stragglers seem to be derived mainly from binary systems, even in dense cluster cores.[3]

13.6 Alternative Constraints on Formation Channels

Let us accept for the moment that the scaling of blue straggler numbers with cluster parameters tends to favour a binary formation channel. Are there other strands of evidence that would challenge this idea?

As discussed elsewhere in this book, it is extremely difficult to confidently assign a specific formation mechanism to a particular blue straggler. The only convincing cases are the Carbon/Oxygen-depleted blue stragglers, which were initially discovered by Ferraro et al. (2006) in 47 Tuc. This chemical anomaly is an expected consequence of mass transfer, since this process can dredge up CNO-processed material from the stellar interior. By contrast, no unique spectroscopic signature for dynamically/collisionally formed blue stragglers is known.

Nevertheless, there are at least two other types of observations that may shed light on blue straggler formation in globular clusters. They are (a) the radial distribution of blue stragglers in a given cluster, and (b) the discovery of a double blue straggler sequence in M30 (and perhaps other clusters). Both of these observations are discussed in much more detail elsewhere in this book, so here we will merely ask whether (or to what extent) they conflict with the idea that most blue stragglers derive from binaries, rather than from dynamical encounters.

[3] We were careful not to rule out the possibility that the relevant binary population may be affected by dynamical encounters. However, we also noted that the absence of a scaling with collision rates seemed hard to understand in any scenario involving lots of dynamical encounters (see Sect. 13.1).

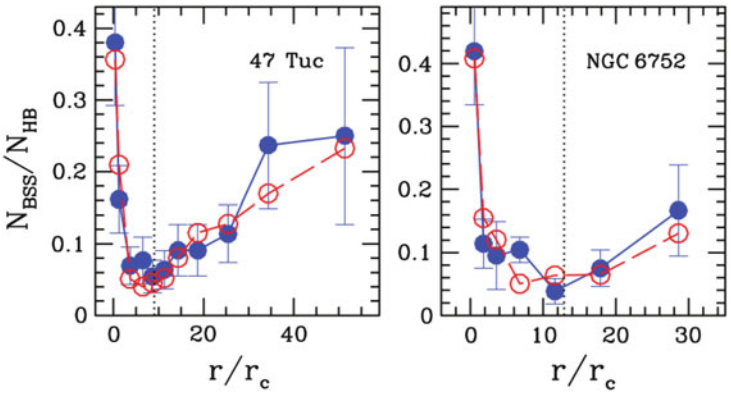

Fig. 13.9 The radial distribution of blue straggler frequencies in the globular clusters 47 Tuc and NGC 6752. Blue straggler frequencies are defined here as the number of blue stragglers normalised to the number of horizontal branch stars. The *filled blue point* and *solid blue lines* are the observational data, while the *open red circles* and *red dashed lines* are the best-fitting models of Mapelli et al. (2006). The *dotted lines* mark the location of the minimum in the radial distributions. See text for details. Figure adapted from Figure 2 of Mapelli et al. (2006), *The Radial Distribution of Blue Straggler Stars and the Nature of their Progenitors*, MNRAS, 373, 361

13.6.1 Radial Distributions

In most globular clusters, the dependence of blue straggler *frequency* on radius is bimodal (Fig. 13.9; e.g. Ferraro et al. 1997; Sabbi et al. 2004; Warren et al. 2006; Lanzoni et al. 2007a,b). These distributions have been modelled quite successfully by Mapelli et al. (2004, 2006). Their simulations follow the motion of blue stragglers in a static cluster potential, assuming that collisional blue stragglers form only within the core, while binary-derived blue stragglers all start their lives outside the core. The ratio of collisional to binary blue stragglers is a free parameter of the model.

Mapelli et al. (2004, 2006) obtained the best fits to the observed distributions with both channels contributing a comparable number of blue stragglers to the total population. Moreover, they also found that collisional blue stragglers completely dominate the population in the cluster core, while binary blue stragglers are dominant in the cluster halo, beyond the minimum in the radial distribution. Yet this conclusion seems incompatible with the lack of a correlation between core blue straggler numbers and cluster collision rates.

It is useful to take a step back at this point and consider the physics that produces the bimodal blue straggler distributions. As discussed by Mapelli et al. (2004, 2006) and described in more detail elsewhere in this book, the key dynamical process is dynamical friction. Since blue stragglers are relatively massive, they tend to sink towards the cluster core. The time scale on which this happens, t_{df}, changes as a function of radius. We can therefore define a critical radius, $R_{min} \simeq R(t_{dc} = t_{gc})$,

where t_{gc} is the lifetime of the cluster. Binary blue stragglers born well inside R_{min} have had plenty of time to sink to the core, while those born well outside this radius have barely moved from their original location. The minimum in the blue straggler distribution therefore corresponds roughly to R_{min}.

These considerations highlight an important point: a blue straggler population containing *only* binary blue stragglers should still produce a bimodal radial distribution. So why are collisional blue stragglers needed at all in the simulations? The answer is that not enough binary blue stragglers were seeded inside R_{min}. But this is just an assumption. If the birth distribution of binary blue stragglers is allowed to be centrally peaked, a population consisting exclusively of such systems may be able to match the data as well (see Mapelli et al. 2006).

It is perhaps also worth emphasising here that the scenario preferred by Mapelli et al. (2004, 2006) is very different from that suggested by Davies et al. (2004). Both scenarios do favour a combination of binary-derived and collisional blue stragglers. However, in Davies et al. model, different formation channels dominate in different *clusters*, whereas in Mapelli et al.'s model, different channels operate in different locations *within* a given cluster. In any case, the key point for our purposes here is that a bimodal radial distribution does not necessarily require distinct formation channels for the core and halo blue straggler populations.

13.6.2 Double Blue Straggler Sequences

One other recent discovery is highly relevant to the question of blue straggler formation channels. Ferraro et al. (2009) showed that the colour magnitude diagram of the globular cluster M30 appears to contain *two* distinct blue straggler sequences (Fig. 5.6). Their interpretation of this observation is that objects on the blue sequence were formed via collisions, while those on the red sequence are derived from binaries.

Why should there be such a clean separation between these two types of systems in M30? The idea put forward by Ferraro et al. (2009) is that, in M30, the collisional blue stragglers all formed recently in a short burst, most likely when the cluster underwent core collapse. All of these objects therefore share the same evolutionary state, so that all of them line up on a well-defined main sequence. By contrast, the red sequence lies roughly 0.75 mag above the extension of the cluster zero-age main sequence, as expected for a population of roughly equal-mass binaries. If this idea is correct, then both sequences could be present in many/most clusters, but would usually overlap too much to be noticeable as distinct entities.

The double blue straggler sequence in M30 is almost certainly an important clue, and Ferraro et al. present new data elsewhere in this book (see Chap. 5) that appear to show a similar double sequence in another cluster. If confirmed, it would be nice if each of the two sequences really does correspond to a distinct formation channel, even if this may make it harder to understand other results, such as the core mass correlation. However, there is at least one surprising aspect to the double

sequence in M30. As noted by Ferraro et al. (2009), their blue straggler sample for this cluster contains 3 W UMa binaries and two other variables that are likely binaries. However, these are not all located on the red (binary) sequence. Rather, one W UMa and one other binary are located nicely on the collisional sequence. Perhaps this simply means that these two binaries were produced in (or affected by) dynamical encounters, while the others are mostly primordial. Nevertheless, if each sequence corresponds cleanly to a particular formation channel, it does seem surprising that the known binaries should be split nearly evenly between them.

13.7 The Search for the Smoking Gun Correlation III: Once More, with Binary Fractions…

Binaries are key to the study of cluster dynamics. In fact, the late dynamical evolution of globular clusters is thought to be *driven* by binary systems (e.g. Hut et al. 1992). It was therefore a major breakthrough when Milone et al. (2012) presented photometric estimates of binary fractions for 59 clusters, based on the HST/ACS survey of Galactic globular clusters already mentioned in Sect. 13.5.

Three trends discovered by Milone et al. are of immediate relevance to the blue straggler formation problem. First, core binary fractions correlate only weakly with $\Gamma_{coll,1+1}$. Second, they anti-correlate more strongly with total cluster luminosity (and hence mass). Third, they correlate very strongly with blue straggler *frequency* (Fig. 13.10). All of these trends are quite promising for the idea that binaries dominate blue straggler production, as suggested in Knigge et al. (2009).

However, the availability of binary fractions makes it possible to test the key formation scenarios much more directly. For example, we can now compare the number of core blue stragglers directly to the number of binaries in the core, rather

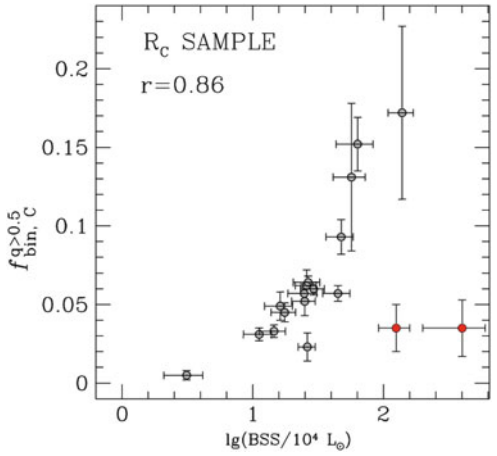

Fig. 13.10 The fraction of binaries with mass ratios $q > 0.5$ in the cluster core versus the blue straggler frequency in the core. The two red points near the bottom right of the plot correspond to post-core-collapse clusters. Figure reproduced from Figure B5 of Milone et al. (2012), *The ACS Survey of Galactic Globular Clusters XII: Photometric Binaries along the Main Sequence*, A&A, 540, A16

than just to the total core mass. Similarly, we can now directly estimate 1 + 2 and 2 + 2 encounter rates (Γ_{1+2} and Γ_{2+2}; see Sect. 13.1). If blue straggler production is dominated by encounters involving binaries (e.g. exchange encounters; see Sect. 13.4), blue straggler numbers should correlate strongly with Γ_{1+2} or Γ_{2+2}.

We carried out these tests in Leigh et al. (2013). For this purpose, we combined the core blue straggler numbers derived by Leigh et al. (2011) with the core binary fractions obtained by Milone et al. (2012). These data sets are ideally matched, since both are based on the HST/ACS survey of Galactic globular clusters (Sarajedini et al. 2007).

Let us first look at the results for dynamical formation scenarios. Figure 13.11 shows plots of $N_{BSS,core}$ against each of $\Gamma_{coll,1+1}$ (top left panel), Γ_{1+2} (top right

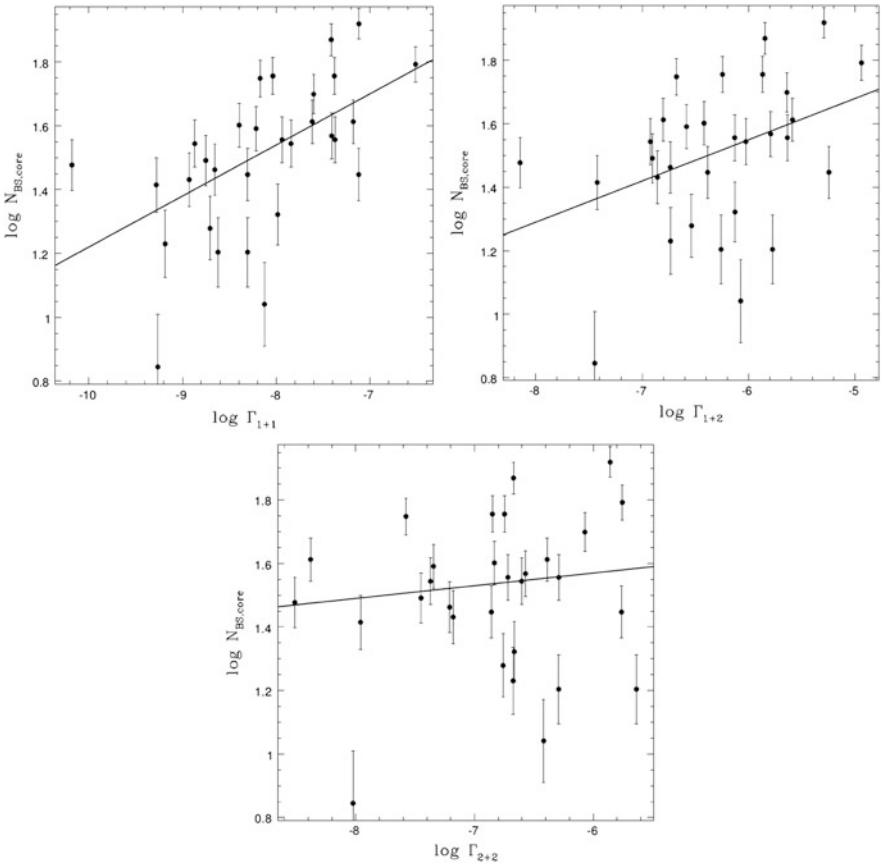

Fig. 13.11 The number of blue stragglers in the core versus the 1 + 1 collision rate (*top left panel*), the 1 + 2 encounter rate (*top right panel*) and the 2 + 2 encounter rate (*bottom panel*). Figure reproduced/adapted from Figures 6, 7 and 8 of Leigh et al. (2013); *The Origins of Blue Straggler and Binarity in Globular Clusters*, MNRAS, 428, 897

panel) and Γ_{2+2} (bottom panel). None of the encounter rates correlate cleanly with the number of blue stragglers in cluster cores.[4]

Now let us look at the binary evolution scenario. The top left panel in Fig. 13.12 shows that the ACS data confirms the existence of a strong correlation between $N_{BSS,core}$ and core mass, with $N_{BSS} \propto M_{core}^{0.4}$ (also see Leigh et al. 2011). The top right panel in Fig. 13.12 shows that the data also confirm the prediction of a strong *anti-correlation* between core binary fraction and M_{core}. A power-law fit to this relation gives roughly $f_{bin,core} \propto M_{core}^{-0.4}$, a little shallower than predicted, but not too far from the expected $M_{core}^{-0.6}$ dependence. So far, so promising. However, the bottom panel in Fig. 13.12 shows what happens when we directly compare $N_{BSS,core}$ to $N_{bin,core} \propto f_{bin,core} M_{core}$. Instead of improving on the correlation with core mass alone, the addition of empirical binary fractions actually *degrades* it!

This is a surprising result. One possibility is that it simply means that all of our straw-man models are too simplistic after all (although, as noted in Sect. 13.1, it seems quite hard to avoid all of the expected correlations, even in more complex formation scenarios). However, before we accept that we need "new physics", we should check if we can somehow reconcile one of the existing models with our new findings.

Since the binary evolution model predicts at least the observed correlation with core mass (and the lack of a correlation with collision rate), let us imagine that all blue stragglers are exclusively formed from (primordial) binaries. In this case, $N_{BSS,core} \propto N_{bin,core} \propto f_{bin,core} M_{core}$, with just some modest intrinsic scatter. We already know empirically that $f_{bin,core}$ anti-correlates quite strongly with M_{core}. But now suppose that the intrinsic anti-correlation is even stronger than the observed one, i.e. that the scatter in the middle panel of Fig. 13.12 is mostly due to observational errors on $f_{bin,core}$, rather than any intrinsic dispersion. In this limit, *M_{core} actually becomes a better predictor of the true core binary fractions than the observationally estimated values.* The number of binaries in the core—and hence the number of blue stragglers—will then also be predicted more accurately by M_{core} alone than by the empirically estimated combination of $f_{bin,core} M_{core}$.

We have carried out some simple simulations to test and illustrate this idea. In these simulations, we create mock data sets of similar size and dynamic range as the real data and assume that the number of blue stragglers scales perfectly and linearly with the number of binaries, i.e. $N_{BSS,core} \propto N_{bin,core}$. We also assume that $f_{bin,core} \propto M_{core}^{0.6}$, with only a slight intrinsic dispersion, σ_{int}. Finally, we assume that our observational estimates of $f_{bin,core}$ are subject to an observational uncertainty σ_{obs}, which we vary in the range $0.1\sigma_{int} \leq \sigma_{obs} \leq 10.0\sigma_{int}$. We then analyse each mock data set to estimate the correlation coefficients of $N_{BSS,core}$ against the "observationally estimated" M_{core} and $N_{bin,core} = f_{bin,core} M_{core}$. We also fit the latter correlation with a power law and estimate the power law index.

[4] As noted by Leigh et al. (2011), the correlation between $N_{BSS,core}$ and $\Gamma_{coll,1+1}$ is formally significant, but probably induced by the intrinsic correlation between $\Gamma_{coll,1+1}$ and M_{core} (see Sect. 13.1).

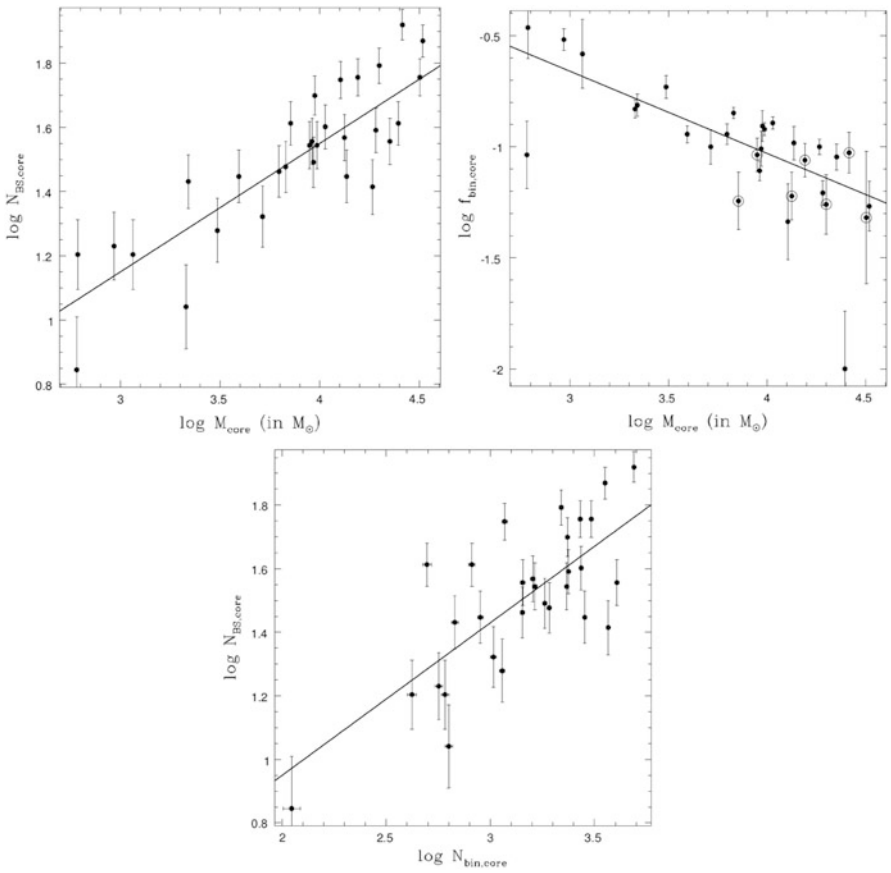

Fig. 13.12 Diagnostic plots for the binary evolution scenario for blue straggler formation, based on the HST/ACS survey of Galactic globular clusters (Sarajedini et al. 2007). *Top left panel*: The number of blue stragglers in the core versus the mass of the core. *Top right panel*: Core binary fraction versus core mass. *Bottom panel*: The number of blue stragglers in the core versus the estimated number of binaries in the core. Figure reproduced/adapted from Figures 2, 3 and 4 of Leigh et al. (2013); *The Origins of Blue Straggler and Binarity in Globular Clusters*, MNRAS, 428, 897

Figure 13.13 shows how the ratio of the estimated correlation coefficients, and also the inferred power law index of the $N_{BSS,core}$ vs $N_{bin,core}$ relation, depend on the ratio of $\sigma_{obs}/\sigma_{int}$. As expected, when $\sigma_{obs} \ll \sigma_{int}$, the "empirical" core binary fractions add value. In this case, the correlation coefficient between $N_{BSS,core}$ and $N_{bin,core}$ is larger than that between $N_{BSS,core}$ and M_{core}. Also, the inferred power law index of the $N_{BSS,core}$ vs $N_{bin,core}$ relation is unity, i.e. we correctly infer that the intrinsic relation is linear. However, when $\sigma_{obs} \gg \sigma_{int}$, the empirical binary fractions only serve to degrade the underlying signal. In this limit, the correlation of N_{BSS} with M_{core} is stronger than that with the estimated $N_{bin,core}$, and the relationship between

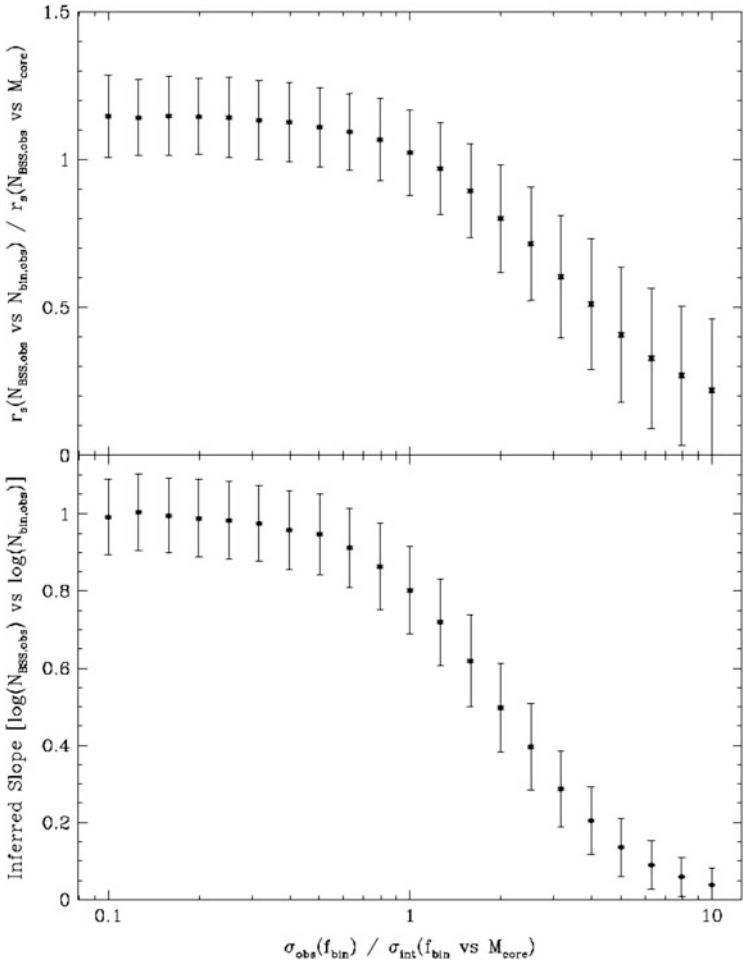

Fig. 13.13 The effect of observational uncertainties in binary fractions on correlations between blue straggler numbers and cluster parameters. The data shown in both panels are derived from simulations designed to roughly mimic the data shown in Fig. 13.12 (see text for details). The ordinate in both panels is the ratio of the assumed observational uncertainty, σ_{obs}, to the assumed intrinsic dispersion in the relation between $f_{bin,core}$ and M_{core}. *Top panel*: The ratio of the correlation coefficients between $N_{BSS,core}$ and $N_{bin,core}$, on the one hand, and $N_{BSS,core}$ and M_{core}, on the other; note that the correlation with $N_{bin,core}$ will only seem stronger than that with M_{core} if $\sigma_{obs} \ll \sigma_{int}$. *Bottom panel*: The inferred power law index of the $N_{BSS,core}$ versus $N_{bin,core}$ correlation; note that the correct value of unity is only obtained if $\sigma_{obs} \ll \sigma_{int}$. Figure reproduced from Figure 9 of Leigh et al. (2013); *The Origins of Blue Straggler and Binarity in Globular Clusters*, MNRAS, 428, 897

$N_{BSS,core}$ and $N_{bin,core}$ is incorrectly inferred to be sub-linear. So the binary evolution *might* still be consistent with the observations, *but only if (core) binary fractions correlate extremely cleanly with cluster (core) masses.*

13.8 Summary and Outlook

What are the key points to take away from our look at blue straggler statistics? On the observational front, we have seen that (a) blue straggler numbers do *not* correlate with dynamical encounter rates; (b) they *do* correlate strongly with cluster (core) masses; (c) empirically estimated core binary numbers (obtained by combining core masses with photometrically determined core binary fractions) correlate *less* strongly with blue straggler numbers than core masses alone.

The first point would seem to argue against a dynamical origin for most blue stragglers in globular clusters. Yet presumably encounters and collisions must happen in such dense environments at roughly the predicted rates. So can the efficient production of blue stragglers via this channel actually be avoided? Sills et al. (2001) followed the evolution of a simulated stellar collision products. One of their key findings was that, if left to their own devices, such objects tend to exceed the break-up velocity and can be completely disrupted if unbound mass shells are successively removed from the surface. In their words: "either blue stragglers are not created through physical off-axis collisions or some mechanism(s) can remove angular momentum from the star on short timescales" (Sills et al. 2001). Thus perhaps stellar collisions occur, but do not produce blue stragglers.

On the other hand, recent dynamical simulations of globular clusters suggest that, even if blue stragglers are produced predominantly by (mainly binary-mediated) collisions, their numbers may scale only weakly with $\Gamma_{coll,1+1}$ (Chatterjee et al. 2013; Sills et al. 2013). The reason for this is not immediately apparent, however, and it is also not clear if a strong scaling with Γ_{1+2} could be avoided as well.

The second point—the core mass correlation—can be explained most naturally in the context of a binary scenario for blue straggler formation.[5] However, the third point—the poor correlation obtained when core masses are combined with empirically estimated binary fractions—seems at first sight inconsistent with a binary scenario. We have seen that this discrepancy can be resolved if core binary fractions are extremely tightly coupled to core masses. If this idea is correct, it would have significant implications for our understanding of cluster dynamics, well beyond the realm of blue stragglers.

Acknowledgements I am extremely grateful to the organisers of the ESO workshop that led to the production of this book. Special thanks are due to Henri Boffin, whose patience as an editor was almost literally unlimited.

[5]We should note, however, that Chatterjee et al. (2013) and Sills et al. (2013) argue that the dynamically-formed blue stragglers in their simulations also produce a core mass correlation.

References

Chatterjee, S., Rasio, F. A., Sills, A., Glebbeek, E.: ApJ **777**, 106 (2013)
Clark, G. W.: ApJL **199**, L143 (1975)
Davies, M. B., Piotto, G., de Angeli, F.: MNRAS **349**, 129 (2004)
Eggleton, P. P., Fitchett, M. J., Tout, C. A.: ApJ **347**, 998 (1989)
Eggleton, P. P., Fitchett, M. J., Tout, C. A.: ApJ **354**, 387 (1990)
Fabian, A. C., Pringle, J. E., Rees, M. J.: MNRAS **172**, 15P (1975)
Ferraro, F. R., Beccari, G., Dalessandro, E., et al.: Nature **462**, 1028 (2009)
Ferraro, F. R., Paltrinieri, B., Fusi Pecci, F., et al.: A&A **324**, 915 (1997)
Ferraro, F. R., Sabbi, E., Gratton, R., et al.: ApJL **647**, L53 (2006)
Hurley, J. R., Pols, O. R., Tout, C. A.: MNRAS **315**, 543 (2000)
Hut, P., McMillan, S., Goodman, J., et al.: PASP **104**, 981 (1992)
Katz, J. I.: Nature **253**, 698 (1975)
Knigge C., Leigh N., Sills A.: Nature **457**, 288 (2009)
Lanzoni, B., Dalessandro, E., Ferraro, F. R., et al.: ApJ **663**, 267 (2007a)
Lanzoni, B., Dalessandro, E., Perina, S., et al.: ApJ **670**, 1065 (2007b)
Leigh N., Geller A. M.: MNRAS **425**, 2369 (2012)
Leigh N., Knigge C., Sills A., et al.: MNRAS **428**, 897 (2013)
Leigh N., Sills A., Knigge C.: ApJ **661**, 210 (2007)
Leigh N., Sills A., Knigge C.: ApJ **678**, 564 (2008)
Leigh N., Sills A., Knigge C.: MNRAS **415**, 3771 (2011)
Leigh N., Sills A.: MNRAS **410**, 2370 (2011)
Mason, E., Diaz, M., Williams, R. E., Preston, G., Bensby, T.: A&A **516**, A108 (2010)
Mapelli, M., Sigurdsson, S., Colpi, M., et al.: ApJL **605**, L29 (2004)
Mapelli, M., Sigurdsson, S., Ferraro, F. R., et al.: MNRAS **373**, 361 (2006)
Milone, A. P., Piotto, G., Bedin, L. R., et al.: A&A **540**, A16 (2012)
Milone, A. P., Piotto, G., Bedin, L. R., Sarajedini, A.: Mem. Soc. Astron. Ital. **79**, 623 (2008)
Nakano, S., Nishiyama, K., Kabashima, F., et al.: IAU Circ. **8972**, 1 (2008)
Piotto, G., De Angeli, F., King, I. R., et al.: ApJL **604**, L109 (2004)
Piotto, G., King, I. R., Djorgovski, S. G., et al.: A&A **391**, 945 (2002)
Pooley, D., Hut, P.: ApJL **646**, L143 (2006)
Pooley, D., Lewin, W. H. G., Anderson, S. F., et al.: ApJL **591**, L131 (2003)
Sabbi, E., Ferraro, F. R., Sills, A., Rood, R. T.: ApJ **617**, 1296 (2004)
Sarajedini, A., Bedin, L. R., Chaboyer, B., et al.: AJ **133**, 1658 (2007)
Sills, A., Faber, J. A., Lombardi, J. C., Jr., Rasio, F. A., Warren, A. R.: ApJ **548**, 323 (2001)
Sills, A., Glebbeek, E., Chatterjee, S., Rasio, F. A.: ApJ **777**, 105 (2013)
Sollima, A., Beccari, G., Ferraro, F. R., Fusi Pecci, F., Sarajedini, A.: MNRAS **380**, 781 (2007)
Sollima, A., Lanzoni, B., Beccari, G., Ferraro, F. R., Fusi Pecci, F.: A&A **481**, 701 (2008)
Tylenda, R., Hajduk, M., Kamiński, T., et al.: A&A **528**, A114 (2011)
Udalski, A.: Acta Astronomica **53**, 291 (2003)
Warren, S. R., Sandquist, E. L., Bolte, M.: ApJ **648**, 1026 (2006)

Chapter 14
Blue Stragglers in Clusters and Integrated Spectral Properties of Stellar Populations

Yu Xin and Licai Deng

14.1 Introduction

Evolutionary population synthesis (EPS) has been widely used as a powerful tool to study the stellar contents of galaxies. In essence, EPS compares the observed, integrated spectrum of a galaxy with a combination of spectra of simple stellar populations (SSPs; single-age, single-metallicity populations) of different ages and metallicities, and decomposes the complex stellar contents into SSPs of known ages and metallicities to infer the galaxy's star-formation history. Over the past two decades, much work has been done to improve the accuracy of EPS and SSP models in various contexts (e.g., Bica and Alloin 1986; Bruzual and Charlot 2003; Leitherer et al. 1999; Thomas et al. 2003; Vazdekis 1999; Worthey 1994).

Unfortunately, population synthesis models still suffer from a number of limitations. One is our poor understanding of some advanced single-star evolutionary phases, such as of supergiants and asymptotic giant branch stars (Yi 2003), while a second is an absence in the models of the results of stellar interactions, such as the so-called "stragglers" formed through mass transfer in binaries or stellar collisions. Such stars are usually very bright and can strongly affect the integrated-light properties of the entire system. The potential uncertainties inherent to EPS caused by ignoring these components could be much larger than those still remaining and due to the variety of input physics among different models.

In this chapter, we focus on the second limitation to the standard SSP models. With the updated knowledge of stars, in particular on the physical properties of binary and collisional interactions that eventually create the exotic blue straggler stars (BSSs) discussed in previous chapters in this book, a more realistic prescription

Y. Xin • L. Deng (✉)
National Astronomical Observatories, Chinese Academy of Sciences, Beijing, China
e-mail: xinyu@bao.ac.cn; licai@bao.ac.cn

H.M.J. Boffin et al. (eds.), *Ecology of Blue Straggler Stars*, Astrophysics and Space Science Library 413, DOI 10.1007/978-3-662-44434-4_14

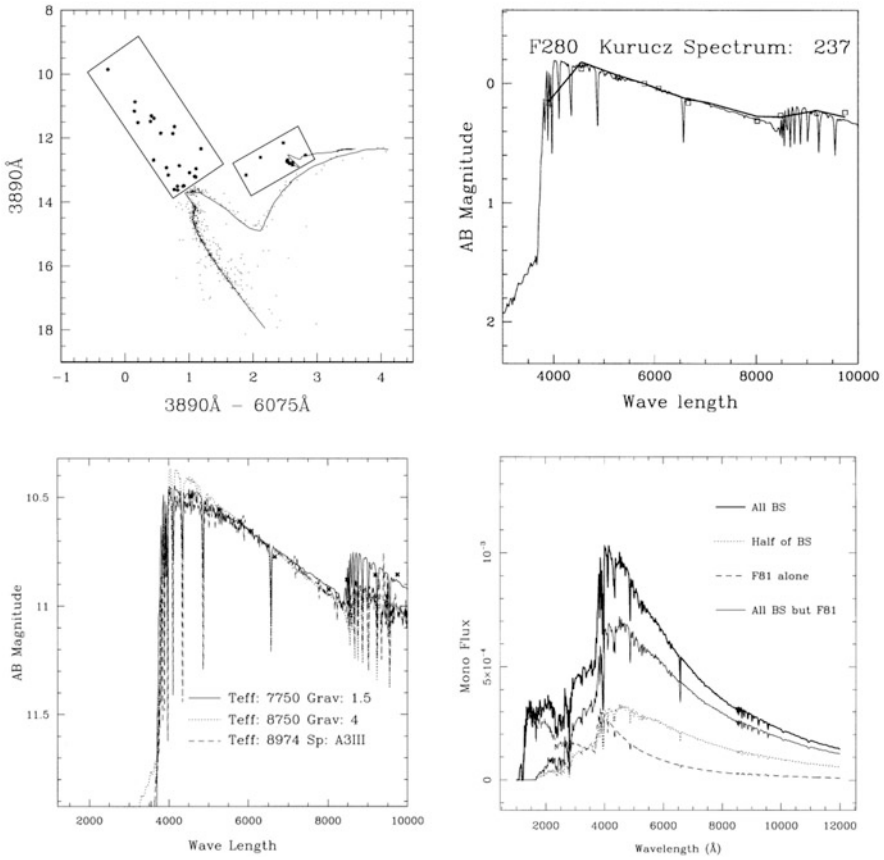

Fig. 14.1 This is an example of building up the integrated spectral energy distribution (ISED) of a star cluster based on accurate spectrophotometry from the BATC survey (Fan et al. 1996). *Upper left panel*: CMD of M67 with all highly probable members, the left box along the extension of the main sequence marks the region of BSSs. *Upper right panel*: assigning a Kurucz spectrum to the star F280. In such a way we can actually determine the parameters of the stars (*lower-left panel*). *Lower right panel*: the ISEDs of the cluster with different combinations of spectral energy contribution to account for the stochastic effect

of stellar populations is now possible. The goal of this chapter is to present a new set of SSP models which include contributions from BSSs.

BSSs are common and easily identified in colour-magnitude diagrams (CMDs) of star clusters. They are members of the host cluster and located above and blueward of the cluster's main-sequence (MS) turn-off. BSSs in a cluster are obviously the most luminous blue stars in the CMD (see the top-left panel of Fig. 14.1), therefore they are the primary contributors in the total light of the cluster. The standard theory of single-star evolution cannot explain the presence of BSSs in SSPs' CMDs, and thus the standard SSP models do not include the contributions of BSSs. All currently

accepted scenarios of BSS formation are related to stellar interactions. Coalescence in primordial binaries can launch BSSs to positions up to 2.5 magnitudes brighter than the MS turn-off (McCrea 1964; Chen and Han 2009). Mergers of binary-binary systems can produce possible BSSs with masses four times those of stars at the MS turn-off (Leonard and Linnell 1992). Given the high luminosities and common presence of BSSs in stellar systems (e.g., Ahumada and Lapasset 1995 for open clusters; Piotto et al. 2002 for globular clusters; Mapelli et al. 2009 for dwarf galaxies), we believe that we must consider the effects of BSSs in studies of stellar populations using population synthesis in unresolved observations. The key issue is how to accurately include BSS contributions in SSP models.

Studies show that no single mechanism can account for the entire BSS population observed in any one star cluster (Stryker 1993). This means that it is not easy to theoretically measure the respective contribution of BSSs in SSPs of different ages and metallicities. Although the detailed physical properties of BSSs can be better understood now (see Chaps. 3, 8, 9, and 12), a comprehensive and robust model for BSS content in star clusters is still missing. Therefore, building up BSS population characteristics empirically from the statistics of a large sample of star clusters could be more practical and reliable than relying on incomplete theoretical approaches. In this way, the behaviour of BSSs (in terms of their specific frequency and relative distribution with respect to the MS turn-off in CMDs) can be modelled. Open clusters (OCs) in the Galaxy have a number of advantages for use as a working sample: (a) most have photometric data, thus enabling accurate determination of their fundamental parameters; (b) many have multi-epoch proper motion and/or radial velocity data, so that their cluster membership probabilities can be measured accurately; and (c) they are representative of the environments of stellar populations shortly after their birth. Compared to OCs, globular clusters (GCs) are usually much more massive and often contain multiple stellar populations (e.g., Piotto 2008), which renders them questionable as SSPs.

Preliminary modelling of BSS effects has been done on the basis of individual clusters in our previous papers (Deng et al. 1999; Xin and Deng 2005; Xin et al. 2007, 2008), where we (a) introduced the method used for calculating the realistic, integrated spectrum of a star cluster including the contribution of BSSs; (b) analysed the modifications to the integrated spectra and the broad-band colours caused by BSSs; and (c) estimated the possible uncertainties in the conventional SSP models, showing that the ages of star clusters can be underestimated by up to 50 % if BSS contributions are not considered. To overcome such a great discrepancy, we present a set of BSS-SSP models based on a statistical study of galactic OCs. Our models cover the wavelength range from 91 Å to 160 μm, ages from 0.1 to 20 Gyr and metallicities $Z = 0.0004, 0.004, 0.008, 0.02$ (solar metallicity) and 0.05.

This chapter is organised as follows. In Sect. 14.2, we demonstrate how BSSs can affect the integrated spectral properties of a star cluster, taking one of the most studied old clusters, M67, as an example. In Sect. 14.3, we present the

statistical results of the properties of BSS populations based on 100 Galactic OCs, supplemented by a few rich GCs in Magellanic clouds in Sect. 14.4. In Sect. 14.5, we describe the construction procedure of our models, as a generalised method based on that for M67, and we discuss our model results and compare them with those of Bruzual and Charlot (2003, hereafter BC03). Finally, a summary, brief discussion and prospectives are presented in Sect. 14.6.

14.2 M67: Setting Up the Scheme

We started to consider quantitatively the effects of BSS on the integrated spectral properties of star clusters, and to constrain the theoretical models of SSPs in 1999 using the well studied and relatively rich galactic OC, M67 (Deng et al. 1999).

Almost all bright stars in the cluster region (about 1° in diameter) have reliable membership information, which is very important to the argument we want to pursue. This cluster was observed using a 15 intermediate-band filter photometric system covering the whole optical wavelength range between 3,000 and 10,000 Å (BATC survey, Fan et al. 1996). Such an observation is ideally suited for our purpose. Figure 14.1 demonstrated the key steps to build the integrated spectral energy distribution (ISED) of the cluster:

- First of all, we need to find out the BSS members in the cluster. The upper left panel is a CMD of the cluster in two passbands (centred at 3,890 and 6,075 Å, respectively), with the x-axis being the colour—defined as the difference between magnitudes in two bands. All the BSSs confined by the left box at the upper bluer extension of the MS are almost sure members of M67.
- The upper right panel show how precisely we can anchor a *Kurucz* spectrum to the observed spectral energy distribution (SED) determined in all the filters for the famous BSS member F280 in M67. In fact, a BSS star may not be a single star, therefore it is not possible to have parameters that are defined for single stars, such as effective temperature and gravity. Thus, the spectrum assigned to the star this way is a "pseudo" but still constitutes an useful approximation. The spectrum assigned is indeed close enough and can represent the star's spectral property.
- In this way, we can then accurately derive its "physical parameters", given the metallicity is solar as measured by numerous other observations (presumably also treated as single stars). This is demonstrated in the lower left panel. In our work, we assumed that the BSSs can be taken as single stars in terms of spectral properties.
- The ISED of the cluster is obtained by summing up individual SED of all bright members. To account for possible stochastic effects due to the low number of BSSs, we plotted different combinations of BSS sample in M67 (lower right panel).

As a conclusion, the ISED of M67 built this way is apparently different from that of the theoretical SSP model corresponding to its age and metallicity. We further point out that, with the existence of BSSs, and when observed at unresolved conditions (such as in remote galaxies), the actual stellar population may appear substantially younger and/or more metal poor, sometimes containing less total mass compared to standard SSP models. M67 is just a typical old age cluster in our Galaxy, that can represent real stellar population of similar age and metallicity in any other galaxies, which means, the widely used conventional SSP models in EPS need to be modified in order to be correctly applied to the analysis of stellar content in galaxies.

Thanks to the accurate but elaborate 15 intermediate band photometry (Deng et al. 1999), the technique to build the ISED of M67 based on photometric observations is very unique and reliable. However, BATC photometry is not available for the entire galactic OC sample. Other photometry, including broadband, can also be helpful. The methodology is defined in Sect. 14.5.2.

14.3 ISEDs of Galactic Open Clusters

Building up a library of ISEDs of a large sample of star clusters is an observational approach towards realistic SSP models. Such a library can also be used to constrain theoretical efforts towards the same aim. By using the existing photometry and membership information of galactic star clusters, we have carried out a series of work in the past few years (Xin and Deng 2005; Xin et al. 2011, 2008, 2007).

Galactic OCs are the most studied stellar systems in the Galaxy, and have relatively more information about their physical properties including membership, age, metallicity, etc. However, the content of BSSs in OCs is rather stochastic due to the limited number of stars and BSSs, while all the BSS population may involve different ways of formation, and can be affected by dynamical processes in the cluster and with their environment.

In Xin and Deng (2005), a small sample of 27 Galactic OCs from Ahumada and Lapasset (1995; AL95 in the following) was selected to discuss the BSS contribution in a statistical way. The BSS population is better presented in the CMD of older OCs, thus the 27 OCs are all older than 1 Gyr, and provide a constraint to SSP models of the same age and metallicity range.

The basic parameters of the selected clusters are given in Table 1 of Xin and Deng (2005), where columns (1)–(3) give the cluster name, right ascension, and declination (J2000.0); columns (4)–(7) are the ages, colour excesses $[E(B-V)]$, distance moduli (DMs) and metallicities (Z) of the clusters; the number of BSSs, $N_{\rm BSS}$, and N_2 values are listed in columns (8) and (9), respectively; and finally, column (10) is the reference number. Values of $N_{\rm BSS}$ and BSS photometric data for selected clusters are quoted directly from AL95. The N_2, defined as the number

of stars within an interval of two magnitudes below the turn-off point for a given cluster (see detailed discussion in Sect. 14.5), is also from AL95. The other basic parameters of the selected clusters, specifically the age, Z, $E(B-V)$, and DM, are extracted from the more recent photometric and theoretical work when results newer than AL95 are available.

N_2 is regarded as a very important parameter that indicates the richness of the theoretical stellar component in the simple population synthesis scheme. For each cluster, this count is made in the same CMD from which the BSSs are selected. Then the ratio $N_{\rm BSS}/N_2$ can be taken as a specific BSS frequency in a cluster and can be used as a probe for the cluster internal dynamic processes concerning BSS formation.

It is worth emphasising here that not all the clusters have complete membership determinations in terms of both proper motion and radial velocity. The selection of BSS candidates in AL95 is basically according to where they appear in the observed CMDs. In our work, all the BSSs are treated equally, without any further detailed membership measurements and BSS identification.

In order to demonstrate the effects of BSSs on the conventional ISEDs in the case of old OCs, we construct the ISED of the normal star and the BSS population in one cluster separately. The steps of how we build the composite SSP models including BSS contribution will be presented in details in Sect. 14.5. The results with the OC samples were rather stochastic due to the small number of BSSs, or because of the small total number of stars in a given cluster. The ISEDs vary from BSS dominant—one or a few very bright BSSs—or one in which BSSs contribute nothing to the ISED (see Fig. 4 in Xin et al. 2007), and discussions on statistics there. This remind us that rich star clusters should be used, or find a proper way to enhance statistics of the OC sample such as binning the clusters in parameter space (see Sect. 14.5.1).

14.4 The Massive Star Clusters in the LMC and SMC

Star clusters in the Magellanic Clouds are massive and have a large span in age. Unlike the globular clusters in the Galaxy, they represent much better stellar populations in age coverage, and therefore serve as great targets for our work. In this section, the LMC cluster ESO 121-SC03 is analysed as the first example to detect BSS contributions to the conventional SSP models using a massive intermediate-age cluster in a low-metallicity environment. ESO 121-SC03 is a distant northern Large Magellanic Cloud (LMC) cluster, lying at a projected angular separation of 10 degrees from the LMC centre. It is described as a unique LMC cluster by Mackey et al. (2006), because it is the only known cluster to lie in the LMC age gap. A significant number of previous studies (e.g., Bica and Alloin 1986; Mateo et al. 1986; Mackey et al. 2006) claim an absolute age for ESO 121-SC03 in the

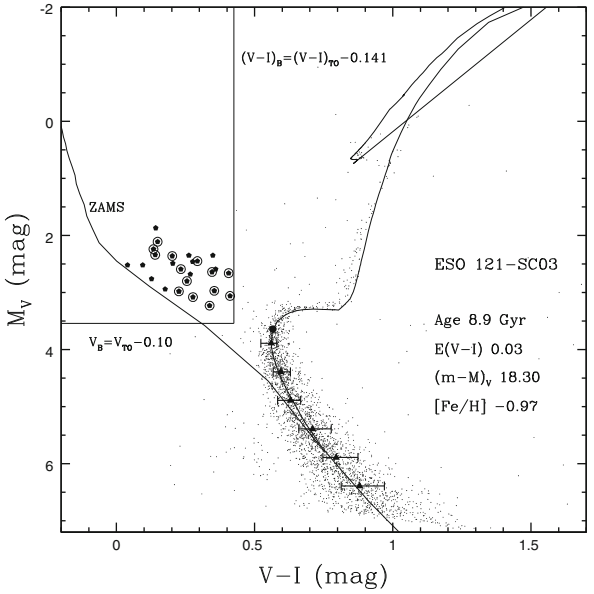

Fig. 14.2 Cleaned CMD for ESO 121-SC03. The best-fitting Padova 2000 isochrone is overplotted. The corresponding fit parameters are included in the figure legend. In the CMD, we define a region that we will use for the identification of the cluster's BSS population. The ZAMS is the Padova 1994 isochrone at $\log(\text{age year}^{-1}) = 6.60$ and $[\text{Fe/H}] = -0.97$ dex. The *solid bullet* is the cluster's MS turn-off. The *solid triangles* represent the MS ridge line of the cluster. Pentagons are BSSs. *Pentagons with circles* are BSSs inside the half-light radius (R_{HL}) of the cluster

range of 8–10 Gyr. Mateo et al. (1986) obtained $[\text{Fe/H}] = -0.9 \pm 0.2$ combined with a reddening of $\text{E}(B-V) = 0.03$ mag. Mackey et al. (2006) derive $[\text{Fe/H}] = -0.97 \pm 0.01$ and $E(V-I) = 0.04 \pm 0.02$ for the cluster. They also mark a region in the CMD used to define BSS candidates in the cluster, but they do not study the BSS population in detail.

As shown in Fig. 14.2, ESO 121-SC03 is a "clean" cluster and includes an obvious population of BSS candidates, which is very advantageous for our main aim of analysing the BSS contributions to the ISED of the cluster. This example demonstrated that, with statistics better than Galactic OCs, BSSs may have significant contributions to a stellar population (Xin et al. 2008). Figure 14.3 shows the ISED of the cluster and how it is affected. With either BSSs only in the half-light radius (R_{HL}) or full sample in the cluster, apparent alternation due to BSSs to the theoretical ISED of its SSP model (the think solid line) is present. The change is stronger for the full sample, and the changes are always more prominent in the shorter wavelengths. This may actually infer either a younger age or lower metallicity when observed at unresolved conditions.

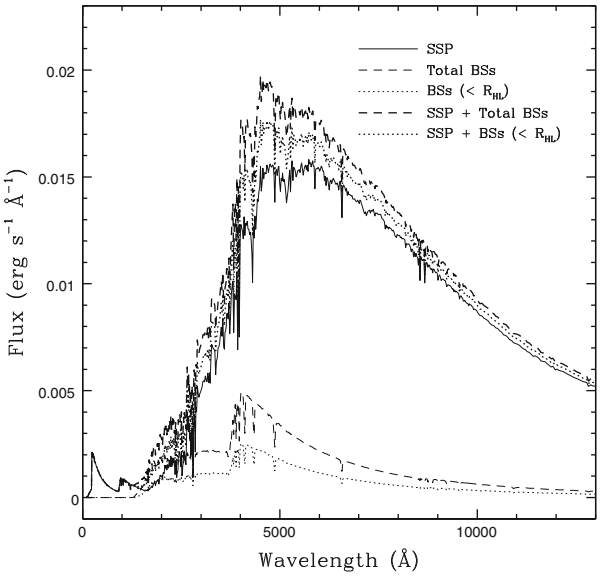

Fig. 14.3 ISED modifications. The BSS contributions are presented for two cases. The *solid line* is the ISED of the SSP component. The *thin dotted line* is the ISED of the BSS component for case (i): BSSs within $R_{\rm HL}$. The *thin dashed line* is the ISED of the BSS component for case (ii): all BSSs in the cluster. The *heavy dotted line* is the synthetic ISED of the SSP component and the case (i) BSS component. The *heavy dashed line* is the synthetic ISED of the SSP component and the case (ii) BSS component

Figure 14.4 concludes our work on individual cluster's base. If we fit the ISED of star clusters by using the conventional SSP models, and we compare the ages of the cluster measured by observations of clusters (taking as true age, the horizontal axis), to that of the best fit SSP model (the vertical axis), it is very clear that the fitted ages are substantially younger than the true ages of the clusters for the whole sample of clusters (all types). Quantitatively, at the true age of $\sim$1 Gyr, the deviation is 47 % and it is 63 % at the age of $\sim$10 Gyr. This fact tells us that EPS may have seriously underestimated ages for populations within the age range covered by our sample.

Certainly, a larger sample of such rich clusters with good coverage in both age and metallicity is highly desired in order to constrain the method we proposed. Observational aspects, including detailed individual BSS, statistics of all BSSs in, and their dynamical effects on, rich GCs can be found in Chap. 5.

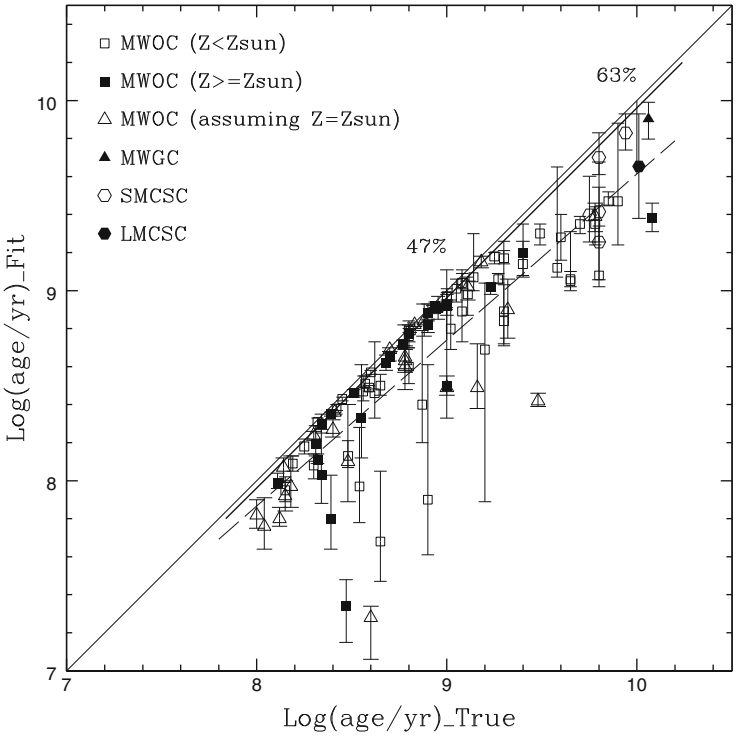

Fig. 14.4 The underestimation of age value by the conventional SSP models. The x-axis is the real age of star clusters, while the y-axis is the best-fitting age from the conventional SSP models. *Different symbols* mean different working samples. The *dashed line* is the least-square fitting of all the data points. The *heavy solid line* is given according to the formula of $t_b = (0.17 + 8.27Z_s) + (1.38 - 14.45Z_s)t_s$ (Li and Han 2008), assuming 50 % binaries in stellar populations and using solar metallicity ($Z_s = 0.02$). Distances between the *diagonal* and the *dashed line* are measured to detect the age uncertainty—$(age_{real} - age_{fit})/age_{real}$. The underestimation of age value by the conventional SSP models becomes larger for older population. It is 47 % at 1 Gyr, and 63 % at 10 Gyr

14.5 Building Up an Empirical SSP Library

In order to create empirically a library for use in EPS, a dataset of observed star clusters covering wide enough parameter space (age, metallicity) has been made available in our previous work. In this section, we are going to describe how the library is actually built.

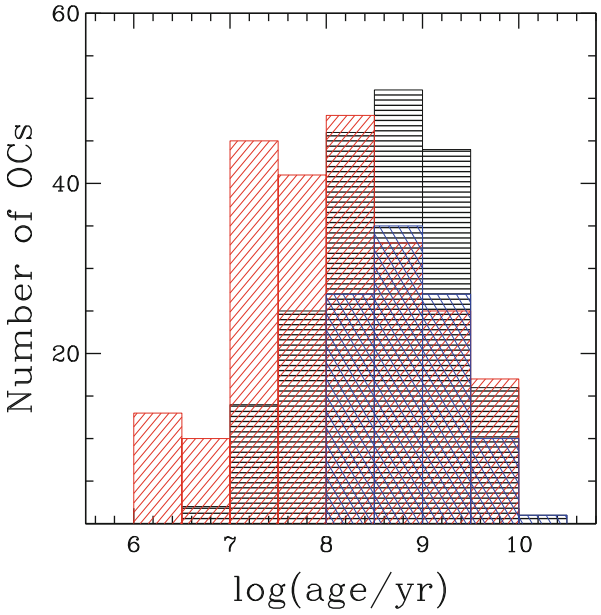

Fig. 14.5 Number distributions of Galactic OCs containing BSSs as a function of age. *Horizontal shading* represents the statistics from the Ahumada and Lapasset (2007) catalogue. The hatching from the *bottom left* to the *top right* represents the statistics from AL95, while that from the *top left* to the *bottom right* shows the number distribution of our working sample (100 Galactic OCs)

14.5.1 A General BSS Distribution Function in Stellar Populations

Basically, two properties of BSS populations are relevant to the modelling of BSS behaviour in SSPs, i.e. the number of BSSs ($N_{\rm BSS}$) in the SSP and their distribution in the SSP's CMD. In this paper, both properties are obtained empirically from the observed OCs' CMDs. A working sample including 100 Galactic OCs from the catalogue of AL95 is adopted to secure the reliability of the statistical results.

Figure 14.5 shows the differences among the number distributions of OCs containing BSSs versus age for the Ahumada and Lapasset (2007, hereafter AL07) catalogue (horizontal hatching), the AL95 catalogue (slanted hatching from bottom left to top right) and our sample (slanted hatching from top left to bottom right). AL95 and AL07 published the most complete catalogues to date in terms of photometric data of BSSs in Galactic OCs. They include almost all OCs containing BSSs in the solar neighbourhood. Figure 14.5 shows that, compared to AL95, AL07 dramatically reduced the number of young OCs containing BSSs, mainly because of the difficulty of identifying BSSs in the CMD of a star cluster that does not exhibit at least a fully developed red giant branch (RGB) phase (particularly when information on membership probability is lacking). Moreover, most of the BSSs in

young OCs (i.e., log(age/year) < 8.0 in this work) from both catalogues are located close to the MS turn-off point in the CMD, which means that it is hard to distinguish BSSs from MS stars. Such BSSs cannot effectively modify the spectral intensity of a cluster. Therefore, we start the selection of our working sample based on OCs with log(age/year) ≥ 8.0.

Meanwhile, to construct a spectrum of the BSS population for a given OC, we need to obtain the physical parameters of the BSSs in the CMD of the OC. To do this, we need the age, metallicity, colour excess and distance modulus for each OC, which are not all included in either AL95 or AL07. Therefore, we decided to keep only the photometric data of BSSs from AL95, to ensure a homogeneous selection of the BSS sample. We collected the remaining OC parameters from the recent literature (see Table 1 in Xin et al. 2007). In practice, OCs with log(age/year) ≥ 8.0 from AL95 are included as sample clusters if reliable parameters can be found, in the sense that most of the BSSs are located at reasonable positions in the CMD with respect to the Padova 1994 isochrone for the OC's age and metallicity.

There are 33 OCs with age $\geq$ 1.0 Gyr in the combined catalogue comprised of AL95, AL07 and our working sample. Older OCs have better statistics as regards their BSS populations. Using the photometric data of the BSSs in these 33 OCs as an example, we analysed the BSS distribution functions versus the MS turn-off point, as a function of M_V and $(B-V)$. In such a way, we can detect differences in the BSS distributions in the CMD between the AL95 and AL07 statistics. It is shown that the distribution functions of both M_V and $(B-V)$ do not exhibit any essential differences between the AL95 and the AL07 catalogues. Therefore, we continue on the basis of the results from our previous work, i.e. the parameters of the sample clusters and the BSS population from AL95.

Details of the BSS properties are presented in Figs. 14.6, 14.7, and 14.8. Figure 14.6 shows $N_{\rm BSS}$ as a function of the age, metallicity and richness of the sample OCs. The richness of a star cluster is represented by N_2, which is the number of cluster member stars within two magnitudes below the cluster's MS turn-off. The open circles represent the results for the 100 Galactic OCs. Because of the small number of member stars and even smaller number of BSSs in the individual OCs, the results directly derived from Fig. 14.6 are very stochastic, and thus we use the ratio of $N_{\rm BSS}/N_2$ to reduce the effects of stochasticity. We use this ratio as definition of the specific frequency of BSS components in SSPs. We calculated the standard deviation (σ) of the ratio for the entire sample, i.e., $\sigma = \sqrt{\frac{\sum_{i=1}^{N}(\frac{N_{\rm BSS}}{N_2}_i - \overline{\frac{N_{\rm BSS}}{N_2}})^2}{N\times(N-1)}}$ and $N = 100$. We marked the OCs with $\frac{N_{\rm BSS}}{N_2} \leq \overline{\frac{N_{\rm BSS}}{N_2}} + 1\sigma$ with filled circles in Fig. 14.6.

The left-hand panel in Fig. 14.6 shows $N_{\rm BSS}$ versus cluster age on a logarithmic scale. $N_{\rm BSS}$ seems largely insensitive to age until a sudden increase for ages greater than 1.0 Gyr. Based on this figure it is hard to discern any correlation between the two parameters, and it is also risky to jump to the conclusion that $N_{\rm BSS}$ is not correlated with age. The seemingly constant $N_{\rm BSS}$ for age <1.0 Gyr could be caused by the confusion of defining an accurate MS turn-off point and a BSS population in relatively young star clusters. In our model construction, we have not adopted

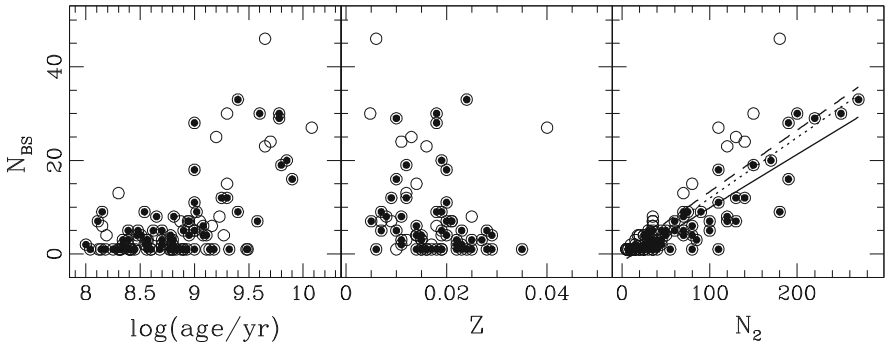

Fig. 14.6 Correlations (if any) between $N_{\rm BSS}$ and the age, metallicity and richness (N_2) of Galactic OCs, respectively. The *open circles* show the results for the 100 OCs in our working sample. The *filled circles* mark the OCs with $N_{\rm BSS}/N_2$ less than the average ratio plus 1σ (standard deviation). The *solid line* in the right-hand panel is the least-squares fit to the *filled circles*; it is given by Eq. (14.1). For reference, the *dotted line* in the right-hand panel is the least-squares fit to all OCs (*open circles*), and the dashed line is the fit to OCs with ages $\geq$ 1.0 Gyr

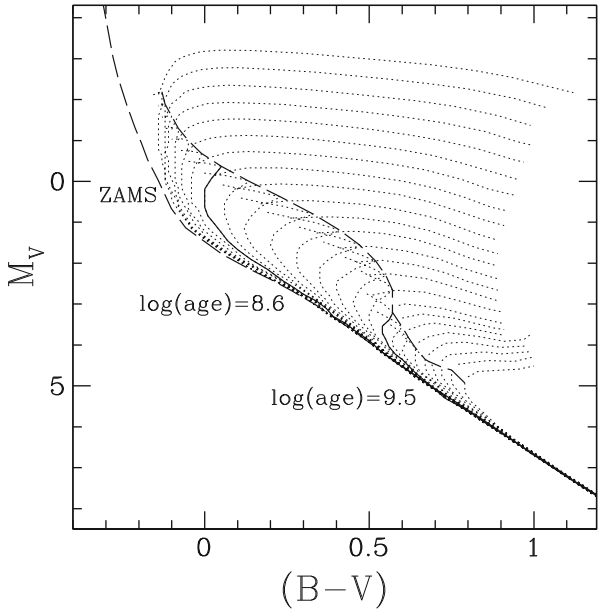

Fig. 14.7 Criteria used for our age-bin selection. The *dotted lines* are the isochrones for ages between 0.1 and 20 Gyr, truncated at the bottom of the RGB phase. The *two dashed lines* mark the MS stage between the zero-age MS (ZAMS) and terminal-age MS (TAMS). The choice of age bin is shown as the *solid lines*

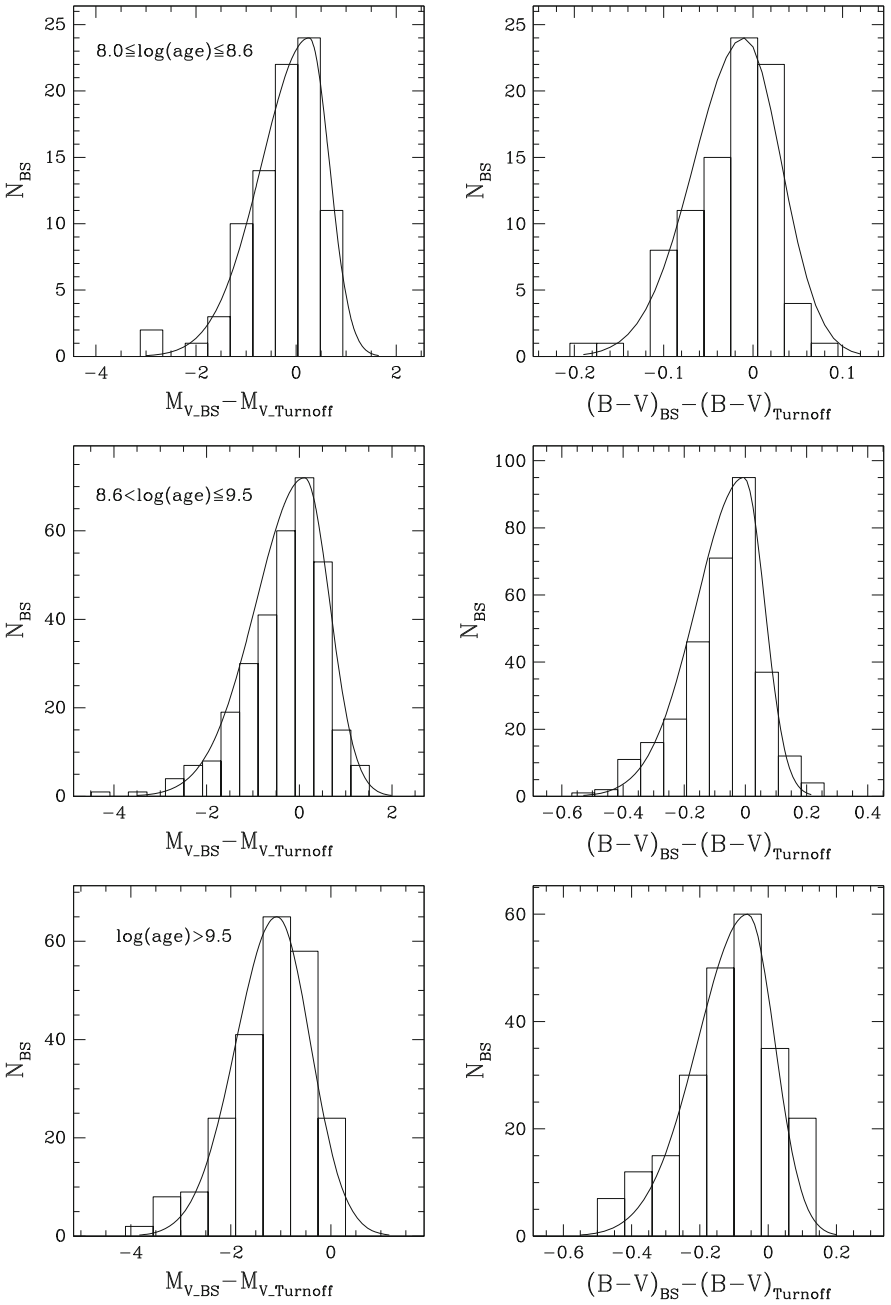

Fig. 14.8 BSS distribution functions in our OCs' CMDs in three different age bins as a function of M_V (*left panels*) and the $(B-V)$ (*right panels*). In each panel, a Gaussian profile is used to describe either side of the peak separately

any correlation between $N_{\rm BSS}$ and age. The only correlation we used is that between $N_{\rm BSS}$ and N_2 (shown in the right-hand panel in Fig. 14.6; see below). In fact, for SSPs, $N_{\rm BSS}$ and age are related through the SSP's N_2. N_2 increases following the initial mass function (IMF) slope as the SSP ages, and so does $N_{\rm BSS}$ through the correlation between $N_{\rm BSS}$ and N_2.

The middle panel of Fig. 14.6 shows $N_{\rm BSS}$ as a function of metallicity for our sample OCs with published metallicity information. No correlation can be established. We previously studied whether the BSS strengths are sensitive to metallicity. We did not find any obvious correlation between these two parameters either (see Fig. 18 in Xin and Deng 2005).

The right-hand panel of Fig. 14.6 clearly shows that only $N_{\rm BSS}$ and N_2 are correlated. The implication of this correlation is that $N_{\rm BSS}$ is proportional to the richness of an SSP, but not (at least not obviously) to any other parameter, such as age or metallicity. The solid line in the right-hand panel is the least-squares fit to the filled circles. For reference, we present two more fits for different samples. The dotted line is the least-squares fit to all OCs (open circles), while the dashed line is the fit to those OCs that are older than 1.0 Gyr. It is hard to tell which fit is most accurate. We choose the solid line for estimating $N_{\rm BSS}$ in an SSP simply to avoid exaggeration of the BSS-enhanced intensity in our SSPs. The correlation can be empirically described as

$$N_{\rm BSS} = (0.114 \pm 0.006) \times N_2 - (1.549 \pm 0.731). \tag{14.1}$$

The uncertainties in the coefficients result from the 1σ uncertainty in $N_{\rm BSS}/N_2$.

The loci of BSSs in cluster CMDs are fixed by their formation and evolutionary processes (Ferraro et al. 2009), which could still be stochastic owing to the varying physical conditions among star clusters. Thus, it is impossible to construct the specific distribution function of the BSS population for each individual SSP. A feasible approach to generate a BSS population in the CMD is to work out a uniform BSS distribution function.

The dotted lines in Fig. 14.7 are isochrones with ages between 0.1 and 20 Gyr, truncated at the bottom of the RGB phase. The two dashed lines, i.e. the zero age MS (ZAMS) and the boundary between the MS and post-MS phases, highlight the entire MS stage for all isochrones. The distance between the two dashed lines becomes narrower in the colour range in the CMD for older—$\log(\text{age/year}) \geq 9.5$—and younger—$\log(\text{age/year}) \leq 8.6$—SSPs, which means that a uniform BSS distribution function will certainly push a BSS population towards red colours for SSPs with a MS turn-off close to the ZAMS. To avoid uncertainties associated with the distance between the MS turn-off points and the ZAMS, we consider BSS distribution functions in three different age bins, i.e., $8.0 \leq \log(\text{age/year}) \leq 8.6$, $8.6 < \log(\text{age/year}) \leq 9.5$, and $\log(\text{age/year}) > 9.5$. The solid lines in the figure show the age-bin selection.

Since the bin selection is done empirically, we tested that a small change in the age-bin selection, i.e., $\Delta \log(\text{age/year}) = 0.1$, cannot effectively modify the BSS distribution in the CMDs and, consequently, affect our model results. Specifically,

we construct the BSS distribution functions with log(age/year) = 8.6 included in the older age bin and calculate the $(U - B)$ and $(B - V)$ colours of the SSP with $Z = 0.02$ and log(age/year) = 8.6. The colour changes resulting from adopting different distribution functions are <0.0001 mag for both colours. The same result is found for a test with log(age/year) = 9.5.

We align the MS turn-off points of all OCs in our working sample to obtain a sufficient number of BSSs for good statistics. Figure 14.8 shows the distribution functions of BSSs versus the MS turn-off point in three different age bins as a function of M_V (left panels) and $(B-V)$ (right panels). For each of the distributions, a Gaussian profile is adopted to fit either side of the peak separately, based on which we construct the BSS population in the CMD of an SSP using Monte Carlo simulations in two dimensions (M_V and $(B - V)$). All Gaussian profiles have the same standard format,

$$f(x) = \exp\left[-\frac{(x-\mu)^2}{2\sigma^2}\right], \tag{14.2}$$

where μ is the peak position and σ the standard deviation. The notation $x = \Delta M_V = M_{V_{\rm BSS}} - M_{V_{\rm TO}}$ refers to the increment in luminosity (M_V) of a BSS with respect to the SSP's turn-off luminosity; $x = \Delta(B-V) = (B-V)_{\rm BSS} - (B-V)_{\rm TO}$ is the equivalent increment in colour index $(B - V)$. The specific values of μ and σ for different x ranges are listed in Table 14.1. Here, $f^-(x)$ and $f^+(x)$ refer to the left- and right-hand sides of the Gaussian profiles, respectively.

Since the distribution functions are constructed empirically from observational statistics, the values of both μ and σ are inevitably sensitive to the selection of the bin size. To find reasonable descriptions for the Gaussian profiles, we start exploring the statistics of M_V and $(B - V)$ in each age bin with a bin size of $\Delta M_V = 0.20$ and $\Delta(B - V) = 0.010$ mag, and we subsequently increase the bin size in steps of $\Delta M_V = 0.05$ and $\Delta(B - V) = 0.005$ mag until the distribution resembles a Gaussian function. The adopted bin sizes for ΔM_V and $\Delta(B - V)$ for each age bin are given in column (3) of Table 14.1. The μ and σ values listed in the table are calculated based on the corresponding bin size.

In addition to the distribution function, a further boundary that also constrains BSS positions in the CMD is the ZAMS. Any BSSs located beyond the ZAMS, i.e., with bluer colours than the ZAMS for the same luminosity, will not be generated by our program. This assumption is made mainly because we treat BSSs as MS stars and describe them using standard MS models.

Our sample of 100 Galactic OCs has limited parameter coverage in age and metallicity, i.e. it covers ages from 0.1 to 12 Gyr and metallicities from $Z = 0.0048$ to 0.035 (Xin et al. 2007, their Table 1). To consider the BSS contributions for the full set of SSP models, some extrapolations of the parameter space have been adopted based on the results from OCs and some reliable working assumptions: (a) ages from 0.1 to 20 Gyr, with the lower limit set by the difficulty to identify BSS components in star clusters younger than 100 Myr, while the BSS properties are not

Table 14.1 Gaussian profile parameters for BSS distribution functions in different age bins

Age bin (year)		Bin size (mag)	μ (mag)	$f^-(x)$		$f^+(x)$	
				σ	x range	σ	x range
$8.0 \leq \log(\text{age}) \leq 8.6$	M_V	0.45	0.26	0.9454	[−3.00, 0.26]	0.4056	[0.26, 1.65]
	$(B-V)$	0.03	−0.01	0.0563	[−0.19, −0.01]	0.0418	[−0.01, 0.12]
$8.6 < \log(\text{age}) \leq 9.5$	M_V	0.40	0.112	1.0464	[−3.50, 0.112]	0.5470	[0.112, 2.00]
	$(B-V)$	0.075	−0.005	0.1544	[−0.530, −0.005]	0.0678	[−0.005, 0.220]
$\log(\text{age}) > 9.5$	M_V	0.55	−1.08	0.8155	[−3.83, −1.08]	0.6711	[−1.08, 1.20]
	$(B-V)$	0.08	−0.06	0.1472	[−0.55, −0.06]	0.0837	[−0.06, 0.20]

expected to change dramatically in very old stellar populations; and (b) metallicities $Z = 0.0004, 0.004, 0.008, 0.02$ and 0.05. We extend the metallicity to a lower boundary of $Z = 0.0004$ and a maximum value of $Z = 0.05$ because the statistics of OCs show that BSS behaviour is not sensitive to metallicity. ($Z = 0.0001$ is not included in the models because horizontal branch stars, instead of BSSs, dominate the energy in the ultraviolet and blue bands in extremely metal-poor populations.)

14.5.2 Building the Empirical SSP Library

With the distribution functions of BSS in a population, it is now possible to build an empirical library of stellar populations. The fundamental ingredients of our models are listed in Table 14.2. For convenience, we use the widely adopted BC03 models as reference. Modifications owing to BSSs are calculated as increments to the BC03 SSPs of the same age and metallicity. We adopted the Padova 1994 isochrones (Bertelli et al. 1994) and the `BaSeL` spectral library (Lejeune et al. 1997) because they homogeneously cover the widest ranges of age and metallicity, and the longest wavelength range. The Padova 2000 isochrones (Girardi et al. 2000) are based on a more recent equation of state and low-temperature opacities compared to Padova 1994. However, we decided against adopting them for our model construction, because BC03 do not recommend to use their SSPs based on the Padova 2000 isochrones. They state that their models based on the Padova 2000 isochrones

> tend to produce worse agreement with observed galaxy colours.

High-resolution observational spectral libraries (e.g., Pickles 1998; Le Borgne et al. 2003) suffer from problems related to limited parameter coverage. Instead of combining spectra from different libraries to enlarge our parameter coverage, we decided to use only the theoretical library.

For consistency with BC03, we adopted the Salpeter (1955) and Chabrier (2003) IMFs. As clearly shown by Dabringhausen et al. (2008),[1] the Chabrier IMF is

Table 14.2 Fundamental ingredients of the BSS-SSP models

Name	Property	Source
Padova1994 isochrones	$Z = 0.0001$–0.05 Age $= 4$ Myr to 20 Gyr	Bertelli et al. (1994)
BaSeL spectral library	91 Å to 160 μm Median resolution $\lambda/\Delta\lambda \approx 300$	Lejeune et al. (1997)
Initial mass function	$\xi(\log\ m) \propto m^{-1.35}$ Table 1 in Chabrier (2003)	Salpeter IMF (1955) Canonical IMF (Kroupa 2002)

[1] See their Fig. 8.

almost indistinguishable from the Kroupa IMF (2001, 2002) when normalised as $\int_{0.1}^{100} \xi(m)\mathrm{d}m = 1\,\mathrm{M}_\odot$, which is exactly how both BC03 and we normalise the SSP models. Using such a normalisation, the slight differences between the two IMFs cannot cause any effective modifications as regards the BSS contribution to SSPs. Therefore, we refer to the IMF (in addition to the Salpeter IMF) as the "Canonical IMF" throughout this work. It can be conveniently described by a two-part power law, $\xi(m) \propto m^{-\alpha_i}$, with $\alpha_1 = 1.3$ for the stellar-mass range $0.08 \leq m/\mathrm{M}_\odot < 0.5$ and $\alpha_2 = 2.3$ for $m \geq 0.5\,\mathrm{M}_\odot$ (Kroupa 2001), or in terms of a power law plus a lognormal form as presented in Table 1 of Chabrier (2003).

Our construction procedure for SSP models including BSS contributions is summarised as follows: (a) We use the standard models (we use BC03 in this work, but we can in principle use any other SSP flavour as well) to represent the integrated spectrum of the "normal" SSP member stars. We subsequently use the statistical properties of BSSs from Galactic OCs to generate the BSS population for the appropriate SSP; and (b) We calculate the spectrum of the BSS population and combine it with the spectrum of the normal member stars after the appropriate flux calibration. The composite spectrum is the integrated spectrum of the BSS-corrected SSP.

In detail, the model construction includes the following steps:

1. We assume that any given model SSP contains 10^5 original member stars. The corresponding normalisation constant, A, for a given IMF is calculated as

$$10^5 = A \times \int_{m_\mathrm{l}}^{m_\mathrm{u}} \phi(m)\,\mathrm{d}m, \tag{14.3}$$

   where $\phi(m)$ is the IMF, $m_\mathrm{l} = 0.1\,\mathrm{M}_\odot$ and $m_\mathrm{u} = 100\,\mathrm{M}_\odot$.
2. The SSP's N_2 number is calculated using

$$N_2 = A \times \int_{m_1}^{m_2} \phi(m)\,\mathrm{d}m, \tag{14.4}$$

   where m_2 is the mass of the SSP's MS turn-off point and m_1 is the mass on the MS 2 mag below the turn-off point.
3. The SSP's N_BSS then follows from Eq. (14.1).
4. The distribution of the BSS population in the CMD is generated using Monte Carlo simulations in two dimensions in the CMD, i.e., M_V and $(B - V)$, based on the Gaussian profiles described by Eq. (14.2) and Table 14.1.

Figure 14.9 shows the comparison between the observed and modelled BSS populations in the CMDs of four representative Galactic OCs. In each panel, the fundamental cluster parameters are listed in the top right-hand corner, the solid curve is the Padova 1994 isochrone for the cluster's age and metallicity, the dashed line is the ZAMS, the solid circles are the observed BSSs from AL95 and the open squares are the BSSs generated by the Monte Carlo simulation. We calculate $N_\mathrm{BSS\_model}$ from the observed N_2 and Eq. (14.1). Apparently, the BSS distribution fluctuates significantly for different simulations because of the small $N_\mathrm{BSS\_model}$

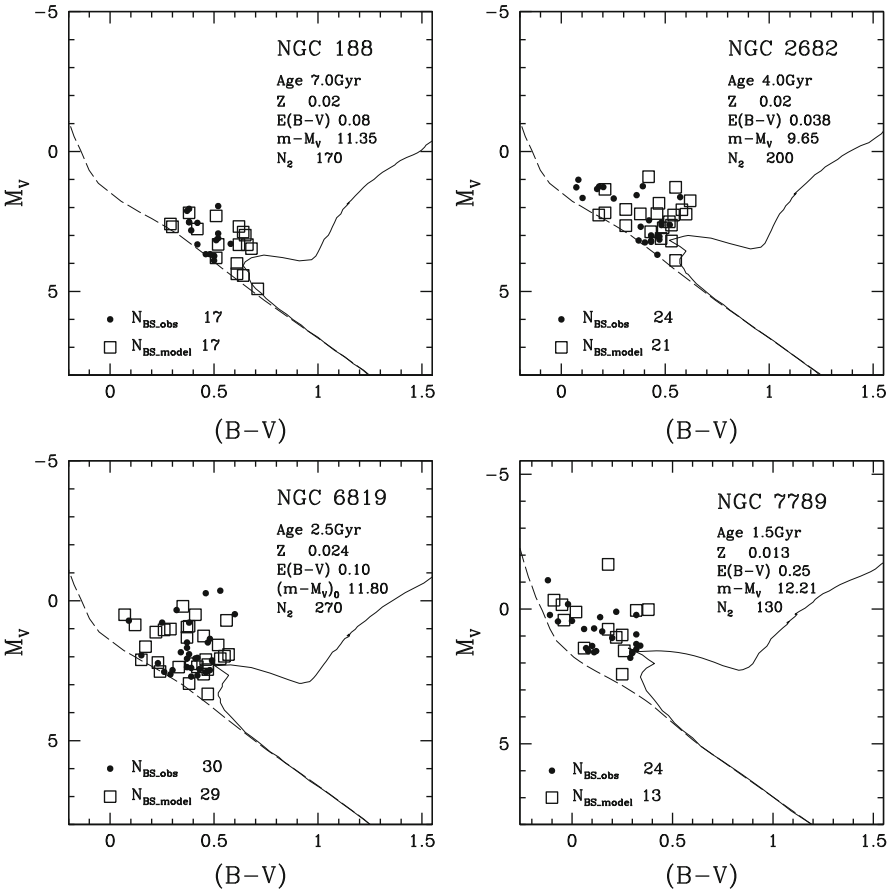

Fig. 14.9 Comparison between the observed and modelled BSS populations in the CMDs of four representative Galactic OCs. In each panel, the fundamental cluster parameters are given in the *top right-hand corner*, the *solid curve* is the isochrone representing the cluster's age and metallicity, the *dashed line* is the zero-age MS, the *solid circles* are the observed BSSs from AL95, and the *open squares* are the model BSSs based on Monte Carlo simulations. $N_{\rm BSS\_model}$ is calculated using the observed value of N_2 in Eq. (14.1)

numbers. What we intend to show with this figure is that the modelled BSS population is quite reasonable and comparable with that observed.

5. Calculate the spectrum of the SSP's BSS population.

For an SSP initially consisting of 10^5 stars, $N_{\rm BSS}$ always spans the range from dozens to at most hundreds of stars for ages between 0.1 and 20 Gyr, which still gives rise to stochastic fluctuations when we generate the BSS population in the CMD. These fluctuations can influence the stability of the spectrum of the BSS population. One of the best ways to reduce this stochastic effect is by using the

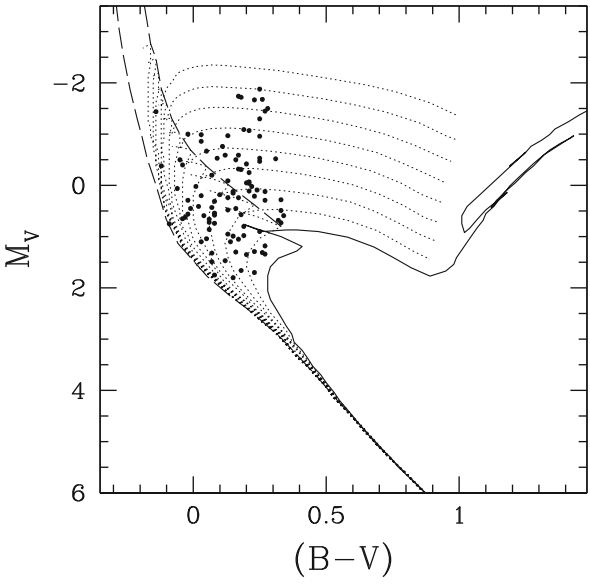

Fig. 14.10 Derivation of the basic parameters of BSSs in the CMD of a given cluster. The *solid dots* are the model BSSs, the *solid curve* is the isochrone for the SSP's age and metallicity corresponding to the cluster, and the *dotted lines* are isochrones representing ages younger than the SSP and truncated at the bottom of the RGB phase, that determine the fitted parameters and spectra of the BSSs. The *dashed lines* are the ZAMS and boundary between the MS and the end of the MS stages, respectively

average of a large number of models. To find the optimum number of realisations, (a) we repeat the generation of BSS populations in the CMD for a given SSP 500 times (500 models) and we subsequently calculate the corresponding composite spectrum of the SSP. This implies that the 500 models yield 500 different spectra for the same SSP. (b) We calculate the broad-band colours $(U - B)$, $(B - V)$ and $(V - R)$ for the SSP based on the average of the spectra of a successively increasing number till 500. This calculation results in 500 values for each colour. (c) We calculate the average of each colour using the colour values for between 200 and 500 models, thus quantifying the differences (δ) of the 500 colour values and the average colour. Finally, (d) we identify the number of models adopted to repeat generating the BSS population in the CMD as the number for which $\delta < 0.0005$ mag. Using the solar-metallicity SSPs as templates, we conclude that combining 100 models is a safe choice for SSPs characterised by different ages and IMFs.

To construct the spectrum of the model BSS population, we use Padova 1994 isochrones of the same metallicity but younger ages than the SSP to fit the position of each BSS in the CMD. We then derive the effective temperature ($T_{\rm eff}$) and surface gravity ($\log g$) by interpolation between two isochrones straddling the BSS. A demonstration of this procedure is included in Fig. 14.10. The solid dots are the model BSSs, the solid line is the isochrone for the SSP's age and metallicity and the dotted lines are isochrones with ages younger than the SSP and truncated at the bottom of the RGB phase. The dashed lines are the ZAMS and the boundary of the MS and post-MS stages, respectively. In our model construction, BSSs located

between the dashed lines are modelled strictly assuming that they can be represented by the MS phases of the isochrones and the remainder of the BSSs located outside the boundary are fitted with post-MS (and pre-RGB) phases.

Depending on the values of $T_{\rm eff}$ and $\log\, g$, a spectrum is extracted from the Lejeune et al. (1997) spectral library and assigned to the BSS. The flux of the BSS spectrum is then calibrated using the BSS's absolute magnitude and, finally, the spectrum of the BSS population is obtained by adding up all flux-calibrated BSS spectra, i.e., $F_{\rm BSS} = \sum_{i=1}^{N_{\rm BSS}} f_{\rm BSS}^{i}$.

The approximation to use the spectra of single MS stars to represent the spectra of BSSs is made based on both theoretical (e.g., Benz and Hills 1987, 1992) and observational (e.g., Liu et al. 2008; Shetrone and Sandquist 2000) considerations. The major formation scenarios of BSSs, such as mergers of primordial binaries and dynamical encounters between stars, can replenish fresh hydrogen fuel in the core and rejuvenate BSSs to the MS stage. Liu et al. (2008) studied the spectral properties of a complete sample of 24 BSSs in M67 based on spectroscopic observations with a resolution of 3.2 Å pixel^{-1} and covering wavelengths of 3,600–6,900 Å. They concluded that BSS spectra can be well represented by the theoretical spectra of single stars, at least at medium resolution.

6. We use BC03 models to represent the spectrum of the population of normal member stars in an SSP (i.e., all member stars except the BSSs).

For a conventional SSP of age t and metallicity Z, the integrated spectrum is given by

$$F_{\rm SSP}(\lambda, t, Z) = B \times \int_{m_{\rm l}}^{m_{\rm u}} \phi(m)\, f(\lambda, m, t, Z)\, {\rm d}m, \tag{14.5}$$

where $\phi(m)$ is the IMF, $f(\lambda, m, t, Z)$ is the spectrum of a single star of mass m, age t and metallicity Z, $m_{\rm u}$ and $m_{\rm l}$ are the upper and lower integration limits in mass, respectively, and 'B' is the normalisation constant required to restore the real intensity of the flux of the conventional SSP.

Since BC03 normalised the total mass of their model SSPs to 1 $\rm M_{\odot}$ at $t = 0$, 'B' is the total mass of the model SSP containing 10^5 stars at $t = 0$:

$$M_{\rm tot} = B = A \times \int_{m_1}^{m_2} \phi(m) m\, {\rm d}m, \tag{14.6}$$

where 'A' is the normalisation constant from Eq. (14.3), $m_1 = 0.1$ and $m_2 = 100\, \rm M_{\odot}$.

Similarly as for the calibration of the BSS spectra, the flux of the conventional SSP is also calibrated based on its absolute magnitude. $M_{\rm tot}$ is used to calculate M_V

of the conventional SSP (M_{V_SSP}) based on Eq. (14.7), in which $M_{V\_\mathrm{SSP(BC03)}}$ is the absolute magnitude of the corresponding BC03 SSP[2]:

$$M_{V\_\mathrm{SSP}} = M_{V\_\mathrm{SSP(BC03)}} + 2.5 \times \log_{10}(1/M_{\mathrm{tot}}) \tag{14.7}$$

7. After flux calibration, direct combination of the spectra of the BSS population and the conventional SSP yields the spectrum of the BSS-corrected SSP. As our final step, the composite spectra are normalised to the BC03 models by adopting the flux-calibration constant derived from Eq. (14.7) for each SSP.

As an SSP ages, the SSP's BSS population evolves to redder colours in the CMD following the movement of the SSP's MS turn-off, which implies that the "blue" in "blue stragglers" only means "bluer than the MS turn-off", not necessarily blue in colour. Since young SSPs (age <0.1 Gyr) are not included in our models, and because of the presence of "yellow stragglers" in the AL95 catalogue, we decided to explore the BSS contributions to the integrated-light properties involving U-, B- and V-band energies, because they may all be significant. Specifically, we present and discuss in detail the differences in the ISEDs, broad-band colours and mass-to-light ratios (M/L_V) between our models and those published by BC03 in this section.

Using the $Z = 0.02$ models with a Salpeter IMF as example, the differences in the ISEDs between two models of different age (top left-hand panel) and metallicity (top right-hand panel) are given in Fig. 14.11. The solid lines in the top panels represent the BC03 ISEDs, while the dashed lines represent the ISEDs from our models. Since the BSS contribution is calculated as an increment to the BC03 models, the intensities of the corresponding BC03 ISEDs of different age (bottom left-hand panel) and metallicity (bottom right-hand panel) are also given in the figure.

The differences presented in the top left-hand panel show a tendency for a stronger BSS contribution for younger SSPs. BSSs have a significant effect on ISEDs for ages between 0.1 and 1.0 Gyr. A sharp enhancement appears in the UV range at 1.0 Gyr for our models, while the UV intensity remains very low in the BC03 ISEDs. During SSP evolution, all massive single stars have left the main sequence and evolved into the red supergiant or the red giant phases in conventional SSPs of 0.1–1.0 Gyr, the UV light declines and the near-infrared intensity increases, and thus BSSs are the most luminous and bluest objects in the populations. For SSPs older than 2.0 Gyr, the intensity of the BSS contribution decreases smoothly and slowly as the population ages. The bottom left-hand panel presents the BC03 ISEDs for different ages, which show that ISEDs are stronger (brighter) for younger SSPs. This tendency is consistent with that found for the BSS contribution to ISEDs of different ages.

[2] M_{tot} actually quantifies the relative increase in M_V with respect to the M_V of an initially 1 $\mathrm{M}_\odot$ SSP.

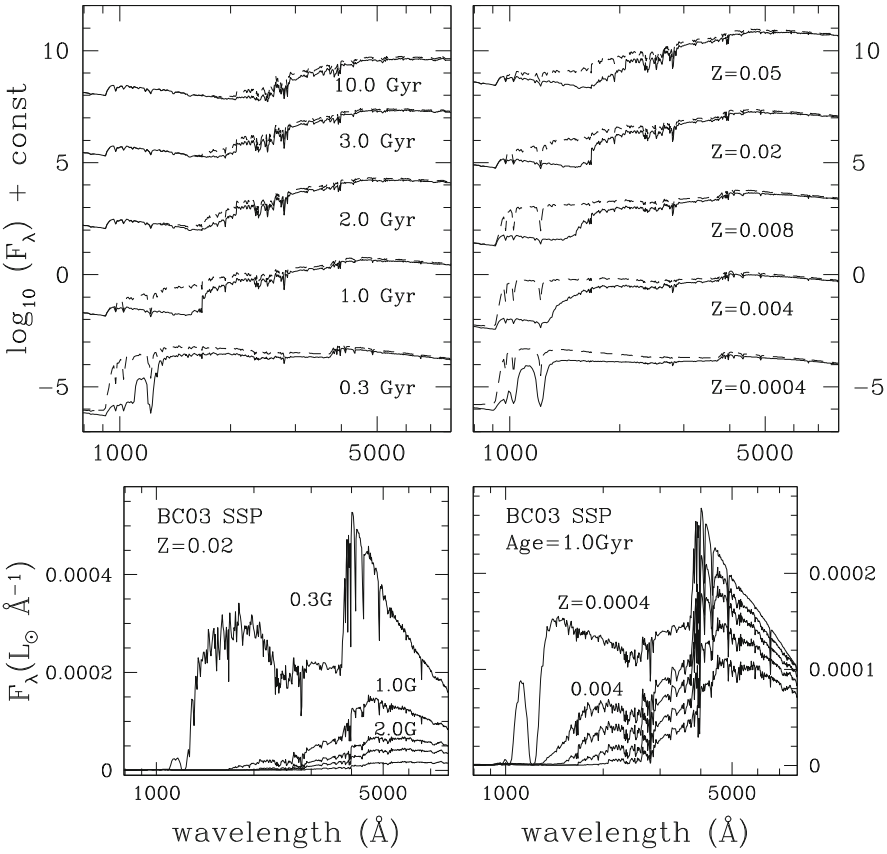

Fig. 14.11 Differences of the integrated spectral energy distributions (ISEDs) between BC03 and our models for different ages (*top left-hand panel*) and metallicities (*top right-hand panel*). The *solid lines* in the top panels are the BC03 ISEDs, while the *dashed lines* are the ISEDs resulting from our models. Because the BSS contribution is calculated as an increment to the BC03 models, the corresponding BC03 ISEDs are shown in the *bottom panels* for reference

14.6 Discussions and Prospectives

Fitting the spectra of unresolved galaxies using SSP models to extract information of their star formation history and current stellar contents has been a routine practice in astrophysics, but stellar populations are never simple as the current theory of stellar evolution (basically of single stars) can predict. BSSs is one of the less understood type of stars, and they are probably one of the most important contributors to the uncertainties in EPS. The other chapters in this book addressed the complicated nature of individual BSSs in both observational and theoretical aspects.

Based on observations of individual star clusters with determinations of BSSs in both numbers and photometric properties, we established a practical method to

build ISED of these clusters and to use them as a constraint for the conventional SSP models and EPS analysis of galaxies. We have shown here the contents of BSSs actually altered the host stellar populations in terms of integrated light. Although there is still a very large uncertainty in the empirical treatment, our results show that EPS really should be built on more realistic SSP models that have all possible stars included properly. By analysing distribution of BSSs in a general composite CMD of all star clusters, we also developed a way to estimate BSS contributions in any stellar populations, and made a spectral library of BSS-SSP models that bares observationally constrained BSS content. The basic description of our BSS-SSP models includes:

1. The models cover the wavelength range from 91 Å to 160 μm, ages from 0.1 to 20 Gyr and metallicities $Z = 0.0004, 0.004, 0.008, 0.02$ (solar metallicity) and 0.05. The metallicity $Z = 0.0001$ is not included, because extended horizontal branch stars, instead of BSSs, dominate the energies in the UV and blue bands in such extremely metal-poor SSPs.
2. The models are constructed as increments to the BC03 standard SSP models using the Padova 1994 isochrones and the Lejeune et al. (1997) stellar spectra. They can thus be used directly in EPS studies as replacement of BC03 for the same parameter coverage. Application of the models should be limited to the "low-resolution" regime. As each BSS spectrum is approximated by the theoretical spectrum of a single MS star, the models cannot fully account for changes in the spectral lines that are related to the formation scenarios of BSSs.
3. The essential effect of BSSs is to make an SSP's ISED hotter in the UV, blue and optical bands, and consequently turn the broadband colours much bluer. Taking the SSP models with $Z = 0.02$ as an example, the differences in the broadband colours between BC03 and our models are 0.10 ± 0.05 mag in $(U - B)$, 0.08 ± 0.02 mag in $(B - V)$, 0.05 ± 0.01 mag in $(V - R)$, 0.12 ± 0.05 mag in $(u - g)$, 0.09 ± 0.02 mag in $(g - r)$ and 0.17 ± 0.03 mag in $(g - z)$.

Given the universal presence of BSSs in various stellar systems, the BSS-SSP models will enable the community to uncover interesting results in studies of stellar populations, despite the number of limitations of the current set of models.[3] The main source of the uncertainties in our work is true BSSs in star clusters. The current catalog of BSSs in star clusters (AL95, AL07) actually came from observations taken with different instruments at different accuracy. A survey of star clusters producing a uniform and accurate catalog is needed. An update to the catalog can be expected in a near future (Deng et al. 2013). Also limited by small numbers of both BSSs and member stars, the statistics of BSS contribution to a cluster (population) is poor. This can be much improved by spectroscopy surveys of a substantially large number of individual stars (including BSSs) in our Galaxy, such as SDSS, LAMOST, Gaia, which can give direct census of BSSs in the Milky Way Galaxy.

[3] Available at: http://sss.bao.ac.cn/bss.

Acknowledgements This work is supported by National Science Foundation of China through grants No. Y111221001 and 10973015. We are also grateful for being invited to this ESO workshop, thanks to the organisers, in particular Giovanni Carraro and Henri Boffin.

References

Ahumada, J. & Lapasset, E.: A&AS **109**, 375 (1995)
Ahumada, J. & Lapasset, E.: A&A **463**, 789 (2007)
Benz, W. & Hills, J.G.: ApJ **323**, 614 (1987)
Benz, W. & Hills, J.G.: ApJ **389**, 546 (1992)
Bertelli, G., Bressan, A., Chiosi, C., Fagotto, F., Nasi, E.: A&AS **106**, 275 (1994)
Bica, E., & Alloin, D.: A&AS **66**, 171 (1986)
Bruzual, G. & Charlot, S.: MNRAS **344**, 1000 (2003)
Chabrier, G.: PASP **115**, 763 (2003)
Chen, X. & Han, Z.: MNRAS **395**, 1822 (2009)
Dabringhausen, J., Hilker, M., Kroupa, P.: MNRAS **386**, 864 (2008)
Deng, L., Chen, R., Liu, X.S., Chen, J.S.: ApJ **524**, 824 (1999)
Deng, L., Xin, Y. , Zhang, X. B., Li, Y.; Jiang, X.J.; Wang, G.M.; Wang, K.; Zhou, J.L.; Yan, Z.Z.; Luo, Z.Q.: IAUS, **288**, 318 (2013)
Fan, X., Burstein, D., Chen, J.S., Zhu, J., Jiang, Z., Wu, H., Yan, H., Zheng, Z., Zhou, X. Fang, L.Z., et al.: AJ **112**, 628 (1996)
Ferraro, F.R., Beccari, G., Dalessandro, E., Lanzoni, B., Sills, A., Rood, R.T., Pecci, F.F., Karakas, A.I., Miocchi, P., Bovinelli, S.: Nature **462**, 1028 (2009)
Girardi, L., Bressan, A., Bertelli, G., Chiosi, C.: A&AS **141**, 371 (2000)
Kroupa, P.: MNRAS **322**, 231 (2001)
Kroupa, P.: Science **295**, 82 (2002)
Le Borgne, J.F., Bruzual, G., Pello, R., Lancon, A., Rocca-Volmerange, B., Sanahuja, B., Schaerer, D., Soubiran, C., Vilchez-Gomez, R.: A&A **402**, 433 (2003)
Leitherer, C., Schaerer, D., Goldader, J.D., González Delgado, R.M., Robert, C., Kune, D.F., de Mello, D.F., Devost, D., Heckman, T.M.: ApJS **123**, 3 (1999)
Lejeune, T., Cuisinier, F., Buser, R.: A&AS **125**, 229 (1997)
Leonard, P.J.T. & Linnell, A.P.: AJ **103**, 1928 (1992)
Li, Z. & Han, Z.: ApJ **685**, 225 (2008)
Liu, G.Q., Deng, L., Chávez, M., Bertone, E., Davo, A.H., Mata-Chávez, M.D.: MNRAS **390**, 665 (2008)
Mackey, M.C., Payne, M.J., Gilmore, G.F.: MNRAS **369**, 921 (2006)
Mapelli, M., Ripamonti, E., Battaglia, G., Tolstoy, E., Irwin, M.J., Moore, B., Sigurdsson, S.: MNRAS **396**, 1771 (2009)
Mateo, M., Hodeg, P., Schommer, R.A.: ApJ **311**, 113 (1986)
McCrea, W.H.: MNRAS **128**, 147 (1964)
Pickles, A.J.: PASP **110**, 863 (1998)
Piotto, G.: IAUS **246**, 141 (2008)
Piotto, G., King, I.P., Djorgovski, S.G., Sosin, C., Zoccali, M., Saviane, I., De Angeli, F., Riello, M., Recio-Blanco, A., Rich, R.M., Meylan, G., Renzini, A.: A&A **391**, 945 (2002)
Salpeter, E.E.: ApJ **121**, 161 (1955)
Shetrone, M.D. & Sandquist, E.L.: AJ **120**, 1913 (2000)
Stryker, L.L.: PASP **105**, 1081 (1993)
Thomas, D., Maraston, C., Bender, R.: MNRAS **339**, 897 (2003)
Vazdekis, A.: ApJ **513** 224 (1999)
Worthey, G.: ApJS **95**, 107 (1994)

Xin, Y. & Deng, L.: ApJ **619**, 824 (2005)
Xin, Y., Deng, L., de Grijs, R., Kroupa, P.: MNRAS **411**, 761 (2011)
Xin, Y., Deng, L., de Grijs, R., Mackey, A.D., Han, Z.: MNRAS **384**, 410 (2008)
Xin, Y., Deng, L., Han, Z.: ApJ **660**, 319 (2007)
Yi, S.K.: ApJ **582**, 202 (2003)

Index

H.M.J. Boffin et al. (eds.), *Ecology of Blue Straggler Stars*, Astrophysics and Space Science Library 413, DOI 10.1007/978-3-662-44434-4